ASSESSMENT OF SUB SEA ECOSYSTEM IMPACTS

Technical Study

Report No. 2008/8

March 2009

INTERNATIONAL ENERGY AGENCY

The International Energy Agency (IEA) was established in 1974 within the framework of the Organisation for Economic Co-operation and Development (OECD) to implement an international energy programme. The IEA fosters co-operation amongst its 26 member countries and the European Commission, and with the other countries, in order to increase energy security by improved efficiency of energy use, development of alternative energy sources and research, development and demonstration on matters of energy supply and use. This is achieved through a series of collaborative activities, organised under more than 40 Implementing Agreements. These agreements cover more than 200 individual items of research, development and demonstration. The IEA Greenhouse Gas R&D Programme is one of these Implementing Agreements.

ACKNOWLEDGEMENTS AND CITATIONS

COPYRIGHT

ACKNOWLEDGEMENTS AND CITATIONS

This report describes research sponsored by the IEA Greenhouse Gas R&D Programme. This report was prepared by:

Dr Rachel Dunk

To ensure the quality and technical integrity of the research undertaken by the IEA Greenhouse Gas R&D Programme (IEA GHG) each study is managed by an appointed IEA GHG manager. The report is also reviewed by a panel of independent technical experts before its release.

The IEA GHG manager for this report: Toby Aiken

The expert reviewers for this report:

Stephen Widdicombe, Plymouth Marine Labs,
Martin Hovland, StatoilHydro,
Peter Brewer, MBARI,
Chris Vivian, CEFAS,

The report should be cited in literature as follows:

IEA Greenhouse Gas R&D Programme (IEA GHG), "Assessment of Sub Sea Ecosystem Impacts", 2008/8, August 2008.

Further information or copies of the report can be obtained by contacting the IE Greenhouse Gas R&D Programme at:

IEA Greenhouse Gas R&D Programme, Orchard Business Centre, Stoke Orchard, Cheltenham, Glos., GL52 7RZ, UK
Tel: +44 1242 680753 Fax: +44 1242 680758
E-mail: mail@ieaghg.org
www.ieagreen.org.uk

ASSESSMENT OF SUBSEA ECOSYSTEM IMPACTS

Background to the Study

One of the key elements required before receiving permission to commence underground storage of CO_2, will be the ability of the operator to predict the behaviour of the injected CO_2 and demonstrate a thorough understanding of the risks of leakage, and the associated impacts of these leaks. Also, CO_2 Capture and Storage (CCS) operators must be able to demonstrate that CO_2 can be injected into suitable storage reservoirs both safely and with minimal or no environmental impact. The safety aspect predominantly relates to good design and operational practices and strict adherence to accepted health and safety procedures.

In July 2007, the IEA Greenhouse Gas R&D Programme (IEA GHG) published a report compiled by the British Geological Society (BGS) assessing the impacts of leaks from on-shore geological storage sites on terrestrial ecosystems[1]. This report showed that any environmental impacts that may arise will occur as a result of CO_2 migration from a geological storage reservoir followed by subsequent seepage to the surface. If seepage is to occur, it will most likely be at low levels over long time periods (possibly 100's to 1,000's of years) and could result in localised environmental impacts. The evidence for these statements comes from those natural accumulations of CO_2 that have been observed to have migration and seepage occurring[2]. It is expected that migration and seepage on-shore can be minimised or prevented through a combination of effective site selection and design, risk assessment and monitoring.

Whilst it is expected that there will be similarities regarding seepage from off shore geological storage reservoirs there is still a need to attempt to quantify the migration/seepage conditions that might lead to environmental impacts on the seafloor from sub-seafloor geological storage projects. For CCS technologies to be acceptable to the general public, environmental bodies, commercial operators and regulatory bodies alike, it may be necessary for operators to be able to demonstrate a deep and thorough understanding of the possible long and short term effects of CO_2 seepage on ecosystems, both at the surface and subsurface level. However, this requirement would be a project-specific decision, based on the individual site assessment, and some sites may not require such stringent understanding in order to justify a permit.

This study aims to assess the extent of information currently available on the effects of CO_2 seepage on subsea ecosystems, and assess what gaps in knowledge exist, along with providing recommendations for further research to address these gaps.

The study was undertaken by Dr Rachel Dunk, The Crichton Carbon Centre, UK.

---

[1] IEA Greenhouse Gas R&D Programme (IEA GHG), "Study of Potential Impacts from Onshore CO_2 Storage Projects on Terrestrial Ecosystems, 2007/3, July 2007".

[2] For the purpose of this overview, migration is defined as movement from the storage reservoir through the surrounding geology, and seepage refers to migration that passes through or around the caprock and reaches the atmosphere or, in this case, the ocean floor.

Figure 2: The percentage of regional storage capacity in oil and gas reservoirs that occurs offshore versus the percentage of regional storage capacity in saline aquifer that occurs offshore (based on data from Hendriks et al., 2004 & Dooley et al., 2005). Shaded areas define the 50% and 66.6% boundaries.

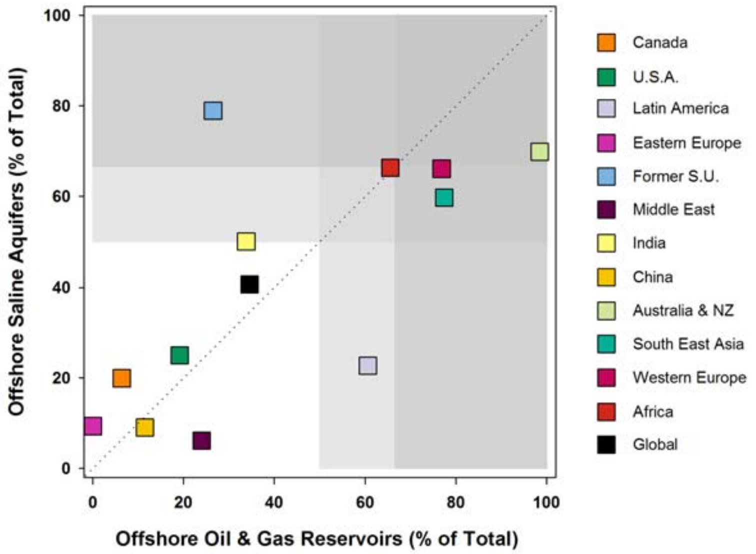

From this plot, it can be expected that Africa (specifically West Africa), South East Asia, Western Europe and Oceania are will have significant offshore storage potential, in each case offshore storage represents over 50% of their respective total regional storage capacities.

Fluxes of CO_2 to the Global Ocean

Fluxes to the oceans are either atmospheric or subterranean in origin. Atmospheric fluxes occur in the form of non-purposeful sequestration direct from the air to the ocean surface. The role of the world's oceans in sequestering atmospheric CO_2 has long been accepted, and numerous efforts have been made to limit this uptake[4]. Estimates and data sets taken from these experiments were combined by Sabine et al. (2004) to suggest a total uptake between the years of 1800 and 1994 of 433±70 $GtCO_2$, which equates to approximately 50% of the CO_2 produced by fossil fuel combustion in the same period. The IPCC Fourth Assessment Report estimates fluxes of 6.6±2.9 $GtCO_2$/yr, 8.1±1.5 $GtCO_2$/yr and 8.1±1.8 $GtCO_2$/yr for the 1980's, 1990's and the period 2000-2005 respectively.

Natural fluxes of CO_2 to the ocean bottom waters are derived through hydrothermal circulation[5], and this can occur in four different ways; submarine volcanism (volcanic arcs), Mid Ocean Ridges (MOR's), subduction zones (back arc basins) and hotspots. The methodologies to determine the extent of these fluxes is a complex procedure and is explained in detail in the main report.

Estimating global fluxes of volcanic CO_2 requires an understanding of the $CO_2/^3He$ ratio of volcanic emissions at the different types of hydrothermal vent sites, and there have been numerous studies carried out (see main report for more information), but using average values from the published data, the calculations for volcanic CO_2 fluxes to the ocean can be

---

[4] World Ocean Climate Experiment (WOCE), and the Joint Global Ocean Flux Survey (JGOFS).

[5] The heat driven transport of water through the earths crust.

determined as shown below in Table 1 which transposes these ratios into CO_2 fluxes in terms of Mt/yr.

Table 1: The Flux of Volcanic CO_2 to the Ocean

	$F(^3He)$	$CO_2/^3He$	$F(CO_2)$		
	mol/yr	10^9 mol/mol	10^{12} mol/yr	Mt CO_2/yr	*(%)*
MORs	489 ± 217	2.1 ± 0.9	1.0 ± 0.6	45 ± 28	***(27.8)***
Back-Arc Basins	109 ± 48	12.8 ± 10.7	1.4 ± 1.3	61 ± 58	***(37.8)***
Volcanic Arcs	53 ± 28	23.5 ± 10.0	1.3 ± 0.8	55 ± 37	***(34.1)***
Hotspots	2 ± 1	4.5 ± 2.6	0.01 ± 0.01	0.5 ± 0.4	***(0.3)***
TOTAL			**3.7 ± 1.7**	**162 ± 74**	

Comparison of these two sources of CO_2 flux to the ocean indicates that the main flux is atmospheric in origin, with an estimated 8.1±1.8 $GtCO_2$/yr for the present day, compared with 162±74 $MtCO_2$/yr for volcanic fluxes. This equates to an atmospheric flux of 50 times that of sub-seafloor sourced fluxes. However it is noted that these fluxes and in fact approximately 600-1000 times the amount of CO_2 injected into sub-seafloor reservoirs to date and are significantly higher than the expected maximum permissible seepage rates from geological storage reservoirs[6]. Also most of these volcanic fluxes occur in the Australasian and South East Asian regions which are prospective areas for offshore storage. In these regions therefore there will be existing natural emissions of CO_2 that have the potential to mask the impacts of leaks from geological storage systems. It could therefore be suggested that the effect of man-made leaks would be analogous to the effects of similar natural leaks in the same ecosystem.

Analogues for Leakage or Seepage of CO_2 from Sub-Seafloor Storage Sites

There are two possible analogues for leakage from sub-seafloor geological storage site which are; release from natural CO_2 vents and purposeful release experiments. In order to determine the validity of these as analogues, the physical and chemical characteristics must be compared and examined for similarities and differences.

Natural vents are usually found along faults in regions of high tectonic activity, and are understood to occur at shallow, intermediate and deep zones. The zones can be recognised by the following:

- Shallow zones are typically less than 200m deep, and can also be recognised by the absence of vent obligate taxa, which are organisms usually present around hydrothermal vents, and the CO_2 will be in the gas phase,
- Intermediate zones are between 200 and 600m deep, and at these vents it is likely that some vent obligate taxa will be present and the phase state of the CO_2 is determined by the local temperature,
- Deep zones are characterised as being deeper than 600m, the majority of biota present will be vent obligate taxa, and the CO_2 will be in the liquid phase.

---

[6] Assuming widespread deployment of CCS by 2100, then the total mass of stored CO_2 could reach 250-500 $GtCO_2$, and assuming that all storage reservoirs meet performance requirements of >99% of CO_2 retained for 1000 years, then maximum leakage flux should total 2.5-5 $MtCO_2$/yr which is around 20-100 times lower than the natural volcanic flux to the ocean. It must also be noted that these calculations, while based on leakage of 1% of stored volume, are not expected to be typical leakage rates, and good initial site characterisation and selection should result in the overwhelming majority of storage reservoirs not suffering from leakage at all.

To compare a vent to leakage from a geological storage reservoir, three aspects must be considered; firstly does the environment reflect that likely to be found at a leakage site? Does the scale of leakage in terms of area, rate and duration equate to that of an expected leakage event? And thirdly, what extent of variation exists between the vents and the expected leakage site in terms of physical and chemical properties? These three questions must be addressed in order to determine suitability of a vent as a natural analogue for CO_2 storage.

The report identified West Africa, Western Europe, South East Asia and Oceania as potential regions for near future deployment of sub-seafloor storage, and vents can be readily found in the Mediterranean and Pacific regions due to tectonic activity so there is a potentially good correlation between natural vents and potential CO_2 storage sites. Examples of this correlation are shown in figure 3, a cropped version of figure 3.2 in the main report.

Figure 3: Map showing analogous vent sites for Western Europe, South East Asia and Oceania

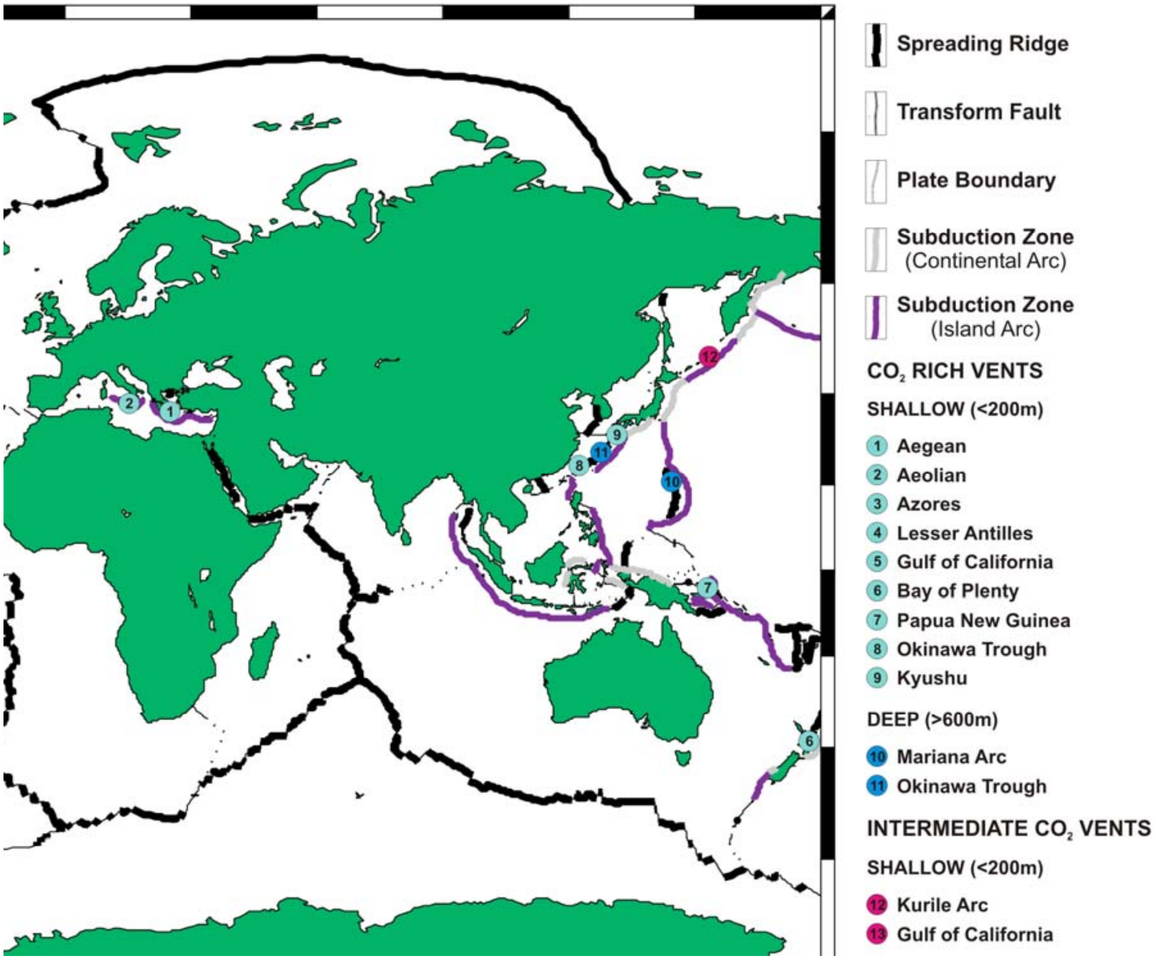

There are numerous problems encountered when attempting to carry out purposeful release experiments of an appropriate scale. To imitate seepage through the sediment column would essentially need an engineered leakage, and in addition to the difficulties of setting up such a procedure, adverse public opinion and permitting for the procedure could encounter further issues. Despite these issues, numerous purposeful release experiments have been carried out, and although these experiments are transient in nature, they have contributed to the understanding of the effects of CO_2 on various species. However the differences in characteristics between purposeful release and an engineered leak dictate a need for further study of the potential impact from engineered leaks to better comprehend the difference between acute (short term) and chronic (longer term) exposure to elevated levels of CO_2.

Both types of analogue can be a good source of data, and both should be the subject of further research as they provide a good balance; where vents are weak in some aspects, purposeful release experiments are strong, and vice versa.

Primary Leakage or Seepage of CO_2 from Sub-Seafloor Geological Storage Reservoirs

The potential mechanisms for trapping of CO_2 in geological storage reservoirs both on-shore and off-shore are well documented - see the IPCC Special Report on CO_2 Capture and Storage (IPCC SRCCS). The mechanisms that can facilitate leakage are also well understood.

However, in the case of subsea geological storage, when migrating CO_2 encounters the sediment column, there is a possibility that further trapping mechanisms come into play which can restrict or prevent the further migration of CO_2 into the ocean. Also, different forms of migration pathways can exist that facilitate the movement of CO_2 from the storage reservoir into the bottom ocean waters. The buoyancy of the CO_2 bares a great impact on the migration rate, and the buoyancy is dependant on the density and viscosity of the CO_2, and these in turn are impacted by the temperature and pressure. Different combinations of conditions result in affected buoyancy, and subsequent changes to the migration rate of CO_2. These are illustrated by example cases in the main report.

A leak of CO_2 into a water saturated sediment column will instigate residual trapping[7]. The capacity of residual trapping is dependant on in-situ conditions, but the main report demonstrates that a $1m^2$ sediment column at a depth of 1000m will have the capacity to trap 116±23 tCO_2. In conditions of slow leakage (i.e. approximately $10tCO_2/yr$), it would be possible for all the CO_2 that leaked over a 10 year leakage event to be effectively trapped in the sediment column. However, as leakage of this rate is unlikely to be detected, it is reasonable to assume that the leakage event would continue for longer than 10 years, and could be in the range of 100-1000 years. In this situation, the amount of CO_2 that could be trapped by this method would only equate to between 1-10% of the total leaked volume. This can be illustrated on a graph, and is shown in Figure 4 below.

---

[7] In this context, residual trapping refers to the CO_2 that has leaked from the storage reservoir, but remains in the sediment column, and does not reach the ocean waters.

Figure 4: The efficacy of residual trapping as a function of leakage rate and duration of leakage.

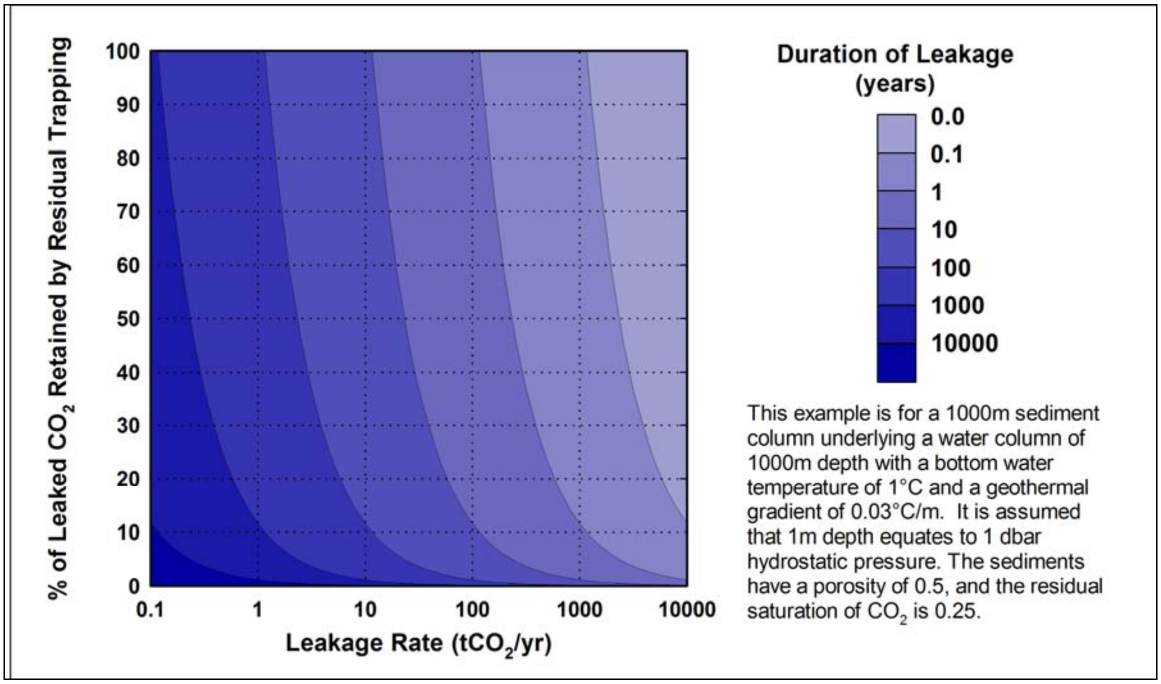

Another secondary trapping mechanism which can account for the eventual fate of CO_2, is gas hydrate trapping. CO_2 readily forms a gas hydrate, which is a solid phase which forms at low temperature and high pressure, conditions which are often encountered at potential leakage sites in deep waters. This hydrate formation can limit the escape of CO_2 to the ocean, and in some cases may prevent it completely. Theoretically, as CO_2 migrates upwards through the sediment column into an area where the conditions are suited to hydrate formation, hydrate crystals will begin to form, and they can block the pre space, slowing the potential for further upward CO_2 migration; it is possible that these hydrates can form to such an extent that they form a hydrate cap capable of withstanding considerable pressure from below as more CO_2 migrates through the sediment column to the base of this hydrate layer.

Other mechanisms that can affect the trapping include dissolution and mineral trapping. These are both subject to complex controlling mechanisms, and not all of these are understood to a degree whereby they can be incorporated into models. There is more detail of these methods in the main report. Currently, each of the trapping mechanisms discussed in this section are considered in isolation, due to this lack of understanding. They represent an area for future research to facilitate the incorporation of these mechanisms into a comprehensive dynamic model.

The Release of Leaked CO_2 to the Ocean

If the various trapping mechanisms in both the geological storage reservoir and sediment column do not prevent the migration of CO_2, then the ultimate result will likely be a leak into the ocean waters. Comparisons have been made between this situation and that of purposeful storage in the oceans under similar conditions; however differences between the two situations exist and must be considered:

- Chemistry of the CO_2; purposeful ocean storage would include stringent controls on the chemical make-up of the CO_2, and although sub-seafloor injection would be subjected to similar controls, migration through the overburden and sediment column could alter the CO_2 chemistry by mobilising heavy metals and other toxic substances.
- Volume location and depth characteristics; these factors would be dictated by the site selection of ocean storage, whereas leakage could occur in a less predictable location, without external controls.
- Monitoring techniques; a combination of methodologies would be necessary to detect a leak, both sub-surface and water column monitoring, continuous and periodic. Although the total amount of CO_2 would be lower that purposeful ocean storage, the risks due to lack of controlling mechanisms would equate to a higher risk factor.

Impacts on organisms and ecosystems are highly complex and can occur at any level from the molecular to the entire community. Effects can also be as severe and easily detectable as organism death, to less discernable effects such as decreased growth or development rates. Tolerance levels are a vital element of determining impacts of CO_2 leaks, and Figure 5 illustrates the possible effects on different organisms and ecosystems.

Figure 5: Possible hierarchy of functional limits at increasing CO_2 levels (after Pörtner et al., 2004). Categorisation of CO_2 dependant effects on ocean biota based on the concept of a molecular to systematic hierarchy of tolerance limits. The widest tolerance windows are at the lowest hierarchical or functional levels. As system complexity increases, the combined effect of on numerous different functions leaks to narrow tolerance windows at high hierarchical levels. Thus while individual mortality might only be observed at significantly elevated CO_2 levels, changes in community structure and ecological functions may well occur at considerably lower CO_2 concentrations. Pejus thresholds (long term tolerance) mark the CO_2 concentration where performance limitations are first observed. Critical thresholds (short term tolerance) mark the onset of metabolic depression. Both pejus and critical thresholds are likely to vary between species and phyla.

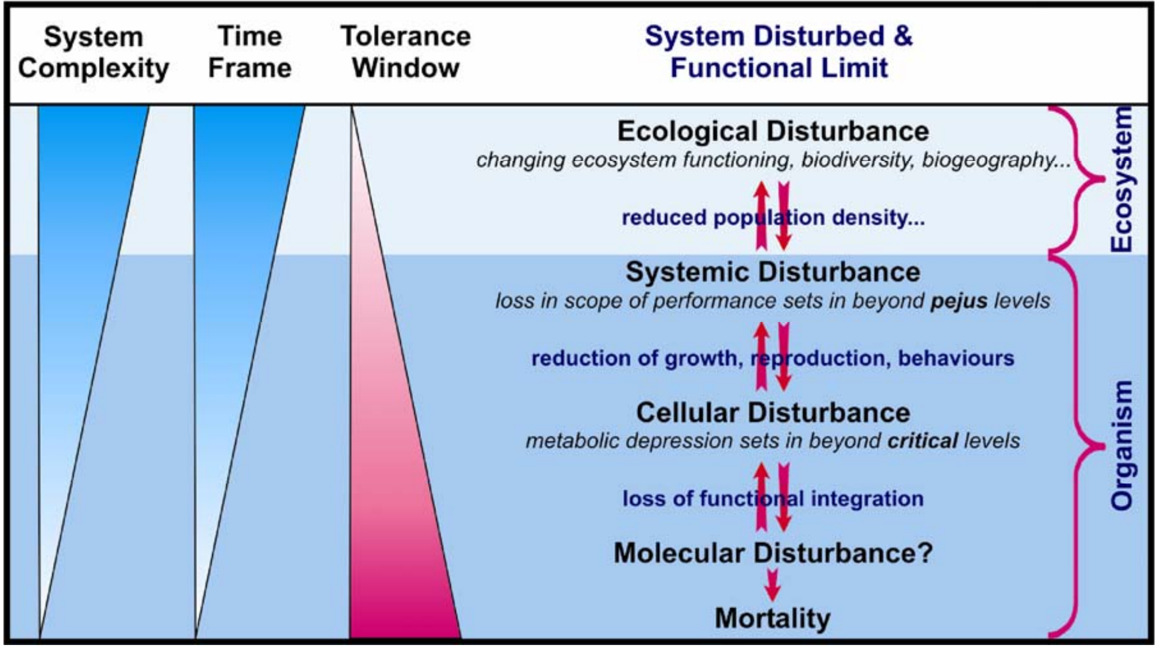

Results and Discussion

The study covers 6 areas, and they are briefly outlined in this overview. Full details are presented in the main report. The subjects are as follows:

- Near Future Sub-Seafloor CO_2 Storage Sites,
- Fluxes of CO_2 to the Global Ocean,
- Analogues for Leakage or Seepage of CO_2 from Sub-Seafloor Storage Sites,
- Primary Leakage or Seepage of CO_2 from Sub-Seafloor Geological Storage Reservoirs,
- The Release of Leaked CO_2 to the Ocean,
- Vulnerable Objects and High Risk Scenarios.

Near Future Sub-Seafloor CO_2 Storage Sites

Offshore storage of CO_2 depends on many physical factors and conditions, and the map shown in Figure 1 illustrates the most prospective basins for offshore storage of CO_2.

Figure 1: Prospective Offshore Basins for Storage of CO_2 (Bradshaw & Dance, 2005).

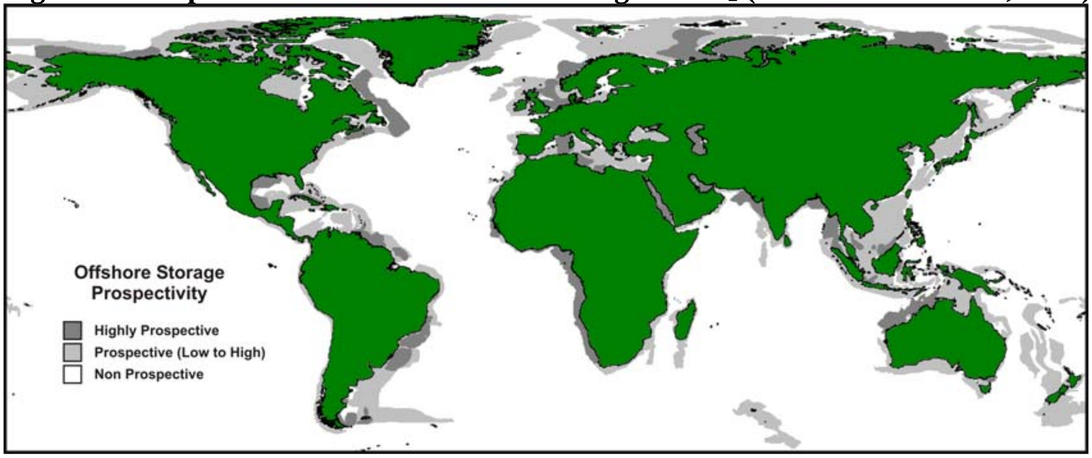

Storage can be undertaken in both offshore oil and gas fields and deep saline aquifers[3]. The regional distribution of potential storage capacity offshore is illustrated in Figure 2.

---

[3] The term deep saline aquifers in this overview is used to maintain consistency with the main report, and refers to aquifers containing only saline water with no links to potable water supplies and of no value as an underground source of drinking water (USDW).

Vulnerable Objects & High Risk Scenarios

It can be stated that the risks associated with a leakage event can be defined as high when a high possibility of leakage coincides with the presence of one or more vulnerable objects (species) in the leakage path. The key determining factor for a high risk scenario is therefore likely to be the presence of a vulnerable object. An example that illustrates this is the scenario of CO_2 migrating out of the storage formation through a leakage pathway such as a fault; the CO_2 could be subsequently immobilised by secondary trapping mechanisms in the sediment column, resulting in the leakage event being defined as low risk; but the same leakage without the secondary trapping mechanisms could result in escape to the ocean, whereby the presence of a vulnerable object would determine whether the leakage event was low or high risk.

An example of a potentially high risk situation is that of leakage in areas with a proliferation of deep water coral reefs. These coral reefs occur in the vicinity of nearly all areas both currently being used for CCS, and those identified as likely to commence sub-seafloor storage in the near future. These often occur in proximity to hydrocarbon seeps which could also act as possible migration pathways. Leakage of CO_2 to a deep water coral reef could cause impact an entire ecosystem. The presence of CO_2 in this instance could lower the pH of the sea water which would inhibit calcification (the process by which coral reefs are formed) and even lead to dissolution of the reef. For this reason, the presence of coral reefs equate to a potentially high risk at the level of damage to organisms, but furthermore, the coral reefs play an important role in the greater ecosystem; the reefs sustain an extremely high level of biodiversity, and also act as nurseries for many species of fish, including those of importance to commercial fishing. As a very slow growing species, damage to coral reefs could take as much as 100's to 1000's of years to recover, if at all.

Key Knowledge Gaps and Future Research Requirements

The report has highlighted where the key knowledge gaps exist, and also outlines the issues that need to be considered before commencement of a sub-seafloor storage project. The key conclusions and needs for further research can be summarised as:

- Site specific assessment; due to the potential for wide ranging variations in temperature, pressure, and presence of vulnerable species, site specific assessments are vital before permitting storage operations. Although generic guidelines could potentially provide a high level screening process, the complexity of storage under the sea-floor would require in-depth analysis of the likely conditions experienced, the susceptibility of a reservoir to leak, the possibility of the leak reaching the ocean, and the presence of CO_2 tolerant / vulnerable species. Effects of leaked CO_2 on the pH would also need significant attention.
- Capacity of the sediment column to provide secondary trapping mechanisms; it is explained in the report how trapping mechanisms in the sediment column can account for secure and permanent immobilisation of CO_2 leaking from the storage reservoir, and the potential for this could provide a strong indication of secondary storage security. Whether this would be considered acceptable under a storage permit is not known, but possibly further research could help to develop the knowledge on the potential of this storage mechanism.
- Species identification; as with all CCS activities, the identification of key indicator species to determine the presence and extent of impacts from leaks will greatly assist in determining the potential effects of leakage. Sub-seafloor geological storage could cover such a wide diversity of environments and ecosystems around the world, that many species may be needed depending on the precise situation encountered. Certain

coral species for example could be vulnerable to CO_2, and even small decreases in ocean pH may have significant effects.

Expert Review Comments

The key findings of the report were presented at a recent workshop organised by IEA GHG and BGS, addressing the impacts of potential leakage on both terrestrial and marine ecosystems. The report was also sent to a panel of exert reviewers, whose comments concluded that the report was a very thorough piece of work, and would be of benefit to the R&D community.

Some comments were made regarding the omission of some more recent research, and this is due to the timescale the project has run for. In the interests of publishing the report, this was accepted but no action has been taken.

Conclusions

The report has highlighted the areas of the world that are likely to be used for sub-seafloor geological storage in the near future, which are: West Africa, Western Europe, South East Asia and Oceania.

It is noted that there are sub seafloor leaks of CO_2 from natural sources which are several orders of magnitude lower than the ocean surface sequestration of CO_2, and further that leaks from sub seafloor geological storage of CO_2 are unlikely to equate to even 2% of this level of naturally occurring leakage. These natural analogues (such as volcanic arcs and hydrothermal vents) occur in many of the areas where subsea geological storage is likely to take place, and can therefore be used as analogies for leaks from geological storage reservoirs. This will allow operators to perform assessments on the likely implications of leakage events before storage commences. It also suggests that any leaks in these areas will have a relatively low significance, as the leaked CO_2 will represent a lower percentage change to the seawater chemistry in these areas.

It will be necessary to identify a range of key indicator species to act as target organisms for monitoring programmes. Such monitoring programmes will prove beneficial in early detection of leakage, should it occur, and detailed study of these organisms will facilitate greater understanding of the potential risks of longer term exposure. Associated with this study will be the determination of exposure limits and recovery rates of affected species. This will allow much more accurate quantification of risk during the initial risk assessment and site characterisation process.

It should be noted that the potential immediate impacts on ocean ecosystems of CO_2 currently released into the atmosphere is significantly higher than any potential impacts of leakage from storage reservoirs in the future. Predictions of potential impacts in the future cannot be quantified; site selection criteria will focus activities on reservoirs that are likely to perform to high standards, minimising the risks of leakage and ecosystem impacts.

Recommendations

Further research is needed into the identification of key-indicator species for different regions around the world, tolerance levels of these species, and recovery rates when normal conditions are reinstated.

The recent IEA GHG / BGS workshop on environmental impact assessments highlighted areas for future research, and it is recommended that further workshops will be held to monitor progress towards these research goals.

Contents

1: Near Future Sub-Seafloor CO_2 Storage Sites

Over the last decade, carbon capture and storage (CCS) in geological formations has grown from a concept of limited interest to one that is regarded as a potentially important greenhouse gas mitigation option. With regard to sub-seafloor storage, initial interest in CCS has focused on gas fields with naturally high CO_2 contents, where the CO_2 has to be separated from the supply gas stream to create a saleable product. This includes the two currently operational facilities injecting CO_2 into sub-seafloor geological formations, the Sleipner project (Norway) and the K12-B project (Netherlands), both located in the North Sea, and three further projects at the development or planning stage; Snøhvit (Barents Sea, Norway), Gorgon (Australia), and Natuna (Indonesia). More recently, the possibility of combining CO_2 storage with offshore Enhanced Oil or Gas Recovery (EOR or EGR) is being considered, and power companies have also started to investigate offshore CCS as a mitigation option of relevance to their industry.

This chapter provides a brief overview of the global possibilities for offshore geological storage of CO_2, before focusing on regions where sub-seafloor storage of CO_2 is currently occurring, or is planned for the near future, at either the field experiment or commercial scale.

1.1 Global Potential for Offshore CO_2 Storage

While a detailed review of current knowledge regarding global geological CO_2 storage capacity and criteria for identification of potential CO_2 storage sites is beyond the scope of this report, a summary of information pertinent to offshore storage is presented below and a first order attempt is made to identify those regions where offshore storage may be utilised in the future.

The primary control on the extent to which sub-seafloor storage of CO_2 could be implemented in the future is the geographical location and capacity of potential offshore storage sites. Generally, the geological provinces of interest are sedimentary basins that have undergone only minor tectonic deformation and are at least 1000m thick with adequate reservoir/seal pairs to allow for the injection and trapping of CO_2. Within this, the following types of storage reservoirs are usually distinguished: natural gas and oil fields, aquifers, and deep unmineable coal seams. Although some research is being conducted into potential storage in other geological provinces, for example storage in seafloor basaltic crust (e.g. Matter et al., 2006), this research is in its infancy and is unlikely to contribute significantly to storage capacity in the near future.

1.1.1 Prospectivity

Bradshaw & Dance (2005) provided a qualitative assessment of potential storage sites defined in terms of 'prospectivity', or the likelihood that a suitable storage location is present in a given area based on available information. In this study the sedimentary basins of the world were divided into provinces that are considered to be (i) highly prospective, (ii) prospective, or (iii) non-prospective for CO_2 storage capacity based on the following criteria:

(i) Highly prospective basins: major hydrocarbon provinces that are "high priority" or "frontier" basins identified in the United States Geological Survey World Petroleum Assessment (USGS, 2000). Such basins have adequate reservoir / seal pairs and suitable traps for hydrocarbons (liquids or gases) and are expected to have substantial CO_2 storage potential.

(ii) Prospective basins (low to high): minor petroleum basins but not world class, as well as other non-petroliferous sedimentary basins that have not been highly deformed.

(***iii) Non-prospective basins:*** highly deformed sedimentary basins (and other geological provinces principally comprising fold belts, metamorphic and igneous rocks).

The offshore prospective regions identified by this study are shown in Figure 1.1. This map reveals that there are prospective storage sites along the majority of the worlds coastlines, and allows a qualitative assessment of the worlds regions that are rich (e.g. European Countries bordering the North Sea) or poor (e.g. Chile, the Somali Republic) in terms of prospective offshore storage sites. However, as capacity is not solely a function of the areal extent of sedimentary basin, it does not provide information on the relative capacity of the identified areas (Bradshaw & Dance, 2005).

Figure 1.1: Prospective offshore basins for storage of CO_2 (Bradshaw & Dance, 2005).

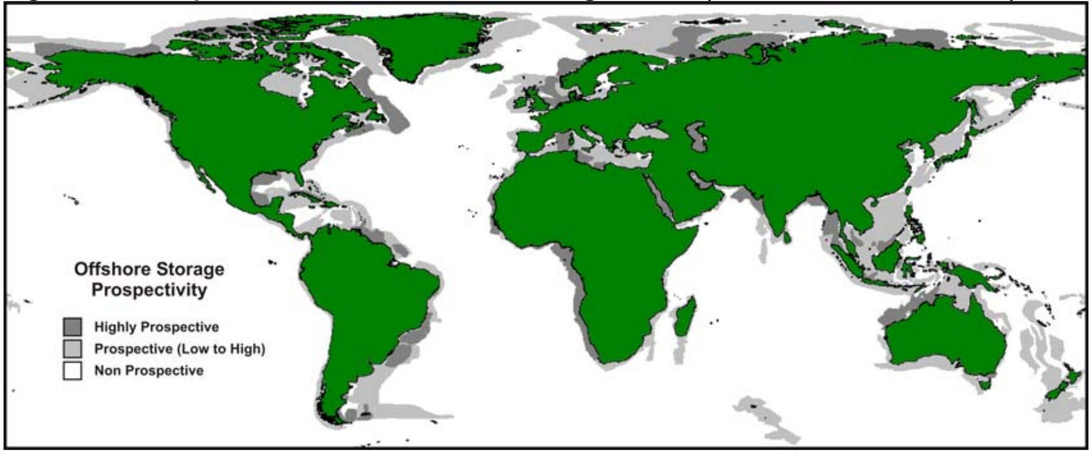

1.1.2 Technical Storage Capacity

While various high level estimates of the global CO_2 storage capacity of prospective geological formations have been made, these estimates cover a very broad range in values. This is due to the current lack of detailed geological and geophysical data in many world regions; hence various assumptions (which carry a high degree of uncertainty) have to be made regarding probable reservoir characteristics. A selection of estimates of the global CO_2 storage capacity within the four principal reservoir types are presented in Table 1.1 (Hendriks et al., 2004; Manancourt & Gale, 2005; IPCC, 2005; Dooley et al., 2005).

Table 1.1: Global CO_2 storage capacity in geological formations ($GtCO_2$).

Reservoir			IPCC (2005)	Manancourt & Gale (2005)	Dooley et al. (2005)		Hendriks et al. (2004)			
							Best Estimate			Range
Coal Beds			3-15 – 200	150 – 250	176		267			0 – 1480
Saline Aquifers			1000 – 10000	200 – 200000	9530		240			30 – 1081
Oil & Gas Fields	**Depleted**	**Gas**	675 – 900 (900 – 1200) *including undiscovered reserves*	500 – 1000	810	700	1153	332	239	24 – 423
		Oil				110			93	42 – 151
	Remaining	**Gas**		Not Reported	Not Reported			821	672	368 – 1703
		Oil							149	12 – 1043

The estimated storage capacities in oil and gas reservoirs show good agreement (within a factor of 2-3), reflecting the high quality of input information available for these economically important provinces, and providing confidence that the storage capacity is reasonably well defined. Conversely, the storage capacity available in coal beds and deep saline aquifers are very poorly constrained, with estimates encompassing 3 to 4 orders of magnitude. The range in values for coal bed storage reflects uncertainty in both the size of this reservoir and assumptions made regarding the feasibility of using it (i.e. the number of injection wells required to access the storage potential). At present no comprehensive realistic survey has been made of global storage capacity in coal beds, and no commercial CO_2 – Enhanced Coal Bed Methane (ECBM) recovery operation exists (IPCC, 2005). It is therefore unlikely that this storage type will play a significant role in near future operations, and it is not discussed further here.

Upper limits on the storage capacity of saline aquifers suggest that this reservoir type provides the greatest storage potential, up to 10 to 100 times larger than that available in oil and gas reservoirs. Furthermore, the majority of current or planned future offshore storage projects involve injection of CO_2 into a deep saline aquifer. The wide range in estimated capacity of aquifers reflects a number of issues. Firstly, as these geological formations do not hold valuable hydrocarbon reserves, they have received relatively little attention with regards to surveying etc., thus data are severely limited. Secondly, there are multiple mechanisms for storage in aquifers, including physical trapping beneath a low permeability cap rock, dissolution and mineralisation. Different authors have applied different assumptions regarding the type of trapping considered and used different assumed values for the physical properties of the aquifers. The lower estimates tend to consider storage only within physical traps, while the upper limits include dissolution based storage. Even within the subset of storage mechanism, widely different values have been applied to key reservoir characteristics. For example, Hendriks et al. (2004) assumed that only 1% of an aquifer formed part of a structural trap, while other authors have used values of 2-6% (IPCC, 2005 and references therein). Nevertheless, based on the principal of proportionality and the more detailed regional assessments available, the IPCC considers a storage capacity in the region of 1000 $GtCO_2$ to be a robust lower limit.

1.1.3 Technical Capacity of Offshore versus Onshore Storage Potential

The relative capacity (availability) of potential offshore and onshore storage sites may have a significant bearing on the extent to which offshore storage is utilised.

Due to the differing degree of uncertainty associated with global estimates of CO_2 storage within different reservoir types it is difficult to make a meaningful assessment of total offshore versus onshore storage capacity. Nevertheless, in a like to like comparison (i.e. using the same set off assumptions) and within the subset of reservoir type, a first order assessment can be made. This discussion is restricted to oil and gas reservoirs and deep saline aquifers.

1.1.3.1 Natural Gas and Oil Fields

The capacity estimates presented by Hendriks et al. (2004) are used as an example here. These authors evaluated storage capacity in 18 world regions, and explicitly considered offshore versus onshore storage, and depleted versus remaining fields (see Figures 1.2 -1.3 and Table 1.2; all numerical data are given in Appendix 1.A and the details of calculations and assumed values are given in Appendix 1.B). Hendriks et al. (2004) based their assessment of oil and gas fields on the USGS Digital Data Series (USGS 1995; 2000), thus these data correspond to the prospective storage regions identified by Bradshaw and Dance (2005) and illustrated in Figure 1.1.

Globally, over a third of the potential CO_2 storage capacity in oil and gas fields (depleted and remaining) is located offshore, including nearly one quarter of the storage capacity available in currently depleted fields (see Figure 1.2 and Table 1.2). Near future storage opportunities are likely to focus on depleted fields, or fields nearing depletion, as these sites: (i) have available capacity; (ii) may have existing infrastructure that can be adopted, and; (iii) may provide opportunities for EOR and EGR. Indeed, the use of gas fields may well be restricted to depleted fields due to the potential for contamination of the gas feed stream by injected CO_2 (current research is addressing the application of EGR - see discussion of K12-B). Conversely, the storage capacity of remaining oil fields will be 3 to 10 times larger if utilised immediately via EOR, and this should perhaps be considered in the exploration and exploitation of new oil reservoirs (Hendriks et al., 2004).

Figure 1.2: Global distribution of CO_2 storage capacity in oil and gas reservoirs (a) between onshore and offshore storage sites for depleted and remaining fields (b) a regional breakdown of offshore storage capacity (after Hendriks et al. 2004).

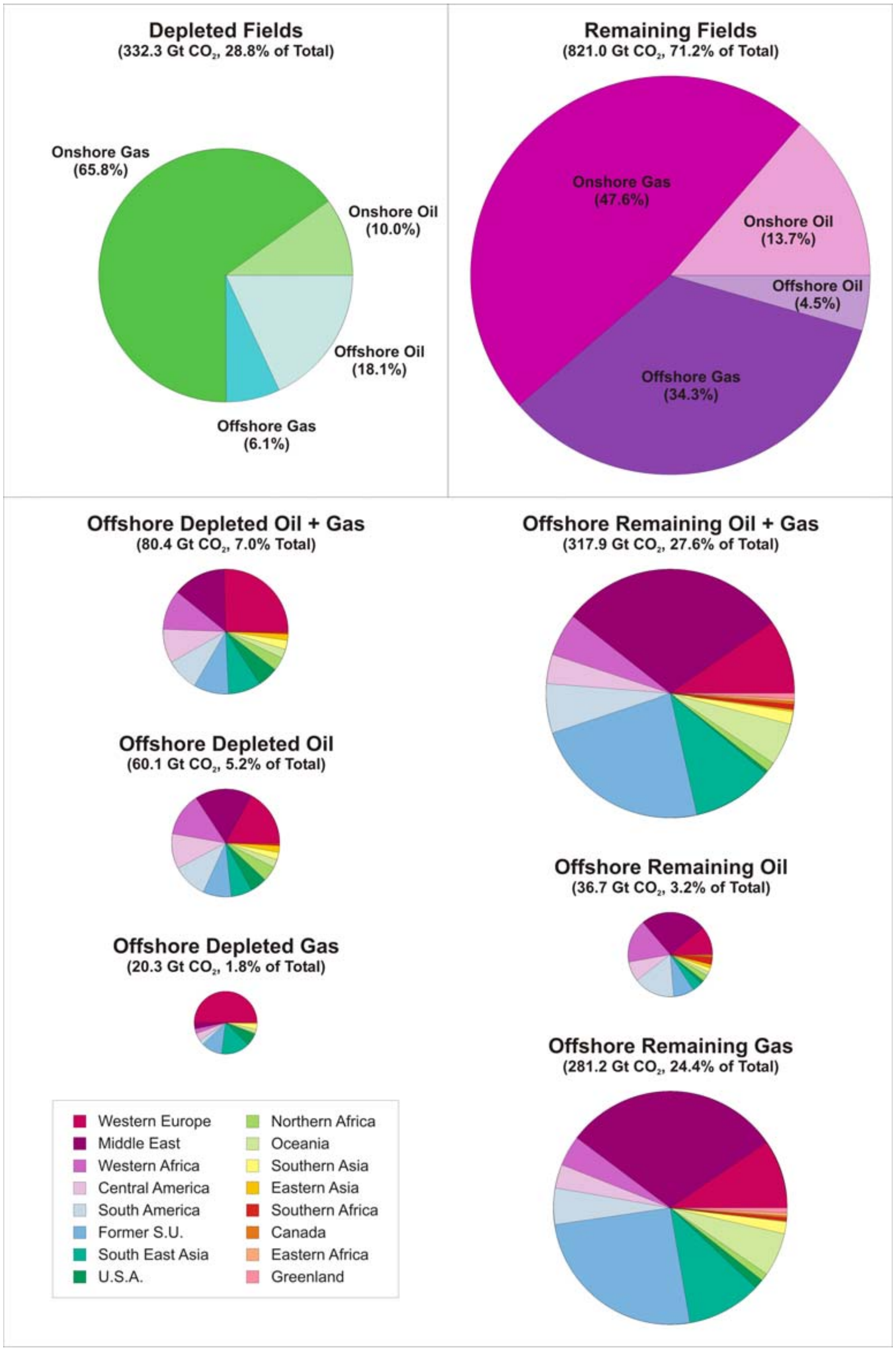

Figure 1.3: Regional distribution of CO_2 storage capacity between onshore and offshore storage sites in depleted and remaining oil and gas fields (after Hendriks et al. 2004).

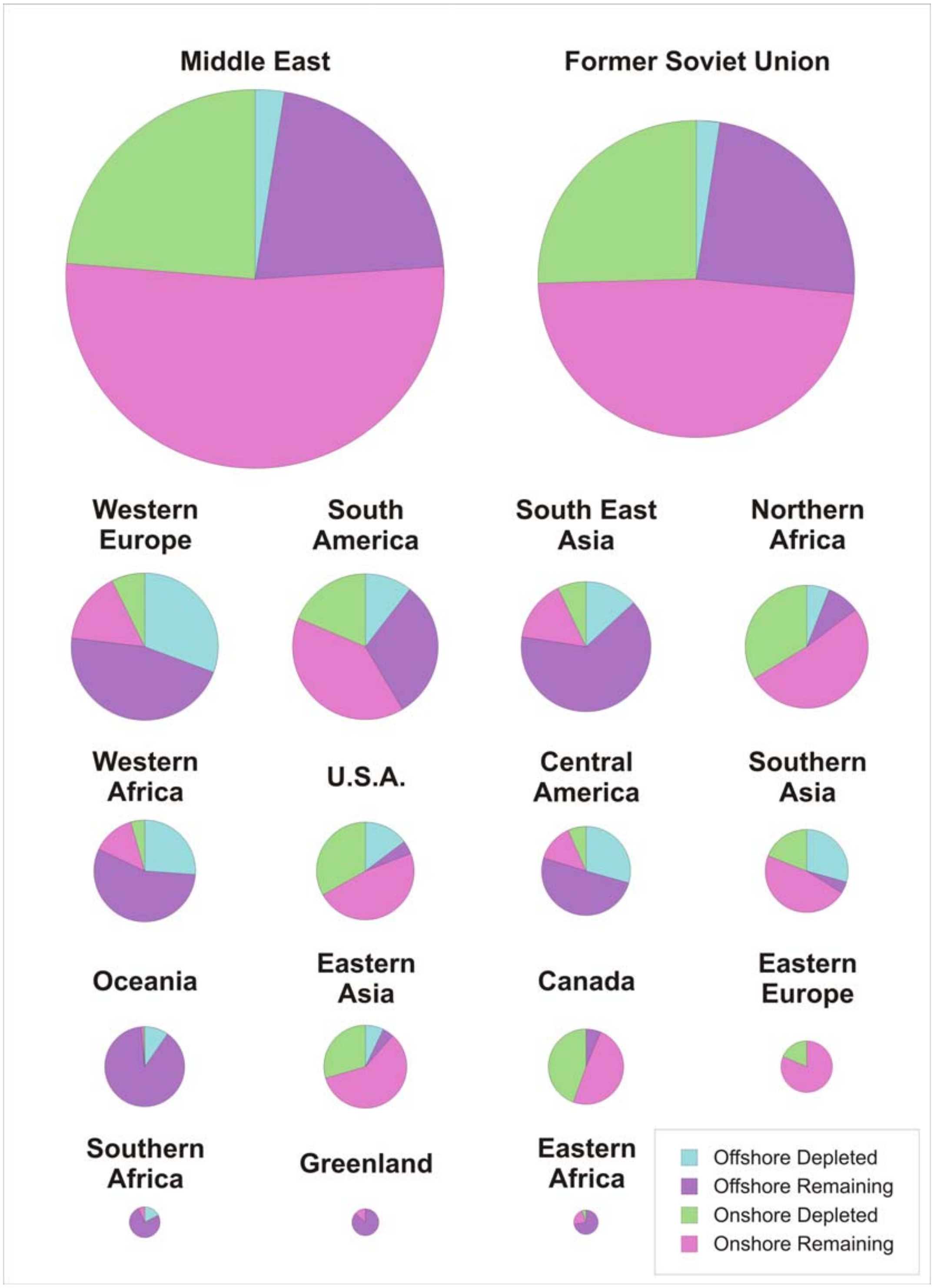

Table 1.2: Regional CO_2 storage capacity in offshore geological formations.

Region	Oil & Gas Reservoirs[a]						Saline Aquifers[b]		Region
	Depleted		Remaining		All				
	$GtCO_2$	*(%)*[c]	$GtCO_2$	*(%)*[c]	$GtCO_2$	*(%)*[c]	$GtCO_2$	*(%)*[c]	
Canada	0.0	*(0)*	1.1	*(11)*	1.1	*(6)*	249.3	(20)	**Canada**
U.S.A.	4.3	*(31)*	1.3	*(9)*	5.6	*(19)*	909.3	(25)	**U.S.A.**
Central America	7.1	*(82)*	12.2	*(79)*	19.3	*(80)*	55.0	(23)	**Latin America**
South America	6.8	*(36)*	20.1	*(44)*	26.9	*(41)*			
Northern Africa	2.8	*(15)*	4.0	*(14)*	6.8	*(15)*	231.0	(66)	**Africa**
Western Africa	8.3	*(86)*	17.8	*(81)*	26.1	*(82)*			
Eastern Africa	0.0	*(0)*	1.3	*(76)*	1.3	*(72)*			
Southern Africa	0.5	*(100)*	2.2	*(92)*	2.7	*(93)*			
Western Europe	20.4	*(81)*	30.8	*(75)*	51.2	*(77)*	143.0	(66)	**Western Europe**
Eastern Europe	0.0	*(0)*	0.0	*(0)*	0.0	*(0)*	11.0	(9)	**Eastern Europe**
Former S.U.	7.3	*(9)*	74.2	*(33)*	81.5	*(26)*	1386.0	(79)	**Former S.U.**
Middle East	11.0	*(10)*	94.3	*(29)*	105.3	*(24)*	14.7	(6)	**Middle East**
Southern Asia	1.9	*(32)*	5.2	*(34)*	7.1	*(34)*	187.0	(50)	**India**
Eastern Asia	1.3	*(19)*	0.8	*(7)*	2.1	*(11)*	33.0	(9)	**China**
South East Asia	6.8	*(65)*	33.3	*(81)*	40.1	*(77)*	179.7	(60)	**South East Asia**
Oceania	1.9	*(95)*	17.4	*(99)*	19.3	*(98)*	476.7	(70)	**Australia & New Zealand**
Japan	0.0	–	0.0	–	0.0	–	0.0	–	**Japan**
Greenland	0.0	–	1.9	*(86)*	1.9	*(86)*	–	–	–
TOTAL	**80.4**	***(24)***	**317.9**	***(39)***	**398.3**	***(35)***	**3875.7**	**(41)**	**TOTAL**

[a]Data of Hendriks et al. (2004); [b]Data of Dooley et al. (2005); [c]Percentage of total (onshore + offshore) regional capacity that is located offshore.

Examination of Figure 1.2 shows that 6 regions comprise 75% of the global storage capacity in offshore depleted oil and gas fields: (i) Western Europe (ii) the Middle East (iii) Western Africa (iv) Central America (v) South America (vi) the Former Soviet Union. These same regions are also comparatively ‘rich’ in remaining offshore fields. However, it does not necessarily follow that offshore storage is most likely in these regions. For three of these regions (Western Europe, Western Africa, Central America) examination of the regional breakdown of storage capacity and location (see Figure 1.3 and Table 1.2) shows that offshore storage capacity accounts for over 75% of the regionally available storage (in both depleted and remaining fields), suggesting that offshore storage may play a significant role in these regions. However, for two of the regions (the Middle East and the Former Soviet Union), offshore sites account for only one quarter of the regional storage volume, and if this is restricted to depleted fields only ~10% of available capacity. Conversely, while Oceania (Australia and New Zealand) and Southern Africa account for only a small proportion of global capacity, the regional breakdown reveals that over 90% of available storage is located offshore.

1.1.3.2 *Deep Saline Aquifers*

The capacity estimates presented by Dooley et al. (2005) are used as an example here. These authors evaluated storage capacity in 14 world regions and explicitly considered offshore versus onshore storage (see Figure 1.4 and Table 1.2; all numerical data are given in Appendix 1.C).

Globally, over 40% of the potential CO_2 storage capacity in deep saline aquifers is located offshore (see Figure 1.4 and Table 1.2). Examination of Figure 1.4 shows that 4 regions comprise over 75% of the global storage capacity in aquifers: (i) the Former Soviet Union (ii) the U.S.A. (iii) Australia and New Zealand (Oceania) (iv) Canada. However, as with the oil and gas reservoirs, evaluation of the regional assessments shows that for two of these regions (the U.S.A. and Canada), offshore storage accounts for a minority (≤25%) of available capacity. Nevertheless, for the former Soviet Union, nearly 80% of available storage capacity in aquifers is located offshore, and for Australia and New Zealand around 70% is located offshore. Of the remaining regions, offshore storage accounts for at least half of the available capacity in Africa, India, South East Asia and Western Europe, and for less than 10% in China, the Middle East and Eastern Europe.

1.1.3.3 *Regions where Offshore Storage may Prove Attractive*

As previously stated, it is not necessarily appropriate to consider the capacity of all offshore storage reservoirs versus all onshore storage reservoirs due to the high degree of uncertainty in estimates of aquifer capacity. For example, it may be that the capacity of depleted oil and gas fields is directly comparable to that of aquifers, or that the capacity of aquifers is dominant. Nevertheless, the breakdown of storage capacity into offshore and onshore sites discussed above allows a first order identification of regions where offshore storage may prove particularly attractive based on the available storage resources. In Figure 1.5, the percentage of regional storage capacity in oil and gas reservoirs that occurs offshore is plotted against the percentage of aquifer storage capacity that occurs offshore. This allows identification of those regions where the majority of all available storage capacity occurs offshore.

Over half of the available storage capacity in Africa, South East Asia, Western Europe and Oceania (Australia and New Zealand) occurs offshore, suggesting that these regions could see significant utilisation of sub-seafloor geological sequestration of CO_2 in the future. Together these regions account for over one quarter of the world's potential offshore CO_2 storage capacity.

Figure 1.4: Global and regional distribution of CO_2 storage capacity between onshore and offshore deep saline aquifers (after Dooley et al. 2005).

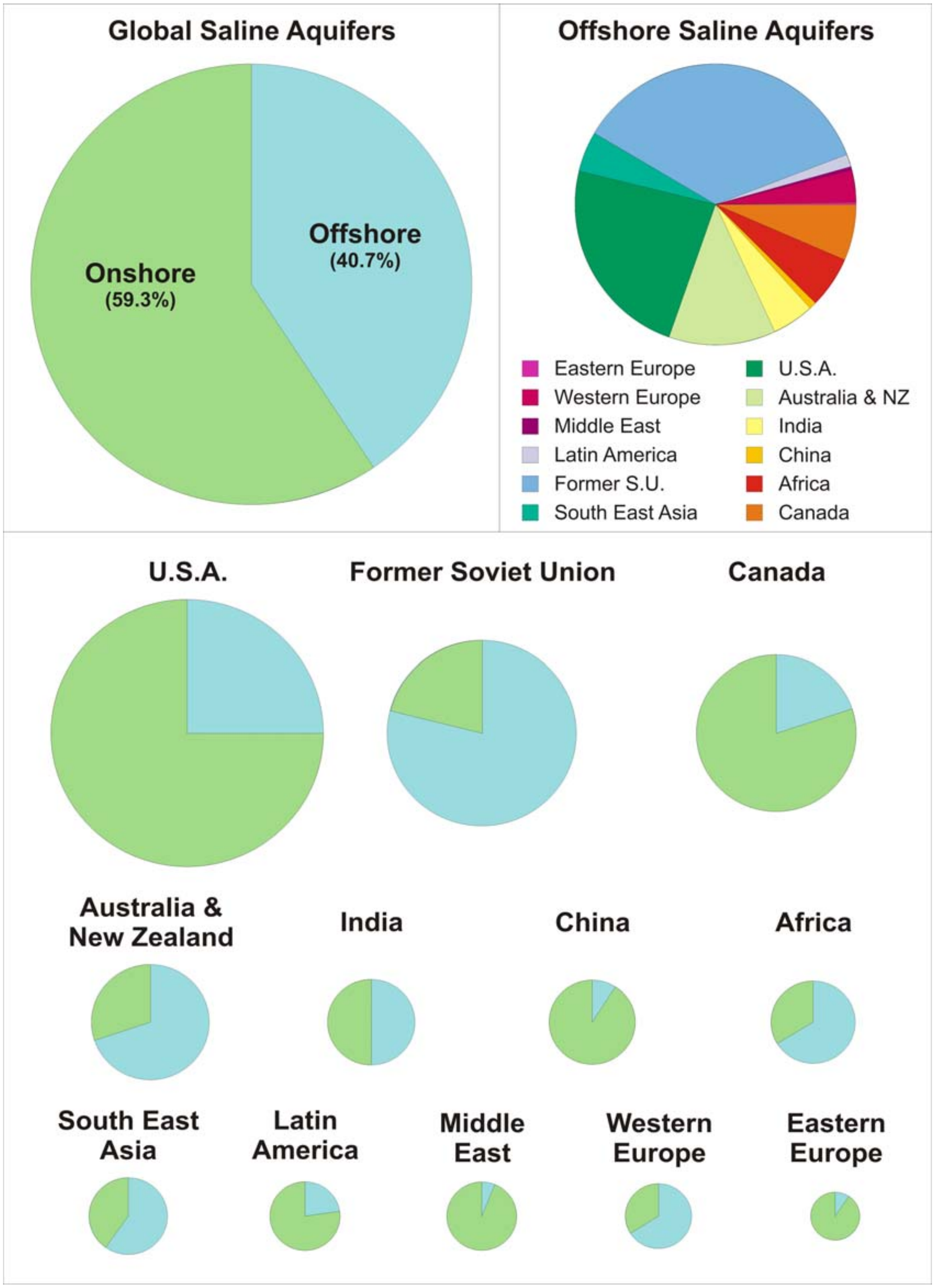

Figure 1.5: The percentage of regional storage capacity in oil and gas reservoirs that occurs offshore versus the percentage of regional storage capacity in saline aquifer that occurs offshore (based on data from Hendriks et al., 2004 & Dooley et al., 2005). Shaded areas define the 50% and 66.6% boundaries.

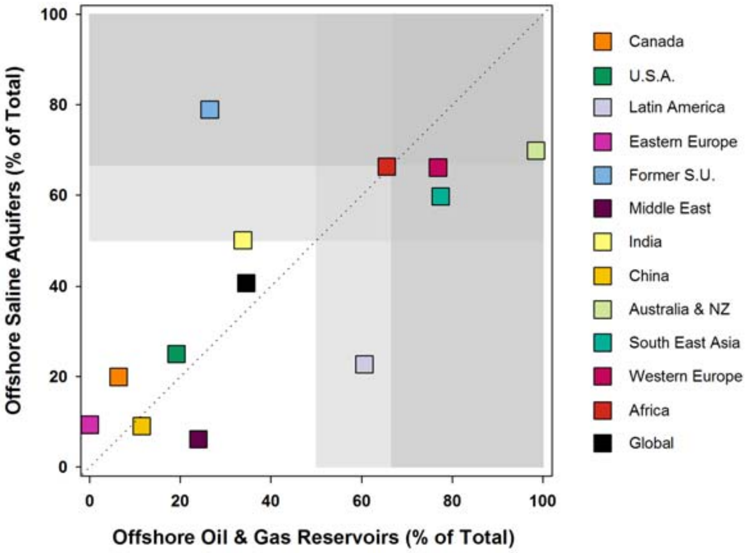

1.1.4 Technical Capacity versus Actual or Economic Capacity

The discussion above has focused on global and regional technical storage capacity. There are of course numerous other factors that will determine whether or not offshore storage of CO_2 is implemented in a given region, and not all of the potential storage sites will be useable.

To turn technical storage capacity into economical storage capacity (to realise the potential), the storage project must be cost effective, technically feasible, demonstrably safe, environmentally sustainable, capable of being broadly applied, and acceptable to the community (IPCC, 2005).

Storage safety is an important factor, where offshore storage would significantly reduce the risk to human health in the event of a leakage (Holloway, 2005). For this reason sub-seafloor storage may be utilised in preference to onshore storage sites (for example it would appear that at present Japan only intends to perform commercial scale CO_2 sequestration in offshore storage locations).

Economic criteria are of prime importance – it does not matter how good the storage site would be if it is not economically feasible to fill it with CO_2. In particular, the relative costs of onshore versus offshore storage may strongly influence the uptake of sub-seafloor geological sequestration. For example, Bachu (2003) considers it likely that offshore basins will be used for CO_2 geological storage much later than onshore basins, if at all, due to poor accessibility and possible lack of infrastructure (note this supports the supposition that implementation of offshore storage will be focused in areas where the majority of possible sites are located offshore). Criteria for identifying possible storage sites are thoroughly reviewed in the IPCC Special Report on CCS (IPCC, 2005), and a very brief overview of the key points are given below.

Any geological storage project will incur costs associated with:

(i) Capture of CO_2 from emission point sources followed by dehydration and compression.

(ii) Transportation of the CO_2 by pipeline to the storage site.

(iii) Injection and storage of the CO_2 in the geological reservoir.

Numerous researchers are working on optimising source sink matching to achieve maximum storage at minimum cost within specific regions. To a large degree, the economic criteria for site selection are dependent on capture and transport costs. Very simply, the closer the emission source is to the storage sink, and the cleaner the source (higher purity CO_2), the lower the costs.

The IEA-GHG has compiled a database of the major anthropogenic stationary sources of CO_2 (IEA-GHG, 2002). At a global level, Bradshaw & Dance (2005) compared their assessment of prospective geological storage sites to the locations of the world's current large stationary CO_2 emissions point sources. These point sources can be grouped into emissions clusters, bounded by a 'reasonable' transport distance, where the IPCC selected a radius of 300km as a guide for likely transport distances for potentially viable source to storage matches (IPCC, 2005). These cluster emissions for 12 regions of the world are overlaid on the prospectivity map in Figure 1.6.

Van Bergen et al. (2004) note that one of the key barriers to the introduction of CCS is the high cost of CO_2 capture, where this is principally associated with the extensive equipment required to scrub CO_2 from power plant exhaust gas streams containing CO_2 in low concentrations (8–14% by volume). These authors pre-selected a subset of the stationary CO_2 emissions sources known to have high purity (close to 100% CO_2) exhaust gas streams that can directly be dehydrated and compressed, thereby lowering capture costs significantly (van Bergen et al., 2004). They also applied a minimum emissions selection criterion of 100 ktCO_2/yr to reduce transport costs. These emission sources represent the 'low hanging fruit' and may provide the best opportunities for early implementation of CCS. Those pre-selected sites that fall near the coast are also shown in Figure 1.6.

Figure 1.6: Regional emissions clusters (300km radius) and near coast high purity CO_2 point sources (>90% CO_2, minimum 100 kt/yr) in relation to offshore CO_2 storage prospectivity (after van Bergen et al., 2004; Bradshaw & Dance, 2005; IPCC, 2005).

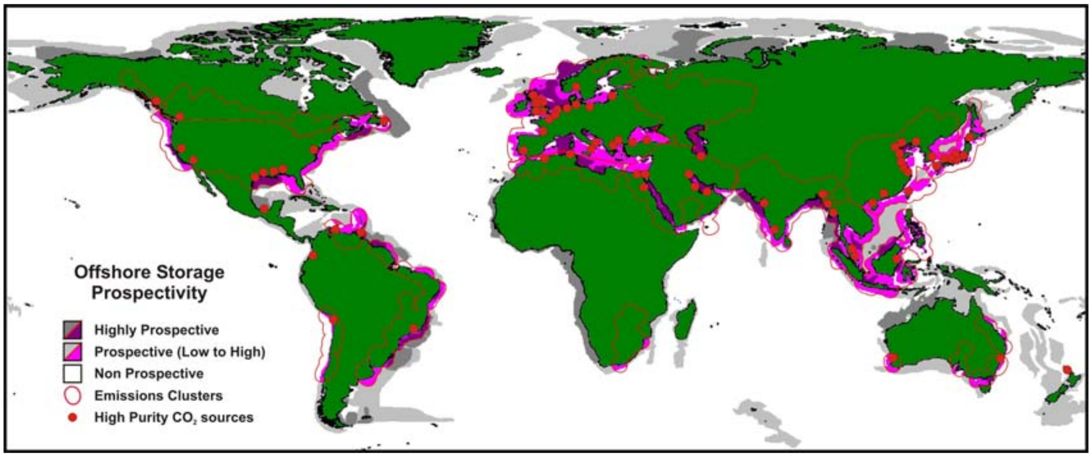

Overlaying the geographical distribution of potential source CO_2 emission points and offshore geological storage sinks provides a useful guide for locating the probable regions where subsea floor storage of CO_2 may, or may not, occur in the near future. For example, it would appear that the vast majority of the high purity near-coast CO_2 emissions sources occur in regions where offshore storage would be available. This is particularly true for the high density of emissions sources in Western Europe along the shores of the North Sea and the Mediterranean Sea. Conversely, while Western Africa has a high prospectivity/technical storage capacity, these data suggest there are no corresponding 'low hanging fruit', thus sub-seafloor storage is unlikely to occur in this region in the near future. Whether or not sub-seafloor storage is utilised in those areas where it appears possible will depend on detailed regional assessments as to the quality and viability of each sedimentary basin and specific proposed sites, and the relative costs/benefits of offshore versus onshore storage.

Finally, it should be noted that this analysis is severely limited in one important respect. Due to data unavailability, the pre-selection of high CO_2 emission sources does not include the locations of gas fields with naturally high CO_2 contents (van Bergen et al. 2004). For example, high CO_2 concentrations are encountered in petroleum reserves in (among others) South East Asia, Australia and New Zealand, and the North Sea (Thrasher & Fleet, 1995). Although costs of CO_2 capture at these sites are also high, CO_2 has to be cleaned from the feed gas stream in order to create a saleable product. High purity CO_2 streams are therefore available at a number of producing gas fields with high CO_2 contents, and more may become available as new fields are exploited. In such instances, the CO_2 emission source may well be located on a platform offshore, thus were CCS to be implemented, sub-seafloor storage would become the favoured option. Indeed, such operations account for the only currently operating offshore CCS projects, and for numerous future planned projects, as is discussed further in Section 1.2.

1.2 Currently Operating & Near Future Offshore CCS Projects

The remainder of this Chapter focuses on those regions where sub-seafloor geological storage of CO_2 is currently occurring, or is planned for the near future. This includes Japan, South East Asia, Oceania and Western Europe. Of these regions, South East Asia, Oceania and Western Europe were identified above as key regions where offshore storage could play a significant role in CCS due to the dominance of offshore with respect to onshore storage capacity.

1.2.1 Japan

An assessment of potential geological storage sites in the Asia-Pacific Economic Cooperation (APEC) region excluded the possibility of geological storage in Japan due to the lack of storage capacity in hydrocarbon reservoirs and minimal sedimentary basins that would meet the criteria for geological storage of CO_2 (Bachu, 2003). Indeed, in the assessment of Dooley et al. (2005), Japans technical storage capacity in saline aquifers is rated at 0 $GtCO_2$. These evaluations reflect concerns regarding the security of CO_2 storage in tectonically active areas such as the Pacific Rim due to the complexity of geological structures and the risk of reactivating faults during injection of CO_2 (e.g. Bradshaw & Dance, 2005). Nevertheless, there are several petroleum provinces that are tectonically active and have stored substantial volumes of hydrocarbons (e.g. California and parts of South East Asia) and such locations should not be automatically dismissed as unsuitable CO_2 storage locations (Bradshaw & Dance, 2005).

While perhaps not providing the optimum storage sites at the high level of the APEC region, at the national level Japan considers CCS to be one the key technologies that could be employed to reduce net emissions post-2010, and is actively pursuing the geological storage of CO_2 in deep saline aquifers. Offshore storage sites also appear to be preferred to onshore sites due to both adequate storage capacity and a greater margin of safety with respect to human health in the event of a possible leakage. To the author's knowledge no commercial scale projects have been announced as yet. Nevertheless, Japan is included in the discussions here as it is one of few countries that have conducted detailed work on the regional potential (technical and economic) CO_2 storage capacity and has a clearly stated mission to implement offshore storage in the near future. The dynamic research and development program on CO_2 sequestration in Japan is coordinated by the Research Institute of Innovative Technology for the Earth (RITE).

An early assessment of Japans geological storage capacity, carried out by the Engineering Advancement Association of Japan (ENAA), identified 60 potential sites, including oil and gas fields and aquifers, with an estimated capacity of ~91.5 $GtCO_2$ (Tanaka et al., 1995). 29 of these sites, with a capacity in excess of 72 $GtCO_2$, were located offshore (Tanaka et al., 1995). Encouraged by the large potential storage capacity, RITE and ENAA undertook a 5 year joint R&D project (2000-2005) entitled 'Underground Storage of Carbon Dioxide' (Kaya et al., 2001). One of the main objectives of this project was to identify candidate storage sites for large-scale demonstration projects followed by commercial implementation in the near future, where site selection would be based on both safety and economic criteria. While further outputs are expected from this project, two assessments of the 'realisable' CO_2 storage potential in Japan have been published (Akimoto et al., 2002; Li et al., 2005). The principal findings of these various assessments are summarised below (Section 1.2.1.1). At present, RITE is conducting a field demonstration test of CO_2 sequestration into an onshore anticlinal aquifer (Nagaoka site). However this is not regarded as the target site in the implementation phase – where the most likely aquifer targets are located offshore to the southeast and northwest of Honshu. Deep unmineable coal seams, many of which extend offshore, are also being considered as future targets for CO_2 sequestration; however there remains much work to be done before this becomes a realisable option (Yamazaki et al., 2006).

1.2.1.1 Offshore Storage Potential in Japan

The assessments of offshore storage potential in Japan have considered storage in four reservoir types (Category I-IV, after Tanaka et al., 1995 and Li et al., 2005), including both supercritical based storage in systems with structural traps (oil and gas fields and aquifers containing anticlinal structures) and dissolution based storage in systems without structural traps (monoclinal aquifers). Li et al. (2005) also graded the aquifers according to storage capacity and distance from an emissions source to identify the optimal ‘Rank 1’ sites (in economic terms) for near future development. For Rank 1 status, the storage site must be located within a reasonable distance of a stationary CO_2 source equivalent to or greater than the emissions from a medium-scale power plant (~2-2.5 $MtCO_2$/yr) and the technical capacity must be greater than 50 Mt CO_2 (20-25 years of storage). The ‘Rank 1’ grading criteria for supercritical based storage requires an emission source within 50km, while that for dissolution based storage requires an emission source within 0km (within or on the aquifer boundary). This allows the lower transport costs to offset the higher injection costs associated with this type of storage (CO_2 not in supercritical phase). The location and capacity of these storage sites are summarised below and in Figure 1.7.

Figure 1.7: Location and capacity of CO_2 storage sites in saline aquifers, Japan (after Tanaka et al., 1995; Akimoto et al., 2002; Li et al., 2005).

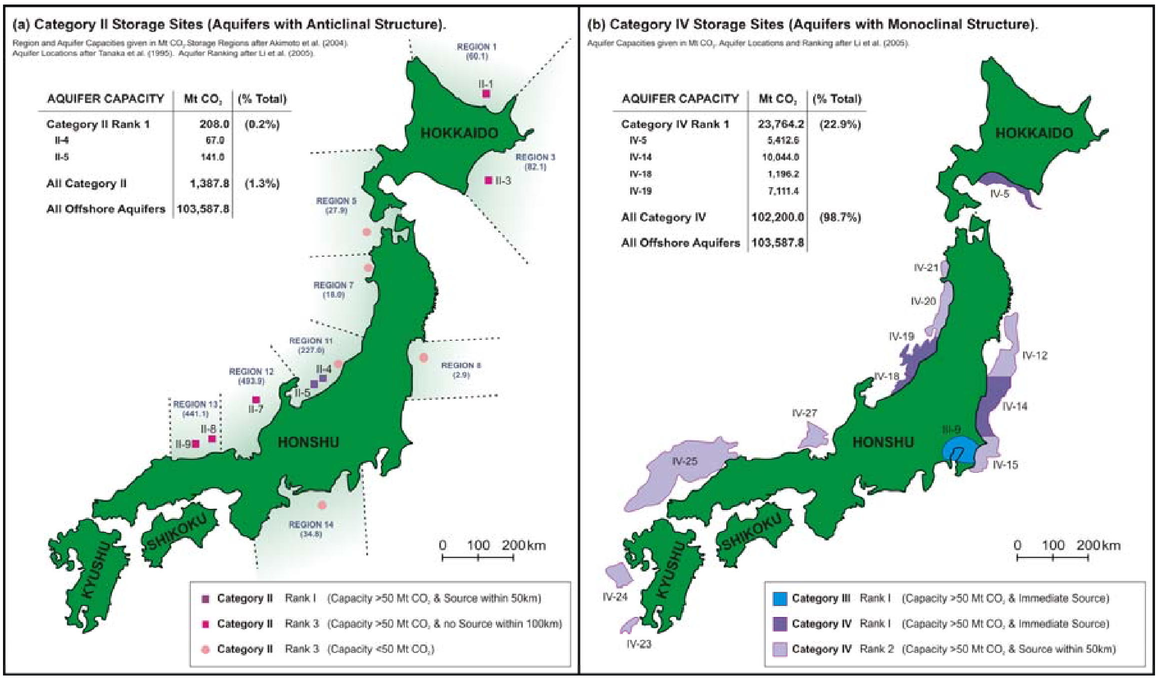

(a) Category II Storage Sites (Aquifers with Anticlinal Structure).

Region and Aquifer Capacities given in Mt CO_2 Storage Regions after Akimoto et al. (2004). Aquifer Locations after Tanaka et al. (1995). Aquifer Ranking after Li et al. (2005).

AQUIFER CAPACITY	Mt CO_2	(% Total)
Category II Rank 1	208.0	(0.2%)
II-4	67.0	
II-5	141.0	
All Category II	1,387.8	(1.3%)
All Offshore Aquifers	103,587.8	

(b) Category IV Storage Sites (Aquifers with Monoclinal Structure).

Aquifer Capacities given in Mt CO_2. Aquifer Locations and Ranking after Li et al. (2005).

AQUIFER CAPACITY	Mt CO_2	(% Total)
Category IV Rank 1	23,764.2	(22.9%)
IV-5	5,412.6	
IV-14	10,044.0	
IV-18	1,196.2	
IV-19	7,111.4	
All Category IV	102,200.0	(98.7%)
All Offshore Aquifers	103,587.8	

Category I: oil and gas reservoirs and neighbouring aquifers (supercritical based storage)

Tanaka et al. (1995) considered 13 sites, of which 1 is located offshore. However, these oil and gas fields are still active and are not expected to become CO_2 storage sites in the near future (Tanaka et al., 1995; Li et al., 2005). Once depleted, EOR may be considered, or they may be used for natural gas storage, a likely option as Japan imports much of its fossil fuel (Tanaka et al., 1995; Li et al., 2005).

Category II: Aquifers in anticlinal structures (supercritical based storage)

Tanaka et al. (1995) identified 29 Category II sites, 16 on land and 13 offshore, with a potential offshore storage capacity of ~1.4 $GtCO_2$. The offshore Category II sites perhaps represent the most secure storage option. Indeed this is the only category to be considered by Akimoto et al. (2002), where their conservative site selection criteria required offshore aquifers with known structural traps. The offshore area was divided into 19 regions, of which 10 were excluded due to a lack of reliable data. The remaining 9 regions included the 13 known Category II aquifers (see Figure 1.7a). An optimisation model was then applied to match emission sources with the offshore aquifer traps. The model results indicated that geological sequestration at these sites would be an economically viable greenhouse gas mitigation option for Japan (Akimoto et al., 2002). However, it should be noted that for a 0.5%/yr emissions reduction scenario, the total storage capacity of these aquifers would be reached within ~50 years.

Only 2 of the 13 offshore sites meet the ‘Rank 1’ criteria of Li et al. (2005). Although 5 other sites have a capacity in excess of 50 $MtCO_2$, these were rejected on the basis of distance from an emissions source (>100km) and the cost of laying pipeline offshore.

Category III: Aquifers in monoclinal structures on land (dissolution based storage)

This category is included here as one ‘Rank 1’ site (III-9) extends offshore into the Bay of Tokyo, thus possible leakage at this site could occur subsea. The storage capacity of this site is estimated to be 12,351 $MtCO_2$ (Li et al., 2005).

Category IV: Aquifers in monoclinal structures offshore (dissolution based storage)

Tanaka et al. (1995) identified 15 Category IV sites within the sedimentary basins surrounding Japan with a potential storage capacity of 72 $GtCO_2$. Li et al. (2005) present a revised assessment based on higher resolution mapping of the area, identifying 28 sites with a potential storage capacity of 102.2 $GtCO_2$. Four of these sites are graded as ‘Rank 1’, with a storage capacity of 23.8 $GtCO_2$, and a further eight sites are graded as ‘Rank 2’ (capacity in excess of 50 $MtCO_2$ and within 50km of an emission source).

Given the high capacity of Category IV sites, dissolution-based storage could become the primary sequestration method in Japan (Li et al., 2005). However, compared with supercritical storage, dissolution-based storage has not been well studied in either the laboratory and in the field. Therefore further research is required to decrease knowledge gaps between theory, simulation, and practical implementations.

1.2.1.2 Likely Sub-Seafloor Storage Sites and Rates of Sequestration in Japan

The likely regions where geological storage of CO_2 will occur beneath Japanese waters are summarised in Figure 1.7. Panel (a) shows the Category II sites and panel (b) shows the Category III and IV aquifers. The Rank 1 sites are those most likely to be developed in the near future, where the most promising aquifer targets are located offshore to the southeast and northwest of Honshu. Given current experience in geological sequestration it also seems likely that the Category II sites (northwest of Honshu) would be developed in preference to Category IV. As Japan is a tectonically active province, the geomechanical properties of these target aquifers will require detailed examination to assess site security, in particular the likelihood of leakage up faults or reactivation during injection due to increased reservoir pressures (Bradshaw & Dance, 2005).

With no development plans yet announced the amount of CO_2 to be sequestered in Japan is difficult to assess. The modelling work of Akimoto et al. (2002) indicates a mean sequestration rate of 6.6–35 $MtCO_2$/yr from 2010-2050 would be required to achieve an emissions reduction of 0.5%/yr based on different future economic and population scenarios. The work of Li et al. (2005) indicates a supply potential for Category II Rank 1 sites of 7.4 $MtCO_2$/yr (within a 50km radius), and 49.7 $MtCO_2$/yr for Category IV Rank 1 sites (within 0km). These numbers suggest a sequestration rate on the order of ~7 $MtCO_2$/yr could be achieved in the near future, increasing to ~35-50 $MtCO_2$/yr if dissolution based storage is utilised. Nevertheless, given the concerns regarding the implementation of CO_2 storage in tectonically active areas, it seems likely that CO_2 storage in Japan will fall toward the lower limit of these ranges.

1.2.2 South East Asia

Following the methodology described above (Section 1.1.4), 30 sedimentary basins in East and South East Asian APEC economies have been selected as primary targets for CO_2 geological sequestration based on their proximity to major CO_2 sources (both emission cluster analysis and high purity CO_2 sources, Bradshaw et al., 2004a). Of these target sites, 7 are located offshore, and a further 12 have an offshore and onshore component (see Figure 1.8). It has been suggested that 13 of these basins should be excluded from near future considerations due to poor accessibility and/or lack of infrastructure (Bachu, 2005). However, this region has numerous offshore gas fields that are naturally rich in CO_2 (Imbus et al., 1998; JAPEX, 2003), which may provide good targets for early implementation of CCS. Figure 1.8 shows the location of the sedimentary basins that are considered primary targets, those that have been excluded on the basis of poor accessibility/infrastructure, and those that may become targets if CO_2 point sources associated with the future development of natural gas fields are included. The Natuna East sedimentary basin has been included in the latter category here. This basin did not feature in the list of primary targets – yet it as at present the only location in South East Asia where a CCS project is planned, albeit with an uncertain future, and this site is discussed further below.

Figure 1.8: Target sedimentary basins for potential CO_2 Storage in East and South East Asia (modified from Bradshaw et al., 2004a).

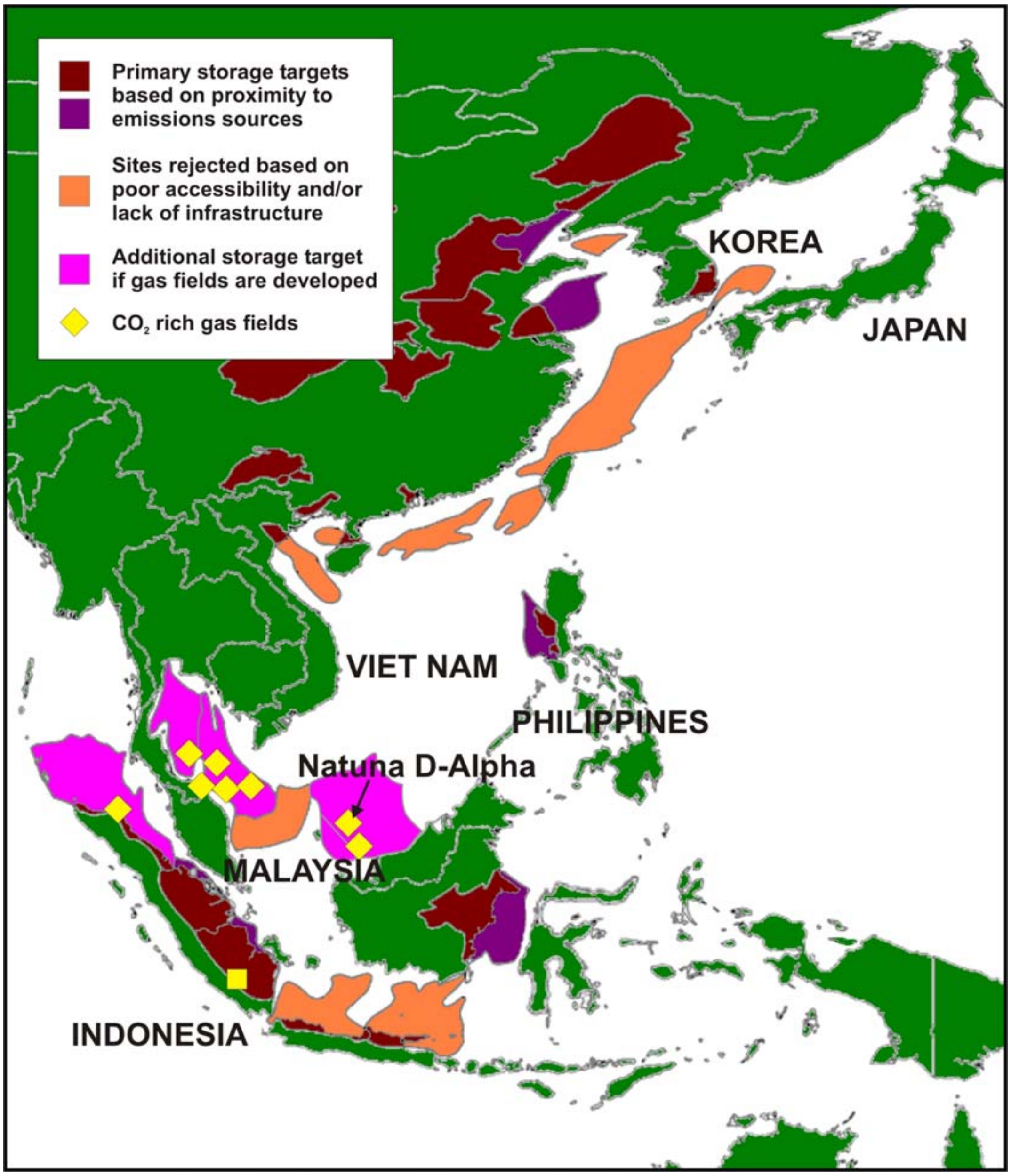

1.2.2.1 *Natuna D-Alpha*

Natuna D-Alpha is an offshore gas field located in Indonesia's East Natuna Sea approximately 1,100km north of the Indonesian capital Jakarta and 225 km northeast of Natuna Island. The Natuna D-Alpha block contains ~6.3 x10^{12} m^3 of gas (222 x10^{12} cubic feet). However the fuel deposit is extremely impure, with a CO_2 content of around ~70% by volume (Herzog *et al.,* 1997). Allowing for separation of the CO_2, Exxon Mobil has estimated that the recoverable natural gas reserves are ~1.3 x10^{12} m^3 (46 x10^{12} cubic feet), accounting for about 25% of Indonesia's total gas reserves.

At present the status of this gas field is uncertain. Nominally, Exxon Mobil owns a 76 % stake, while the Indonesian state-run oil company Pertamina holds 24%. However, in late 2006 the

Indonesian government terminated ExxonMobil's contract to develop the gas block. This appears to have been due to slow movement on the development of the block. At present, Indonesia and ExxonMobil are negotiating a new contract. It seems likely that a new agreement will be reached, with Exxon Mobil Indonesia Inc. stating that the company is progressing with a four-year plan to deliver natural gas from the Natuna D-Alpha block to foreign buyers by 2014.

Furthermore, it is clear that the Indonesian government is keen to see gas production from this area, thus it is a question of when, rather than whether, this field will be developed.

Current plans for the development of the Natuna D-Alpha field include capture of 90% of the CO_2 and injection into two neighbouring deep saline reservoirs ~900 m beneath the bed of the Natuna Sea (Chargin & Socolow, 1997; RCEP, 2000). The decision to employ CCS at this project is in part related to the volume of CO_2 that will be produced, where direct venting of the CO_2 to the atmosphere would create a massive point source equal to ~0.5% of the current global CO_2 emissions from fossil fuels (Chargin & Socolow, 1997). The danger to the local area from such a release (in addition to likely associated political difficulties and economic factors such as possible future taxation on emissions) drove the decision to employ CCS. The large quantities of CO_2 to be separated from the gas would be pumped back into the ocean floor using dedicated deep-sea platforms. The project calls for the construction of at least 18 offshore platforms, comprising six for drilling, six for treating and four for injection work. Operations would take place where the water is at least 145 m deep.

Output and injection rates are as yet essentially unknown, although they are likely to be very high. Pertamina has been quoted as projecting an initial output of 5 Mt LNG, which could be increased later to 15 Mt. Other sources suggest a yield as high as 22.2 Mt LNG each year, or around 30% of the world's output. Thus if the project goes ahead, at full production around 100 $MtCO_2$ would be disposed of annually into a sub-sea bed aquifer (Table 1.3; Chargin & Socolow, 1997; Hanisch, 1998). This is equivalent to 100 'Sleipners', and no other currently announced project would rival this in scale.

Table 1.3: Potential CO_2 Sequestration Rates at Natuna D-Alpha (calculated based on projected LPG production rates and assumes the gas feed stream is a binary mixture composed of 30% CH_4 and 70% CO_2, with capture and storage of 90% of the CO_2).

Extraction	LPG	CO_2 Extracted	CO_2 Stored (90%)	
	Mt/yr	Mt/yr	Mt/yr	t/day
Initial Rate	5.0	32.1	28.9	79,110
Future Rate	15.0	96.3	86.6	237,329
Maximum Rate	22.2	142.5	128.2	351,247
	Mt	Mt	Mt	
Total Reserve	929	5963	5367	

1.2.3 Oceania (Australia)

As with Japan, Australia is one of the world leaders in the field of CCS, with active research, a roadmap for CCS implementation and pilot studies underway. This program is lead by The Cooperative Research Centre for Greenhouse Gas Technologies (CO2CRC), a collaborative research organisation focused on CO_2 capture and geological storage. A detailed regional assessment of storage capacity, CO_2 sources, and source to sink matching have been performed, and details are readily available and clearly presented (see for example Bradshaw et al., 2002, 2004b, and the CO2CRC website www.co2crc.com.au).

In brief, Australia's CO_2 storage capacity in depleted hydrocarbon reservoirs is small, and there are only niche opportunities for CO_2-EOR (Bradshaw and Rigg, 2001; Bradshaw *et al*., 2002). In regard to deep saline aquifers, an Australia-wide study of sedimentary basins conducted by

CO2CRC (previously GEODISC) assessed 100 sites for their suitability for the safe, long-term storage of CO_2. This initial study identified 65 potentially viable Environmentally Sustainable Sites for CO_2 Injection (ESSCIs) within 48 basins, with an estimated storage capacity of 740 $GtCO_2$ (see Figure 1.10 below; Bradshaw et al., 2001).

Source to sink matching and a ranking exercise have also been performed in order to identify those ESSCIs that appear to be the most viable, based on geotechnical, environmental and economic risk factors (Bradshaw et al., 2004b and references therein). This assessment explicitly included potential future LNG sources of CO_2 from unproduced gas fields with naturally high CO_2 contents located on the North Western Shelf (NWS), the Gorgon, Scott Reef and Evans Shoal fields (see Figure 1.9). Including only the CO_2 emissions nodes with large emission volumes, within 300km of a technically viable ESSCI and with low storage costs indicates that Australia has the potential to realistically store between 100 and 115 $MtCO_2$, equivalent to ~25% of its annual total net CO_2 emissions. Within this, the unproduced gas fields of the NWS were identified as prime targets for future CCS operations. These fields are likely to be developed in the near future, where if the separated CO_2 were simply released to the atmosphere, the production of natural gas could contribute around 4% of Australia's current CO_2 emissions. However, Gorgon & Scott Reef lie within 100km of a technically viable offshore ESSCI, while Evans Shoal lies within 300km, thus providing the ability to sequester the CO_2 sub-seafloor with relatively low transport costs (Bradshaw et al., 2002, 2004b). Furthermore, the development of these fields would shift the balance in energy production, with a higher proportion of Australia's energy requirements being supplied from gas rather than coal. Thus if CCS were implemented at the production stage, this would result in a true decrease in Australia's CO_2 emissions. Plans for the development of the Gorgon field are already at an advanced stage and include CCS as an integral part of the project. This project is discussed in more detail below.

Figure 1.9: Location of potentially viable Environmentally Sustainable Sites for CO_2 Injection (ESSCIs) in relation to stationary emission nodes and unproduced high CO_2 gas fields (image provided by CO2CRC, copyright retained by CO2CRC). The three unproduced gas fields located on the North Western Shelf are (from southwest to northeast) Gorgon, Scott Reef and Evans Shoal.

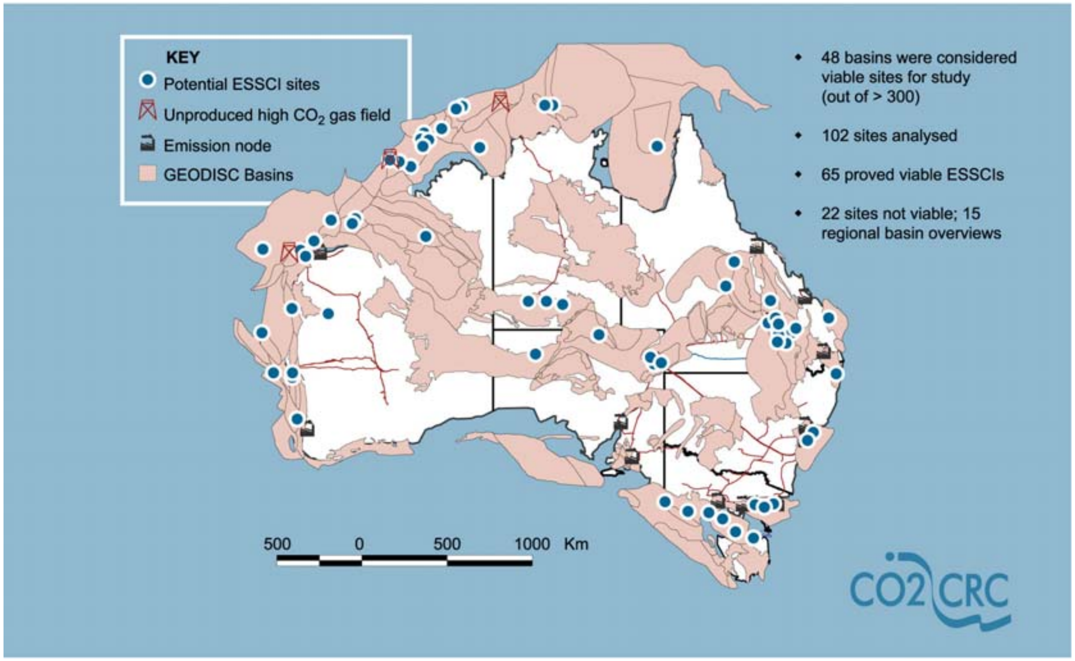

1.2.3.1 The Gorgon Project

The Gorgon Project plans to develop the Greater Gorgon gas fields, located between 130km and 200km off the north-west coast of Western Australia. This project is being pursued by the Australian subsidiaries of three major international oil companies (the Joint Venturers), Chevron (operator of the project holding a 50% interest), ExxonMobil (25%) and Shell (25%). The project proposal includes greenhouse gas management via injection of carbon dioxide into the Dupuy formation (a saline aquifer) beneath Barrow Island (Oen, 2003). There appear to be multiple driving forces for the implementation of CCS within this project. Firstly, the CO_2 has to be removed from the gas stream prior to processing (liquefaction) and marketing. Secondly, in the absence of a CO_2 emission abatement or mitigation strategy, the Australian EPA made a strong recommendation against further development of the Barrow Island nature reserve site (see current status below). Thirdly, as major international energy companies the Joint Venturers have a vested interest in the development and demonstration of CCS technology, where incentives provided by the Australian Government through the Low Emissions Technology Demonstration Fund (LETDF), encourages industry investment in this region, offering $1 for every $2 spent by industry for projects that demonstrate new low greenhouse emissions technology. Chevron was recently awarded a $AU 60m grant to demonstrate CO_2 capture from the Gorgon gas field development and sequestration in a saline aquifer under Barrow Island.

The gas fields of the Greater Gorgon area (comprising the Gorgon area and Jansz field among others) represent Australia's largest-known undeveloped gas resource, containing ~1.1 $x10^{12}$ m^3 of natural gas (40 $x10^{12}$ cubic feet). While the CO_2 content of the Jansz field is low (0.25% by volume), gas in the Gorgon area has a high CO_2 content ranging from 10-15% by volume, with a typical composition of 14-15% CO_2 and 2-3% N_2. The technically proven and certified recoverable gas resource of the Gorgon area is 0.37 $x10^{12}$ m^3 (12.9 $x10^{12}$ cubic feet), corresponding to a reservoir CO_2 volume of approximately 65 $x10^9$ m^3, or ~125 Mt CO_2. The CO_2 (and other trace contaminants such as H_2S) will be removed from the raw gas feed stream as part of the gas pre-treatment before processing, where the recovered CO_2 will be injected back into the subsurface below Barrow Island. The maximum anticipated rate of CO_2 removal is 3.4 Mt/yr, with an average rate of 3.1 Mt/yr over the life of the project. Under routine operations, it is expected that all CO_2 removed from the incoming gas stream would be injected into the subsurface. However, venting of reservoir CO_2 may be required during commissioning, maintenance periods, unplanned downtime and in the event of reservoir or injection well constraints. The long term goal is to achieve injection of 95% of the reservoir gas (Chevron, 2005). However, the reference case adopted by the Joint Venturers is based on a worst-case scenario that assumes venting of 20% of reservoir CO_2 to the atmosphere, providing an allowance of ~5% for maintenance and compressor down time plus ~15% assuming one of the seven planned injection wells is offline. Thus CO_2 injection at this site is expected to range between 2.7-3.4 $MtCO_2$/yr.

Injection Site

Extensive investigations of the feasibility of CO_2 injection at the Gorgon project have been carried out, both by the Joint Venturers (Chevron 2005) and via an independent report (Curtin University of Technology, 2004) commissioned by the Australian Department of Industry and Resources (DoIR). This has included assessment of potential CO_2 injection sites, subsurface geology and stratigraphy, injectivity, storage capacity and likely CO_2 behaviour and movement in the subsurface.

The intention is to inject reservoir CO_2 into the Dupuy Formation, approximately 2300m below Barrow Island, with the CO_2 injection facility located on the central eastern coast of Barrow Island. This site was selected to maximise the migration distance from major geological faults and to limit disturbance to areas around the proposed gas processing plant. The injection wells are planned to be directionally drilled from two surface locations, with a total of 7 (6-8) injection wells. It is likely that a monitoring well (or wells) will be drilled from each cluster of injection wells to provide a sample point within the area of injection

The Dupuy Formation appears to have adequate capacity to contain the ~125 Mt CO_2 that will be potentially available for injection over the life of the project, where the Basal Barrow Group seal which overlies the Dupuy Formation should be adequate to contain the injected CO_2 for thousands of years (Curtin University of Technology, 2004).

Although the injection site is located on land, the migration of CO_2 within the Dupuy formation will result in CO_2 storage beneath both Barrow Island and the adjacent shallow waters of the coast, i.e. the intended storage site is both sub-terrestrial and sub-seafloor. The Joint Venturers also note that the Greater Gorgon gas fields themselves would provide significant additional CO_2 storage capacity once the hydrocarbon reservoirs are depleted. Thus if carbon storage in sub-sea geologic formations proves successful, this region may see significant further development as a storage site in the future.

Project Status

The Gorgon Project is now nearing the end of a lengthy and thorough environmental approval process. The associated documents are publicly available and provide detailed information on the project. This includes the independent report commissioned by the DoIR (Curtin University of Technology, 2004) in addition to the following documents prepared by the Joint Venturers:

- The draft Environmental Impact Statement/Environmental Review and Management Program (EIS/ERMP) document. This meets the requirements of environmental impact assessment processes under the *Commonwealth Environment Protection and Biodiversity Conservation Act 1999* and the *Western Australian Environmental Protection Act 1986.*

- An Additional Information Package containing supporting technical information that became available following the release of the Draft EIS/ERMP.

- The Final Environmental Impact Statement/Response to Submissions on the Environmental Review and Management Program.

In June 2006, the Western Australia Environmental Protection Authority (WA EPA) published an advisory bulletin (Bulletin 1221) recommending against the Gorgon project's EIS/ERMP. This was largely due to negative impacts on the Barrow Island Nature Reserve (Barrow Island is a Class A internationally significant nature reserve recognised for its very high conservation values, where the waters around Barrow Island are also recognised for their conservation values, with parts included in marine conservation reserves and a marine park). The EPA also noted that the opportunity to inject reservoir CO_2 was a key argument for the use of Barrow Island, and made a clear statement that should the project proceed the EPA considers it essential that injection or equivalent greenhouse gas mitigation action occurs.
The Western Australia Environment Minister has since upheld the Gorgon Joint Venturers appeal against the EPAs advisory bulletin. However, in response to the recommendation of the EPA, geological sequestration of CO_2 has now been made a condition of the development.

Prior to this decision, the Gorgon Joint Venturers were publicly committed to injection of 80% of the reservoir CO_2 unless it proved "technically infeasible or cost prohibitive". The successful injection of CO_2 is now an integral part of the Gorgon Project, without which development of the gas field cannot proceed as planned. A test well was drilled into the Dupuy Formation in early 2006 and comprehensive tests and analysis to assess the ability to inject the CO_2 at Barrow Island are now underway. Assuming that test results are positive and CO_2 injection is possible, the final decision on the Gorgon Project is in the hands of the federal Environment Minister. Given the Australian governments support for CCS, including funding awarded to Chevron via the LETDF specifically for the purposes of demonstrating CCS at the Gorgon site, it seems likely that this project will proceed as planned with production commencing in 2008-2010.

1.2.4 Western Europe (North Sea, Barents Sea & Mediterranean Sea)

Western Europe is a world leader in the field of offshore CCS, where the only two currently operating sub-seafloor CO_2 storage projects in the world are located in the North Sea. The dynamic European CCS research community includes national programs, industry led projects (in particular by Statoil, a true world leader in CCS technology) and academic-industrial collaborations, which are supported at the regional level through the European Commission Framework Programs (see European Communities (2004) for an overview of programs funded via FP5 (1999-2002) and FP6 (2002-2006), calls for FP7 opened in December 2006). In light of the wealth of both available storage opportunities, and available information regarding European CCS activities, this subject matter could form the basis of an individual report. Here the focus has therefore been restricted to specific current and planned future projects.

Two major projects have assessed European CO_2 storage capacity (including depleted oil and gas fields and deep saline aquifers), JOULE II (1996) and GESTCO (2003). These studies examined specific case studies, and do not represent a comprehensive coverage of all storage potential in Europe. Nevertheless, estimates of the regional storage potential clearly demonstrate that the vast majority of Western Europe's CO_2 storage capacity occurs in offshore formations; with the majority of offshore storage sites occurring within the UK and Norwegian sectors of the North Sea (see Table 1.2; Holloway, 1996; Bøe et al., 2002; IEA-GHG 2004; Wildenborg et al., 2005). This region represents an ideal candidate for sub-seafloor storage of CO_2 due to a good understanding of its geology (proven storage capabilities over geological time) and proximity to stationary CO_2 sources. Furthermore, many of the North Sea oil and gas fields are now nearing depletion. While this provides opportunities for enhanced oil and gas recovery (EOR and EGR), it also creates a finite time window within which existing infrastructure can be adopted and converted to accommodate CO_2 injection (rather than removed, as is required on decommissioning). Thus rapid development of the North Sea as a major CO_2 storage site might be expected. Indeed, in late 2005, government and industry representatives from Denmark, Germany, The Netherlands, Norway and the UK reached an agreement to promote large-scale CCS as an effective way to tackle global climate change and signed a joint declaration on geological storage beneath the North Sea. This declaration agreed to set up a 'North Sea Basin Task Force' to develop common principles to regulate CO_2 storage and to explore possible areas of co-operation.

Current offshore CCS schemes in Europe include the first example of a geological CO_2 storage facility (the Sleipner project) and a pilot scale project investigating the potential for CO_2 storage combined with EGR (the K12-B project), with numerous other projects either under development or under consideration. Of these, three sites fall under the umbrella of the European CASTOR (CO_2, from capture to storage) project, the K12-B project in the North Sea, the Snøhvit project in the Barents Sea, and the Casablanca project in the Mediterranean Sea. One of the principal objectives of the CASTOR project is to develop and apply a methodology for the selection and the secure management of storage sites by improving assessment methods, defining acceptance criteria, and developing a strategy for safety-focussed, cost-effective site monitoring. As such, these sites have been chosen to reflect a broad range of reservoir characteristics. Source-sink matching and cost benefit analysis are also highly developed in this region, as is illustrated by the concept of the CO_2 value chain. For example, near-future European projects will extend the role of CCS to include schemes that link the generation of CO_2 at large power stations (fueled by North Sea hydrocarbon reserves) to the application of EOR within the North Sea, and strive to create zero emissions systems (see for example the Tjeldbergodden/Heidrun/Draugen and Miller/Peterhead Projects). Various European sub-seafloor CO_2 storage projects are described briefly below and summarised in Figure 1.10 and Table 1.4.

Figure 1.10: CCS Operations in the North, Norwegian and Barents Seas.

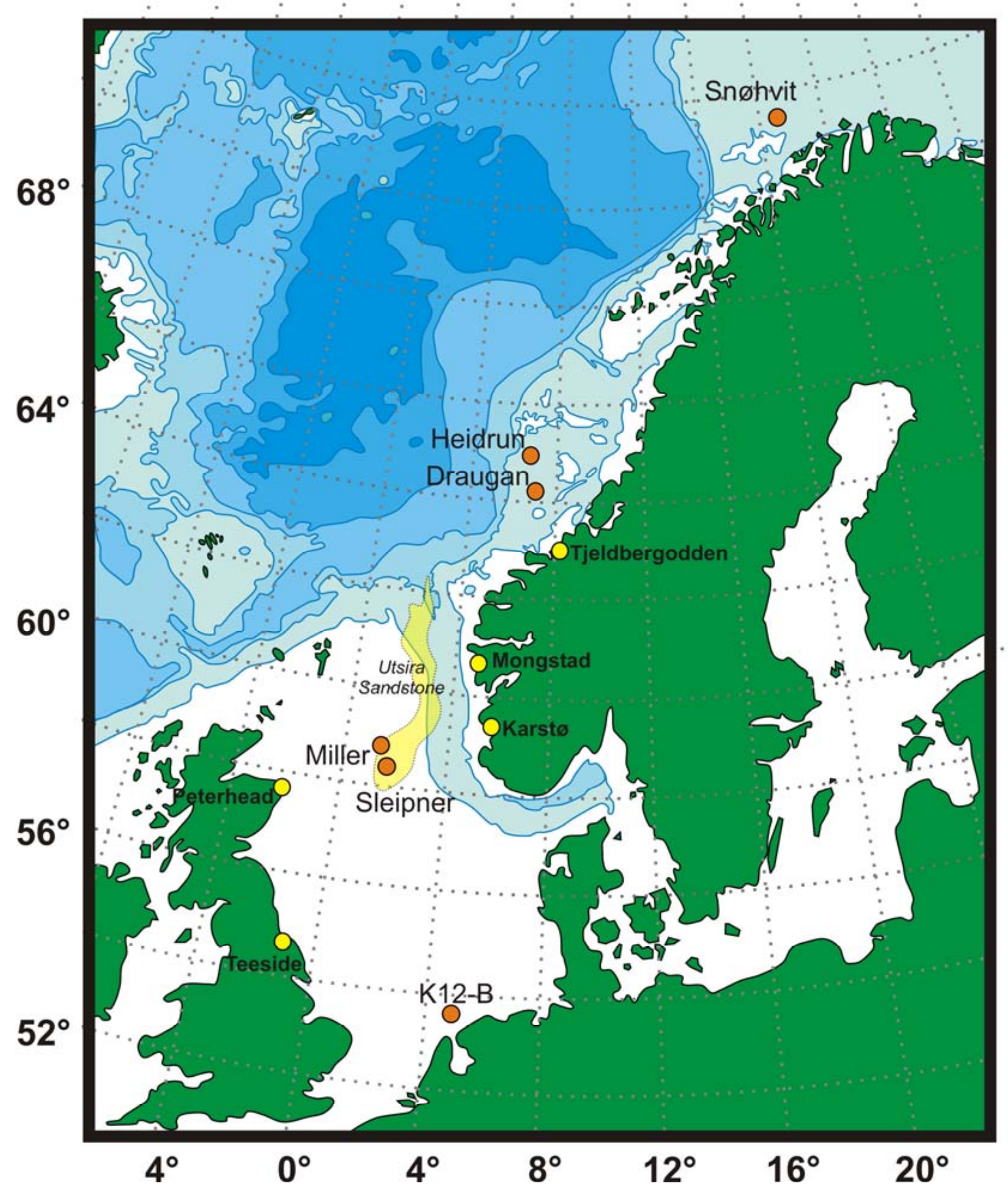

Table 1.4: Current & future offshore CO_2 storage projects.

Project Status	**Location**	**Storage Rate $MtCO_2/yr$**	**Project Start**
Current Projects			
Sleipner	**Norway**	1.00	1996
K1-2B	**Netherlands**		
Initial		0.02	2004
Increasing to		0.31 - 0.48	2007-2008
Snøhvit	**Norway**	0.75	2007
Future Planned/Proposed			
Gorgon	**Australia**	2.70 - 3.40	2008-2010
Miller/Peterhead	**UK**	1.80	**2009**
Teeside	**UK**	4.00	2011
Tjeldbergodden/Heidrun/Draugen	**Norway**	2.50	2012
Mongstad	**Norway**		
Initial		0.10	2010
Increasing to		1.30	2014
Kårstø	**Norway**	1.00 - 1.20	2011-2012
Uncertain Future			
Natuna	**Indonesia**	28.9 - 86.6	post 2014?
Japan	**Japan**	~7	post 2010?
Casablanca	**Spain**	0.50	?

1.2.4.1 The Sleipner Project, North Sea

Initial practical experience in the geological storage of CO_2 beneath the seafloor is being obtained in the Norwegian sector of the central North Sea area, where CO_2 from the Sleipner West gas field (owned and operated by Statoil) is extracted, captured, and injected back into a deep saline aquifer located at a depth of ~1000m.

The Sleipner West natural gas field has a naturally high CO_2 content of ~4.0-9.5% by volume. For natural gas to be fed directly into pipelines for sale in Europe, the CO_2 content must be less than 2.5% by volume, thus development of this field required removal of CO_2 from the produced gas by necessity. Furthermore, at the time of development (1990), it was known that the Norwegian government would shortly be introducing significant CO_2 emissions taxation on the offshore petroleum industry (~$ 40/t CO_2, introduced in 1991). In response to these factors, a team of technical experts came up with the then unprecedented idea of capturing the CO_2 offshore and injecting it into a saline aquifer beneath the Sleipner installations. Statoil proceeded with this pioneering project (for both environmental and financial benefit) and since project start up in 1996 around ~1$MtCO_2$/yr has been injected into the Utsira aquifer.

The Sleipner West field is produced through two installations; the Sleipner B (SLB) wellhead platform and the Sleipner T (SLT) gas treatment facility. The carbon dioxide removal plant installed on the SLT platform is the first employed in the North Sea and was the largest offshore facility of its kind (a Total patented amine separation process) at the time of commissioning. The CO_2 extracted from the natural gas feed stream is injected into the water-bearing Upper Miocene Utsira Formation, located at a depth of 1,000 metres above the Sleipner West reservoir, and overlain by an 80 m thick Nordland Group shale cap rock. The Utsira Formation forms an elongated sand-body about 450 km long and 90 km wide, with a maximum thickness of 250-330 m. According to Statoil, the estimated capacity of this aquifer is several $GtCO_2$.

In order to learn as much as possible from this first endeavor in the realm of geological storage a collaborative research project, the Saline Aquifer CO_2 Storage Project (SACS) was established in 1998 to examine and monitor the behaviour of injected CO_2 within the Utsira Formation. The SACS project finished in 2003, and this work is now being continued by the partly EU funded CO2STORE project.

1.2.4.2 K12-B – The ORC Project, North Sea

In the Netherlands a pilot scale CO_2 injection program is being carried out by Gaz de France Production Netherland B.V. (GPN) at the K12-B offshore gas field in the Dutch sector of the North Sea (van der Meer et al., 2005).

The K12-B platform, located 150 km NW of Amsterdam, is the test facility for GPN's ORC project (Offshore Reinjection of CO_2). This project forms part of the Dutch CRUST program (CO_2 Re-use through Underground STorage) and the European CASTOR program, and was jointly funded by GPN (10%) and The Ministry of Economic Affairs of the Netherlands (90%). The aims of the ORC project were to assess (i) the feasibility of CO_2 storage in a depleted gas reservoir and (ii) the possibility of using CO_2 injection for Enhanced Gas Recovery (EGR). If the ORC project is deemed successful CO_2 could also be injected into other fields in this area for both storage and EGR purposes.

K12-B was selected as a potential CO_2 injection test site as the gas field was nearing depletion and the platform was already equipped with a CO_2 removal plant due to the high CO_2 content of the reservoir gas (~13%). A feasibility study conducted in 2002-2003 concluded that excellent facilities were available for a demonstration project, that the reservoir has good characteristics for CO_2 re-injection and storage, and that there were no significant legal or social barriers to the project (van der Meer, 2004). Pilot scale CO_2 injection was initiated in May 2004. This is the first site in the world where CO_2 has been injected into the same reservoir from which it originated, the Rotliegend sandstone located at a depth of ~3800m (Upper Slochteren Member, Permian age).

The pilot phase involved two injection tests. Test 1 (initiated in May 2004) involved CO_2 injection into a single-well depleted reservoir compartment (K12-B8) and demonstrated reasonable CO_2 injectivity despite the low permeability of the reservoir, where the reservoir response and behavior of the injected CO_2 were within the expected range (Van der Meer, 2005). Test 2 (initiated in March 2005) involved CO_2 injection into a producing compartment of the reservoir to evaluate the potential for EGR in K12-B (Van der Meer 2006). This test involved three wells, a CO_2 injection well (K12-B6) and two producing gas wells (K12-B1 and K12-B5). Tracer experiments were also carried out to enable monitoring of any breakthrough of injected CO_2 into the methane production wells. Results from the 2005 injection period demonstrated that CO_2 breakthrough could be modelled accurately, where simulation results indicate that CO_2 increase in the gas-production wells would be slow and gradual, and the volumetric consequences of CO_2 breakthrough in K12-B1 were undetectable within the test period. However, at the end of 2005 there was no clear evidence of measurable improvement in the gas-production performance of the tested compartment and it was concluded that this test phase should be continued into 2006 to increase the EGR potential of CO_2 injection (Van der Meer, 2006). Results from the 2006 injection program should be available in the near future.

During the pilot test phase CO_2 injection at this site has been restricted to 20 kt CO_2/yr, with an injection rate of ~50 to 60 t/day. However, with the successful completion of the test injection, the K12-B project is expected to enter into commercial phase operation in the near future, with an injection potential of 310 to 475 kt CO_2/yr and a total estimated reservoir size of 8Mt CO_2 or ~17-25 years of storage (van der Meer 2006).

1.2.4.3 The Snøhvit Project, Barents Sea

Statoil and its partners are involved in a second offshore CO_2 storage venture, the Snøhvit project, which is due to commence in June 2007. This project (part of the European CASTOR project) will be the first oil and gas development in the environmentally sensitive Barents Sea, the first LNG gas-field development in Europe, and the first LNG production site where the captured CO_2 will be stored. The Snøhvit Field, located in the Barents Sea, contains natural gas with a CO_2 content of 5-8% by volume. A full subsea solution is being used for the development of this site, with all production equipment residing at water depths of 250 to 345 m. The produced gas will be fed to an onshore reception terminal on Melkøya. Here the CO_2 will be removed from the natural gas feed stream (as at Sleipner, the CO_2 will be captured by amine absorption), dewatered, compressed, sent back offshore via a dedicated pipeline, and injected into the Tubåen Formation. This storage aquifer is located beneath the gas-bearing strata at a depth of ~2,600 m and is capped by 75-125 m of thick impermeable shale. It is expected that ~0.75 $MtCO_2$ will be reinjected per annum.

1.2.4.4 Tjeldbergodden/Heidrun/Draugen, Norwegian Sea

This joint venture between Shell and Statoil plans to establish a complete CO_2 value chain in Norway. The proposed project involves a new 850MW gas-fired power station at the Tjeldbergodden industrial complex facility in Mid Norway, which currently comprises a gas receiving terminal, methanol plant, an air separation facility and a gas liquefaction unit. Natural gas will be piped to the power station via the existing Haltenpipe pipeline. Around 85% of post-combustion CO_2 emissions from the power station will be captured, in addition to capture of CO_2 from the methanol production facility. The CO_2 will be dewatered, compressed, and transported offshore via a pipeline for CO_2-EOR based storage, first at the Shell operated Draugen field and later at the Statoil-operated Heidrun field. Currently Shell and Statoil are undertaking a feasibility study and will decide upon a final concept if the project is deemed to be commercial. A decision to award the project sanction will be taken at the end of 2008, which could allow project start-up by 2010 and full operation by 2012. If the project proceeds, up to 2.5 $MtCO_2$ (including ~ 0.3 $MtCO_2$/yr from the existing methanol plant) could be injected annually.

1.2.4.5 Miller/Peterhead (BP-DF1), North Sea

The BP Miller/Peterhead Power Station project, referred to as DF1 (decarbonised fuels 1), aims to generate electricity using hydrogen manufactured from North Sea natural gas, where the CO_2 created in the gas reforming process is captured and utilised for CO_2-EOR at the Miller field. The project, if it goes ahead, will be the first industrial scale decarbonised fuel project in the world and will be able to reduce CO_2 emissions from the electricity generation process by around 90%. North Sea gas will be supplied via an existing link from the St. Fergus terminal to a new reformer based at the Peterhead Power Station. The CO_2 captured from the gas reforming process will be transported via an existing gas export pipeline to be injected for EOR and long-term geological storage in the Miller field reservoir which lies at a depth of around 3,500 metres. The Miller field was selected as a CO_2 storage site as (i) it is uniquely positioned with an existing, dedicated high-grade steel pipeline connected to a suitable power station (ii) the high specification pipeline is able to handle the corrosive properties of a high-CO2 content gas stream (iii) Miller has gas re-injection facilities (iv) CO_2 naturally present in the field has been proven to be held in the reservoir on a geological timescale (v) the application of CO_2-EOR could increase recoverable oil reserves by around 60 million barrels and extend the life of the field by around 20 years. This development could commence as early as 2009, with a projected CO_2 sequestration rate of ~1.8 $MtCO_2$/yr.

1.2.4.6 Other North Sea Projects

Plans have recently been announced for the UK's first complete clean coal power generation project (Centrica PLC, Progressive Energy Ltd., Coastal Energy Ltd., and Coots Ltd). If progressed, this project would involve the construction of a new 800 MW Integrated Gasification Combined Cycle (IGCC) power station (located in Teesside, UK) combined with CO_2 capture, transport via a new pipeline, and storage in the North Sea. The project has a projected start date of 2011, and no further details are as yet available. However, a CO_2 storage rate of ~4 $MtCO_2$/yr can be estimated based on the expected annual energy output (6 TWh/yr) and applying the representative figures provided by the IPCC for emissions reductions associated with new IGCC power plants combined with CSS (86% - equivalent to capture of ~0.665 $kgCO_2$/kWh; IPCC, 2005).

In Norway, all new-build gas fired power stations are now expected to be ‘carbon recovery ready’. For example, the recently approved combined heat and power (CHP) plant at Kårstø (Naturkraft; ~3.5 TWh/yr) is being built to allow retrofitting of carbon capture systems. At full production this plant will have emissions of ~1.0-1.2 $MtCO_2$/yr, where CCS is expected to implemented post 2011-2012. At a similar new CHP plant at Mongstad (Statoil; ~2.2 TWh/yr) carbon capture systems are to be built simultaneously with the power plant, where the emissions permit from the Norwegian government requires capture of at least 0.1 $MtCO_2$/yr to start at the same time as power production, with full emissions capture (1.3 $MtCO_2$/yr) in operation by 2014. The storage plans for these projects have not yet been announced.

1.2.4.7 The Casablanca Project, Mediterranean Sea

The Casablanca oil field is operated by Repsol-YPF and is situated off the coast of northeastern Spain in the Mediterranean Sea, approximately 43 km from Tarragona. This carbonate hosted oil field, located at a depth of ~2500m below the seafloor, and is nearing the end of its productive life, where the economic limit of the field will be reached in the next few years. Repsol-YPF is therefore considering using this field for storage of approximately 0.5 $MtCO_2$/yr, which is to be captured at the company's Tarragona refinery (~20% of the refinery's annual production). At present, this is the only project planned for the Mediterranean Sea.

Evaluation of the Casablanca oil fields' suitability as a CO_2 storage site is being carried out as part of the CASTOR project (Mignot et al., 2006). This field case has been divided into several steps, including a geological study, reservoir modeling, forecast of CO2 injection, well integrity, and long term behavior of CO_2 in the subsurface (Mignot et al., 2006). To date, early results have been reported from the first three steps of the study (Mignot et al., 2006). There is not (as yet) a projected start date for CO_2 injection as a full evaluation of the ability of this field to be safely used as a geological storage site awaits the results of the full study (Mignot et al., 2006),.

1.2.4.8 The Rate of Sub-Seafloor Storage of CO_2 in Western Europe

The injection of CO_2 into sub-seafloor geologic reservoirs in Western Europe is currently occurring at a rate of ~1 $MtCO_2$/yr (see Table 1.4). If all current and future planned projects proceed according to projected timescale, this will increase to 2.1-2.2 $MtCO_2$/yr by the end or 2007, 4.0-4.1 $MtCO_2$/yr by 2010, and 12.7-13.0 $MtCO_2$/yr by 2015 (13.2-13.5 $MtCO_2$/yr if Casablanca is included).

1.3 Projected Rate of Near Future Sub-Seafloor CO_2 Storage

The current, future planned and potential CO_2 storage rates discussed above are summarised in Table 1.4, where the storage projects have been categorized as Current, Future Planned/Proposed and Uncertain Future. The cumulative CO_2 storage that would be achieved by 2050 is plotted in Figure 1.11. Considering only the current projects, ~100 $MtCO_2$ will have been stored by 2050. Including the Gorgon Project, which has nearly completed the planning and approvals process, this increases to 225 $MtCO_2$, and including the future plans for the North Sea area that have been announced to date, the total storage would reach ~650 $MtCO_2$. The storage that could be achieved by Japan or at the Natuna Field in Indonesia has not been included in Figure 1.11 due to the uncertain future of these projects where development of the Natuna field progress. If these projects were to proceed on schedule, then assuming the upper limit on injection rates, the annual sequestration rate would on the order of 100 $MtCO_2$/yr, with ~3.8 $GtCO_2$ stored by the year 2050.

It seems probable that Carbon Capture and Storage (CCS) will play an increasingly significant role in greenhouse gas emissions reduction strategies over the course of the 21st Century. Indeed some models estimate that for stabilisation of atmospheric CO_2 at levels of 490-540 ppmv, the total emissions abatement achieved via CCS may be on the order of 1000 $GtCO_2$ by the year 2100 (IPCC, 2007). Should CCS be deployed at this level then a reasonable upper limit on the offshore storage utilisation might be ~25-50% of the total mass of CO_2 stored (in proportion to the fraction of total storage capacity that occurs offshore, giving an offshore cumulative storage of 250-500 $GtCO_2$ by 2100). If it is assumed that new projects come online at a constant rate, each injecting some ~1-4 $MtCO_2$/yr, an effort of this order would require between 15-120 offshore storage projects

to start injecting CO_2 every year from 2010 to 2100. Under this scenario, there would be between 600 and 5000 projects by the year 2050, with an annual storage rate of 2.5-5 $GtCO_2$/yr, and a cumulative mass of CO_2 stored between 50 and 100 $GtCO_2$. By the year 2100, the total number of projects would increase to 1400-11000, with a total storage rate of 5.5-11 $GtCO_2$/yr.

Figure 1.11: Projected cumulative CO_2 storage likely to be achieved by 2050 (including only current and future planned projects).

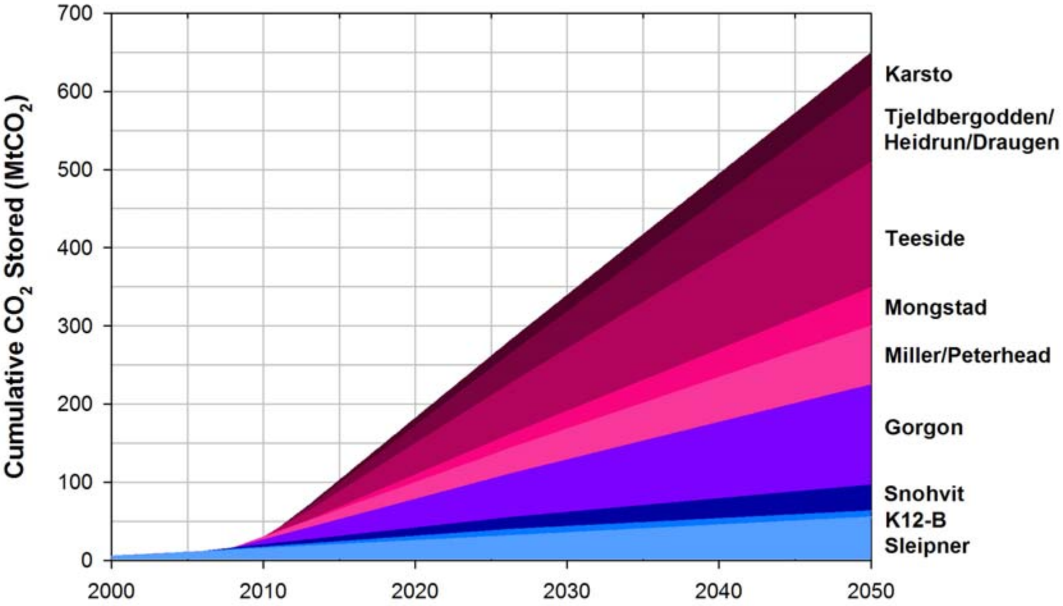

2: Fluxes of CO_2 to the Global Ocean

Two key questions regarding the security and safety of sub-seafloor geological sequestration of CO_2 are (i) the likelihood of leakage or seepage of CO_2 from the storage reservoir to the seafloor and ocean bottom waters, and (ii) the impact this might have on ocean chemistry and ecosystems. When evaluating the potential impact of leakage or seepage of CO_2 from sites of purposeful sequestration it is useful to consider the contextual setting, and to ask how potential leakage fluxes compare to the pre-existing fluxes of CO_2 to ocean waters. There are two principal CO_2 inputs of interest. Firstly, the indirect (non purposeful) sequestration of fossil fuel CO_2 into the surface ocean, and secondly, the natural emissions of CO_2 to ocean bottom waters that occur via hydrothermal exhalations. The ocean uptake of fossil fuel CO_2 has been the subject of a recent report by the Royal Society, and is briefly summarised here before focussing on the hydrothermal flux, where this chapter presents a comprehensive analysis and revised estimate for the total flux of volcanic CO_2 to the seafloor. Chapter 3 discusses specific sites of CO_2 venting to the seafloor in more detail, examining whether these sites could provide a useful analogue for sites of leakage from sub-seafloor storage reservoirs.

2.1 Current Input of Fossil Fuel CO_2 to the Surface Ocean

The indirect (non-purposeful) sequestration of fossil fuel CO_2 into the surface ocean occurs via air-sea gas exchange as a result of increasing atmospheric CO_2 concentrations. The role of the ocean in moderating the atmospheric CO_2 signal has long been recognised, and in the 1990s a major international effort was made to constrain this uptake through the World Ocean Climate Experiment (WOCE) and the Joint Global Ocean Flux Survey (JGOFS). Sabine et al. (2004)

used the global data set resulting from these programmes to estimate a cumulative oceanic sink from 1800 to 1994 of ~433±70 GtCO_2, or around half the fossil fuel emissions over this time period. Recently, the Intergovernmental Panel on Climate Change Fourth Assessment Report (IPCC AF4) estimated mean air to sea fluxes of 6.6±2.9 GtCO_2/yr, 8.1±1.5 GtCO_2/yr and 8.1±1.8 GtCO_2/yr for the 1980s, 1990s and the period 2000-2005 respectively (equivalent to average daily uptake rates of 18.1±8.0 MtCO_2/day, 22.1±4.0 MtCO_2/day and 22±5.0 MtCO_2/day respectively; Denman et al., 2007). As the concentration of total CO_2 in the surface ocean increases, the waters become more acidic, and the concentration of carbonate ions decreases (through the equilibration of the oceanic carbonate system $CO_2 + H_2O \Re HCO_3^- + H^+ \Re CO_3^{2-} + 2H^+$). The impact of this CO_2 input on surface ocean chemistry and biology has recently been the topic of a public report published by the Royal Society (Raven et al., 2005). These impacts are discussed in comparison to the potential impact of leakage or seepage of CO_2 to bottom waters in later Chapters.

2.2 Natural Flux of Volcanic CO_2 to Ocean Bottom Waters

CO_2 is delivered to the ocean through hydrothermal circulation (the heat driven transport of water through the earths crust), where hydrothermal fluids are highly enriched in CO_2 and exhibit low pH with respect to ambient seawater. There are three principal requirements for hydrothermal activity to occur; a heat source, permeable conduits for fluid flow, and an advecting fluid. These conditions are met in four distinct active lithosphere regions where submarine volcanism occurs (see Figure 2.1); at the Mid Ocean Ridges (MORs), at subduction zones (associated with both back-arc basin spreading centres and arc volcanism), and at hotspots (intraplate volcanism). During hydrothermal circulation, cold seawater gradually percolates downward through fractures in the permeable ocean crust. As the seawater penetrates basement, it comes in to contact with hot rock, and may come close to a zone of active magma intrusion, or magma chamber (Lister, 1972). Rapid heating then forces the buoyant hot water (the hydrothermal fluid) to the surface as a hydrothermal vent. Mantle degassing releases gases such as helium (He), methane (CH_4), hydrogen (H_2), carbon monoxide (CO), and carbon dioxide (CO_2), and volatile elements such as mercury (Hg) and arsenic (As). The composition of the fluid is further changed through reaction with the host basalt as it circulates (e.g. Elderfield and Schultz, 1996, see Figure 2.2). Thus, in addition to thermal transfer, hydrothermal circulation facilitates a major chemical exchange between the circulating seawater and the ocean crust and plays an important role in regulating the chemistry of the oceans (e.g. Elderfield et al., 1993; Elderfield and Schultz; 1996).

Figure 2.1: A cartoon illustrating the zones of seafloor magmatic emplacement that may represent a significant source of CO_2 to ocean waters (not to scale).

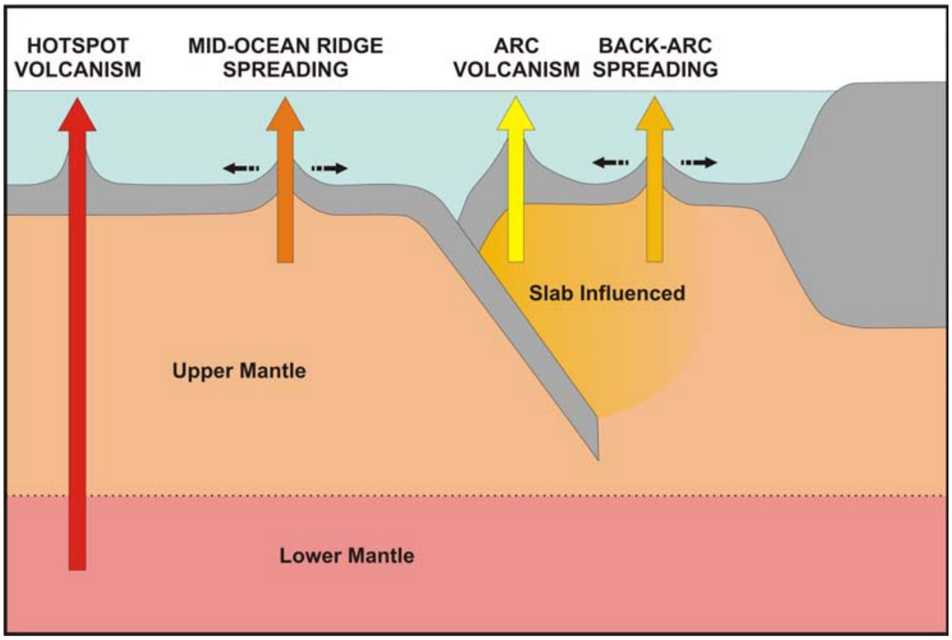

Figure 2.2: A Schematic diagram of hydrothermal circulation.

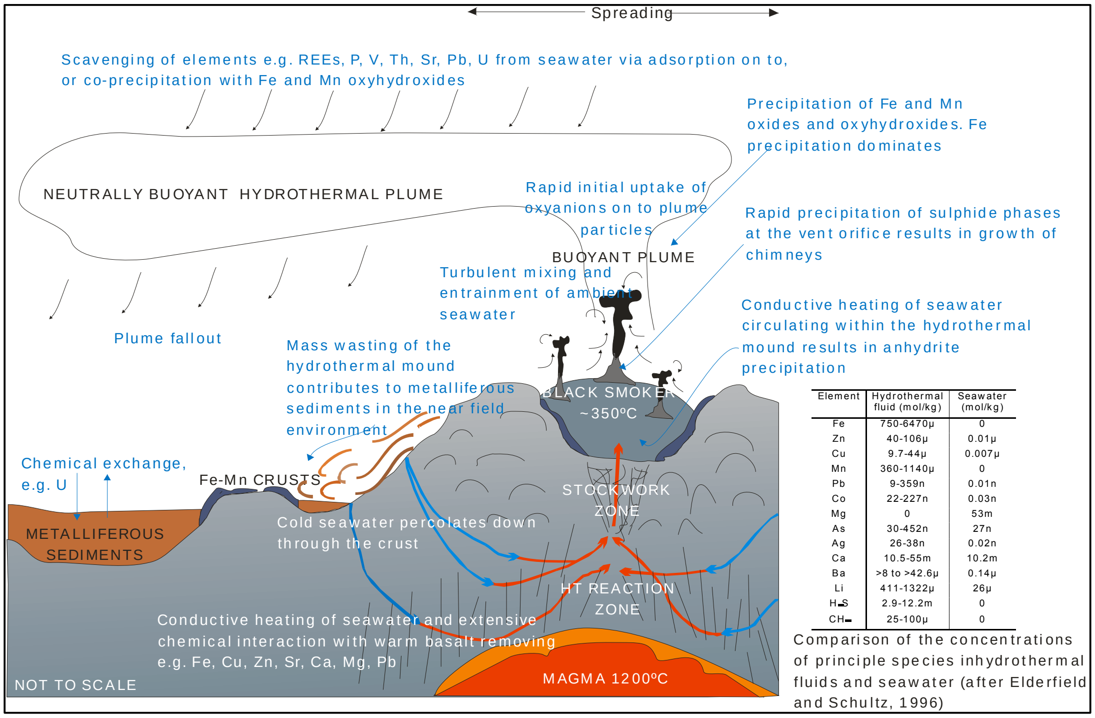

Element	Hydrothermal fluid (mol/kg)	Seawater (mol/kg)
Fe	750-6470µ	0
Zn	40-106µ	0.01µ
Cu	9.7-44µ	0.007µ
Mn	360-1140µ	0
Pb	9-359n	0.01n
Co	22-227n	0.03n
Mg	0	53m
As	30-452n	27n
Ag	26-38n	0.02n
Ca	10.5-55m	10.2m
Ba	>8 to >42.6µ	0.14µ
Li	411-1322µ	26µ
H_2S	2.9-12.2m	0
CH_4	25-100µ	0

Comparison of the concentrations of principle species inhydrothermal fluids and seawater (after Elderfield and Schultz, 1996)

Determining the flux of volatiles to ocean bottom waters is a difficult task. The solubility of CO_2 and ^{3}He in magmas is low, where these species are thought to escape the magma while it resides in the magma chamber, and are quantitatively degassed during eruptions (e.g. Gerlach, 1989; Kingsley & Schilling, 1995). In subduction zones, the downgoing slab can represent a significant and variable source of additional CO_2. This means that the original CO_2 content of magmas cannot be measured directly, and the CO_2 flux has to be estimated indirectly.

Furthermore, estimates of the flux of CO_2 to the ocean typically consider only the MORs, where intraplate volcanism is considered negligible, and the subduction zone contribution is treated as a subaerial (as opposed to submarine) flux (e.g. Marty & Tolstikhin, 1998). However, the recent discovery of submarine CO_2 rich vent sites associated with back-arc spreading centres (e.g. Sakai et al., 1990a), volcanic arcs (e.g. Lupton et al., 2006), and hotspots (e.g. Staudigel et al., 2006) suggests that these fluxes may have been significantly underestimated. Here a current best estimate of the CO_2 flux to ocean waters is determined. However, it should be noted that there remain a number of obstacles in determining an accurate estimate of the total CO_2 flux, and as such this estimate is subject to significant revision in the future.

2.2.1 Basis of the Estimate

A number of different approaches have been taken to estimate volcanic CO_2 fluxes:

(1) Estimating the abundance of CO_2 (C) in the mantle combined with the magmatic production rate. This approach has been applied to the MORs (e.g. Javoy et al., 1982) and hotspots (mantle plumes; e.g. Aubard et al., 2005). However, it is not applicable to determining the CO_2 flux in regions influenced by subduction as it does not account for additional sources of CO_2.

(2) Using average hydrothermal vent fluid compositions combined with estimates of the mass flux of hydrothermal fluids. This approach has been applied to the MORs (e.g. Elderfield & Schultz, 1996). While a similar approach could be applied to subduction zones and hotspots, it would carry a high level of uncertainty as the number of CO_2 vent sites is essentially unknown.

(3) Estimating the $CO_2/^3He$ ratio of the volcanic emissions combined with the flux of magmatic ^3He. This approach has been applied to the MORs, subduction zones and hotspots, where the use of the observed $CO_2/^3He$ ratio accounts for additional (non-mantle) sources of CO_2 (e.g. Sarda & Graham, 1990; Graham & Sarda, 1991; Marty & Jambon, 1987; Marty & Zimmerman, 1999; Des Marais & Moore, 1984; Marty & Tolstikhin, 1998).

While each of these approaches carries intrinsic uncertainties associated with the assumptions made in the calculation and the quality/quantity of available data, the latter approach appears both the most robust and broadly applicable, and is thus favoured here. In this calculation the total flux of CO_2 to ocean bottom waters is given by the sum of individual fluxes at the MORs (MOR), back-arc basin spreading centres (BAB), volcanic arcs (ARC), and hotspots (HOT):

$$F(CO_2)_{TOTAL} = F(CO_2)_{MOR} + F(CO_2)_{BAB} + F(CO_2)_{ARC} + F(CO_2)_{HOT} \quad \textbf{[Eq. 2.1]}$$

The individual fluxes are determined from:

$$F(CO_2)_X = (CO_2/^3He)_X \times F(^3He)_X \quad \textbf{[Eq. 2.2]}$$

Where X denotes the region of volcanic activity, $(CO_2/^3He)_X$ is the ratio of CO_2 to magmatic ^3He, and $F(^3He)_X$ is the flux of magmatic ^3He. To a first approximation, $F(^3He)_X$ is assumed to be proportional to the rate of magmatic emplacement (M_X) and the magmatic He content ($^3[He]_X$):

$$F(^3He)_X = f_X\,(^3He)_{TOTAL} \quad \textbf{[Eq. 2.3]}$$

Where:

$$f_X = \frac{M_X[^3He]_X}{M_{MOR}[^3He]_{MOR} + M_{BAB}[^3He]_{BAB} + M_{ARC}[^3He]_{ARC} + M_{HOT}[^3He]_{HOT}} \quad \textbf{[Eq. 2.4]}$$

This chapter therefore first reviews magmatic emplacement in the submarine environment (Section 2.2.2), before apportion the total flux of magmatic ^3He (Section 2.2.3) and presenting a revised assessment of the volcanic flux of CO_2 to ocean waters (Section 2.2.4).

2.2.2 Magmatic Emplacement Rates

One of the most frequently used compilations of magma emplacement rates is that of Crisp (1984), presented below in Table 2.1. However, there is now a significant amount of additional information available, and these estimates are updated here.

Table 2.1: Global rates of magma emplacement and volcanic output.

Location	Crisp (1984)			This estimate		
	Volcanism km^3/yr	**Plutonism** km^3/yr	**Total** km^3/yr	**Best** km^3/yr	**Range** km^3/yr	**% of submarine**
Ocean Ridge	3	18	21	20.6	17.7 - 23.4	88
Mid Ocean Ridges				16.8	14.5 - 19.2	72
Back-Arc Basins				3.8	3.2 - 4.3	16
Subduction-zone	0.4 - 0.6	2.5 - 8.0	2.9 - 8.6	4.7	3.5 - 5.9	
Oceanic†	0.2 - 0.3	1.1 - 3.6	1.3 - 3.9	2.9	2.2 - 3.6	
Submarine				2.0	1.1 - 2.9	8.5
Oceanic intraplate	0.3 - 0.4	1.5 - 2.0	1.8 - 2.4	1.5	1.1 - 1.9	
Submarine				0.8	0.4 - 1.2	3.4
Continental intraplate‡	0.0 - 0.1	0.1 - 1.5	0.1 - 1.6	0.5	0.3 - 0.6	
Total Global			**25.8 - 33.6**	**27.3**	**22.7 - 29.5**	
Oceanic			**24.1 - 27.3**	**24.9**	**21.0 - 27.5**	
Submarine				**23.35**	**19.2 - 27.5**	**100**

†The Crisp (1984) estimate assumes 45±5% of total subduction-zone magma emplacement occurs in oceanic crust after statement "about 50-60% of Benioff zone magmatism occurs in continental crust". ‡Intra-continental magmatism estimated following same method as described for oceanic intraplate, assuming 1 large hotspot, and 45 minor hotspots.

2.2.2.1 *The Magmatic Flux at Oceanic Spreading Ridges (M_{MOR} & M_{BAB})*

Igneous activity along divergent (constructive) margins where new ocean crust is formed is overwhelmingly the largest contribution to global magmatism. Oceanic Spreading Ridges (OSRs) include both the MOR system and spreading in back-arc basins (see Figures 2.1 and 2.3), where the rate of magmatic emplacement can be estimated from:

$$M_{OSR} = L_{OSR} \times T_C \times \mu_S = (L_{MOR} + L_{BAB}) \times T_C \times \mu_S \qquad \textbf{[Eq. 2.5]}$$

Where M_{OSR} is the volume of magma emplaced per year, L_{OSR} is the length of the OSR system, T_C is the mean crustal thickness, and μ_S is the mean full crustal spreading rate. Crisp (1984) used an L_{OSR} of 53,700 km, a crustal thickness of ~7 km, and a spreading rate of 55 mm/yr to estimate a total magmatic emplacement of 21 km^3/yr.

Here, L_{OSR} is taken to be 76,620.5 km (L_{MOR} = 61,327.9 km, L_{BAB} = 15,292.6 km). This revised length is based on the digital data series of Bird[1] (2003), where the significant increase in length is primarily due to the inclusion of back-arc basin spreading centres.

The full spreading rate along the OSR system shows a wide degree of variation, ranging from ultra-slow (<20 mm/yr) to super fast (>200 mm/yr) spreading sections. The crust generated at

---

[1] Note that Bird (2003) defines oceanic spreading ridges as those lying entirely: (1) within seafloor whose age is known from linear magnetic anomalies to be less than 180 Ma; and/or (2) at water depths exceeding 2000 m. Any spreading centres that do not meet these criteria are defined by default as continental rift boundaries (CRB) The Okinawa Trough falls in this category, where only 56.4 km of the total ~1066.1 km length is defined as an OSR. However, for the purposes of this estimate the most important criteria is whether a spreading section is submarine in nature, for example there are five known sites of submarine CO_2 discharge located in the Okinawa Trough, thus the full length is included here. Other examples include the Red Sea Rift and the South Sandwich Back-arc Spreading Centre to the west of the South Sandwich Islands. In total 9274.8 km of CRB sections are included in this estimate of the total OSR length.

ultra-slow segments is significantly thinner than that generated at slow to super-fast spreading sections, and is therefore considered separately.

Using the digital data set of Bird (2003) the total length of ultra slow ridge segments is estimated at 21719.4 km with a mean spreading rate of 10.9 mm/yr (L_{US} = 21719.4 km, μ_{US} = 10.9 mm/yr; $L_{MOR\text{-}US}$ = 17405.0 km, $\mu_{MOR\text{-}US}$ = 10.9 mm/yr; $L_{BAB\text{-}US}$ = 4314.4 km, $\mu_{BAB\text{-}US}$ = 11.1 mm/yr). Baker and German (2004) suggest a nominal crustal thickness at ultra-slow spreading centres (T_{US}) of 4 km (White et al., 2001), but also note that seismic observations indicate thicknesses less than 2 km (Muller et al., 1999; Jokat et al., 2003), while dredging and magnetic surveys suggest that large sections may have near-zero crustal thickness (Dick et al., 2003). Here, a value for T_{US} of 3±1 km is used to reflect this uncertainty.

The remainder of the OSR system has a length of 54901.1 km with a mean spreading rate of 57.4 mm/yr (L_{OSR*} = 54901.1km, μ_{OSR*} = 57.4 mm/yr; L_{MOR*} = 43922.9 km, μ_{MOR*} = 58.7 mm/yr; L_{BAB*} = 10978.2, μ_{BAB*} = 52.2 mm/yr) and exhibits a relatively constant crustal thickness (T_{C*}) of 6.3±0.9 km (White et al., 1992, 2001). Magmatic emplacement along the MORs and in back-arc basins can then be estimated from:

$$M_{OSR} = \left(L_{OSR*} \times T_{C*} \times \mu_{OSR*}\right) + \left(L_{US} \times T_{US} \times \mu_{US}\right) \qquad \textbf{[Eq. 2.6]}$$

Giving a total magmatic emplacement of 20.6±2.8 km^3/yr, of which approximately 15-20% is associated with spreading in back-arc basins (M_{OSR} = 20.6±2.8 km^3/yr; M_{MOR} = 16.8±2.3 km^3/yr; M_{BAB} = 3.8±0.5 km^3/yr).

2.2.2.2 The Magmatic Flux at Volcanic Arcs (M_{ARC})

Subduction zones exist at convergent plate boundaries (also referred to as consuming margins), where one plate of oceanic lithosphere converges with another plate and sinks below into the mantle (see Figures 2.1 and 2.3). Chains of volcanoes form above subduction zones, typically at a location where the subducted slab has reached a depth of about 100 km. These volcanic chains are often curved, hence the term volcanic or island arc.

Figure 2.3: Map of global oceanic plate boundaries (after Bird, 2003).

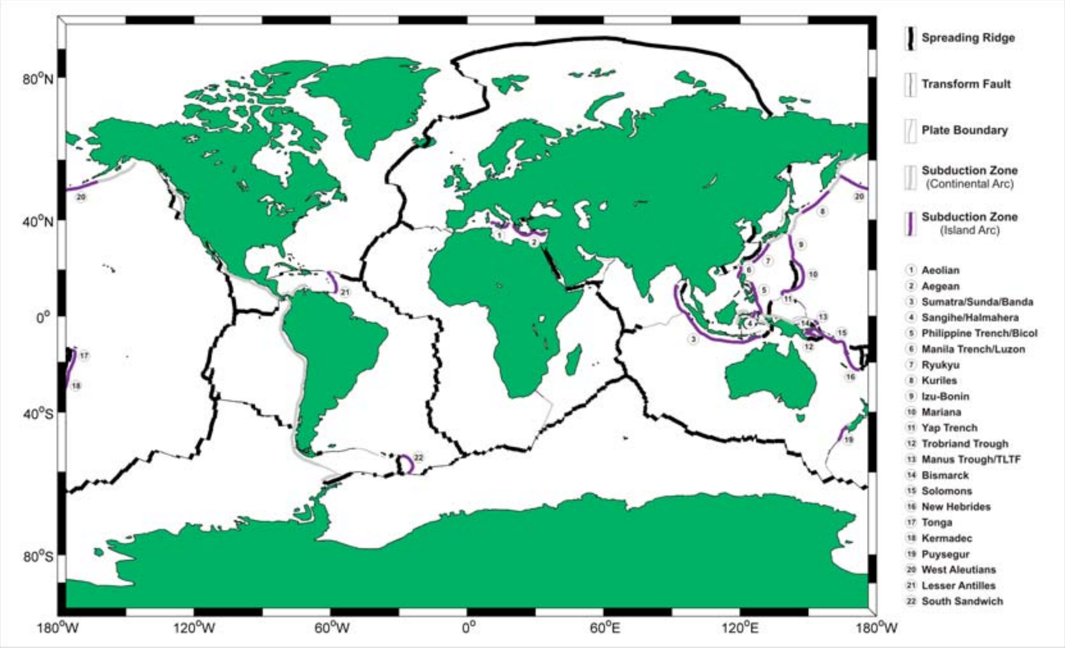

Volcanic arcs are typically divided into two types based on the nature of the over-riding plate. In areas where oceanic lithosphere is subducted beneath oceanic lithosphere the volcanism is expressed on the surface as chains of islands referred to as an **island arc**. In areas where oceanic lithosphere is subducted beneath continental lithosphere volcanism occurs as chains of volcanoes near the continental margin, referred to as a **continental margin arc**. However, many submarine subduction zones lie close to continental margins, or contain thickened arc crust which may be considered to have some continental character. The distinction of arc type can thus be somewhat arbitrary. Nevertheless, within the context of this report, the subdivision of arc types is useful, where a further distinction can be made which considers the submarine versus subaerial components of the arc system (after de Ronde et al., 2003):

(1) **Intra-oceanic arcs**, with oceanic crust on either side which are almost entirely submarine in nature (e.g. Tonga-Kermadec arc).

(2) **Transitional or island arcs** that have developed along the margins of island chains of which parts are submarine but most are subaerial (e.g. Sunda arc).

(3**) Continental arcs** that develop along the margins of the continents which are entirely subaerial in nature (e.g. Andean arc).

It is the first two types that are of interest here, where we also require an estimate of the proportion of subaerial versus submarine volcanism that occurs along these intra-oceanic and island arc systems.

■ Comments on previous estimates of subduction related volcanism

The lower limit on volcanic emplacement at subduction zones of Crisp (1984) was based on the summed volcanic output for sections of island arcs and plate margins for which estimates were available (0.1 km^3/yr, see Table 1 in Crisp, 1984). Crisp states that the length of margin included in this total corresponds to less than ¼ of the total length of active margin, giving a minimum estimate of 0.4 km^3/yr, however the margin lengths used were not explicitly stated. The upper limit was quoted from the compilation of data on volcanism along plate margins between 1500 and 1914 AD of Sapper (1927). An arc plutonism (intrusives) to volcanism (extrusives) volume ratio of 6:1 to 13:1 (based on the Andes (continental arc) and Kuriles (island arc)) was then applied to give a total emplacement of 2.9-8.6 km^3/yr. Although this estimate was not explicitly broken down in to continental and oceanic components, Crisp makes the statement "about 50-60% of Benioff zone magmatism occurs in continental crust", suggesting an oceanic subduction zone emplacement rate of 1.3-3.9 km^3/yr (note this division is not strictly equivalent to submarine versus subaerial activity). However, the ratios of plutonism to volcanism used were based on extremely limited data, and thus this estimate carries a high degree of uncertainty. Indeed, in the recent update of the Crisp (1984) data set, White et al. (2006) highlight that the ratio of intrusives to extrusives requires considerable further work, and note that there does not appear to be a systematic variation between eruptive style, volcanic setting, or total volume. These authors suggest that a ratio of 5:1 could be viewed as common to most magmatic systems, while values greater than 10:1 are rare. Furthermore, the revised data set excluded the Kuriles data, and gives an estimated ratio for the Aleutians (island arc) of 1:1-3:1 (White et al., 2006). Applying a ratio of 1:1 to 5:1 suggests a much reduced magmatic emplacement of ~0.4-2.5 km^3/yr, of which ~0.16-1.25 km^3/yr occurs in an oceanic setting.

A second widely cited estimate is that of Reymer and Schubert (1984), who calculated a magma emplacement rate of 20-40 km^3 per km of active margin per million years (20-40 km^3/kmMa) based on a global compilation of arc crustal volume. These authors estimated the total length of consuming margin with active volcanism was 37,000 km, giving a total emplacement rate of 0.7-1.5 km^3/yr, somewhat lower than the original Crisp (1984) estimate, but directly comparable to the revised estimate.

For the purposes of this report, these estimates are limited in the information they provide. For example, the Crisp (1984) data set includes only two direct estimates for the total magmatic emplacement at major island arc systems, the Kuriles (47.5 km^3/kmMa) and the Aleutians (30.0 km^3/kmMa), equivalent to ~15% of the total length of intra-oceanic and island arc systems.

Furthermore, recent research indicates that these rates are somewhat low. For example, Dimalanta et al. (2000) have used satellite gravity data in conjunction with improved seismic data from a number of island arc systems in the western Pacific to provide an improved estimate of crustal volumes, reporting an average crustal growth rate of ~60 km^3/kmMa in this region. With regard to individual arc systems, Jicha et al. (2006) have revised the estimate for the Aleutian islands upwards to 89-182 km^3/kmMa based on new geochemical data constraining the duration of arc magmatism to the last 46 Ma (80 Ma used in Crisp compilation). Similarly, Taira et al. (1998) used new seismic data to estimate a rate of igneous addition to the Northern Izu-Bonin arc of 80 km^3/kmMa. These authors also present preliminary estimates of 80 km^3/kmMa for the Mariana arc, 60-80 km^3/kmMa for Tonga and the New Hebrides (Vanuatu) of, and 50-300 km^3/kmMa for the Northeast Japan arc. Similarly, Stern (2006) has presented a revised time integrated rate of crust formation for the Izu-Bonin-Mariana Arc system (IBM) of 100 km^3/kmMa. Weighting these estimates according to arc length suggests a mean arc growth rate on the order of 95±27 km^3/kmMa, where the lower limit is in good agreement with the regional average of Dimalanta et al. (2000), and significantly higher than the Reymer and Schubert (1984) or revised Crisp (1984) estimates.

- **This estimate – a global approach**

The question remains as how best to obtain a good estimate of global arc magmatism, and then how to apportion this between subaerial and submarine emplacement. The estimate presented in this report draws heavily on three recent papers that have approached various aspects of this problem, combining the separate approaches to determine a current best estimate of submarine magma emplacement in an arc setting.

Clift and Vannucchi (2004) present an excellent review paper on the origin and recycling of the continental crust. They argue that to maintain the current volume of continental crust, subduction related magmatism must equal the rate of destruction via tectonic erosion. Furthermore, they note that to account for the constant level of the continental freeboard, net continental crustal growth must be occurring, thus the rate of magmatic emplacement must exceed the tectonic erosion rate. Based on a detailed analysis of 32 major arc systems (total length 40,225 km), these authors estimate a mean global tectonic erosion rate of 90 km^3/kmMa, where allowing for a moderate amount of continental growth, they infer an average magmatic emplacement rate of 91 km^3/kmMa. Clift and Vannucchi (2004) also observe that magmatic emplacement is not uniformly distributed, but is instead higher in faster converging margins. They conclude that the orthogonal convergence rate is the primary control on magmatic emplacement, and can be used to apportion global magmatic emplacement between individual arc systems. Following this method within their data set, Clift and Vannucchi report a magmatic production rate within oceanic arcs of 81-149 km^3/kmMa – in good agreement with the mean of the individual arc emplacement estimates discussed above (95±27 or 68-122 km^3/kmMa).

The digital model of plate boundaries presented by Bird (2003) defines subduction zones as plate boundary steps with a convergent component of velocity and a Benioff zone of intermediate to deep earthquakes and/or a parallel volcanic arc with Quaternary activity. The total length of subduction zone in Birds (2003) model is 51309.2 km. However, close examination of the Bird (2003) data set reveals some minor discrepancies when compared to other compilations of arc systems, and some minor variations have been made to the data set used here. These changes are detailed below giving a revised total subduction zone length of 52007.6 km, an increase of 698.4 km (~1.4%).

(i) Bird (2003) includes the Seram Trough as a subduction zone. However, other authors have recently concluded that this is not a subduction zone (e.g. Pairault et al., 2003), and it is not included here, decreasing the total length by 563.0 km.
(ii) The section of plate boundary corresponding to the Banda/Java arc is classified as an Oceanic Convergent Boundary (OCB) by Bird (2003). Including this section increases the total length of subduction zone by 949.8 km.

(iii) The section of plate boundary corresponding to the Tabar-Lihir-Tanga-Feni (TLTF) arc is categorised as an Oceanic Convergent Boundary in the Bird (2003) model. The TLTF is a recent addition to the Bismark-Solomon arc system, formed by the subduction of the Pacific

Plate under the Northern Bismark microplate along the Manus Trench, and is identified by de Ronde et al. (2003) as an island arc where 40% of the volcanoes are submarine and there is evidence for hydrothermal activity. Here the length of the TLTF subduction zone is chosen to match the arc length given by de Ronde et al. (2003), increasing the total length of subduction zone by 266.6 km.

It should also be noted that the Bird (2003) data set refers to strictly defined plate boundaries, whereas trenches, troughs and arcs appear to follow a somewhat more arbitrary naming convention. There are often multiple names for a given system, where quoted lengths show a wide degree of variation, and in the case of contiguous systems, the boundary between one arc and another is not necessarily clear. For example, moving from the northwest to southeast along the subduction zone lying along the Eastern boundary of the Indian Ocean, Clift and Vannucchi (2004) use the classification Burma (1800 km) – Sumatra (1800 km) – Java (2100 km), with a total length of 5700 km, while de Ronde et al. (2003) use the naming convention Sumatra (1620 km) – Sunda (2200 km) – Banda (580 km), with a total length of 4400 km. Similarly, Clift and Vannucchi (2004) appear to include the New Hebrides arc within their classification of the Solomon arc system. To aid future revision of the estimate presented here, the segment identifiers of Bird (2003) for each subduction zone system considered (only those corresponding to intra-oceanic and island arcs) are given in Table 2.2, and the subduction systems are illustrated in Figure 2.2. For those instances where a continuous subduction zone plate boundary transitions from continental to island/oceanic arc types, the following assumptions have been made:

(i) The boundary between the East Aleutian (Alaskan) and the West Aleutian arcs is assumed to correspond to the tip of the Alaskan Peninsula.

(ii) The Kurile arc is assumed to stretch from the Kuril straight at the southern tip of the Kamchatka peninsula to the eastern point of Hokkaido.

(iii) The Aeolian and Aegean subduction zones in the Mediterranean are considered to have a submarine component. It would appear that Clift & Vannucci (2004) classified this system as a continental arc. Similarly, de Ronde et al. (2003) list only the Aeolian (length of 180km) as having a submarine component. Inclusion of both the Aeolian and Aegean for the purposes of this estimate is justified by the numerous CO_2 rich gasohydrothermal vent sites known to occur in this region (e.g. Dando et al., 1999; see Chapter 3).

de Ronde et al. (2003) present the first systematic attempt to quantify the amount of submarine hydrothermal venting that occurs along volcanic arcs. These authors identify 21 volcanic arcs (15 island arcs and 6 intra-oceanic arcs) with submarine components, with an estimated total length of 21,690 km (>40% total subduction zone length, or approximately 1/3rd of the total spreading centre length). Although de Ronde et al. (2003) do not assess magmatic emplacement, they provide a valuable compilation of data giving the number of known volcanoes along each arc, and the percentage of volcanoes that are submarine versus subaerial in nature. Only one modification has been made to this compilation. For the Kurile Arc, de Ronde et al. (2003) report a total of 48 volcanoes, of which 19% are submarine. A more recent review by Glasby et al. (2006) suggests that ~50% of volcanic activity in the Kuriles is submarine, with 100 submarine volcanoes and a further 5 submarine calderas, compared to 105 subaerial volcanoes. On average, there is 1 known volcano per 25 km of arc length, where 44% of those volcanoes are submarine. For intra-oceanic arc systems, approximately 63% of volcanoes are submarine, whereas for island-arc systems approximately 33% are submarine.

Here it is assumed that the percentage of submarine volcanic activity provides a good first order estimate of the proportion of total magmatic emplacement that occurs in the submarine environment. For those systems where individual estimates are not available, the average values calculated above have been applied.

- **This estimate – the calculation**

Bird (2003) provides a detailed breakdown of information for each 'step' in his plate boundary model, including the convergent component of relative velocity of the plates (mm/a or km/Ma), thus this data set can be used to calculate magmatic production at individual subduction zones following the method of Clift and Vannucchi (2004).

The total magmatic production along arc systems is calculated from:

$$M_{ARC} = L_{SUB} \times E_{SUB} \qquad \textbf{[Eq. 2.7]}$$

Where M_{ARC} is the total volume of magma emplaced per year, L_{SUB} is the total length of subduction zone systems (52007.6 km) and E_{SUB} is the mean magmatic emplacement rate per year per km of L_{SUB} (91 km^3/kmMa), giving a total magmatic emplacement rate of 4.7 km^3/yr, equivalent to 23% of M_{OSR}.

Magmatic emplacement within an individual arc system, Y, can be determined from:

$$M_{ARC(Y)} = L_{SUB(Y)} \times E_{SUB(Y)} \qquad \textbf{[Eq. 2.8]}$$

Where $E_{SUB(Y)}$ is the mean magmatic emplacement rate per km of system Y, and is determined by prorating E_{SUB} in proportion to the convergence rate:

$$E_{SUB(Y)} = \frac{E_{SUB}}{\mu_{SUB}} \times \mu_{SUB(Y)} = 1.74 \times \mu_{SUB(Y)} \qquad \textbf{[Eq. 2.9]}$$

Where μ_{SUB} is the mean convergence rate of the global subduction zone system (52.3 km/Ma) and $\mu_{SUB(Y)}$ is the mean convergence rate of system Y (from the Bird (2003) data set). Here 25 subduction zone systems are considered to have a significant marine component (see Figure 2.3, note the Sumatra, Sunda and Banda systems are considered as a contiguous section, and the Sangihe and Halmahera systems are considered together). This includes the 21 arcs identified by de Ronde et al. (2003), with the addition of the Aegean, Ryukyu, Yap, and Trobriand systems. A comparison of the system length and convergence rate used here to those given by de Ronde et al. (2003) and Clift and Vannucchi (2004) is presented in Figure 2.4. In general, there is a reasonable agreement between the various data sets. The lengths used in this data set are based on the length of the subduction zone and as such are more comparable to those of Clift & Vannucci (2004) than de Ronde et al. (2003) who describe the arc length. Although there is significant scatter in the convergence rate comparison, the mean convergence rate (normalised to system length) is directly comparable.

Figure 2.4: Comparison of Subduction Zone Length and Convergence Rate between this study and (i) Clift & Vannucchi (2004) *[circles]* (ii) de Ronde et al. (2003) *[squares]*. Large hatched square indicates weighted mean values.

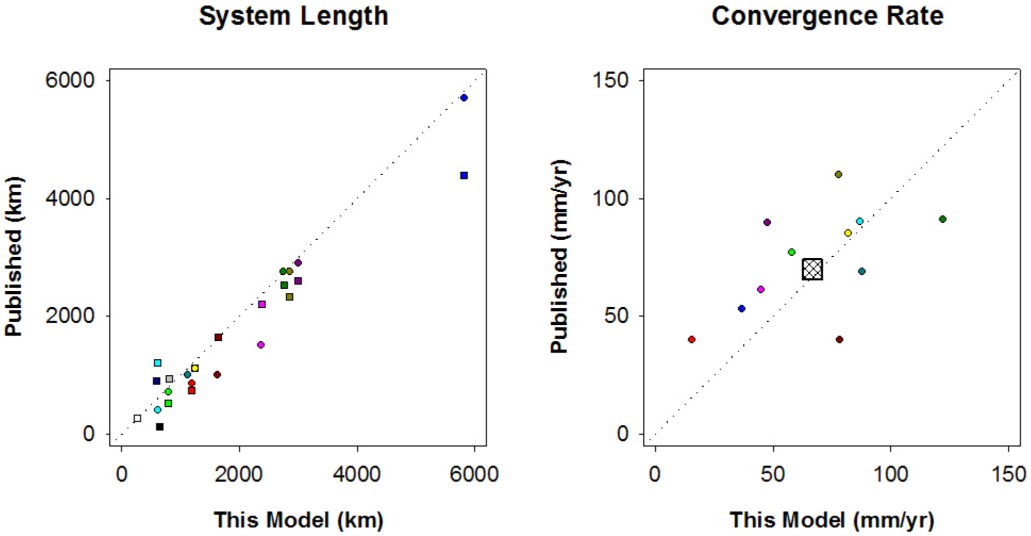

Direct comparison of the estimated $M_{ARC(Y)}$ does not give such favourable results, where the values calculated here (Table 2.2) are consistently 20-30% higher than those presented by Clift and Vannucchi (2004). This is due to the different values used for the mean global convergence rate. The data set used here has a mean global convergence rate of 52.3 mm/yr, in comparison to a value of 66.6 km/Ma for the subset considered by Clift and Vannucchi (2004). As the convergence rates of those arcs with submarine components are directly comparable (see Figure 2.4), and as magmatic emplacement is prorated based on the global convergence rate (see Eq. 2.9), this results in higher magmatic emplacement estimates in this study. Nevertheless, the mean (length normalised) magmatic emplacement rate calculated here of 97.7 km^3/kmMa shows excellent agreement with the range presented above of 95±27 km^3/kmMa (based on individual arc systems), and suggests an uncertainty of ~25% on this estimate is reasonable.

Table 2.2: Submarine magmatic emplacement rate in subduction zones.

	Subduction Zone / Arc Name	Length[a]	Covergent velocity[a]	Total Magmatic Emplacement Rate[b]		% of Arc that is Submarine[c]	Submarine Emplacement
	(Bird (2003) Data Segment Identifiers)	(km)	(km/Ma)	$km^3/kmMa$	km^3/Ma	%	km^3/Ma
①	**Aeolian** *(399-411, 419-429, 3403)*	781.6	6.2	10.7	8396.7	46.0	3862.5
②	**Aegean** *(5438-5466)*	1553.3	21.4	37.3	57890.8	33.0	19104.0
③	**Sumatra/Sunda/Banda** *(1375-1419,3739-3768, 4152-4163)*	5823.3	37.0	64.3	374590.0	33.0	123614.7
④	**Sangihe/Halmahera** *(3991-3993, 4024-4026, 4172-4173)*	597.6	54.8	95.4	57028.1	33.0	18819.3
⑤	**Philippine Trench/Bicol** *(3964-3985)*	1634.0	78.3	136.2	222579.2	21.0	46741.6
⑥	**Manila Trench/Luzon** *(3942-3951)*	609.9	87.2	151.7	92499.5	9.0	8325.0
⑦	**Ryukyu** *(3141-3156, 4388-4393)*	1125.5	87.7	152.6	171784.5	33.0	56688.9
⑧	**Kuriles** *(2752-2769)*	1241.9	82.2	142.9	177529.6	50.0	88764.8
⑨	**Izu-Bonin** *(3225-3242)*	1127.9	47.8	83.1	93784.0	58.0	54394.7
⑩	**Mariana** *(3199-3224)*	1866.7	47.6	82.8	154634.2	78.0	120614.7
⑪	**Yap Trench** *(3189-3198)*	690.8	15.7	27.4	18921.3	63.0	11920.4
⑫	**Trobriand Trough** *(1615-1633)*	590.8	10.6	18.4	10896.7	63.0	6864.9
⑬	**Manus Trough/TLTF** *(4525-4532)*	266.6	5.9	10.3	2732.8	40.0	1093.1
⑭	**New Britain Trench (S&N Bismarck)** *(1596-1610)*	814.4	94.8	164.9	134335.2	33.0	44330.6
⑮	**San Cristobel Trench (Solomons)** *(1611-1614, 1644-1744)*	1505.7	64.0	111.3	167598.6	31.0	51955.6
⑯	**New Hebrides** *(1745-1841)*	1350.8	93.2	162.2	219059.6	28.0	61336.7
⑰	**Tonga** *(1500-1532)*	1126.0	165.4	287.7	323988.5	73.0	236511.6
⑱	**Kermadec** *(1465-1499)*	1627.9	92.4	160.8	261750.0	87.0	227722.5
⑲	**Puysegur** *(4293-4325)*	651.4	16.9	29.4	19123.9	80.0	15299.1
⑳	**West Aleutians** *(2779-2817)*	2379.0	44.8	78.0	185611.2	7.0	12992.8
㉑	**Lesser Antilles** *(1912-1934)*	1192.4	15.5	27.0	32176.3	30.0	9652.9
㉒	**South Sandwich** *(5253-5265)*	790.7	58.1	101.2	79996.1	33.0	26398.7
	TOTAL	**29348**	**56.1**	**97.7**	**2866907**	**43.5**	**1247009**

(a) From the digital data set of Bird (2003) with modifications as described in the text; (b) Calculated here following the method of Clift & Vannucchi (2004); (c) From de Ronde et al. (2003), except for the Kurile Arc form Glasby et al. (2006).

The total magmatic emplacement in intra-oceanic and island arcs is estimated to be 2.9±0.7 km^3/yr, equivalent to 14% of M_{OSR}. Applying the estimated percent submarine gives a submarine magmatic emplacement rate of 1.2±0.3 km^3/yr, or approximately 5% of M_{OSR}. This may be considered a lower limit as this estimate inherently assumes that for all volcanoes that break the ocean surface the total volatile flux is released to the atmosphere, where this is not necessarily the case as significant venting may occur on the volcano flanks. The true flux is therefore most likely bounded by these estimates, falling in the range 1.2-2.9 km^3/yr. It is also noted that other subduction zone systems (e.g. Sulawesi, Papua New Guinea, NE Japan, SW Honshu etc.) may have some submarine components. However, it is assumed here that the contribution made by these systems falls within the large uncertainty on this estimate.

2.2.2.3 *The Intraplate Magmatic Flux (M_{HOT})*

Hotspots are relatively small areas of volcanism scattered across the Earths surface, generally defined as sites of intraplate volcanism or excessive volcanism along divergent plate boundaries. Hydrothermal venting of CO_2 rich fluids or direct venting of a discrete CO_2 phase has been observed at a number of hotspot locations including Hawaii, Iceland, the Azores, and the Samoan archipelago (see Chapter 3).

Crisp (1984) reported a total oceanic intraplate magmatic emplacement rate of 1.8-2.4 km^3/y from an estimated extrusive emplacement of 0.3-0.4 km^3/yr (Menard, 1964; Batiza, 1982) and an intrusive to extrusive ratio of 5:1. Schilling (1978) took a different approach, estimating a mean production rate for two classes of hotspots ('large' such as Hawaii and all other 'smaller' hotspots) and extrapolating to the total flux based on the number of hotspots. The latter approach is followed here. Table 2.3 provides a list of the oceanic hotspots for which estimates of magmatic emplacement rates and/or the ratio of intrusives to extrusives are available (after Schilling et al. (1978), Crisp (1984) and White et al. (2006)). This includes total emplacement rates for 5 of the larger hotspots (Hawaii, Iceland, Galapagos, Azores, Kerguelen), and the extrusive emplacement rate for a further 10 hotspots.

The Holocene emplacement rate at the Iceland hotspot is ~0.2-0.4 km^3/yr (Schilling et al., 1978; White et al., 2006). That at Hawaii appears similar, with an estimated emplacement rate at Mauna Loa of 0.05-0.08 km^3/yr (over the past 4 ka), where Kilauea (0.14 km^3/yr over the past 400 ka) and Loihi are also currently active, suggesting a total emplacement rate on the order of ~0.2-0.3 km^3/yr. Estimated emplacement rates for the Galapagos and Azores are also comparable, at 0.24 and 0.1-0.2 km^3/yr respectively. Although the estimated Kerguelen emplacement rate is also high (0.26 km^3/yr), this includes underplating with an intrusive to extrusive ratio of 28:1, and is thus an overestimate of the magma supply. Following the approach of Schilling et al. (1978) and applying an estimated 25% partial melting suggests a magmatic emplacement rate of 0.07 km^3/yr. Reunion is also considered to be a large hotspot, and is likely to have a comparable magmatic emplacement rate of ~0.2 km^3/yr. Combining these estimates gives a total emplacement rate for these 6 hotspots on the order of 1.0-1.6, or 1.3±0.3 km^3/yr. For the remaining 10 hotspots, the extrusive emplacement rates are considerably lower than those observed at the major hotspots, and range over 2-3 orders of magnitude, from 5 $\times 10^{-6}$ km^3/yr (Fernando Noronha) to 7.5 $\times 10^{-3}$ km^3/yr (Canary Islands), with a mean of ~1.14 $\times 10^{-3}$ km^3. Examination of the intrusive:extrusive ratios suggests a value of 4:1 is reasonable (range of 2:1 to 6:1), indicating a mean total emplacement rate of 0.006±0.002 km^3/yr at each ‘small’ hotspot.

There are at least 38 active (Holocene activity) oceanic hotspots (see Figure 2.5, after hotspot lists of Hagstrum (2005) and Anderson & Schramm (2005)), suggesting a minimum of 32 smaller hotspots with a combined flux of ~0.2±0.1 km^3/yr, giving a total hotspot magmatic emplacement rate of ~1.5±0.4 km^3/yr (1.1 to 1.9 km^3/yr), slightly lower than the Crisp (1984) estimate. Here simple assumptions are made to provide a first order estimate of the proportion of the magmatic volatile flux associated with oceanic intraplate volcanism that occurs in the submarine environment. Firstly, it is noted that only the major oceanic hotspots form volcanic structures that break the ocean surface and vent to the atmosphere. Secondly, most, if not all, oceanic hotspots will have some form of submarine volcanic and/or hydrothermal activity, where the volatile flux is not associated with high temperature crater degassing but with medium and low temperature vent sites located on the flanks of the volcanoes. Thus a significant proportion of the volatile flux associated with all oceanic hotspots will occur below sea-level. Here it is assumed that 50±25% of the oceanic intraplate magmatic flux, or 0.8±0.4 km^3/yr (0.4-1.2 km^3/yr), occurs in the submarine environment.

Table 2.3: Magmatic emplacement rates at oceanic hotspots (after White et al., 2006).

Hotspot	Location		Duration	Magma Volumes			Magmatic Emplacement Rates		
	Lat. (°N)	Long. (°E)	(ka)	Extrusives (km^3)	Instrusives (km^3)	Ratio	Extrusives (km^3/yr)	Intrusives (km^3/yr)	Total (km^3/yr)
Ascension[a,b]	-8	-9	1500	90			6.0×10^{-5}		
Azores[c]	38	-28							0.10 to 0.20[†]
Sao Miguel[d]			4.55	4.5			9.9×10^{-4}		
Terceira[d]			23	5.46			2.4×10^{-4}		
Bouvet I.[a]	-54	3	700	28			4.0×10^{-5}		
Canary Is.[d,e]	28	-17	20000	150000			7.5×10^{-3}		
La Palma[f,g]			123	125			1.0×10^{-3}		
La Gomera[h]			1400	350			2.5×10^{-4}		
Gran Canaria[d,e,i]			600	200			3.3×10^{-4}		
Cape Verde Is.	16	-25							
Santo Antao[j]			1750	68			4.0×10^{-5}		
Fernando Noronha[§,a]	-4	-32	12000	60			5.0×10^{-6}		
Galapagos Is.[c]	1	-89							0.24[†]
Gough[§,k,l]	-40	-10	2420	99			4.1×10^{-5}		
Hawaii	19	-155							
Hawaii-Emperor Smt. Chain[d,m,n]			73600	1080000	5900000	6:1 [‡]	1.5×10^{-2}	8.0×10^{-2}	0.09[‡]
Kilauea[o,p]			400	20000	36000	2:1	5.0×10^{-2}	9.0×10^{-2}	0.14
Kohala, Hawaii[d]			400	14000			3.5×10^{-2}		
Mauna Kea, Hawaii[d]			300	24800			8.3×10^{-2}		
Mauna Loa, Hawaii[d]			500	42500			8.5×10^{-2}		
Mauna Loa, Hawaii[q,r]			4	80	110 to 240	>1:1 to 3:1	2.0×10^{-2}	2.8 to 6.0×10^{-2}	0.05 to 0.08
Koolau, Oahu[d]			600	20900			3.5×10^{-2}		
Iceland[c]	65	-19							0.23 to 0.45[†]
Iceland[d,s,t,u]			11	484		4:1 to 8:1	4.4×10^{-2}		0.22 to 0.40
Iceland[d]			1000	20000			2.0×10^{-2}		
Iceland[v]							2.6×10^{-2}		
Juan Fernandez Is.[a]	-34	-81	1000	72			7.2×10^{-5}		
Kerguelen Is.	-49	69							
Kerguelen Archipelago[w]			11000	99000	2750000	28:1 [‡]	9.0×10^{-3}	3.0×10^{-1}	0.26[‡]
Kerguelen Island[a]			26000	5720			2.2×10^{-4}		
Marquesas Is.[§,x]	-9	-139		330000	620000	2:1 [‡]			
Reunion[a]	-21	56	2000	4800			2.4×10^{-3}		
Ross[a]	-78	167	4000	4800			1.2×10^{-3}		
St. Helena[§,a]	-17	-9	8000	192			2.4×10^{-5}		

[§] no documented activity in the Holocene; [†] estimated from mantle plume flux and assuming 25% partial melting (Schilling, 1978); [‡] includes underplating.

(a) Gerlach 1990; (b) Nielson & Sibbett, 1996; (c) Schilling, 1978; (d) Crisp, 1984; (e) Hoernle & Schmincke, 1993; (f) Carracedo et al., 1999; (g) Guillou et al., 1998; (h) Paris et al., 2005; (i) Freundt & Schmincke, 1995; (j) Plesner et al., 2002; (k) Chevallier, 1987; (l) Maund et al., 1988; (m) Bargar & Jackson, 1974; (n) Vidal & Bonneville, 2004; (o) Quane et al., 2000; (p) Dvorak & Dzurisin, 1993; (q) Klein, 1982; (r) Lipman, 1995; (s) Bjarnason et al., 1993; (t) Darbyshire et al., 1998; (u) Menke et al., 1998; (v) Jakobsson, 1972; (w) Nicolaysen et al., 2000; (x) Caress et al., 1995.

Figure 2.5: Map showing location of oceanic hotspots with Holocene activity.

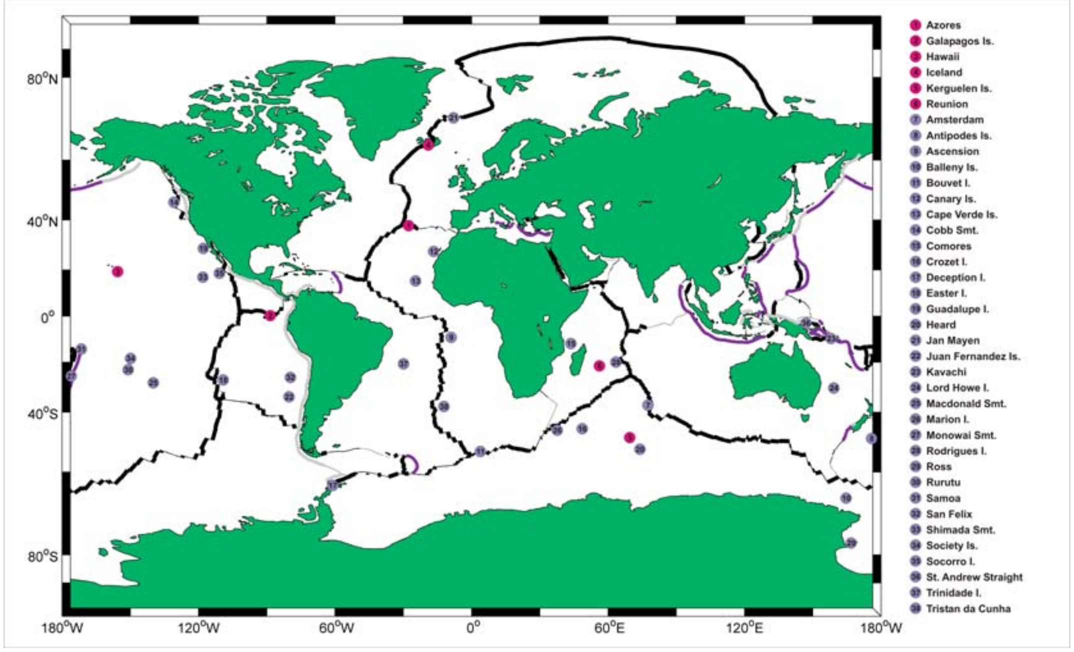

2.2.3 The Global Flux of Volcanic He to Ocean Bottom Waters

In comparison to the direct determination of a CO_2 flux, the ^{3}He flux to the oceans is relatively well constrained, and can be calculated from the excess ^{3}He present in the ocean.

Excess ^{3}He is the enrichment in ^{3}He relative to the ratio of ^{3}He to ^{4}He in the atmosphere, and is typically expressed in terms of the ratio R/R_a, or the ratio anomaly δ^3He:

$$\frac{R}{R_a} = \frac{(^3He/^4He)_{sample}}{(^3He/^4He)_{atmosphere}} = \frac{(^3He/^4He)_{sample}}{1.39 \pm 0.01 \times 10^{-6}} \quad \textbf{[Eq. 2.10]}$$

$$\delta^3He = \left(\frac{R}{R_a} - 1\right) \times 100(\%) \quad \textbf{[Eq. 2.11]}$$

The excess ^{3}He in the oceans is due to the flux of He degassed or extracted from the mantle during submarine volcanic and hydrothermal activity, where mantle He exhibits a high R/R_a due to incomplete degassing of primordial (original) ^{3}He following Earth condensation 4.5 Gyr ago (Clarke et al., 1969). As an inert gas He therefore provides a conservative and sensitive tracer of magmatic inputs to the ocean.

The magmatic flux of ^{3}He to the ocean can be calculated from the He saturation anomaly (ΔHe), which is the observed deviation from the equilibrium solubility concentration for seawater in contact with water saturated air (Craig et al., 1975). For total He, a large proportion of ΔHe reflects a contribution from air injection by bubbles. Nevertheless, examination of noble gas ratios (He/Ne) allows an excess saturation anomaly (Δ_EHe) to be determined (Craig et al., 1975). This Δ_EHe ranges from 0% in juvenile North Atlantic deep waters to 5% in older deep waters overlying the East Pacific Rise, where Craig et al (1975) adopted a mean global ocean value of 2.5%. The ^{3}He flux (F(^{3}He)) can then be calculated following two different approaches. In the first case, Δ_EHe is used to determine F(^{4}He), which is then multiplied by the ^{3}He/^{4}He ratio of the mantle to obtain F(^{3}He). In the second case, F(^{3}He) is calculated from Δ^3He, which is estimated from Δ_EHe and the δ^3He of ocean bottom waters. Both methods are outlined below.

2.2.3.1 *Estimate 1: determining F(^{3}He) from F(^{4}He) and the ^{3}He/^{4}He of the mantle*

The flux of excess ^{4}He, F(^{4}He), is first estimated from Δ_EHe (expressed as a fraction, 0.025) using an advective flux calculation (Craig et al., 1975; Elderfield & Schultz, 1996):

$$F(^4He) = \frac{\rho_{sw} \times {}^4He^* \times (\Delta_E He) \times \omega \times A_{ocean}}{V} = 8.4 \times 10^7 \, mol/yr \quad \textbf{[Eq. 2.12]}$$

Where ρ_{sw} is the density of seawater (1.04 g/cm^3), ω is the mean vertical advective water velocity (500 cm/yr), A_{ocean} is the area of the ocean (3.61 x10^{18} cm^2), V is the molar volume of an ideal gas (22,414 cm^3 STP/mol), and ^{4}He* is the equilibrium concentration of ^{4}He (4x10^{-8} cm^3 STP/g). Craig et al. (1975) give an estimated uncertainty in this value on the order of 50%, giving a ^{4}He flux of 8.4±4.2 x10^7 mol/yr. However, this flux includes both a magmatic and radiogenic source term, where ^{4}He is also produced by radioactive decay of U and Th series nuclides. Well et al. (2001) estimate that the radiogenic ^{4}He flux out of deep-sea sediments and the ocean crust is ca. 2.7±1.1 x10^7 mol /yr, giving a magmatic ^{4}He flux of 5.7±4.1 x10^7 mol/yr.

The ^{3}He flux is then determined by multiplying the ^{4}He flux by the (^{3}He/^{4}He) of the mantle source (often quoted as $(R/R_a)_{mantle}$):

$$F(^{3}He) = F(^{4}He) \times (^{3}He/^{4}He)_{mantle} = F(^{4}He) \times R_{a} \times \left(\frac{R}{R_{a}}\right)_{mantle} \quad \textbf{[Eq. 2.13]}$$

The average ^{3}He/^{4}He observed at the MORs is generally accepted as the He signature for the upper mantle and can be determined from the observed ^{3}He/^{4}He of basaltic glasses (MORB) and hydrothermal fluids (vents and plumes). In their original calculation, Craig et al. (1975) used an $(R/R_a)_{mantle}$ of 11.2±2, whereas more recent data compilations suggest that a range in $(R/R_a)_{mantle}$ of 8±1 is more accurate (Kurz & Jenkins 1981, Lupton 1983, Elderfield and Schultz 1996), giving a F(^{3}He) of 630±460 mol/yr. A more detailed analysis, allowing for the different isotope ratios and concentrations of He in the source magmas is presented below, although it is noted that this introduces a minor variation that falls well within the uncertainty on this estimate.

2.2.3.2 *Estimate 2: determining F(^{3}He) from Δ_EHe and the δ^{3}He of the oceans*

F(^{3}He) can also be calculated using the ^{3}He analogue of **Eq. 2.12**:

$$F(^{3}He) = \frac{\rho_{sw} \times {}^{3}He^{*} \times (\Delta^{3}He) \times \omega \times A_{ocean}}{V} \quad \textbf{[Eq. 2.14]}$$

The equilibrium concentration ^{3}He* is equal to ^{4}He* multiplied by αR_a, where α is the solubility fractionation factor 0.988:

$$^{3}He^{*} = {}^{4}He^{*} \times \alpha \times R_{a} \quad \textbf{[Eq. 2.15]}$$

Δ^{3}He is calculated from Δ_EHe and δ^{3}He:

$$\left(\frac{^{3}He}{^{4}He}\right)_{ocean} = \frac{(1+\Delta^{3}He) \times {}^{3}He^{*}}{(1+\Delta_{E}He) \times {}^{4}He^{*}} = \left(\frac{\delta^{3}He}{100}+1\right) \times R_{a} \quad \textbf{[Eq. 2.16]}$$

Where substituting for ^{3}He* and rearranging gives:

$$\Delta^{3}He = \frac{\left(\frac{\delta^{3}He}{100}+1\right) \times (1+\Delta_{E}He)}{\alpha} - 1 \quad \textbf{[Eq. 2.17]}$$

As with Δ_EHe, the δ^{3}He of ocean bottom waters reflects a combination of two factors (1) the source distribution of magmatic He and (2) ocean ventilation and deep water circulation patterns (Farley et al., 1995; Lupton, 1998). Baker & German (2004) compared the global distribution of deep-water (2000-3000 m) ^{3}He to the spreading rate trend along the MORs (see Figure 9 in Baker & German, 2004). In general there is a good correlation between spreading rate (proportional to hydrothermal activity; Baker & German, 2004) and the distribution of δ^{3}He.

The young bottom waters of the North Atlantic Ocean exhibit the lowest δ^{3}He (<5%), which increases slightly along the slow spreading MAR to ~10% in the South Atlantic (Jenkins et al., 1972; Östlund et al., 1987; Rüth et al., 2000). The influence of Atlantic deep water and vigorous vertical and circumpolar mixing around Antarctica results in a relatively low δ^{3}He of 8-9% extending across the Southern Indian Ocean (despite vigorous seafloor spreading), which increases to 15-18% in the Central and North Indian Ocean due to hydrothermal inputs (Jamous et al., 1992; Farley et al., 1995; Lupton, 1998). Similarly, δ^{3}He in the Pacific Ocean increases from 15% in the South to 25% in the North, with intense δ^{3}He plumes spreading westward from super-fast spreading ridge segments on the southern EPR, the fast spreading northern EPR and the intermediate-rate JDFR (Clarke et al., 1969; Craig et al., 1975). Using mean δ^3He values for the Atlantic Ocean, Indian Ocean, South Pacific and North Pacific of 5%, 14%, 15% and 25% respectively, and normalising to ocean area, gives a global mean δ^3He of ~15%, corresponding to a Δ^3He of 19%, and a F(^{3}He) of 880±440 mol/yr (assuming an error of 50%).

2.2.3.3 Apportioning of the magmatic He flux

Of interest here is the proportion of total ^{3}He that is delivered to the ocean via submarine volcanic activity at the Ocean Spreading Ridges, Island Arcs and Hotspots (f_{MOR}, f_{BAB}, f_{HOT}, and f_{ARC}). If complete degassing is assumed, the apportioning of the total He flux is dependent on the magmatic volume fluxes, and the relative concentrations and isotope ratios of He in the different magmas (see **Eq. 2.4**).

The ^{3}He/^{4}He ratios observed at back arc spreading centres such as the Lau Basin and Mariana trough are isotopically indistinguishable from MORB He, indicating that these zones of crustal expansion extract He from the upper mantle in much the same way as normal MOR spreading centres (Lupton, 1983). Based on this observation, the Ocean Spreading Ridges can be treated as a single magma type with a uniform $[^4He]_{OSR}$ and an R_{OSR}/R_a of 8±1.

Subduction zones exhibit a ^{3}He/^{4}He ratio slightly lower than that observed at the MOR, with a range in R/R_a of ~2-11, and a mean of ~6 (Lupton, 1983). The constancy of this ratio across different regions indicates uniform proportions of recycled down-going slab and primary mantle material are involved in the generation of subduction zone volcanics. Here an R_{ARC}/R_a of 6±2 is used, where it is assumed that the down-going slab has a radiogenic isotope ratio, with $R_{ARC(r)}/R_a$ of 0.050±0.025, and that the primary melt has an isotopic composition equal to MORB, with $R_{ARC(p)}/R_a$ of 8±1. Unfortunately, little is known regarding the He concentration of undegassed subduction zone volcanics. However, it is reasonable to assume that $[He]_{ARC(p)}$ is comparable to $[He]_{OSR}$ (c.f. Torgersen, 1989; Marty & Tolstikhin, 1998). Two end-member cases can then be considered. In case 1 it is assumed that $[^4He]_{ARC}$ (and therefore $[^4He]_{ARC(r)}$) is equal to $[^4He]_{OSR}$, and that R_{ARC} is less than R_{OSR} is due to mixing of primary melt with a ^{3}He depleted down-going slab. In case 2 it is assumed that $[^3He]_{ARC}$ (and therefore $[^3He]_{ARC(r)}$) is equal to $[^3He]_{OSR}$ and that R_{ARC} is less than R_{OSR} is due to mixing of primary melt with a ^{4}He enriched down-going slab.

The observed R/R_a at Hotspots varies considerably with a range of 15-30, although only a fraction of samples exhibit the highest ratios (for example Loihi seamount, the current location of the Hawaiian hotspot, with R/R_a = 20-32). It is thought that Hotspots exhibit extreme ^{3}He/^{4}He because they are tapping a deeper primitive (or undepleted) part of the mantle that is more enriched in ^{3}He (Craig and Lupton 1976). However, somewhat paradoxically, the absolute concentrations of He in plume magmas are around 25 times lower than in upper mantle magmas (0.03 to 4.5 μcc/g with respect to 1 to 80 μcc/g; Anderson, 1998 and references therein). Here a $[^4He]_{HOT}$ equal to $(0.04\pm0.02)*[^4He]_{OSR}$ and an R_{HOT}/R_a of 20±5 are assumed to be representative.

Combining the above assumptions with the magmatic fluxes determined in section 2.2.2, and noting that the portion of the subduction zone He flux attributable to the recycled down-going slab is accounted for in the radiogenic He flux, allows the He fluxes calculated above to be apportioned between the submarine components of the OSRs, Volcanic Arcs, and Hotspots. The results are given below in Table 2.4, where the fraction of He attributed to the OSRs, Arcs, and Hotspots (f_{OSR}, f_{ARC} and f_{HOT}) is an average of that determined from the Case 1 and Case 2 assumptions. Combining the estimates of f_X with the two estimates of the total He fluxes (Estimate 1 and Estimate 2 above) and assumed R/R_a ratios then gives best estimates for the magmatic F(^{4}He) and F(^{3}He) of 68±28 x10^6 mol/yr and 760±310 mol/yr respectively.

Table 2.4: The estimated flux of ^{4}He and ^{3}He delivered to the ocean via volcanic activity at the Mid Ocean Ridges, Back-Arc Basin spreading centres, Island Arcs, and Hotspots. Estimate 1 is determined from F(^{4}He) and Estimate 2 is determined from F(^{3}He).

	^{4}He Flux (×10^3 mol/yr)			**^{3}He Flux (mol/yr)**		
	Estimate 1	**Estimate 2**	**Average**	**Estimate 1**	**Estimate 2**	**Average**
F(He)$_{total}$	83,781 ± 41,890	87,429 ± 31,719	85,605 ± 26,272	635 ± 425	889 ± 444	762 ± 307
F(He)$_{radiogenic}$	27,000 ± 11,000	27,000 ± 11,000	27,000 ± 7,778	2 ± 1	2 ± 1	2 ± 1
F(He)$_{magmatic}$	56,781 ± 40,420	60,429 ± 29,751	58,605 ± 25,094	633 ± 425	887 ± 444	760 ± 307
F(He)$_{OSR}$	52,147 ± 37,471	55,297 ± 29,557	53,722 ± 23,863	580 ± 423	615 ± 320	597 ± 265
MOR	42,643 ± 30,642	45,218 ± 24,171	43,931 ± 19,514	474 ± 346	503 ± 261	489 ± 217
BAB	9,506 ± 6,800	10,080 ± 5,388	9,793 ± 4,338	106 ± 77	112 ± 58	109 ± 48
Fe(He)$_{ARC}$	6,082 ± 4,891	6,743 ± 4,985	6,413 ± 3,492	51 ± 42	56 ± 37	53 ± 28
primary	4,552 ± 3,715	5,047 ± 3,392	4,799 ± 2,515	51 ± 42	56 ± 37	53 ± 28
recycled	1,530 ± 1,751	1,696 ± 2,135	1,613 ± 1,381	0 ± 0	0 ± 0	0 ± 0
Fe(He)$_{HOT}$	81 ± 71	86 ± 68	84 ± 49	2 ± 2	2 ± 2	2 ± 1

2.2.4 The Global Flux of Volcanic CO_2 to the Ocean

To obtain an estimate for the global flux of volcanic CO_2 to the ocean from F(^{3}He) requires knowledge of the $CO_2/^3He$ ratio of volcanic emissions at the MORs, Back-Arc Basin spreading centres, volcanic arcs and hotspots (see **Eq. 2.2**). Measurements of $(CO_2/^3He)_X$ can be obtained from analysis of the residual gas trapped in vesicles in basaltic glasses, hydrothermal fluids, CO_2 rich phases (e.g. liquid CO_2 droplets), or volcanic gases. A compilation of available data is presented in Figure 2.6, and best estimates are discussed below.

At the MORs both ^{3}He and CO_2 are magmatic in origin. Thus at a given location on the MOR, a good correlation is expected (and observed) between the $CO_2/^3He$ of residual gases trapped in MORB glasses, and the $CO_2/^3He$ of hydrothermal vent and plume fluids (e.g. Resing et al., 2004). Furthermore, if the $CO_2/^3He$ ratio is relatively constant in the mantle and there is little fractionation of CO_2 from ^{3}He during magmatic and hydrothermal processes, then ^{3}He and CO_2 are expected to be well correlated along the entire MOR system.

$CO_2/^3He$ measurements in MORB give a range of 0.2 to 3.0 x10^9 (mol/mol) with a mean ratio of 2.2±0.6 (n=38, Marty and Zimmerman 1999), similar to previous estimates based on a more restricted data set (Marty and Jambon, 1987; Marty and Tolstikhin, 1998; Trull et al., 1993).

$CO_2/^3He$ measurements in hydrothermal vent and plume fluids are available from 9 locations, with a range of 0.7 to 8.1 x10^9 and a mean of 2.1±1.8 x10^9 (Resing et al., 2004). Although this data set is limited, it includes both slow (Mid Atlantic Ridge, MAR) and super-fast (27°S to 32°S on the Southern East Pacific Rise, SEPR) spreading ridges, and both CO_2 poor (TAG site, MAR) and CO_2 rich (Axial Volcano) vent sites, and is therefore most likely representative of the range in values expected for the MOR system.

Gerlach (1991) highlighted fractionation as a potential problem in the use of $(CO_2/^3He)_{MOR}$ to determine CO_2 fluxes. Indeed, $(CO_2/^3He)_{MOR}$ does show significant variation among the sites studied to date (0.2 to 8.1 x10^9), and some fractionation of ^{3}He from CO_2 has been observed in hydrothermal fluids following magmatic and tectonic events at Endeavour Ridge and along the northern East Pacific Rise (Lilley et al., 2003). Nevertheless, Marty and Zimmerman (1999) argue that heterogeneity of the mantle source is the major factor controlling the spread of data, where magmatic degassing appears to cause only a small amount (factor of 2) of fractionation of ^{3}He from CO_2. This is supported by Resing et al. (2004), who note that the close agreement between the overall average $CO_2/^3He$ in MORB and hydrothermal vent fluids and plumes suggests that significant fractionation between ^{3}He and CO_2 has not occurred during magma chamber degassing, eruption and hydrothermal convection. Combining the basalt and fluid data (with equal weighting) thus gives a best estimate for $(CO_2/^3He)_{MOR}$ of 2.1±0.9 x10^9.

The $CO_2/^3He$ ratio for samples from volcanic arcs shows a large degree of variation and can be significantly greater than that observed at the MORs, with $(CO_2/^3He)_{ARC}$ ranging over 5 orders of magnitude from 3 $x10^8$ to greater than 6 $x10^{13}$ (see Figure 2.6). This reflects variable inputs from different CO_2 sources in arc systems, where CO_2 is derived from degassing of subducted slab and magma and additional crustal and/or sedimentary CO_2 inputs (e.g. Varekamp et al., 1992, Plank & Langmuir, 1993; Sano & Marty, 1995; Sano & Williams, 1996). The subducting slab carries C-rich material (limestones, slab carbonates and organic matter) into the magma generation zone, where thermal alteration produces CO_2 (decarbonation of limestone and thermal cracking of organic matter). Further CO_2 may also be added by the incorporation of volatiles from the overlying crust and sediments through which the magma then erupts. The total CO_2 flux in arcs can be de-convolved to the individual source contributions by considering the observed $(CO_2/^3He)$ and $\delta^{13}C$ and a three component mixing model between MORB ($\delta^{13}C$ = -6.5%), marine carbonates ($\delta^{13}C$ = 0%), and organic sediment ($\delta^{13}C$ = -30%). Following the method described by Sano and Williams (1996), and assuming a $(CO_2/^3He)$ for marine carbonates and organic matter of $1x10^{14}$, but using the revised $(CO_2/^3He)_{MORB}$ of 2.1 $x10^9$ presented above, gives a mean contribution to arc CO_2 from MORB of 12±10%, marine carbonates of 56±11%, and organic rich sediments of 32±9% (based on data presented in Figure 2.6 for which $\delta^{13}C$ values are also available, from Sano & Williams, 1996; Shaw et al., 2003; Snyder et al., 2001; Van Soest et al., 1998).

Figure 2.6: Observed (CO_2/^{3}He) Ratios at Mid Ocean Ridges, Back-Arc Basin Spreading Centres, Island and Continental Volcanic Arcs, and Hotspots. (Hotspots, Marty & Tolstikhin (1998); MOR Basalts, Marty & Zimmerman (1999); MOR Fluids, Resing et al. (2004); Back Arc Basin Basalts from top down, Manus Basin, Shaw et al. (2004), Eastern Manus Basin, Marty et al. (2001), North Fiji Basin, Marty & Zimmermann (1999), Nishio et al. (1998), Mariana Trough, Sano et al. (1998); Okinawa Trough JADE site (Fluids and CO_2 droplets), Sakai et al. (1990b); Okinawa Trough Minami Ensei Knoll, Glasby & Notsu (2003); NW Eifuku Champagne vent (Fluids and CO_2 droplets), Lupton et al. (2006); Arc high T volcanic gases, fumaroles and geothermal springs, after compilation of Sano & Williams 1996, with additional data from Clor et al. (2005), Shaw et al. (2003), Snyder et al. (2001), and Van Soest et al. (1998). On the range bars, vertical black lines indicate arithmetic mean values for MOR Basalts and MOR Fluids. For Hotspots and Arcs, the 25th, 33rd, 50th (median), 67th and 75th percentiles are shown.

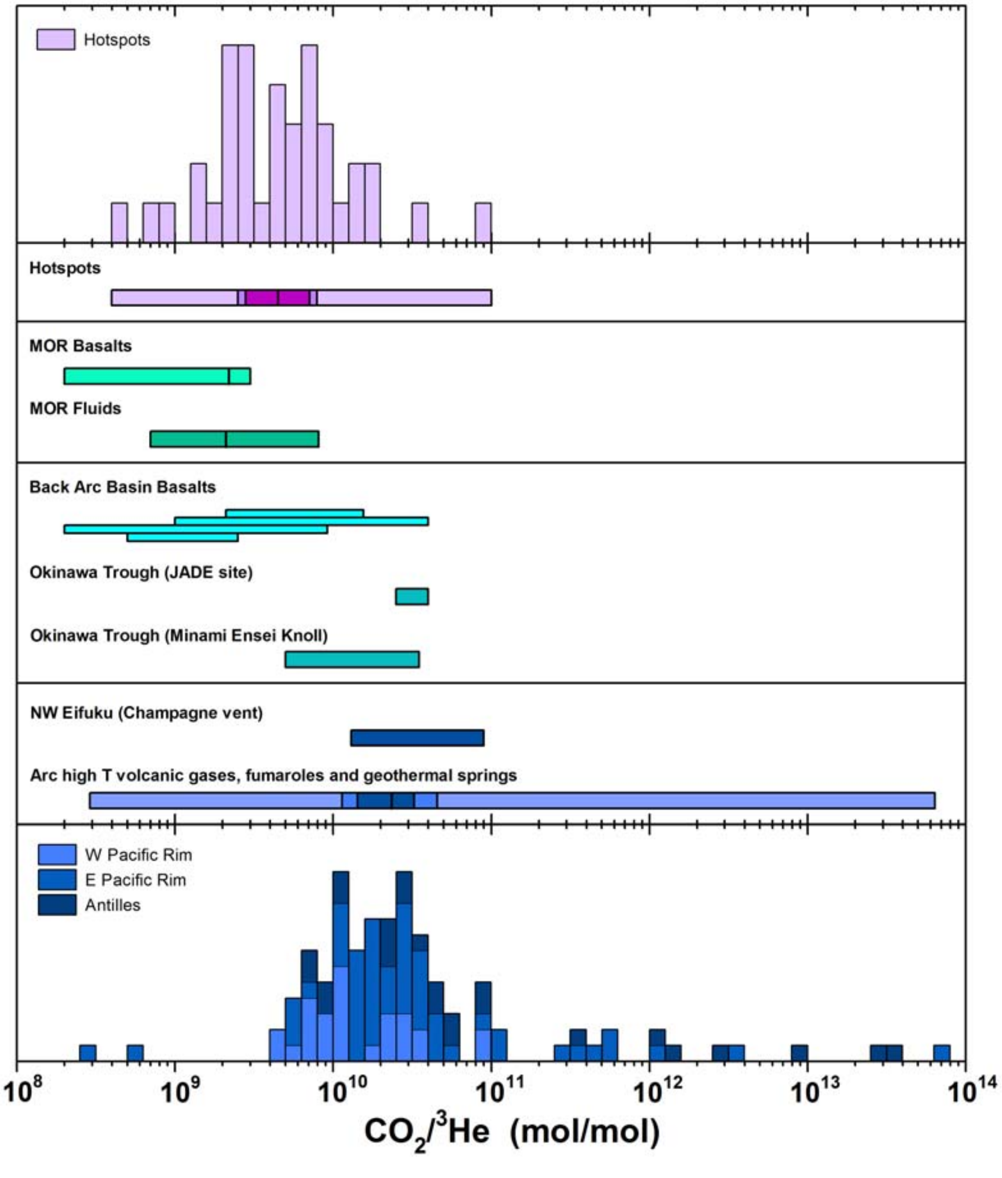

It is noted that the arc data presented in Figure 2.6 corresponds to subaerial systems. At present there is a marked shortage of $CO_2/^{3}He$ measurements from submarine arc volcanoes with data available from a single location, the Champagne vent site at NW Eifuku (Lupton et al., 2006). Nevertheless, the range in $(CO_2/^{3}He)$ observed in Champagne vent fluids and CO_2 droplets (13-90 $x10^{9}$) shows good agreement with the observations of subaerial arc systems, bracketing over 50% of the arc measurements (from 30th-81st percentile, n=107). Furthermore, a number of the arc systems included here have submarine components (the Antilles arc, New Zealand, the Sangihe arc and Indonesia). The subaerial data are therefore thought to be representative of the likely $CO_2/^{3}He$ ratio in submarine arc systems. That $(CO_2/^{3}He)_{ARC}$ varies over 5 orders of magnitude makes the use of an arithmetic mean inappropriate (the mean of the data presented here is 1.39 $x10^{12}$, 2 orders of magnitude higher than that observed at the Champagne vent site, where only 5% of all arc measurements exceed this value). Instead, the median value of $23.5x10^{9}$ is considered the best estimate of $(CO_2/^{3}He)_{ARC}$. The uncertainty on this estimate is likely large, where a value of $\pm 10x10^{9}$ (encompassing the 33rd and 67th percentiles, see Figure 2.6) is considered reasonable here.

Spreading centres in back-arc basins can also be influenced by the down-going slab (see Figure 2.1) and display a considerable variation in $(CO_2/^{3}He)$, ranging from MORB type ratios to arc type ratios (see Figure 2.6). It is assumed here that $(CO_2/^{3}He)_{BAB}$ is bounded by $(CO_2/^{3}He)_{MOR}$ and $(CO_2/^{3}He)_{ARC}$, giving a best estimate of 12.8 ± 10.7 $x10^{9}$.

The $(CO_2/^{3}He)_{HOT}$ is somewhat higher than that observed at the MORs, where the median value of 4.5 ± 2.6 $x10^{9}$ is considered the best estimate here.

Combining the estimates of $F(^{3}He)_X$ and $(CO_2/^{3}He)_X$ presented above gives a best estimate for the flux of volcanic CO_2 to the ocean of 3.7 ± 1.7 $x10^{12}$ mol/yr (2.0-5.4 $x10^{12}$ mol/yr), or 162±74 $MtCO_2$/yr (see Table 2.5). This estimate falls within the range of previous estimates (0.1-15 $x10^{12}$ mol/yr), and toward the upper end of those estimates based on the magmatic flux of ^{3}He and $CO_2/^{3}He$ ratios (0.4-6 $x10^{12}$ mol/yr, see review of Resing et al., 2004). This assessment agrees with previous analyses that the flux of volcanic CO_2 from hotspot magmatism is negligible in comparison to the flux from the MORs. However, this estimate highlights the potentially large flux from volcanic arcs and back-arc basins, where the contribution from these regions is directly comparable to (if not larger than) the CO_2 flux at the MORs.

Table 2.5: The flux of volcanic CO_2 to the ocean.

	$F(^{3}He)$	**$CO_2/^{3}He$**	**$F(CO_2)$**		
	mol/yr	**10^{9} mol/mol**	**10^{12} mol/yr**	**Mt CO_2/yr**	***(%)***
MORs	489 ± 217	2.1 ± 0.9	1.0 ± 0.6	45 ± 28	***(27.8)***
Back-Arc Basins	109 ± 48	12.8 ± 10.7	1.4 ± 1.3	61 ± 58	***(37.8)***
Volcanic Arcs	53 ± 28	23.5 ± 10.0	1.3 ± 0.8	55 ± 37	***(34.1)***
Hotspots	2 ± 1	4.5 ± 2.6	0.01 ± 0.01	0.5 ± 0.4	***(0.3)***
TOTAL			**3.7 ± 1.7**	**162 ± 74**	

2.3 Comparison of CO_2 Fluxes to Projected Storage Rates

The most significant flux of CO_2 to the surface ocean is via air-sea gas exchange, with an estimated uptake rate of 8.1±1.8 $GtCO_2$/yr for the present day. This annual flux of CO_2 to the surface ocean is approximately 600-1000 times greater than the mass of CO_2 that has been injected into subseafloor geological storage reservoirs to date, and is higher by a factor of 2 than the projected storage utilisation by the year 2050 if it is assumed that all potential storage projects that have been announced proceed on forecast timelines and store CO_2 at the maximum projected rate (including all current, planned, and potential future projects, the storage rate by the year 2050 will be ~100 $MtCO_2$/yr, with a total volume stored of 3.8 $GtCO_2$, see Chapter 1, Section 1.3).

This estimate of the flux of volcanic CO_2 to the ocean gives a range of 88-236 $MtCO_2$/yr, with a best estimate of 162 $MtCO_2$/yr[2]. This annual flux of CO_2 to the seafloor is approximately 8-23 times greater than the mass of CO_2 that has been stored in subseafloor geological storage reservoirs to date, and is equivalent to the projected storage utilisation by the year 2050 for all current projects that have completed, or nearly completed, the planning and approvals process (225 $MtCO_2$, see Chapter 1, Section 1.3). The cumulative emissions of volcanic CO_2 to the ocean from the present day to 2050 will be in the region of 6.9±3.2 $GtCO_2$, comparable to the projected storage utilisation if both the Natuna gas field is developed, and Japanese offshore storage projects proceed as intended (3.8 $GtCO_2$ by 2050).

Should Carbon Capture and Storage (CCS) see widespread utilisation as a greenhouse gas emission reduction strategy, then by the year 2100 the subseafloor geological storage rate could reach levels comparable to the current rate of atmospheric CO_2 invasion into the surface ocean, and approximately 5 times greater than the volcanic flux of CO_2 to the ocean, with a total mass stored of ~250-500 $GtCO_2$ (see Chapter 1, Section 1.3). If it is assumed that all storage reservoirs meet recommended performance levels (that >99% of the CO_2 stored is retained for a period of at least 1000 years), then the maximum 'allowable' leakage flux would be 2.5-5 $MtCO_2$/yr, around 20-100 times lower than the natural volcanic flux of CO_2 to the ocean. Conversely, if it is assumed that all storage sites are inherently leaky, delivering some ~200 tCO_2 to the ocean each year (potential leakage rate via a wellbore – see Chapter 4), then the total leakage flux in 2100 could be in excess of 2 $GtCO_2$/yr, or around 10 times the volcanic flux. These data suggest that with proper site selection criteria, and in the absence of catastrophic storage failure, the leakage or seepage flux of CO_2 from sub-seafloor storage sites to ocean waters is likely to fall well within the natural flux of CO_2 to the seafloor, and would not therefore result in a major perturbation to the global CO_2 budget of the oceans.

3: Analogues for Leakage or Seepage of CO_2 from Subseafloor Storage Sites

To evaluate potential impacts of the leakage or seepage of CO_2 on seafloor systems (including physical, chemical and biological impacts) it would be useful to have good analogues from which high quality observational information can be obtained.

This Chapter considers two possible analogues for the leakage or seepage of CO_2 to ocean bottom waters from a storage reservoir; (1) sites of natural CO_2 venting, and (2) small scale purposeful CO_2 release experiments (some examples are illustrated in Figure 3.1). To determine whether either natural CO_2 vents or purposeful releases of CO_2 are good analogues for leakage/seepage events both the similarities and differences with respect to expected physical and chemical conditions during a leakage/seepage event are discussed.

---

[2] It is noted that a part of this flux will not be retained as in shallow water volcanic systems a significant fraction of the vented CO_2 will outgas to the atmosphere. To determine the fraction retained over a given time period would require knowledge of the depth distribution of venting, which cannot yet be constrained with any certainty. Nevertheless, this represents an appropriate number to compare the possible leakage flux to as, similar to natural vent sites, the water depth overlying potential CO_2 storage reservoirs will likely range from deep waters to shallow waters in direct contact with the atmosphere.

Figure 3.1: CO_2 in the Deep-Sea - vent sites & release experiments

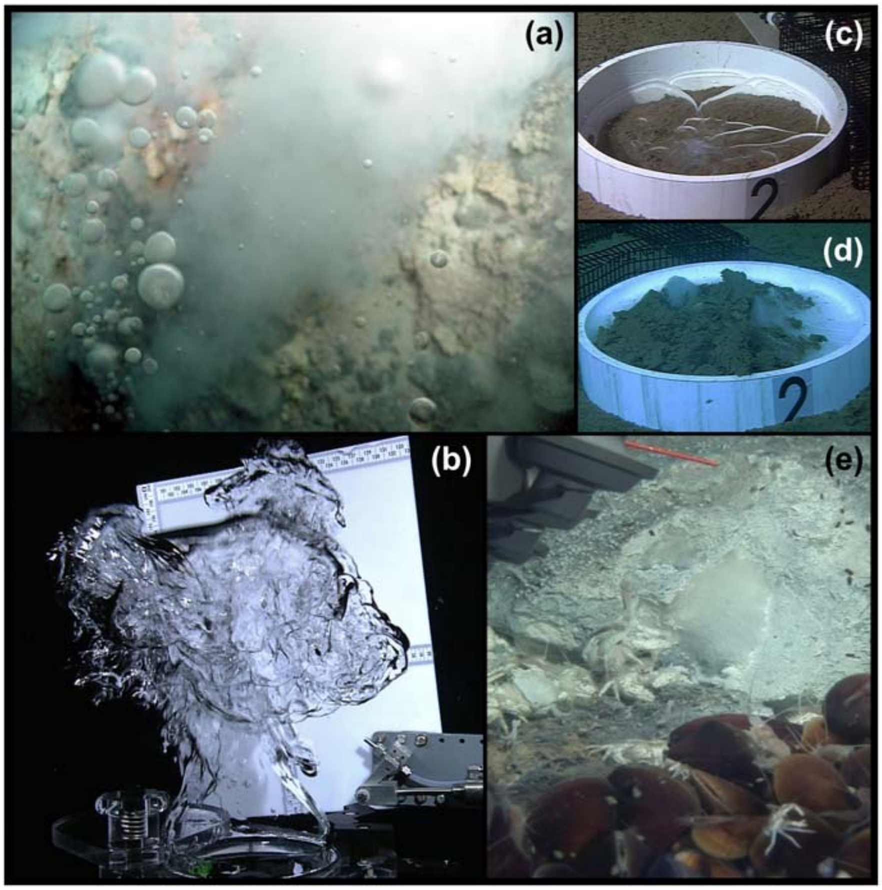

(a) Buoyant liquid CO_2 droplets rising out of the sediment surrounding small white chimneys at the Champagne vent site, NW Eifuku, Mariana Arc (Lupton et al., 2006). Photograph courtesy of NOAA (http://oceanexplorer.noaa.gov/explorations/04fire/logs/april10/media/bubbles.html); (b) A small scale release of buoyant CO_2 liquid in a droplet plume experiment (Brewer et al., 2006); (c) A small scale release of CO_2 below the neutrally buoyant point forming a pool of CO_2 on the seafloor; (d) The same pool approximately 24 hours later, where the liquid CO_2 has converted to hydrate. Photographs (b), (c) and (d) courtesy of MBARI; (e) A natural formation of CO_2 hydrate at Hatoma Knoll in the Okinawa Trough (Shitashima & Maeda, 2005). Photograph courtesy of Shitashima-san.

3.1 Seafloor CO_2 Vent Sites

This Section provides a state of play assessment of current knowledge regarding the global occurrence of natural CO_2 vent sites. Here we assess the spatial distribution of known vent sites in relation to the phase behaviour and chemistry of the CO_2 rich phase. Summaries of the additional information available for individual vent locations are provided in Appendix 3.A.

3.1.1 Global distribution of seafloor CO_2 vent sites

The natural venting of CO_2 to the ocean occurs along faults and fractures in tectonically active regions, and is typically associated with volcanic and/or hydrothermal activity at Oceanic Spreading Ridges (OSRs), Island Arcs, and Hotspots (see Chapter 2).

Venting of a discrete CO_2 rich phase is now known to occur at depths ranging from the inter-tidal zone to the deep ocean (see Table 3.1). Traditionally, a division is made between 'shallow' and 'deep-water' vent sites. For example, Tarasov et al. (2005) defined shallow sites as those occurring in water depths of less than 200m, based on the observation that vent obligate taxa (organisms restricted in occurrence to hydrothermal vent sites) are absent or rare at these sites. For the purposes of this report, it is important to consider both the biota associated with the vent sites, and the physico-chemical behavior of the expelled CO_2. Therefore, we consider three broad categories based on the depth of venting; shallow systems (<200m), where the CO_2 is expelled as a discrete gas phase and the biota is unlikely to include vent obligate taxa; intermediate systems (200-600m), where the biota are likely to include a significant proportion of vent obligate taxa, and where the behavior of CO_2 will be strongly dependent on local temperature in the vicinity of the vent site (i.e. whether CO_2 is expelled in the gas or liquid phase, and whether hydrates will form in the sediment column); and deep systems (>600m), where the biota are most likely to include vent obligate taxa, and where CO_2 is expelled as a liquid and has the potential to form hydrates in the upper sediment column.

At shallow water hydrothermal vent sites, discrete streams of gas bubbles are often discharged along with hot hydrothermal fluids, where this type of activity is described as gasohydrothermal venting (Dando et al., 1995a). Bubble plumes in shallow water may be seen as streams of bubbles breaking the surface, even from depths of 100 m, and are clearly visible to divers and Remotely Operated Vehicles (ROVs) (Dando et al., 1995b). Since gas bubble plumes are also clearly visible on echo sounders this often provides the simplest way of mapping vent locations (Dando et al 1995b, 1995c). CO_2 comprises the major gas component within most known gasohydrothermal exhalations (e.g. Dando et al., 1995b; Pichler & Dix, 1996; see Table 3.1), although nitrogen (N_2), methane (CH_4) and hydrogen (H_2) may also be present in significant concentrations (e.g. Vidal et al., 1981; Prol-Ledesma et al., 2002; Minissale, 1989), and hydrogen sulphide (H_2S), a toxic gas, is often present at trace to low levels (see Table 3.1). The locations where CO_2 is the dominant constituent (defined here as >60 mol% of total gas[3]) are shown in Figure 3.2, including vents in the Mediterranean Sea, the Atlantic Ocean, the Caribbean Sea, and from both the Eastern and Western margins of the Pacific Ocean. Also shown are two sites where, although not dominant, the CO_2 concentration is significant (40-60 mol% of total gas), Kraternaya Bight, Ushishir volcano in the Kurile Arc (Zhirmunsky & Tarasov, 1990), and the El Requeson fault zone, Baha California Sur (Forrest et al., 2005). Figure 3.3 shows those sites where CO_2 venting has been inferred, either from observations of gas bubbles or high bottom water CO_2 contents. To determine whether or not venting of CO_2 as a discrete gas phase actually occurs at these sites would require further investigation. It should be noted that the CO_2 content of gas bubbles cannot be reliably inferred by comparison to nearby systems. For example, it was originally suggested that gas vents offshore Kolbeinsey Island (North of Iceland) might be CO_2 rich based on the reported gas composition of an onshore geothermal system (Dando et al., 1995b). However, later analysis demonstrated that these vents have a comparatively low CO_2 content of <2 mol% (Botz et al., 1999).

Figure 3.2: Map showing global distribution of gas and liquid vent sites where CO_2 is a dominant (CO_2 rich >60 mol%) or a significant (intermediate CO_2 = 40-60 mol%) component. For references see Table 3.1.

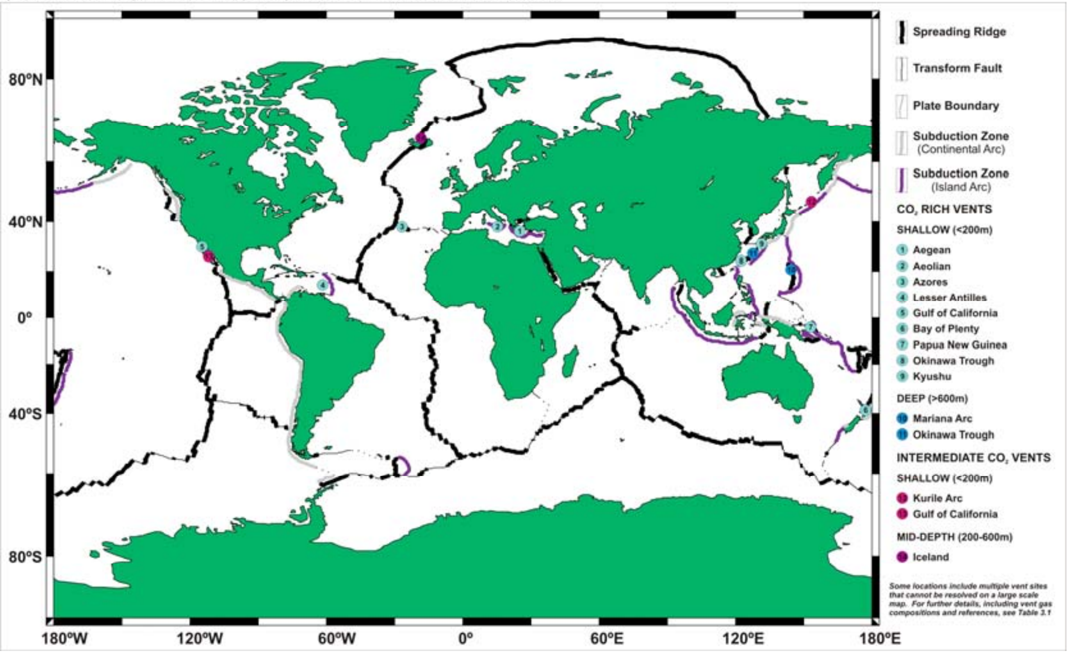

Some locations include multiple vent sites that cannot be resolved on a large scale map. For further details, including vent gas compositions and references, see Table 3.1

---

[3] Mol% is approximately equal to percent volume, where 1 mole of an ideal gas occupies 22.4L at standard temperature and pressure (273.15K, 1 atm). 1L of gas with a CO_2 content of 60 mol% will therefore contain ~600 ml of CO_2.

Figure 3.3: Map showing global distribution of vent sites where the venting of CO_2 gas or liquid is thought to occur (based on visual observation of bubbles, droplets, seafloor hydrates and/or high bottom water CO_2 concentrations).

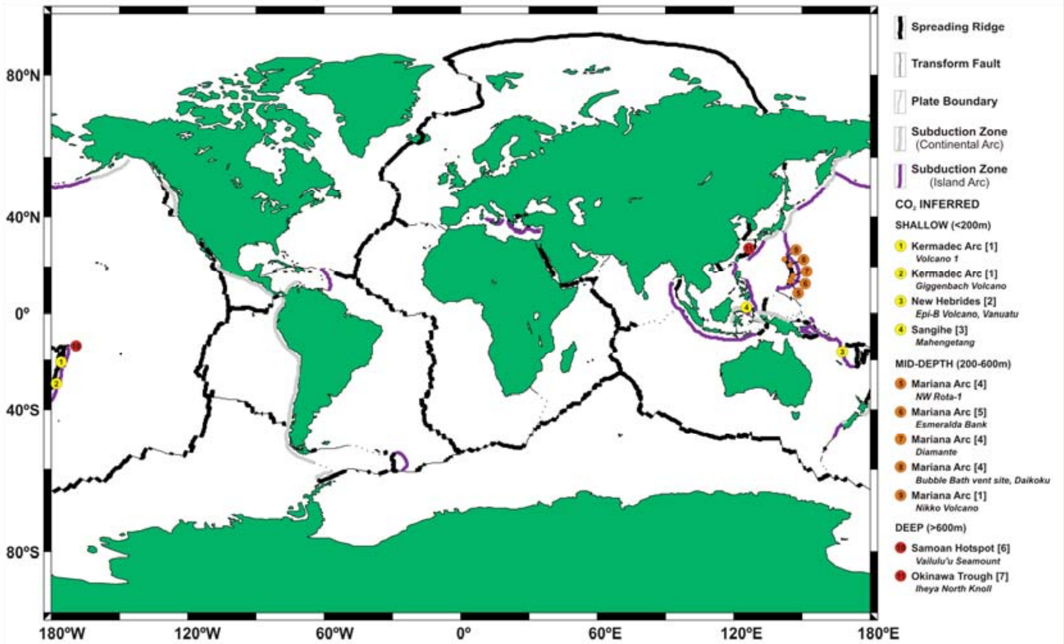

[1] Lupton et al., (2005); [2] Obzhirov (1992b); [3] Heikoop et al., (1996); [4] Embley et al., (2006); [5] Stuben et al., (1992); [6] Staudigel et al., (2006); [7] Chiba et al., (1996).

With respect to the known distribution of hydrothermal vent fields along the OSRs, sites of CO_2 discharge in deeper waters are comparatively rare (see Figures 3.2 and 3.3 and Table 3.1). The venting of liquid CO_2 was first observed at the JADE hydrothermal site in the Okinawa Trough (Sakai et al., 1990). There are now four further sites where venting of liquid CO_2 has been confirmed by chemical analysis; Minami-Ensei Knoll, Yonaguni Knoll IV, and Hatoma Knoll in the Okinawa Trough (Figure 3.1; Chiba et al., 1992; Shitashima & Maeda, 2005; Inagaki et al., 2006), and the Champagne vent site on the Mariana Arc (Figure 3.1; Lupton et al., 2006). In addition, there are two more sites where venting of liquid CO_2 is thought to occur (based on visual observations and bottom water chemistry) but is yet to be confirmed by chemical analysis; Iheya North Knoll in the Okinawa Trough (Fujikura et al., 2001; Chiba et al., 1996), and Vailulu'u Seamount, the current location of the Samoan Hotspot (Staudigel et al., 2006).

At present, there are no mid-depth gas vent sites where CO_2 is known to be the dominant constituent, and only a single site where CO_2 approaches a significant concentration; offshore Grimsey Island to the North of Iceland, where gas vents at a depth of ~400m have a reported CO_2 content of 1-41 mol% (Botz et al., 1999). This lack of well-characterised mid-depth sites most likely reflects the current limits of ocean exploration. A large proportion of the known shallow sites are coastal, and therefore easily identified (by bubble bursting at the surface), easily accessible, and well explored. Since the first discovery of hydrothermal venting on the Mid Atlantic Ridge in the late 1970s, offshore exploration of hydrothermal vent sites has focused on the OSRs, which fall almost exclusively within the deep-water category. Only recently has the research community turned the same level of focus to exploring subduction zones, where

Table 3.1: Composition of high CO_2 content gases and liquids from submarine vents

Site Characteristics			Composition of Vent Gas (mmol/mol)							
Type/Name	**Depth (m)**	**Fluid T† (°C)**	**CO_2**	**H_2S**	**CH_4**	**N_2**	**H_2**	**He**	**Ar**	**O_2**
CO_2 RICH - SHALLOW (<200m)										
① Northern Aegean & Hellenic Arc										
Nigrita, Strimon Basin, Greece[a]			944		0.08	33.7				22.7‡
Elephetere, Greece[a]			941		0.80	56.9				7.6‡
Thermopilae, Sperkios Basin, Greece[a]		**40**	799	0.15	0.20	198.0				2.5‡
Euobea Island, Greece[a]		**80**	969		0.20	25.6				4.6‡
Milos[b]										
Palaeochori Bay	**3**		766	13.40	2.70		27.50			
Milos Bay	**60.3**		749	0.00	4.80		0.00			
East of Spathis Point	**110**		919	1.40	8.60		4.30			
Yali[c]			944	<0.05	0.03	35.78	<0.01			20.18‡
Kos[c]			939	<0.05	3.62	48.2	<0.01			9.12‡
② Aeolian Islands										
Vulcano[d]		**86-101**	980 – 1000							
Panarea										
Lisca Banca[e]		**27**	966	26.40	<0.01	6.4	0.03			0.80
Basiluzzo[e]		**26**	932		<0.01	61.8	0.21			6.10
La Calcara[e]		**27**	901		30.10	55.0	0.17			13.10
Between Dattilo & Lisca Bianca[f]			930	60.00	0.14	8.0	<0.01			<0.1
③ Azores										
D. Joao de Castro Seamount[g] *bubble plumes also observed at ~170m*	**18-45**	**26.5-63.3**	~900							
④ Lesser Antilles										
Champagne Hot Springs, Dominica[h]	**1-5**	**41.0-71.4**	741 – 934	16.4 – 42.5	1.5 – 7.2	44 – 211	0.00 – 0.02	0.01 – 0.03	0.8 – 4.7	0.8 – 4.5
Average (n=4)			844	31.6	4.2	118	0.01	0.02	2.2	1.9
⑤ Gulf of California										
San Felipe[i] *offshore submarine vents also reported*[j]	**intertidal**	**48**	992	0.038	0.993	6.51	0.0	0.000	0.411	
⑥ Bay of Plenty, New Zealand										
White Island[k]			830		140					
White Island[l]		**111**	808	4.47	8.9	9.8	0.2	0.002	0.03	
Whale Island[k]			880		95					
Whale Island[m]	**34**		680 – 734		120 – 193	119 – 131	0.1 – 0.3		0.8 – 1.2	7.5 – 14.1
Average (n=2)			707		157	125	0.2		1.0	10.8
⑦ Papua New Guinea										
Luise Harbour, Lihir Island[n]	**3-10**	**60-96**	949 – 975	3.2 – 12.8	2.4 – 6.7	15.7 – 24.1	1.01 – 1.20	0.02 – 0.02		3.4 – 5.9
Average (n=2)			962	8.0	4.6	19.9	1.11	0.021		4.7
Tutum Bay, Ambitle Island[o]	**5-10**	**89-98**	927 – 979	<0.3	6 – 20	22 – 47	<0.01	<0.01 – 0.02		4.3 – 7.3
Average (n=5)			949	<0.3	15	37	<0.01	0.01 – 0.01		5.8
Matupi Harbour, New Britain Island										
Tavurvur[p]	**2-9**	**50-60**	623 – 884	0.0 – 70	0.07 – 0.10	95 – 288	0.01 – 0.34			18 – 28
Average (n=3)			744	43	0.08	187	0.12			24
Rabalankaia[p]	**7-27**	**90**	827 – 865	0.0	0.40 – 0.45	117 – 141	1.43 – 1.54			15 – 29
Average (n=2)			846	0.0	0.43	129	1.49			22
⑧ Okinawa Trough										
Kueishantao, Taiwan[q]	**10-20**	**48-107**	916 – 992	8.5 – 84	b.d.l. – 0.34	0.02 – 2.23	0.001 – 0.11	0.01 – 0.03	0.0002 – 0.025	0.002 – 0.195
Average (n=5)			970	29.3	0.081	0.655	0.028	0.016	0.007	0.049
⑨ Kyushu, Southern Japan										
Kagoshima Bay, Sakurajima volcano[r]	**78**	**24-30**	806 – 843	0.7 – 4.7	125 – 153	26 – 40	0.0		0.03	0.4 – 0.6
Average (n=2)			825	2.7	139	33	0.0		0.03	0.5
Kagoshima Bay, Sakurajima volcano[r]	**200**	**40-215**	713 – 926	3.2 – 13.7	49.2 – 199	16.9 – 73.7	2.0 – 8.1	0.001 – 0.003	0.01 – 0.4	0.2 – 5.4
Average (n=10)			857	5.9	95.3	36.7	3.61	0.002	0.02	1.6
CO_2 RICH - DEEP (>600m)										
⑩ Mariana Arc										
Champagne vent site, NW Eifuku[s]	**1604**	**103**	980	8	<0.1		<0.1	0.006		
⑪ Okinawa Trough										
Minami-Ensei Knoll[t]	**690-705**	**265-278**	872	10						
Yonaguni Knoll IV[u]	**1370-1385**	**upto 323**	851 ± 21		140 ± 21					
JADE vent site, Izena Cauldron[v]	**1300-1450**	**upto 320**								
free droplets in water column			860 ± 50	30						
droplets released from sediment			920 ± 10	44						
Hatoma Knoll[w]	**~1500**	**upto 301**	950 – 980	20 – 30						
INTERMEDIATE CO_2 - SHALLOW (<200m)										
⑫ Kurile Arc										
Kraternaya Bight, Ushishir volcano[x]	**0-22**	**10-34**	440 – 660		0.1 – 0.3	270 – 420	0.5 – 2.0	0.1 – 0.3		
⑬ Gulf of California										
Bahia Concepcion[y]	**7**	**upto 92**	429 – 441	n.d.	21.3 – 22.8	526 – 541	0.05 – 0.09	0.41 – 0.44	6.84 7.22	1.21 2.41
Average (n=2)			435		22.1	534	0.1	0.4	7.0	1.8
INTERMEDIATE CO_2 - MID-DEPTH (200-600m)										
⑭ Iceland										
Grimsey island vent field[z]	**395-407**	**238-250**	10.6 – 412		71.7 – 243					
Average (n=3)			169		159					

†Temperature quoted is that of associated hydrothermal fluids, and may not provide a good measure of the temperature at which CO_2 is expelled, see text for further discussion. ‡ O_2 + Ar

(a) Minnisale, 1989; (b) Dando et al. 1995b; (c) Minissale et al., 1997; (d) Baubron et al., 1990; (e) Italiano & Nuccio, 1991; (f) Calanchi et al, 1995; (g) Cardigos et al., 2005; (h) McCarthy et al., 2005; (i) Barragan et al. 2001; (j) Gastil & Bertine, 1982; (k) Giggenbach et al., 1993; (l) Giggenbach & Matsuo; (m) Lyon et al., 1977; (n) Pichler et al., 1999a; (o) Pichler et al., 1999b; (p) Obzhirov, 1992a; (q) Chen et al., 2005; (r) Ossaka et al., 1992; (s) Lupton et al., 2006; (t) Chiba et al., 1992; (u) Inagaki et al., 2006; (v) Sakai et al., 1990; (w) Shitashima & Maeda, 2005; (x) Zhirmunsky & Tarasov, 1990; (y) Forrest et al., 2005; (z) Botz et al., 1999.

subduction related volcanism spans a much larger depth range, and mid-depth venting of CO_2 might be expected. Indeed, the recent NOAA Submarine Ring of Fire expeditions have already led to the discovery of five mid-depth sites on the Mariana Arc, where bubbles venting from the seafloor are thought to be composed dominantly of CO_2 (see Figure 3.2).

Initial examination of Figures 3.2 and 3.3 might suggest that CO_2 vent sites are concentrated in the Mediterranean (Aeolian Islands and the Hellenic Arc), and along the Okinawa Trough and Kermadec and Mariana Arcs. However, it would appear that the general global distribution of all known or inferred CO_2 vent sites also strongly reflects the intensity of scientific exploration. For example, the Mediterranean systems are easily accessible and have been studied in detail (see the review by Dando et al., 1999). Similarly, the Japanese research community has made an extensive study of the Okinawa Trough (see the review by Glasby & Notsu, 2003), with numerous dives of both ROVs and manned submersibles, resulting in the discovery of 4 deep-water sites where venting of CO_2 is known and 1 where it is inferred. Likewise, the NOAA Submarine Ring of Fire expeditions from 2003 to 2006 focused on exploration of the Mariana and Kermadec Arcs with the extensive use of ROV and submersible technology resulting in the discovery of 1 confirmed and 7 possible CO_2 vent sites (for expedition summary from year 200**X** see www.oceanexplorer.noaa.gov/explorations/0**X**fire/welcome.html). This pattern suggests that vent sites may well exist in comparable locations that have not yet been fully explored. Further CO_2 rich vents may also be associated with other hot-spot locations. CO_2 is expelled in the gas or liquid phase at the Azores (D. Joao de Castro Seamount, ~90 mol%, Cardigos et al., 2005), Iceland (offshore Grimsey Island, 1-41 mol%, Botz et al., 1999), and Samoan (Vailulu'u Seamount, inferred, Staudigel et al., 2006) hotspots, while hydrothermal fluids particularly enriched in CO_2 are vented at both the Hawaiian (Loihi Seamount, up to 418 mmol/kg, Sedwick et al., 1992) and Cobb (Axial Seamount, up to 285 mmol/kg, Butterfield et al., 1990) hotspots.

To summarise, CO_2 vents have been located in the majority of tectonically active areas where extensive scientific surveying has been carried out, with a high proportion of sites occurring in subduction zones (associated with both island arcs and back-arc basin spreading centres). This geographic distribution raises an interesting question. Although CO_2 storage might be considered less safe in tectonically active regions due to a higher probability of leakage (e.g. Bradshaw & Dance, 2005), should leakage occur is it perhaps less likely to result in a negative impact on the local ecosystem? Given that natural venting is known, and in some cases appears quite widespread at the regional scale, it might be concluded that a higher possibility of leakage would be offset by a lower risk of significant negative impact on local ecosystems[4].

3.2 A Good Analogue?

In a review paper Tyler (2003) addressed whether or not disposal of various types of waste in the deep sea, including CO_2, could be considered an analogue of natural processes. While Tyler (2003) drew the general conclusion that "the natural processes and their apparent anthropogenic counterparts are false analogies", he also emphasized that both a better understanding of natural processes and appropriately scaled experiments were vital to determine the impact of disposal (of any waste) in the deep sea.

However, Tyler (2003) was examining oceanic disposal of CO_2, i.e. the creation of seafloor lakes or storage of CO_2 in the hydrate phase on the seafloor at a large scale, not the possibility of a leak from a sub-seafloor storage site. While some of the Okinawa Trough CO_2 vent sites had been discovered, these were considered a rarity, with no other deep sea CO_2 vent sites known at that time. Furthermore, while the slow release of CO_2 at the deep water vent sites bears little comparison to a large CO_2 lake or massive CO_2 hydrate deposit (as envisaged in direct ocean sequestration scenarios), they seem likely to provide a much better comparison to a small to medium scale CO_2 leak. This section therefore returns to the question of whether or

---

[4] It is noted here that negative impacts on ocean ecosystems are not the only reason that leakage is undesirable. For geological storage to be an effective greenhouse gas mitigation strategy, the CO_2 must stay isolated from the atmosphere for a sufficiently long period of time – desirably a minimum of ~1000 years. However, leakage from the primary reservoir to the overburden is not necessarily followed by leakage to the seafloor, nor is leakage to the seafloor necessarily followed by escape to the atmosphere. Thus there will be cases where leakage to the seafloor could be classed as possible, while escape to the atmosphere is classed as highly unlikely (on a timescale of 1000 years, the turnover time of the ocean).

not natural releases of CO_2 could act as a good analogue for determining potential impacts of leakage or seepage of CO_2 from sub-seafloor storage sites. The role of in-situ experiments is discussed in Section 3.3.

In determining whether or not a natural CO_2 vent provides an analogue for a leakage/seepage event it is important to identify both the similarities and the differences between these modes of CO_2 release. In particular:

(1) ENVIRONMENT: To what extent does the whole environment reflect that likely in the vicinity of leakage or seepage from sub-seafloor storage sites?

(2) SCALE OF RELEASE: Does the area over which CO_2 is released, the rate of release, and the duration of release, reflect potential leakage or seepage events?

(3) PHYSICAL & CHEMICAL CONDITIONS: To what extent do the physical conditions in the vicinity of a vent site differ from that expected at a leakage/seepage site? Does the chemistry of the released CO_2 reflect the likely composition of CO_2 leaking from a sub-seafloor storage reservoir?

3.2.1 The Whole Environment

The analysis presented in Chapter 1 identified Africa, South East Asia, Western Europe and Oceania as key regions where offshore storage could play a significant role in CCS due to the dominance of offshore with respect to onshore storage capacity. With the exception of Africa, all of these regions have current or planned sub-seafloor CO_2 storage programs. Despite some assessments rating the offshore storage capacity of Japan as negligible (based on the regions active tectonism and perceived lack of storage security), sub-seafloor storage is also being actively pursued in this region and seems likely to occur in the near future.

The natural venting of CO_2 occurs in tectonically active areas. Thus for potential storage sites located in such areas (e.g. The Pacific Rim, The Mediterranean Sea) there is likely to be a natural site of CO_2 venting within reasonable proximity (at the local to regional scale), with the current best match occurring between the Casablanca oil field and the Aeolian Island vent sites in the Mediterranean Sea.

This regional scale match-up provides a good probability that possible leakage sites could be correlated to nearby CO_2 vent sites with comparable characteristics (e.g. similar water depth, latitude, substrate, and within the same biogeographic province), hence providing possible analogue sites for studying impacts of CO_2 leakage. However, care must be taken when deciding whether or not these sites do in fact represent a reasonable comparison.

For example, deep-sea venting of CO_2 is known to occur to the south of Japan over much of the length of the Okinawa Trough (see Section 3.2.1 above). Thus, at the regional scale, there are numerous CO_2 vents located in reasonable proximity to Japan. However, the primary targets for Japanese offshore CO_2 storage reservoirs lie to the northwest of Honshu in the Sea of Japan. Although the Okinawa Trough and the Sea of Japan are neighbouring deep basins, they are semi-isolated, with different primary energy sources, and different hydrographic and faunistic histories (see review by Tyler, 2002). The Sea of Japan was isolated from the main Pacific during the last ice age and became anoxic, with the only link today through narrow shallow straits. As a result the fauna is impoverished and is believed to be composed of cold-adapted eurybathic (capable of living in a wide range of water depths) species rather than true deep-sea species (Tyler, 2002). In contrast, in the Okinawa Trough the most noticeable fauna is associated with hydrothermal activity and chemosynthesis forms the base of the food chain for the bathyal community (Tyler, 2002).

In tectonically stable potential storage regimes the case is somewhat simpler - there are no proximal sites of CO_2 venting at the regional scale. For example, the closest site of CO_2 venting to the North Sea would be the Iceland Hotspot, or the Mediterranean vent sites. Both of these systems exhibit markedly different characteristics (in terms of geology, oceanography, and biology) to the North Sea. In these locations, impacts of CO_2 would need to be inferred based on similar or model sites, and known biotic responses (for similar or model species) or based on experimentation, e.g. controlled CO_2 release experiments or laboratory experiments.

In the absence of a natural vent site located in close proximity and within a similar environment to an intended storage reservoir, it remains possible that an analogue vent site exists. The rapid advances that have been made in the fields of remote surveying techniques, habitat mapping and GIS (Geographical Information Systems) over recent years would be of great assistance in the assessment of inter-site comparability, and thus in selecting similar or model sites and in determining the validity of 'impact' comparisons. A habitat is defined as a place and its living and non-living surroundings where an individual or population lives. Thus a particular habitat type combines the essential physical, geological and biological data required to determine how comparable two sites are. There is now a growing recognition of the need for such data to aid policy decision making and regulatory processes in the marine environment. For example, habitat mapping in the North Sea is now well advanced, with two major projects currently underway.

The Mapping European Seabed Habitats (MESH – see Box 3.1) programme is funded by EU INTERREG IIIB and involves 12 partners from the five countries within the north-west Europe area (UK, Ireland, the Netherlands, Belgium and France). MESH aims to produce seabed habitat maps for north-west Europe and develop international standards and protocols for seabed mapping studies. The project started in spring 2004 and will end in January 2008, although outputs are being made publicly available as they are completed at the excellent project website (www.searchmesh.net). These include a meta database of mapping studies and a web-delivered geographic information system (webGIS) showing the habitat maps (see Box 3.1 for examples). The MESH programme is also producing an interactive guide to marine habitat mapping (web hosted version to be available in June 2007), including Recommended Operating Guidelines (ROGs), and a Habitat Matching Programme (currently in the testing phase) in an effort to introduce standardised methods and protocols, vital to ensure that true comparisons can be made between different data sets.

Similarly, in 2005 the Norwegian government launched the MAREANO Programme which will run to 2010 (http://www.mareano.no/english/index.html), a collaborative project between the Institute of Marine Research, the Geological Survey of Norway and the Norwegian Hydrographic Service. The objectives of the MAREANO Programme are to survey and study the physical, biological and chemical environment of the seabed in Norway's coastal and marine regions. As with the MESH programme, this information will be made publicly accessible via a web portal and marine area database. The early stages of the MAREANO Programme focussed on key environmentally sensitive areas of the Barents Sea and Lofoten in which offshore activities are now underway (e.g. development of the Snøhvit and Goliat offshore petroleum fields). This programme also includes a specific research component to examine deep sea corals and biotopes[5], and to assess relationships between biotopes, sediments, and oil and gas spills.

---

[5] A biotope defines the area of uniform environmental conditions that provide living space for a biological community (as opposed to a habitat defining living space for a population or species).

Box 3.1: Examples of Habitat Information for the North Sea from the MESH webGIS.

MESH: Mapping European Seabed Habitats

Information contained here has been derived from MESH Consortium webGIS data (www.searchmesh.net/webGIS) which received funding from the INTERREG IIIB NWE programme (www.nweurope.org).

A: MESH EUNIS Model (displays at scales from 1:30,000,000 to 1:500,000).

The MESH EUNIS (European Nature Information System) Model map layer is a predictive map based on combining physical data layers. The EUNIS habitat types classification is a comprehensive pan-European system to facilitate the description and collection of data across Europe through the use of criteria for habitat identification. Level A describes all Marine Habitats. The aim of the MESH EUNIS Model was to use 'habitat envelopes' to predict/ model the distribution of broad-scale EUNIS marine habitat types, across the MESH area. Through the development of the EUNIS marine habitat classification, key physical and environmental variables have been identified which are known to drive the distribution of biological communities, and thus EUNIS habitat types in our seas. Each habitat type within EUNIS is defined by its unique combination of environment variables (referred to as the habitat envelope) together with its associated biological community. Please note that at this stage the EUNIS habitat types shown in this map have NOT been validated. The validation process using biological point sample data is due to be completed before the end of the MESH Project (January 2008).

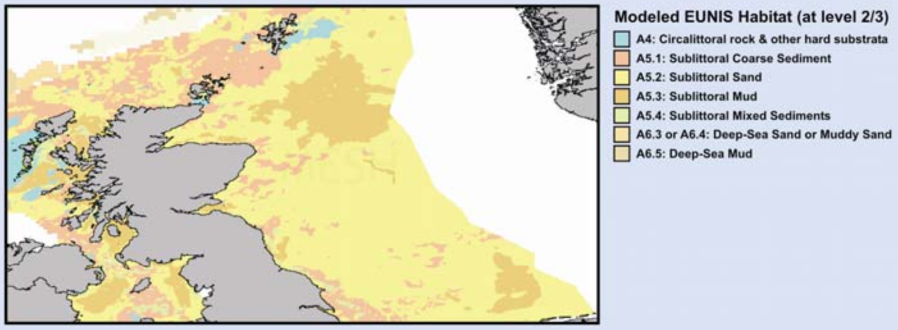

B: UK Marine Landscapes (displays at scales from 1:30,000,000 to 1:500,000).

The UK Marine landscapes map layer is a predictive map based on combining physical data layers and was created as part of the UKSeaMap project. The aim of the UKSeaMap project was to use available geological, physical and hydrographical data, combined where possible with ecological information, to produce simple broadscale and ecologically relevant maps of the dominant seabed features for the whole sea under UK jurisdiction. To create the UK Marine landscapes layer a classification tree was developed, based on the following categorised data sets: seabed substrata, photic depth, wave base, bathymetry, bottom temperature and tide-generated bed-stress. The data were biologically validated with seabed sample data and confidence assessment carried out. For full details see: Connor, D.W., Gilliland, P.M., Golding, N, Robinson, P., Todd, D., & Verling, E. 2006. UKSeaMap: the mapping of seabed and water column features of UK seas. Joint Nature Conservation Committee, Peterborough, or www.jncc.gov.uk/UKSeaMap

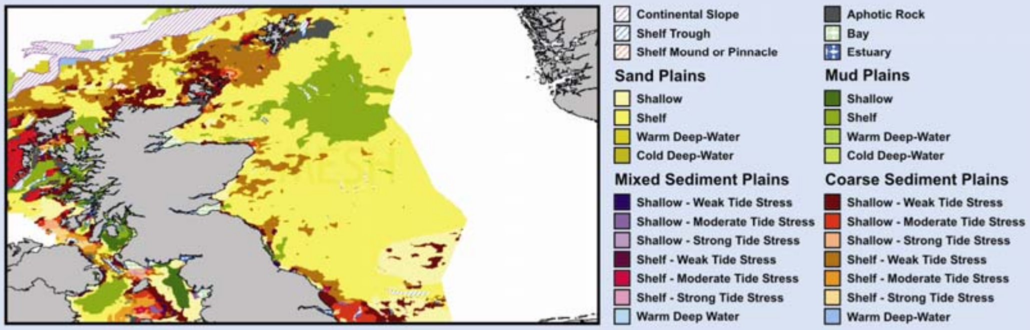

One of the key questions that will need to be addressed is the comparability of biota between natural CO_2 vent sites and sites of potential leakage. In general, at deep vent sites the biota is highly unlikely to be comparable as vent obligate taxa tend to dominate the area of the hydrothermal field (i.e. tube worms, clams). However, in mid depth and shallow systems this is not the case. In mid-depth systems, there may be a mixed hydrothermal/pelagic community (e.g. Minami Ensei Knoll, Okinawa Trough), and vent obligate taxa are generally absent from shallow sites (Tarasov et al., 2005). Thus a comparison between community assemblages in the vicinity of CO_2 vents to the general local species distribution in the surrounding area (outside the area chemically or physically influenced by the vents) is likely to provide valuable information on tolerant and intolerant species.

3.2.2 The Scale of CO_2 Release

The impact of leakage or seepage of CO_2 to the ocean will depend on the scale of the leakage/seepage event, including the area over which CO_2 is released, the rate at which it is released, and the duration of the leakage/seepage event. For example, the impact of a large release of short duration (acute exposure) is likely to be very different to a small release of long duration (chronic exposure). Furthermore, the impact (or consequences) of a single leakage/seepage event may evolve significantly over time and could conceivably pass through different stages where the 'direction' of the system response changes. For example, in the case of a small to moderate leak occurring at a seafloor depth and temperature where CO_2 is a buoyant liquid, but where hydrate formation is possible, the impact on the local environment will be (among other factors) dependent on whether or not hydrate is formed, where this may change over time.

Potential rates of CO_2 release to the ocean range from slow seepage (e.g. from the overburden through a self-limiting hydrate capped system) to vigorous or rapid release through a flow conduit (such as an opened fault, gas chimney or well bore) following cap-rock failure, tectonic displacement, or well-seal failure (see Chapter 4 for further discussion of these processes). The duration of leakage will reflect a combination of factors, including site monitoring, the scale of leakage (small leaks being harder to detect), and whether remedial action is possible, or natural cessation occurs. It is widely acknowledged that the most probable site of large scale leakage is via a well bore. As a recognized risk, well sites are those most likely to be continually monitored, thus such a leak is also the most likely to be detected (except in the case where the well bore is unmapped), and also allows remedial action to be taken. CO_2 leakage occurring away from well bores could be detected as new sub-surface features in full site seismic surveys. In this case, early detection is dependent on the frequency of monitoring. For example, at the Sleipner project, time-lapse 3-D seismic surveys (also referred to as 4-D seismic surveys) have been successfully employed to image the migration of CO_2 in the Utsira formation (Chadwick et al., 2006). Surveys have been carried out on an approximately biennial basis since injection commenced in 1996 (Chadwick et al., 2006). Compared to expected migration rates in the subsurface, this frequency of monitoring should ensure early detection of any CO_2 leakage through the caprock and provide prior warning of potential leakage to the seafloor. In the event of release at the seafloor, CO_2 liquid droplets and gas bubbles in the water column could also be readily detected using sonar. Nevertheless, despite the potential for detection, it is currently unclear what could be done to 'plug' a non-well site leak.

Natural vent sites represent the transfer of CO_2 from a reservoir at depth (sourced from magma chambers or thermal cracking of organic/carbonate rich sediments) through the overburden, across the sediment-seawater interface, to the ocean. Given the high heat flow and the presence of open faults and fractures through which the fluids migrate, these sites could be considered representative of the upper limit on the rate at which leaked CO_2 might be expelled from the seafloor. However, the deeper sites, where hydrates form in the uppermost sediments, could also give an indication of expected rates of seepage through an impeding hydrate cap. Visual descriptions provide anecdotal information, with release rates ranging from slow and intermittent bubbling through a hydrate cap or hydrate pipes at deep water sites (e.g. Okinawa Trough, Jade site, Sakai et al., 1990), to vigorous bubbling churning the upper sediment column in shallow sites (e.g. Paleohori Bay Site 4, Milos, Mediterranean, Dando et al., 1995b). Although estimates of volumetric CO_2 release rates at these end member sites are not available (not reported for JADE site, and release rates too fast to measure at Paleohori Bay Site 4), venting rates have been reported for more intermediate vent sites. For example, at the moderate shallow water vent sites (3-110m) in the vicinity of Milos Island, measured total gas release rates (of which ~80% is CO_2) range from 0.09 to 17 L per hour per bubble stream under in-situ conditions, equivalent to 0.16 to 26.23 L/hr at STP or 2-360 $kgCO_2$/yr (Dando et al., 1995b). At the deep water (1600m) Champagne Vent site on the Mariana Arc, estimated volumetric release rates at in-situ conditions are directly comparable at ~12 L per hour per droplet stream, however given the high compressibility of CO_2 this corresponds to a significantly higher flux, and is equivalent to over 6000 L/hr at STP or ~100 tCO_2/yr (Lupton et al., 2006).

The density of venting and the total area over which CO_2 release occurs also varies widely among the natural systems, and seems likely to bracket that which could be expected in a leakage event, ranging from localized venting restricted to an area of 10s of m^2, to regions where venting extends over a total area of 10s of km^2. For example, in the waters surrounding Milos Island, CO_2 venting extends over an area of ~34 km^2, consisting of numerous bubble fields with up to ~6 gas outlets per m^2, interspersed with regions where no venting occurs. Average bubble stream densities are on the order of 0.2-0.9 outlets per m^2, with an estimated total flux on the order of 920-4620 $ktCO_2/yr$, or ~30-140 $kgCO_2/m^2/yr$ (Dando et al., 1995b). Conversely, at the Champagne Vent site, CO_2 venting occurs over an area of only ~30m^2, with around 10 droplet streams per m^2, giving a total flux on the order of 30 $ktCO_2/yr$ or ~3500 $kgCO_2/m^2/yr$ (Lupton et al., 2006).

On the question of scale and duration of venting, the primary limitation on whether a natural vent site is an analogue for leakage may well be when venting of CO_2 commenced, and therefore for how long the local environment has been exposed to elevated CO_2 levels. Many of these systems may have been experiencing CO_2 release over long periods of time. They may therefore provide an analogue for re-equilibration of a system following an initial perturbation – but not provide information on the impact of the initial perturbation. Nevertheless, valuable information on site history and evolution over time may be obtained through geochemical and biological surveys and return visits.

3.2.3 The Physical & Chemical Conditions

As CO_2 rich vents occur in association with hydrothermal venting there are obvious questions to ask regarding differences between physical and chemical conditions at the vent sites and potential leakage sites, where hydrothermal fluids have elevated temperatures and altered chemistry with respect to ambient bottom seawater (see Box 3.2). The implications of these altered physical and chemical conditions are discussed below.

3.2.3.1 The Thermal Regime

In the case of leakage/seepage, it is expected that the CO_2 released to the seafloor will be at ambient temperature. Conversely, venting of CO_2 typically occurs in association with venting of hydrothermal fluids (~10-320°C, see Table 3.1). The question is then can the impacts of CO_2 release on seafloor systems be separated from the effects exerted by injection of hot water?
The first point to be made here is that within a given system the venting of CO_2 is not necessarily co-located with the high temperature hydrothermal vents. In some systems CO_2 droplets are indeed expelled from the same orifice as high temperature fluids or emerge (at lower temperatures) from the base of black or white smoker chimneys. However, in other regimes CO_2 discharge occurs in association with diffuse low temperature fluid flow, or indeed as separate streams of gas bubbles or liquid droplets emerging from the seafloor at ambient or near ambient temperatures (see site summaries in Appendix 3.A).

The second point to consider is that mixing of high temperature hydrothermal fluids with ambient bottom water quickly dissipates the temperature anomaly (the temperature difference between waters influenced by hydrothermal fluids and ambient seawater; $\delta T = T_{observed} - T_{ambient}$). High temperature hydrothermal fluids are buoyant (due to the low density with respect to bottom seawater) and rise rapidly through the water column in a focused plume. Shear flow at the boundary between the ascending fluids and bottom waters produces eddies (Lupton, 1995) causing turbulent mixing and the entrainment of large quantities of ambient seawater into the plume (Kadko, 1993). This rapidly dilutes the rising plume, with typical mixing ratios of 100:1 to 1000:1 within the first 5 to 10 m of plume rise (Feely et al., 1994), causing temperatures and particle concentrations within the plume to decrease within a short distance from the vent orifice. For example, for a hydrothermal fluid with a high chimney exit temperature of ~400°C venting into ambient bottom waters of 1°C, the temperature of the plume fluid would decrease to 1.4 to 5.0°C within 5-10m above the vent orifice (δT = 0.4-4.0°C), while a fluid with a lower exit temperature of 100°C would reach near ambient temperatures within 5-10m (δT = 0.1-1.0°C). The plume will continue to rise through the water column until sufficient entrainment of ambient seawater has taken place for the hydrothermal plume to reach neutral buoyancy (typical mixing ratios of ~10,000:1) at a height of around 200-300m above the vent site. At this point the plume is dispersed laterally by prevailing bottom currents and can be identified as both a hydrographic and chemical anomaly in the water column (German et al., 1991; Baker et al., 1995).

Large water column temperature anomalies are therefore generally restricted to the immediate vicinity of the hydrothermal vent and extend vertically through the water column above the vent orifice, exerting little lateral influence at near seafloor depths. Nevertheless, both sediments and near seafloor water temperatures in the near-field region are likely to be slightly elevated compared to ambient levels due to the influence of low temperature diffuse fluid flow (see Box 3.2). Clam beds, which are often observed at CO_2 rich vents sites, form in this region. A broadly consistent pattern of temperature anomalies has been reported for clam beds along the OSRs, with near ambient temperatures near the clams' siphons, and warmer temperatures in the sediments beneath the shells (e.g. Fisher et al., 1988a; Hessler et al., 1985). For example, at the Rose Garden vent site (Galapagos Rift) temperature anomalies below the clam shells were 8-9°C, decreasing to 0-2.4°C between the shells, and 0-0.25° at the clam siphons (Fisher et al., 1988a). At the Clam Acre site (21°N East Pacific Rise), temperature anomalies were slightly higher, at up to 14.5°C at a depth of 20-30cm below the clam shells, decreasing to 0.6-4.7°C between the shells and 0.9°C at the clam siphons (Hessler et al., 1985).

Box 3.2: Hydrothermal Circulation.

Hydrothermal Circulation is the heat driven circulation of water through the Earths crust.

During hydrothermal circulation, cold seawater percolates downward though fractures in the permeable ocean crust. As the seawater penetrates basement, it comes into contact with hot rock and may come close to a magma chamber (Lister, 1972). Mantle degassing releases gases such as helium (He), methane (CH_4), hydrogen (H_2), carbon monoxide (CO), and carbon dioxide (CO_2), and volatile elements such as mercury (Hg) and arsenic (As). In the reaction zone alteration temperatures are high (300-400°C), and the fluid composition is further changed though reaction with the host basalt. Magnesium and sulphate are removed from solution, and fluids become acidic and enriched in ore forming metals and sulphide leached from the host rock (Von Damm, 1990). At these high temperatures the altered fluids also expand, viscosity is reduced, and buoyancy is increased, with densities about two thirds that of seawater. The hot buoyant fluids rise rapidly with the return flow to the seafloor often focused through high permeability channels in the ocean crust.

The location of the zone in which the sulphide rich high temperature solutions mix with oxygen rich bottom water is critical in determining the composition of the hot-spring water that vents onto the seafloor. A continuum between three types of venting are typically observed at active hydrothermal zones, representing different plumbing systems through which the upwelling fluids are returned to the seafloor; high temperature black smoker chimneys; (2) mid to low temperature white smoker chimneys; and (3) low temperature, diffuse fluid flow. A typical vent field might comprise several black and white smoker chimney structures in an area of 100 to 150m^2, with areas of diffuse fluid flow visible through the shimmering of relatively warm fluids (~10-30°C) as they enter bottom waters (e.g. Murton et al., 1995; Schultz et al., 1992).

The concentrations of metals in hydrothermal fluids & seawater (Elderfield & Schultz, 1996)

Element	Seawater (ymol/kg)	y	Hydrothermal Fluid (xmol/kg)	x
Iron (Fe)	0		750-6470	μ
Zinc (Zn)	0.01	μ	40-106	μ
Copper (Cu)	0.007	μ	9.7-44	μ
Manganese (Mn)	0		360-1140	μ
Lead (Pb)	0.01	n	9-359	n
Cobalt (Co)	0.03	n	22-227	n
Magnesium (Mg)	53	m	0	
Arsenic (As)	27	n	30-452	n
Silver (Ag)	0.02	n	26-38	n
Calcium (Ca)	10.2	m	10.5-55	m
Barium (Ba)	0.14	μ	>8 to >42.6	μ
Lithium (Li)	26	μ	411-1322	μ

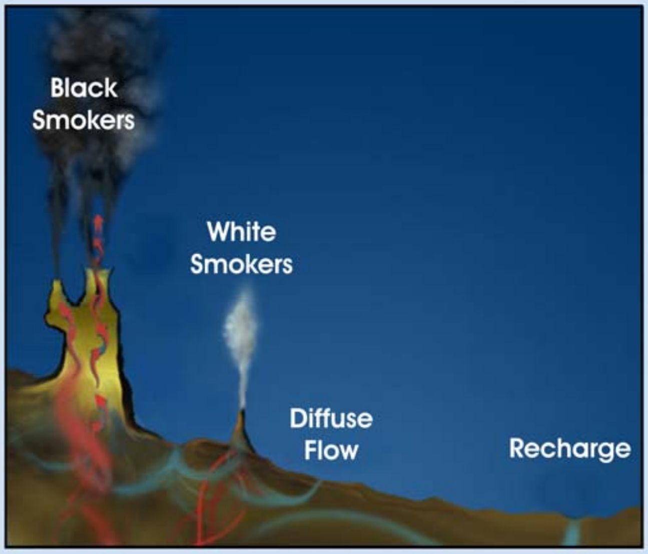

At black smoker chimneys, high temperature fluids (300-400°C) are expelled directly onto the seafloor at a rate of ca. 1-5 ms^{-1} and with a chemical composition that reflects that of the basement fluid (MacDonald et al., 1980). These plumes of hot, reducing, acidic hydrothermal fluids immediately entrain cold, alkaline, oxygenated seawater, resulting in instantaneous precipitation of fine grained metal rich sulphides and sulphates and (hydr)oxides that give the rising plumes their characteristic colour and smoke like appearance (Feely et al., 1987, Lilley et al., 1995).

Low to mid temperature fluids also vent through focused flow paths directly on to the seafloor. In these white smoker systems the hot hydrothermal fluid has either cooled or undergone sufficient sub-seafloor mixing with seawater to deposit the metal rich sulphide precipitates in the walls of the channel up which the fluid is rising. When the ascending fluid emerges at the seabed, amorphous silica and various sulphate and oxide minerals are precipitated, giving the appearance of white smoke (Thompson et al., 1988; Tivey et al., 1995; Edmond et al., 1995).

Low temperature diffuse source venting results from the increased mixing of upwelling hydrothermal fluids with seawater at depth, and can produce sub-surface mineralization where the chemical composition of the fluids may be significantly modified by reaction with the sediments (Edmond et al., 1979; Schultz et al., 1992; Mills and Elderfield, 1995). Diffuse fluid flow can also result from the conductive heating of seawater (or altered fluid) circulating through the sediment column (Murton et al., 1999; Cooper et al., 2000). In this second mode of diffuse fluid flow, heat is transported from the vent site without a pronounced geochemical exchange between the fluid and the host system (Cooper et al., 2000; Murton et al., 1999).

Some efforts can be made to carry out purposeful experiments at low temperature vent sites that include an element of design intended to determine which is the dominant factor controlling animal responses. For example, Vetter & Smith (2005) conducted a series of experiments (using ROV technology) at the Loihi seamount vent site, where vent fluids are particularly rich in dissolved CO_2 (not separate venting of a CO_2 phase). In their experiments Vetter & Smith (2005) collected amphipods in baited traps then placed the traps directly over and only 20cm above low temperature vent outlets for periods of ~60 minutes. The amphipods were thus exposed to CO_2 rich vent fluids with a moderately elevated temperature (vent fluids had an average pH of 6.18 (minimum 5.7) and average temperature of 5°C (maximum 8°C) compared to bottom water pH of 7.11 and temperature of 3.7°C). After 10-20 minutes of exposure the amphipods became inactive and dropped to the bottom of the trap in a state of torpor. Following removal of the trap from the vent plumes all amphipods recovered and began actively swimming within 30 minutes. The question was then was torpor induced by the elevated CO_2 or the elevated temperature of the vent fluids? As temperature also increases with decreasing water depth (i.e. surface waters are warmer than deeper waters), while the partial pressure of CO_2 remains approximately constant, Vetter & Smith (2005) compared the observed response of the amphipods to plume exposure to the observed response of the amphipods during ascent through the water column. Following recovery of the amphipods from 'plume' intoxication, the traps were taken up through the water column, where amphipods remained active until ascent yielded temperatures of ~10-11°C (300m), at which point amphipod swimming activity decreased rapidly until all amphipods lay at the bottom of the trap at 13°C (250m). This result suggests that the torpor induced by exposure to the lower temperature vent plumes (~6°C) can be attributed to the elevated CO_2 concentration (Vetter & Smith, 2005).

3.2.3.2 The Chemistry of the CO_2 Rich Phase

The dominant effect exerted by hydrothermal circulation on biota in the near field region is not necessarily temperature related. Rather it is the chemical composition of the vent fluids and gases, and how these may differ to that observed in the case of CO_2 leakage that may be of most significance. In particular, the presence (or absence) and concentration of both toxic species and those compounds which constitute the basic building blocks of chemosynthesis (i.e. heavy metals, H_2S, CH_4; pers. comm. George Somero).

Constraining the expected chemistry of CO_2 that has leaked or seeped out of a subseafloor storage reservoir, and determining the extent to which it is similar or dissimilar to a CO_2 rich phase vented from the seafloor, poses a complex problem.

The chemistry of 'leaked' CO_2 will depend on the initial purity of the injected CO_2, and the nature of both the storage reservoir and sediment column through which the CO_2 has migrated before reaching the seafloor.

Recent amendments to international agreements pertaining to the storage of CO_2 in subseafloor geological formations have implications for the chemistry of the CO_2 to be stored (see Box 3.3). Both the London Protocol and the OSPAR Convention state that the CO_2 to be injected must consist 'overwhelmingly' of CO_2, but make allowance for the presence of additional compounds derived from the source material or from the capture and sequestration processes (see Box 3.3). However, there is no clarification (as yet) on what constitutes an 'overwhelming' amount of CO_2, or if limits will be set on the permissible levels of additional substances. For example, in the case of CO_2 removal from sour hydrocarbon streams and re-injection (e.g. in the production of natural gas from CO_2 rich gas fields), it might be decided to re-inject the extracted acid gas with no further purification. In this case, the CO_2 may contain significant amounts of H_2S in addition to small amounts of hydrocarbons, treating solvents, and absorbents.
However, even if the CO_2 were injected as a chemically pure phase, in the event of leakage or seepage it is highly unlikely to emerge as such. Indeed, supercritical fluid extraction using CO_2 is a promising technology for the decontamination of environmental wastes, capable of extracting organic contaminants (e.g. petroleum hydrocarbons, polyaromatic hydrocarbons, polychlorinated biphenyls) and inorganic contaminants (e.g. heavy metals and radioactive elements) from soils, sludge's and aqueous solutions (Anitescu & Tavlarides, 2006; Erkey, 2000; Librando et al., 2004; Babel & del Mundo Dacera, 2006; Saldana et al., 2005).

Box 3.3: Regulatory Issues

International agreements pertaining to sub-seafloor CO_2 storage have implications for the chemical purity of the CO_2 to be stored and may impact the ability to carry out controlled release experiments at the seafloor and in the water column.

A. The London Convention and London Protocol

The 1972 Convention on the Prevention of Marine Pollution by Dumping of Wastes and Other Matter, also called the 'London Convention', is a global agreement designed to protect the marine environment, regulating the dumping and disposal of waste and any other material to the sea. Currently, 82 states are parties to this convention (IMO, 2007). In 1996 the London Protocol was agreed to modernise and ultimately replace the London Convention. In 2006 the London Protocol was amended to allow the storage of CO_2 in geological formations beneath the seafloor, where the amendment was adopted on 2 November 2006 and came into force on 10 February 2007. The 2006 Amendment to Annex 1 of the 1996 London Protocol states that:

> ***Carbon dioxide streams from carbon dioxide capture processes for sequestration may only be considered for dumping, if:***
>
> ***(1) disposal is into a sub-seabed geological formation; and***
>
> ***(2) they consist overwhelmingly of carbon dioxide. They may contain incidental associated substances derived from the source material and the capture and sequestration processes used; and***
>
> ***(3) no wastes or other matter are added for the purpose of disposing of those wastes or other matter***

Aware of the need for more precise regulation, the Convention also agreed that further guidance for the conduction of sub-seabed geological sequestration of CO_2 ' in a manner that is safe for the marine environment in the short and long term' should be developed. These guidelines will be considered for adoption at the 2nd Meeting of the Contracting Parties in November 2007 and will form part of the regulatory scheme.

B. The OSPAR Convention

The Convention for the Protection of the Marine Environmental of the North-East Atlantic, the 'OSPAR Convention' (1992) regulates the dumping of pollutants into the Northeast Atlantic Ocean. In June 2007 amendments were agreed to Annex II and Annex III of the Convention to allow for the storage of CO_2 in subseafloor geological formations, such that:

> ***The dumping of carbon dioxide streams from carbon dioxide capture processes for storage is not prohibited, provided:***
>
> ***(1) disposal is into a sub-soil geological formation;***
>
> ***(2) the streams consist overwhelmingly of carbon dioxide. They may contain incidental associated substances derived from the source material and the capture, transport and storage processes used;***
>
> ***(3) no wastes or other matter are added for the purpose of disposing of those wastes or other matter;***
>
> ***(4) they are intended to be retained in these formations permanently and will not lead to significant adverse consequences for the marine environment, human health and other legitimate uses of the maritime area.***

The OSPAR Commission also adopted two decisions related to CO_2 disposal in the marine environment, which will enter into force on 15 January 2008. The first decision (2007/1) legally rules out placement of CO_2 into the water column or on the seabed:

> ***The placement of carbon dioxide streams in the water column or on the seabed is prohibited, unless it results from normal operations as described in Article 1(g)(i) of the Convention or is for a purpose other than the mere disposal thereof as described in Article 1(g)(ii) of the Convention and is in accordance with the relevant provisions of the Convention.***

The second decision (2007/2) provides a regulatory framework to ensure that point 4 above is met, stating that:

> ***The storage in geological formations of carbon dioxide streams from carbon dioxide capture processes shall not be permitted by Contracting Parties without authorisation or regulation by their competent authorities. Any authorisation or regulation shall be in accordance with the OSPAR Guidelines for Risk Assessment and Management of Storage of CO_2 Streams in Geological Formations, as updated from time to time.***

Furthermore, the solvent properties of supercritical CO_2 can be extensively modified by the addition of co-solvents (often polar compounds) resulting in a substantial increase in extraction efficiency. Crude oil consists of ~90% hydrocarbon compounds such as napthenes, paraffins, and aromatic hydrocarbons and ~10% polar compounds containing N, O, and S heteroatoms (including H_2S), and metal atoms (Hughey et al., 2002, 2004). The storage of CO_2 in a depleted oil or gas reservoir is therefore likely to result in the uptake of a range of organic non-polar and polar compounds, and possible extraction of metals. In the case of storage in a hydrocarbon free reservoir, such as a deep saline aquifer, leaching of metals from the host rock may still occur. In a leakage event, the CO_2 will migrate upwards through the overburden, and the chemistry of the CO_2 phase will be further modified by interactions with the host sediment and porewaters. For example, if the CO_2 passes through organic rich sediments a significant uptake of organic compounds and microbially produced gases such as H_2S and CH_4 can be expected.

As an example of the propensity of trace gases to partition into the CO_2 rich phase, the results from a series of flash calculations are presented below in Table 3.2. The calculations were carried out by Dr. Edward Peltzer (Monterey Bay Aquarium Research Institute) using Infochem Multiflash to determine the equilibrium distribution of common volcanic gases between 1 litre of seawater (salinity of 34.7) and 1 litre of the given CO_2 phase. Three cases were considered:

Case 1: Supercritical CO_2 in the sediment column – total depth of 1500m (15.247 MPa) and temperature of 50°C.

Case 2: Liquid CO_2 at the sediment-seawater interface – water depth of 1000m (10.187 MPa) and bottom water T of 2°C.

Case 3: Same conditions as Case 2, but considering CO_2 hydrate rather than CO_2 liquid.

For supercritical and liquid CO_2, He (and other non-polar gases) and H_2S both partition strongly into the CO_2 phase. However, in Case 3, we see a different picture. He does not form hydrates (it is too small to be ‘trapped’ in the cages), thus all He resides in the aqueous phase. Conversely, H_2S is a hydrate former and remains strongly partitioned in the CO_2 phase.

Table 3.2: Partitioning of trace gases between aqueous (seawater) and CO_2 rich phases.

	CASE 1: Supercritical CO_2			**CASE 2: Liquid CO_2**			**CASE 3: CO_2 Hydrate**		
	S = 34.7, Z = 1500 m, T = 50 °C, P = 15.25 MPa			*S = 34.7, Z = 1000 m, T = 2.0 °C, P = 10.19 MPa*			*S = 34.7, Z = 1000 m, T = 2.0 °C, P = 10.19 MPa*		
Component	**Aqueous**	**SC-CO_2**	**X_{CO2} (%)**	**Aqueous**	**L-CO_2**	**X_{CO2} (%)**	**Aqueous**	**H-CO_2**	**X_{CO2} (%)**
H_2O (mol)	54.6	0.0	0.0	55.3	0.0	0.0	55.3	44.9	44.8
CO_2 (mol)	0.8	16.0	95.5	1.2	20.1	94.5	0.6	6.7	92.2
He (µmol)	0.0	1.0	99.8	0.0	1.0	99.9	1.0	0.0	0.0
N_2 (mmol)	5.9	595.7	99.0	14.1	587.5	97.7	13.7	587.9	97.7
H_2S (mmol)	0.7	11.8	94.1	0.5	12.0	95.6	0.1	12.4	99.3
Density (g/cm^3)	1.015	0.575		1.035	0.884		1.030	1.106	

To a first approximation, it seems likely that naturally vented CO_2 that has interacted with the bedrock and sediment column is likely to provide a better analogue for CO_2 that has leaked from a sub-seafloor storage site than a pure CO_2 phase. However, this requires significant further investigation. While a number of researchers are investigating CO_2 reactions in storage reservoirs, little attention has yet focused on interactions with sediments in the event of leakage. The simple model presented above assumes chemical equilibrium is reached, whereas a natural system is dynamic and may be far from equilibrium. Detailed geochemical models of CO_2 interaction with the bedrock and overburden, incorporating fluid flow and kinetic constraints are therefore required. The influence of altered chemistry on expected physical behaviour and potential environmental impacts in the event of CO_2 leakage are discussed further in later Chapters. In brief, the uptake of hydrate forming compounds such as H_2S and CH_4 can significantly alter the hydrate stability field, thereby altering the conditions under which secondary trapping mechanisms may operate. It may also prove that the leakage of CO_2 poses a greater threat to ocean ecosystems through acting as a carrier of other toxic substances such as H_2S or heavy metals to the ocean, as opposed to the direct impact of the CO_2 itself (bioaccumulation of Hg for example). This report therefore recommends that the likely contamination of a pure CO_2 phase that would result from storage in a particular reservoir and/or transfer through the overburden should be included in assessments of site suitability and Environmental Impact Assessments. This would require site specific modeling and perhaps additional directed research on the solvent properties of CO_2 under the intended storage conditions with a given reservoir rock and/or hydrocarbon reserve composition.

3.3 Purposeful CO_2 Release Experiments

In the case of CO_2 leakage to the oceans there are inherent problems in designing and carrying out an ‘appropriately scaled’ release experiment, as suggested by Tyler (2003). It seems difficult to conceive a purposeful experiment that would completely mimic a leakage or seepage event. For example, to determine the impact of CO_2 migrating upwards through the sediment column on deep sediment infauna and microbial communities would essentially require engineering a leakage event. Nevertheless, in-situ experiments can provide valuable information, although conducting these experiments is a difficult task. Not only are there major technical barriers to overcome, there is also the problem of permitting, where negative public opinion has proved a substantial barrier to research in the past (e.g. de Figueiredo et al., 2003). The question of permitting and regulation is non trivial. A decision recently adopted by the OSPAR commission explicitly prohibits the placement of CO_2 streams in the water column or the seafloor in the North East Atlantic (see Box 3.3). Although this decision is intended to prevent large scale oceanic sequestration of CO_2, it seems likely that this would also have the (possibly unintended) side effect of preventing any purposeful release experiments from being carried out in this region.

Notwithstanding the technical and regulatory challenges, a number of release experiments have been successfully designed and carried out by scientists and engineers working at the Monterey

Bay Aquarium Research Institute (MBARI) and their research partners. Over the past few years (since 2001), the Ocean Chemistry of Greenhouse Gases Group, led by Dr Peter Brewer, and the Benthic Biology Group, led by Dr. James Barry, have conducted a number of experiments to examine the physico-chemical behaviour of CO_2 gas, CO_2 liquid and CO_2 hydrate in the ocean, and the impact of CO_2 release on seafloor sediments and local biota.

Various aspects of these experiments are described in Boxes 3.4 (Transport and Delivery of CO_2 in the Ocean), 3.5 (Monitoring Techniques), and 3.6 (Sustained Release Experiments). Here we evaluate whether or not seafloor release of CO_2 can be considered an analogue of leakage/ seepage under the same criteria used to assess natural vent sites.

Box 3.4: Transport & Delivery of CO_2 at Depth in the Ocean.

Carrying out controlled CO_2 release experiments in the ocean is technically challenging. The information presented here provides a summary of the techniques developed over the last 10 years by scientists and engineers at the Monterey Bay Aquarium Research Institute (MBARI) to transport and deliver small volumes (~128 ml to ~50 L) of CO_2 in the ocean using Remotely Operated Vehicle (ROV) technology, thereby enabling a variety of release experiments to be carried out across a range of water depths.

Small volumes (<1L)

This system consists of two hydraulic cylinders mechanically connected in tandem. One cylinder is filled with CO_2. The second cylinder is controlled using the hydraulic system on the ROV. When this device is activated, it moves the piston in the first cylinder, expelling liquid CO_2 into the ocean.

Larger Volumes (up to ~50L)

For larger volumes, the core delivery system consists of two components - a piston accumulator and a tandem pump - mounted in the tool sled of an ROV. The size of the piston accumulator determines the total volume of CO_2 that can be delivered to the ocean on a single ROV dive, while the size of the tandem pump provides controls on the volume dispensed.

Two accumulators have been developed (see figure below). A steel 9L accumulator provides a medium sized CO_2 reservoir, delivering ~8L CO_2 at 1000m depth, or ~7L at 3000m (see Table below). While this is sufficient for many experimental needs, to provide the larger volumes required for many release experiments, a 56 L accumulator was designed to allow transport of the maximum possible volume of CO_2 to the seafloor, limited only by the ROV payload capacity in terms of weight and size. This system consists of a carbon-fibre composite piston accumulator of 56L internal capacity constructed by Hydratech Fresno CA. At 23cm outside diameter and 194cm length it is close to the largest object the ROV can carry within the tool-sled. The use of a carbon fibre reinforced fiber glass composite for construction of the accumulator barrel provides sufficient strength (3000 psig rating) at a fraction of the weight of a steel cylinder of comparable size. Tandem cylinder pumps are used to actuate both the 9L and the 56L accumulator.

9L Accumulator & Single Tandem Pump

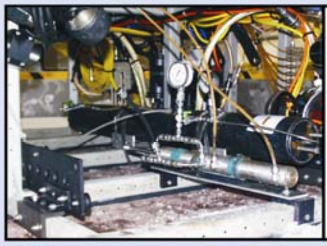

Piston Accumulators

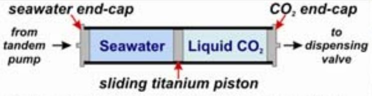

On deck, the accumulator is initially filled with seawater, pushing the piston flush to the CO_2 end-cap. Liquid CO_2 is then added through the CO_2 end-cap, pushing the piston back and expelling seawater until the entire accumulator is filled with CO_2. During the ROV dive, seawater is pumped into the seawater side (using the tandem pump) to maintain P,T conditions within the accumulator such that CO_2 remains in the liquid phase. To dispense CO_2, the hydraulic dispensing valve is opened, and seawater is pumped into the seawater side to push the piston forward and expel CO_2.

56L Accumulator & Twin Tandem Pumps

Tandem Cylinder Pumps - Controlled Delivery

A tandem cylinder pump (pushing on both the forward and backward stroke) is used to force seawater into the seawater side of the piston accumulator. This pumping action drives the internal piston and expels liquid CO_2 from the other end. The use of a tandem pump allows delivery of CO_2 free from the constraints of the ROV hydraulic system reservoir and provides a precise measure of the amount of liquid CO_2 dispensed.

Two tandem pumps provide a choice of dispensing volume, with a small pump dispensing 128 ml per stroke, and a large pump dispensing 970ml per stroke. Using the two pumps together in a twin configuration (see photograph of 56L accumulator above) provides a choice between fine control of small dispensing volumes, and the capacity to deliver larger volumes relatively quickly. This also provides a level of redundancy should one of the pumps fail during a dive.

Delivery Volumes

Because of the compressibility of liquid CO_2, the volume of CO_2 delivered at depth is dependent on the pressure and temperature of the CO_2 at the time the accumulator is filled, and the ambient PT conditions at depth. Theoretical delivery volumes for the 9 L and 56 L accumulators are given below.

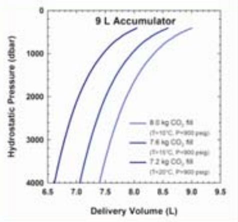

9L Fill @ 900 psig		Theoretical Delivery Volume for 9 L Accumulator @ Depth			
Fill T (°C)	Mass CO_2 (kg)	1000m, 3.9°C (L)	2000m, 2.1°C (L)	3000m, 1.7°C (L)	4000m, 1.6°C (L)
10	8.0	8.3	7.9	7.6	7.4
15	7.6	8.0	7.5	7.2	7.1
20	7.2	7.5	7.0	6.8	6.6
56L Fill @ 900 psig		**Theoretical Delivery Volume for 56 L Accumulator @ Depth**			
Fill T (°C)	Mass CO_2 (kg)	1000m, 3.9°C (L)	2000m, 2.1°C (L)	3000m, 1.7°C (L)	4000m, 1.6°C (L)
10	49.8	51.9	49.0	47.3	46.5
15	47.5	49.5	46.7	45.1	44.4
20	44.5	46.4	43.8	42.3	41.6

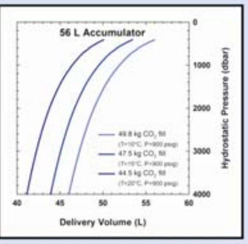

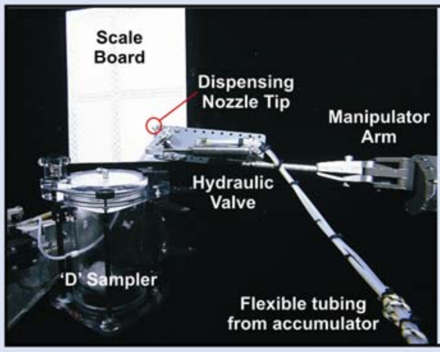

Dispensing

The CO_2 outlet on the accumulator is attached to a dispensing nozzle via flexible tubing. This allows the dispensing nozzle to be moved into the required position for CO_2 release using the manipulator arm on the ROV. A hydraulically actuated valve on the end of the nozzle is opened to allow CO_2 to be dispensed, and kept closed at all other times to prevent water from entering the system (if water entered the system at depth CO_2 hydrate could form inside the tubing or accumulator). In the image to the left, the 'D' Sampler has already been filled with ~10L of buoyant CO_2. In the image to the right, the lid of the 'D' Sampler has been opened (hydraulically actuated), releasing the 10L of CO_2 in one go. Immediately after release the buoyant liquid begins to break down into small cm size droplets.

Key Reference: Peltzer et al. (2002).

Box 3.5: CO_2 Monitoring Techniques in the Ocean.

This Box provides an overview of some of the in-situ techniques that have been developed and used in both small scale release experiments and at natural vent sites to detect and track CO_2 releases in the ocean, and to investigate the chemical behaviour of CO_2 in the ocean. It does not provide an exhaustive summary of all techniques that may be relevant to the monitoring of CO_2 leakage or seepage from a subseafloor storage site.

Visual Observations

Careful visual observations can provide excellent information on the behavior of CO_2 in the ocean. For example, HD video footage has been used to determine the *in-situ* dissolution rates of both rising CO_2 droplets (Brewer et al., 2002 and see below) and CO_2 hydrate (Rehder et al., 2004). The information obtained from such experiments serves as input for sophisticated models of CO_2 behaviour in the ocean environment (e.g. Alendal & Drange, 2001; Chen et al., 2003; Sato, 2004; Gangstø et al., 2005).

Examining droplet behaviour using a bubble box (see figure opposite): Observing free CO_2 droplets in the ocean can be a difficult task (see panel A - this figure shows a small cloud of CO_2 droplets that are almost impossible to see against a backdrop of marine snow and jelly fish). To allow clear imaging of CO_2 droplets MBARI scientists and engineers developed an approach using a specially constructed 'bubble box'(panel B). The bubble box, which is open at the top and bottom, is mounted at the front of an ROV within the field of view of the HD camera. CO_2 droplets are injected at the base of the box and the ROV is flown upwards (or downwards) through the water column so as to keep the freely rising (or sinking) droplets within the field of view. The ROV ascent/descent rate then gives the rise/sink rate of the CO_2 droplets, while detailed analysis of frame grabs (still pictures acquired from the HD video footage - panel C) allows the shrinkage rate (and therefore dissolution rate) of the droplets to be calculated. This technique has since been adopted by scientists investigating the fate of CO_2 at natural vent sites in the Okinawa Trough (Shitashima & Maeda, 2005).

Tracking a free release of CO_2 using a bubble box

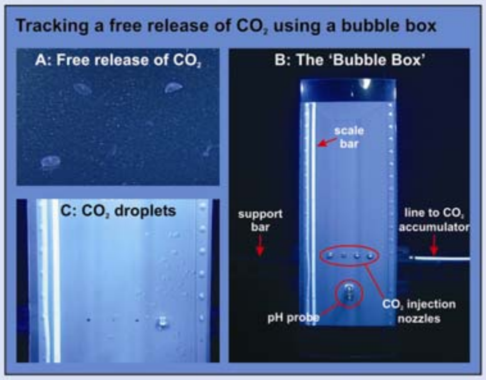

Tracking a free release of CO_2 using 3-dimensional acoustic monitoring

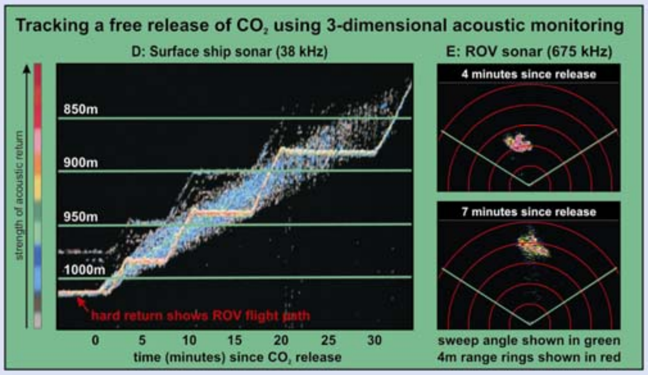

Acoustic Monitoring (Sonar)

Sonar has been widely used to locate naturally occurring gas bubble streams (CO_2 or other gases such as CH_4) rising from the seafloor. Similarly, should leakage of CO_2 from a subseafloor storage site to the ocean occur, acoustic monitoring would provide a valuable tool with which to locate and determine the extent of the resultant CO_2 droplet/bubble plume.

3-D imaging of a CO_2 droplet cloud (see figure opposite): Sonar can also be used in release experiments to investigate the development and dispersion of a CO_2 droplet cloud as it rises through the water column. In a novel experiment Brewer et al. (2006) used a downward looking ship sonar (panel D) in combination with a forward looking sonar mounted on an ROV (panel E) to obtain 3 dimensional information on a CO_2 droplet cloud over a 150 m (30 minute) ascent. The ships sonar provides information on the vertical extent of the cloud, while the ROV sonar provides a cross section through the cloud giving the lateral extent. Experiments such as this provide important information with which to test and validate theoretical models.

Tracking dissolved CO_2 in the ocean

The eventual fate of CO_2 released to the ocean is to dissolve into seawater, increasing the total amount of dissolved CO_2 (TCO_2) and decreasing pH. pH probes can therefore be used to track and map the flow of seawater rich in dissolved CO_2 during both small scale release experiments (e.g. Brewer et al., 2000; see also Box 3.6) and at natural vent sites (e.g. Shitashima & Maeda, 2005). The figure opposite (reproduced with kind permission of Shitashima-san) shows the pH anomaly (ambient seawater pH - observed pH) mapped at the Hatoma Knoll CO_2 vent site. It can be seen that large decreases in pH (0.5-0.6 units) are limited to the immediate vicinity of the vent outlets, with plumes of low pH water extending upwards through the water column with little lateral dispersion (panels F & G). While pH probes certainly provide a valuable tool, there are also limitations to their use. Firstly, response drift and sensor failure frequently occurs during long term deployments (e.g. Barry et al., 2005). Secondly, the slow kinetics of CO_2 hydration (Zeebe & Wolf Gladrow 2001) means that in a dynamic open system, pH measurements will significantly underestimate the TCO_2 loading (e.g. Brewer et al., 2005a). Work therefore continues on developing robust, accurate, rapid response pH and pCO_2 sensors for in-situ measurements of the CO_2 system in seawater (e.g. Someya et al., 2004; Shitashima et al., 2005).

Mapping pH anomalies at the Hatoma Knoll CO_2 vent site

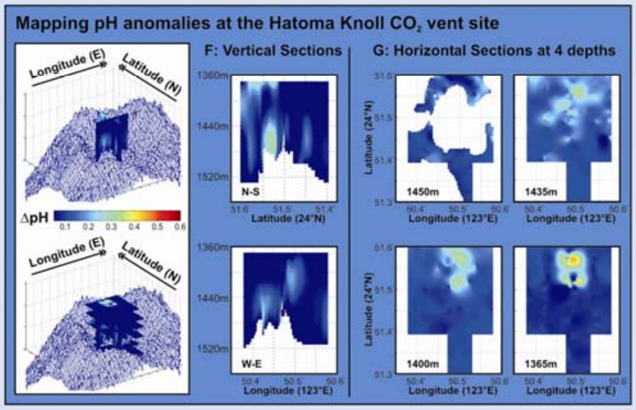

The DORISS Instrument (Deep Ocean Raman In-Situ Spectrometer)

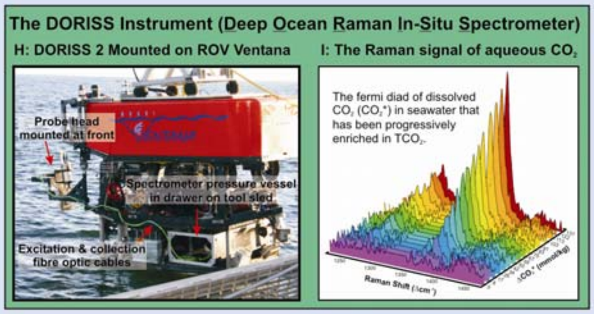

Raman Spectroscopy in the Ocean

MBARI's Deep Ocean Raman In Situ Spectrometer (DORISS) and the 2nd generation instrument DORISS 2 have now been deployed on numerous ROV dives (panel H) with the successful acquisition of spectra from a wide range of targets including minerals, gases, gas hydrates and dissolved species (e.g. Brewer et al., 2004a; Dunk et al., 2005; Hester et al., 2006, 2007a,b; White et al., 2005, 2006a,b). Of particular interest here is the potential for direct detection of the CO_2 system, since each species has a characteristic Raman signal (e.g. Brewer et al., 2004b; Dunk et al., 2005). While current instrument sensitivity does not permit detection of the CO_2 system at ambient seawater concentrations, it does allow detection at the elevated levels that might be expected in the vicinity of a release site (see panel I). Furthermore, Raman spectroscopy would provide an extremely valuable tool in investigating the chemical composition of leaked CO_2, allowing identification of minor components (e.g. H_2S), and investigation of chemical fractionation during processes such as dissolution or hydrate formation (e.g. White et al., 2006a).

Box 3.6: Investigating Impacts of CO_2 Release on Ocean Biota.

This Box provides an overview of the methods used during small scale release experiments to investigate the impact of sustained exposure to elevated CO_2 on ocean biota. In addition to these in-situ techniques, laboratory and mesocosm studies also provide valuable information on the biological impacts of elevated CO_2, particularly with respect to surface water ecosystems. For example, the Pelagic Ecosystem CO_2 Enrichment Study (PeECE - see peece.ifm-geomar.de/index.htm) conducted a range of experiments at the Bergen Marine Mesocosm Laboratory (www.bio.uib.no/eksternesider/bergenmarine/inst2.html) that focused on the impact of elevated CO_2 on plankton communities (e.g. Riebesell 2004), while experiments conducted at the Biosphere-2 facility in Arizona (www.b2science.org) investigated the impacts of elevated CO_2 on a large coral reef mesocosm (Langdon et al., 2003).

Sustained release from pools of liquid CO_2

Scientists at MBARI have investigated the impact of CO_2 on deep sea biota in a series of release experiments conducted off the coast of central California at water depths of ~3100-3600m (Barry et al., 2001, 2004, 2005; Barry & Drazen, 2007; Carmen et al., 2004; Fleeger et al., 2006; Thistle et al., 2005; 2006, 2007). The intention of the experiments was to perturb the CO_2 content of bottom seawater for a period of around 1 month through exposure to the dissolution plume advected from pools of CO_2 on the seafloor. Details on experimental designs are given in Barry et al. (2005) and a brief overview is provided here.

The CO_2 pools: At the depths of these experiments CO_2 is more dense than the surrounding seawater and will sink to form gravitationally stable pools of liquid CO_2 on the seafloor. To contain the pools (and prevent the CO_2 from flowing downslope or being 'blown' away by bottom currents) the CO_2 was injected into plastic corrals (panel A). Various sizes and clusters of corral have been used to create CO_2 pools with total volumes of ~20L to ~100L. On injection a hydrate film immediately forms at the interface between the CO_2 and seawater (panel A(a)). In some instances the formation of massive hydrate was also observed during the deployment (panel A(b)). The trapped CO_2 slowly dissolves, producing a plume of CO_2-rich low-pH seawater that is advected and dispersed by near-bottom currents. The CO_2-rich plume is more dense than ambient seawater and sinks, thus surficial sediments downstream from the CO_2 pools are also exposed to high CO_2 conditions. To date all experiments have lasted for ~1 month (27- 41 days), sometimes requiring the CO_2 pools to be refilled during the deployment. Although accurate dissolution rates cannot be determined (due to uncertainties in the volume of CO_2 dispensed, the surface area of the CO_2, infrequent imaging, and in some cases all CO_2 being dissolved by the time of the return visits), apparent dissolution rates were on the order of 0.1-0.2 $\mu mol/cm^2s$. This is significantly lower (by an order of magnitude) than the dissolution rate of liquid CO_2 through a fresh hydrate membrane as determined by pH measurements during one of these experiments (Dunk et al., 2002) and is more comparable to that determined for CO_2 hydrate (Rehder et al., 2004). This difference could be due to the formation of a thick hydrate membrane, or the presence of a protective thin layer of sediment deposited on top of the hydrate membrane, or may simply reflect the difference between initial and steady state dissolution rates.

A: CO_2 corral on the seafloor

(a) liquid CO_2 immediately after injection with hydrate membrane clearly visible

(b) massive hydrate in the same corral approximately 24 hours later

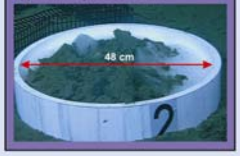

B: Examples of experimental layout

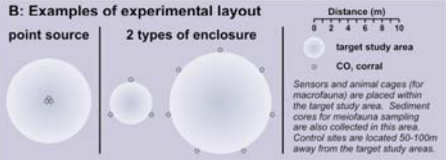

Sensors and animal cages (for macrofauna) are placed within the target study area. Sediment cores for meiofauna sampling are also collected in this area. Control sites are located 50-100m away from the target study areas.

C: ΔpH measured ~1m from a cluster of CO_2 corrals

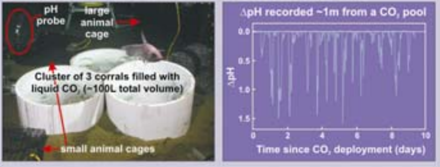

Monitoring the CO_2-rich low-pH plume & the extent of perturbation: Experimental designs can be divided into two groups (panel B): in ***point source experiments*** the CO_2 pool is located at the centre of the target study area, while in ***enclosure experiments*** the study area is encircled by multiple CO_2 pools. The intensity and variability of the CO_2 dissolution plume within the study area is monitored using an array of pH probes positioned above the seafloor (~5cm) at various distances from the CO_2 pools (<1m to ~10m, with background conditions being measured at a distance of 50-100m from the pools). In some experiments a vertical array was also used, with pH probes positioned at heights up to 50cm above the seafloor. The magnitude and variability of pH perturbations observed has varied widely between different experiments, reflecting the experimental layout, the rate of CO_2 dissolution, and the extent of mixing between the CO_2 rich plume and ambient bottom water. The two latter factors both increase with increasing speed and turbulence of near bottom flow. In point source experiments sensors and study organisms were exposed to high-CO_2 low-pH water for around 30 minutes every ~12 hours (panel C, $\Delta pH = pH_{seawater} - pH_{observed}$). This pattern of exposure reflects the inertial and tidal periodicity of bottom currents in this location, with a given point falling downstream of the CO_2 pool every 12 hours and near background pH experienced the rest of the time. Acute perturbations with a decrease of up to 1.7 pH units have been recorded in the immediate vicinity (<1m) of the CO_2 pools (panel C), with more moderate decreases at distances of 5-10m (ΔpH_{max} ~0.3). Enclosure experiments were designed to achieve a more stable pH regime within the target study area. The use of multiple CO_2 sources in these designs means that a given location within the study area is exposed to a dissolution plume more frequently than in the point source experiments, thus damping the tidal periodicity of exposure.

Impacts on megafauna: The impact of CO_2 release on megafauna has been evaluated by comparing the survival rate and physiological conditions of animals held in cages within the study area to those held in control locations some 50-100m distant from a CO_2 pool. Slow moving benthic animals are collected using a 'slurp' sampler and deposited in small cages, while more mobile benthopelagic species are caught in larger baited traps (panel D). This approach has been used to investigate the impact of high CO_2 on two echinoderms (a sea urchin and a sea cucumber; Barry et al., 2001) and three abyssal scavengers (Barry & Drazen, 2007), an octopus (*Benthoctopus* sp.) and two fish species (eelpout and grenadier). Rates of survival for sea urchins and cucumbers held in cages adjacent to CO_2 pools were very low, with decalcification of urchin spines and skeletal elements also evident. All grenadiers (CO_2 and control cages) died, possibly due to stress, predation (from *Benthoctopus* in the same cage), or exposure to the CO_2 dissolution plume. Conversely, high survival of *Benthoctopus* and eelpout over a month-long experiment indicates a physiological capacity to cope (at least temporarily) with exposure to seawater enriched in CO_2.

Impacts on sediment infauna: The tolerance of sediment infauna to high CO_2 conditions has been evaluated by comparing the abundance of live taxa found in near surface sediments close to the CO_2 pools to that in control locations 40-75m from a CO_2 pool. Mortality rates for 3 major meiofaunal groups (nematodes, amoebae, flagellates) were determined from changes in biovolume along a point source exposure gradient. In sediments adjacent to a CO_2 pool (<0.5m) the impact of exposure was severe with ~90% mortality in all 3 groups (Barry et al., 2004). At distances of 5-10m from the CO_2 pools the abundance of nematodes showed no significant difference to that at control sites (0% mortality), while amoebae and flagellate mortality decreased from ~70% at 5m to ~25% at 10m (Barry et al., 2005). This suggests that either the latter two taxa are sensitive to relatively small brief changes in pH or that pH perturbations in surface sediments are greater than those measured in bottom waters (Barry et al., 2005). The impact of CO_2 exposure on another important infaunal group, the harpacticoid copepods, has also been investigated. In this case mortality rates were determined from analysis of striated muscle appearance, a technique developed to allow individuals that were alive (or recently dead) at the time of collection to be distinguished from those that had been dead for many days (Thistle et al., 2005). Copepod mortality in sediments from the centre of an enclosure experiment (~2m from the CO_2 pools with a measured porefluid ΔpH of ~0.6) was around 50-80% (Thistle et al., 2005). Some harpacticoid copepod species were found to be significantly less susceptible to CO_2 exposure than others, with 6 out of 34 species showing no difference in mortality between study and control sites (Thistle et al., 2006). These differences most likely reflect different physiological capacities to withstand high CO_2 conditions and could affect the pattern of recovery following an exposure event.

D: Impacts on megafauna

(a) depositing echinoderms collected in a 'slurp' sampler in a small animal cage

(b) *Benthoctopus* sp. & grenadier (rattail) trapped in a large fish cage, with sensor array positioned to the left.

Experiments above the depth of CO_2 neutral buoyancy

Baited plume release experiment: The first empirical in-situ study that directly examined animal responses to CO_2 dissolution plumes was a small scale release experiment conducted at a water depth of ~625m above the CO_2 point of neutrally buoyancy (Tamburri et al., 2000). Animals were attracted to a release point by pumping fish odour solution into the water column. Liquid CO_2 was then rapidly injected into an inverted 4L beaker to form a buoyant flocculent hydrate. The fish odour solution continued to be discharged through the porous hydrate material, to create a CO_2 rich odour plume (ΔpH of ~1 at the beaker opening). After hydrate formation there was no noticeable change in animal behaviour, with animals continuing to accumulate at the release site. One hagfish that entered the CO_2 beaker quickly lost consciousness (~5s) and sank to the seafloor, recovering after it had rolled downstream away from the CO_2. This narcotic effect was most likely a result of respiratory stress caused by elevated seawater pCO_2 (e.g. Burnett, 1997). A similar approach to in-situ studies has also been taken at Loihi seamount near Hawaii, where hydrothermal vent solutions are rich in dissolved CO_2 (Vetter & Smith, 2005). In these experiments, the authors created odor plumes by placing bait balls within the CO_2 rich vent plumes, and also placed trapped animals directly within the plumes (see main text and Chapter 6 for further discussion of these experiments).

3.3.1 The Whole Environment

In principal, CO_2 release experiments can be performed in any area, providing it is accessible to research vessels and ROVs. This could be considered a major advantage, allowing experiments to be carried out in areas immediately overlying storage reservoirs. In practice, the issue of permitting may well prevent release experiments from being carried out in certain areas (see Box 3.3).

3.3.2 The Scale of CO_2 Release

At present, all purposeful release experiments are transient in nature. Given the current technical limitations on the amount of CO_2 that can be transported to depth (see Box 3.4), the duration of release is inherently limited. It is helpful to consider release experiments in two categories: those taking place above and below the neutrally buoyant point of CO_2 in the ocean.

3.3.2.1 Experiments Above the Neutrally Buoyant Point

Discrete releases of CO_2 at depths above the neutrally buoyant point to form a rising droplet or bubble plume can provide valuable information regarding droplet and bubble rise rates and shrinkage rates, and allow new detection and monitoring methods to be tested in-situ (see Box 3.5). However, given the limited volumes of CO_2 that can be transported to depth in the ocean, the release cannot be sustained for long periods. As an illustrative example, we can compare

the flux of CO_2 observed at a natural vent site, to that which could be achieved in a release experiment using current available technology.

The Champagne vent site, located on NW Eifuku at a water depth of 1600m, consists of a ~10 m^2 field within which ~300 individual streams of CO_2 droplets emanate from the seafloor with an exit temperature of ~4°C (Lupton et al., 2006). Each droplet stream is releasing CO_2 at a rate of 2 droplets with a diameter of 1.5 cm every second. This gives a CO_2 release rate of ~3.5 g/s for an individual stream, 105 g/s per m^2 of the vent field, and a little over 1 kg/s (~33 kton CO_2/yr) for the entire vent field.

In comparison, if the 56L accumulator is used, and filled to a pressure of 900 psig at 10-20°C, this gives a total mass of 44.5-49.8 kg CO_2 transported to depth (see Box 3.4). If a purposeful experiment were then to attempt to simulate an individual droplet stream at the Champagne vent site, a 1m^2 area of the vent field, or the entire vent field, the release would last for 3.5-4.0 hours, 7-8 minutes, or 45 seconds respectively.

The short duration of such a release means that (at present) biological impacts can not be assessed in free release experiments at depths above the neutrally buoyant point. However, an inverted container (open to seawater on its bottom face), can be used to trap a buoyant volume of CO_2, thereby modifying the CO_2 content of a seawater plume that passes beneath the container (e.g. Tamburri et al., 2000), where this technique is similar to that employed in deep release experiments below the neutrally buoyant point (see Box 3.6).

3.3.2.2 Experiments Below the Neutrally Buoyant Point:

At depths below the neutrally buoyant point, CO_2 is more dense than seawater and will sink, forming a pool of liquid CO_2 on the seafloor.

Under these conditions, it becomes somewhat easier to design and carry out a wide range of experiments to examine the physico-chemical behaviour of CO_2 in the deep ocean (including measurements of the in-situ dissolution rate of liquid CO_2, hydrate formation and dissolution processes, and the creation of plumes of CO_2 enriched seawater) and to investigate the impacts of CO_2 release on seafloor biota (see Box 3.6). For example, creating small contained pools of CO_2 on the seafloor (~20-100L) allows experiments and observations to be carried out over a period of days to weeks (before the CO_2 has fully dissolved and requires replenishing). In addition, multiple deliveries of CO_2 to the seafloor can be made, thereby increasing the total volume of CO_2 that can be incorporated into the experimental design.

It is noted that the formation of a pool of liquid CO_2 on the seafloor as a consequence of leakage or seepage from a geological storage site is highly unlikely. If the sediment-seawater interface is deeper than the point of CO_2 neutral buoyancy, then leaked CO_2 will be trapped at some depth in the sediments, whereas if the interface is shallower, then the CO_2 will remain buoyant and rise up through the water column. Nevertheless, the dissolution plume of CO_2 enriched seawater (and the impact that this exerts on local bottom water conditions, the surficial sediments, and local biota) that is formed from a static pool of CO_2 emplaced on the seafloor will share numerous similarities with that formed from a constant stream of CO_2 droplets emanating from the seafloor, or a CO_2 saturated sediment-seawater interface. Similarly, the impact of elevated CO_2 levels on surficial sediments (and associated infauna) will also provide some insights into the impact of elevated CO_2 levels deeper in the sediment column. Thus these experiments provide the ability to assess the initial perturbation of oceanic systems on addition of CO_2, i.e. what happens when CO_2 is first released to the seafloor. As such, they provide information complementary to that gained by studying CO_2 vent sites.

3.3.2.3 Sustained Release Experiments

Barry et al., (2005) assessed the utility of deep sea CO_2 release experiments in understanding the effects of elevated CO_2 levels on deep sea biota. In their discussion these authors noted that the high spatial and temporal variability of CO_2 and pH that animals in release experiments are exposed to (see Box 3.6) impairs the ability to interpret dose tolerance responses of animals to hypercapnia (excess CO_2 in the bloodstream). Furthermore, it is not possible to distinguish the importance of episodic moderate hypercapnia from chronic mild hypercapnia on animal survival (Barry et al., 2005). Such information is certainly necessary to develop a clear understanding of the consequences of elevated CO_2 concentrations on marine ecosystems, and would significantly improve confidence in our ability to predict the full extent of impacts related to either leakage of CO_2 from a sub-seafloor storage reservoir, ocean disposal scenarios or the future high-CO_2 low-pH ocean.

Of the three elevated oceanic CO_2 scenarios (leakage - local, storage - regional, the high-CO_2 low-pH ocean - global), the current methods employed in release experiments perhaps simulate most closely the conditions expected in a leakage event (e.g. a point source of CO_2 resulting in the formation of a relatively narrow dissolution plume that oscillates with bottom currents, periodically exposing the local seafloor and water column to elevated CO_2 and decreased pH). Nevertheless, experimental designs that allow either a controlled release of CO_2 sustained over longer periods of time and/or provide relatively stable perturbations (of CO_2 and pH) within the range of variation expected would allow significant advances in our general understanding of the impacts of high CO_2 on ocean biota. The enclosure design experiments described in Box 3.6 represented the first step towards this goal by damping the high pH variation observed in point source experiments. Furthermore, although at present release experiments cannot simulate CO_2 emissions over an extended time period, particularly at water depths above the point of neutral buoyancy, they may be able to do so in the future.

Current research efforts are focused on the design and testing of a Free Ocean Carbon Dioxide Enrichment (FOCE) experimental system that would enable creation of a lowered seawater pH environmental condition, control it within discrete limits, and allow for in-situ multi-disciplinary science experiments while also conducting monitoring observations (Brewer et al., 2005b; Kirkwood et al., 2005, 2007). A FOCE experiment can be considered analogous to the on-land Free Air Carbon Dioxide Enrichment (FACE) experiments used to measure the response of terrestrial ecosystems to elevated atmospheric CO_2 levels (e.g. McLeod & Long, 1999; cdiac.esd.ornl.gov/programs/FACE/face.html). FACE experiments regulate the partial pressure of atmospheric CO_2 (pCO_2) over a control zone through sophisticated feedback between rapid response pCO_2 and wind sensors located within the control zone and CO_2 injectors that encircle the control zone, such that additional CO_2 is added across the upwind sector of injectors so as to maintain near constant pCO_2 within the control zone. Similarly, a FOCE system would elevate the H^+ and TCO_2 concentration in a free volume of sea water using active feedback of current velocity and pH data. A FOCE system would provide a knowledge base for predictive experiments to better understand the impacts of elevated CO_2 on ocean biota and important biogeochemical processes, allowing studies (for example) on coral reefs, benthic fauna, and carbonate dissolution. Primarily targeted at investigating the future high-CO_2 low-pH ocean, such data could also provide valuable information regarding the impact of moderately depressed pH ($\Delta pH = 0.1\text{-}0.3$) in the vicinity of a leakage or seepage site. If successful, this project will provide the ability to conduct mid to long term (weeks to years) CO_2 release experiments. For short term testing small volumes of acid or CO_2 may be delivered from self-contained packages. Looking to the future, the promise of cabled observatories in the ocean, which would provide the power and communications necessary for extended experimental control, in combination with a small bore pipeline delivering CO_2 (or acid) to the observatory would allow long term experiments to be carried out over a number of years. Furthermore, continued monitoring following cessation of CO_2 (or acid) delivery would allow the rate and extent of system recovery from any negative impacts to be evaluated.

3.3.3 The Physical and Chemical Conditions

To date the vast majority of CO_2 release experiments have been conducted using a pure CO_2 phase. However, unlike a natural vent site, a purposeful release experiment does provide the opportunity to define the composition of the CO_2 rich phase. For example, it would be extremely interesting to conduct experiments using CO_2 from an impure capture stream, and compare behaviour (and impacts) to that of the pure CO_2 phase, thus perhaps informing decisions on what should constitute an 'overwhelming' proportion of CO_2 (see overview of regulations in Box 3.3). Similarly, mixtures could be created to simulate the expected composition of CO_2 emerging from a given storage reservoir or sediment column. Indeed, targeted experiments on CO_2 mixtures have the potential to provide valuable information regarding the physico-chemical behaviour (and potential impacts) of the 'leakage' fluid or gas.

For example, a study on the differential dissolution of CO_2 and H_2S using in-situ Raman spectroscopy (see Box 3.5) could provide insight into the extent to which a leaking CO_2 phase could act as a carrier for reservoir H_2S. Such experiments have already been carried out on CH_4/N_2 mixtures (White et al., 2006a) and CH_4/H_2S mixtures (Dunk et al., in prep).

In summary, release experiments can provide a wealth of information regarding the physico-chemical behaviour of CO_2, allow the ability to develop and improve on experimental and monitoring techniques, and allow a first order assessment of the immediate impact of CO_2 on biota. To date they do not provide information on the longer term impacts of continuous CO_2 emissions, although some progress has now been made toward establishing the required technology.

3.4 Summary & Recommendations

Both natural CO_2 vents and purposeful release experiments can provide valuable information regarding the behavior, impact, and fate of CO_2 in the environment. In general, the weaknesses of CO_2 vents as analogues are offset by the strengths of purposeful release experiments and vice versa.

Further investigation of both the expected composition of 'leaked' CO_2 and the composition of CO_2 emitted at natural vent sites is needed. A combination of experiments and modeling is most likely required to determine the possible chemical composition of the leakage fluid. In particular, interactions between supercritical CO_2 and depleted hydrocarbon reservoir rocks should be explored in more detail to determine if leakage of CO_2 will act as an efficient transport mechanism delivering toxic substances from the storage reservoir to the ocean.

The creation of a CO_2 vent site database, including details regarding the hydrothermal regime, chemical composition of the CO_2 rich phase, an estimate of the CO_2 flux, and a full habitat/biotope description could provide an invaluable tool with which to assess potential impacts of leakage or seepage of CO_2 from a subseafloor storage reservoir for the purposes of Environmental Impact Assessments. A summary of currently known sites is provided in Appendix 3.A.

This report raised the question that although CO_2 storage might be considered less safe in tectonically active regions due to a higher probability of leakage (e.g. Bradshaw & Dance, 2005), should leakage occur is it perhaps less likely to result in a negative impact on the local ecosystem? This question warrants further investigation, and could perhaps be usefully addressed in site selection criteria and Environmental Impact Assessments in tectonically active regions (e.g. Japan, South East Asia, New Zealand). This would require a site specific understanding of the likelihood of leakage, the potential rate of leakage, the natural flux of CO_2 to bottom waters, and the impact of CO_2 venting on the biota (at the local and regional scales). To determine regional fluxes of CO_2 for this purpose would require a more detailed consideration than that presented in Chapter 2. It is worth noting that the intermediate and deep-water CO_2 vent sites have been discovered primarily through the use of ROVs and manned submersibles. As deep-ocean exploration, and in particular the exploration of island arc systems, continues, it seems likely that new CO_2 vent sites will continue to be discovered. Indeed, if the rate at which new discoveries have been made over the least 2 years is sustained, then reasonably robust regional CO_2 flux estimates may be available in the near future.

4: Primary Leakage or Seepage of CO_2 from Subseafloor Geological Storage Reservoirs

This Chapter examines the possibility of primary leakage or seepage of CO_2 from a subseafloor storage reservoir – that is the movement of CO_2 out of the target storage formation.

The global distribution and storage capacity of potential offshore CO_2 storage reservoirs (in particular depleted natural gas and oil fields, and deep saline aquifers) have been discussed in Chapter 1. Within these target storage reservoirs, the retention of CO_2 is achieved through a number of different trapping mechanisms (IPCC, 2005):

- trapping below an impermeable confining layer (caprock)
- retention as an immobile phase trapped in the pore spaces of the storage formation
- dissolution in the in situ formation fluids
- adsorption onto organic matter (i.e. in coal and shale)
- reacting with the minerals in the reservoir and seal rocks to produce carbonate minerals

Here we focus on the first of these mechanisms. When supercritical CO_2 is injected into a storage reservoir it is more buoyant than the formation fluid in the pore spaces and will rise to the top of the reservoir. Initial retention of CO_2 is therefore almost entirely dependent on physical trapping beneath the caprock, and the primary characteristic of a secure CO_2 storage reservoir is a good reservoir/seal pair: that is the presence of a permeable high porosity reservoir rock that is capped by an extensive cover of impermeable low porosity rocks acting as a seal and preventing the CO_2 from migrating vertically. Indeed, all possible mechanisms for CO_2 leakage or seepage from the primary storage are related to breaching or bypassing of the caprock seal. Over time, the amount of CO_2 trapped via the other mechanisms (and therefore the overall security of storage) will increase, and the possibility of leakage will diminish.

As it is vital that site selection criteria ensure that a target storage reservoir is confined by an adequate caprock, this Chapter first considers the desired characteristics of the caprock seal. Potential leakage mechanisms related to the seal and wellbores are then discussed.

When we consider migration of CO_2 out of the primary storage reservoir we also need to make a distinction as to whether the CO_2 leaks (or seeps) to the overburden, to the ocean, or to the atmosphere. It does not necessarily follow that leakage to the overburden will result in the release of CO_2 to the ocean, nor does it follow that release to the ocean will automatically result in escape to the atmosphere. Secondary trapping mechanisms and the fate of CO_2 in the overburden and the water column are discussed in later chapters.

4.1 Characteristics of the Caprock

A large amount of expertise regarding caprock performance is available from hydrocarbon exploration, production, and storage operations. However, while there are many similarities in seal performance criteria, there are also key differences that must be considered when storage of CO_2 is being evaluated, as a caprock that is adequate for hydrocarbon storage may not be adequate for CO_2 storage. For example, in terms of seal capacity and resistance to fracturing, the most effective sedimentary seals for hydrocarbons are gas hydrates followed by evaporites (Figure 4.1; Downey 1984; Warren 2007). In comparison, methane gas hydrates should not under any circumstances be considered as a potential seal for CO_2 storage reservoirs due to the high probability of an exchange reaction occurring, indeed they should be classed as a geohazard and avoided (see Chapter 7 for further discussion). To form an effective seal for CO_2 storage purposes the sealing lithology needs to be:

- impermeable to CO_2
- unfaulted and relatively ductile (resistance to fracturing)
- laterally continuous, maintaining a constancy of properties over a large area

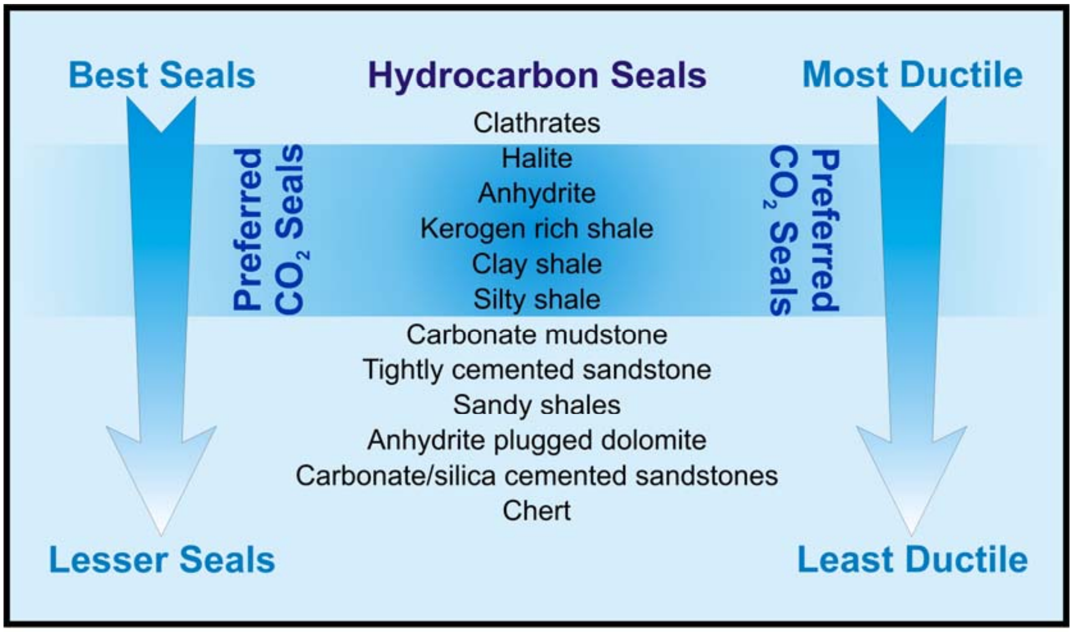

Figure 4.1: Preferred seals for CO_2 storage reservoirs in comparison to hydrocarbon reservoir seals. Differing ability to form a hydrocarbon seal is related to inherent ductility in the subsurface (after Warren, 2007 & Downey, 1984). For CO_2 storage additional factors must be taken into account - most notably potential chemical interactions with methane hydrates and carbonates.

Caprocks considered suitable for CO_2 storage operations include evaporites (e.g. halite or anhydrite), shales and mudstones (e.g. Bachu, 2005). In their site selection framework, Pawar et al. (2006) also include carbonates. These caprock types are discussed below in relation to their ability to form an effective seal for CO_2 storage purposes.

4.1.1 Seal Capacity & Permeability

A fundamental requirement for an effective seal is that the entry pressure of the caprock be greater than the buoyancy pressure of the CO_2 stored in the reservoir beneath.

The seal entry pressure or seal capacity is the capillary pressure at which CO_2 will leak into the pore space of the caprock. This is dependent on both rock and fluid parameters. Rock parameters include the size distribution of continuous pore throats – the small space at the point where two grains meet which connects two larger pore spaces. Fluid parameters include the fluids (or gases) present (e.g. CO_2, hydrocarbons, water), the density of the fluids, and the interfacial tension of the fluids.

The permeability of a rock is a measure of its ability to transmit fluids, and is a function of pore space distribution and connectivity (e.g. porosity and pore throat distribution). The units of permeability are length^2, and it is typically quoted in darcies (d) or millidarcies (md), where 1 d (10^3 md) is approximately equal to 10^{-12} m^2. Formations that transmit fluids readily, such as sandstones, are described as permeable and tend to have many large, well-connected pores. Impermeable formations, such as evaporites, shales and siltstones, tend to be finer grained or of a mixed grain size, with smaller, fewer, or less interconnected pores.

Massive bedded halite (sodium chloride; NaCl) units contain few if any interconnected pore throats, and the permeability of halite is very low with typical values less than 10^{-6} md, and some of the tighter halites having permeabilities as low as 10^{-7} to 10^{-9} md (Ehgartner & Tidwell, 2000; Beauheim and Roberts, 2002; Warren, 2007). Massive anhydrites (calcium sulphate; $CaSO_4$) also have low permeabilities in the region of 10^{-5} md (Beauheim and Roberts, 2002), and entry pressures for massive evaporite deposits are correspondingly high (Warren, 2007). Molecular diffusion of CO_2 through halite is also restricted, as the distance between NaCl lattice units is 2.8 x10^{-10} m (2.8 Å), while the molecular diameter of CO_2 is somewhat larger at 3.34 x10^{-10} m (3.34 Å).

A typical shale seal has a permeability of 10^{-1} to 10^{-5} md, with rare values as low as 10^{-8} (Warren, 2007). Shales tend to be water bearing, and typically have entry pressures that are lower than those of evaporites by a factor of 2-3 (Warren, 2007). Even though shales are respectable seals, over time shale can allow substantial diffusive leakage of methane and even liquid hydrocarbons via inherent microporosity (less so if the shales are organic rich), and could be expected to also allow diffusive leakage of CO_2.

4.1.2 Faulting & Fracturing

The caprock should ideally be unfaulted, as faults could provide migration pathways for the CO_2 to leak out of the reservoir. Thus, extensively faulted and fractured sedimentary basins are not good candidates for CO_2 storage, unless the faults and fractures are sealed (closed) and CO_2 injection will not reopen them (Bachu, 2005). It is this selection criterion that makes seismically active areas unattractive as potential storage targets (Bachu, 2005).

In some situations, for example in faulted halite layers, faults can become resealed, and therefore do not present a migration pathway. Other types of sealed faults also exist (e.g. clay or shale fault smears or gouges), and are indeed often responsible for the formation of structural traps. However, their sealing nature would need to be confirmed by detailed analysis to ensure the integrity of the storage site. In some instances, while the fault itself is effectively impermeable and sealed to lateral cross-fault flow, there may be a high permeability damage zone in the adjacent rocks that will act as a migration pathway through the top seal (e.g. CO_2 leakage in the northern Paradox Basin, Utah; Shipton et al., 2005). As highlighted by Fisher & Knipe (2001), there is a lack of definitive models to explain why in some circumstances faults act as conduits for fluids, whereas in others they form barriers. In an effort to improve understanding, these authors recommended the creation of a quality controlled database containing examples of how faults affect fluid flow in petroleum reservoirs, noting that ultimately any method developed to predict fluid flow properties of faults requires an understanding of the main controls on fault permeability (Fisher & Knipe, 2001).

The importance of faults as flow conduits can be simply illustrated by comparing flow through a rock with low permeability to flow through an unsealed fault or damage zone. Assuming Darcian flow (flow is directly proportional to permeability), then if we consider a rock unit 1 km in length on each side with a relatively low permeability of 10^{-8} md, and cut by a fault with a permeability of 1 md (low compared to a typical reservoir permeability of ~100-200 md), then that fault only has to be 10 μm wide for flow through the fault to equal flow through the entire rock unit (or looking at it another way, flow through a unit area of the fault will be 10^{8} times faster than flow through the rock).

With the probable exception of thick halite deposits, almost all potential caprocks will at some time in their burial history be subject to microfracturing and leakage – i.e. most reservoirs are inherently 'leaky'. In a study considering the world's giant oilfields, Macgregor (1996) concluded that on a geological timescale oil pools are dynamic short lived phenomena, where the median age of 350 giant oilfields is 35 Ma, and one third of these fields show evidence for post-entrapment destructive processes. Indeed, only 1 in 10 prospective hydrocarbon reservoirs (where geological surveys indicated the presence of potential source, reservoir and seal rocks) are found to actually contain petroleum reserves, suggesting that up to 90% have leaked over geological time (Deffeyes, 2005). In the present day petroleum leakage to the surface is thought to be occurring in roughly 50% of the 370 basins worldwide (both onshore and offshore) with known petroleum reserves (Clarke and Cleverly, 1991). Migration through faults also represents the principal mechanism that delivers CO_2 to the seafloor at natural CO_2 vent sites (see Chapter 3 and the summary of known vent sites provided in Appendix 3.A).

Further understanding of fluid and gas migration through fault zones can be obtained through the study of leaking systems as an analogue for failed storage reservoirs. To date, detailed studies on CO_2 migration pathways in natural systems have focused on the more readily accessible on land systems, such as the Paradox Basin in Utah (e.g. Shipton et al., 2005). Nevertheless, hydrocarbon migration from subseafloor storage reservoirs through the seal and overburden has been widely studied and can provide valuable information on potential pathways for CO_2 leakage. In particular, the identification of hydrocarbon leakage sites above a target storage reservoir (e.g. the presence of cold seeps, gas chimneys, pock marks or carbonate mounds) could signal the presence of flow paths through both the seal and overburden. Such a site should not be considered for CO_2 storage, unless it can be proven that the hydrocarbons originate from a different reservoir (e.g. if the target CO_2 storage reservoir underlies the hydrocarbon reserve and is separated from it by an intact seal).

4.1.3 Seal Thickness and Continuity

Theoretically, the thickness of a seal does not contribute to seal capacity. In reality, a bed only a few cm thick is unlikely to be laterally continuous unbroken unit capable of maintaining a stable lithic character over a sizeable area. Thus seal continuity rather than measured seal capacity (e.g. entry pressure) becomes the most important factor in assessing seal quality. Indeed, as noted by Warren (2007), average values of seal properties measured on discrete core samples are next to useless without a reliable geological model for the reservoir - what is needed is the knowledge of the likeliest weakest point in the seal across the structure of interest. A thicker seal provides many layers of contingent sealing beds and so gives a larger probability of a sealing surface being continuous over an entire target storage reservoir. In hydrocarbon exploration, shale seals more than 50m thick and evaporate seals more than 10m thick are considered adequate for hydrocarbon trapping, while evaporate seals more than 30m thick are considered excellent (Warren, 2007).

4.1.4 The Preferred Seal Type I - Halite Caprocks

Macgregor (1996) found the main controls on oilfield preservation to be post-entrapment tectonism and seal type, concluding that the potential for giant oilfields is the greatest in quiescent basins with evaporite seals. By the same token, the greatest potential for secure storage of CO_2 on geological timescales would also be in quiescent basins with evaporite seals (personal communication S. Hazledine & Z. Shipton).

Evaporite seals with their extremely high entry pressures, very low permeability, and large lateral extents can maintain seal integrity over wide areas even when exposed to a wide range of subsurface temperature and pressure conditions. Furthermore, unlike most other rock types, halite is ductile at relatively low temperatures and pressures and will flow under differential pressure at (geologically) rapid rates of up to meters per year. This not only gives halite a low susceptibility to fracturing, but even if a halite bed fractures, those fractures will quickly reanneal and crystal lattice binding will be reestablished by a combination of flow and pressure solution induced recrystallisation (Warren, 2007). Indeed, it would appear that the only way that CO_2 could migrate through an unfractured halite bed, even by diffusion, is if the halite contains impurities than render it locally porous and make it brittle during deformation.

The ability of evaporites to form highly efficient seals is clearly demonstrated by consideration of the number of hydrocarbon reserves that are sealed by evaporites. Even though evaporites constitute less than 2% of the worlds sedimentary rocks (compared to mudstones and shales which comprise 65%), 14 of the worlds 25 largest oil fields and 9 of the worlds 25 largest gas fields are sealed by evaporites (Grunau, 1987; Warren, 2007). The plastic self sealing properties of halite have also been exploited in salt cavern storage operations, where purpose made salt caverns (formed by dissolution mining of large salt deposits) have been used as hydrocarbon storage facilities and contaminated waste repositories for over 60 years (see for example the US Waste Isolation Project Plant www.wipp.energy.gov). Salt caverns have also been discussed as potential CO_2 sequestration sites (Dusseault et al., 2002; Shi & Durucan, 2005). A large body of literature regarding the self sealing behaviour of halite in relation to cavern closure is available – see for example the Bibliography for Cavern Abandonment compiled by the Solution Mining Research Institute (SMRI) and available at the Salt Cavern Information Centre at web.ead.anl.gov/saltcaverns/studies.

Despite the excellent properties of halite seals with respect to safety of CO_2 storage, they may not be widely utilized as storage reservoir caprocks due to economic driving forces (personal communication S. Haszledine). For example, the North Sea Basin contains a widespread Permian salt layer (the Zechstein Salt) which stretches from the East Coast of England to Northern Poland and reaches a depositional thickness of *c.* 1 km in the basin centre (salt tectonics in the North Sea Basin are discussed by Stewart, 2007). Indeed, this formation forms the seal of the K1-2B demonstration storage project in the North Sea. However, the Permian salt layer is overlain by other potential storage targets such as sandstone aquifers capped by mudrocks (e.g. the Triassic Bunder Sandstone in the southern North Sea). These shallower sites may well be utilized more widely for CO_2 storage, despite the better sealing qualities of the deeper salt layer, as the costs of storage would be significantly lower.

4.1.5 The Preferred Seal Type II - Multiple Confining Layers

The ideal storage reservoir would be overlain by multiple confining layers, where if primary leakage were to occur, the CO_2 would migrate vertically through the overburden and become trapped under a second confining layer (and so on).

The new CO_2 storage facility at the Snøhvit LNG Project (operated by Statoil) is an example of a storage reservoir overlain by multiple confining layers. The following summary of the Snøhvit storage project is after Maldal & Tappel (2004):

In the Snøhvit field, the main recoverable gas volume is located in the Stø Jurassic formation. This reserve is CO_2 rich, where CO_2 is separated from the well stream and re-injected into the subsurface. The target CO_2 storage reservoir is the Tubåen formation, which is located approximately 60m beneath the Stø formation and separated from it by the Nordmela 1 and 2 formations. The Tubåen formation is dominantly sandstone, with a formation thickness of 45-75m and is expected to store 23 Mt of CO_2 over the lifetime of the Snøhvit project. Nordmela 1 and especially Nordmela 2 contain extensive shale layers (25–30 m thickness of massive shale) providing barriers to vertical migration of CO_2. A CO_2 content of 5 mol% in an existing gas cap in the Tubåen formation, as well as proven gas reservoirs in the area with up to 80 mol% of CO_2, are strong indicators that CO_2 will be permanently sealed in this formation. Nevertheless, should leakage through the caprock occur, the CO_2 will enter the Stø formation from which it was initially extracted, i.e. it will remain separated from the ocean and atmosphere. Furthermore, primary leakage would be readily identified through an increase in the CO_2 content of the producing well streams.

4.1.6 Cautionary Note - The Importance of High Quality Seismic Surveys

Targeted discovery of a potential storage site must conduct a detailed seismic survey of the caprock seal, specifically a high resolution 3D seismic survey. The spatial resolution of traditional 2-D seismic techniques is on the order of 30m at reservoir depths of 3-4 km (at shallower depths resolution will be correspondingly better). This may well prove insufficient to resolve key features that are determinant in the performance of the caprock (personal communication, Z. Shipton & S. Haszeldine). For example, if a salt deposit is interbedded with permeable layers with thicknesses on the order of 10m, this would most likely appear as a continuous salt deposit in a 2-D seismic survey. Similarly, faulting where the fault throw is less than the seismic resolution would not be identified. Either of these scenarios (or a combination of the two) could result in the deposit being assessed as a suitable seal, where in fact low permeability flow paths are present. In comparison, 3-D seismics offer spatial resolution on the order of ~10m, and should provide sufficient resolution for correct caprock assessment.

4.2 Failure of the Caprock Seal

4.2.1 Mechanical Failure

The most likely way in which a shale or mudrock seal could fail is fracturing induced by a change in the pressure differential across the seal (personal communication, S. Haszledine).

The initial pressure in potential target storage reservoirs may vary widely, ranging from zero overpressure (hydrostatic pressure) to hard overpressured (up to 10s of MPa greater than hydrostatic, e.g. natural gas reservoirs). As a general guideline, CO_2 storage operations should not exceed the initial pressure of the reservoir, as this demonstrates a known pressure that the caprock is capable of withstanding. However, this constraint (a) may be hard to meet and (b) may not in itself ensure safe operating pressures are established.

Firstly, during pipeline transport and injection, CO_2 will likely be pressured to ~200 atm (20 MPa, 2000 dbar) to ensure the supercritical phase for ease of pumping. Secondly, storage in saline aquifers requires injection at pressures higher than the initial value to compress and displace water from the pore space (Katz and Tek, 1981). This overpressuring increases the risk of leakage to overlying strata and the surface. Indeed, leakage due to overpressuring has occurred in natural gas storage operations. For example, at the Leroy Aquifer natural gas storage facility in Wyoming, the initial pressure in the storage reservoir (sandstone aquifer in the Lower Thaynes Formation at a depth of 900m) was 10.3 MPa (~hydrostatic). When the reservoir pressure reached 12.6 MPa (22% overpressured with respect to the initial pressure) leakage of natural gas occurred, detected through the appearance of gas bubbling at a pond and creek over the storage reservoir site (Araktingi et al., 1984). After the initiation of leakage, although the rate of leakage could be controlled by limiting the maximum pressure in the reservoir, it could not be eliminated, with a loss rate on the order of 0.7% of the volume of gas injected per year (Araktingi et al., 1984). The relationship between reservoir pressure and leakage rate indicated hydraulic failure of the caprock seal through pressure induced faulting (Araktingi et al., 1984).

Depleted oil and gas reservoirs also pose some potential problems. Firstly, as the reserves are extracted water invasion can occur, and the reservoir becomes like an aquifer, requiring an overpressure to achieve injection. Secondly, in systems that are initially overpressured, the reservoir pressure decreases as the reserves are extracted. This decrease in reservoir pressure may damage the integrity of the caprock seal, potentially causing fracturing, particularly in the immediate vicinity of the bore hole. If a reservoir were then re-pressured to its initial virgin pressure (pressure prior to extraction), the seal could well prove to be 'leaky'. This potential weakening of caprocks represents a known unknown, and requires further investigation (personal communication, S. Hazledine). Precautionary measures should be taken. For example, although detailed characterization of the caprock was most likely carried out during exploration, all depleted reservoirs that are CO_2 storage targets should be resurveyed prior to injection. For reserves that are not depleted, an alternative (and attractive) strategy would be to initiate CO_2 storage via EOR or EGR in the early stages of reserve extraction. This would not only maintain reservoir pressure, but also maximise storage capacity by limiting water invasion (see discussion of storage capacity in Chapter 1). During injection, monitoring of micro-seismicity would alert the operator if faults or fractures were activated, and injection rates and pressures could be reduced accordingly (c.f. Hooper et al., 2005).

4.2.2 Chemical Interactions - Impacts on Seal Integrity

Chemical interactions between CO_2, formation water, the reservoir host rock and the caprock are potentially of importance to storage integrity and may impact the quality of the seal in a number of ways (e.g. Watson, 2004; Bentham & Kirby, 2005; van der Meer, 2005; Kharaka et al., 2006; Haszeldine et al., 2006; Busch et al., 2007).

As discussed in Chapter 3 (Section 3.2.3.2), supercritical CO_2 is a highly efficient solvent capable of extracting organic contaminants (e.g. petroleum hydrocarbons) and inorganic contaminants (e.g. heavy metals) from soils, sludge's and aqueous solutions. Furthermore, the solvent properties of supercritical CO_2 can be extensively modified by the addition of co-solvents resulting in a substantial increase in extraction efficiency. However, little (if anything) is yet known regarding interactions between supercritical CO_2 and storage formations, and this topic warrants further investigation.

While little is known regarding the direct impact of supercritical CO_2, more information is available regarding reactions involving CO_2 in the aqueous phase. Unlike hydrocarbons, CO_2 readily dissolves in water, where the circulation of CO_2-rich saline waters can lead to geochemical reactions with the surrounding rocks, resulting in either mineral dissolution or mineral precipitation. Dissolution usually yields an increase in porosity/permeability, while precipitation yields a decrease. Depending on where such reactions occur they can have either negative or positive effects with respect to storage integrity:

Potential Negative Consequences

1. Dehydration of the cap rock by reaction with the dry injected CO_2 (dry to minimise well corrosion issues and ensure hydrate is not formed), leading to shrinkage and the creation of new flow pathways for CO_2.

2. Corrosion of the reservoir rock matrix by CO_2/water mixtures, leading to the compaction or collapse of the formation and thus to the development of cracks and new migration paths through the cap rock.

3. Dissolution of components of the cap rock by CO_2/water mixtures, leading to its collapse or failure as a seal.

Potential Positive Consequences

4. Infilling of faults and fractures in the seal due to precipitation of secondary minerals

With respect to point 1 above, any reaction between CO_2 and a water bearing caprock could change the characteristics of the water and so change the impervious properties of the seal. This has led some authors to recommend that only gas fields where the original gas contained high CO_2 should be considered as target geological storage sites (e.g. van der Meer, 2005).

With respect to point 2, dissolution of minerals in the reservoir host rock could lead to an increase in storage capacity without resulting in failure of the caprock seal.

With respect to point 4, precipitation of carbonate minerals within the reservoir rock could also confer a positive benefit (mineral trapping), although a reduction of porosity and permeability due to mineral precipitation near to the injection well could yield technical problems during the injection of CO_2.

In addition (although not specifically seal failure), dissolution of CO_2 into the pore fluid and transport out of the structure by natural or induced pore fluid flow would also represent CO_2 leakage (Bentham & Kirby, 2005).

Understanding how CO_2 potentially affects reservoir and seal rocks is therefore a crucial component of successful long term containment of injected CO_2 (Watson, 2004). The reactions that may occur are dependant on geochemical and physical conditions such as the composition of the formation water, pH, redox status, mineralogy and texture of the formation rock and caprock, temperature, pressure, fluid flow rates, and the timing of the reactions (e.g. Bentham & Kirby, 2005; van der Meer, 2005). They are therefore highly site specific, and within a specific storage site are likely to vary both spatially (according to the exact mineralogy and petrography of the reservoir and seal) and temporally.

Information on potential chemical reactions can be obtained by studying natural analogues (e.g. CO_2 rich reservoirs), monitoring reactions in current storage projects, and carrying out laboratory experiments on mineral samples (preferably samples of specific reservoir and seal rocks). It should be noted that a number of reactions are likely to occur on very long timescales, thus monitoring and laboratory experiments are inherently limited in the data they can provide, and long timescale interactions can only be directly investigated through evaluation of natural analogues. Nevertheless, all of these sources of information can be used to refine predictive geochemical models of CO_2-water-rock interactions. At present, such models are somewhat inadequate, where predicted mineral assemblages in CO_2 altered rocks do not match with observations (e.g. Haszeldine et al., 2005).

The potential interactions that are likely of most importance with respect to CO_2 storage security are reactions with carbonates (either in the reservoir or seal) and shale or mudrock seals. These are discussed further below.

4.2.2.1 Reaction with Carbonates

Possible reservoir storage formations include limestones, chalks and carbonate-cemented sandstones. In addition, some hydrocarbon caprocks include carbonate materials (see Figure 4.1). Czernichowski-Lauriol et al. (1996) made the following generalisations regarding reaction of aqueous CO_2 with carbonate reservoir rocks (see also the discussion of carbonate dissolution in the overburden in Chapter 5):

In areas where the CO_2 pressure is high, carbonate will dissolve and the formation water will become saturated with CO_2. The carbonate may reprecipitate if the pressure falls or the temperature rises[6], for example in areas further from the well. Because of this local dissolution, the porosity and the permeability will increase near the injection point, but can decrease further along the flow path because of carbonate precipitation.

This dissolution of carbonate can have a negative impact on storage integrity through multiple mechanisms. Firstly, dissolution of seal carbonate could open high permeability flow channels through the seal, or indeed lead to seal compaction and structural collapse. Similarly, dissolution of reservoir carbonate may lead to reservoir compaction, potentially also resulting in seal collapse and failure.

---

[6] Note that calcite ($CaCO_3$), the most common carbonate mineral in sedimentary rocks, exhibits retrograde solubility, becoming less soluble as the temperature increases.

Based on experimental observations, Kharaka et al. (2006) highlight that rapid dissolution of carbonate (and other minerals) could ultimately create leakage pathways in reservoir seals. The Frio CO_2 Test Injection Site on the U.S. Gulf Coast is an on land facility designed to investigate the potential for CO_2 storage in saline aquifers and to achieve experience in CO_2 storage and monitoring operations. As such it is a valuable source of information regarding early stage reactions between CO_2 and the reservoir rocks. Following injection of a relatively small volume (1600 t) of CO_2 into a Frio Formation sandstone (1500 m depth), the chemical composition of the formation water was shown to change markedly (Kharaka et al., 2006). Comparison of water chemistry from before and after CO_2 injection showed sharp drops in pH (from 6.5 to 5.7) and pronounced increases in alkalinity (from 100 to 3000 mg/dm^3 as HCO_3) and Fe (from 30 to 1100 mg/dm^3). Geochemical modeling indicated that brine pH would have dropped lower but for buffering by dissolution of carbonate and iron oxyhydroxides.

Liteanu et al., (2007) highlight the potential for reservoir compaction leading to collapse. They note that in addition to minor dissolution effects, modelling work has suggested that CO_2 injection into carbonate can enhance compaction creep by 7 orders of magnitude due to acidification of the pore fluid. They therefore carried out an experimental study of compaction in carbonates in order to provide essential data to inform models of the long term behaviour of carbonate reservoirs. The results demonstrated that compaction of calcite in the presence of water is dependent on grain size, applied stress and the pH of the solution, where injection of CO_2 into the system increased compaction rates by up to 3 orders of magnitude.

In summary, the propensity of CO_2 rich aqueous solutions to dissolve carbonate minerals, in addition to predicted and observed increases in the rate of carbonate compaction as a function of pH and CO_2 content, strongly suggests that both carbonate reservoir formations and caprocks should be avoided.

4.2.2.2 Reaction with Shales & Mudstones

Shales and mudstones seem likely to comprise the dominant form of seal in offshore CO_2 storage operations. Indeed, all of the commercial scale projects currently in operation or at the advanced planning stage (Sleipner, Snøhvit, Gorgon, see Chapter 1) are sealed by shales or mudstones, while the smaller K1-2B demonstration project is sealed by the Zechstein Salt. Furthermore, there are numerous known CO_2 rich (or indeed CO_2 dominant) reservoirs that are sealed by shales and mudrocks. Such reservoirs provide (a) surety that CO_2 can be safely stored in these systems and (b) valuable analogues for studying CO_2 – caprock interactions.

The Miller oilfield in the North Sea may form the first offshore CO_2 storage site located in UK waters (see Chapter 1). This field is CO_2 rich, with ~20 mol% CO_2 in the oil phase and 60-70 mol% in the water phase (representing equilibrium partitioning). Haszeldine et al. (2006) report an investigation of long-timescale interactions between CO_2 and the mudrock seal of the Miller oilfield. These authors examined mudrock samples from a number of oilfield wells and compared them to mudrocks from the same stratigraphic level obtained from a well bore located some 20 km distant in an area with 'normal' CO_2 levels (<5 mol% in water). While the control bore hole showed no evidence for vertical changes in mudrock mineralogy, some of the oilfield samples were depleted in feldspar, and enriched in kaolin and calcite, which could be due to the CO_2 induced reaction of feldspar to kaolin and calcite.

Another storage project due to start injecting in the near future (this time on-shore) will also be utilising a caprock known to be capable of retaining CO_2. The Otway Basin Pilot Project in Australia will inject CO_2 into the depleted Naylor Gas Field (for more information see www.co2crc.com.au/pilot/OBPP.html). The target reservoir is the Late Cretaceous Waarre C Sandstone at a depth of about 2100 m, which is overlain and sealed by the Belfast Mudstone. The Belfast Mudstone forms a regional seal, and indeed comprises the main seal for natural CO_2 accumulations in the Otway Basin. In a fractured form, it is also the reservoir rock at the Pine Lodge Gas Field, which comprises 97% CO_2 of volcanic origin (Watson et al., 2004). Watson et al., (2004) investigated the effects of CO_2 on the lithology of the Belfast Mudstone using core samples and well data from a Pine Lodge exploration well. These authors report substantial CO_2 – seal rock interaction, with alteration of feldspar, clays, and volcanic fragments. Overall, they found that precipitation of CO_2 in the form of siderite (iron carbonate, $FeCO_3$) has enhanced the capacity of the seal, where capacity enhancement correlated with the original (pre-CO_2 influx) porosity and permeability of the rock. This indicates that CO_2 influx migrated predominantly to the natural fractures present in the mudstone, and only infiltrated a small way into the low permeable units proximal to the fractures. Dissolution – precipitation reactions generated through CO_2 – brine – rock interactions then led to siderite cement filling fractures and all available pore space near facture edges. Watson et al. (2004) highlight that enhancement of seal capacity only occurred due to the availability of Fe^{2+} cations (most likely sourced from Fe rich volcanogenic fragments) for siderite precipitation. They note that labile mineral dissolution (i.e. feldspar, calcite) could also lead to a decrease in seal capacity in the absence of appropriate cations for secondary mineral formation.

As noted above, shales could be expected to allow diffusive leakage of CO_2, although this process will be slow in comparison to flow through porous faults and fractures. Busch et al. (2007) measured molecular diffusion of CO_2 in water saturated shales, reporting effective diffusion coefficients between 10^{-9} and 10^{-11} m^2/s. These values agree with those reported for other pelitic rocks by Hildenbrand & Kroos (2003), who concluded that diffusive transport is not an important process for CO_2 leakage, even on geological timescales, although these authors also noted that diffusion does represent a rate controlling factor in the deterioration of caprocks and cements. Busch et al. (2007) also investigated the sorptive storage potential of shales, reporting capacities up to 0.14 mmol CO_2/g sample, significantly higher than the solubility of CO_2 in water present in the system. The large capacities were not solely related to organic carbon content, with significant sorption to clay minerals such as montmorillonite and kaolinite also observed. Thus in addition to their sealing properties, natural non-sealing shale sequences within a storage reservoir could represent a sink for CO_2 deposited in the subsurface by fixing and immobilising it, hence reducing the risk of leakage to the surface (Busch et al., 2007).

4.3 Leakage via Wellbores

In addition to leakage of CO_2 from reservoirs via the 'natural' pathways discussed above, potential release via wellbores must also be considered. There are two principal ways in which wellbore leakage can occur. The first is catastrophic well failure, or blowout, resulting in the rapid release of large volumes of CO_2 to the atmosphere. The second is leakage or seepage of CO_2 along high permeability channels associated with the wellbore, delivering CO_2 to higher stratigraphic levels, and potentially delivering CO_2 to the seafloor or the ocean surface. Indeed, while the probabilities of catastrophic release are slight, the migration of CO_2 along preferential pathways associated with the wellbore is widely accepted to be the most likely mode of leakage or seepage of CO_2 from a geological storage reservoir.

4.3.1 Well Blowout

A well blowout is the uncontrolled flow of reservoir fluids into the wellbore, and sometimes catastrophically to the surface. If reservoir fluids flow into another formation and do not flow to the surface, the result is called an underground blowout. In this case, if the wellbore has significant openhole intervals, it is possible that the well will bridge over downhole (seal itself with rock fragments from collapsing formations). However, in the event of catastrophic failure, large volumes of CO_2 would be released directly to the atmosphere. Due to the possibility of severe accidents, the main concern in the event of blowout must be the hazard to workers in the vicinity of the release (both at the time of blowout and during remediation).

The likelihood of well blowout can be assessed from offshore Oil & Gas experience through the use of an analogue database from which the relative frequency, duration, and magnitude of well releases for a given well category can be ascertained. Combining this with the number and type of wells in the storage reservoir then allows a site specific risk of blowout to be estimated (e.g. FutureGen, 2007). Commercial databases (restricted access) are available to the industry sector, such as the SINTEF Offshore Blowout Database which includes information on 515 offshore blowouts and well releases that have occurred world-wide since 1955 (see www.sintef.no for more details). Table 4.1 shows the mean well blowout frequency from North Sea and US Offshore Oil & Gas experience (after Holland, 1997). The frequency of production well blowout is low, at 1 event every 16,000-20,000 well-years, with slightly higher frequencies of blowout in the US during well workover (repair and maintenance). Blowout frequency during drilling suggests 1 event for every 150-600 wells drilled. While these frequencies indicate that the likelihood of catastrophic well blow-outs is exceedingly slight, the eventuality that stored CO_2 escapes rapidly in great amounts at once cannot be completely neglected.

Table 4.1: Offshore well blowout frequency - Oil & Gas experience (after Holland, 1997)

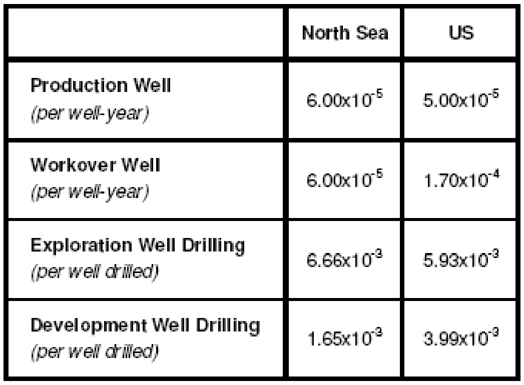

	North Sea	US
Production Well *(per well-year)*	6.00×10^{-5}	5.00×10^{-5}
Workover Well *(per well-year)*	6.00×10^{-5}	1.70×10^{-4}
Exploration Well Drilling *(per well drilled)*	6.66×10^{-3}	5.93×10^{-3}
Development Well Drilling *(per well drilled)*	1.65×10^{-3}	3.99×10^{-3}

In the event of blowout, the maximum rate at which CO_2 will vent to the atmosphere is constrained by choked flow through the well bore. For an ideal gas, the mass flow rate under choked flow is given by[7]:

$$Q_{CO_2} = CA\sqrt{\gamma_{CO_2}\rho_{CO_2}P_{CO_2}\left(\frac{2}{\gamma_{CO_2}+1}\right)^{\left(\frac{\gamma_{CO_2}+1}{\gamma_{CO_2}-1}\right)}} \qquad \textbf{[Eq. 4.1]}$$

Where

$$\gamma_{CO_2} = \frac{C_{p(CO_2)}}{C_{v(CO_2)}} \qquad \textbf{[Eq. 4.2]}$$

Where Q_{CO2} is the mass flow rate of CO_2 (kg/s), C is the discharge coefficient for the orifice (typical values are near 1), A is the cross sectional area of the orifice (m^2), γ_{CO2} is the specific heat ratio (the specific heat capacity of CO_2 at constant pressure divided by the specific heat capacity of CO_2 at constant volume, $C_{p(CO2)}/C_{v(CO2)}$, 1.308 at STP), ρ_{CO2} is the density of CO_2 (kg/m^3), and P_{CO2} is the pressure of CO_2 in the wellbore (Pa).

CO_2 will continue to flow at this maximum rate while pressure in the wellbore meets the pressure criterion:

$$P_{CO_2} \geq P_{atm}\left(\frac{\gamma_{CO_2}+1}{2}\right)^{\left(\frac{\gamma_{CO_2}}{\gamma_{CO_2}-1}\right)} \qquad \textbf{[Eq. 4.3]}$$

For example, for γ_{CO2} of 1.308, choked flow will continue while P_{CO2} is more than 1.84 times higher than atmospheric pressure (P_{atm}). Thus in the case of storage in an overpressured reservoir, choked flow could be expected to continue until the wellbore is controlled.

---

[7] Note: As CO_2 is a non-ideal gas this equation provides an approximation for the mass flow rate under choked flow. For an accurate description of CO_2 mass flow rates real gas effects such as compressibility and variable specific heats need to be taken into account, where these effects can make a significant difference to the mass flow rate. Nevertheless, this equation allows an order of magnitude calculation to be made for illustrative purposes.

Although the rate of CO_2 release is very fast in the event of blowout, such events are readily detected (primarily due to the rapid rate of release) and remedial action is possible, where Offshore Oil and Gas experience indicates that the typical duration of a high release event (time from blowout to control) ranges from 0.5 to 5 days (Holland, 1997; average duration for all North Sea and US well blowouts). The total amount of CO_2 likely to be released in the event of a catastrophic blowout can be estimated from the mass flow rate and the duration of the leakage event. For a simple illustration, Figure 4.2 shows the mass flow rate of CO_2 assuming choked flow at typical injection conditions (T=35°C, P=15-20 MPa) as a function of wellbore diameter. If it is assumed that pressure in the wellbore does not decrease significantly over time, then for a wellbore diameter of ~10cm approximately 50 ktCO_2 would be released per day.

Figure 4.2: CO_2 release rate under choked flow conditions.

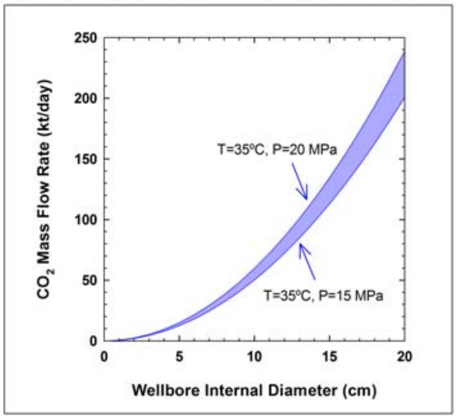

4.3.2 Leakage or Seepage along a Wellbore

As noted above, existing well penetrations represent the most likely pathway for CO_2 migration out of the storage reservoir. When CO_2 dissolves in water it creates an acidic environment that is detrimental to the long term integrity of both cement and casings (e.g. Davis & McDonald, 2005; Scherer et al., 2005). Over time, cement degradation and casing corrosion could create preferential channels for CO_2 migration. In addition, there may be formation damage due to drilling of the well, and wells may be poorly completed, with poor bonding between the cement and formation or cement and casing, contaminated cement, or the absence of cement altogether (e.g. Watson et al., 2002). Potential leakage pathways along an individual wellbore include (see Figure 4.3):

- through damage zones in the formation immediately adjacent to the wellbore
- between the cement sheath and the formation
- between the cement sheath and the casing
- through the cement (sheath and plug)
- through corroded casing
- through fractures in the cement or regions without cement

Figure 4.3: Potential CO_2 leakage pathways via wellbores (after Celia et al., 2004).

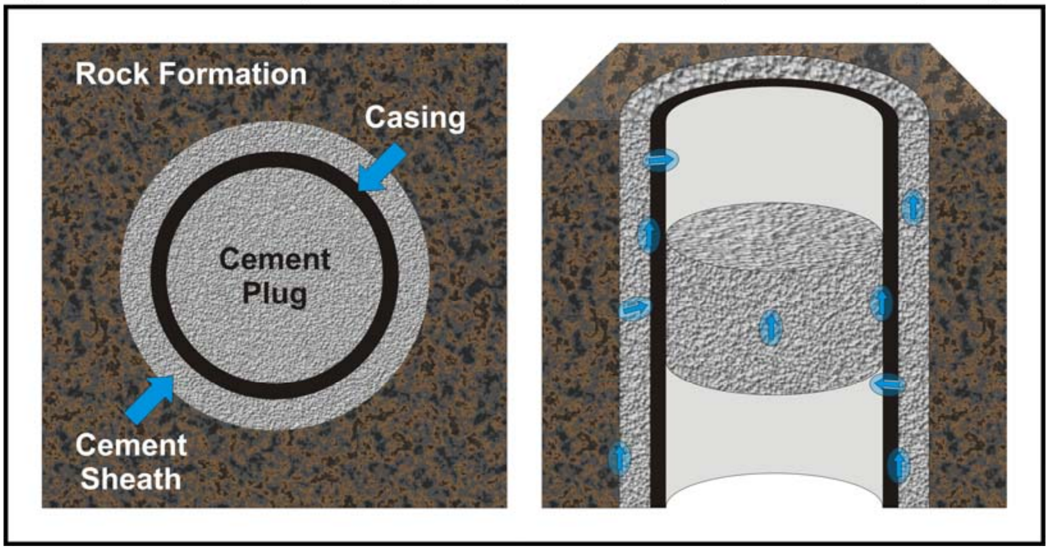

Any wellbore within the spatial footprint of the storage reservoir may act as a conduit for leakage. This includes wells that penetrate either deeper or shallower strata than the target storage reservoir, abandoned wells, exploration wells, producing wells, and the CO_2 injection wells themselves. In the case of leakage up an improperly abandoned wellbore, the CO_2 could leak through a corroded casing wall and travel upward through the casing to the surface. This represents a potential escape route that not only breaches the seal, but also the overburden, thereby bypassing any potential secondary trapping mechanisms that may act in the overburden (see Chapter 5). Alternatively, migration outside the casing could deliver CO_2 into shallower formations, which may eventually release CO_2 to the sediment-seawater interface. Similarly, in the case of leakage up a poorly sealed or failed injection well casing, the CO_2 could leak out the well through a corroded casing wall travel upward outside the casing or migrate into adjacent formations, again potentially reaching the seafloor.

The principal control on the actual migration path is the distribution of high and low permeability segments both along a single well and between different wells (Celia et al., 2006). For example, CO_2 may migrate out of the storage formation along one wellbore, then migrate laterally through a permeable formation and find another flow path along a second wellbore to the sediment-seawater interface. While intact cements have low permeability (~10^{-5} md), degraded cements will have significantly increased permeability, and an annular opening (a ring shaped gap) around 1mm wide between the rock and the cement sheath (due to poor bonding) has an effective permeability on the order of 100 d (10^5 md) (Celia et al., 2004). Furthermore, at the 10s of cm scale there could be large pockets with no cement between the formation and the casing.

4.3.3 Relative Risk of Leakage along Different Wellbore Types

Decommissioned wellbores are the most likely to have high permeability segments along the wellbore, and therefore the probability of leakage is highest along these wells. Specifically, the highest probabilities of leakage are associated with:

- Undocumented Wells
- Poorly Constructed &/or Improperly Abandoned Deep Wells (penetrates primary seal)
- Poorly Constructed &/or Improperly Abandoned Shallow Wells (above primary seal)

In comparison, the likelihood of leakage along currently producing wells is expected to be lower, and the lowest probability of leakage is associated with the CO_2 injection wells themselves.

4.3.3.1 Undocumented Wells & House Keeping Records

Undocumented wells represent the highest risk of leakage as no remedial action can be taken to ensure seal and plug integrity prior to CO_2 injection. Furthermore, should leakage along an undocumented wellbore occur, it is highly unlikely to be detected. Thus to determine the overall likelihood of leakage from a storage reservoir an assessment of the number of undocumented wells within the plume footprint will need to be made.

For the North Sea, the number of undocumented wells is expected to be low, if not zero, as house keeping records are understood to be excellent. In areas where records are not as good, a judgement will have to be made using information based on historical exploration in the area (c.f. FutureGen, 2007).

In all cases, care should be taken both to preserve and catalogue existing documentation of drilling activities, and to ensure excellent records are kept and maintained in the future. Indeed, a continuously updated record of storage sites, including wellbore characteristics, monitoring and repair activities, can be considered vital to the long term success and stewardship of storage projects. Given the importance of such records, and the need to preserve them over long timescales (1000+ years) it seems sensible to suggest they should be lodged with a regulatory body (be it national or international).

4.3.3.2 Decommissioned Wells & Abandonment Procedures

At present there are no specific abandonment procedures for 'CO_2' wells (defined here as any well that falls within the footprint of a target CO_2 storage reservoir), and a review and adaptation of standard plugging-and-abandonment (P&A) procedures is required to ensure that both sheaths and plugs are fit for purpose (e.g. Barlet-Gouédard et al., 2006).

At abandonment, the well is typically sealed by a cement plug. For the vast majority of abandoned wells, CO_2 injection would not have been contemplated at the time of decommissioning. Thus inappropriate decommissioning of wells (e.g. insufficient plug) seems likely to be a widespread problem (Barlet-Gouédard et al., 2006). For all 'CO_2' wells, an assessment should be made of the location, thickness and material (e.g. type of cement) of the plug and casing sheath, and the likely continuity of the sheath. If required, remedial action can be taken prior to CO_2 injection, where documented wellbores can be re-entered and re-plugged. Barlet-Gouédard et al., (2006) suggest that if deemed necessary by the criticality of the plug, the casing and cement can be milled all the way to the storage formation before placing a cement plug directly in contact with the formation. Ideally, all 'CO_2' wells should be resealed using chemically resistant cements (see Section 4.3.3.5 below). However, given the expense of this procedure it seems more likely that existing wells with intact Portland cement seals will be monitored for leakage during storage operations, and if leakage is detected, then the wellbore will be re-entered and resealed (see for example the Gorgon project risk assessment, ChevronTexaco Australia Pty Ltd., 2005).

4.3.3.3 Current Wells & CO_2 Injection Wells

For current producing or exploration wells that penetrate a potential future CO_2 storage reservoir, there exists an opportunity while the wells remain accessible to ensure that both the plug and casing sheath are of sufficient quality for CO_2 storage purposes. For example, for a well that will continue to produce during CO_2 storage operations (e.g. via EOR, or if it penetrates a hydrocarbon reservoir that either over or underlies the storage reservoir) an assessment should be made of the quality of the sheath prior to CO_2 injection, and remedial action taken if necessary. Likewise, for a well that is to be decommissioned, the sheath should be checked (or the casing removed altogether) prior to plugging.

As CO_2 injection wells will be specifically engineered and constructed to withstand the corrosive conditions in the storage reservoir (e.g. using chemically resistant cements), these wells can reasonably be considered to represent the lowest risk of leakage.

4.3.3.4 Other Drill Holes

In addition to Offshore Oil & Gas operations, there may be other drill holes located in a target storage reservoir. For example, the Integrated Ocean Drilling Program (previously the Deep Sea Drilling Program, then the Ocean Drilling Program) is an international research program that explores the history and structure of the earth as recorded in seafloor sediments and rocks. These scientific drilling programs have now cored seafloor sediments and rocks at over 1300 sites. While the majority of drill holes at these sites only extend a few hundred metres into the overburden, 28% have drill holes that extend beyond 500m, and 5% have drill holes that extend beyond 1000m. While the likelihood of a deep DSDP/ODP/IODP drill hole occurring within the footprint of a target storage reservoir is low, it should nevertheless be checked.

4.3.3.5 Cement Integrity

Traditionally wells have been sealed (both sheaths and plugs) with standard Portland cement, a material that is inherently unstable with respect to reactions with CO_2. New materials are now becoming available that offer either flexibility and expansion (lightweight or foam cements, of benefit to ensure good cement distribution in horizontal or deviated wells) or long term durability to CO_2 attack (chemically resistant cements). Data is needed on the long-term integrity of these materials when exposed to a CO_2-rich environment. At the decade scale, this can be obtained either by studying the condition of cement seals that are known to have been exposed to CO_2 over a given period of time (e.g. Carey et al., 2006), or by carrying out laboratory testing, and using data obtained over a comparatively short period to extrapolate to long term seal performance (e.g. Barlet-Gouédard et al., 2006).

Carey et al. (2006) investigated the impact of CO_2-cement interactions on wellbore samples from the world's second oldest continuous CO_2-flooding operation, the SACROC unit, located in the Permian Basin of West Texas. The SCAROC unit is a limestone oil reservoir with a shale caprock. Samples were analysed from a region extending from the limestone-shale contact, to 6m above the reservoir, where the well from which samples were taken was drilled and cemented in 1950 (using an additive-free Portland type 1 cement) and first exposed to CO_2 in 1975. The analytical results (structural integrity, permeability, and petrography) indicate that the cement retained its capacity to prevent significant flux through the cement matrix itself. However, significant carbonate precipitation was observed at both the interface between the shale caprock and the cement, and between the casing and cement, indicating migration of CO_2 along the shale-cement and casing-cement interfaces. The origin of the CO_2 at the casing-cement interface may have been derived by migration along this interface from the reservoir or from the interior of the well at casing joints or regions of casing corrosion (Carey et al., 2006). Carey et al. (2006) therefore concluded that the integrity of these interfaces appears to be the most critical issue in wellbore performance for CO_2 sequestration (Carey et al., 2006).

In a laboratory study, Barlet-Gouédard et al. (2006) tested the integrity of Portland cement and a new resistant cement with respect to both CO_2 saturated aqueous fluid and wet supercritical

CO_2. They conducted their experiments over a range of temperatures and pressures that encompass expected in-situ conditions (T = 30-300°C, P = 1-50 MPa) with experiment durations ranging from 2 days to 3 months. The evolution of the cement chemical composition and porosity with time was fully characterized by scanning electron microscopy, chemical analyses, backscattered electron image analysis and Hg-porosimetry measurements (Barlet-Gouédard et al., 2006). The alteration observed was then used to create a predictive model of cement integrity over longer time periods. They found that Portland cement was not mechanically resistant to either wet supercritical CO_2 or to CO_2-saturated water, where an initial sealing by carbonation is followed by a dissolution stage, which starts earlier in CO_2-saturated water than in wet supercritical CO_2. The model predicts an alteration front of 100 mm after 20 years of CO_2-attack possibly, potentially destroying zonal isolation and triggering casing corrosion. In contrast, the CO_2 resistant cement was found to be comparably inert, where the good stability of this material was confirmed by weight, density, compressive strength, microstructural characterizations and Hg porosity measurements.

The differences between these two studies, with the laboratory tests indicating Portland cement failure after a period of 20 years, and the SACROC data indicating the cement itself had maintained its integrity over a period of 30 years, will reflect a number of different parameters, the most obvious of which will be CO_2-water-cement ratio (e.g. a cement plug completely immersed in either wet supercritical CO_2 or to CO_2-saturated water versus a cement plug where supply of CO_2 is limited by migration). Nevertheless, the laboratory study indicates that carbonation does not continuously plug Portland cement, suggesting that the SACROC cement can be expected to deteriorate further over time. Given the requirement for secure storage over 1000+ years, all new wells and any remedial measures taken to reseal existing wells should utilise chemically resistant cements.

4.3.3.6 Site Screening

The existence of multiple known wellbores and/or a high possibility of multiple undocumented wells may render a site unsuitable for storage purposes (i.e. if the cumulative probability of leakage along wellbores is deemed too high, or if costs of any required remedial action outweighs any economic benefits associated with that site).

Based on analysis of documented wellbore leakage in Alberta Canada, a mature on-shore sedimentary basin with a statistically significant number of wells (over 300,000), Bachu et al. (2006) recommended that risk assessments should be based on the following criteria:

- Well age
- Well status (active, inactive, abandoned)
- Well casing, or lack thereof
- Well direction (vertical, deviated, horizontal)
- Cementing intervals
- Level of drilling activity
- Global and local events that may have affected drilling practices
- Regulations and their timeline of being introduced.

While offshore basins do not generally face the same level of difficulties as onshore basins in North America (e.g. generally lower drilling densities), these criteria seem equally valid for preliminary screening of offshore storage sites. In the absence of hard data, the categorisation of wells according to this scheme, combined with the use of an analogue database, would allow a preliminary assessment of the likely distribution of permeability along the wellbores that fall within the footprint of the storage reservoir.

If the permeability distribution along all wellbores is known, then potential leakage pathways and rates can readily be determined using computationally fast semi-analytical models (e.g. Celia et al., 2006). The use of such a model at the site selection stage would allow identification of any critical wellbores that require remedial action prior to CO_2 injection.

As an illustrative example, Figure 4.4 shows a simulated permeability distribution for 1000 segments along wellbore casings. This example assumes a log-normal distribution for two classes of cement segments (1) intact cement segments with a mean permeability κ_1 of 10^{-5} md and a variance (σ^2) of var[$\log_{10}\kappa_1$]=1^2 and (2) degraded or poorly bonded cement segments with a mean permeability κ_2 of 0.1 md and a variance of var[$\log_{10}\kappa_2$]=2^2 (after Celia et al., 2006). In the example shown in Figure 4.4(a) a 1:1 ratio of intact to degraded segments is assumed. Figure 4.4(b) shows the cumulative permeability distribution for varying proportions of intact to degraded segments. If we compare these permeability distributions to caprock permeabilities, the following becomes apparent: All well segments (even when 100% intact segments) are more permeable than the best evaporite seals (halite, 10^{-8} to 10^{-9} md). A significant proportion of well segments will be more permeable than the poorest quality shale seals (~10^{-1} md), where as the proportion of degraded segments increases from 25% to 50% to 75%, the number of segments with relatively high permeability (≥0.1 md) increases from 12.5% to 25% to 37.5%.

Figure 4.4: (a) Permeabiity distribution for 1:1 ratio of intact to degraded cement segments (b) Cumulative permeability distribution for varying proportions of intact to degraded cement segments (after Celia et al., 2006).

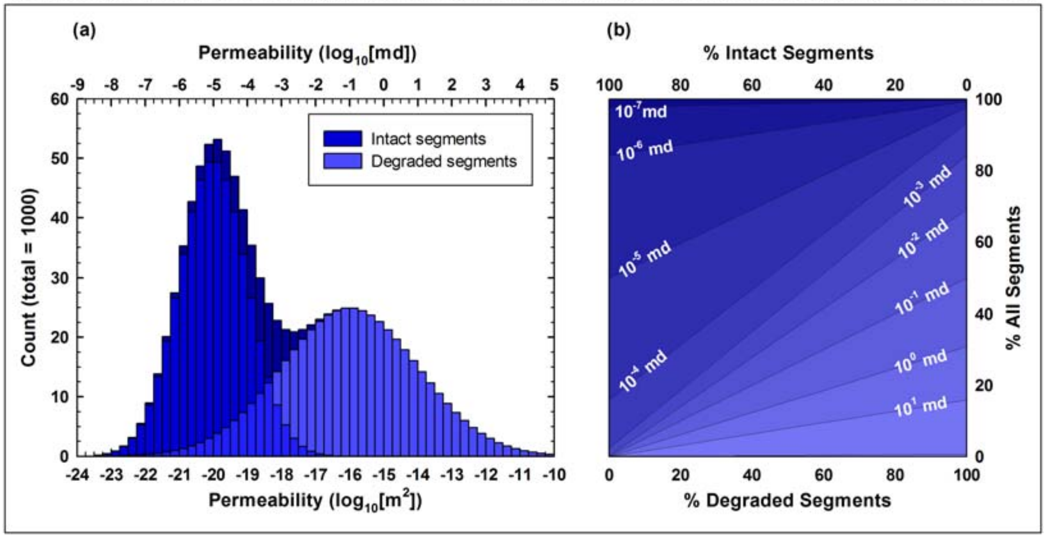

4.3.3.7 *Well Monitoring & Repair*

Evaluating and monitoring the integrity over time of steel casings and cement sheaths and plugs is of the utmost importance for the long term security of CO_2 storage.

In CO_2 injection wells, and other active wells in the footprint of the storage reservoir, well integrity should be regularly checked across the injection interval, the cap rock and shallower zones (Barlet-Gouédard et al., 2006). Over the past 20-30 years there has been considerable improvement in the tools available for this task, and in active wells it is possible to assess the integrity of both the steel casing and the sealing material in the annulus behind the casing (see review by Vu-Hoang et al., 2006). For example, modern tools such as the Isolation Scanner and Sonic Scanner enable both identification of channelling and examination of the full cement sheath between the casing and formation, with high vertical and azimuthal resolution, thus providing the ability to create a detailed Cement Bond Log (Vu-Hoang et al., 2006). In addition, casing corrosion can be evaluated by combining electromagnetic and ultrasonic measurements of the metal thickness (Vu-Hoang et al., 2006).

However, as these techniques require passing the measurement instrument down the wellbore (wireline logging), they cannot be readily employed on decommissioned wells. Monitoring the integrity of abandoned wells thus requires more attention, and new research on appropriate monitoring techniques will most likely be required. Methods for monitoring these aspects are currently under investigation within the Carbon Dioxide Capture project (www.co2captureproject.org/), the results of which are not yet publicly available.

Adequate remedial operations must also be concurrently developed to re-establish zonal isolation when a potential leakage path has been detected. For instance, squeeze jobs will allow repair of any faulty primary cement job (Barlet-Gouédard et al., 2006).

4.3.3 Scale & Duration of Leakage along Wellbores

The potential scale of leakage along wellbores ranges from relatively slow migration through a high permeability pathway, to faster flow along an annulus or via surface casing vent flow, to rapid release due to well blowout. Based on expert opinion, a number of risk assessments for on-shore geological storage sites have estimated probable slow leakage rates on the order of ~200 tCO_2/yr (e.g. Hooper et al., 2005; FutureGen, 2007). Release of CO_2 at such low rates (~6 gCO_2/s) is likely to go undetected, and could therefore remain active for long periods of time (in excess of 1000 years). Conversely, rapid release (at rates in excess of 10,000 tCO_2/yr, or over 300 gCO_2/s) due to well blowout, can be assumed to be detected and mitigated, and therefore be active for short periods only (e.g. 0.5 to 5 days).

4.4 Summary

The relative likelihood of leakage or seepage via the different mechanisms discussed in this Chapter is summarised in Figure 4.5. This assessment is based on published risk assessments for geological CO_2 storage projects (ChevronTexaco Australia Pty Ltd., 2005; Hooper, 2005; FutureGen, 2007), and represents a general case, where site specific criteria may result in a different assessment of the probability of leakage or indeed a re-ordering of the likelihood of leakage via the various different mechanisms.

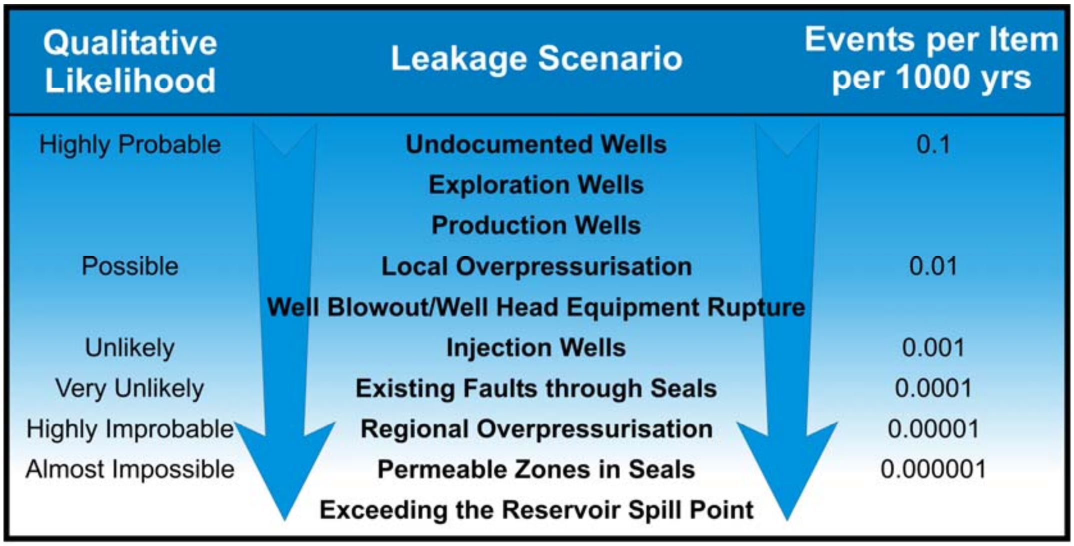

Qualitative Likelihood	Leakage Scenario	Events per Item per 1000 yrs
Highly Probable	Undocumented Wells	0.1
	Exploration Wells	
	Production Wells	
Possible	Local Overpressurisation	0.01
	Well Blowout/Well Head Equipment Rupture	
Unlikely	Injection Wells	0.001
Very Unlikely	Existing Faults through Seals	0.0001
Highly Improbable	Regional Overpressurisation	0.00001
Almost Impossible	Permeable Zones in Seals	0.000001
	Exceeding the Reservoir Spill Point	

Figure 4.5: Qualitative likelihood of leakage via different mechanisms and probability of a leakage event occurring per item per 1000 years.

The low probability of leakage or seepage via existing faults through seals or via permeable zones in seals assumes an appropriate storage reservoir has been selected, i.e. the presence of a laterally continuous low permeability caprock has been confirmed by a 3-D seismic grid over the entire footprint of the storage reservoir, and that therefore the probability of faults or high permeability zones remaining undetected is minimal. Similarly, the leakage of CO_2 along faults or fractures activated due to regional scale overpressurisation is considered to be low if (and only if) an appropriate storage reservoir is selected (i.e. the presence of faults that may be reactivated by the pressure required for injection should automatically disqualify a site from CO_2 storage activities). Should leakage occur via any of these mechanisms, the loss rate is expected to be low (<10 tCO_2/yr). Leakage at such low rates is unlikely to be detected, and can be expected to continue over the life of the storage reservoir. If we consider a storage reservoir with

50 years of injection at a rate of ~1MtCO_2/yr, this would be equivalent to a percentage loss rate of less than 0.00002% per year, where 99.8% of the stored CO_2 would remain trapped after 10,000 years of leakage, thus meeting storage performance targets (retention of greater than 99% CO_2 over a period of at least 1,000 years).

The possibility of fault activation due to earthquake activity should also be assessed, and in tectonically active areas this could be significant. The approach taken in other risk assessments is to evaluate the frequency of magnitude 5 earthquakes occurring in the area of the storage reservoir (e.g. Hooper et al., 2005). In the instance of earthquake induced faulting, initially high loss rates (~1000 tCO_2/yr) might be expected during the earthquake, but once the earthquake has stopped, leakage rates might decrease to lower values typical for leakage through faults (<10 tCO_2/yr) (e.g. Hooper et al., 2005).

A further low probability leakage mechanism that has not been discussed here is exceeding the spill point of a storage reservoir, that is the CO_2 spilling out underneath a structural trap into an unconfined formation. Again, with adequate site selection, and ongoing monitoring of the CO_2 plume, such an event should not occur (classed as almost impossible), although in this case potential loss rates are high (essentially equivalent to the rate of injection, on the order of ~MtCO_2/yr).
Local overpressurisation resulting in faulting or fracturing in the immediate vicinity of an injection well is generally thought possible, and it is recommended that continuous monitoring for micro-seismicity be carried out during CO_2 injection to allow early detection. Potential loss rates via this mechanism are on the order of 10s tCO_2/yr.

By far the most probable leakage mechanism is via wellbores, where slow leakage along undocumented, exploration and production wells is classed as highly probable to possible and wellblow out is possible, with potential release rates ranging from ~200 tCO_2/yr to in excess of 10,000 tCO_2/yr. Rapid release of CO_2 via wellbores is highly likely to be detected, and as remedial action is possible, these events are expected to be mitigated in a matter of hours to days, thereby limiting the total volume of CO_2 released. For example, if we consider a worst case scenario, that is release at choked flow rates for a period of 5 days, then the total volume released will be on the order of ~250 ktCO_2. For the storage reservoir considered above, with 50 years injection at a rate of 1Mt/CO_2 per year, this represents 0.5% of the total volume stored, and thus (in the absence of other leakage events) the reservoir would still meet required retention standards. However, slow leakage at a rate of ~200 tCO_2/yr may remain undetected, particularly if it occurs via an undocumented wellbore. If leakage at rates of this order were to continue unmitigated, and potentially at multiple locations across the footprint of the reservoir, then storage sites may not meet required performance standards. This illustrates the importance of adequate screening of wellbores during site selection and ongoing monitoring of wells during CO_2 injection and long-term stewardship of storage sites. It would appear that new research is required to develop methods to allow detection of leakage at low rates along wellbores.

5: The Fate of CO_2 in the Overburden

This Chapter considers what might happen in the event of CO_2 leakage from a geological storage reservoir into the unconfined overburden. In these discussions it is assumed that the overburden consists of sedimentary rock overlain by unconsolidated sediments (referred to hereafter as the sediment column).

When CO_2 migrates into the sediment column, a number of additional or secondary trapping mechanisms may come into effect, acting to either limit or prevent the release of CO_2 to the ocean. Indeed, purposeful storage of CO_2 in deep-sea sediments has been proposed (e.g. Koide et al., 1997a,b; House et al., 2006; Camps et al., 2006), and as such, under certain circumstances the leakage or seepage of CO_2 from a geological formation to the sediment column could be viewed as a transfer between two valid storage reservoirs, albeit unplanned. Conversely, there may exist high permeability channels through the overburden, providing a preferential flow path along which CO_2 could migrate to the sediment-seawater interface at relatively rapid rates.

Here we first examine CO_2 ascent profiles and migration pathways, including the possibility of buoyancy trapping, the existence of preferential flow paths, residual gas trapping, and an assessment of the maximum rate at which CO_2 could migrate upwards through the sediment column. This is followed by a discussion of CO_2 hydrate formation, potentially the most effective of all the secondary trapping mechanisms. These processes are then discussed in reference to site specific case studies, examining the fate of CO_2 in the event of leakage or seepage from a sub-seafloor storage reservoir, including the likely CO_2 ascent rate, potential for secondary trapping mechanisms, and probability of CO_2 escape to the ocean and atmosphere. Finally, we discuss the reaction of CO_2 with carbonates, another important process that could act to significantly limit CO_2 escape. In general, both the rise rate and the efficacy of sediment column trapping mechanisms will depend to a large extent on in-situ temperature (T) and pressure (P) as together these factors determine the physical properties and phase behavior of CO_2, including the potential to form CO_2 hydrate.

In some instances, leakage of CO_2 into the sediment column could have serious negative consequences. An example of this is if CO_2 migrates into methane hydrate bearing sediments. This is discussed further in Chapter 7 as an example of a high risk scenario.

5.1 CO_2 Migration Pathways

In this section we focus on CO_2 buoyancy and the rate at which CO_2 migrates upwards through the sediment column, where these parameters are dependent on the density (which defines buoyancy forcing) and viscosity (resistance to flow) of the CO_2. For further details on the physical properties of CO_2 please see the background information.

5.1.1 Density & Viscosity of CO_2

CO_2 density and viscosity increase with increasing P and decreasing T, where the P-T conditions within the sediment column are dependent on:

(i) The depth of the overlying water column
(ii) The temperature of bottom waters (defining the sediment-water interface)
(iii) The depth within the sediment column
(iv) The geothermal gradient

T decreases and P increases with depth in the water column, where 1m of water depth is approximately equivalent to 1 dbar of hydrostatic pressure. In the sediment column, P continues to increase with depth and is approximately equal to hydrostatic pressure. However, T increases with depth due to the geothermal gradient, which typically varies from 0.02°C/m to 0.04°C/m, although in areas influenced by volcanic activity a significantly higher thermal gradient might be expected. An important consequence of the geothermal gradient is that the minimum temperature point in the system occurs at the sediment-seawater interface and is defined by the bottom water temperature.

At depth in the sediment column both P and T are high and are likely to exceed the critical temperature and pressure for CO_2 (T_C = 30.98°C, P_C = 737.73 dbar absolute or 727.60 dbar hydrostatic), thus CO_2 will be in the supercritical phase. Supercritical CO_2 is less dense (more buoyant) than the surrounding pore fluids and will rise through the sediment column. As the leaked CO_2 migrates upwards it moves into a lower P, lower T regime. Eventually, temperatures will fall below T_C and (if P remains greater than P_C) the CO_2 will become a liquid as opposed to a supercritical fluid. In the liquid phase, the decrease in T (defined by the geothermal gradient) exerts a stronger effect than the decrease in P (~1 dbar/m) on the physical properties of CO_2, and the CO_2 will become both more dense and more viscous as it continues to ascend, and the rise rate will slow accordingly. In the general case, the liquid CO_2 will continue to rise at a gradually slowing rate until one of three things happens:

CASE 1: In deep/cold sediments the density of the rising CO_2 will eventually equal that of the surrounding pore fluid. At this point the net buoyancy force is zero and the CO_2 will stop moving upwards. This is the point of neutral buoyancy or gravitational stability. Above this depth, the CO_2 would be more dense that the surrounding pore fluids and would sink. Thus under these conditions the CO_2 is trapped (buoyancy trapping) in the sediment column and will not leak to the ocean. Remembering that the minimum temperature in the system is defined by the sediment-seawater interface, this scenario requires a minimum water depth of ~2300-2800m (depending of the temperature profile of the water column – see BACKGROUND INFORMATION for a regional breakdown). It is therefore the least likely to occur in the case of leakage from near future sub-seafloor geological storage sites as the vast majority of current and planned sites are located in near coastal regions underlying relatively shallow water columns. Nevertheless, two examples are considered in Section 5.3 where cold deep waters are found comparatively close to shore and geological storage of CO_2 may occur in the future – see the Japan (Sea of Japan) and North West Europe (Norwegian Sea) case studies.

CASE 2: In mid-depth/mid-temperature sediments the point of neutral buoyancy is not reached, and the CO_2 will continue to migrate upwards, eventually leaking to the ocean. See the Japan (Sea of Japan), South East Asia (East Natuna Sea) and North West Europe (Norwegian Sea) case studies below. For a discussion of the fate of CO_2 in the water column see Chapter 6.

CASE 3: In shallow **or** warm sediments, the CO_2 continues to become more dense and more viscous until the CO_2 liquid-gas phase transition is reached, at which point there is an abrupt decrease in CO_2 density and viscosity and increase in buoyancy forcing. The volume increase on the transition from CO_2 liquid to CO_2 gas is large and depends on the P-T conditions at which the phase boundary is reached. The shallower the transition (comparatively cold sediments), the greater the volume increase. See the Australia (North Western Shelf), and North West Europe (North Sea and Barents Sea) case studies in Section 5.3. In these examples, the predicted volume increase ranges from a factor of 3.72 in relatively warm deep sediments (Australian Shelf: 575.5m total depth and 21.3°C), to a factor of 6.42 in relatively shallow cold sediments (Barents Sea: 432.0 m and 9.7°C). This will pressurize the pore fluids and presumably under certain circumstances could have an effect similar to that of methane hydrate dissociation, destabilizing the sediment column and potentially causing sediment slides (see discussion presented in Chapter 7).

There is also a fourth case, corresponding to warm and shallow sediments. In this type of environment, P will fall below P_C while T still exceeds T_C, thus the CO_2 will change from a supercritical fluid to a superheated vapour, eventually becoming a gas when T falls below T_C.

CASE 4: In shallow **and** warm sediments, the CO_2 will not become a liquid, but will pass from a supercritical fluid to a superheated vapour to a gas. Under this scenario the density and viscosity of CO_2 will always decrease with decreasing depth, thus the rise rate of CO_2 increases as it ascends through the sediment column. See the South East Asia (East Natuna Sea) and Australia (North Western Shelf) case studies in Section 5.3.

5.1.2 Single-Phase and Two-Phase Flow

Here we examine in more detail the principal controls on the CO_2 rise rate. For a single phase flowing through a porous media, such as CO_2 flowing through a sediment column, the flow velocity is governed by Darcys law:

$$u_{CO_2} = -\frac{\kappa}{\mu_{CO_2}}\left(\nabla p + \rho_{CO_2} g\right) \qquad \textbf{[Eq. 5.1]}$$

Where u_{CO_2} is the flow rate of CO_2 (in m/s), κ is the intrinsic permeability of the sediments (typical range in values of ~10^{-15} to 10^{-12} m^2), μ_{CO_2} is the viscosity of CO_2, (a function of T and P, in Pa.s or kg/ms), Λp is the pressure gradient, ρ_{CO_2} is the density of CO_2 (a function of T and P in kg/m^3), and g is gravity (9.8 m/s^2). This equation is valid when the fluid is homogenous (a single phase), fluid flow is of seepage type (low flow rates, or more specifically low Reynolds number), and the permeability of the porous phase is low (κv1).

However, this equation does not account for the presence of the pore fluid. The presence of more than one fluid generally inhibits flow due to occupation of pore space and the reciprocated drag forces that the phases exert on each other. When two immiscible phases are present (referred to as a wetting or liquid phase, and a non-wetting or gas phase) the flow is described as two-phase, and in the case we are considering the flow of CO_2 (the non wetting phase) is described by Darcys law with the addition of a relative permeability parameter, K_{CO_2} :

$$u_{CO_2} = -\frac{\kappa K_{CO_2} g}{\mu_{CO_2}}\left(\nabla p + \rho_{CO_2}\right) \qquad \textbf{[Eq. 5.2]}$$

Where K_{CO_2} is a multiplier (between 0 and 1, 1 representing single phase flow) which accounts for the reduction in flow due to the mutual interaction of the CO_2 and the pore fluid. At the simplest level, K_{CO_2} is a function of the proportion of pore space that the CO_2 phase occupies:

$$K_{CO_2} = \left(1 - S^*\right)^2 \left(1 - S^{*2}\right) \qquad \textbf{[Eq. 5.3]}$$

Where:

$$S^* = \frac{\left(S_p - S_{pr}\right)}{\left(1 - S_{pr} - S_{CO_2r}\right)} \qquad \textbf{[Eq. 5.4]}$$

Where S_p is the saturation of the pore fluid (the proportion of the pore-space occupied by the pore fluid), S_{pr} and S_{CO_2r} are the residual saturations (the saturation below which the phase becomes immobile) of the pore fluid and CO_2 respectively. Values of K_{CO_2} calculated according to Eqs. 5.3 and 5.4 are presented in Figure 5.1. It is noted that K_{CO_2} will depend on many other sediment and fluid descriptors, including wettability, possible additional phases (e.g. hydrocarbons), fluid viscosity, interfacial tension, flow rate and saturation history (Avraam & Payatakes, 1995). However, a detailed discussion of two-phase and multi-phase flow is beyond the scope of this report, and the reader is referred to the growing literature base addressing multiphase flow with respect to CO_2 storage and leakage, and in particular with regard to the development of fluid flow models such as TOUGH2 (e.g. Doughty, 2007). Here discussion is limited to general points that can be clearly illustrated by the simple forms of these equations.

5.1.2.1 Single Phase Flow & Preferential Flow Paths

For a given sediment column, single phase flow represents the fastest potential CO_2 flow rate. As such, the existence of dry channels through the overburden (or a portion thereof) would act as a conduit, leading to rapid migration of CO_2 through the overburden to the seafloor.

Subsurface leakage of gas from a poorly sealed hydrocarbon accumulation can efficiently dry the sediments through which it travels, creating a ‘gas chimney’. These features can reach the seafloor, creating a preferential flow path linking a leakage point (e.g. fault) directly to the ocean. Gas chimneys can be recognized in seismic data as areas of poor quality data or push downs. Indeed, seismic detection of chimneys is now being used to detect fluid migration pathways and assess the sealing quality of faults in reservoir exploration (Ligtenberg & Connolly, 2003).

If a CO_2 storage facility has either a modern or paleo gas chimney located above it, then any CO_2 that leaks from the reservoir may find the preferential flow pathway. This would not only result in the fastest possible escape time for CO_2 to reach the seafloor, but would also bypass secondary trapping mechanisms that would operate in water bearing sediments. As such, care should be taken during site selection to assess the possible occurrence of methane seeps and gas chimneys in the overburden.

Detailed seismic surveying of the overburden, and in particular the upper ~100 m, is highly unlikely to have featured as part of hydrocarbon exploration surveys. Furthermore, fluid migration structures on reflection seismic data are often difficult to map manually, and subtle features that are related to hydrocarbon migration are often overlooked (Ligtenberg & Connolly, 2003). Best Practice would therefore be to carry out a seismic survey of the overburden, and to utilize advanced analytical tools in combination with other indicators of gas seepage to assess potential flow paths (e.g. the ChimneyCube processing technique; Ligtenberg & Connolly, 2003). Other potential expressions of shallow gas and gas seepage include seafloor pock marks, seepage plumes in the water column, acoustic blanking, shallow enhanced reflectors (e.g. Schroot et al., 2005), carbonate mounds (Naeth et al., 2005), and deep water coral reefs (Hovland & Risk, 2003).

5.1.2.2 Two Phase Flow & Residual Trapping

In wet sediments, before leakage occurs the sediment column will be water saturated (S_p=1), and the residual saturation of CO_2 (S_{CO_2r}) will be zero. At the point of leakage, two-phase flow will be initiated when the capillary entry pressure of the sediment is exceeded. This is called a drainage process, where the non-wetting phase (CO_2) is replacing the wetting phase (pore fluid). Initially, the flow rate of CO_2 (u_{CO_2}) will be low, and if the supply rate of CO_2 is sparse u_{CO_2} is likely to remain low. However, if there is a sufficient and continuous supply of CO_2 (where the amount of CO_2 entering a unit volume of sediment from below is greater than that leaving it from above), then the saturation of CO_2 (S_{CO_2}), the relative permeability of CO_2 (K_{CO_2}) and u_{CO_2} will increase over time (see 'Slippery Plume' curve in Figure 5.1). Eventually, the sediment column will become saturated in CO_2 ($S_{CO_2} = 1 - S_{pr}$), at which point u_{CO_2} is at its maximum value. Should the flow of CO_2 into the sediment column cease (e.g. due to suspension of CO_2 injection and reduction of reservoir pressure), then the behavior of the system will change, switching from a drainage process to a wetting process (the wetting phase replacing the non-wetting phase). As water re-enters the sediment column (due to the continuing upward flow of the CO_2 already within the sediment column), the flow rate of CO_2 will slow. However, for a given water saturation, the flow rate will now be slower than that experienced during the drainage phase (see 'Sticky Plume' curve in Figure 5.1). This is due to residual trapping of CO_2 occupying pore space, where a proportion of the CO_2 present in the sediment column at the point that the flux of 'new' CO_2 into the system ceases will become permanently trapped in the sediments.

Figure 5.1: The Relative Permeability of CO_2 as a Function of CO_2 and Pore Fluid Saturation.

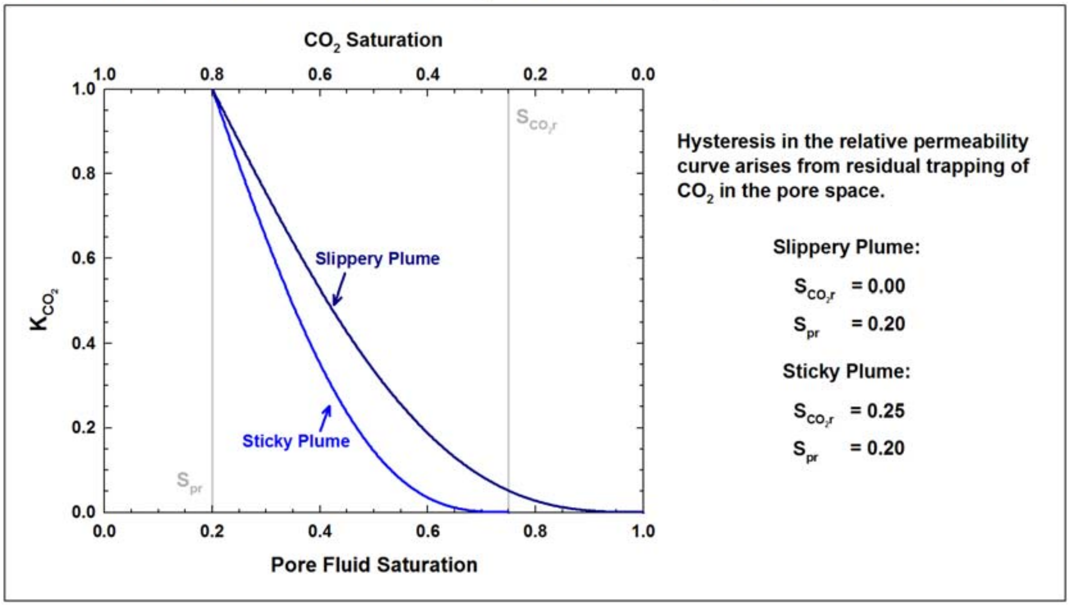

Hysteresis in the relative permeability curve arises from residual trapping of CO_2 in the pore space.

The efficacy of residual trapping (the proportion of total leaked CO_2 that is retained) depends on the trapping capacity of the sediments and the total volume of leaked CO_2. For example, if we consider a 1m^2 sediment column of 1000m depth with a porosity of 0.5, then for an S_{CO_2r} of 0.25±0.05, the residual trapping capacity of the sediments will be 125±25 m^3 of CO_2. Assuming a water depth of 1000m, a bottom water temperature of 1°C and a geothermal gradient of ~0.03°C/m, this is equal to 116±23 tCO_2. Order of magnitude calculations of trapping efficacy for this example are shown in Figure 5.2. For slow leakage rates of ~10 tCO_2/yr (e.g. through faults), all of the CO_2 would be trapped for leakage events lasting up to ~10 years. However, if leakage is sustained over longer periods of ~100 to ~1000 years (highly likely as leakage at such low rates is unlikely to be detected), then between 10% and 1% of the total leaked volume would be retained via this mechanism. Similarly, for leakage rates of ~100 tCO_2/yr (e.g. through high permeability flow paths such as poorly sealed wellbores), 100%, 10% and 1% of the leaked CO_2 would be retained for leakage events lasting ~1, ~10 and ~100 years respectively.

Figure 5.2: The Efficacy of Residual Trapping as a Function of Leakage Rate & Duration of Leakage

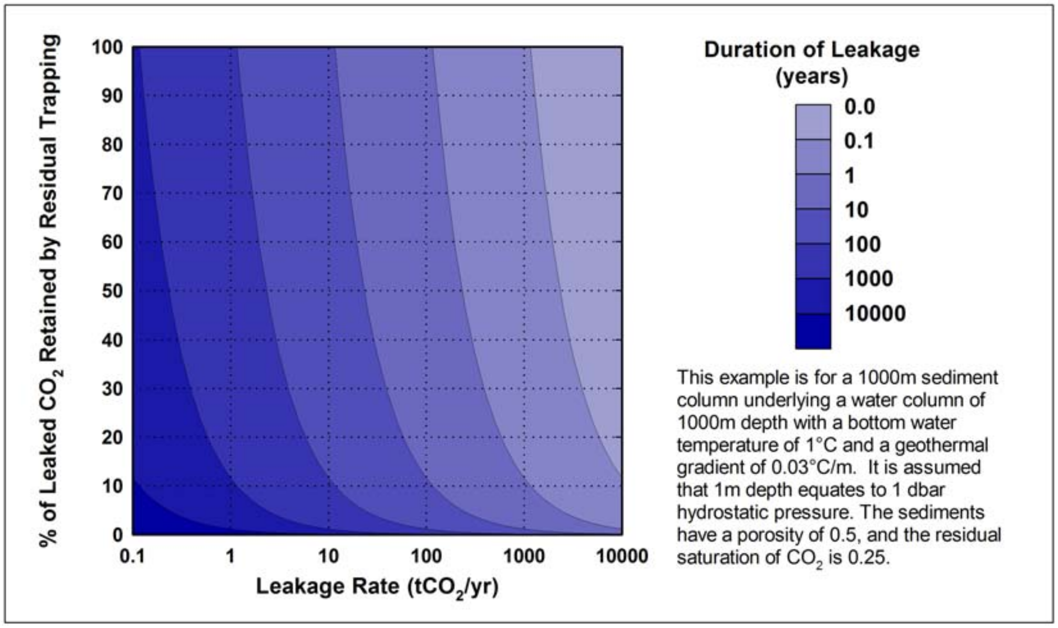

This example is for a 1000m sediment column underlying a water column of 1000m depth with a bottom water temperature of 1°C and a geothermal gradient of 0.03°C/m. It is assumed that 1m depth equates to 1 dbar hydrostatic pressure. The sediments have a porosity of 0.5, and the residual saturation of CO_2 is 0.25.

5.1.3 CO_2 Escape Times

Here we consider illustrative examples of CO_2 escape times, that is the period of time it will take for CO_2 to travel from the top of a caprock seal to the seafloor.

As an order of magnitude calculation for the instantaneous flow rate at a particular point in space and time, the driving force of the flow is the difference between the density of CO_2 and the porefluid, and Eq. 5.2 can be approximated by (after equation 3 in House et al., 2006):

$$u_{CO_2} \approx -\frac{\kappa K_{CO_2} g}{\mu_{CO_2}}\left(\rho_{CO_2} - \rho_{H_2O}\right)$$ **[Eq. 5.5]**

Given the large range in values for the intrinsic permeability of seafloor sediments, the CO_2 rise rate that will be observed for a given set of physical conditions is strongly dependent on this parameter. This is illustrated in Figure 5.3 where rise parameters are given as a function of κ for the upper ~1000 m of a model sediment column. This simple model is based on a water column depth of 1000 m, a bottom water temperature of 1°C, a geothermal gradient of 0.03°C/m, and assumes a uniform seawater and pore fluid density of 1.04 g/cm^3. This example also assumes single phase flow with K_{CO2} set to 1 (that is either transport through a dry or CO_2 saturated sediment column), and thus represents maximum potential flow rates, and shortest potential escape times.

Panel A shows the density (ρ_{CO_2}) and viscosity (μ_{CO_2}) of CO_2 as a function of depth in the sediment column, and the rise rate (u_{CO_2}) as a function of depth and κ. For a given value of κ, the CO_2 rise rate decreases by a factor of ~2.9 from 1000 m depth in the sediments to the sediment-seawater interface due to the decrease in buoyancy forcing and increase in viscosity of CO_2 as it moves into colder sediments. For example, for a reasonable value of κ for sandy sediments of ~10^{-13} m^2 (~10^2 md; Fetter, 1994) the rise rate slows from ~52 m/yr at 1000 m sediment depth to ~18 m/yr in the upper 10 m of the sediment column. However, the migration rate is a much stronger function of the value of κ. For example, silts have a permeability approximately two orders of magnitude lower than sands, with a κ of ~10^{-15} m^2 (~1 md; Fetter, 1994), thus the rise rate is also two orders of magnitude lower, decreasing from ~52 cm/yr at 1000m depth to 18 cm/yr in the upper sediments. As the permeability of marine sediments can vary over at least 7 orders of magnitude, with κ ranging from ~10^{-19} m^2 to 10^{-12} m^2, (~10^{-4} to 10^3 md; e.g. Bryant and Rack, 1990), the rise rate of liquid CO_2 may also vary over more than 7 orders of magnitude, ranging from significantly less than 1 mm/yr to 100s of m/yr. If we also consider migration along high permeability flow paths such as poorly sealed wellbores, degraded cement segments are likely to have permeabilities similar to high permeability sediments, extending upwards to ~10^{-10} m^2 for a 1 mm wide annulus (10^5 md; Celia et al., 2004), thus a continuous narrow annulus would result in extremely rapid migration rates on the order of 10s of km/yr, or 100s m/day.

Panel B shows the estimated time that it would take for CO_2 to migrate through the upper 1000m of sediments and escape into the ocean as a function of κ. For a κ of 10^{-15}, 10^{-14}, 10^{-13} and 10^{-12}, the escape times are 3130 yrs, 313 yrs, 31.3 yrs (31 years 111 days), and 3.13 yrs (3 years 48 days) respectively. Thus CO_2 leakage through low permeability sediments such as silts is relatively slow, taking on the order of 1000 years or longer. However, migration through high

Figure 5.3: Rise parameters for buoyant CO_2 migrating upward through the sediment column. All calculations are based on a water depth of 1000 m, a bottom water temperature of 1°C and a geothermal gradient of 0.03°C/m. It is assumed that 1 m depth is equal to 1 dbar pressure.

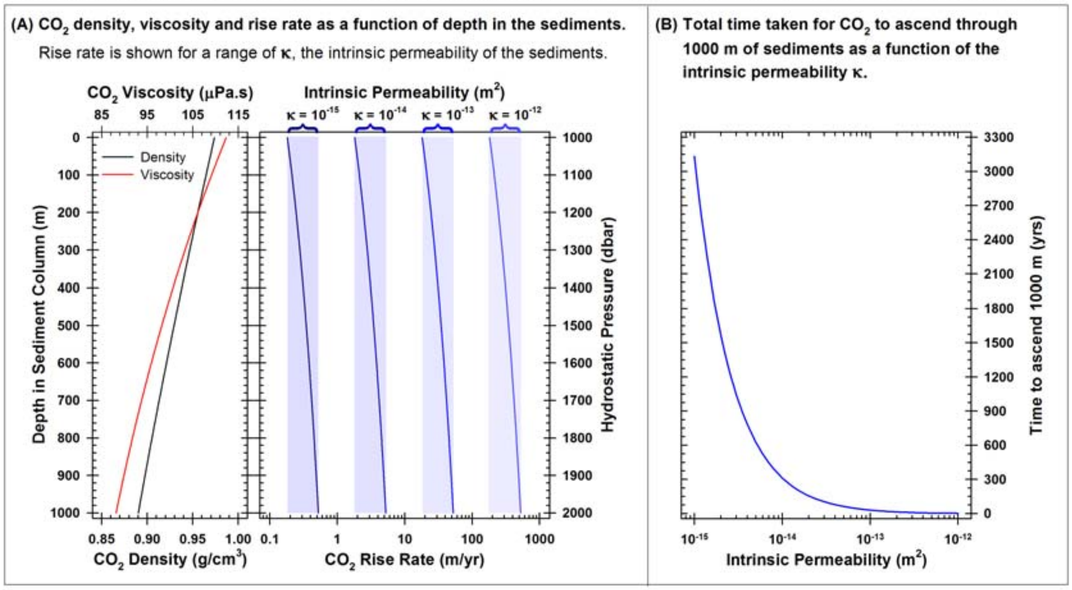
(A) CO_2 density, viscosity and rise rate as a function of depth in the sediments. Rise rate is shown for a range of κ, the intrinsic permeability of the sediments.

(B) Total time taken for CO_2 to ascend through 1000 m of sediments as a function of the intrinsic permeability κ.

permeability sandy sediments or via a high permeability pathway (e.g. associated with degraded cement segments along a wellbore) could result in delivery of CO_2 to the seafloor on a years to decades timescale. For leakage along a narrow annulus, delivery times would be substantially shorter, on the order of 1-2 weeks.

5.2. Hydrate Trapping

Gas hydrates are ice-like solid phases that form at low T and high P in a reaction between the 'host' water molecules and 'guest' gas molecules. CO_2 readily forms a gas hydrate, where the stability conditions for CO_2 hydrate are reasonably well known, and overlap significantly with expected T, P conditions in the upper layers of cool/deep sediments. Thus in cool marine sedimentary basins deeper than two or three hundred meters, CO_2 migrating upwards through the sediment column will move into a T, P regime where hydrate formation is possible (e.g. Koide et al., 1995). The formation of CO_2 hydrate in the sediment column would limit, and may even prevent, CO_2 escape to the ocean.

The reaction for CO_2 hydrate formation is:

$$CO_2 + nH_2O \rightarrow CO_2 \cdot nH_2O \qquad \textbf{[Eq. 5.6]}$$

Where n is the hydration number (average moles of water required to cage one mole of CO_2). In a perfect crystalline hydrate (full cage occupancy) n will be 5.75, but typically varies from 6.1 to 7.8 (Yamamuro & Suga, 1989; Sloan 1991; Uchida et al. 1995), i.e. CO_2 hydrate formation requires an approximate ratio of 6-8 moles of water to 1 mole of CO_2. Therefore in addition to high pressures and low temperatures, CO_2 hydrate formation also depends on the extent of CO_2 saturation, requiring the presence of a free CO_2 phase (liquid or gas) to generate and sustain (super)saturated conditions in the aqueous phase.

CO_2 hydrate has a density of 1.054-1.143 g/cm^3 (Chen, 1972; Bozzo et al., 1975; Uchida et al., 1995; Aya et al., 1997; Circone et al., 2003; Rehder et al., 2004). Thus unlike CH_4 hydrate, CO_2 hydrate is more dense than the expected density of pore fluids or seawater. This means that any CO_2 hydrate formed in the sediment column or at the sediment-seawater interface is gravitationally stable, and does not rely on the overburden or cementation of sediment grains to hold it in place.

This section explores in more detail the potential for hydrate trapping in the overburden.

5.2.1 Hydrate Trapping & Capping – a Self Sealing System?

When CO_2 migrating upwards through the sediment column enters the hydrate stability zone, CO_2 hydrate will begin to precipitate. These hydrate particles will block pore spaces, reducing the permeability of the sediments and impeding further upwards flow of buoyant liquid or gaseous CO_2. Indeed, the hydrate could create an impermeable 'cap', effectively trapping buoyant liquid or gaseous CO_2 below. The CO_2 hydrate may also cement sediment grains, increasing the mechanical strength of the sediment, and potentially forming a cap capable of withstanding a significant build-up of pressure beneath the hydrate layer.

The potential of CO_2 hydrate to act as a cap capable of preventing leakage of CO_2 to the ocean has recently gained significant interest, with a number of researchers examining the possibility of CO_2 storage under a self forming hydrate layer in deep-sea sediments (e.g. Koide et al., 1996; Camps et al., 2006; House et al., 2006; Someya et al., 2006). These studies provide a direct analogue for a leakage or seepage event, in that they require injection of CO_2 into sediments at a depth beneath the hydrate formation zone, where the CO_2 then migrates upwards into cooler sediments where hydrate formation is possible. In the general model (summarised from House et al., 2006) the assumption is that hydrate formation will start as soon as upwardly migrating CO_2 enters the hydrate formation zone, resulting in the formation of an impermeable barrier. Additional CO_2 flowing up beneath this 'cap' would then be forced to spread laterally. As the CO_2 flows laterally, the hydrate cap will grow, where the hydrate cap will be stable as long as it is in contact with CO_2 or CO_2 saturated pore fluid. Should the CO_2

supply cease (e.g. cessation of leakage or cessation of injection in the direct storage case) the hydrate cap is therefore expected to remain intact until the trapped plume of CO_2 has fully dissolved. As the plume (followed by the hydrate cap) dissolves, the surrounding pore fluids will become saturated in CO_2 and will sink (as they are more dense than either liquid CO_2 or the pristine pore fluids). Thus formation of a hydrate cap followed by dissolution dissipation of the trapped CO_2 is expected to prevent any transport of CO_2 to the seafloor.

Research in this area is at an early stage, and further studies should be encouraged. In particular, the current simple models need to be developed to include the complexity of the real system and differences between the leakage case and direct storage need to be explored. The most important question is whether or not CO_2 hydrate formation will prevent leakage to the ocean. This is likely to depend on the supply rate of CO_2, the permeability of the sediments, and the thickness of the potential hydrate formation zone, among other factors (e.g. Liu & Flemings, 2007). As highlighted by Camps et al. (2006), although there have been numerous studies on CO_2 hydrate, few merge sediments, water of appropriate salinity, and conditions appropriate to geological storage. The principal factors that will exert a strong influence on hydrate formation (and the prediction thereof) are discussed below.

5.2.2 Small Scales – Hydrate within Pore Spaces

The initial permeability of the hydrate free sediments may exert a strong control on whether or not an impermeable barrier is formed (Liu & Flemings, 2007). The capillary entry pressure of a sediment is inversely proportional to the square root of the permeability, thus a hydrate free sand (κ ~10^{-13} m^2) has a capillary entry pressure 10 times lower than a hydrate free silt (κ ~10^{-15} m^2). As hydrate is formed, permeability decreases and the capillary entry pressure increases, where for the same amount of hydrate formation silt will experience a greater increase in capillary pressure than sand (Liu & Flemings, 2007). Thus not only is the initial permeability lower for silt, the decrease in permeability is more rapid, and an impermeable barrier (high capillary entry pressure) will be formed more readily. Indeed, in their model of CH_4 hydrate formation in marine sediments Liu & Flemings (2007) predict that hydrate formation in coarse-grained sandy sediments cannot form an effective capillary barrier to upward migration of free gas. Although the same conclusion cannot be simply extrapolated to CO_2 hydrate formation (due to the different properties of CH_4 and CO_2, such as the interfacial tension with water), the possibility of a sediment permeability threshold above which CO_2 hydrate formation cannot form an impermeable barrier should be explored.

As recognised by Camps et al., (2006) there is a need for more information on the impact of CO_2 hydrate formation on sediments. This includes determining whether hydrate will form in the centre of pores or on grain surfaces (pore filling results in a more rapid decrease in permeability than pore coating; Kleinberg et al., 2003), whether it will cement grains thereby increasing the strength of the sediment, and ultimately whether precipitation will indeed create an effective impermeable barrier to upward CO_2 migration. It may also be important to consider whether the state of the CO_2 influences hydrate precipitation (Camps et al., 2006). For example, there may be differences in the nature of the hydrate when formed purely from dissolved CO_2 (i.e. in water-saturated rock or sediments adjacent to any CO_2 'pool'), compared to that formed from within the CO_2-rich phase (i.e. within the CO_2 'pool').

To gain some insight into these processes, Camps et al., (2006) conducted a series of laboratory-based studies examining CO_2 hydrate formation within synthetic sandy sediments under seawater-saturated and seawater-poor conditions. Cryogenic scanning electron microscopy revealed that complex hydrate fabrics were formed. Where CO_2 was abundant, but water was limited, hydrate appears to cement the sediment grains together, filling inter-granular pores, and in some larger pores forming crystals of ~100μm in size. In water-rich areas of lower CO_2 abundance, hydrate appears to form in the centre of the pores. The formation of complex dendritic crystals of halite disseminated within the hydrate suggests that in some areas hydrate growth was sufficiently fast that Na and Cl ions were not able to diffuse away from the growth front. The experimental results also indicated that a very thin (~2mm) hydrate layer was enough to impede flow of CO_2, at least over timescale of days to weeks, supporting the concept that a relatively thin 'cap' of CO_2 hydrate may be able to trap a slightly buoyant pool of liquid CO_2 beneath it (Camps et al., 2006).

5.2.3 Influences on CO_2 Hydrate Stability in the Sediment Column

Most studies examining CO_2 hydrate formation as a potential trapping mechanism compare expected T,P conditions in the sediment column to stability fields for pure CO_2 hydrate in the bulk phase, either based on a fit to data for CO_2 hydrate in seawater or model calculations for CO_2 hydrate in 3.5 wt% sodium chloride (NaCl). Indeed, this is the approach taken in the case studies presented later in this Chapter. While these simple comparisons are valuable in that they provide a broad picture for the potential to form hydrate, the results must be treated with caution. Firstly, all model predictions carry some error (e.g. Ballard & Sloan, 2004). Secondly, P, T conditions that define a hydrate-gas-water or hydrate-liquid-water equilibrium curve will depend on dissolved ion and trace gas concentrations (Sloan, 1990). Thirdly, the actual hydrate stability in sediment pore spaces may differ considerably from the predicted bulk phase stability (e.g. Llamedo et al., 1997). Finally, the supply rate of CO_2 is likely to exert a strong control on the location of hydrate formation in the sediment column in relation to the predicted hydrate stability zone (e.g. Liu & Flemings, 2007). The variation introduced by these parameters is significant and will not only impact the depth to which hydrates are stable in the sediment column, but may be the controlling influence on whether or not hydrate formation prevents CO_2 escape to the ocean. These considerations should therefore be kept firmly in mind when examining the simple models of hydrate prediction presented later in this Chapter.

5.2.3.1 Hydrate Stability Prediction Programs

There are a variety of programs available to predict hydrate stability. For an assessment of five of the most frequently used programs (CSMHYD, CSMGem, DBRHydrate, Multiflash and PVTSim) see Ballard & Sloan (2004). In a comparison to experimental data, these authors found CSMGem to be the most accurate, where the most notable differences between CSMGem and the other programs are for CO_2 and CH_4 single hydrates (Ballard & Sloan, 2004). All of the programs under- or over-predict the effect of adding an inhibitor such as NaCl on hydrate stability. However, for nearly all inhibited systems, CSMGem predicts the data with less error than the other programs (Ballard & Sloan, 2004).

The upper panel of Figure 5.4 presents a comparison of the stability fields for CO_2 and CH_4 single hydrates in 3.5wt% NaCl predicted by CSMHYD and CSMGem. The plotted lines show the hydrate-gas-water (for CO_2 and CH_4) and hydrate-liquid-water (for CO_2) equilibrium curves, where hydrate is stable below and to left of the line (low temperature, high pressure). It can be seen that while the models agree well at low pressure (up to ~300 and ~600 dbar hydrostatic pressure for CO_2 and CH_4 hydrates respectively), at higher pressures the models diverge, with a difference in T of ~1°C for a given P. For a typical geothermal gradient of ~0.03°C/m, this is equivalent to a difference in the predicted depth of hydrate formation of ~30m.

Figure 5.4: Hydrate stability curves for pure CO_2 and pure CH_4 hydrate. Upper panel - a comparison of two models, CSMGem and CSMHYD. Lower panel - the inhibitory effect of salt on hydrate formation.

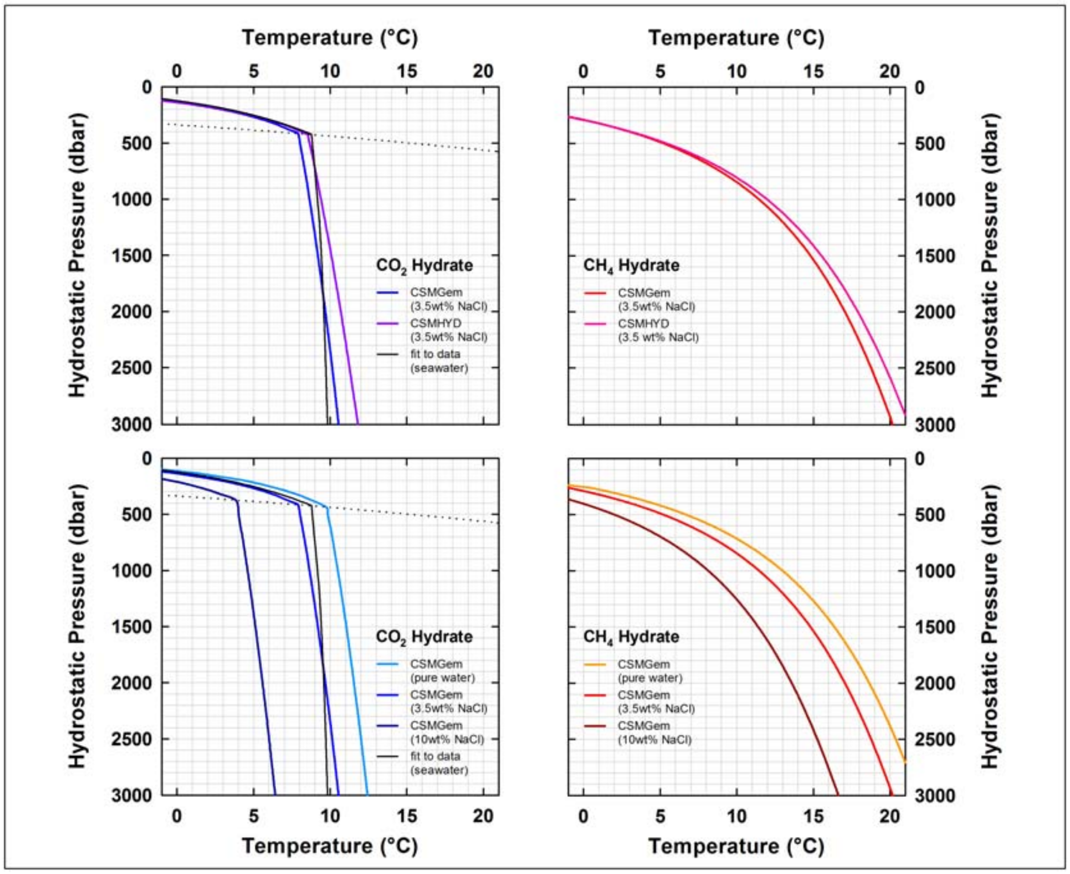

5.2.3.2 *The Effect of Inhibitors*

Addition of dissolved ions to water (salinity) shifts the hydrate equilibrium curve such that the hydrate will form and/or dissociate at a lower T for a given P, i.e. hydrate in salt water is less stable than hydrate in pure water. Most evaluations of CO_2 hydrate formation in the sediment column assume that pore fluid salinity is well approximated by 3.5 wt% NaCl solution. Similarly, the approach taken in the case studies presented in this Chapter is to assume that pore fluid salinity approximates to seawater salinity. However, pore fluids are chemically distinct from seawater due to processes such as fluid flow, diagenetic reactions, and ionic diffusion. In near coast sediments there may be a significant influx of meteoric (rain) waters through coastal aquifer systems, and pore fluid salinity may be near zero. Sedimentary diagenesis can significantly change the ionic composition of the pore fluids. For example, organic matter degradation proceeds via oxic respiration, denitrification, Fe-Mn oxide reduction, sulphate reduction and methanogenesis, and the porewaters become depleted in O_2 and SO_4^{2-}, deficient in Ca^{2+} and Mg^{2+} (via carbonate precipitation), enriched in NH_4^+ and various trace metal ions and elevated in Br^-, and enriched in the trace gases H_2S and CH_4 (see below for further discussion of the influence of trace gases on hydrate stability). Furthermore, salt rejection during hydrate formation in confined sediment pore-spaces will also increase the ionic strength of the porewaters in proportion to the volume of hydrate formed. Thus actual conditions may range from near zero salinity to hypersaline, where not only the total ionic strength but also the ions present in solution may be significantly different to seawater.

For methane hydrate it has been shown that hydrate stability is dependent on the activity of water in the solution, which can be calculated if the ionic composition of the solution is known (Dickens & Quinby-Hunt, 1997). Thus predictions of hydrate stability in simple ionic solutions such as NaCl can still be used if the concentration of NaCl is chosen to reflect the water activity (rather than the ionic strength) of the pore fluid. The lower panel of Figure 5.4 shows a comparison of the hydrate stability curves for CO_2 and CH_4 hydrate in pure water, 3.5 wt% NaCl and 10 wt% NaCl as predicted by CSMGem. The activity of water in these solutions is equivalent to oxic water/seawater with salinities of 0, 31.5 and 97.7 (following the methods described in Dickens & Quinby-Hunt (1997)). The strong inhibitory effect of salt on hydrate stability can be clearly seen. For a given P in the CO_2 hydrate-liquid-water system, the addition of 3.5 wt% NaCl decreases the temperature of hydrate formation by ~2°C in comparison to the pure water system. Increasing the salt concentration from 3.5 wt% to 10 wt% (e.g. by consuming ~2/3rds of the water) decreases hydrate stability by a further ~4°C. This implies that (in a closed system) there may be a salinity-imposed limit to hydrate growth, as the expulsion of salts during the crystallization process increases the concentration of salts in the remaining pore waters to a point beyond which continued formation of gas hydrate cannot be sustained.

5.2.3.3 *The Effect of Capillary Inhibition*

As noted above, the models and data used to predict potential hydrate formation in the sediment column are typically based on the bulk (unconfined) phase. However, hydrate stability conditions in confined pore spaces can be significantly different. In tight capillaries, the high curvature of phase interfaces results in a higher fugacity and chemical potential of components. This can cause a significant shift in the T,P conditions at which solid-liquid transitions occur with respect to bulk (unconfined) conditions. The magnitude of this shift depends on numerous factors, including pore radius, pore shape, phase contact angles, and surface properties. Indeed, capillary inhibition of hydrate stability in narrow pores is considered a possible explanation for reported differences between predicted (from bulk data) and actual CH_4 hydrate stability zones in marine sediments (e.g. Clennell et al. 1999; Henry et al. 1999). For an accessible discussion of the effect of capillary inhibition on hydrate stability the reader is referred to Llamedo et al. (2004).

5.2.3.4 *The Effect of Minor/Trace Gas Components*

Incorporation of traces gases (e.g. CH_4, H_2S, N_2) into the hydrate lattice will also displace the hydrate equilibrium curve. Whether the shift is such that the hydrate will form and/or dissociate at a higher or lower temperature is dependent on the gas or combination of gases added.

As discussed in Chapter 3, many compounds, including hydrate forming gases, will preferentially partition into a CO_2 rich phase (gas, liquid or hydrate). Thus the conditions under which hydrates can or will form (in either natural systems or in the case of leakage/seepage) may differ considerably from those for the pure CO_2 phase. The effects exerted by three hydrate forming gases N_2, CH_4 and H_2S are discussed below. These gases were chosen for illustrative purposes as (1) all three gases are common components in naturally occurring CO_2 vent systems, which provide potentially valuable analogues to leakage/seepage events (see Section 5.2.4); (2) in the case of leakage or seepage, it is reasonable to suppose that the CO_2 may well contain minor amounts of CH_4 and H_2S (see Chapter 3 Section 3.4.4.2).

Calculations of incipient hydrate formation temperatures ($T_{hydrate}$) for various mixtures of CO_2 with the hydrate forming gases N_2, CH_4 and H_2S are presented in Figure 5.5. All calculations were carried out by Dr. Keith Hester using the Colorado School of Mines Gibbs energy minimization program (CSMGem; Ballard & Sloan, 2003). To approximate seawater, a salt content of 3.5 wt% NaCl in the water phase was used. Note these calculations are based on the mol% additional gas in the hydrate phase – not in the precursor gas phase.

Figure 5.5a shows the hydrate stability curves for the single hydrate phases, and Figure 5.5b shows the curves for binary mixtures of 95% CO_2 + 5% trace gas. Comparison of these curves demonstrates that the stability of a mixed gas hydrate cannot be simply derived from the stability of the individual hydrate phases. Nevertheless, the influence exerted by including a minor component in a CO_2 mixture does broadly correspond to the relative stability of the individual hydrate phases, where the addition of H_2S strongly stabilizes the CO_2 hydrate, while the addition of CH_4 and N_2 exert little effect at low pressures and are moderately stabilizing at higher pressures.

The influence of trace gas content and composition was then examined by considering a variety of gas mixtures (binary, tertiary and quaternary, with total trace gas contents of 0-20%) at two fixed pressures, 2.5 and 10MPa, roughly equivalent to 250 and 1000 m total depth. In simple binary mixtures, the addition of 1-20 mol% of either CH_4 or N_2 (the most common secondary gas components in natural CO_2 rich vents, see Table 3.1 in Chapter 3) results in a destabilization of the hydrate phase at 2.5 MPa, reducing $T_{hydrate}$ by 0.0-0.3°C and 0.1-1.7°C respectively (Figure 5.5c). Conversely, at 10 MPa the presence of these gases increases hydrate stability (Figure 5.5d). For N_2, a poor hydrate former, the effect is minor, with an increase in $T_{hydrate}$ of 0.6°C at 5 mol%. For CH_4, the effect is more significant, with an increase of 0.6°C at 1 mol%, and 2.0°C at 20 mol%. The inclusion of a small amount of H_2S, a particularly strong hydrate former, leads to a more stable hydrate phase at both pressures, where addition of 1-5 mol% increases $T_{hydrate}$ by 2.1-6.0°C at 2.5 MPa and 2.2-6.2°C at 10 MPa.

In more complex mixtures (Figure 5.5e-h), the combined addition of CH_4 and N_2 has an effect intermediate between the single additions of these gases, where the addition of 1-20 mol% CH_4 + N_2 lowers $T_{hydrate}$ by 0.0-0.9°C at 2.5 MPa and increases $T_{hydrate}$ by 0.4-2.5°C at 10MPa. When H_2S is added, the effect of this strong hydrate former is dominant.

Figure 5.5: The effect of trace gas (N_2, CH_4, H_2S) content on CO_2 hydrate stability.

(a) & (b) - hydrate stability curves for single phase hydrates and simple binary mixtures; (c), (e) & (g) - hydrate stability as a function of trace gas content for binary, tertiary and quaternary mixtures at 2.5 MPa; (d), (f) & (h) - hydrate stability as a function of trace gas content for the same mixtures at 10 MPa.

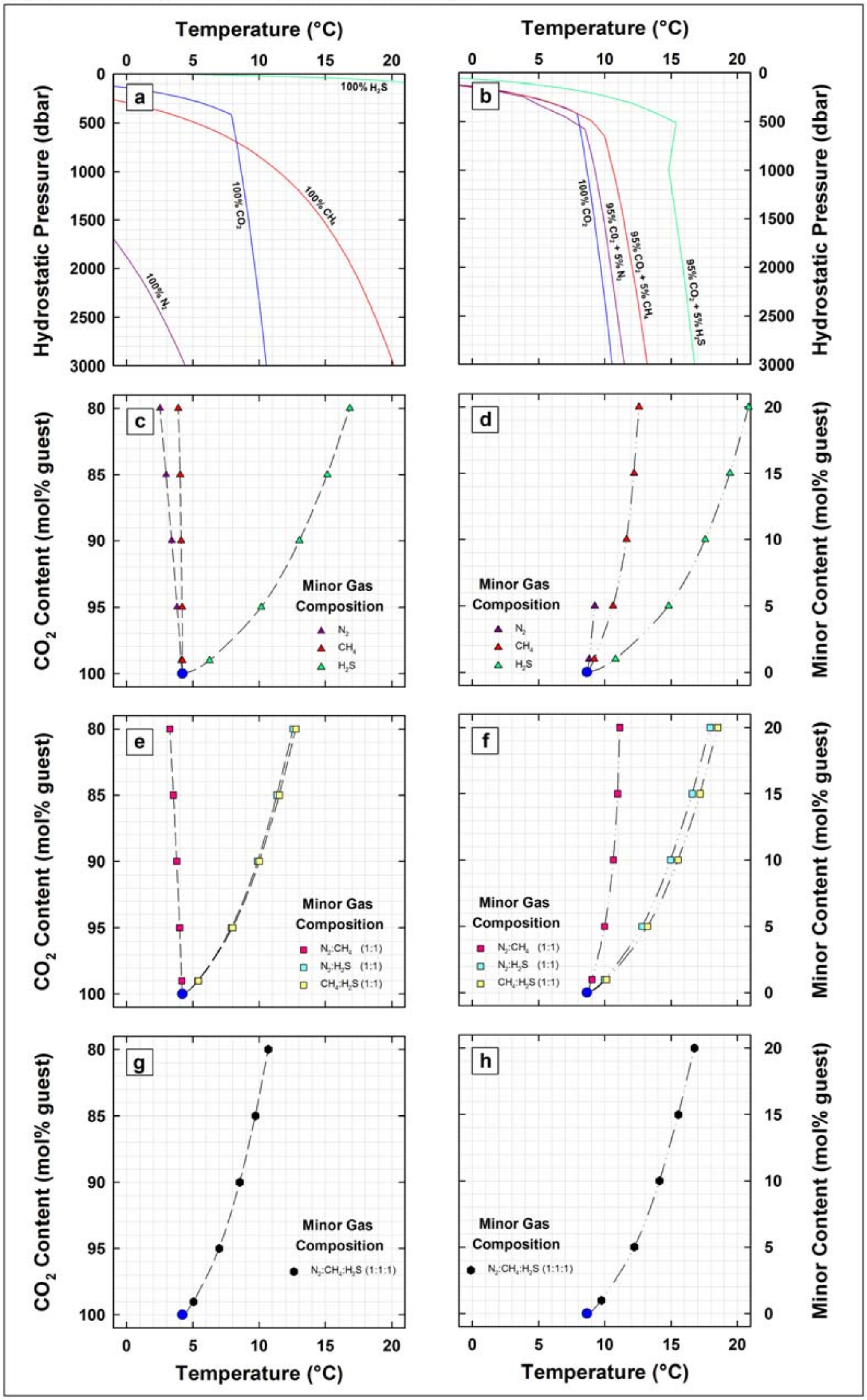

These calculations underline the large differences in CO_2 hydrate stability that arise from the consideration of additional minor gas components, in particular the stabilising effect exerted by the presence of H_2S. Given the efficiency of both supercritical and liquid CO_2 as solvents, a significant partitioning of species such as H_2S into the CO_2 phase can be expected to occur, both within the storage reservoir, and as the CO_2 ascends through the sediment column. Note also that the stability data considered here are quoted in terms of the proportion of gases present within the hydrate structure, where to achieve an H_2S content of 5 mol% in the hydrate requires a feedstock with a significantly lower concentration of ~0.5 mol%. Thus current models considering a pure CO_2 phase are likely to under predict the extent of the hydrate stability zone.

5.2.3.5 The CO_2 Supply Rate

The rate at which the CO_2 is supplied to the hydrate formation zone is also likely to exert a strong influence on where, when and how much hydrate is formed. For example, at high flow rates equilibrium conditions may not be met, and hydrate formation could become limited by the availability of water, or inhibited by an increase in salinity. For example, Liu & Flemings (2007) model of CH_4 hydrate formation indicates that under high gas flux conditions, rapid hydrate formation consumes water and increases salinity, inhibiting further hydrate formation, and allowing the transport of free gas upwards through the hydrate stability zone. Thus in the event of leakage at fast rates, it might be expected that both salinity and CO_2 hydrate concentration will increase upwards from the base of the hydrate stability zone to the seafloor, with delivery of the free CO_2 phase to the ocean (c.f. Liu & Flemings, 2007). In general, there is a need to develop dynamic models of CO_2 hydrate formation within the sediment column that account for the various factors discussed above, in addition to other parameters such as the possibility of pore fluid advection, which may also significantly perturb the base of the hydrate stability zone.

5.2.4 A Potential Analogue: Hydrate Formation at Natural Vent Sites

Natural CO_2 hydrate deposits have been observed at a number of locations, including Minami-Ensei Knoll (695-705m), Iheya North Knoll (970m), Yonaguni Knoll IV (1370-1385m), the JADE hydrothermal field (1300-1450m), and Hatoma Knoll (~1500m) in the Okinawa Trough, and have been inferred to exist in the subsurface at the Champagne Vent site (1604m) on the Mariana Arc (for site locations and composition of the CO_2 phase see Chapter 3, Figure 3.1, Figure 3.2, and Table 3.1, for further site information see Appendix 3.A).

At Minami-Ensei Knoll (695-705m) CO_2 rich droplets emerge from the sandy seafloor and mussel beds among crowded hydrothermal chimneys (Hashimoto et al., 1995). CO_2 hydrate has also been observed at the seafloor in this region, where the hydrate texture is described as a 'sherbet-like' substance (Chiba et al., 1992; Hashimoto et al. 1995). The hydrate material was seen to intermittently emerge from the seafloor and rise up through the water column, where this phenomenon decreased with increasing distance from the most active vent (Hashimoto et al. 1995). The description of the hydrate fabric and its positive buoyancy strongly suggests that buoyant CO_2 liquid is trapped inside void spaces within the hydrate, or that the 'hydrate' material is actually formed through the amalgamation of hydrate coated droplets.

Chiba et al., (1996) report the occurrence of CO_2 hydrates at the seafloor at Iheya North Knoll (970m), with no mention of CO_2 venting as a discrete phase, suggesting that the hydrate may well form a barrier to flow in this region.

At Yonaguni Knoll IV (1370-1385m), small liquid CO_2 droplets emerge from the seafloor in the immediate vicinity of two black smoker chimneys, with a hydrate formation zone some distance from the vent sites (Inagaki et al., 2006). First descriptions of the possible presence of CO_2 hydrate in the subsurface at this site reported 'bubbles' from gas hydrates being released from the sediment after sampling it with a corer (Fujikura et al., 2001, Glasby & Notsu, 2003). A later study established the existence of a CO_2 hydrate layer in the shallow subsurface, where this layer traps a pool of liquid CO_2 beneath it (Inagaki et al., 2006). The 'CO_2-hydrate-zone' is located approximately 50m down-slope from the black smoker chimneys and covers an area of ~200m^2 (Inagaki et al., 2006). The zone is characterized by a thin sediment cover (~5cm), with abundant white patches and pavements, and a temperature gradient increasing from 3.9°C at the sediment-seawater interface to 9.9°C at 35cm sediment depth (at the in-situ pressure, CO_2 hydrate formation can occur at temperatures less than 10°C). Small CO_2 droplets were seen to emerge from cracks in the pavement, and coring of the material confirmed the presence of a thin CO_2 hydrate layer of less than 10cm thickness beneath the sediment cover. When the hydrate layer was punctured by the collection of the sediment core, a continuous emission of liquid CO_2 was observed from the cored hole, indicating that the hydrate layer was acting as a cap with a pool of buoyant liquid CO_2 trapped beneath.

At the JADE site (1300-1450m) CO_2 liquid droplets are expelled to the ocean through hydrate pipes that grow out of the sediments (Sakai et al., 1990). Sakai et al. (1990) and Hou et al. (1999a,b) suggested that an impermeable CO_2 hydrate layer forms beneath the seafloor in the vicinity of these hydrate pipes, where this hydrate layer was assumed to act as a trap. However, Glasby & Notsu (2003) argued that temperatures in the sub-surface are likely to be too high for CO_2 hydrate to form as this site occurs in close proximity to a black smoker discharging hydrothermal fluids at a temperature of 320°C. Nevertheless, Sakai et al. (1990) report a temperature of 3.8°C at the sediment-seawater interface, with a temperature gradient of ~0.8°C/cm, indicating that hydrate formation would be possible in the upper 8cm of the sediments where temperatures are below 10°C. They suggest that leakage of droplets through the impeding hydrate layer occurs when the seal is ruptured, most likely due to shifts in hydrothermal fluid circulation patterns leading to elevation of the 10°C isotherm, where this hypothesis is consistent with the general observation that seepage of CO_2 is occurring in areas of high heat flow (Sakai et al., 1990).

At the Hatoma Knoll site (~1500m) both CO_2 venting and hydrate deposits at the sediment-seawater interface have been observed, with small droplets of CO_2 leaking through the hydrate layer (Shitashima & Maeda, 2005 and personal communication).

A photograph of the hydrate deposit outcropping at the seafloor in close proximity to a clam bed is shown in Figure 5.6 (reproduced by kind permission of Shitashima-san). It can be seen that the hydrate outcrops in close proximity to a healthy clam bed. Galatheid crabs can also be seen on the clam bed and sediment surface close to the hydrate deposit.

Figure 5.6: CO_2 Hydrate outcropping at the seafloor, Hatoma Knoll, Okinawa Trough. Photograph reproduced by kind permission of Shitashima-san.

More recently, Lupton et al. (2006) hypothesized the existence of a CO_2 hydrate layer in sediments at the Champagne vent site, NW Eifuku, on the Marina Arc. At this site CO_2 droplets were seen to emerge out of crevices in the seafloor, where the flux of droplets increased dramatically whenever the seafloor was disturbed. Lupton et al. (2006) interpret this phenomenon as being consistent with the presence of a layer of liquid CO_2 beneath the surface capped by an impeding layer of CO_2 hydrate. Careful probing of the sediments in this region give temperatures less that 4°C, consistent with the presence of CO_2 in either the liquid or hydrate states (at the in-situ pressure, CO_2 hydrate formation can occur at temperatures less than 9°C).

Figure 5.7 shows a simple cartoon illustrating the formation of an impeding hydrate cap in these environments, and comparing it to expected conditions in a non hydrothermal 'leakage' location. The natural vent sites span a range in bottom depths from ~700m to ~1600m, with cold ambient bottom water temperatures of 1-4°C. As such these sites provide a reasonable analogue for deep waters overlying a storage reservoir.

Figure 5.7: Schematic diagram comparing hydrate formation and distribution at deep water CO_2 vent sites to potential leakage sites. The general case considered is for a water depth of 1000m and a bottom water temperature of 2°C, with a geothermal gradient of 0.03°C/m at the leakage site.

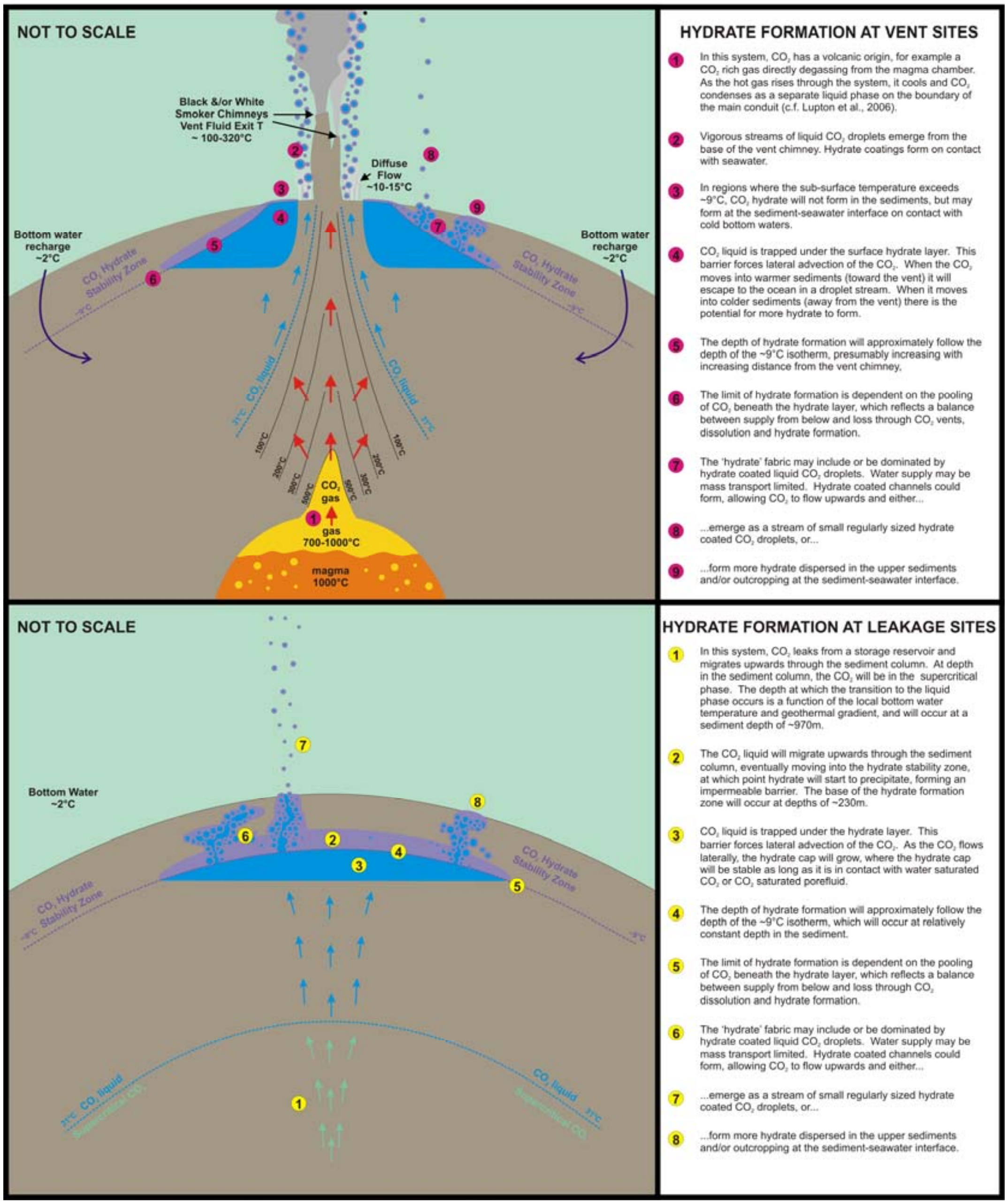

HYDRATE FORMATION AT VENT SITES

① In this system, CO_2 has a volcanic origin, for example a CO_2 rich gas directly degassing from the magma chamber. As the hot gas rises through the system, it cools and CO_2 condenses as a separate liquid phase on the boundary of the main conduit (c.f. Lupton et al., 2006).

② Vigorous streams of liquid CO_2 droplets emerge from the base of the vent chimney. Hydrate coatings form on contact with seawater.

③ In regions where the sub-surface temperature exceeds ~9°C, CO_2 hydrate will not form in the sediments, but may form at the sediment-seawater interface on contact with cold bottom waters.

④ CO_2 liquid is trapped under the surface hydrate layer. This barrier forces lateral advection of the CO_2. When the CO_2 moves into warmer sediments (toward the vent) it will escape to the ocean in a droplet stream. When it moves into colder sediments (away from the vent) there is the potential for more hydrate to form.

⑤ The depth of hydrate formation will approximately follow the depth of the ~9°C isotherm, presumably increasing with increasing distance from the vent chimney.

⑥ The limit of hydrate formation is dependent on the pooling of CO_2 beneath the hydrate layer, which reflects a balance between supply from below and loss through CO_2 vents, dissolution and hydrate formation.

⑦ The 'hydrate' fabric may include or be dominated by hydrate coated liquid CO_2 droplets. Water supply may be mass transport limited. Hydrate coated channels could form, allowing CO_2 to flow upwards and either...

⑧ ...emerge as a stream of small regularly sized hydrate coated CO_2 droplets, or...

⑨ ...form more hydrate dispersed in the upper sediments and/or outcropping at the sediment-seawater interface.

HYDRATE FORMATION AT LEAKAGE SITES

① In this system, CO_2 leaks from a storage reservoir and migrates upwards through the sediment column. At depth in the sediment column, the CO_2 will be in the supercritical phase. The depth at which the transition to the liquid phase occurs is a function of the local bottom water temperature and geothermal gradient, and will occur at a sediment depth of ~970m.

② The CO_2 liquid will migrate upwards through the sediment column, eventually moving into the hydrate stability zone, at which point hydrate will start to precipitate, forming an impermeable barrier. The base of the hydrate formation zone will occur at depths of ~230m.

③ CO_2 liquid is trapped under the hydrate layer. This barrier forces lateral advection of the CO_2. As the CO_2 flows laterally, the hydrate cap will grow, where the hydrate cap will be stable as long as it is in contact with water saturated CO_2 or CO_2 saturated porefluid.

④ The depth of hydrate formation will approximately follow the depth of the ~9°C isotherm, which will occur at relatively constant depth in the sediment.

⑤ The limit of hydrate formation is dependent on the pooling of CO_2 beneath the hydrate layer, which reflects a balance between supply from below and loss through CO_2 dissolution and hydrate formation.

⑥ The 'hydrate' fabric may include or be dominated by hydrate coated liquid CO_2 droplets. Water supply may be mass transport limited. Hydrate coated channels could form, allowing CO_2 to flow upwards and either...

⑦ ...emerge as a stream of small regularly sized hydrate coated CO_2 droplets, or...

⑧ ...form more hydrate dispersed in the upper sediments and/or outcropping at the sediment-seawater interface.

However, the difficulty in drawing direct comparisons to these sites arises from the difference in thermal regime when compared to the regime expected in sediments overlying a storage site. All of these sites are associated with hydrothermal activity, and are characterised by both high and spatially variable heat flow in the sediment column. As such, the hydrate stability zone will also be spatially variable and generally shallow, most likely limited to the sediment-seawater interface in near proximity to the hydrothermal vents.

In contrast, for a 'leakage' site at the same water depth, rising CO_2 will enter the hydrate formation zone at considerable depth. Indeed, when considering the liquid CO_2-hydrate stability curve, the base of the hydrate formation zone will likely always occur at significant depth in the sediment (due to the generally low temperature of ocean bottom waters). For example, if we consider a shallow water column of 500m with a relatively warm bottom water temperature of

~5°C, and a comparatively high geothermal gradient of 0.04°C/m, then the base of the hydrate stability zone (~8°C in this case) occurs at the still considerable depth of ~75m. However, by comparison to disseminated and massive methane hydrate deposits, the formation of flow pathways through the hydrate is conceivable (for example, hydrate coated pipes, where liquid CO_2 flowing through the pipe does not come into contact with water), delivering liquid CO_2 into upper levels of the sediments and potentially to the ocean. Under these circumstances CO_2 hydrate may well extend throughout the potential hydrate formation zone, and potentially outcrop at the seafloor.

Despite the difference in thermal regimes, observations of CO_2 behaviour at vent sites (particularly in the far field region at some distance from a high temperature vent) seem likely to provide information regarding hydrate formation that would be of considerable relevance to a leakage/seepage event. Of particular interest would be a detailed analysis of hydrate composition, fabric, and distribution in the sediments, and how these relate to the composition of the CO_2 feed liquid and the CO_2 supply rate. Although the base of the hydrate formation zone is likely to be shallow at these sites (even in the far field), that nearly all observations report droplets emerging through the hydrate cap and overlying sediments suggests that leakage of CO_2 can still occur, albeit at a slower rate, in areas where hydrate formation is possible. A cross site comparison of the depth of the hydrate stability zone, the thickness of the hydrate cap and the rate at which CO_2 is leaking through the cap, may provide valuable information regarding the conditions required (e.g. minimum thickness of hydrate cap, maximum limit on CO_2 supply) to prevent CO_2 leakage.

5.3 Case Study Examples

The analysis presented in Chapter 1 identified Japan, South East Asia (Natuna), Australia (Gorgon), and Western Europe as key regions where sub-seafloor storage of CO_2 is either in the active or planning stage. The phase behaviour and possibility of secondary trapping mechanisms operating in the sediment column in these regions is discussed below and summarised in Table 5.1. In all cases, water column depth and temperature profiles were extracted from the BODC (British Oceanographic Data Centre) and NODC (National Oceanographic Data Center) data bases.

For each region, typical water and sediment column T-P profiles are presented overlaid on a CO_2 phase diagram. Figure 5.8 provides the colour key to all phase diagrams in this section, where different keys are used to define the CO_2 phase space in the water column and the sediments. The hydrate stability zone is based on a simple fit to stability data for bulk phase CO_2 hydrate in seawater (Ohgaki et al., 1993; fit of type $P = \exp(a + b/T)$. For a comparison of this stability curve to those predicted by CSMHYD and CSMGem, and a discussion of the sources of uncertainty in this simplistic model of hydrate behaviour, see Section 5.2.3 above.
Also shown are the changes in CO_2 viscosity and density as a function of depth (for the free CO_2 phase, i.e. supercritical fluid, liquid, superheated vapour and gas phases). T-P profiles and the corresponding viscosity and density of CO_2 are described by solid black lines, with uncertainties arising from a difference in geothermal gradient of ±0.01°C/m shown by dashed black lines. The seawater-sediment interface is marked by a thick horizontal brown line, with 500m depth intervals in the sediment column marked by dashed brown lines. The dark blue vertical line on the density plots marks the range of expected seawater density.

Figure 5.8: CO_2 phase diagram colour key for case study examples.

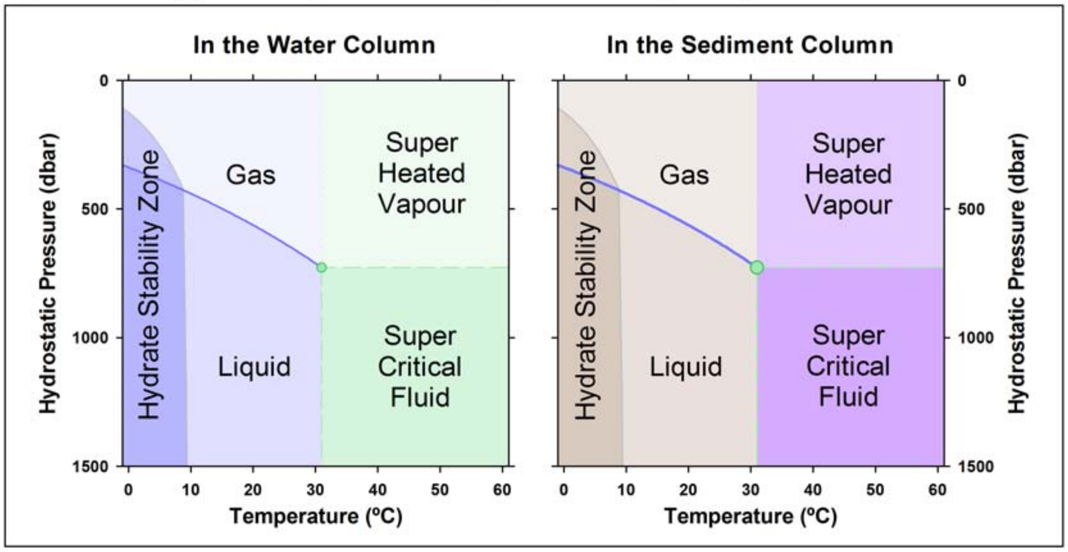

Each case study profile is categorized according to the buoyancy regime (CASE 1-4 scenarios described in Section 5.1.1) and the potential to form hydrate: In brief, hydrate formation is possible in all CASE 1 and CASE 2 sediments, and in cold and shallow CASE 3 sediments. Hydrate formation is not possible in warm CASE 3 sediments and all CASE 4 sediments.

CASE 1: The upper few hundred metres of these cold deep sediments will lie within the hydrate stability zone. Thus CASE 1 sediments will benefit from both buoyancy and hydrate trapping mechanisms.

CASE 2: If CO_2 remains in the liquid phase at the sediment-seawater interface, then the conditions will typically be such that they also fall within the hydrate stability zone. Thus although CASE 2 sediments do not benefit from buoyancy trapping, they do benefit from a gradually slowing migration rate and the possibility of hydrate trapping.

CASE 3: In warm CASE 3 sediments, temperatures are too high for hydrate formation. See the Australia (North Western Shelf), and North West Europe (North Sea) case studies below. However, in very cold shallow CASE 3 sediments, the upper sediments can lie within the hydrate stability zone. See the North West Europe (Barents Sea) case study below. In this case, the CO_2 crosses the liquid to gas transition before entering the hydrate stability zone.

CASE 4: Hydrate formation is not possible in any CASE 4 type sediments.

5.3.1 The Sea of Japan

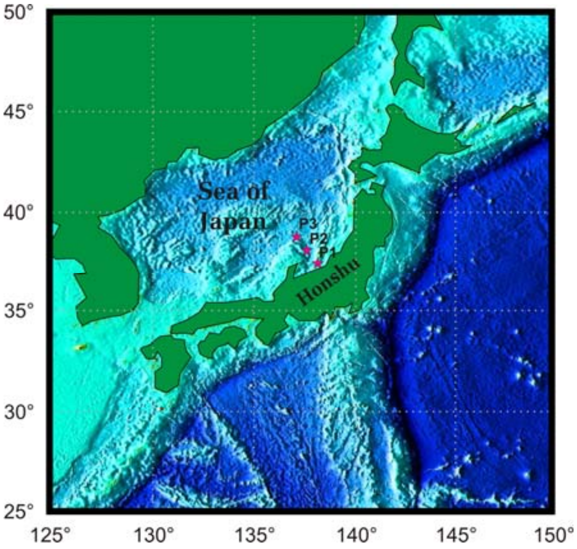

The offshore region to the north west of Honshu is the most likely target for sub-seafloor storage in this region. This area includes the only Category II Rank 1 aquifers located in Japanese waters (anticlinal structure, technical capacity > 50 Mt/CO_2, distance to source < 50 km). Here we consider 3 profiles in a north-west transect extending offshore from Honshu into the progressively deeper waters of the Sea of Japan (see map opposite). T-P conditions and CO_2 behavior as a function of depth are shown in Figure 5.9. The water column profiles are from April 2002 (NODC, originators Japan Meteorological Agency). A geothermal gradient of 0.03±0.01 °C/m was assumed.

P1: Water depth 982 m. CASE 2 scenario – CO_2 remains a buoyant liquid throughout the sediment column. Density and viscosity maxima at the sediment-water interface are 0.98 g/cm^3 and 114 μPa.s respectively. For κ of 10^{-13}, this gives a rise rate in near surface sediments of ~15 m/yr. Hydrate formation is possible, with a potential hydrate layer thickness of 303 m.

P2: Water depth 1822 m. CASE 2 scenario – CO_2 remains a buoyant liquid throughout the sediment column. Density and viscosity maxima at the sediment-water interface are 1.02 g/cm^3 and 129 μPa.s respectively. For κ of 10^{-13}, this gives a rise rate in near surface sediments of ~4 m/yr. Hydrate formation is possible, with a potential hydrate layer thickness of 315 m.

P3: Water depth 2368 m. CASE 1 scenario – CO_2 reaches the point of neutral buoyancy at a depth of 9 m in the sediment column. This provides an effective buoyancy cap, and in the absence of other disturbance, CO_2 will not leak to the ocean. Hydrate formation is possible, where the hydrate stability zone extends to 321 m depth in the sediment column. Allowing for the buoyancy cap, this gives a potential hydrate layer thickness of 312 m.

JAPAN SUMMARY: Cold deep waters occur relatively close to shore and secondary trapping mechanisms will operate at all locations along this transect. Hydrate formation

Table 5.1: The potential for buoyancy and hydrate trapping in regions where storage is occuring, or is likely to occur in the near future

Profile Location				The Sediment-Seawater Interface				The Sediment Column						
										Point of Neutral Buoyancy			Hydrate Stability Zone	
Region		Lat (°N)	Lon (°E)	Hydrostatic Pressure (dbar)	Depth (m)	Bottom Water T (°C)	Salinity (PSS'78)	Geothermal Gradient (°C/m)	Buoyancy Scenario	ρ_{CO2} (g/cm^3)	Depth (m)	Thickness (m)	Depth (m)	Thickness (m)
Japan	P1	37.5	138.2	992	982	0.25	34.1	0.03±0.01	*CASE 2*				1285 *1208 - 1440*	303 *226 - 458*
	P2	38.2	137.7	1844	1822	0.20	34.1	0.03±0.01	*CASE 2*				2137 *2057 - 2296*	315 *235 - 474*
	P3	38.8	137.2	2400	2368	0.23	34.1	0.03±0.01	*CASE 1*	1.039	2377 *2374 - 2386*	9 *6 - 18*	2689 *2609 - 2850*	321 *241 - 482*
SE Asia	P1	3.7	109.9	85	84	21.1	34.2	0.045±0.01	*CASE 4*					
	P2	7.4	109.9	1413	1400	3.3	34.8	0.045±0.01	*CASE 2*				1536 *1511 - 1575*	136 *111 - 175*
Australia	P1	-21.0	115.6	17	17	21.5	35.3	0.03±0.01	*CASE 4*					
	P2	-20.5		201	200	10.0	35.3	0.03±0.01	*CASE 3*					
North West Europe	P1	59.0	0.6	160	158	6.2	34.7	0.03±0.01	*CASE 3*					
	P2	59.3	4.0	303	300	6.5	35.3	0.03±0.01	*CASE 3*					
	P3	63.0	3.9	849	839	-0.8	34.9	0.03±0.01	*CASE 1*				1175 *1091 - 1348*	336 *252 - 509*
	P4	64.4	0.7	2567	2526	-0.9	34.9	0.03±0.01	*CASE 2*	1.040	2645 *2606 - 2761*	119 *80 - 235*	2883 *2793 - 3063*	357 *267 - 537*
	P5	72.0	25.0	263	260	4.6	35.0	0.03±0.01	*CASE 3*		4		369 *309 - 473*	109 *49 - 213*

is predicted to occur at all sites, with a thick potential hydrate formation layer of ~300 m. In the deeper waters further offshore buoyancy trapping will also occur. This suggests that in the event of CO_2 leakage from a sub-seafloor storage site, secondary trapping in the sediment column is likely to be efficient and CO_2 release to the ocean will be limited.

Figure 5.9: T-P conditions and CO_2 behavior for 3 profiles in a transect offshore Honshu into the Sea of Japan.
Upper Panel - P1 (water depth 982 m). Centre Panel - P2 (water depth 1822 m). Lower Panel - P3 (water depth 2368 m).

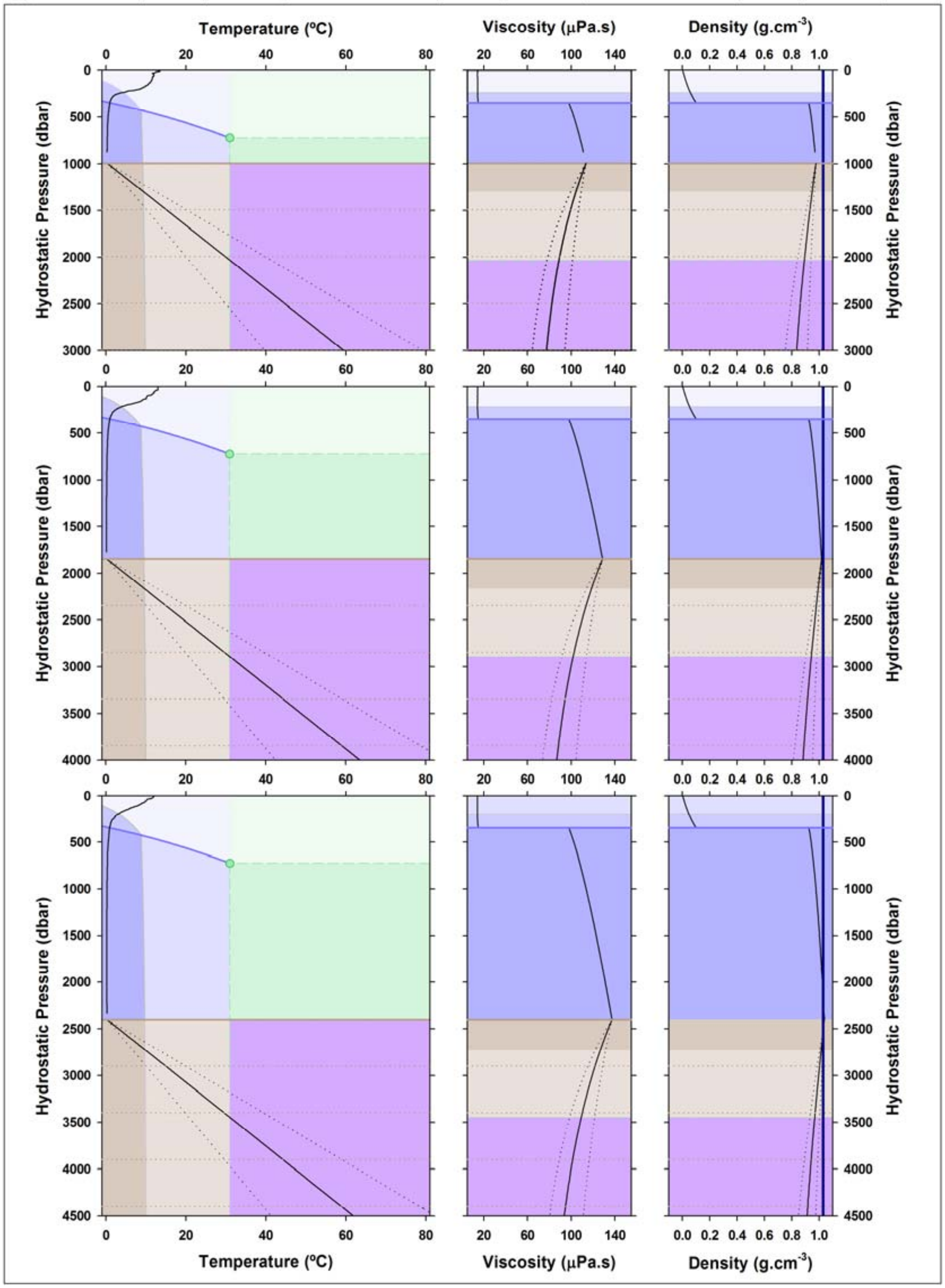

5.3.2 South East Asia

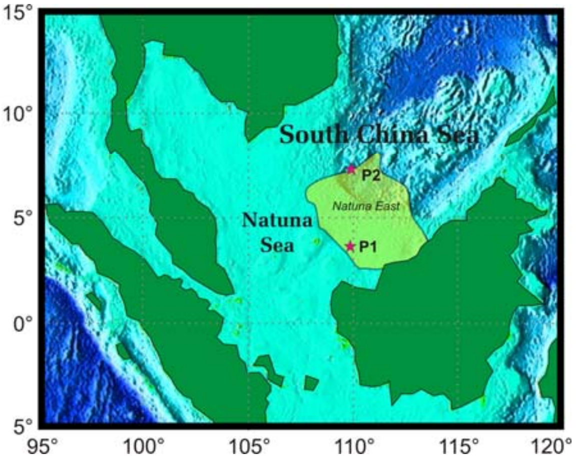

If the Natuna-D Alpha field is developed, CO_2 storage will occur in neighbouring deep saline aquifers at a depth of ~900m below the sediment surface. Precise locations of potential storage targets are not available. Here we consider two profiles representative of the range of conditions in the Natuna East basin. T-P conditions and CO_2 behavior as a function of depth are shown in Figure 5.10. The water column profiles for P1 and P2 are from July 1989 and October 1985 respectively (NODC, originators Pacific Oceanological Institute and Far East Scientific Research Institute). A high geothermal gradient of 0.045±0.01 °C/m was used to reflect known conditions in this basin (APEC, 2005).

P1 (East Natuna Sea): Water depth 84 m. CASE 4 scenario – due to high temperatures and low pressures in the sediments of this shallow warm shelf sea, any CO_2 that leaks to the sediment column will rise rapidly becoming less dense and less viscous as it ascends. The supercritical fluid to superheated vapour transition occurs at ~ 723 m sediment depth and the superheated vapour to gas transition at ~304 m depth. Density and viscosity of the CO_2 gas at the sediment-water interface are ~0.018 g/cm^3 and ~14.8 μPa.s respectively, indicating rapid rise of buoyant gas. Thus in the event of leakage from a sub-seafloor storage site, CO_2 escape to the ocean is inevitable. Given the shallow water column, a significant proportion of the CO_2 is also likely to escape to the atmosphere.

P2 (South China Sea): Water depth 1400 m. CASE 2 scenario – CO_2 remains a buoyant liquid throughout the sediment column. Density and viscosity maxima at the sediment-water interface are 0.99 g/cm^3 and 116 μPa.s. For κ of 10^{-13}, this gives a rise rate in near surface sediments of ~13 m/yr. Hydrate formation is possible, with a potential hydrate layer thickness of 136 m.

NATUNA EAST BASIN SUMMARY: If CO_2 is stored in geological formations beneath the Natuna Sea, then storage security will be entirely dependent on the integrity of the primary storage site. This shallow shelf sea is characterized by high bottom water temperatures (P1 = 21.1°C). When combined with the high geothermal gradient and low hydrostatic pressures, this means that CO_2 will become less dense and less viscous as it rises, and will ascend at an accelerating rate through the sediment column. In the event of primary leakage, escape of CO_2 to the ocean seems inevitable, and release to the atmosphere likely. In comparison, storage security would be enhanced for sites located within the deeper, colder basin of the South China Sea in the north-eastern sector of the Natuna East area (see map above). In this region, hydrate formation is possible, with a potential hydrate layer thickness on the order of ~100 m. Thus in the event of primary leakage, CO_2 release to the ocean may be significantly reduced through efficient secondary trapping mechanisms operating in the sediment column.

Figure 5.10: T-P conditions and CO_2 behavior for 2 profiles in the Natuna East basin, in the East Natuna Sea (P1) and South China Sea (P2). Upper Panel - P1 (water depth 84 m). Lower Panel - P2 (water depth 1400 m).

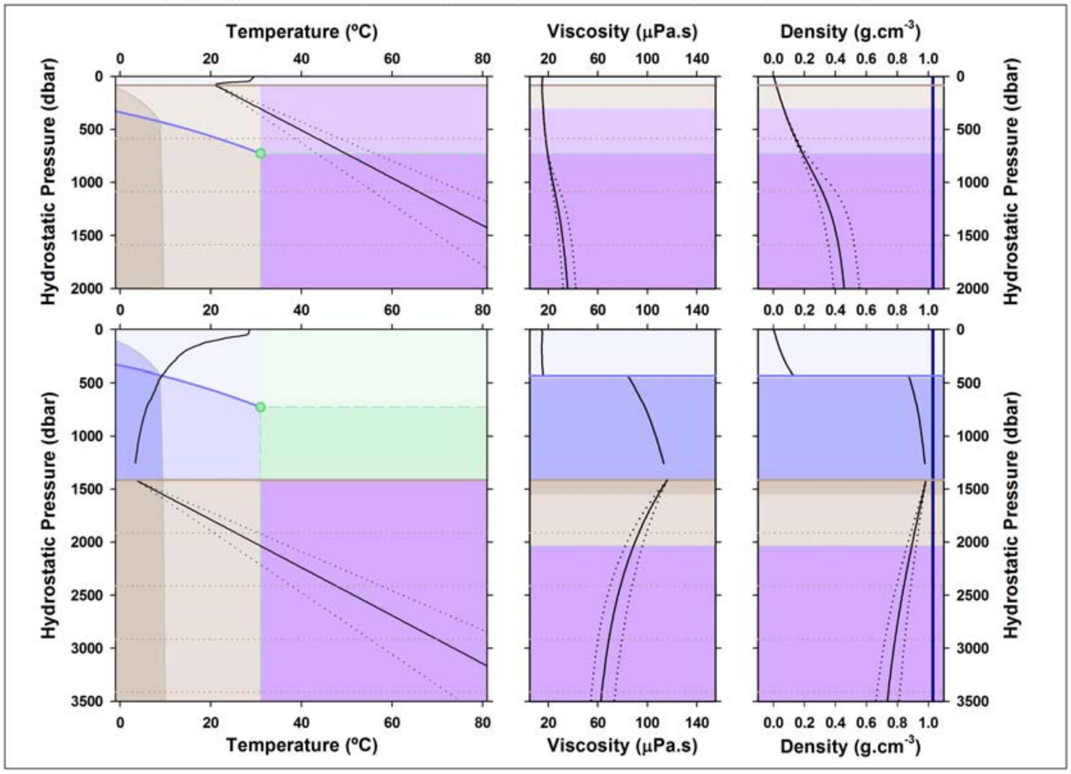

5.3.3 Australia

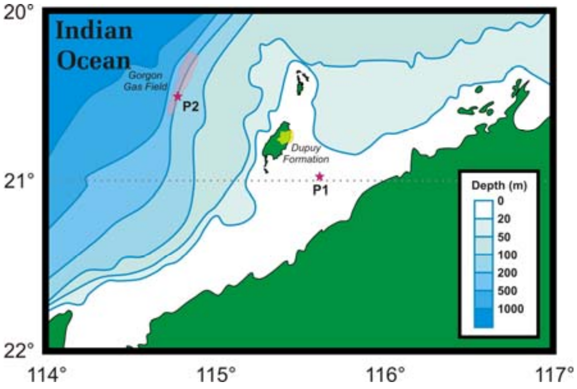

The Gorgon Project is planned with CO_2 storage under Barrow Island, where the storage reservoir (the Dupuy Formation) extends offshore and underlies the shallow warm seas of the North Western Australian Shelf. The waters immediately surrounding Barrow Island and extending between Barrow Island and the mainland are very shallow and do not exceed 20m depth. The water column is well mixed, with uniform temperatures throughout the water column, ranging from ~30°C in Austral summer to ~21°C in Austral winter (ChevronTexaco Australia, 2003). For example, the water column profile for P1 is from July 1999 (NODC, originators Commonwealth Scientific and Industrial Research Organization (CSIRO)), with a bottom water temperature of 21.5°C.

As noted in Chapter 1, if carbon storage in sub-sea geologic formations proves successful, the Greater Gorgon gas fields themselves would provide significant future additional CO_2 storage capacity once the hydrocarbon reservoirs are depleted. The Gorgon gas field lies on the continental slope at a water depth of approximately 200 m (see map above). Surface water temperatures in the vicinity of the Gorgon gas field and the offshore portions of the proposed feed gas pipeline vary between 22°C and 31°C. From the surface to a depth of 100 m, the water column is generally well-mixed. The mean temperature for depths between 200 and 250 m is around 10°C (ChevronTexaco Australia 2003). P2 is a theoretical profile chosen to be representative of expected conditions at this site, located in water depth of 200m with an assumed bottom water temperature of 10°C.

For both P1 and P2 a geothermal gradient of 0.03±0.01°C/m has been assumed. However, it is noted that the Dupuy formation lies at a depth of 2200m with a temperature of ~100°C (Chapter 13, ChevronTexaco Australia Pty Ltd., 2005), consistent with a geothermal gradient of 0.03-0.04°C/m. Thus for P1 the CO_2 behavior is unlikely to fall towards the colder limit shown. T-P conditions and CO_2 behavior as a function of depth for both profiles are shown in Figure 5.11.

P1: Water depth 17 m. CASE 4 scenario – due to high temperatures and low pressures in the sediments of this shallow warm shelf sea, any CO_2 that leaks to the sediment column will rise rapidly becoming less dense and less viscous as it ascends. The supercritical fluid to superheated vapour transition occurs at ~ 703 m sediment depth (720 m total depth) and the superheated vapour to gas transition at ~316 m sediment depth (333 m total depth). Density and viscosity of the CO_2 gas at the sediment-water interface are ~0.005 g/cm^3 and <14.8 μPa.s respectively, indicating rapid rise of buoyant gas. Thus in the event of leakage from a sub-seafloor storage site, CO_2 escape to the ocean seems inevitable. Given the shallow water column, a significant proportion of the CO_2 is also likely to escape to the atmosphere.

P2: Water depth 200 m. CASE 3 scenario – any CO_2 that leaks to the sediment column will become more dense and viscous as it ascends until it reaches the liquid-gas transition. The liquid to gas transition occurs at ~375 m sediment depth (575 m total depth). The volume will increase by a factor of 3.72 at the transition, from ~1.31 cm^3/g (density 0.76 g/cm^3) in the liquid phase to ~4.88 cm^3/g (density 0.21 g/cm^3) in the gas phase. Once in the gas phase, the ascending CO_2 will become less dense and less viscous as it rises, with a further increase in volume to 21.68 cm^3/g at the sediment-seawater interface. Density and viscosity of the CO_2 gas at the sediment-water interface are ~0.046 g/cm^3 and ~15.3 μPa.s respectively, indicating rapid rise of buoyant gas..

GORGON SUMMARY: If CO_2 is stored in the Dupuy formation beneath Barrow Island, then storage security will be entirely dependent on the integrity of the primary storage site. This shallow shelf sea is characterized by high bottom water temperatures (21-30°C). When combined with the high geothermal gradient and low hydrostatic pressures, this means that CO_2 will become less dense and less viscous and ascend at an accelerating rate through the sediment column. In the event of primary leakage (in the offshore sector of the storage reservoir), escape of CO_2 to the ocean seems inevitable, and release to the atmosphere likely. However it is also noted that the sedimentary rocks in this region are predominantly limestone, thus reaction may occur during CO_2 ascent, acting to neutralise the CO_2 (see Section 5.4). Storage security would only be moderately improved in the slightly deeper and colder Gorgon Gas Field Area, due to slower ascent rates and the increased depth of the water column.

Figure 5.11: T-P profiles and CO_2 behavior for 2 profiles in the vicinity of the Gorgon CO_2 storage project.
Upper Panel - P1 (water depth 17 m). Lower Panel - P2 (water depth 200 m).

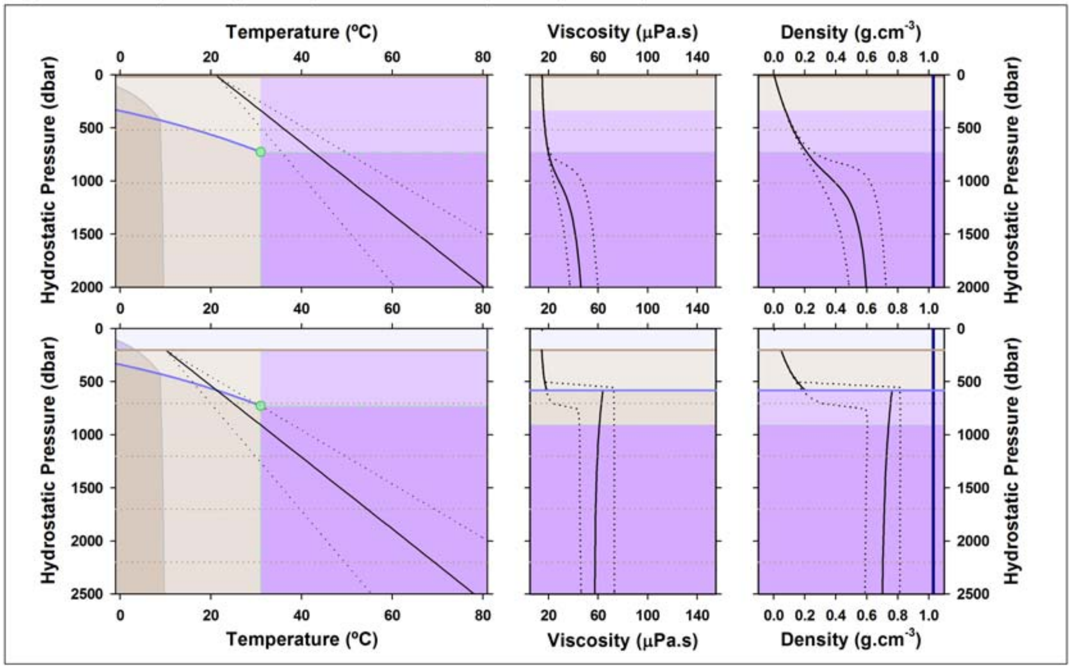

5.3.4 Western Europe

Western Europe is currently the most active world region in terms of offshore storage. A regional scale assessment of potential hydrate formation has been carried out for sediments offshore Western Europe (Camps et al., 2006). This project involved the development of a computer program to calculate CO_2 hydrate stability zones on a high resolution one-minute grid. Detailed bathymetry was extracted from the GEBCO global bathymetry data sets, bottom water temperature data were extracted from the BODC database, a geothermal gradient of 0.03°C/m was assumed, and stability conditions for CO_2 hydrate were calculated using CSMHYD (Camps et al., 2006). The results of this intensive effort are presented below in Figure 5.12 as a map of potential hydrate thickness (reproduced by kind permission of the authors).

Figure 5.12: Predicted Carbon Dioxide Hydrate Thickness (m) Offshore Western Europe (from Camps et al., 2006)

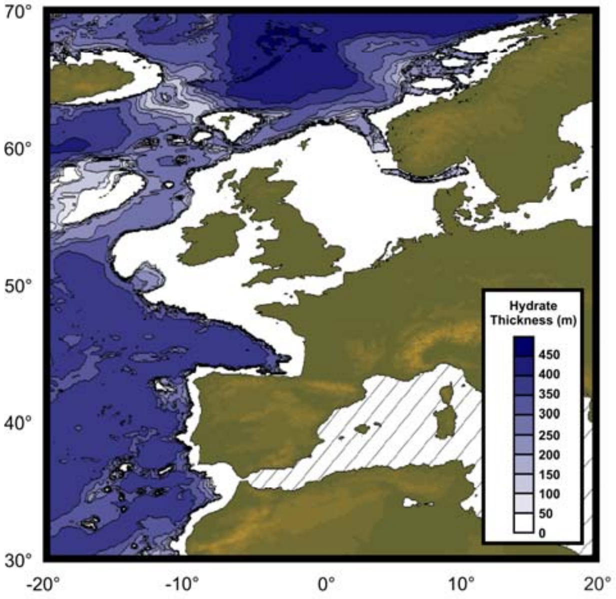

Results predict that CO_2 hydrate will be stable over large areas, with the base of the stability zone reaching a depth of up to ~450m below the ocean floor. The greatest potential for hydrate formation in near shore sediments is found offshore Portugal, Northern Spain, South West France and parts of Norway where relatively deep water lies close to shore. Conversely, there is little potential for hydrate formation in sediments underlying the shallow waters of the North Sea, with potential hydrate formation restricted to the deeper waters offshore southern Norway.

While this analysis strongly indicates that sub-seafloor storage sites located offshore Portugal, Northern Spain, and South West France would benefit from the possibility of effective secondary trapping mechanisms in the event of a primary leakage; these areas do not (at present) correspond to current or planned sub-seafloor storage sites. Rather, European interest in sub-seafloor storage is focused in the north-west of the region, with multiple current and planned future storage sites located in the North Sea, Norwegian Sea & Barents Sea. Here we look in more detail at the behavior of CO_2 in these regions.

The map opposite shows the locations of the five profiles considered. P1 and P2 are located in the North Sea in reasonable proximity to the Utsira Sandstone, where sub-seafloor storage of CO_2 is already occurring (Sleipner project). P3 and P4 have been selected as representative profiles for the deeper waters to be found in the Norwegian Sea. These profiles are also in reasonable proximity to the Heidrun and Draugan sites, which may be used for CO_2 storage in the future. P5 is representative of conditions in the Barents Sea, where sub-seafloor CO_2 storage will commence shortly at the Snøhvit site.

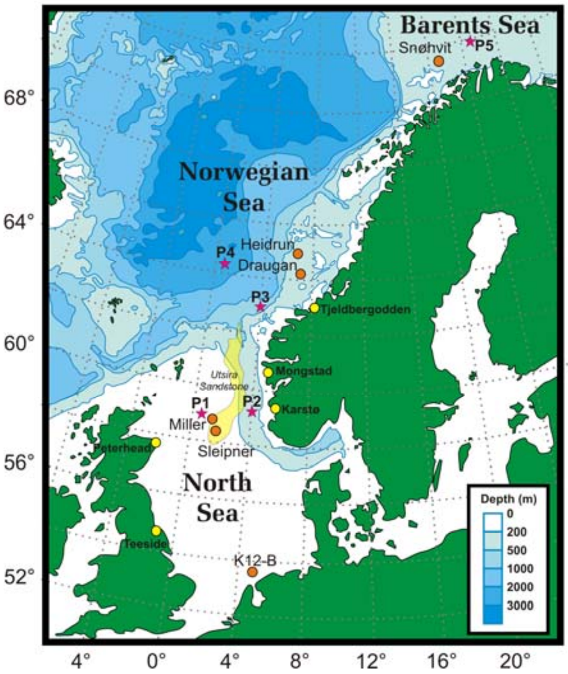

5.3.4.1The North Sea

Although relatively cold, the vast majority of the North Sea is shallower than 200m, which is too shallow for hydrate formation (see Figure 5.12). Nevertheless, the North Sea also contains the deeper waters found in the Norwegian Trench and the Skagerrak Strait at the southern end of Norway, where hydrate formation is possible (Camps et al., 2006). Profiles P1 and P2 are located in reasonable proximity to the Utsira Sandstone. P1 represents a typical shallow North Sea profile and is also relatively close to the Miller Oil Field, where CO_2 storage in combination with EOR is being considered. P2 is located in the deeper waters of the Trench (although not within a region of potential hydrate formation) offshore from Karstø, where a CCS ready power station is in the planning/construction phase. T-P conditions and CO_2 behavior as a function of depth for both profiles are shown in Figure 5.13.

P1: Water depth 158 m. CASE 3 scenario – any CO_2 that leaks to the sediment column will become more dense and viscous as it ascends until it reaches the liquid-gas transition at ~359 m sediment depth. At the liquid-gas transition the volume will increase by a factor of 4.66 from ~1.24 cm^3/g (density 0.81 g/cm^3) in the liquid phase to ~5.78 cm^3/g (density 0.17 g/cm^3) in the gas phase. Once in the gas phase, the CO_2 will become less dense and less viscous as it continues to rise, with a further increase in volume to 27.41 cm^3/g at the sediment-seawater interface. Density and viscosity of the CO_2 gas at the sediment-water interface are ~0.036 g/cm^3 and 14.2 μPa.s respectively, indicating rapid rise of buoyant gas.

P2: Water depth 300 m. CASE 3 scenario – any CO_2 that leaks to the sediment column will become more dense and viscous as it ascends until it reaches the liquid-gas transition at ~145 m sediment depth. At the liquid-gas transition the volume will increase by a factor of 6.14 from ~1.16 cm^3/g (density 0.86 g/cm^3) to ~7.16 cm^3/g (density 0.14 g/cm^3). Once in the gas phase, the CO_2 will become less dense and less viscous as it continues to rise, with a further increase in volume to 12.84 cm^3/g at the sediment-seawater interface. Density and viscosity of the CO_2 gas at the sediment-water interface are ~0.078 g/cm^3 and ~14.8 μPa.s respectively, indicating rapid rise of buoyant gas.

NORTH SEA SUMMARY: For CO_2 stored in the North Sea basin, storage security will be entirely dependent on the integrity of the primary storage site. This shelf sea is characterized by shallow water depths, typically less than 200m, and CO_2 will enter the gas phase at depth in the sediment column. In the event of primary leakage, escape of CO_2 to the ocean seems inevitable, and some release to the atmosphere likely.

Figure 5.13: T-P profiles and CO_2 behavior for 2 profiles in the North Sea in proximity to the Utsira Formation.
Upper Panel - P1 (water depth 158 m). Lower Panel - P2 (water depth 300 m).

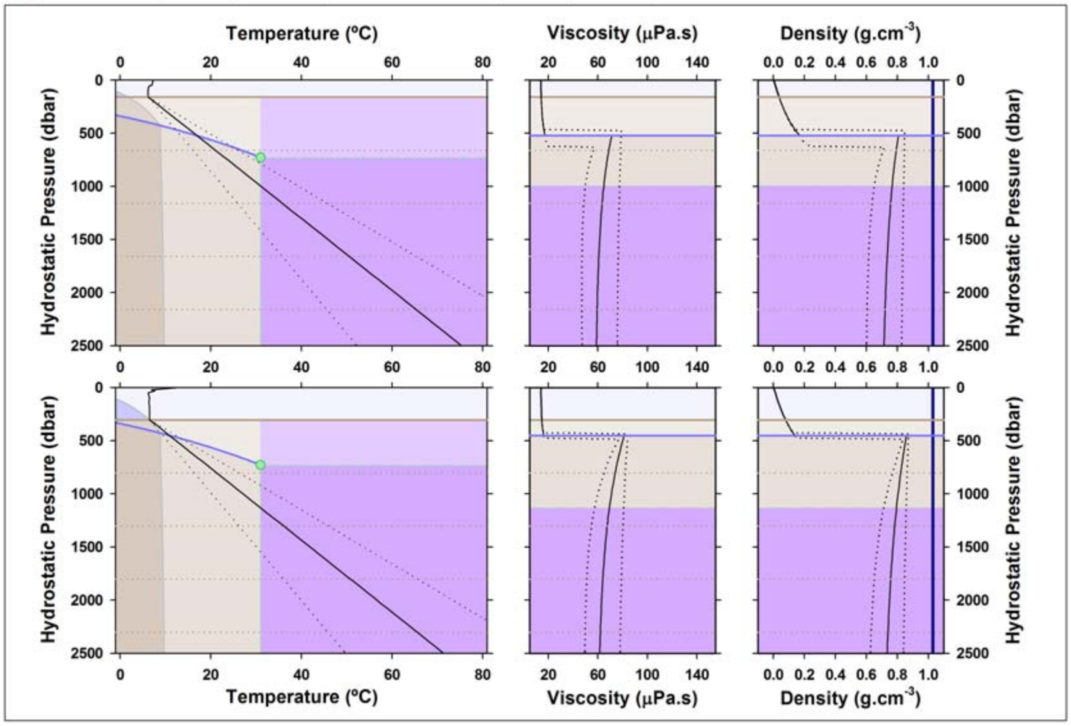

5.3.4.2 The Norwegian Sea

The deeper waters of the Norwegian Sea are combined with sub-zero temperatures at the sediment-seawater interface. Here we consider two representative profiles, where T-P conditions and CO_2 behavior as a function of depth for both profiles are shown in Figure 5.14.
P3: Water depth 839 m. CASE 2 scenario – CO_2 remains a buoyant liquid throughout the sediment column. Density and viscosity maxima at the sediment-water interface are 0.97 g/cm^3 and 113 μPa.s respectively. For κ of 10^{-13}, this gives a rise rate in near surface sediments of ~16 m/yr. Hydrate formation is possible, with a potential hydrate layer thickness of 336 m.

P4: Water depth 2526 m. CASE 1 scenario – CO_2 reaches the point of neutral buoyancy at a depth of 119 m in the sediment column, thus CO_2 will not leak to the ocean. Hydrate formation is possible, where the hydrate stability zone extends to 357 m depth in the sediment column. Allowing for the buoyancy cap, this gives a potential hydrate layer thickness of 238 m.

NORWEGIAN SEA SUMMARY: Secondary trapping mechanisms will operate in the cold deep waters of the Norwegian Sea. Hydrate formation is predicted to occur, with a potential hydrate formation layer of ~200-300 m. In deeper waters buoyancy trapping will also occur. This suggests that in the event of CO_2 leakage, secondary trapping is likely to be efficient and CO_2 release to the ocean will be limited or prevented.

5.3.4.3The Barents Sea

The Barents Sea offers an unusual case study when compared to the other sites considered. Profile P5 is located in shallow cold sediments and is representative of conditions in this region. T-P conditions and CO_2 behavior as a function of depth for this profile are shown in Figure 5.15.

P5: Water depth 260 m. CASE 3 scenario – any CO_2 that leaks to the sediment column will become more dense and viscous as it ascends until it reaches the liquid-gas transition at ~172

Figure 5.14: T-P profiles and CO$_2$ behavior for 2 profiles in the Norwegian Sea.
Upper Panel - P3 (water depth 839 m). Lower Panel - P4 (water depth 2526 m).

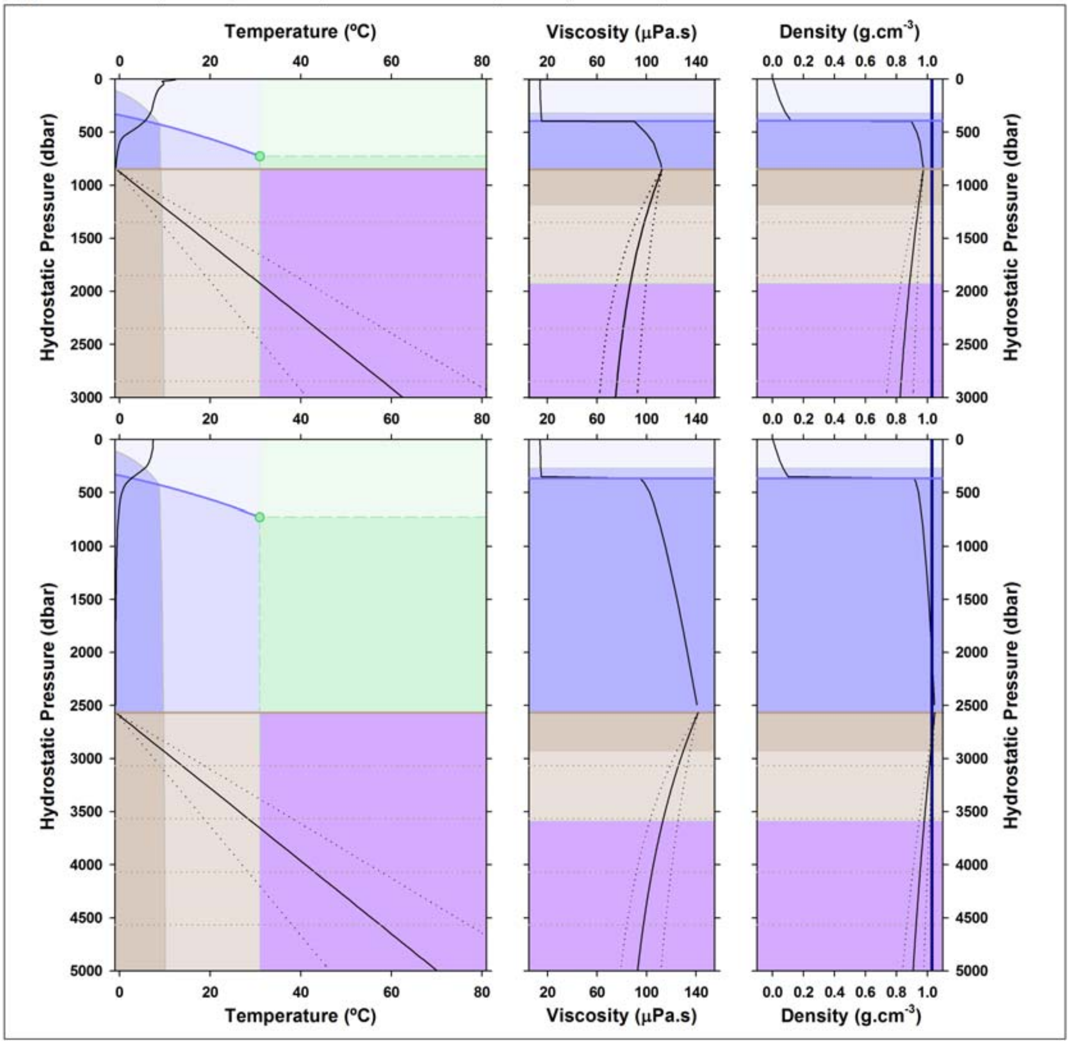

m sediment depth. At the liquid-gas transition the volume will increase by a factor of 6.42 from ~1.15 cm^3/g (density 0.87 g/cm^3) in the liquid phase to ~7.41 cm^3/g (density 0.14 g/cm^3) in the gas phase. Once in the gas phase, the CO$_2$ will become less dense and less viscous as it continues to rise. At shallower depths hydrate formation is possible, where the base of the hydrate stability zone occurs at ~109 m sediment depth. Thus secondary trapping mechanisms are likely to operate in these sediments, with a potential hydrate layer thickness of 109 m.

BARENTS SEA SUMMARY: In the shallow cold sediments of the Barents Sea CO$_2$ will enter the gas phase at depth. Hydrate formation is predicted to occur where the base of the hydrate formation zone is some 70m above the depth of the gas to liquid transition. The ability of a CO$_2$ hydrate layer to impede flow of CO$_2$ gas remains to be seen.

5.4 Reaction with Carbonates

Additional physico-chemical processes that can act to limit CO_2 escape include dissolution (also called solubility trapping) and reaction with minerals (e.g. carbonates) in the host rock or sediments. Both of these processes have complex controls, a number of which are not yet well enough understood (under the conditions of interest) to be accurately incorporated into models in order to predict the fate of CO_2 in the sediment column. Efforts are being made to address this knowledge gap, for example House and co-workers are intending to extend their model of a hydrate capped liquid CO_2 reservoir (described in House et al., 2006) to determine the rate of CO_2 dissolution when buoyancy driven advection is accounted for – that is the mixing and entrainment of pristine pore fluids that arises from either the sinking of dense CO_2 saturated pore fluids and/or the rising of the CO_2 plume. Here we focus on the reaction between CO_2 and sedimentary calcium carbonates, highlighting areas where an improved understanding is required in order to determine the eventual fate of CO_2 in carbonate bearing sediments..

5.4.1 Controls on the Reaction between CO_2 & Calcium Carbonate

NOTE: for further discussion of the thermodynamics of the CO_2 system in seawater see BACKGROUND INFORMATION.

The leakage or seepage of CO_2 from a sub-seafloor storage reservoir into carbonate rich sediments will lead to carbonate dissolution. This has two important consequences. Firstly, the dissolution of carbonate acts to buffer the injected CO_2, reducing the acidifying effect of adding CO_2 to the system. Secondly, carbonate dissolution will alter the physical structure of the sediment column, in particular increasing the porosity and permeability of the sediments. While the relationship between porosity and permeability in carbonates is highly variable (Enos & Sawatsky, 1981), small increases in porosity can lead to large increases in permeability. Thus a small amount of carbonate dissolution could significantly change both flow paths and flow rates through the sediment column, and thus the rate and extent of further carbonate dissolution, and the amount of CO_2 that reaches the seafloor.

In the long-term (thousand year time-scales), the dissolution of sedimentary carbonates is likely to (partially) reverse ocean acidification due to surface invasion of fossil fuel CO_2 (Archer et al., 1998). The limitation of this process with respect to surface invasion is that it requires the injected CO_2 to have been mixed into deep waters where it comes into contact with $CaCO_3$ rich seafloor sediments. Furthermore, only a limited proportion of the total seafloor carbonate reservoir is available for neutralization as the depth of downward mixing (and therefore dissolution) is limited to the upper bioturbated layer. However, for CO_2 migrating upwards through a $CaCO_3$ rich sediment column, these limitations do not apply, and the reaction will exert an immediate effect.

Figure 5.15: T-P profile and CO_2 behavior for a profile in the Barents Sea. P5 (water depth 260 m).

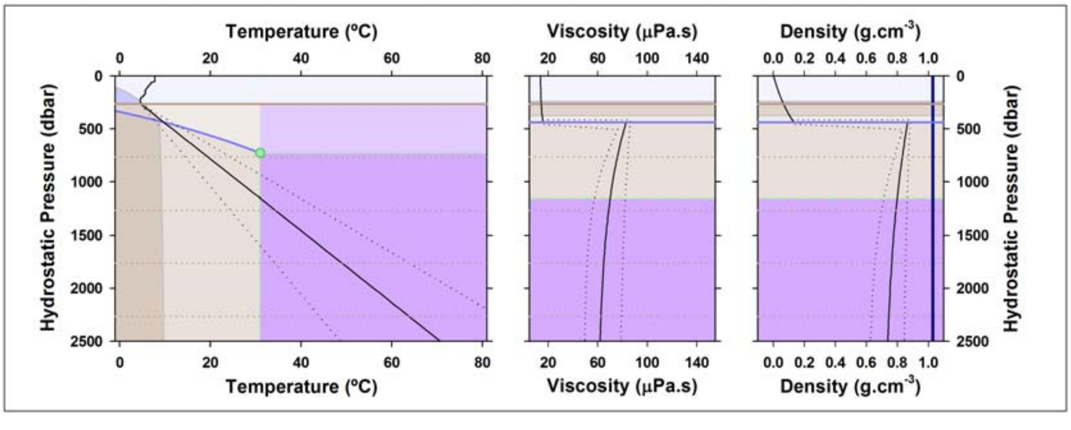

If we consider a sediment pore fluid in equilibrium with a separate CO_2 phase, the pore fluid will be saturated in CO_2 and have a low pH. The CO_2 speciation of the pore fluid will be dominated by CO_2^* ($CO_{2(aq)}$ + H_2CO_3) with minor bicarbonate (HCO_3^-), and the carbonate (CO_3^{2-}) concentration will be zero.

The dissolution of calcium carbonate is controlled by the saturation state of the pore fluids with respect to $CaCO_3$ (Ω), which is expressed as:

$$\Omega = \frac{[Ca^{2+}]_{pf}[CO_3^{2-}]_{pf}}{K_{SP}^*} \qquad \textbf{[Eq. 5.7]}$$

Where $[Ca^{2+}]_{pf}$ and $[CO_3^{2-}]_{pf}$ are the actual concentrations of calcium and carbonate ions in the pore fluid, and K^*_{SP} is the stoichiometric solubility product for the equilibrium reaction:

$$CaCO_3 \Leftrightarrow Ca^{2+} + CO_3^{2-} \qquad \mathrm{K}_{\mathrm{SP}}^* = [Ca^{2+}][CO_3^{2-}] \qquad \textbf{[Eq. 5.8]}$$

K^*_{SP} is not constant, but varies as a function of temperature, salinity and pressure. At the reference pressure (hydrostatic pressure = 0 bar, absolute pressure = 1 atm), $K^*_{SP,0}$ is given by (Mucci, 1983):

$$\log K_{SP,0}^* = -a - bT_K + \frac{c}{T_K} + d\log T_K + \left(-e + fT_K + \frac{g}{T_K}\right)S^{\frac{1}{2}} - hS + iS^{\frac{3}{2}} \qquad \textbf{[Eq. 5.9]}$$

Where T_K is the temperature in degrees Kelvin, S is salinity, and values of the constants *a* to *i* are given in Table 5.2. The effect of pressure can be calculated from the equation (Millero, 1995):

$$\ln\left(\frac{K_{SP,P}^*}{K_{SP,0}^*}\right) = -\frac{\Delta V_{SP}}{\hat{R}T_K}P + 0.5\frac{\Delta\kappa_{SP}}{\hat{R}T_K}P^2 \qquad \textbf{[Eq. 5.10]}$$

Where:

$$\Delta V_{SP} = -a_0 + a_1T_c \quad \text{and} \quad \Delta\kappa_{SP} = -b_0 + b_1T_c$$

Where P is the hydrostatic pressure in bars, ΔV_{SP} is the molal volume change, $\Delta\kappa_{SP}$ is the compressibility change, R is 83.131 cm^3 bar mol^{-1} K^{-1}, and T_C is the temperature in degrees Celsius. Values of the constants a_0, a_1, b_0 and b_1 are given in Table 5.2.

Table 5.2: Coefficients for determining the solubility products of calcite & aragonite

	Calcite	Aragonite
As function of T and S (see Eq. 5.9)		
a	171.9065	171.945
b	0.077993	0.077993
c	2839.319	2903.293
d	71.595	71.595
e	0.77712	0.068393
f	0.0028426	0.0017276
g	178.34	88.135
h	0.07711	0.10018
i	0.0041249	0.0059415
The effect of pressure (see equation 5.10)		
a_0	48.76	46.00
a_1	0.5304	0.5304
b_0	0.01176	0.01176
b_1	0.0003692	0.0003692

Table 5.3: Matrix densities for components of marine sediments

Mineral		**Density (ρ)** g/cm_3
Carbonates		
Aragonite	$CaCO_3$	2.93 - 2.94
Calcite	$CaCO_3$	2.71
Dolomite	$CaMg(CO_3)_2$	2.8 - 2.9
Quartz		2.65 - 2.66
Clays		
Montmorillonite		2.2 - 2.7
Kaolinite		2.6 - 2.63
Illite		2.6 2.9
Iron oxyhydroxides		
Ferrihydrite	$Fe(OH)_3$	3.93
Goethite	$FeO(OH)$	4.27
Hematite	Fe_2O_3	5.3

If Ω is less than 1, the pore fluid is undersaturated, and if Ω is greater than 1 the pore fluid is supersaturated. As the addition of CO_2 to the pore fluid reduces the concentration of CO_3^{2-} to zero, Ω is also zero (extreme undersaturation), and $CaCO_3$ will dissolve. For every mole/unit of $CaCO_3$ that is dissolved, one mole/unit of total CO_2 ($TCO_2 = CO_2^* + HCO_3^- + CO_3^{2-}$) and two moles/units of alkalinity (due to the double negative charge on the carbonate ion) are added to the pore fluid. The addition of alkalinity to the pore fluid decreases the concentration of CO_2^* by shifting the carbonate equilibrium toward bicarbonate. The overall reaction, though more complex, can be thought of as:

$$CO_2(aq) + H_2O + CaCO_3 \rightarrow Ca^{2+} + 2HCO_3^- \qquad \textbf{[Eq. 5.11]}$$

The extent of carbonate dissolution, and therefore the extent to which this reaction neutralizes the CO_2 input will be a complex function of numerous factors including:

(i) the type of carbonates present in the sediment column
(ii) the amount of carbonates present in the sediment column
(iii) the degree of saturation in the aqueous phase with respect to $CaCO_3$
(iv) the rate of carbonate dissolution
(v) the migration of the CO_2 rich fluid through the sediment column

These are discussed in the following sections.

5.4.1.1 The Type of Calcium Carbonate Present

There are two polymorphs of $CaCO_3$, aragonite and calcite. These minerals have different properties, where aragonite is more soluble (Table 5.2, higher K_{SP} and therefore lower Ω for the same given conditions) and has a higher density (Table 5.3) than calcite. The presence of other components in the carbonate lattice (e.g. magnesium (Mg) content) will also alter dissolution characteristics.

The vast majority of $CaCO_3$ in the sediment column consists of the skeletal remains of a variety of marine organisms such as coccolithophores, foraminifera and pteropods. The major carbonate minerals in sedimentary rocks are calcite, and to a significantly lesser extent, dolomite ($CaMg(CO_3)_2$). In modern sediments, calcite is by far the most abundant carbonate mineral in the deep sea, while aragonite and high-magnesian calcites dominate in tropical and subtropical shallow water environments. As such, marine carbonate assemblages are multi-phase systems, characterized by a heterogenous mixture of particle sizes, structure, and chemical composition.

5.4.1.2 The Amount of Calcium Carbonate Present

The amount of $CaCO_3$ present in the sediment column gives the upper limit on the possible extent of neutralisation. Figure 5.16 compares global seafloor bathymetry to the distribution of $CaCO_3$ in sediment core tops. The well-known depth dependence of sediment carbonate concentration can be clearly seen. There is a high concentration of calcite in the Atlantic Ocean in response to the high pH, freshly ventilated North Atlantic Deep Water, high concentrations in the eastern equatorial Pacific, in response to high rates of calcite production and a topographic high in that region, and a sharp cut-off in calcite preservation poleward of 50^o south latitude (Archer, 1996).

Figure 5.16: Global seafloor bathymetry (upper panel) & distribution of $CaCO_3$ (wt%) in core top sediments (lower panel).

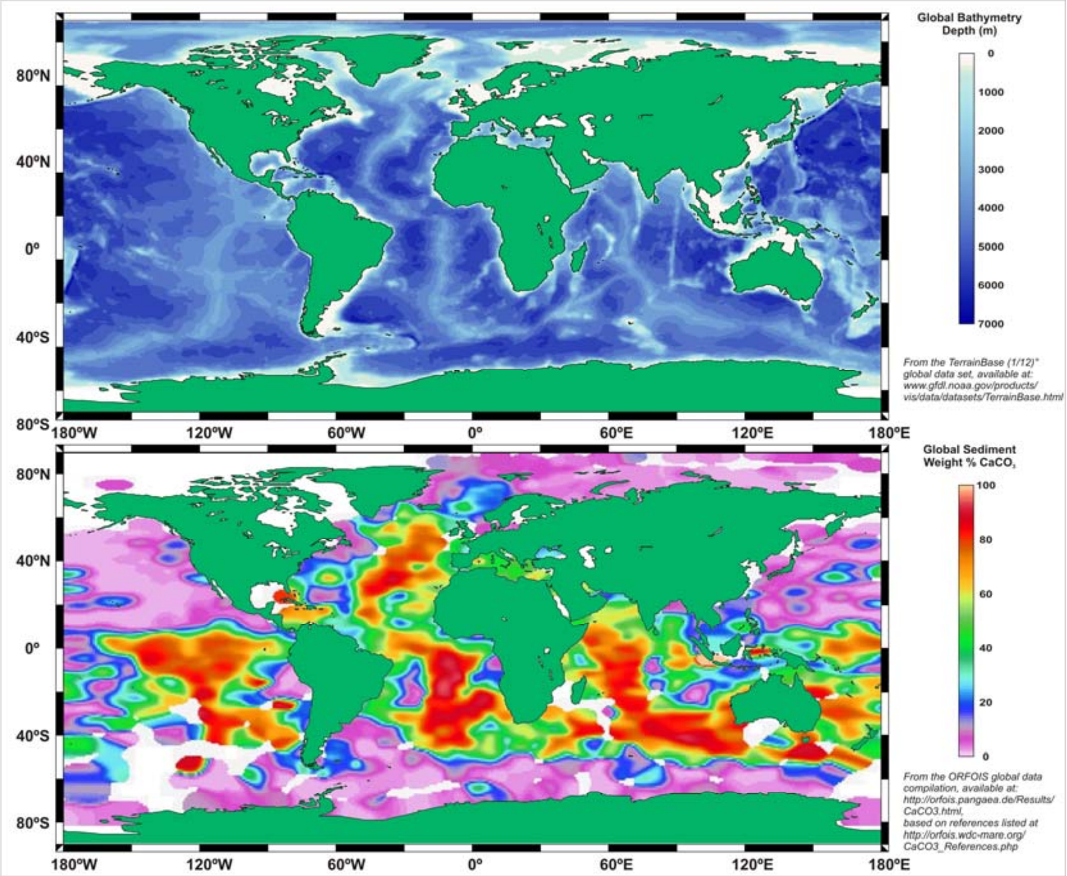

From the TerrainBase (1/12)° global data set, available at: www.gfdl.noaa.gov/products/vis/data/datasets/TerrainBase.html

From the ORFOIS global data compilation, available at: http://orfois.pangaea.de/Results/CaCO3.html, based on references listed at http://orfois.wdc-mare.org/CaCO3_References.php

Comparison of Figure 5.16 to those regions where sub-seafloor storage of CO_2 is occurring, or is expected to occur in the near future, allows a first order evaluation of how significant carbonate neutralisation may be (note this map is of surface sediments only). In the North Sea/Norwegian Sea/Barents Sea sectors and offshore Japan, sediment carbonate concentrations are low at <20 wt%. In the Natuna Sea, concentrations are somewhat higher at ~20-30 wt%. The highest carbonate contents are seen on the North-Western Shelf of Australia, with values of ~60-80 wt% (see also the discussion of coral reefs in Chapter 7).

The maximum neutralising capacity of sea-floor sediments can be evaluated by assuming complete carbonate dissolution, where to neutralise 1 kg of CO_2 would require 2.273 kg of $CaCO_3$ (see Eq. 5.11). Two simple cases of a carbonate rich and carbonate poor sediment column are considered below.

For a sediment column with a typical porosity (at depth) of ~0.5 and a unit volume of 1 m^3, the volumes occupied by the sediment and the pore fluid are equal at 0.5 m^3. Note that in the upper metre(s) the porosity will be significantly higher, and closer to values of 0.9 (only 10% of the volume occupied by solids) at the sediment-seawater interface.

For carbonate rich sediments, a $CaCO_3$ content of ~80 wt% is assigned, where the remaining ~20 wt% consists of quartz ± clay ± iron oxyhydroxides. Using typical matrix densities for these minerals (see Table 5.3) gives an expected carbonate mass of 1070-1290 kg/m^3 wet sediment, with a maximum neutralising capacity of 471-568 kg CO_2. Thus to neutralise 1 ton of CO_2 would require ~2 m^3 of sediment.

For a carbonate poor sediment with a $CaCO_3$ content of ~10 wt%, an iron oxyhydroxide content of 0-10 wt%, and a quartz ± clay content of 80-90 wt%, the expected $CaCO_3$ mass is ~130-140 kg/m^3 wet sediment. This gives a maximum neutralising capacity of 57-62 kg CO_2, or to neutralise 1 ton of CO_2 would require ~16-17 m^3 of sediment.

For comparison, 0.5 m^3 of saline pore fluid at a depth of ~1000-3000 m that is saturated in CO_2 would contain ~850-1000 mol, or 37.4-44.0 kg CO_2. To neutralise this CO_2 loading would require 85-100 kg $CaCO_3$, equivalent to <0.1 m^3 of carbonate rich sediment, or ~1.5 m^3 of carbonate poor sediment.

5.4.1.3 The Degree of Saturation with Respect to Calcium Carbonate

While the calculations above describe the maximum potential neutralising capacity, complete dissolution of carbonates is unlikely to occur. To illustrate this we consider the reaction between a CO_2 saturated pore fluid and a host carbonate rich sediment in a closed system. The initial CO_2 system speciation of the pore fluid (before any dissolution occurs) is dominated by CO_2^* and HCO_3^-, the concentration of CO_3^{2-} is zero, and the Ca^{2+} concentration is assumed to be that of seawater. As dissolution of $CaCO_3$ progresses, both alkalinity and Ca^{2+} are added to the pore fluid. Eventually, the increase in alkalinity is sufficient such that the concentration of CO_3^{2-}, and therefore Ω, becomes non-zero. Once the pore fluids become saturated ($\Omega = 1$), dissolution will cease. Under static conditions in a closed system, the extent of dissolution is therefore fundamentally limited. For example, House et al. (2006) estimate that for limestone with 50% porosity filled with a CO_2-saturated pore water in equilibrium with liquid CO_2 (3°C, 30 MPa pCO_2), only 7.5 kg of $CaCO_3$ will dissolve before the pore fluid is saturated.

This static condition most likely gives a reasonable lower bound on the extent of carbonate neutralisation. However, interaction of a rising CO_2 plume with the surrounding sediments is neither a static nor a closed system, and kinetic factors are likely to come into play.

5.4.1.4 The Rate of Carbonate Dissolution

To date, most kinetic studies have focused on the extent and rate of carbonate dissolution at typical conditions in the water column and at the seafloor, or consideration of potential future rates of dissolution under the high-CO_2 low pH ocean. As yet, little attention has focussed on the rate of carbonate dissolution under CO_2 saturated conditions at the seafloor or in the sediment column. This issue is important, as the rate of reaction may control the extent of dissolution that occurs – particularly under non-static conditions when the system is likely to be far from chemical equilibrium.

Under typical seawater/seafloor conditions, the rate of dissolution is a function of the degree of undersaturation (e.g., Morse and Berner, 1972):

$$R_{diss} = -\frac{\mathrm{d}m_c}{\mathrm{d}t} = \left(\frac{A}{V}k\right)(1-\Omega)^n = k^*(1-\Omega)^n \qquad \textbf{[Eq. 5.12]}$$

Where R_{diss} is the observed dissolution rate normalised to the surface area of the solid (in units of mol per unit area per unit time), m_c is moles of carbonate (calcite or aragonite), t is time, A is the surface area of the solid, V is the volume of solution, k is the rate constant and n is a positive constant known as the order of the reaction. A, V, and k are often combined into a single constant k*, where this simple empirical equation has the advantage that in a plot of $\log R_{diss}$ versus $\log(1-\Omega)$ the intercept will be k* and the slope n. This is one of the most frequently used kinetic expressions for carbonate dissolution in the oceans that is seen in the literature. However, it is only applicable at neutral to alkaline pH, and not at the extreme undersaturations and acidic conditions expected in a CO_2 saturated pore fluid.

The rate at which carbonate dissolution will occur when the sediments are in contact with a CO_2 saturated pore fluid is far from simple to determine. For a detailed review of carbonate mineral dissolution kinetics, the reader is referred to Morse & Arvidson (2002) and references therein. A very brief synopsis is given below.

Reaction kinetics are largely dependent on whether the process is diffusion controlled or surface controlled. We can think of dissolution as a number of discrete steps:

1. diffusion of reactants through the solution to the solid surface,
2. adsorption of the reactants on the solid surface,
3. migration of the reactants on the surface to an ‘‘active’’ site (e.g., a dislocation),
4. the chemical reaction between the adsorbed reactant and solid which may involve several intermediate steps where bonds are broken and formed, and hydration of ions occurs,
5. migration of products away from the reaction site,
6. desorption of the products to the solution,
7. diffusion of products away from the surface to the ‘‘bulk’’ solution.

Under diffusion control, the reaction rate is dependent on either steps 1 or 7. Under surface control, diffusion is comparatively fast, and one of the processes operating at the surface (steps 2 to 6) is the rate limiting step.

Figure 5.17 (panel A) summarises the rate controlling mechanisms for carbonate dissolution as a function of pH and temperature (see Morse & Arvidson (2002) and references therein). At extreme undersaturations, diffusion controlled dissolution kinetics prevail. As equilibrium is approached, there is a transition to surface-controlled dissolution kinetics, and then a region of changing surface-controlled reaction mechanisms until equilibrium is reached.

Figure 5.17: $CaCO_3$ Dissolution Kinetics (after Morse & Arvidson, 2002). (A) Schematic representation of rate controlling mechanisms for calcite dissolution with T and pH. (B) Range in measured values of dissolution rate as a function of pH.

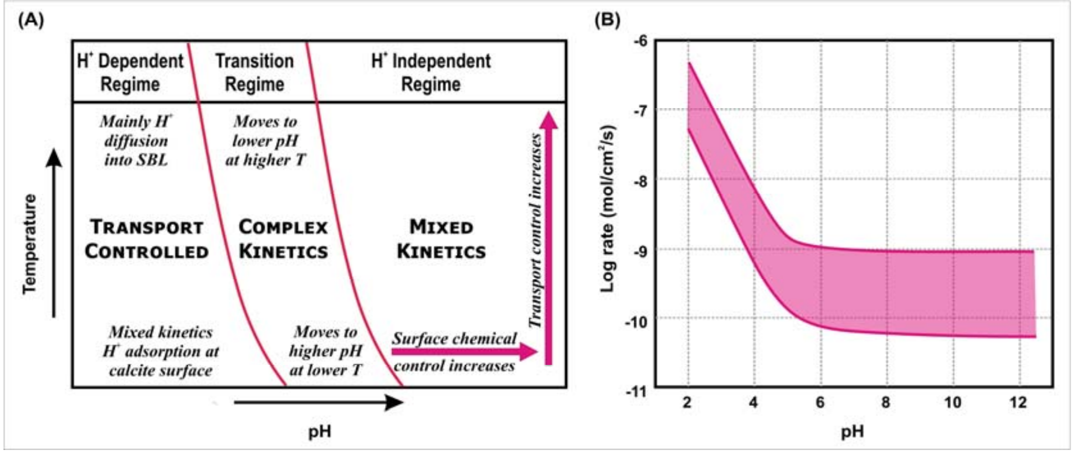

Under diffusion control, the rate of reaction is likely to be strongly dependent on the hydrodynamic conditions in the sediment column. The pore fluids may be either close to stationary (‘‘stagnant’’) or moving with respect to the sediments. In moving solutions, advective transport is substantially faster than molecular diffusion. Therefore, the thickness of a stagnant boundary layer (the region where water movement is slow relative to diffusive transport) between the solid surface and bulk turbulent solution can control the rate of reaction. For carbonates, the situation is further complicated as each of the species involved in the CO_2 system will have a different chemical potential gradient between the near surface region and the bulk solution. Furthermore, the hydration and hydroxylation kinetics of CO_2 are very slow, and may become the rate limiting step.

At low pH in the diffusion controlled region the rate of reaction is dependent on the chemical activity of H^+ ions (a_{H+}), such that:

$$R_{diss} = ka_{H^+}^n \qquad \textbf{[Eq. 5.13]}$$

Where n is the order of reaction and is close to unity.

At extremely low pH (<4), the dissolution control appears to pass from diffusion control to a first order reaction of H^+ at the surface, such that the rate is linearly dependent on the concentration of H^+ at the surface ($[H^+]_S$):

$$R_{diss} = k[H^+]_S \qquad \textbf{[Eq. 5.14]}$$

This linear relationship between rate and H^+ in the low pH region (or –logR and pH) can be seen in Figure 5.17 (panel B), and appears to hold over 3-4 orders of magnitude. The pH at which the transition from H^+ dependence occurs is dependent on the concentration of calcium ions in solution, as the Ca^{2+} concentration increases, so does the transition pH. Sjöberg and Rickard (1985) argue that because flow rates in many natural systems are relatively slow and Ca^{2+} concentrations are often substantial that an end-member transport- controlled dissolution rate for calcite may persist over a substantial pH range.

5.4.1.5 A Comment on Surface Areas

The above rate equations, and the reaction rate plotted in Figure 5.17, are normalised to surface area. This follows the general assumption that dissolution rates are directly proportional to the mineral surface area exposed to the aqueous solution. However, there are a number of difficulties in applying this assumption to natural carbonate materials.

(1) There are two measures of surface area that are routinely used in the literature. Firstly, there is a measure of total surface area (A_{total}), for example as quantified by gas absorption techniques (BET, Brunauer et al., 1938). Secondly, there is the geometric surface area, typically estimated by assuming that all grains are smooth spheres using $A_{geom} = 3 / r^*\rho_c$, where r is the grain radius and ρ_c is the density of the carbonate. The difference between these measures of surface area is substantial (orders of magnitude), where the large discrepancy arises from the complex microporous structures of the shell surfaces – such that a smooth sphere is not a good approximation for total surface area. Care must therefore be taken when applying values of k* and n from the literature, particularly as not all papers explicitly state which measure of surface area has been used in the normalisation procedure.

(2) Recent nanoscale investigations of dissolving mineral surfaces suggest that the relationship between surface area and dissolution rate is not simple, but rather that dissolution of distinct crystallographic faces and/or distinct parts of these faces dissolve at distinct rates (e.g. Ardvison et al., 2003). Thus the reactive surface area (A_{react}) will be different to both A_{total} and A_{geom}, and there will be different types of reactive surface area, each with a different dissolution rate constant. For biogenic carbonates with microporous structures, the relationships between A_{total}, A_{geom} and A_{react} are (very) complex (Walter and Morse, 1984).

5.4.1.6 The Migration of the CO_2 Rich Fluid through the Sediment Column

The lower limit on carbonate dissolution presented above (Section 5.4.4) based on the saturation condition assumes that the CO_2-saturated pore fluid is not flowing. In fact this is unlikely to be the case. If we consider a buoyant plume of CO_2 (liquid or gas) migrating upwards through the sediment column, at the interface between the CO_2 phase and the pore fluids, dissolution of CO_2 into the aqueous phase will result in a CO_2 saturated aqueous boundary layer. The addition of CO_2 to the pore fluids will increase fluid density (Bradshaw, 1973; Haugan & Drange, 1992; Song et al., 2002), and these pore fluids are expected to sink with respect to non-saturated pore-fluids. Thus both the CO_2 phase and the CO_2-saturated pore fluid are expected to flow by buoyancy-driven advection. As a result of that flow, regions in the sediment column may become undersaturated, enabling additional dissolution of the host carbonates.

5.4.2 The Need for Experiments under Expected Conditions

Given the potential benefits (CO_2 neutralisation) and potential negative consequences (damage to physical structure of the reservoir rock, cap rock or sediment column leading to possible creation of preferential flow paths accelerating the leakage of CO_2 to the seafloor) it is important that we can correctly understand and model CO_2 - pore fluid - carbonate interactions. This in turn requires well constrained values for kinetic and thermodynamic parameters under the EXPECTED conditions. This includes temperature, pressure, salinity, pH, TCO_2, and sediment composition. Sediments do not consist of pure carbonates, but include many other materials such as clay minerals, iron-manganese oxyhydroxides, other trace divalent transition metals, and organic matter. The presence of these other materials adsorbed to the carbonate surface or as ions in solution will influence the extent of carbonate dissolution. This issue has already been highlighted in the literature examining mineralisation processes within storage reservoirs, where the use of poorly constrained kinetic and thermodynamic parameters can lead to substantial deviations between predicted and observed responses (e.g. Haszeldine et al., 2005; Bateman et al., 2005).

5.5 Summary

When CO_2 migrates into the sediment column, a number of additional or secondary trapping mechanisms may come into effect, acting to either limit or prevent the release of CO_2 to the ocean. Conversely, there may exist high permeability channels through the overburden, providing a preferential flow path along which CO_2 could migrate to the sediment-seawater interface at relatively rapid rates, with little effective trapping occurring in the sediment column.

The rate at which CO_2 ascends through the sediment column will depend to a large extent on the intrinsic permeability of the sediments (κ), and the in-situ temperature (T) and pressure (P) (together determining the physical properties and phase behavior of CO_2). The efficacy of secondary trapping mechanisms (proportion of total leaked CO_2 that is retained) will depend on these parameters and the ratio of the trapping capacity to the total mass of leaked CO_2.

As the permeability of marine sediments can vary over at least 7 orders of magnitude (κ = ~10^{-4} to 10^3 md), the rise rate of liquid CO_2 may range from less than 1 mm/yr to 100s of m/yr. Migration along degraded cements segments in poorly sealed wellbores would fall toward the upper limit of this range, potentially extending to rise rates of 10s of km/yr (e.g. a continuous 1mm wide annulus with $\kappa = 10^5$ md).

Leakage of CO_2 to a high permeability flow path such as a gas chimney would result in both a rapid rise rate (single phase flow) and bypass secondary trapping mechanisms that would typically operate in water bearing sediments. Best Practice site selection procedures should therefore include a seismic survey of the overburden and utilization of advanced analytical tools (in combination with other indicators of gas seepage) to identify any potential flow paths in the sediments overlying a storage reservoir.

Secondary trapping mechanisms will be most efficient in cold, deep, low permeability sediments where migration rates are slow. Slow migration rates will maximize the

potential for CO_2 dissolution (solubility trapping) and reaction with carbonates, and both buoyancy trapping and hydrate formation will prevent or limit CO_2 escape.

The most efficient secondary trapping mechanism (infinite capacity) is buoyancy trapping. In deep/cold sediments (underlying a minimum water depth of ~2300-2800 m) the density of the rising CO_2 will eventually equal that of the surrounding pore fluid. At this point the buoyancy force is zero, thus the CO_2 is gravitationally stable and will not ascend further. A subseafloor storage reservoir underlying a sediment column with a well defined 'buoyancy cap' perhaps represents the most secure form of storage (if prevention of leakage to the ocean is the primary concern).

In cool marine sedimentary basins deeper than two or three hundred meters, CO_2 migrating upwards through the sediment column will move into a T, P regime where hydrate formation is possible. The formation of CO_2 hydrate in the sediment column would limit, and may even prevent, CO_2 escape to the ocean. However, research in this area is at an early stage, and further studies should be encouraged. In particular, the current simple models need to be developed to include the complexity of the real system and differences between the leakage case and direct storage case need to be explored. In addition, the possibility of a sediment permeability threshold above which CO_2 hydrate formation cannot form an impermeable barrier should be explored.

Additional physico-chemical processes that can act to limit CO_2 escape include dissolution (also called solubility trapping) and reaction with minerals (e.g. carbonates) in the host rock or sediments. Both of these processes have complex controls, a number of which are not yet well enough understood (under the conditions of interest) to be accurately incorporated into models in order to predict the fate of CO_2 in the sediment column.

At present, each potential trapping mechanism tends to be considered in isolation, where our understanding of each process is also incomplete. In particular, an improved understanding of hydrate formation and carbonate dissolution is required. Once knowledge of individual trapping mechanisms is improved, there is a strong need to incorporate these various processes into a combined dynamic model of CO_2 behaviour in the sediment column.

6: The Release of Leaked CO_2 to the Ocean

In the event of CO_2 leakage from a sub-seafloor storage reservoir to the overburden a number of secondary trapping mechanisms may act to limit or prevent the escape of CO_2 to the ocean (see Chapter 5). Nevertheless, under certain circumstances a leakage event could result in delivery of CO_2 to the ocean. This Chapter identifies those scenarios most likely to result in transport of CO_2 to the ocean, and examines how CO_2 release might occur, the fate of any CO_2 released (including the possibility of CO_2 escape to the atmosphere[8]), how leakage might be detected, and potential impacts on ocean biota.

The behaviour, fate and impact of CO_2 in the ocean has been discussed in two recent high profile reports. The IPCC Special Report on Carbon Dioxide Capture and Storage (IPCC, 2005) assessed the possibility of purposefully storing CO_2 in the oceans, while the Royal Society (Royal Society, 2005) examined the surface ocean invasion of CO_2 that occurs as a result of anthropogenic CO_2 emissions to the atmosphere. Here the approach taken is to compare (where appropriate) the case of leakage of CO_2 from a sub-seafloor storage reservoir to the scenarios considered in these reports, highlighting key similarities and differences. Chapter 7 then focuses on specific high risk events particular to leakage from the sub-seafloor.

---

[8] Referring to immediate release to the atmosphere. For a discussion of the timescales on which CO_2 injected into the deep ocean equilibrates with the atmosphere, and estimates of the fraction of CO_2 retained in the ocean, see Chapter 6 of the IPCC SRCCS (IPCC, 2005).

- **A Note on the Chemical Effect of Adding CO_2 to Seawater**

The key information of interest when examining the fate of CO_2 in the ocean is the spatial distribution of changes in the concentration of total seawater CO_2 ($TCO_2 = CO_2$ (aq) + H_2CO_3 + HCO_3- + CO_3^{2-}) and the resultant decrease in seawater pH.

Models examining the impact of CO_2 addition on the seawater system typically report results in terms of the reduction in pH from the background value ($\Delta pH = pH_{initial} - pH_{perturbed}$) that is calculated from the modelled TCO_2. This assumes that the system is in chemical equilibrium. However, the slow hydration kinetics of CO_2 (Zeebe & Wolf-Gladrow, 2001) are such that local advection may remove the reactants far from the release/observing site before equilibrium is reached (see background information). This has two implications. Firstly, while models may accurately simulate the TCO_2 loading, the spatial distribution of ΔpH could be significantly different from that predicted. Secondly, the use of pH sensors to monitor a CO_2 dissolution plume could result in significant underestimation of the true dissolved CO_2 burden. As biological responses to elevated TCO_2 may be distinct to responses to decreased pH (see later section), it is perhaps plausible that the biological impact of a CO_2 dissolution plume that is in chemical equilibrium would be different to that of a plume with the same TCO_2 that is far from chemical equilibrium.

In-situ techniques have been developed to allow measurement of the true TCO_2 loading by either observing the reduction in conductivity caused by the large quantity of non-ionic CO_2 flowing by the sensor (e.g. Brewer et al., 2005) or trapping a sample of the CO_2 enriched water and allowing it to reach equilibrium – thus also allowing measurement of the reaction rate (e.g. Peltzer et al., 2005; Dunk et al., in prep). In recent work the kinetic model of Zeebe and Wolf-Gladrow (2001) has been compared to observed in-situ reaction rates measured at depths from 5 to 1000m in the Pacific Ocean (Peltzer et al., 2005; Dunk et al., in prep). Based upon these comparisons, it is clear that in-situ experimental measurements are in excellent agreement with the model of Zeebe and Wolf-Gladrow (2001). Looking to the future, it would be informative for the CO_2 system kinetics into be incorporated into models of plume dispersion in order to accurately model the distribution of TCO_2 and pH in the near field environment. In the remainder of this Chapter, calculated values for ΔpH for a given addition of CO_2 to a volume of seawater follow the standard approach and assume that the system is in equilibrium.

6.1 Behaviour & Fate of Released CO_2 in the Ocean

In this section we examine the nature of CO_2 release, the circumstances under which release might occur and to what extent that release will modify seawater chemistry. As the physical properties of CO_2 are strongly dependent on conditions such as pressure (P) and temperature (T), the behaviour and fate of CO_2 are discussed here as a function of the depth of release (c.f. Chapter 3).

6.1.1 Comparison to the Ocean Storage Case

In general, once leaked CO_2 has reached the seafloor, the behaviour of that CO_2 in the ocean will be similar to that predicted for the case of direct ocean storage under equivalent conditions. However, there are a number of key differences that must be considered:

6.1.1.1 Chemistry of the CO_2 Phase

In the ocean storage case there would be control over the chemical composition of the CO_2. In the leakage case, while there is control over the composition of the CO_2 injected into the storage reservoir, significant chemical modification of the CO_2 is likely to have occurred during storage and/or migration through the overburden. Leakage may therefore act as a transport mechanism delivering other toxic species such as H_2S or heavy metals to the seafloor (see discussion in Chapter 3).

6.1.1.2 Volume, Location & Depth of Release

In the ocean storage case there would be control over both the volume of CO_2 to be released and the release location. While the total volume of CO_2 released would need to be large in order to achieve a meaningful emissions reduction, control over the release location would provide the ability to devise or choose a release scenario which minimizes ecological damage. Conversely, in the leakage case, both the volume and location of release will be dictated by the failure in the system that resulted in leakage. Thus while the total volume of leaked CO_2 is expected to be significantly less than that considered in ocean storage scenarios (in the absence of catastrophic failure of multiple subseafloor storage sites), leakage could occur in the vicinity of a vulnerable ecosystem, or to a shallow water column resulting in immediate release of CO_2 to the atmosphere.

6.1.1.3 Ease of Monitoring

In the ocean storage case, control over release volume and location would allow the development of comprehensive monitoring schemes to track the fate of the disposed CO_2. In the leakage case, the monitoring challenge is significantly more complex, and will likely need a combination of sub-surface and water column monitoring, incorporating both continuous and periodic observations, and may well require the development of new in-situ analytical techniques.

6.1.2 The Nature of CO_2 Release to the Seafloor

Leakage of CO_2 followed by delivery of CO_2 to the sediment-seawater interface under a deep water column (>600 m) is most likely to result in the formation of a rising plume of liquid CO_2 droplets and/or CO_2 hydrate deposits outcropping at the seafloor.

While the creation of lakes of dense liquid CO_2 on the deep seafloor have been considered in ocean storage scenarios (e.g. IPCC, 2005), a directly analogous situation is not expected in the event of leakage or seepage from a sub-seafloor storage reservoir. This can be simply illustrated by considering whether or not release of CO_2 to the ocean will occur as a function of the depth of the sediment seawater interface – or more specifically the depth of the interface in relation to the neutrally buoyant point of CO_2 in the ocean (NBPO; see Box 6.1).

Consider a leakage scenario where CO_2 is migrating upwards through the sediment column where (a) the sediment-seawater interface lies below the NBPO (b) the sediment-seawater interface lies at the NBPO and (c) the sediment-seawater interface is sufficiently shallow such that the density of CO_2 does not exceed that of seawater – this can be thought of as the sediment-seawater interface lying above the NBPO (see Box 6.1).

Box 6.1: The Nature of Liquid CO_2 Release to the Deep Ocean.

Whether or not leakage of liquid CO_2 to the sediment column results in release to the ocean will depend on the depth of the sediment-seawater interface with respect to the neutrally buoyant point of CO_2 (among other factors - see text). Considering only buoyancy forcing, the delivery of liquid CO_2 to the sediment-seawater interface is most likely to result in the formation of a rising plume of liquid CO_2 droplets. The creation of a seafloor lake of liquid Co_2 is not expected.

The Density & Neutrally Buoyant Point of CO_2

CO_2 is a highly compressible fluid where the density of CO_2 (ρ_{CO2}) increases with depth in the ocean (increasing P and decreasing T), but decreases with depth in the sediments (increasing P and T). The sediment-seawater interface therefore represents the point at which ρ_{CO2} is at its maximum value. The depth at which ρ_{CO2} is equal to the density of seawater (ρ_{SW}) or porefluids (ρ_{PF}) is called the neutrally buoyant point (NBP).

In the ocean, the NBP (NBPO) typically occurs at depths of 2250-2750 m, varying according to local temperature and salinity profiles. If CO_2 is released in the ocean at depths above the NBPO ($\rho_{CO2} < \rho_{SW}$) it will form a rising plume, whereas release at depths below the NBPO ($\rho_{CO2} > \rho_{SW}$) will result in a sinking plume and (potentially) the creation of a CO_2 lake on the seafloor.

The CO_2 density inversion at the sediment-seawater interface means that when the interface lies below the NBPO, there will be a second NBP at depth in the sediments (NBPS), where CO_2 is buoyant below the NBPS ($\rho_{CO2} < \rho_{PF}$), and will sink above the NBPS ($\rho_{CO2} > \rho_{PF}$).

Leakage Case Scenarios

Here we consider 3 possible leakage scenarios where CO_2 is migrating upwards through a sediment column (see panel below) .

In **Case (a)** the sediment-seawater interface lies below the NBPO. In this case, the liquid CO_2 reaches the NBPS at depth in the sediment column and becomes buoyancy trapped. In this case CO_2 will be retained at depth and will not be released to the ocean.

In **Case (b)** the sediment-seawater interface lies at the NBPO. In this case CO_2 will accumulate in the surficial sediments.

In **Case (c)** the sediment-seawater interface is sufficiently shallow such that the density of CO_2 does not exceed that of either the porefluids or seawater. This can be thought of as the interface lying above the regional NBPO. In this case CO_2 liquid will be released to the ocean, forming a rising plume of droplets

The example shown in the panel below is for the Japan Sea (bottom water T=0.23°C, S=34.07) and assumes a geothermal gradient of 0.03°C/m. The brown shaded area represents the sediment column, where the dark brown line indicates the sediment-seawater interface, and bright blue shading represents the presence of CO_2. The dotted black line shows the temperature profile. The pink line shows the density of CO_2. The purple line shows the density of seawater and pore fluids (assuming constant salinity in the sediment column). Droplet streams in (c) are not to scale.

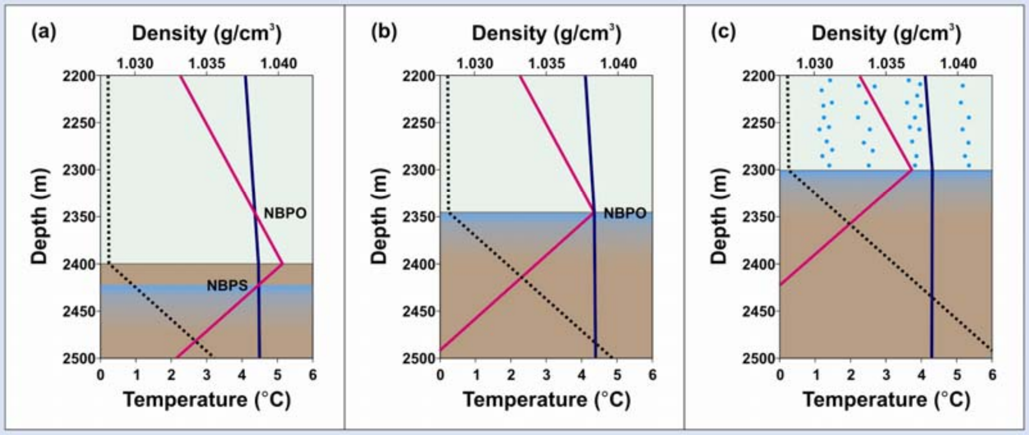

See Chapter 5 for further discussion of buoyancy trapping.

In case (a), the liquid CO_2 becomes buoyancy trapped at depth in the sediments and will not be released to the ocean. In case (b), liquid CO_2 will accumulate at the sediment-seawater interface. In case (c), the CO_2 remains less dense (more buoyant) than either the sediment pore fluids or seawater and will be released to the ocean, forming a rising plume of CO_2 droplets.

Case (b) is most similar to the creation of a CO_2 lake on the seafloor. However, this scenario seems the least likely to occur as it requires the sediment-seawater interface to be precisely collocated with the NBPO. Furthermore, if there is some disturbance such that the CO_2 is physically moved upwards, the CO_2 will become less dense than the surrounding seawater and will rise through the water column. Thus if we consider only buoyancy forcing, the most likely scenario for CO_2 release to the ocean is the formation of a rising plume of CO_2 droplets.

Although the formation of a CO_2 lake is not expected, in both cases (b) and (c) the upper sediments may become saturated in liquid CO_2. The behaviour of a CO_2 saturated sediment-seawater interface may be broadly comparable to that of a CO_2 lake, although the influence of ocean currents and dissolution characteristics will be different (Enstad et al., 2006). As a hydrate membrane is likely to form at the interface between liquid CO_2 and seawater under these conditions, the influence of CO_2 saturated surface sediments on bottom water chemistry is discussed together with the formation and fate of CO_2 hydrate outcrops at the seafloor.

When we include the potential for hydrate formation, then liquid CO_2 will typically enter the hydrate stability zone at significant depth in the sediment column (see the case studies presented in Chapter 5). This could result in the formation of an impermeable hydrate layer that would trap buoyant CO_2 beneath. However, the development of a hydrate cap is by no means inevitable, and transport of free CO_2 through the hydrate stability zone is certainly possible. Thus the growth of CO_2 hydrate outcrops at the seafloor are plausible in any sediment column where the sediment-seawater interface is at or above the regional NBPO (i.e. CO_2 is buoyant in the sediment column) and conditions at the seafloor are within the hydrate stability zone.

At intermediate water depths (~600-200 m), the CO_2 phase behaviour is strongly dependent on local conditions. In warmer deeper waters, CO_2 would be in the liquid phase without the potential to form hydrate, in which case seepage across the sediment-seawater interface would result in a rising plume of liquid droplets. Conversely, in colder shallower waters, CO_2 would be in the gas phase with the potential to form hydrate, in which case hydrate formation in the sediment column and as outcrops at the seafloor could occur, and seepage of free CO_2 across the sediment seawater interface would result in a rising plume of gas bubbles.

At shallow water depths (<200 m), CO_2 would be in the gas phase without the potential to form hydrates, and seepage across the sediment seawater interface would result in a rising plume of gas bubbles.

6.1.3 How Seepage to the Ocean Might Occur

If primary leakage from a sub-seafloor storage reservoir delivers CO_2 into thick sediments underlying a deep water column, then the probability of secondary trapping occurring in the sediment column is high (see Chapter 5). For leakage to sediments underlying an intermediate or shallow water column the probability of efficient secondary trapping decreases as the depth of the sediment-seawater interface decreases and bottom water temperature increases. While the efficacy of secondary trapping mechanisms will depend on local conditions in the sediment column and the rate at which CO_2 is leaking, some general statements regarding the likelihood of CO_2 release to the ocean can be made:

- In sediments underlying a very deep water column (>2250-2750m), CO_2 will become buoyancy trapped and will not escape to the ocean (see Box 6.1).

- In the absence of buoyancy trapping (water column depth <2250-2750m), but at depths where CO_2 is a liquid and hydrate formation is possible, then leakage at comparatively slow rates is unlikely to result in the release of CO_2 to the seafloor. Under slow flow conditions, the combined effects of secondary trapping mechanisms such as CO_2 dissolution, reaction with carbonates, residual trapping and hydrate formation, are likely to efficiently trap the CO_2 in the sediments and prevent (significant) leakage to the ocean.

- In the absence of buoyancy trapping (water column depth <2250-2750m), then leakage at comparatively rapid rates could deliver CO_2 to the seafloor, despite the potential to form hydrates in the sediment column. Under fast flow conditions, rapid hydrate formation at the base of the hydrate stability zone may locally increase salinity, inhibiting further hydrate formation and allowing the upwards transport of free CO_2. It might be expected that both salinity and CO_2 hydrate concentration will increase from the base of the hydrate stability zone to the seafloor, with delivery of the free CO_2 phase to the ocean (c.f. Liu & Flemings, 2007). Furthermore, the proportion of CO_2 consumed through dissolution and/or reaction with carbonates will be limited, and the efficacy of residual trapping will be minimal (proportion of total leaked CO_2 retained).

- In the absence of efficient secondary trapping mechanisms, release of CO_2 to the ocean will occur. Thus for any leakage event that delivers CO_2 to sediments underlying a warm shallow water column, release of CO_2 to the ocean is most likely inevitable.

For leakage to sediments underlying deep and intermediate depth waters, further work is required to determine the flow rate at which the transition from efficient trapping to release of

CO_2 occurs (e.g. dynamic models incorporating all behaviours of CO_2 in the sediment column). This will vary between sites in response to a wide range of parameters including sediment and pore fluid properties, the presence of trace contaminants in the CO_2 phase, P and T conditions, pore fluid advection, etc. Nevertheless, if we assume adequate site selection criteria, reservoir screening, and ongoing monitoring of the subsurface CO_2 plume in the reservoir, then combining the probability of primary leakage (see Chapter 4) with the likelihood of efficient secondary trapping in the sediment column allows identification of those leakage mechanisms most likely to result in release of CO_2 to the ocean.

The probability of leakage via unidentified faults though caprock seals, via faults activated due to regional scale reservoir overpressurisation, or via unidentified high permeability zones in caprock seals, is classed as 'very unlikely' to 'almost impossible' (see Chapter 4). If leakage were to occur, flow rates are expected to be slow - on the order of 10 tCO_2/yr or less – thus secondary trapping mechanisms in the overburden are likely to be effective. Combing the low probability of primary leakage with the high probability of efficient secondary trapping suggests that significant release of CO_2 to the ocean via these leakage mechanisms is unlikely to occur.

Exceeding the spill point of a reservoir, resulting in leakage of CO_2 into a neighbouring unconfined formation, is also classed as 'almost impossible'. However, if leakage were to occur then in this case potential flow rates are very high, being equal to the injection rate and of order ~$MtCO_2$/yr. Therefore, while leakage via this mechanism is not expected, should it occur (due to poor site selection or management) significant release of CO_2 to the ocean seems likely.

In tectonically active regions an earthquake may activate faults through the caprock seal. Initial flow rates could be high at ~1000 tCO_2/yr, potentially decreasing to much lower rates on the order of 10 tCO_2/yr once the earthquake has stopped (e.g. Hooper et al., 2005). Thus significant release of CO_2 to the ocean could be expected during an earthquake, with secondary trapping potentially limiting or preventing release to the ocean once the earthquake has ceased.

Leakage along high permeability pathways associated with abandoned or poorly completed wellbores is classed as highly probable to possible with expected flow rates on the order of ~200 tCO_2/yr. Consequently it seems likely that leakage via wellbores could result in delivery of CO_2 to the ocean. Well blowout is also classed as possible, with expected flow rates on the order of ~50,000 tCO_2/day. Such an event could result in delivery of CO_2 to the ocean (e.g. blowout of an abandoned well) or direct to the atmosphere (e.g. blowout of an active well). Although given the very rapid flow rates well blowouts are expected to be detected and mitigated and will typically be of short duration (less than 5 days).

In all cases, connectivity between a primary leakage point and preferential flow paths that allow rapid migration rates and bypass secondary trapping mechanisms in the sediment column (e.g. gas chimneys) could result in delivery of CO_2 to the ocean (see Chapter 7).

Leakage via a wellbore is used here as the reference scenario as (i) it is the most likely to occur and (ii) flow rates are such that delivery of CO_2 to the ocean might take place while leakage remains undetected. For simplicity, it is assumed that the mass flux of CO_2 at the sediment-seawater interface is equal to the primary leakage flux and is of order ~200 tCO_2/yr.

6.1.4 CO_2 Saturated Surface Sediments & CO_2 Hydrate Outcrops

The influence of CO_2 saturated surface sediments or a CO_2 hydrate outcrop on the chemistry of bottom waters will be dependent on:

- The chemical composition of the CO_2 phase (e.g. does it contain H_2S)
- The dissolution rate or 'shrinkage rate' of the CO_2 phase
- The surface area of CO_2 saturated sediments or exposed hydrate outcrop
- The extent of mixing between the CO_2 dissolution plume and ambient bottom water

Possible trace components in the CO_2 phase are discussed in Chapter 5. The main point to recall is that strong hydrate formers will preferentially enter the hydrate phase, altering the properties of the hydrate with respect to a pure CO_2 hydrate. For example, H_2S is likely to be concentrated by a factor of ~10 in a CO_2 hydrate compared to the stock liquid CO_2 phase. The latter three points are discussed in further detail below. This discussion focuses on hydrate outcrops at the seafloor, where the dissolution behaviour and influence of CO_2 saturated surface sediments may be considered similar to the thin slab hydrate example.

6.1.4.1 *CO_2 Dissolution & Hydrate Shrinkage Rates*

As ambient seawater is under-saturated with respect to CO_2, any CO_2 exposed to seawater is expected to dissolve. For CO_2 hydrate outcropping at the seafloor, decomposition will occur dominantly as a surface phenomenon (Teng et al., 1999). The CO_2 diffuses out of the hydrate lattice cages into seawater until the cage occupancy falls below the stability threshold, at which point the lattice structure collapses releasing the remainder of CO_2 molecules held in the surface layer (Teng et al., 1999). For the purposes of a simple thought experiment it can be assumed that CO_2 hydrate dissolution is mass-transfer limited rather than reaction-limited, i.e. the rate of dissolution is controlled by the transport of dissolved CO_2 away from the hydrate surface, rather than the kinetics of hydrate decomposition (e.g. Rehder et al., 2004 and references therein)[9]. This assumption allows CO_2 hydrate dissolution in turbulent ocean conditions to be approximated by a simple diffusive boundary layer model (Opdyke et al., 1987; Santschi et al., 1991; Egorov et al., 1999; Rehder et al., 2004; see Eq. 6.1 and Figure 6.1):

$$F = \frac{D_{CO_2}}{z}\left([CO_2]_{boundary} - [CO_2]_{seawater}\right) \qquad \textbf{[Eq. 6.1]}$$

Figure 6.1: Schematic diagram showing the diffusive boundary layer at a hydrate outcrop surface.

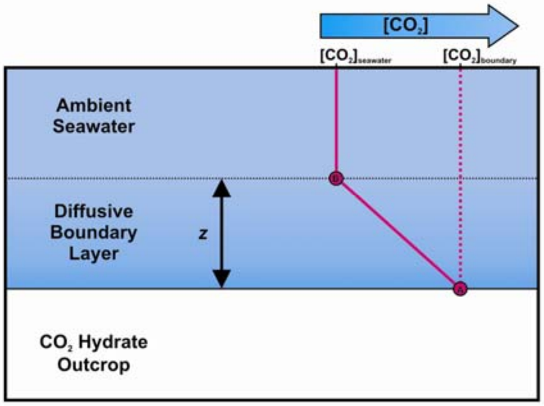

The concentration of CO_2 immediately at the hydrate-seawater interface (point A) is assumed to be in equilibrium with the hydrate phase. Thus $[CO_2]_{boundary}$ is the predicted saturation concentration of CO_2 under the T, P, S conditions of interest.

The equilibrium solubility of CO_2 in the presence of CO_2 hydrate can be determined from flash calculations (e.g. MultiFlash software package from InfoChem Ltd.).

For example, at ~1000 m water depth in the Pacific Ocean ($T = 3.6°C$, $P = 10.48$ MPa, $S = 34.6$), the predicted $[CO_2]_{boundary}$ is ~ 0.728 mol/L (Rehder et al., 2004 - see Figure 6c in this reference for an example profile for the Pacific Ocean).

In comparison, the background concentration of CO_2 in seawater, $[CO_2]_{seawater}$, is several orders of magnitude lower and can be considered negligible (point B).

Where F is the diffusive flux of CO_2, D_{CO2} is the molecular diffusion coefficient of CO_2 in seawater, $[CO_2]_{boundary}$ is the concentration of CO_2 in seawater immediately at the boundary with the hydrate surface and is assumed to be saturated, $[CO_2]_{seawater}$ is the ambient background seawater concentration, and *z* is the thickness of the diffusive boundary layer (Figure 6.1). Typical values for z at the deep-seafloor are on the order of 1 mm or less (Santschi et al., 1991), where z will decrease as the turbulence of bottom flow increases. As z decreases, F, and therefore the hydrate shrinkage rate (SR), will increase (Figure 6.2, order of magnitude guide for SR only). Thus SR is expected to vary in response to physical parameters such as the geometry of the hydrate outcrop surface (as surface roughness increases, turbulence increases and z decreases) and the velocity of bottom currents bathing the hydrate surface (as current velocities increase, z decreases).

---

[9] see Kvamme & Tanaka (1995), Kvamme (2000), & Kvamme et al. (2005) for a detailed model of hydrate dissolution.

Figure 6.2: (a) The molecular diffusion coefficient of CO_2 in seawater (b) An illustrative curve for the Hydrate Shrinkage Rate as a function of the thickness of the Diffusive Boundary Layer, z.

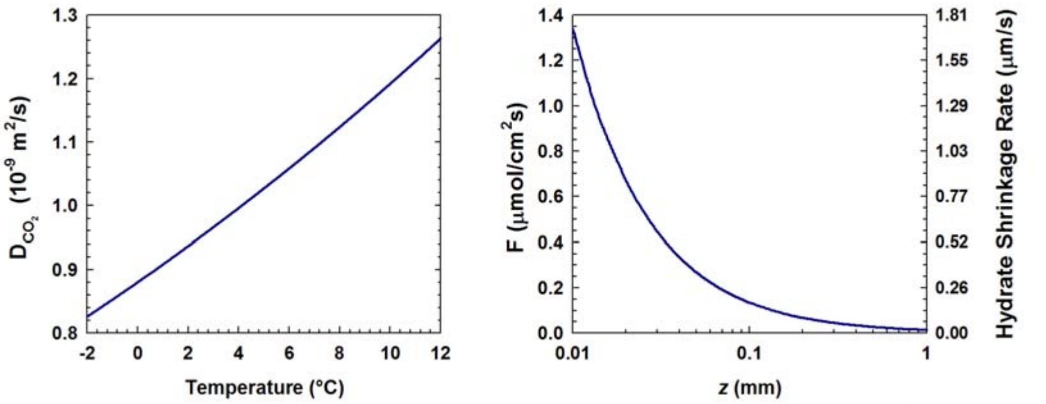

The molecular diffusion coefficient D_{CO_2} is the value for freshwater decreased by ~6% (Jähne et al., 1987). F was calculated from Eq. 6.1 for water depths of ~1000m, with a bottom water T = 3.6°C and $[CO_2]_{boundary}$ = 0.728 mol/L. The hydrate shrinkage rate (SR) was calculated from F using a hydrate density of 1143 kg/m^3 and a hydration number of 5.75 (e.g. Rehder et al., 2004). The curves for F and SR as a function of z are shown for illustrative purposes only.

In-situ measurements of CO_2 hydrate dissolution in the ocean have been made (Rehder et al., 2004). Small cylinders of laboratory grown CO_2 hydrate (density = 1143 kg/m^3, hydration number = 5.75) were transferred to the seafloor in a pressure vessel and exposed to ambient seawater at 1028 m water depth (T = 3.6°C, S = 34.6). The observed radial SR was 0.47-0.60 μm/s, corresponding to a dissolution rate of 0.36-0.47 μmol/cm^{2}s (Rehder et al., 2004). The variation in dissolution rate was attributed to changes in current speed, with periods of faster dissolution corresponding to periods of increased current speeds (Rehder et al., 2004). An in-situ experiment such as this provides advantages over laboratory based studies as the defining boundary conditions of the ocean (such as the extent of CO_2 under-saturation in ambient seawater and local current velocity) are maintained. However, this approach may overestimate the dissolution rate of a CO_2 hydrate outcrop at the seafloor. The presence of a protective thin veneer of sediment or a bacterial mat covering the hydrate surface (as might be expected - see Figure 6.3) would result in a slower dissolution rate. Furthermore, in this experiment the hydrate samples were held in a rack above the seafloor, such that the CO_2 rich dissolution plume (with a greater density than ambient seawater: Bradshaw, 1973; Haugan & Drange, 1992; Song et al., 2002) would tend to sink away from the hydrate samples. Conversely, for a horizontal hydrate surface at the seafloor, the density stratification of CO_2 rich seawater could stabilize the boundary layer, thus suppressing vertical mixing and slowing the rate of hydrate dissolution.

Figure 6.3: (a) Hydrate formation during a small scale release experiment in the Deep-Sea, showing the formation of a rafted block of hydrate covered by a veneer of sediment (photograph courtesy of MBARI).(b) CO_2 Hydrate outcropping at the seafloor, Hatoma Knoll, Okinawa Trough (photograph courtesy of Shitashima-san).

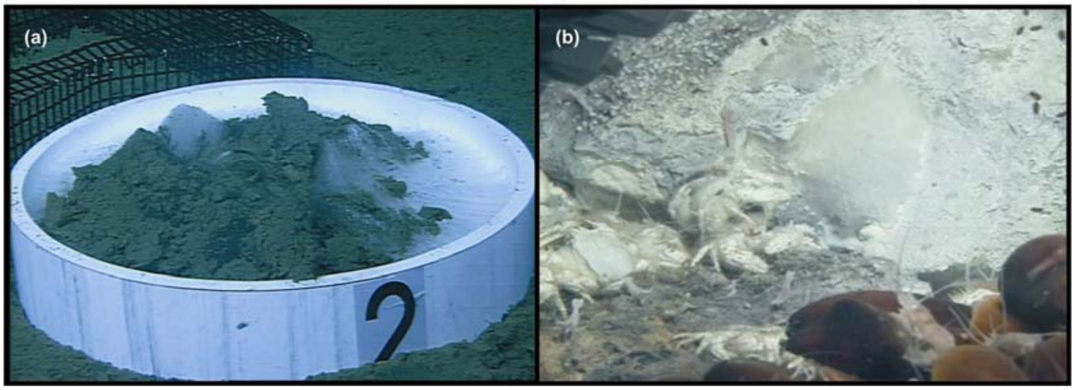

Of relevance here are models examining the fate of liquid CO_2 lakes on the deep seafloor (e.g. Fer & Haugan, 2003; Haugan & Alendal, 2005; Enstad et al., 2006; see Table 6.1). These studies have considered a comparatively large (500m x 500m) lake at a water depth of ~3000m, where the liquid CO_2 is separated from seawater by a thin hydrate membrane. Fer & Haugan (2003) clearly illustrate the damping effect that formation of a stable stratified layer exerts by comparing the steady state dissolution rate achieved when the seawater density increase due to addition of CO_2 is neglected, to that achieved when it is addressed. At a typical bottom current speed of 5 cm/s, including CO_2 induced density stratification decreased the modeled dissolution rate by around two thirds, while at a higher current speed of 20 cm/s (e.g. during a benthic storm) the effect was found to be less marked with a decrease of ~5%.

Over the past few years model complexity has evolved, moving from 2-dimensional advection diffusion models (Fer & Haugan, 2003), to improved 2-dimensional models with numerically resolved boundary layer turbulence and inclusion of internal waves (e.g. Haugan & Alendal, 2005), to 3-dimensional models that include both vertical and lateral mixing (e.g. Enstad et al., 2006). While early models suggested very slow steady state dissolution rates, as model complexity has increased so has the predicted dissolution rate (see Table 6.1), with results from a 3-dimensional model showing reasonable agreement to dissolution rates measured during small scale release experiments (range of ~0.1-3.0 μmol/cm^2/s for liquid CO_2 through a hydrate membrane – see background information and Chapter 3, Box 3.6).

As the key factor limiting dissolution in these models is the development of density stratification in the water column due to addition of CO_2 (Fer & Haugan, 2003; Haugan & Alendal 2005;

Enstad et al., 2006), the steady state dissolution rate for liquid CO_2 through a hydrate membrane is assumed here to be a useful order of magnitude guide for the dissolution rate of massive CO_2 hydrate (see Table 6.1). For the remainder of this chapter an 'expected' range in hydrate shrinkage rate of 0.1-1 μm/s is adopted, with a reference case of 0.5 μm/s to match the experimental observations of Rehder et al. (2004). This allows constraints to be placed on the likelihood of a CO_2 hydrate outcrop forming, and permits a semi-quantitative exploration of the potential fate of any outcrop formed.

Table 6.1: The Modelled Dissolution Rate of Liquid CO_2 through a Hydrate Membrane as a Function of Current Speed (U)

Model	**Liquid CO_2 Dissolution Rate (cm/yr)**		
	U = 5 cm/s	**U = 10 cm/s**	**U = 20 cm/s**
2-D advection-diffusion (Fer & Haugan, 2003)	12		162
2-D increased complexity (Haugan & Alendal, 2005)	55-66	57-193	303-468
3-D (Enstad et al., 2006)	66	264	858
3-D Model Dissolution Rates - Unit Conversions & Equivalent Hydrate Shrinkage Rates			
CO_2 Mass Loss Rate (kg/m^{2}yr)[a]	693	2772	9009
CO_2 Molar Flux (μmol/cm^{2}s)	0.05	0.20	0.65
Equivalent Hydrate Mass Loss Rate (kg/m^{2}yr)[b]	2323	9293	30201
Equivalent Hydrate Shrinkage Rate (cm/yr)[b]	203	813	2642
Equivalent Hydrate Shrinkage Rate (μm/s)	0.06	0.26	0.84

[a] The CO_2 mass loss rate is calculated from the dissolution rate (3-D case) and assumes a liquid CO_2 density of 1050 kg/m^3.

[b] Equivalent hydrate mass loss rates and shrinkage rates are those that would be achieved if the molar flux of dissolved CO_2 were as predicted for the liquid CO_2 lake. The hydrate mass loss rate is the CO_2 mass loss rate multiplied by the ratio of the molar mass of CO_2 hydrate (147.5 g/mol - assuming a hydration number of 5.75) to that of CO_2 (44 g/mol). The hydrate shrinkage rate is then calculated from the mass loss rate assuming a hydrate density of 1143 kg/m^3.

6.1.4.2 The Likelihood of a CO_2 Hydrate Outcrop Forming

Constraints can be placed on the likelihood of a hydrate outcrop forming by considering the mass balance between the flux of CO_2 and the hydrate shrinkage rate. Quite simply, the rate at which hydrate is forming must exceed the rate at which it is dissolving for a deposit to build up. In the simplest case if we assume that all CO_2 delivered to the sediment-seawater interface via leakage or seepage is converted to CO_2 hydrate, then the threshold mass flux is given by:

$$F_L > \frac{44}{147.5} \rho_H SR \qquad \textbf{[Eq. 6.2]}$$

Where F_L is the mass flux of liquid CO_2 per unit area ($kgCO_2/m^2yr$), ρ_H is the CO_2 hydrate density (value used is 1143 kg/m^3), SR is the expected hydrate shrinkage rate (m/yr), 44 is the molar mass of CO_2, and 147.5 is the molar mass of CO_2 hydrate (formula $CO_2.nH_2O$, value of n used is 5.75). Threshold values of F_L as a function of expected SR are shown in Figure 6.4a.

Figure 6.4: (a) The threshold mass flux that must be exceeded for hydate outcrop formation to occur as a function of the hydrate shrinkage rate. (b) The threshold area within which a given mass flux must be constrained for hydrate outcrop formation to occur at hydrate shrinkage rates of 0.1, 0.5 and 1 μm/s. See text for details.

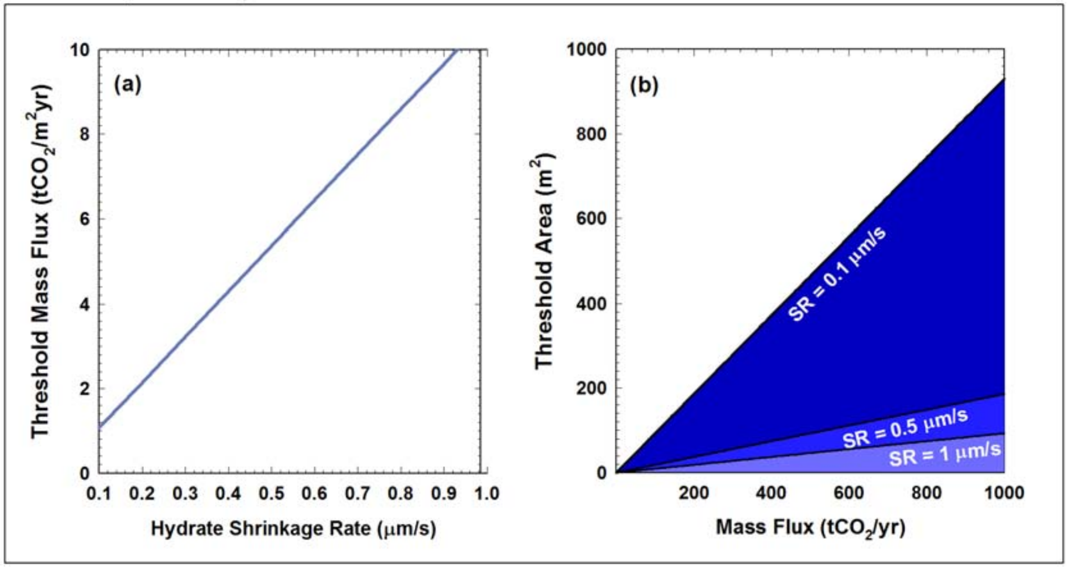

Figure 6.4b shows the threshold area within which a given total CO_2 flux must be contained for hydrate outcrop formation to remain plausible. For slow to moderate leakage rates hydrate formation can only occur if the leakage remains focused within a relatively small area. For example, for a CO_2 flux of ~200 tCO_2/yr the area (width) thresholds are 186 m^2 (13.6 m), 37.2 m^2 (6.1 m), and 18.6 m^2 (4.3 m) for an SR of 0.1, 0.5 and 1 μm/s respectively. However, this simple analysis assumes the upward flux of CO_2 is spatially and temporally uniform. While this would be the case for a CO_2 saturated sediment column, it is likely that real leakage scenarios will be more complex, with multiple CO_2 flow paths resulting in a patchy and temporally variable delivery of CO_2 (see for example reports of intermittent and itinerant droplet streams at natural CO_2 vent sites – with shifts in outlet location from a few to 10s of cm attributed to tortuous flow paths through surface sediments - Appendix 3A; McCarthy et al., 2005; Pichler & Dix, 1996). Thus the total area over which leakage occurs (the leakage field) could be significantly larger than the threshold area, while hydrate formation would remain possible if the upwards flux within any small patch (at any point in time) exceeds the threshold mass flux. This illustrates how seafloor hydrates might be a transient feature, even in the region of a persistent leak with constant total mass flux, where the system could switch between net hydrate formation and net hydrate dissolution in response to changes in either the current speed or in the distribution of CO_2 mass flux across the leakage field.

6.1.4.3 *Outcrop Geometry & Fate of the Hydrate Deposit*

The geometry of a hydrate outcrop will influence its fate in two ways. Firstly, a greater surface roughness will result in increased turbulence and therefore a faster shrinkage rate. Secondly, the geometry is the primary control on the exposed surface area of the hydrate, and therefore also determines the total volumetric rate of dissolution.

In ocean storage scenarios, mounds of hydrate deposited on the seafloor have been modelled as a cone with a radius that is twice the height (e.g. IEA, 2004). This shape is based on sinking blocks of hydrate forming a heap on the seafloor, and represents a different process to emplacement from below. Perhaps the most likely outcrop geometry in the event of leakage is a thin slab, with a comparatively large flat surface area rising only slightly above the seafloor. However, the formation of large hydrate mounds or rafted blocks of hydrate cannot be ruled out.

Below we consider the fate of a hydrate outcrop by applying three scenarios to a range of outcrop shapes that seem likely to encompass the true geometry of a hydrate outcrop at the seafloor, a hemispherical dome (A), 2 cones (B & C), and 3 slabs (D, E & F), where the different cones and slabs are characterised by different height:radius and height:width ratios (see Figure 6.5). The overall rate of dissolution will decrease in the order F>E>D>C>B>A as the volume:surface area ratio increases. End member cases are given by the hemisphere A and thin slab F, while cone C serves as a reference scenario for the standard ocean storage case.

Figure 6.5: The range of possible hydrate outcrop geometries used in example scenario cases (see text for details).

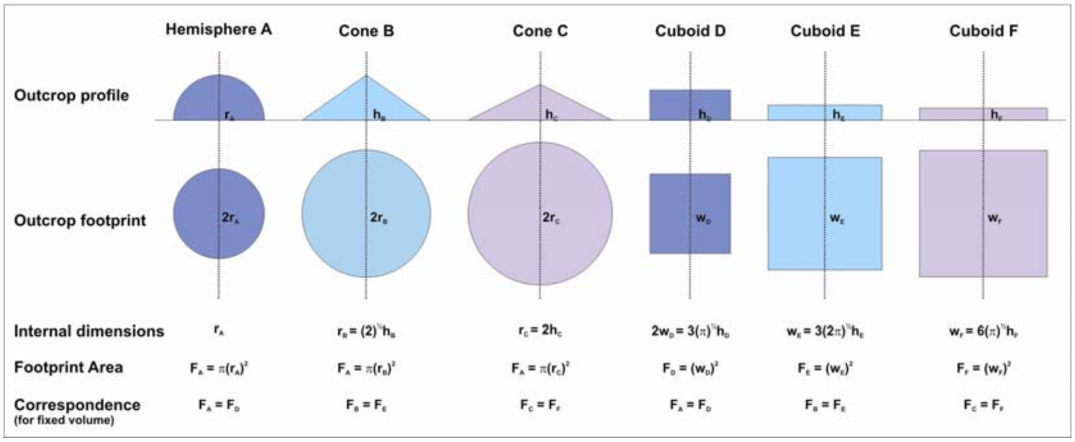

Scenario 1: An isolated leakage event has resulted in the emplacement of a hydrate outcrop at the seafloor. The outcrop lifetime (time to complete dissolution) is calculated as a function of initial deposit size using the reference SR of 0.5 μm/s (Figure 6.6a). A hydrate outcrop containing ~10 tCO_2 (volume ~29.3 m^3) has a lifetime of 15-56 days, depending on whether the outcrop shape resembles a thin slab (F) or a hemispherical dome (A) respectively. Similarly, a hydrate outcrop containing 1000 tCO_2 (volume ~2933 m^3) has a lifetime of ~70-260 days. This variation by a factor of 3-4 in the calculated outcrop lifetime for a given mass of CO_2 illustrates the strong control that geometry exerts on hydrate deposit lifetime.

Scenario 2: An isolated leakage event has resulted in the emplacement of a hydrate outcrop containing 10 tCO_2 at the seafloor. The outcrop lifetime is calculated as a function of expected SR (Figure 6.6b). At the low SR of 0.1 μm/s, the outcrop persists for a period of ~70-280 days, while at the high SR of 1 μm/s, the outcrop would be completely dissipated in ~7-28 days.

Scenario 3: A continuous leak is delivering CO_2 to the seafloor at a rate of 200 tCO_2/yr (548 $kgCO_2$/day). It is assumed that the entirety of this flux is converted to hydrate (hydrate emplacement rate = 1837 kg/day = 1.61 m^3/day). The growth of the deposit (time to steady state[10] and steady state size of the outcrop) is then characterised as a function of SR (Figure 6.6c). At the low SR of 0.1 μm/s, the outcrop would take 3-6 years to reach steady state, at which point the deposit would contain some ~50-115 tCO_2, with a volume of ~150-340 m^3 and a footprint of ~70-170 m^2. At the reference SR of 0.5 μm/s, the outcrop would reach steady state significantly faster (3-8 months) and would be considerably smaller, containing ~5-10 tCO_2, with a volume of ~13-30 m^3 and a footprint of ~15-33 m^2. At the high SR of 1 μm/s, the outcrop would reach steady state in 1-3 months, and would be only 3-10 m^3 in volume, with a footprint of ~7-17 m^2 and a CO_2 content of ~1-4 tCO_2.

Figure 6.6: The influence of hydrate geometry on (a) outcrop lifetime as a function of outcrop size (mass CO_2) (b) outcrop lifetime as a function of hydrate shrinkage rate (c) steady state outcrop size as a function of hydrate shrinkage rate. See text for details.

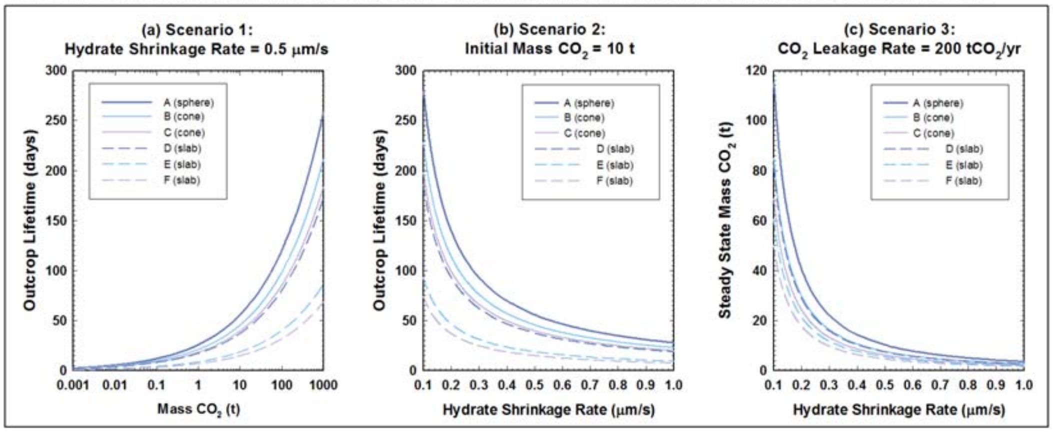

The example mass flux of 200 tCO_2/yr used above is a reasonable value for expected leakage via a wellbore, with the possibility of leakage remaining undetected and therefore unmitigated. In contrast, ocean disposal scenarios have envisaged hydrate emplacement rates 4-5 orders of magnitude greater at ~20 $ktCO_2$/day (e.g. IEA, 2004). It is perhaps a useful exercise to compare the size of the hydrate mounds formed in these two cases to illustrate the difference in scale (and therefore likely impact on the seafloor environment).

Considering the cone C geometry and the reference SR, for the 'leakage' flux of 200 tCO_2/yr the hydrate deposit would reach steady state in ~4-5 months, where the cone would have a volume of 18 m^3 and contain 6.2 tCO_2. If leakage should cease, it would take ~48 days for total dissolution of the hydrate outcrop. For the 'storage' flux of 20 $ktCO_2$/day (7.3 $MtCO_2$/yr), the deposit would take ~80-90 years to reach steady state (reaching 90% of its volume after ~20 years), at which point the mound would have a volume of 1.26×10^8 m^3 and contain ~43 $MtCO_2$. It is perhaps implausible that CO_2 injection would continue over such a long time period. If instead we consider emplacement for a period of 1-5 years, then at the point of cessation, the mound would contain ~6-21 $MtCO_2$. A deposit of this size would take approximately 13-20 years to dissipate, around 100-150 times longer than the 'leakage' case. All other things being equal (e.g. current speeds), the storage mound would alter the chemistry of a significantly larger volume of seawater to a greater extent over a considerably longer period of time.

6.1.4.4 Influence of Hydrate Outcrop Dissolution on Bottom Water Chemistry.

The extent to which dissolution of a hydrate outcrop perturbs the local bottom water chemistry will be dependent on the hydrate dissolution rate and the volume of seawater that the CO_2 dissolves into. This perturbation is therefore a complex function of current speed, outcrop geometry, the orientation of bottom currents with respect to the hydrate footprint, and the extent of both lateral and vertical mixing (degree to which flow is turbulent), and will be both temporally and spatially variable.

---

[10] The time to reach 99.99% of the equilibrium mass as calculated from a simple model using a time step of 1 day.

Figure 6.7 shows a cartoon of the pH field that develops around a large CO_2 lake (500 m x 500 m) based on the model results presented by Enstad et al. (2006) for current speeds of ~10 cm/s (dissolution rate = 0.2 μmol/cm^{2}s, equivalent SR = 0.26 μm/s – see Table 6.1). In this model a marked decrease in pH (ΔpH > 1) extends to a height of ~3m above the lake surface and ~1 km downstream from the lake centre. A significantly larger volume of seawater experiences more moderate changes in pH, where the plume defined by a ΔpH of 0.1 unit or greater extends to a height of 20-25 m, and is ~7 km in length with a width of ~3 km.

Figure 6.7: Cartoon showing the pH field that develops due to dissolution of CO_2 from a large seafloor lake (after model results of Enstad et al. (2006)). Downstream and lateral distances are given from the lake centre. The footprint of the lake is also shown (500m x 500m). Arrows indicate current (10 cm/s) direction. The lower panel shows the vertical cross-section through the centre of the plume in the downstream orientation (along dashed line in upper panel). The upper panel shows a horizontal slice through the plume (along dashed line in lower panel).

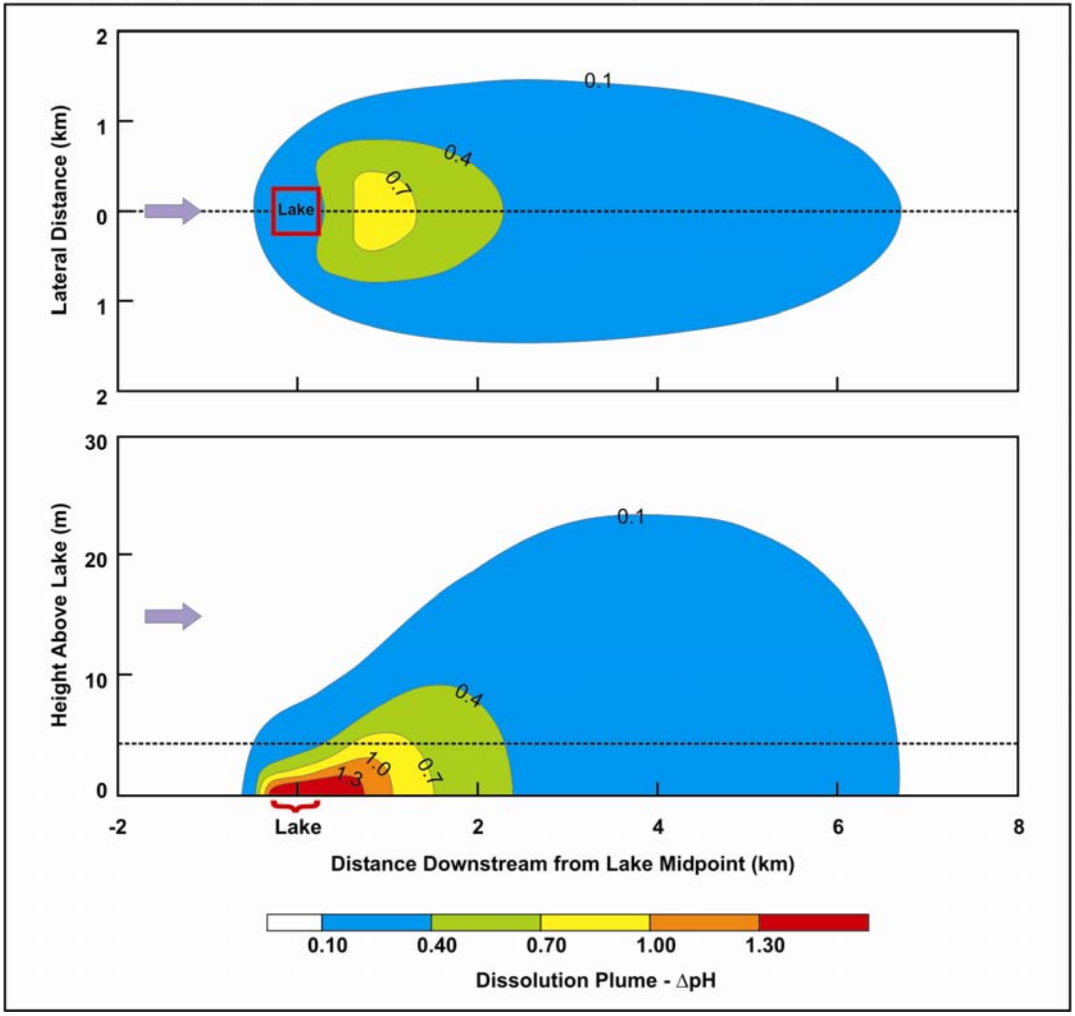

However, this deposit is considerably larger than the probable size of a hydrate outcrop which might form as a result of leakage. Indeed, the total CO_2 dissolution flux from the lake is ~700 ktCO_2/yr, where the only leakage scenario likely to result in a flux of this magnitude would be if the spill point of a reservoir were exceeded. Using the reference leakage rate of ~200 tCO_2/yr and assuming steady state, the more likely outcrop size would have a length scale ~1-2 orders of magnitude smaller and a surface area ~3-4 orders of magnitude smaller than the lake example, with a total CO_2 dissolution flux equal to the leakage rate and some ~3,500 times lower than that from the lake. Thus the spatial extent of the plume, and the volume of seawater that experiences changes in pH, would also be considerably lower.

Small scale field experiments fall at the other end of the scale, where the mass of CO_2 emplaced on the seafloor is significantly less than that which might occur in a leakage scenario (typically 1-100 $kgCO_2$ in any one experiment – see Chapter 3, Boxes 3.4-3.6 and references therein). In these experiments CO_2 is injected into retaining corrals forming smalls pools with a diameter of ~50-100 cm and a surface area of ~0.2-0.8 m^2, around 2 orders of magnitude smaller than the steady state hydrate outcrop surface area for the 200 tCO_2/yr leakage scenario. Large decreases in pH of up to 1.7-1.8 units have been measured in the immediate vicinity of the CO_2 pools (within 1 m), with more moderate decreases of ~0.3 units at a distance of 5-10 m, and background pH at 50-100m. Furthermore, at low current speeds there has been little evidence for significant vertical mixing, with the dense CO_2 rich plume propagating along the seafloor, and ambient pH measured at heights above the seafloor of ~1m.

Ideally models such as those developed to assess dissolution of CO_2 lakes would be applied to hydrate deposits in leakage scenarios to assess the area likely to be affected by a marked decrease in pH under a given set of conditions. In the interim, a comparison of CO_2 deposit footprint and plume extent across the scenarios discussed above (lake, leakage, experiment) suggests that for the 200 tCO_2/yr leakage case, significant changes in pH (ΔpH > 0.5) will be experienced some 10s to 100s of metres downstream from the deposit over an area on the order of 100 m^2 to 1 km^2.

A simple calculation can also be performed to calculate the seawater mixing volumes required to limit the observed pH change assuming well mixed conditions. Threshold seawater mixing volumes for the steady state 200 tCO_2/yr leakage case are shown in Figure 6.8 as a function of ΔpH. The mixing volumes required per day for a ΔpH of 1, 0.5 and 0.1 are ~22 $x10^3$ m^3, ~72 $x10^3$ m^3 and ~400 $x10^3$ m^3 respectively. If we exclude lateral mixing, then for current speeds of 5-20 cm/s, and a hydrate outcrop size of dimension 5-15 m, vertical mixing must extend to ~0.1-1 m, ~0.3-3 m, and ~1.5-18 m to achieve a ΔpH of 1, 0.5 and 0.1 respectively.

Figure 6.8: Threshold seawater mixing volumes required to limit the change in seawater pH for the steady state 200 tCO_2/yr leakage scenario.

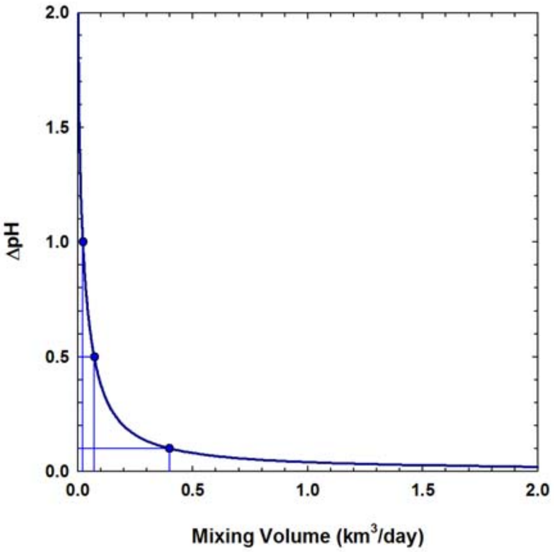

The mixing volume is the volume of seawater required per day into which the CO_2 dissolution flux must be mixed in order to achieve a given ΔpH for the steady state 200 tCO_2/yr leakage scenario. The calculation assumes that the system is both well mixed and at equilibrium.

The change in seawater pH was calculated using CO2SYS (Lewis & Wallace, 1998) with the following input values:

Temperature:	3.6°C
Salinity:	34.6
Pressure:	1047 dbar
Total Alkalinity:	2403 μmol/kg
Initial TCO_2:	2361 μmol/kg
Initial pH:	7.68
Silicate:	142.9 μmol/kg
Phosphate:	3.16 μmol/kg

Results from small scale release experiments have highlighted other factors that need to be taken into consideration when evaluating both the area impacted by the CO_2 dissolution plume, and the ΔpH experienced at a given location in proximity to CO_2 deposit. The potential importance of CO_2 hydration kinetics was highlighted at the beginning of this chapter. In addition, it is important that potential changes in current direction are considered.

Standard dissolution models apply a constant current velocity. That is for a given model run both current speed and direction are held constant. Running the model for different current speeds then allows evaluation of the differing extent of the plume as a function of this parameter. However, the direction of bottom currents can also vary.

Indeed, in small scale release experiments the perturbations in pH observed at a fixed point are periodic, with a given point falling downstream of the CO_2 source for a period of ~30 minutes every ~12 hours and near background pH experienced for the remainder of the time (see Chapter 3, Box 3.6; Barry et al., 2005). This pattern of exposure reflects the inertial and tidal periodicity of bottom currents in the experimental location. In a case such as this the area affected by the CO_2 dissolution plume would be a circle of radius equal to the plume length, rather than the footprint of the plume at any given point in time.

6.1.5 A Rising Plume of Buoyant CO_2 Droplets or Bubbles

Sources of information regarding the behaviour of CO_2 droplets in the ocean include laboratory studies (e.g. Ozaki, 1999; Haljasmaa et al., 2005; Bigalke et al., 2007), in-situ observations (release experiments: Brewer et al., 2002, 2006; vent sites: Lupton et al., 2006; Shitashima & Maeda, 2005), and modelling approaches (e.g. Alendal & Drange, 2001; Chen et al., 2003, 2005; Gangstø, 2004; Gangstø et al., 2005; Zhang, 2005; Brewer et al., 2006).

As a buoyant droplet of liquid CO_2 ascends through the water column it will lose mass due to dissolution. During its ascent the droplet will encounter progressively warmer water, and the remaining liquid CO_2 will expand (became less dense). Hydrate may be present as a thin coating or membrane, or continual conversion of the liquid CO_2 to hydrate may occur. In addition, droplets may collide with each other. Observations during release experiments and at vent sites indicate that when this occurs, hydrate coated droplets do not coalesce into a single larger droplet, but rather adhere to each other forming droplet pairs and rafts (e.g. Brewer, 2002; Lupton et al., 2006). The buoyancy and drag experienced by the droplet during its ascent, and thus the droplet rise rate, will reflect a combination of these processes.

If rising droplets reaches the liquid to gas transition, or indeed if seepage of CO_2 occurs at a depth above the condensation depth, gas bubbles will be formed (Herzog et al., 1991; Haugan & Drange, 1992). These gas bubbles will continue to rise through the water column, and whether or not they fully dissolve or reach the ocean surface will depend largely on the initial size of the gas bubble and the depth of release (or the condensation depth).

As the addition of dissolved CO_2 increases seawater density (Bradshaw, 1973; Haugan & Drange, 1992; Song et al., 2002), we must consider two CO_2 rich plumes; the primary plume of buoyant CO_2 droplets, and the secondary plume of low pH dense seawater that is formed as the droplets dissolve (e.g. Alendal & Drange, 2001; Chen et al., 2003, 2005).

The characteristics of the double plumes are dependent on multiple factors including depth of injection, droplet size, the presence (and nature) of hydrate, current velocity, injection rate, and the local water column temperature and salinity profile experienced during droplet ascent. Indeed, varying combinations of these factors can lead to markedly different behaviours. In the ocean sequestration case (e.g. injection of liquid CO_2 droplets at mid depths) these factors can (to some extent) be controlled or chosen, to engineer droplet and dissolution plumes with a given set of characteristics. In the leakage case, we must consider the most likely behaviour and characteristics. The principle factors that determine double plume characteristics are discussed briefly below, before focusing on in-situ observations of droplet behaviour.

6.1.5.1 Depth of Injection

The depth of ‘injection’, or in this case seepage, will be determined by the leakage event. The discussion below focuses on seepage to deep and intermediate depth waters where CO_2 is a buoyant liquid and hydrate formation may be possible, as it is in this area that further research is particularly required.

6.1.5.2 Expected Droplet Size

Initial droplet size is important for determining the vertical distribution of the CO_2 plumes.

Droplet size is an important parameter in determining the buoyancy forcing experienced by the droplet at a given point in time. Larger droplets have a greater positive buoyancy than smaller droplets, and will ascend through the water column faster. The vertical extent of the droplet plume and associated dissolution plume, and hence the volume of seawater influenced by each plume (the dilution factor), will therefore increase as droplet diameter increases (e.g. Alendal & Drange, 2001). Thus release as large droplets will alter the chemistry of a larger volume of seawater with respect to release as small droplets, while the absolute concentration of CO_2 (both liquid CO_2 and dissolved CO_2) within the double plumes will be lower (more dilute). In addition, very small droplets may be entrained in a sinking CO_2 enriched water plume (e.g. Alendal & Drange, 2001; Chen et al., 2005).

In ocean sequestration scenarios, injection nozzles could be configured to release droplets with a given dimension (e.g. Nishio et al., 2006), and numerical models have examined considered droplets with diameters in the range of ~2 to 60 mm (e.g. Alendal & Drange, 2001; Chen et al., 2005; Gangstø, 2004; Brewer et al., 2006). However, in the seepage case we need to know the expected size of the droplets that would emerge from the seafloor.

When buoyant liquid CO_2 is released directly into the water column it will break down into small droplets due to Taylor instabilities, where observations and model predictions indicate formation of droplets with diameters on the order of 8 to 10 mm (e.g. Brewer et al., 2006). In a water tunnel experiment, droplets larger than 10 mm diameter were observed to shed CO_2 until this size was approximately reached (Halijasmaa et al., 2005). Thus droplets with a diameter on the order of 10 mm might reasonably be expected. Indeed, this shows good agreement with observations at natural vent sites, where droplets emanating from the seafloor at water depths of 1350-1600 m have diameters on the order of 5 to 15 mm (see Table 6.2). The ‘base case’ used in modeling studies typically consider droplet diameters in this range (e.g. 14 mm, Alendal & Drange, 2001; 8 mm, Chen et al., 2005).

Table 6.2: Characteristics of Liquid CO_2 Droplets & Plumes

	Depth of release (m)	Temperature at release (°C)	Initial Droplet Diameter (cm)	Rise Rate (cm/s)	Dissolution Rate ($\mu mol/cm^2/s$)	Methods & Vertical Rise
Release Experiments						
Single droplets, Monterey Bay, California[a]	805	4.4	0.89	10.2 to 14.9	3	Injection of individual droplets. Droplet visually tracked over 460 m ascent. 90% of mass loss occurred within first 200 m of ascent.
Droplet cloud, Monterey Bay, California[b]	1000	3.9	~1	~10		Release of 5 L CO_2 with no attempt to control droplet size. Droplet cloud acoustically tracked over 150 m ascent before signal dissipated.
Natural Vent Sites						
Jade Hydrothermal Field, Okinawa Trough[c]	1350-1550	3.8	~1			
Hatoma Knoll Vent Site, Okinawa Trough[d]	1520	3.9	~0.5-1	~26 to ~20 ~15 to ~10 ~13 to ~4		Droplet visually tracked over 550 m ascent. TCO_2 & pH returns to background values within 10s of m above vents.
Champagne Vent Site, NW Eifuku, Mariana Arc[e]	1604	<4	~1.5			TCO_2 returns to background values within 150 m above vents.

(a) Brewer et al. (2002); (b) Brewer et al. (2006); (c) Sakai et al. (1990); (d) Shitashima & Maeda (2005); (e) Lupton et al. (2006).

6.1.5.3 Influence of Bottom Currents

In a stagnant water column, buoyant CO_2 droplets would simply ascend vertically through the water column until they have completely dissolved, and the CO_2 rich dissolution plume would sink and spread laterally along the seafloor (e.g. Alendal & Drange, 2001). In this case, both plumes experience little dilution, and for a given CO_2 release rate and droplet size the volume of seawater affected is at a minimum, while the decrease in seawater pH is at a maximum.

Under the action of bottom currents, the CO_2 droplets are subjected to horizontal forcing. Both the inclination of the droplet plume and the lateral dispersion of the dissolution plume will increase as current speed increases. As current speed increases, the CO_2 is dissolved into a larger volume of water, and the maximum decrease in seawater pH that is experienced decreases (for a given CO_2 release rate and droplet size). This is illustrated in Figure 6.9, parts (a)-(d), which are based on results from a model with a droplet diameter of 14 mm and a release rate of 1 $kgCO_2/s$, comparing the double plumes predicted for a current speed of 10 cm/s with those predicted for a current speed of 5 cm/s (after Alendal & Drange, 2001). As expected, the water with the highest concentration of droplets and lowest pH is found close to the release point, where the maximum droplet concentration and minimum pH is greater for the lower current speed. While the vertical extent of the droplet plumes (height reached above release point) remains the same as current speed increases, the greater inclination of the droplet plume at 10cm/s results in the plume extending around twice as far downstream than that predicted for the 5cm/s current. In this example, dissolved CO_2 is transported downstream by the background current and downward owing to the increased density of the CO_2-enriched water, where the density of the plume and downward transport is more marked at lower current speeds (as the CO_2 concentration is higher). Eventually, as ambient water entrains the CO_2 enriched water by mixing, the density difference disappears and the dissolved CO_2 follows ocean dynamics as a passive trace (Alendal & Drange, 2001). It is noted that this model does not incorporate the effect of hydrate formation on mass transfer rate (Alendal & Drange, 2001), nevertheless, the illustration of the influence of variable current speed remains valid.

Figure 6.9: Cartoon showing the CO_2 droplet and dissolution plumes resulting from a point source release of buoyant liquid CO_2 at a rate of 0.1-1.0 $kgCO_2/s$ (after model results of Alendal & Drange (2001) and Chen & Akai (2004)). Panel A (after Alendal & Drange (2001)) is for 30 minutes after CO_2 injection commences, with CO_2 release at ~700 m water depth, an initial droplet diameter of 14 mm, and both variable current speed and injection rate: (a & b) current speed 10 cm/s, injection rate 1 $kgCO_2/s$ (c & d) current speed 5 cm/s, injection rate 1 $kgCO_2/s$ (e & f) current speed 5 cm/s, injection rate 0.1 $kgCO_2/s$. Panel B (after Chen & Akai (2004)) is for 100 minutes after CO_2 injection commences, with CO_2 release at ~885 m water depth, an initial droplet diameter of 8 mm, a current speed of 2.3 cm/s, and variable CO_2 injection rate: (g) 0.6 $kgCO_2/s$ (h) 0.1 $kgCO_2/s$. For further details of this model see Chen et al., (2005). CO_2 droplet plumes (a,c,e) are defined by the total mass of liquid CO_2 remaining per m^3 of seawater ($kgCO_2/m^3$). Dissolution plumes (b,d,f,g,h) are defined by the decrease in seawater pH (ΔpH). Arrows indicate current speed and direction.

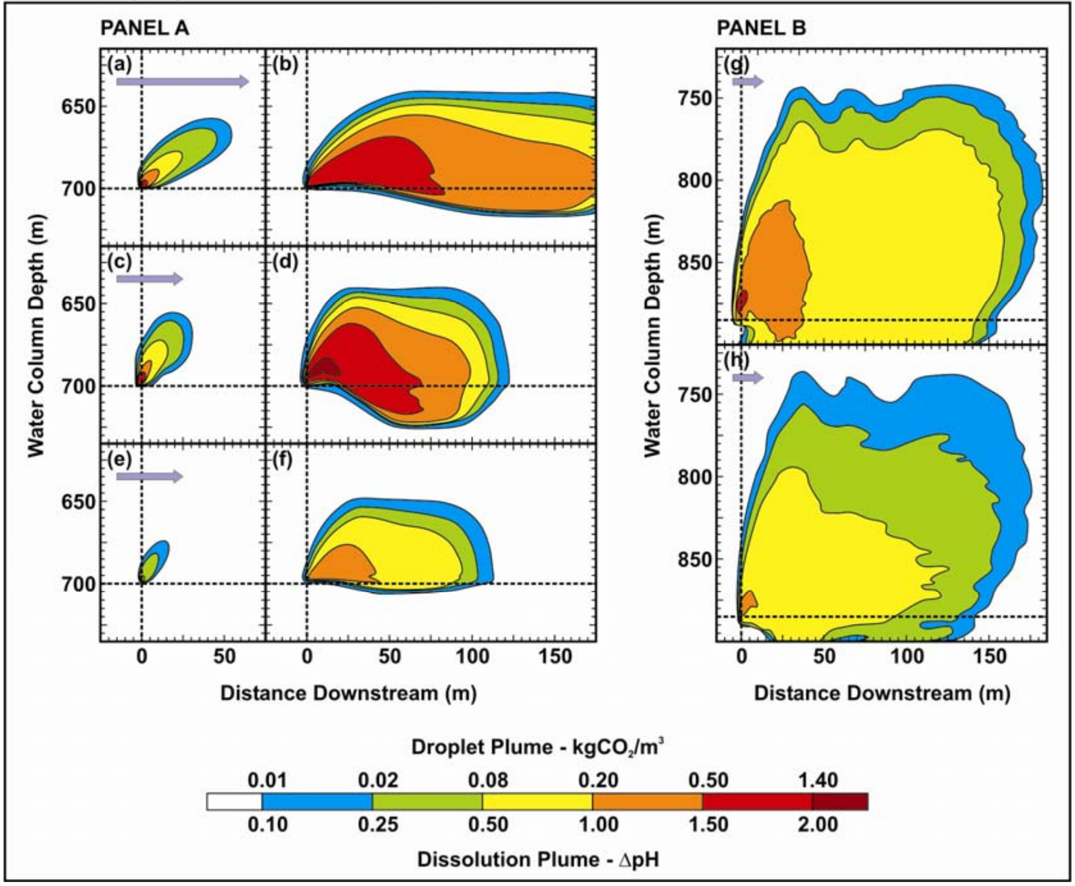

6.1.5.4 *Influence of Release Rate*

The CO_2 release rate, and the area of seafloor over which release occurs (flux of CO_2 per unit area), also exerts a strong control on the extent to which added CO_2 perturbs seawater chemistry. The smaller the mass flux of CO_2, and the larger the area over which it is released, then the greater the dilution factor, and the smaller the resultant reduction in seawater pH.

This is illustrated in Figure 6.9, parts (c)-(h). Parts (c) to (f) are based on results from a model with a droplet diameter of 14 mm and current speed of 5 cm/s, where the influence of hydrate formation on mass transfer rate is not included (Alendal & Drange, 2001). This model compares the double plumes predicted for a point source release rate of 1 $kgCO_2/s$ (~30,000 tCO_2/yr) with those predicted for a release rate of 0.1 $kgCO_2/s$ (~3,000 tCO_2/yr). Figures (g) and (h) are based on results from a model with a hydrate coated droplet diameter of 8 mm and a slower current speed of 2.3 cm/s (Chen & Akai, 2004), comparing the dissolution plume predicted for a point source release rate of 0.6 $kgCO_2/s$ (~20,000 tCO_2/yr) with that predicted for a release rate of 0.1 $kgCO_2/s$ (~3,000 tCO_2/yr). The high release rates of 10s of $ktCO_2/yr$ reflect potential injection rates in ocean storage scenarios, and are considerably greater than expected leakage rates for most failure modes (with the exception of well blowout or exceeding the spill point of a reservoir, where release rates could be significantly larger). The lower release rate of ~3,000 tCO_2/yr is comparable to potential leakage rates in the event of earthquake fault activation, but is still approximately an order of magnitude greater than the reference leakage scenario of ~200 tCO_2/yr (~0.006 $kgCO_2/s$).

Notice that in both models, the decrease in seawater pH is significantly reduced at the low release rate of ~0.1 $kgCO_2/s$, with a maximum predicted ΔpH of <1.5. Furthermore, the addition of dissolved CO_2 to seawater is too low to generate a dense strongly sinking dissolution plume, with the CO_2 enriched seawater tending not to sink (significantly) below the injection depth (Alendal & Drange, 2001; Chen & Akai, 2004).

In addition, the release rate can influence the size of droplet formed, with smaller droplets formed at faster flow rates. For example, laboratory experiments have shown that for the injection of liquid CO_2 through a multiple orifice injector (60 x 4 mm diameter orifices), increasing the flow rate from ~0.1 $kgCO_2/s$ to ~0.2 kg CO_2/s reduced the effective droplet diameter from ~8-20 mm to ~5-15 mm (Nishio et al., 2005).

6.1.5.5 Presence & Nature of CO_2 Hydrate

The presence of a hydrate membrane or ‘shell’ at the interface between a CO_2 droplet and seawater, and/or the formation of composite liquid-hydrate particles, will alter the droplet/particle dissolution rate and rise rate with respect to the liquid only case (e.g. Holder et al., 1995; Ozaki et al., 1999; Chen et al., 2003, 2005; Bigalke et al., 2007).

Numerous small scale release experiments have demonstrated that hydrate formation is ubiquitous within the oceanic hydrate stability zone, with hydrate forming almost instantaneously at the interface between liquid CO_2 and seawater (e.g. Brewer et al., 1999, 2002; personal observation). Similarly, all observations of liquid CO_2 droplets at natural vent sites report the presence of a hydrate membrane on liquid droplets, with the formation of composite liquid-hydrate particles reported at some sites (Sakai et al., 1990; Shitashima & Maeda, 2005; Lupton et al., 2006). It therefore seems reasonable to conclude that under conditions favourable for hydrate formation, seepage of liquid CO_2 to the ocean will result in the formation of hydrate coated droplets and/or composite particles. However it is noted that in regions where P,T conditions lie close to the hydrate stability boundary, hydrate membranes may be partially incomplete or missing due to insufficient thermodynamic forcing and erratic behaviour may occur (Bigalke et al., 2008). Seepage of CO_2 to comparatively warm intermediate depth waters that lie outside the hydrate stability zone (or ascent into this region from below) will result in the formation of buoyant liquid only droplets.

The dissolution of a hydrate coated droplet is a complex phenomenon, involving hydrate formation and dissociation and CO_2 mass transfer across the hydrate membrane (Mori, 1998). While this process has yet to be fully understood, the overall dissolution rate will be proportional to the total interface area, the effective mass transfer coefficient, and the CO_2 concentration difference between the interface and the surrounding seawater, where the CO_2 concentration at the interface is assumed to be saturated (Chen et al., 2005). As CO_2 hydrate is less soluble than liquid CO_2, the dissolution of a hydrate coated droplet (or composite particle) will be slower than that of a liquid only droplet. As hydrate solubility decreases with decreasing temperature this reduction in dissolution rate will be more marked at lower temperatures, where laboratory experiments and models indicate a reduction factor of around 2-3 under the conditions of interest (e.g. Aya et al., 1992, 1997; Nishikawa et al., 1995; Holder & Warzinski, 1996; Gangstø et al., 2005).

The presence of a stiff hydrate membrane also alters the deformation of the droplet (with respect to the liquid only case), and therefore changes the droplet geometry, interface area, and the drag experienced by the droplet during its ascent, hence influencing the overall dissolution rate, the rise rate, and the total ascent of the droplet (e.g. Ozaki et al., 1999; Chen et al., 2003, 2005; Gangstø, 2004; Gangstø et al., 2005).

As the density of CO_2 hydrate is greater than that of buoyant liquid CO_2 (and indeed seawater), the presence of hydrate increases the overall droplet density. For a thin membrane, this density increase can be considered negligible. For example, laboratory measurements of CO_2 hydrate membranes formed at 10 MPa (approximately equivalent to 1000 m water depth) and temperatures of 0 to 10°C indicate a thickness on the order of 7 to 12 μm, where thickness increases as temperature decreases (thermodynamic driving force for hydrate formation increases; Oyama et al., 2004; Abe et al., 2007). For droplets with diameters of 5 to 15 mm, a 12 μm membrane would increase the total droplet density by <0.3% to <0.1% respectively (based on a liquid CO_2 density of 0.950 g/cm^3 and a hydrate density of 1.143 g/cm^3). However, if the hydrate continues to grow with eventual conversion of the liquid CO_2 droplet to a small hydrate particle, the gradual increase in density would slow the rise rate and eventually cause sinking (e.g. Holder et al., 1995). For illustration, using the densities of CO_2 liquid and hydrate given above, and a seawater density of 1.030 g/cm^3, the density of a droplet/particle would exceed that of seawater when approximately 20% of the CO_2 has converted to hydrate.

6.1.5.6 In-Situ Observations of Individual CO_2 Droplets & Droplet Clouds

Individual Droplets/Particles: Observations

In-situ observations indicate a broad spectrum of behaviours, including the formation of hydrate coated droplets and composite particle formation, and are summarised briefly below.

In a small scale release experiment, Brewer et al. (2002) visually tracked CO_2 droplets during their ascent through the water column from a release depth of ~805 m. This experiment utilised a specially designed imaging box or 'bubble box' (see Box 3.5, Chapter 3) mounted on an ROV within the field of view of an HD camera. While the stiffness of the liquid droplet surface and its near spherical shape provided evidence for the presence of a hydrate membrane, gradual conversion of the droplet to a hydrate particle was not observed (Brewer et al., 2002).

Droplets were tracked over a total ascent of ~400 m, where 90% of droplet mass was lost within a period of 30 minutes over the first 200 m of ascent. The droplet dissolution rate was calculated from the measured radial shrinkage rate and was determined to be constant over the ascent at 3.0 $\mu mol/cm^2/s$ (Brewer et al., 2002). This remains at present the only reported in-situ measurement of the dissolution rate of CO_2 droplets. The droplet rise rate increased over the ascent, from a mean of ~10.8 cm/s (6.5 m/min) between 800 m and 700 m, to ~11.5 cm/s (6.9 m/min) between 700 m and 600 m, and 12.7 cm/s (7.6 m/min) between 600 m and 500 m (calculated from Figure 6, Brewer et al., 2002).

While careful injection of liquid CO_2 during in-situ experiments results in the formation of a thin transparent hydrate membrane, the presence of which is inferred from the physical characteristics of the interface (e.g. Brewer et al., 2002; personal observation), observations of droplets at vent sites report a readily visible 'milky skin' (e.g. Lupton et al., 2006), indicating a somewhat thicker membrane.

Utilising the same technique as Brewer et al. (2002), Shitashima & Maeda (2005) tracked droplets emanating from the Hatoma Knoll vents (Okinawa Trough) from a depth of 1470 m over a maximum ascent of ~550 m. Three different droplets were tracked, where the droplets had different initial diameters (in the range 5-10 mm) and displayed different rise characteristics (from presentation by Shitashima & Maeda, 2005). During ascent the droplets gradually converted to small irregularly shaped hydrate particles. The irregular shape was presumably due to a combination of deformation and unevenly distributed hydrate growth. Rise rates were highly variable, although all droplet/particles showed a decreasing rise rate with ascent. As sinking of the droplet/particles was not reported, it can be assumed that conversion of CO_2 to hydrate was not complete (for these droplets). The very rapid ascent of one particular droplet, with an initial rise rate of ~26 cm/s decreasing to ~20 cm/s within a 300 m ascent and remaining approximately constant at shallower depths, seems somewhat difficult to explain. It is perhaps possible that this droplet was influenced by the motion of the ROV, or was entrained in a rising plume of buoyant vent fluids. The two other droplets displayed initial rise rates of ~13 cm/s and ~15 cm/s, decreasing to ~4 cm/s within a 100m ascent and ~10 cm/s within a 300 m ascent respectively.

At the Jade hydrothermal field (Okinawa Trough), translucent hydrate 'horns' were seen growing out of the sediment, with liquid CO_2 emerging from the top of the horns as hydrate coated droplets (Sakai et al., 1990). These horns grew to lengths of ~10 cm, increasing in diameter from a narrow base to about 1 cm at the top, periodically breaking off and rising through the water column (Sakai et al., 1990). As the horns grow in height the proportion of liquid CO_2 (inside the horns) to hydrate (in the horn walls) increases and the average density of the horns decreases, with the horns breaking off when the buoyant force is sufficient to break the hydrate 'root'. Treating the horns as simple inverted cones and assuming that all interior space is occupied by liquid CO_2 suggests a wall thickness less than ~1 mm (i.e. under local conditions, an inverted cylinder with a diameter 1/10th of its length becomes more buoyant than seawater on reaching a length of 10 cm when the hydrate wall thickness is ~1 mm). The droplets and horns were not tracked upwards through the water column, although Sakai et al. (1990) describe the free horns as 'drifting off', suggesting a slow rise rate consistent with a small positive buoyancy.

Finally, at both the Jade vent site and the Champagne vent site (Mariana Arc), droplets trapped in inverted containers have been reported to continuously convert to a white 'sherbet-like' hydrate during ascent (e.g. Sakai et al., 1990; Lupton et al., 2006).

Individual Droplets: Comparison between Observations and Models.

While numerous modelling studies have compared outcomes to the observational data of Brewer et al. (2002), as yet (to the authors knowledge) no attempts have been made to model the behaviour observed at the natural vent sites.

Early work suggested that hydrate coated droplets behave as rigid spheres (Hirai et al. 1997, Mori, 1998). Indeed Brewer et al. (2002) make this assumption for the purposes of a simple thought experiment, and some more recent models are also based on this supposition (e.g. Zhang, 2005). However, the rise characteristics of a rigid sphere do not match the observations of Brewer et al. (2002), where calculating the terminal velocity of a spherical particle (see iterative method outlined in Zhang, 2005) significantly over-estimates the initial rise rate and predicts a decreasing rise rate with decreasing droplet diameter (i.e. decreasing rise rate over ascent). Furthermore, although droplet/particle rise rate did indeed decrease during ascent at the Hatoma Knoll vent site, the irregular shape of these droplet/particles clearly cannot be approximated by a sphere.

The deformation of hydrate coated droplets has been examined in laboratory experiments (Ozaki, 1999; Ozaki et al., 1999; Chen et al, 2003; Nishio et al., 2005). On the basis of these results, Chen et al. (2003, 2005) concluded that CO_2 droplets with a hydrate membrane should be modelled as a rigid irregular ellipse, and calculated terminal velocities using the drag coefficient when droplet deformation was taken into account. In a similar approach, Gangstø (2004) and Gangstø et al. (2005) adapted the bubble model of Bozzano & Dente (2001) to calculate the terminal velocity of hydrate coated CO_2 droplets of differing shapes, where the drag coefficient is defined by the droplet size, interfacial tension, density (of both the droplet and seawater) and the viscosity of seawater. These authors demonstrate a reasonable fit to the rise rates reported by Brewer et al., (2002), with the droplet gradually transitioning from an ellipsoidal regime to a spherical regime as it loses mass during ascent. This conclusion also fits with the observation of Brewer et al. (2002) that on expulsion from the injection nozzle the droplets initially had an elongated shape, gradually becoming more spherical during ascent.

At present, the individual droplet models of Chen et al. (2003, 2005), Gangstø (2004) and Gangstø et al. (2005) provide a reasonable match to the experimental observations (rise rate and shrinkage rate) of Brewer et al. (2002), and clearly demonstrate that shape/deformation must be included in models of droplet behaviour. However, while these models may well provide a strong basis for prediction of hydrate coated droplet behaviour in ocean sequestration scenarios, there are serious limitations in their applicability to the leakage case. Indeed, if the observations at natural vent sites are a true reflection of the variation that can be expected when droplets emerge from the seafloor, this scenario may well frustrate predictive modelling attempts, although end member scenarios could be explored. In particular, it is the variable nature of hydrate formation, which in turn influences all key parameters of the droplet/particles, that may prove problematic.

The reasons for the observed variation in extent and nature of hydrate formation are presently uncertain, and there is clearly a need for additional observational data, including both laboratory and in-situ experiments, and further investigation of natural vent sites. Some possible causes for observed differences and other factors that warrant consideration are suggested below, although this list is by no means exhaustive:

(i) The flow path and flow rate through the sediment and/or accompanying fluid flow (hydrothermal or entrained flow) may promote hydrate formation at the natural vent sites. In an early release experiment, Brewer et al. (1998) expelled a mixture of CO_2 and He through a frit with a 10 μm pore size, which may provide an analogue for expulsion through sediment pore space. The emerging hydrate coated droplets showed a characteristic shape that pinched and narrowed toward the frit/base, and the droplets remained adhered to the frit and to each other to form clusters until they reached a critical size and detached. This behaviour is similar to the hydrate horns described by Sakai et al. (1990). Small scale release experiments have also demonstrated the formation of composite liquid-hydrate-seawater particles using a co-flow injector (Tsouris et al., 2004; Riestenberg et al., 2005), where this experimental work may prove a solid starting point for further examination of composite particle behaviour.

(ii) The presence of trace components in the vented CO_2 that promote hydrate formation (e.g. H_2S), and that are absent in the pure CO_2 used in release experiments.

(iii) Adsorption of contaminants onto the droplet surface - the 'dirty bubble' problem. Experiments have shown that in contaminated water accumulation of surface-active contaminants on a bubble/droplet surface affects the shape and therefore the drag (Clift et al. 1978). While comparison of various numerical models to the observational data of Brewer et al. (2002) implies that surface active contaminants had a negligible effect on the dynamics of the observed droplet (Gangstø, 2004), this may not be the case for droplets emerging from the seafloor.

(iv) The inherent physical properties of the systems under observation. The CO_2 vent sites are located at depths of 1350-1550 m, whereas the release experiment was conducted at a depth of 800 m. The thermodynamic driving force (P and T conditions) for hydrate formation is therefore greater at the natural vent sites, where the difference between the natural and experimental systems would become more marked as the droplets ascend. For example, at Hatoma Knoll the temperature increases only ~0.2°C over the first 200m of ascent from 3.9°C at 1470 m to 4.1°C at 1270 m. In comparison, in the release experiment, temperatures are both higher at the release point and increase more rapidly over the ascent, from 4.4°C at 800 m to 5.2°C at 600 m.

(v) Experimental artefacts. In the Brewer et al. (2002) experiment, the imaging box was fitted with grills at the top and bottom to promote laminar flow through the box and minimise (although not eliminate) turbulence, whereas this was not the case in the Hatoma Knoll experiment (personal communication, Shitashima-san). Turbulent flow (mixing) through the imaging box, and in inverted containers during ROV ascent, could have stimulated further hydrate formation that would not otherwise have occurred. It is noted that numerous in-situ experiments have demonstrated that simply shaking a container holding liquid CO_2 and seawater results in rapid flocculent hydrate formation.

Droplet Clouds: Observations and Comparisons to Models

While the use of an imaging box allows individual CO_2 droplets to be visually tracked during their ascent (or indeed descent) through the water column, this system may also perturb the flow conditions around the droplets, with boundary flow effects potentially altering the dissolution and rise rates from those of a freely ascending droplet (e.g. Brewer et al., 2002; Gangstø et al., 2005). Furthermore, a droplet cloud or plume cannot be so contained, and is impossible to track visually when free to move in all dimensions (Brewer et al., 2002; see also Box 3.5, Chapter 3). While it is commonly assumed that pH sensing may be used to track a CO_2 plume, for small releases of CO_2 droplets the pH signal may be undetectable (e.g. Shitashima & Maeda, 2005; Brewer et al., 2006), thus some other technique is required.

Brewer et al. (2006) recently demonstrated the use of acoustic detection to track a small cloud of CO_2 droplets, using both a surface ship downward looking sonar and an ROV forward looking sonar (see Box 3.5, Chapter 3). The droplet cloud was tracked from a release depth of ~1000 m over an ascent of 150 m (~30 minutes) before the signal was lost. The procedure was to position the ROV directly beneath the ship before releasing ~5 L of liquid CO_2. On release, the liquid mass immediately began to break up into smaller cm scale droplets due to Taylor instabilities, and no attempt was made to control droplet size. The ROV was then backed off to a distance of ~10 m from the cloud (as ascertained by the scanning 675 kHz ROV sonar with a ±15° vertical cone angle) and held stationary. Once the sonar signal indicated the cloud had risen beyond view, the ROV was piloted upwards, positioned immediately above the cloud and held stationary as the cloud transited upward and out of view again. This procedure was repeated throughout the tracking exercise, where both the ascent of the droplet cloud and the ROV flight path were detected by the 38 kHz shipboard sonar. Combining the horizontal slices of the droplet cloud obtained from the ROV sonar with the vertical extent as determined from both the ROV and shipboard sonar provided a detailed 3 dimensional picture of the droplet cloud during its ascent, which was then compared to that predicted using the numerical model of Chen et al. (2005) with randomly set initial droplet diameters of 8 to 10 mm.

Simulated horizontal sections through the centre of the droplet cloud agreed well with the ROV sonar record, increasing from a scale of 4 m x 7 m after 5 minutes to 7 m x 8 m after 15 minutes, and 8 m x 9 m after 25 minutes (see Figure 2, Brewer et al., 2006). Simulated vertical sections also agreed reasonably well with the sonar record images in terms of cloud height and width, however the modelled cloud rose slightly slower than the real cloud, with a mean rise rate over a 25 minute ascent of ~6 cm/s compared to ~10 cm/s (see Figure 3, Brewer et al., 2006). This may be due to two factors. Firstly, while break up of the liquid CO_2 into droplets occurs immediately on release, this shedding process is not instantaneous, thus the real cloud is likely to include globules or droplets larger than the modelled droplet diameters. Secondly, a downward flow of locally dense CO_2 enriched sea water is predicted by the model (Chen et al., 2005), where this develops to a significant level in comparison to the gradually slowing individual droplet rise rates after ~20 minutes (Brewer et al., 2006). Because of a smaller computation domain in the horizontal (20 m x 20 m) than the vertical (200 m), the open boundary conditions at top and bottom make the modelled flow field sensitive to the small negative buoyancy effect (Brewer et al., 2006). In the real ocean no significant down-welling was observed, since the small size of the release produced negligible local density increases (Brewer et al., 2006). Also evident from both the observations and model simulations is the rapid dilution (due to dissolution and dissipation) of the droplet cloud during ascent, where the cloud dilution detected by the ROV sonar corresponded to simulations with maximum droplet numbers per m^3 of 620,160, and 80 at 5, 15, and 25 minutes respectively. The results suggest that very sensitive detection of small amounts of liquid CO_2 leaking from the sea floor may be detected acoustically, but that rapid droplet dissolution results in signal detection only within about 150 m of vertical ascent from the source (Brewer et al., 2006).

This experiment represents the first in-situ assessment of the dynamics of a rising cloud of CO_2 droplets against which a model can be tested. As such, the generally good agreement between the observed and simulated clouds gives increased confidence in our ability to predict plume behaviour. However, the caveat remains that seepage of CO_2 to the ocean is likely to result in more complex behaviour due to the variable nature and extent of hydrate formation.

6.1.5.7 The 'Expected' Behaviour of a CO_2 Droplet or Bubble Plume

Further investigation of CO_2 seepage from sediments to the ocean is required to determine the factors that control droplet formation and composite liquid-hydrate particle formation, and thus allow the most likely behaviour for a given set of circumstances to be predicted with any degree of certainty. Nevertheless, current knowledge and understanding does allow a number of broad statements regarding expected behaviour in the leakage case to be made.

Observations and models indicate that the release of liquid CO_2 to the ocean will result in an initial droplet size on the order of 1 cm diameter.

For seepage of liquid CO_2 to a warm water column (outside the hydrate stability zone) the CO_2 will form a rising plume of buoyant liquid only droplets. Current numerical models are likely to simulate the ascent and dissolution characteristics of these droplets with a reasonable degree of accuracy, although surface contamination may need to be considered.

For seepage of liquid CO_2 to a water column that lies within the hydrate stability zone, hydrate formation will occur. Hydrate may simply be present as a thin membrane at the droplet-seawater interface. Alternatively, composite liquid-hydrate particles with complex geometries could form as the CO_2 emerges from the seafloor. In both cases, continual conversion of CO_2 to hydrate may occur while the droplet/particle remains within the hydrate stability zone. While the proportion of CO_2 present as liquid remains high, the droplet/particles will be positively buoyant and will ascend through the water column. As the proportion of hydrate increases, the rise rate will slow, and if a critical threshold (dependent on the relative density of seawater, liquid CO_2 and CO_2 hydrate under local conditions) is crossed, the droplet/particle will sink. In-situ measurements indicate a droplet/particle rise rate on the order of 5-15 cm/s (Table 6.2).

The ascent rate and dissolution characteristics of hydrate coated droplets can be modelled with a reasonable degree of accuracy, with numerical simulations showing good agreement to the currently limited observational data set. As yet, model studies have focussed on CO_2 release rates appropriate to ocean sequestration scenarios. However, Chen & Akai (2004) presented results from a model run with a release rate of 0.1 $kgCO_2/s$, which is more comparable to the upper end of expected leakage rates (excluding well blowout and exceeding the spill point of a reservoir - see Figure 6.9). As this model run also considered a comparatively slow current velocity of 2.3 cm/s, these results seem likely to represent a good end-member scenario for seepage at relatively rapid rates when CO_2 is released as hydrate coated droplets and plume dilution is low. In this case, the maximum predicted ΔpH is less than 1.5, where the region experiencing a ΔpH of 1-1.5 is restricted to the immediate vicinity of the release point, extending only some 10-15 m in both the vertical and along flow directions. As noted previously, the addition of CO_2 to seawater is not sufficient to generate a dense strongly sinking dissolution plume, where the plume defined by a ΔpH>0.1 extends to a height of ~150 m above the release point, and approximately 175 m downstream (see Figure 6.9).

Observational evidence also supports the conclusion that the vertical influence of a droplet plume (considered here to be the height over which a measurable change in seawater chemistry occurs) is likely to be confined to some 150-200 m above the release point (excluding catastrophic leakage scenarios; see Table 6.2). In release experiments, 90% of droplet mass loss occurred over an ascent of 200 m, while the acoustic signal from a droplet cloud was lost after an ascent of 150 m (Brewer et al., 2002,2006). At Hatoma Knoll, while the pH near the seafloor was significantly depressed (pH 5), the TCO_2 and pH of seawater near the liquid CO_2 vents recovered to background values within several 10s of m from the seafloor (Shitashima & Maeda, 2005). Similarly, water column measurements at NW Eifuku (Champagne vent site) on the Mariana Arc showed that a measurable excess of TCO_2 was confined to depths within 150 m above the vents (Lupton et al., 2006).

This suggests that for seepage of liquid CO_2 to the seafloor at a point more than 200 m below the condensation depth, the majority of liquid CO_2 will have dissolved before the droplet reaches the liquid to gas transition.

Conversely, for seepage of CO_2 to the seafloor at a point less than 200 m below the condensation depth, a significant proportion of the CO_2 may reach the liquid to gas transition, at which point bubbles of CO_2 will be formed (Herzog et al., 1991; Haugan and Drange, 1992). Whether or not the liquid to gas boundary lies within the hydrate stability zone, and thus whether a free gas or hydrate coated gas bubble is formed, will depend on local water column conditions. The gas bubbles will continue to rise through the water column, with a dissolution rate on the order of 0.26 to 1.1 $\mu mol/cm^2/s$ (Teng et al., 1996). Observations of a hydrate coated liquid CO_2 droplet reaching the liquid to gas boundary showed the formation of a gas head, pinching off of a liquid tail, and rapid gas bubble separation and dissolution (Brewer et al., 2002).

Whether the gas bubbles dissolve completely in the water column or reach the ocean surface, will depend largely on the mass of CO_2 remaining in the droplets as they reach the liquid-gas transition (defining bubble size), and the depth of the liquid-gas transition (defining the remaining height of water the bubbles must ascend through to reach the sea surface).

Similarly, for seepage of CO_2 to shallow waters above the condensation depth, a buoyant plume of gas bubbles will be formed. Observations at shallow water CO_2 vent sites suggest that complete bubble dissolution will occur in the water column on a length scale of ~150-350 m, where this variation could be attributed to multiple factors including local conditions, seepage rate, initial bubble size, and bubble gas composition (see Appendix 3.A). For example, at the Grimsey Hydrothermal Field, Iceland, low to intermediate CO_2 vents (CO_2 content of 1-41 mol%) are located at ~400m water depth (Botz et al., 1999). Acoustic profiles over the vents show the most intense scattering near the seafloor, where the signal disperses at depths of 150-50m, indicating complete dissolution on a length-scale of 250-350m (Hannington et al., 2001). In the Bay of Plenty, New Zealand, CO_2 rich gas vents are found at multiple locations and depths (CO_2 content of ~70-90 mol%). The deepest Bay of Plenty vent site where bubble bursting at the surface has been reported is located at 188 m water depth (Glasby, 1971). However, at another site, bubble streams originating at 167 m water depth terminated at 20 m depth, with no bubbles detected at the surface, indicating complete dissolution on a length-scale of ~150 m (W. Giggenbach and I. Menyailov, Bulletin of the Global Volcanism Network, 03/1990 Calypso Mound). In general, it seems likely that seepage to waters shallower than ~ 200 m will result in bubble bursting at the sea surface (direct outgassing). It should also be noted that any CO_2 that dissolves into the surface mixed layer of the ocean will equilibrate with the atmosphere on a comparatively short timescale.

One issue that has not been addressed here is the possibility of rapid transport of large volumes of CO_2 through the water column, resulting in eruptive degassing of CO_2 at the sea surface. The IPCC (2005) concluded that oceanic CO_2 release carries no expectation of risk of catastrophic atmospheric degassing such as that which occurred at Lake Nyos. However, a caveat was included that 'if somehow large volumes of liquid CO_2 were suddenly transported above the liquid-gas phase boundary, there is a possibility of a self-accelerating regime of fluid motion that could lead to rapid degassing at the surface' (IPCC, 2005). It is noted that a catastrophic leakage event (e.g. well blowout, large earthquake) at depths where CO_2 is buoyant may represent a mechanism to transport large volumes of CO_2 rapidly through the water column, and further investigation of this may be warranted.

6.2 Potential Impacts of CO_2 Leakage on Ocean Biota

In this section, we examine the potential impacts of CO_2 leakage on ocean biota. Possible impacts of elevated CO_2 on marine organisms have been addressed in both the IPCC SRCCS (IPCC, 2005) and The Royal Society report on Ocean Acidification (The Royal Society, 2005). As highlighted in these reports, our present understanding of the effects of elevated seawater CO_2 and depressed pH on individual organisms and biological communities is far from perfect and considerable work remains to be done. As the physiological effect of high CO_2 on marine organisms has been the subject of numerous reviews (e.g. Pörtner and Reipschläger, 1996, Seibel and Walsh, 2003, Ishimatsu et al., 2004, 2005; Pörtner et al., 2004, 2005), the approach taken is to be briefly review this material before focussing on potential impacts of leakage at the ecosystem level.

6.2.1 The Physiological Impact of CO_2 on Marine Organisms

Chemical changes to seawater as a consequence of adding CO_2 can directly affect individual organisms through modulation of physiological functions at the molecular level. The effects of elevated CO_2 at the molecular to organism level for a generalised marine water breathing invertebrate or fish are summarised in Figure 6.10 (after Portner et al., 2004) and discussed briefly below.

Both elevated CO_2 and depressed pH (elevated hydrogen ion, H^+, concentration) can exert negative impacts on ocean animals (e.g. Tamburri et al., 2000; see Figure 6.10). Indeed, changes in the concentration of molecular CO_2, the bicarbonate ion (HCO_3^-), and the carbonate ion (CO_3^{2-}), in ambient water and body fluids may each have specific effects on marine organisms (Pörtner and Reipschläger, 1996; IPCC, 2005). Furthermore, the effect of CO_2 induced acidification has been shown to be significantly greater than that caused by the same decrease in seawater pH as a result of addition of mineral acids such as HCl and H_2SO4 (Kikkawa et al., 2004; Ishimatsu et al., 2005). This is due to the much higher biomembrane permeability of gaseous CO_2 compared with that of H^+ (Heisler, 1986; Morris et al., 1989). As highlighted by Ishimatsu et al. (2005), one important consequence of this is that mortality studies based on mineral acid exposure are likely to significantly under predict the effects of hypercapnia induced acidosis. However, there is perhaps a second important consequence – that is if an organism is exposed to a CO_2 rich plume that is far from chemical equilibrium, then uptake of CO_2 and consequent internal acidification may be significantly greater than that predicted for the given total CO_2 loading if equilibrium is assumed. Thus in addition to the total amount of CO_2 added to seawater, the chemical speciation of that CO_2 may be a vital factor in determining the biological impact of leakage.

When an organism is exposed to high external CO_2, (i.e. enters a region where seawater has elevated CO_2 due to leakage), CO_2 rapidly enters the organism by diffusion across body surfaces (especially respiratory surfaces) and equilibrates between body compartments (Figure 6.11; Pörtner et al., 2004). This internal accumulation of CO_2 (hypercapnia) causes an immediate physiological disturbance, and will be responsible for most of the effects observed in animals (reviewed by Pörtner and Reipschläger, 1996; Seibel and Walsh, 2003; Ishimatsu et al., 2004, 2005; Pörtner et al., 2004, 2005). Sensitivity to high CO_2 effects is likely to increase as the organisational complexity, activity level, mobility, and reactivity of the organism increases (e.g. Pörtner et al., 2004). For example, squid generally have a higher sensitivity to elevated CO_2 than fish due to their higher metabolic rate and extremely pH-sensitive blood oxygen transport (e.g. Pörtner et al., 2004).

6.2.1.1 Acid-Base Status & Metabolic Activity

Numerous cellular processes within the organism are directly dependent on the control of pH in intra- and extracellular compartments (acid-base regulation). For example, ion transport mechanisms are dependent on pH or proton (hydrogen ion, H^+) gradients, while enzymes (biomolecules that catalyse chemical reactions) are only active within a relatively narrow range of pH. Good acid-base regulation is therefore vital for proper physiological functioning.

The predominant effect of internal hypercapnia in water breathers is perturbation of acid-base status, where body fluids are acidified through the rapid conversion of CO_2 to carbonic acid, a reaction catalysed by the ubiquitous enzyme carbonic anhydrase. The disturbance of acid-base status across several body compartments can to major effects on the individual, affecting growth, behaviour, reproduction, and development of eggs and larvae (Figure 6.10; see review of Portner et al., 2004).

Figure 6.10: Effects of added CO_2 at the molecular, cellular and organism level for a generalised and simplified marine invertebrate or fish. Redrawn from Pörtner et al. (2004) and IPCC (2005). The purple box represents the organism, and the blue box represents seawater. Cellular processes are shown on the left. These processes occur in various tissues such as the brain, heart or muscle, where the consequences of process depression (indicated by a - sign) or stimulation (indicated by a + sign) are shown on the right and at the top. Black arrows show diffusive transfer of CO_2. Red arrows indicate which of the carbonate system species (CO_2, H^+ or HCO_3^-) modulate the function. Areas shaded green indicate processes relevant for the organisms energy budget and growth.

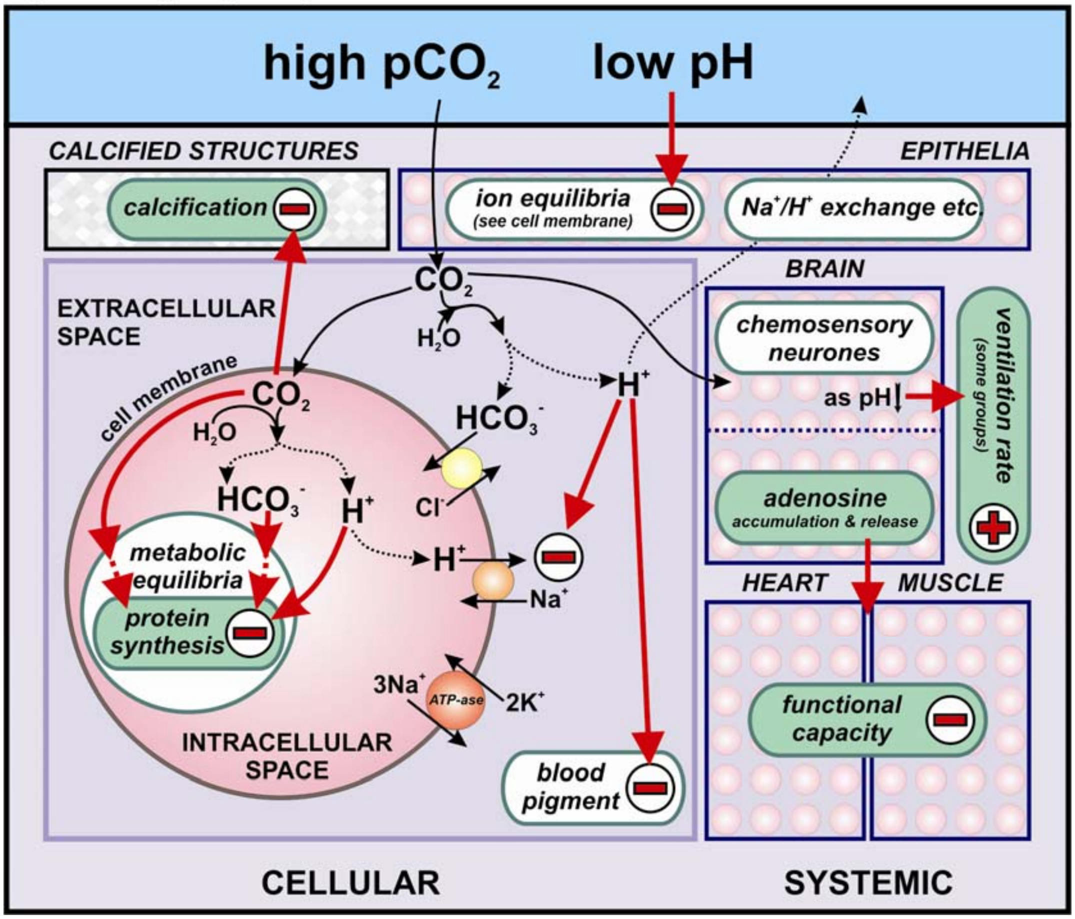

Internal acidification due to CO_2 uptake is compensated for by the same mechanisms used to correct for metabolic or respiratory acidosis, the primary processes being metabolic consumption of protons, buffering of intra- and extracellular compartments, and active proton-equivalent ion transport (Walsh & Milligan, 1989; see Figure 1 in Seibel & Walsh, 2003). Over time, the decrease in internal pH is counteracted by an accumulation of bicarbonate anions in the affected body compartments (Heisler, 1986; Wheatly and Henry, 1992, Pörtner et al., 1998;

Ishimatsu et al. 2004). In calcified organisms the bicarbonate required may be supplied (at least in part) by exoskeleton dissolution (e.g. Spicer et al., 2007). Compensation is not always complete (see review of Pörtner et al., 2004; Miles et al., 2007; Spicer et al., 2007), and for some species may be almost nonexistant (e.g. the deep sea Tanner Crab Chionoecetes tanneri; Pane & Barry, 2007)). Furthermore, the uptake of counter ions can perturb osmoregulation (regulation of salt concentration by osmosis), where this can lead to an increase in steady state salt (NaCl) load of up to 10% in marine fish in high CO_2 environments (Evans, 1984; Ishimatsu et al., 2004). Thus even with near complete compensation of CO_2 related acidification, the change in body fluid ionic concentrations, and/or the energetic costs necessary to maintain the new ionic steady state, could lead to adverse effects including mortality over long time scales (IPCC, 2005; Ishimatsu et al., 2005).

Incomplete compensation of acidosis may result in a depression of aerobic energy metabolism (reviewed by Pörtner et al. 2004, 2005). Central nervous mechanisms may also contribute to metabolic depression, as indicated by the accumulation of adenosine in the nervous tissues of a benthic sipunculid worm *Sipunculus nudus* under hypercapnic conditions (Portner et al., 2004; see Figure 6.10).

The depression of metabolism in marine organisms observed under high CO_2 concentrations also includes inhibition of protein synthesis — a process that is fundamental to growth and reproduction, and thus the maintenance of a population (see reviews of Portner et al., 2004; Ishimatsu et al., 2005 and IPCC, 2005). Reduced protein synthesis under elevated CO_2 conditions has been reported for the Antarctic fish, *Pachycara brachycephalum* and *Lepidonotothen kempi*, and may occur in *S. nudus*, where this effect is best explained by the decrease in intracellular pH (Langenbuch and Pörtner, 2002; Langenbuch and Pörtner, 2003; Portner et al., 2004; see Figure 6.10). Growth suppressions likely (at least in part) to be due to metabolic suppression and reduced protein synthesis have been reported for a number of other species (see review of Ishimatsu et al., 2005), with reduced growth rates under hypercapnia observed for marine penaeid prawns (Wickins, 1984), Mediterranean mussels (Michaelidis et al. 2005), and a number of fresh water and seawater fish (see review of Ishimatsu et al., 2005 and references therein). In the case of juvenile white sturgeon, stimulation of ventilation and the associated increase in oxygen consumption indicated a shift in energy budget towards maintenance metabolism, leading to a reduction in foraging activity and thereby decreasing growth (Crocker and Cech, 1996). Ishimatsu et al. (2005) suggest that CO_2 may also reduce fish growth through decreased chances to detect food based on indications that CO_2 suppresses taste nerve responses to taste stimulants in Japanese eel (Yoshii and Yotsui, 1997). Kurihara et al., (2004) observed a harmful influence of CO_2 on reproductive performance in marine copepods (*Acartia steuri, Acartia erythrea*) and sea urchins (*Hemicentrotus purcherrimus, Echinometra mathaei*), with decreased copepod egg production and hatching rates, and a decrease in the fertilisation rate of sea urchins. Similarly, Ishimatsu et al., (2004) report a decrease in the hatching and survival of fish larvae with increasing CO_2 concentration and exposure time.

6.2.1.2 Ventilation & Oxygen Transport

While ventilation in water breathers is largely driven by the level of water oxygenation, there is growing evidence that the ventilation rate of fish may be stimulated by elevated CO_2, with CO_2 and/or pH sensitive chemoreceptors located in the gills or central nervous system of some fish (Burleson and Smatresk, 2000; Gilmour, 2001; McKendry et al., 2001; McKenzie et al., 2002; Milsom, 2002; Remmers et al., 2001; see also reviews of Pörtner et al., 2004, Ishimatsu et al., 2005 and Figure 6.10). However, as noted by Pörtner et al. (2004), the capacity for ventilatory compensation of hypercapnic acidosis is limited due to the small diffusion gradient of CO_2 between the organism and the water (Scheid *et al*., 1989).

In blue-blooded squid, oxygen transport occurs by use of an extracellular pigment, haemocyanin. The high metabolic rate of squid (due to the high energy demand of jet-propulsion swimming) requires a high oxygen supply. This is achieved through the fine control of pH in arterial and venous blood, where the ability of haemocyanin to bind oxygen decreases markedly with decreasing blood pH (a large Bohr effect), thus oxygen is released in oxygen starved tissues when respiratory CO_2 lowers blood pH. In contrast to fish, there is no venous oxygen reserve in squid as haemocyanin fully releases its O_2 load in the tissue even under resting conditions (Pörtner, 1990). A consequence of the large Bohr effect is that under hypercapnic conditions, blood acidification severely reduces the oxygen carrying capacity of haemocyanin, where animals can asphyxiate at high CO_2 concentrations because the blood cannot transport enough oxygen to support metabolic functions.

Fish are generally less sensitive to CO_2 than squid, most likely due to their lower metabolic rate, the presence of red blood cells which protect their blood pigment (haemoglobin) from excessive pH fluctuations, and the existence of a venous oxygen reserve (IPCC, 2005). Thus fish appear to be able to satisfy the oxygen demand of tissues despite the reduction in the oxygen-binding affinity of hemoglobin due to hypercapnia as long as no exercise is required (see review of Ishimatsu et al., 2005). However, active metabolism, determined as oxygen consumption rate during swimming, may decrease significantly as CO_2 increases (see review of Ishimatsu et al., 2005).

6.2.1.3Calcification

One obvious effect of elevated CO_2 concentrations is the modification of carbonate system speciation, where the concentration of the carbonate ion (CO_3^{2-}) decreases, and hence the carbonate saturation state of seawater (Ω) see Equations 5.7 to 5.10, Section 5.4.1, Chapter 5) also decreases with consequent impacts on calcifying marine organisms.

The various groups of planktonic and benthic marine organisms that form shells or plates of calcium carbonate ($CaCO_3$) are listed in Table 6.3. Also shown is the form of carbonate precipitated, where this varies in crystal structure and chemical composition between the different groups. To make these calcareous structures, seawater must be supersaturated with respect to the relevant carbonate mineral ($\Omega > 1$). Many studies have demonstrated that a decrease in Ω results in a decrease in the rate of calcification, where this occurs even when Ω remains above one (e.g. Borowitzka, 1981; Gao et al., 1993; Langdon et al., 1998, 2000; Gattuso et al., 1998; Marubini and Thake, 1999; Marubini & Atkinson, 1999; Leclercq et al., 2000; Marubini et al., 2003; Feely et al 2004; Langdon & Atkinson, 2005; see Figure 6.10). A decrease in carbonate supersaturation may also weaken carbonate skeletal structures, making them more susceptible to erosion and dissolution. Should seawater become undersaturated ($\Omega < 1$), calcification will cease and dissolution will occur.

Table 6.3: The form of $CaCO_3$ deposited by groups of benthic and planktonic calcified marine organisms (after The Royal Society, 2005).

Organisms	Form of calcium carbonate	Habitat
Coccolithophores	Calcite	Planktonic
Foraminifera	Calcite	Benthic or Planktonic
Calcaerous & Coralline Macroalgae	Aragonite or high Mg Calcite	Benthic
Corals	Aragonite	Benthic
Pteropod Molluscs	Aragonite	Planktonic
Other Molluscs	Aragonite or Aronite + Calcite	Benthic or Planktonic
Crustaceans	Calcite	Benthic or Planktonic
Echinoderms	high Mg Calcite	Benthic

The various carbonate minerals have different solubilites, where aragonite is more soluble than calcite, and the incorporation of magnesium into either form increases the solubility, i.e. under the same seawater conditions $\Omega_{\text{aragonite}}$ will be less than Ω_{calcite} and $\Omega_{\text{Mg calcite}}$ will be less than Ω_{calcite}. Organisms that precipitate aragonite or high Mg calcite will therefore be more vulnerable to elevated CO_2 than those that precipitate calcite. The physical structure of the shell or plates (e.g. porosity and surface area) will also play a significant role in determining solubility, thus organisms precipitating highly porous shells will also be more vulnerable.

Decreased calcification is likely to reduce competitive fitness, where long term exposure to high CO_2 could result in a shift in community structure towards non-calcifying organism (The Royal Society, 2005). Ultimately, the effect that reduced carbonate production has for calcifying organisms will depend on the role of calcification and calcareous skeletons in the cell physiology and ecology of these organisms (Riebesell, 2004; see review of The Royal Society, 2005). In most groups of the calcifying organisms the mechanical function of calcification is obvious, such as providing a structural framework (corals) or mechanical protection (foraminifera, molluscs, crustaceans, echinoderms). However, in other groups such as the corraline algae and coccolithophores, the function of calcification is less clear (The Royal Society, 2005). For a thorough discussion of the impacts of high CO_2 on calcification see The Royal Society (2005). Note also the potential impact of leakage on coral reefs is discussed further in Chapter 7.

6.2.1.4 Other Impacts due to Changes in Ocean Chemistry

Chemical changes to seawater as a consequence of elevated total CO_2 concentrations may also affect marine life through indirect mechanisms (IPCC, 2005). The seawater speciation of over 40 elements (those for which the hydrolyzed form or carbonate complexation is important) will be strongly influenced by pH (Byrne, 2002). For example, a decrease in seawater pH will change the speciation of macronutrients such as phosphate ($H_2PO_4^-/HPO_4^{2-}/PO_4^{3-}$), silicate ($Si(OH)_4/SiO(OH)_3^-$) and ammonia ($NH_4^+/NH_3$), and thus impact nutrient cycling (Zeebe & Wolf-Gladrow, 2001). Indeed, studies have demonstrated a significant decrease in marine nitrification rates (the oxidation of ammonia to nitrite and then nitrate by marine bacteria) under low pH conditions, where this is most likely due to the reduction in the $NH_3:NH_4^+$ ratio (Huesemann et al., 2002). Numerous trace elements are also involved in biological processes, either as essential (and in some cases growth limiting) micronutrients or as potential toxins, where copper is essential at low concentrations and becomes toxic at high concentrations (e.g. Bruland & Lohan, 2004). As the bioavailability of trace elements (i.e. whether or not the elements are taken up by marine organisms) depends on their chemical speciation rather than the total concentration, this will also be altered, where both observations and equilibrium calculations indicate that a decrease in pH generally decreases the association of metals with particles and increases the proportion of biologically available free metals (Sadiq, 1992; Salomons and Forstner, 1984; The Royal Society, 2005).

6.2.1.5 Acute & Chronic Impacts

Acute impacts consider the response of marine organisms to short term exposure (immediate up to a few days) to high CO_2 conditions. The most obvious acute effects are respiratory distress, narcosis and mortality, where these appear to be due to hypercapnia rather than other modulated changes in seawater as a result of decreased pH (see review of Portner et al., 2004; IPCC, 2005). Critical thresholds for impacts such as acute mortality have been investigated through short duration experiments both in the laboratory (e.g. Ishimatsu et al., 2004; Kurihara et al., 2004; Kikkawa et al., 2006; Spicer et al., 2007; Pane & Barry, 2007) and in-situ (e.g. Barry et al., 2004; Carman et al., 2004; Thistle et al., 2007; see Box 3.6, Chapter 3), and evaluated using simulation models (e.g. Caulfield et al., 1997, 2004; Chen et al., 2004; Sato et al., 2004). However, the current knowledge base is limited and significant further work remains to be done in order to gain a comprehensive understanding of the sensitivities of a wide range of marine organisms to high CO_2 conditions.

For one of the most sensitive species known to date, the open-ocean squid *Illex illecebrosus*, lethal effects will most likely occur at a CO_2 partial pressure (pCO_2) of 6,700 µatm, when blood pH decreases by ~0.25 units and oxygenation decreases by ~50% (Pörtner and Reipschläger, 1996; Pörtner et al., 2004). Squid of lower activity appear to be less sensitive, with acute mortality of the coastal squid *Loligo pealei* occurring at a similar drop in blood oxygenation but higher pCO_2 of ~26,500 µatm (Redfield and Goodkind, 1929; Pörtner et al., 2004). Shallow water fish show a generally higher tolerance, with median lethal concentrations (LC_{50}) ranging from ~50,000 to ~70,000 µatm for exposure times of 8 hours to 5 days (see review of Ishimatsu et al., 2005). For a given species, developmental stages appear to be more sensitive than adults, although tolerance of early stages also varies widely between species with measured lethal levels for fish eggs and juveniles ranging from 13,000 to 94,000 µatm (24 hour LC_{50}; Ishimatsu et al., 2005). It therefore seems that acute lethal effects can be expected at a ΔpH of around 1 for the most sensitive squid, around 1.5 for the most sensitive fish eggs, and around 2 for the most sensitive adult fish. Similarly, 100% mortality of the intertidal purple-tipped sea urchin *Psammechinus miliaris* was observed after 7 days exposure to CO_2 acidified seawater with ΔpH of ~1.8, with significant mortality after 8 days exposure to a ΔpH of ~1.3 (Miles et al., 2007), while exposure of the velvet swimming crab *Necora puber* to CO_2 acidified seawater with a ΔpH of ~1.9 resulted in 100% mortality after 5 days (Spicer et al., 2007).

The abruptness with which an animal enters a region of severely depressed pH is also likely to influence acute mortality rates. For example, step-wise exposure of Japanese sillago (*Sillago japonica*) to highly elevated pCO_2 of 70,000-90,000 µatm (corresponding to a ΔpH of 1.60 to 1.64) over a period of 4.5-6.0 hours resulted in 40-67% mortality after 18 hours total exposure time, whereas one step exposure resulted in 100% mortality after only 15 minutes (Kikkawa et al., 2006). Similarly, the European eel (*Anguilla anguilla*) displayed exceptional tolerance to stepwise exposure (over a period of ~3 hours) to a final pCO_2 of 104,000 µatm (McKenzie et al., 2002).

These data suggest that in the case of leakage at slow to moderate rates, where the volume of seawater that will experience a decrease in pH on the order of 1 to 2 units (or greater) is low (see Section 6.1), acute mortality is likely be confined to the immediate vicinity of the leakage site. However, sub-acute mortality, with death occurring on an exposure timescale of weeks to months, seems likely to occur at significantly lower values of ΔpH, particularly for organisms unable to escape such as sessile and slow moving organisms and sediment infauna, and vulnerable groups such as calcifying organisms. For example, exposure of sediment infauna to moderately elevated CO_2 for one month (ΔpH ~ 0.3-0.6) resulted in mortalities within some groups of 25-80% (Barry et al., 2004; Thistle et al., 2006; see also Box 3.6, Chapter 3).

Chronic impacts that limit long term performance and survival under moderately elevated CO_2 are even less well understood than acute impacts, primarily due to the difficulties associated with assessing these effects under experimental conditions. Current knowledge suggests that chronic impacts on marine fauna will likely set in during long-term exposure to moderate pH changes of ~0.1-0.3 units (Pörtner et al. 2005; IPCC, 2005). Expected effects include a reduction in the productivity of calcifying organisms leading to higher ratios of non-calcifiers over calcifiers (Pörtner et al., 2005). In addition, reduced growth rates, reproduction rates, and lifespans may lead to a reduction in population densities among invertebrates, and possibly even species deletion (IPCC, 2005). Consequently food webs may be significantly altered, leading to reduced food availability for high trophic levels, and potentially diminishing resources for local fisheries (IPCC, 2005).

6.2.2 Understanding the Impact of CO_2 Leakage on Marine Ecosystems

An ecosystem is a complex unit that comprises the biological community functioning in a given area together with (and interacting with) the abiotic (chemical and physical) factors of the environment, where a change to the chemical environment through the addition of CO_2 can exert a significant impact on the health, structure and diversity of the biological community.

The biological community will include a number of different species from different trophic levels, where each species performs a particular function(s), and the success of each may depend on complex combinations of multiple factors (e.g. the presence or absence of other species, temperature, light levels, the flux of organic matter to the seafloor, the concentration of O_2, nutrients, CO_2, trace elements, H_2S, etc.). Each species will comprise a number of individuals, where the fitness and performance of each individual relies on correct functioning of tissues and organs (e.g. brain, lungs, heart, reproductive organs), which in turn rely on cellular processes, which in turn rely on molecular processes.

While the direct chemical effects of elevated CO_2 on marine organisms are exerted at the molecular level, they can be propagated across all levels of this complex biological system, from molecules to cells, from cells to tissues and organs, to individual organisms, species and communities (e.g. Pörtner et al., 2004; IPCC, 2005; see Figures 6.10 & 6.11). Furthermore, long-term effects of exposure to elevated CO_2 may only become evident over intervals greater than the duration of the reproduction cycle or the life span of an individual (IPCC 2005). Thus although the death of an individual organism might only occur at significantly elevated CO_2 levels, a combination of sub-lethal effects (e.g. decreased growth rates, poor larval development) may well lead to changes in community structure and ecological functions at considerably lower CO_2 levels (Figure 6.11; Pörtner et al., 2004; IPCC, 2005 and references therein). This supposition follows the concept of a hierarchy of tolerance limits (Pörtner, 2002; Pörtner et al., 2004), where although there may be significant tolerance to high CO_2 conditions at the lowest levels of system complexity (e.g. specific molecular and cellular processes), the combined effect on numerous functions (including the ‘knock-on’ effect of compensatory mechanisms) is likely to lead to a narrower tolerance at higher levels of system complexity (e.g. species and community levels).

Figure 6.11: Possible hierarchy of functional limits at increasing CO_2 levels (after Pörtner et al., 2004). Categorisation of CO_2 dependent effects on ocean biota based on the concept of a molecular to systemic hierarchy of tolerance limits. The widest tolerance windows are at the lowest hierarchical or functional levels. As system complexity increases, the combined effect of CO_2 on numerous different functions leads to narrow tolerance windows at high hierarchical levels. Thus while individual mortality might only be observed at significantly elevated CO_2 levels, changes in community structure and ecological functions may well occur at considerably lower CO_2 concentrations. Pejus thresholds (long term tolerance) mark the CO_2 concentration where performance limitations are first observed. Critical thresholds (short term tolerance) mark the onset of metabolic depression. Both pejus and critical thresholds are likely to vary between species and phyla.

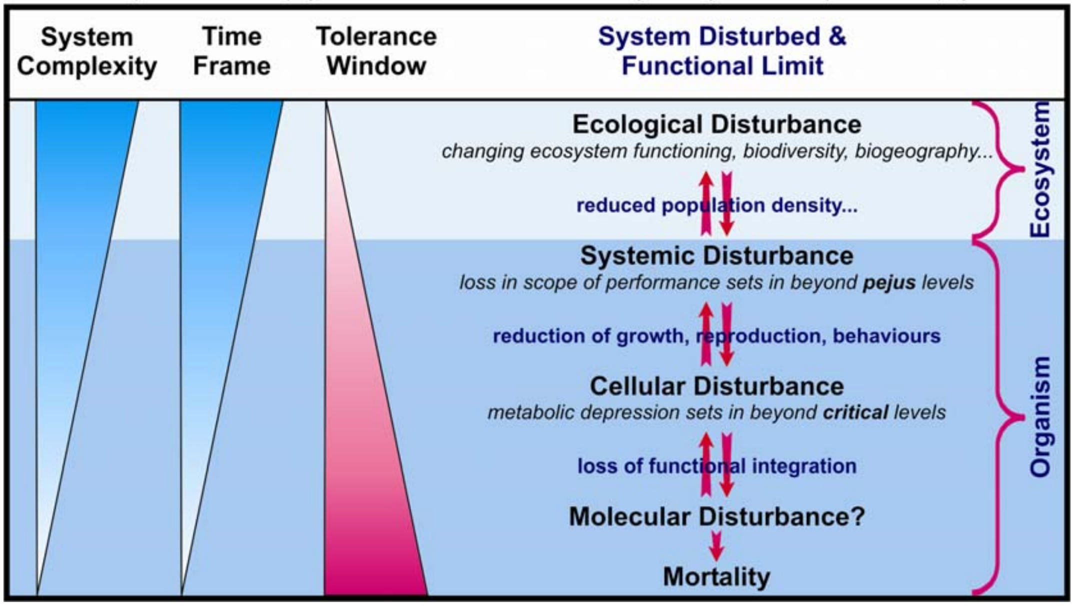

The key factors that will determine the impact of CO_2 release on ocean biota are the extent of changes to seawater chemistry and the length of time an organism (or community) is exposed to high CO_2 conditions, as together these parameters will determine the physiological response of a given individual/species and any consequent impacts on community structure and function (e.g. Auerbach et al., 1997; Caulfield et al., 1997). Thus sessile and slow moving benthic organisms that are either unable or have a limited ability to escape from an area of high CO_2 are likely to be more severely impacted than highly mobile benthic animals and free swimming organisms. In addition to an organisms ability to detect and avoid or escape areas of elevated CO_2, the biological impacts of leakage will depend to a large degree on the characteristics of the leakage event (see Section 6.1 above), that is the rate and nature of leakage (e.g. hydrate outcrop versus rising droplet plume), the extent of plume dilution (which will vary according to the hydrodynamic regime and distance from the leakage site), and the duration of leakage (which in turn depends on the time taken to detect a leak and whether remedial action is possible). As such, the leakage of CO_2 to the sea floor could result in a number of ecological effects, ranging from minor modification of community structure, to wholesale alteration of communities and ecosystem function, and may even lead to the formation of dead-zones (e.g. Shirayama, 1995; Tamburri et al., 2000; IPCC, 2005; Vetter & Smith, 2005).

6.2.2.1 Alteration of Community Structure

With regards to alteration of community structure, the questions that need to be addressed are how and to what extent will the community be changed, and over what area will such changes be experienced. The response timeline also needs to be examined, with an evaluation of immediate impacts on inception of leakage, the evolution of the response during leakage and the possible development of a new steady state community structure, and system recovery (or lack thereof) following cessation of leakage.

In addition, it seems reasonable to suggest that when assessing risks of leakage, consideration should be given to the inherent 'value' of the biological community that currently inhabits a potential leakage point (e.g. in proximity to potential flow paths such as wellbores, faults, fractures, gas chimneys etc.), and how that value may decrease as a consequence of any CO_2-induced changes. Here 'value' is used as a term encompassing the ecosystem services provided by the community, the biological diversity, abundance, fragility and/or rarity of the community and/or any single species within that community, in addition to evaluation of both the direct and indirect commercial value (e.g. commercial shell fish beds or nursery grounds for commercially important fish stocks). Potential impacts of CO_2 leakage on deep water coral reefs, an example high value ecosystem, are discussed further in Chapter 7.

As yet, community level responses are not well understood, particularly in deep-sea ecosystems, and further investigation is clearly warranted. While the biological impact in terms of the number of individuals or species affected will at least partly correspond to the abundance and biodiversity of species present at the site, community changes will also depend on a complex interplay with other factors such as the physical nature and duration of the leakage event, the mobility of organisms within the leakage site, and the relative tolerance (short and long term) of organisms to elevated CO_2 and other concomitant changes in seawater chemistry.

As the numbers of organisms living on the sea floor per unit area decreases exponentially with depth (probably associated with the diminishing flux of food with depth), a simple analysis would suggest that the impact of CO_2 release on ocean biota will also decrease with depth. However, deep sea organisms may be more vulnerable to high CO_2 conditions than their shallow water counterparts as they have adapted to the comparatively stable chemical regime of the deep sea (Seibel & Walsh, 2003; Ishimatsu et al., 2005). Furthermore, deep sea communities are characterized by low biological activities, long life spans, and high biodiversity, where each species has a low number of individuals (Shirayama, 1998). Thus these communities are particularly vulnerable to a decrease in population, where re-colonisation and restoration of ecological function will require a long recovery period, if it occurs at all (Childress, 1995; Haedrich, 1997; Shirayama, 1998; Snelgrove and Smith, 2002; Ishimatsu et al., 2005).

While the tolerance of specific organisms to both short and long term exposure to elevated CO_2 are at present poorly known, it is considered likely that tolerance thresholds will vary between species and phyla in response to the differential impact of changes in seawater chemistry on organism physiology (IPCC, 2005). Indeed, while exposure to high CO_2 levels and severely depressed pH can result in immediate narcosis and death, many species can tolerate more limited shifts, at least in the short term (IPCC, 2005). Conversely, some species that are able to tolerate transient CO_2 fluctuations may not be able to settle and thrive in areas where CO_2 remains permanently elevated due to a drop in metabolic rate (Pörtner et al., 2004; IPCC, 2005). Thus changes in the relative proportions of species are also likely to occur within areas influenced by leakage, where this may include the deletion of species with low tolerance, and the rise to dominance of species with high tolerance, or even the addition of new opportunistic tolerant species (e.g. Vetter & Smith, 2005).

Ecosystem impacts will also vary with distance from the leakage site. The concentration of CO_2 and depression of pH will be at maximum values in the area immediately surrounding the leakage point. As distance from the leakage point increases, the CO_2 plume will become more dilute and have a correspondingly lower CO_2 concentration and smaller decrease in pH, where the extent of dilution increases as a function of current speed. Thus acute impacts of CO_2 exposure will typically be confined to the immediate proximity of the leakage point (see also areas with restricted circulation as discussed in Section 6.2.2.3), while chronic impacts will extend over the larger area influenced by the dissolution plume (Kita & Ohsumi, 2004), and the chemical gradient in CO_2 will also describe a transition in the abundance, diversity and structure of the biological community. The chronic effects on organisms within the plume footprint will evolve over time, becoming more severe the longer the duration of the leakage event.

At high leakage rates, a significant area of surficial sediments may become saturated in CO_2, and/or bathed by dense CO_2 rich dissolution plumes, resulting in the death of sessile and slow moving infauna and epifauna initially present within the affected area, and preventing re-colonisation until leakage slows or stops. The formation of a CO_2 hydrate cap at the seafloor, trapping a lake of buoyant liquid CO_2 beneath, could also exert a similar effect, both by changing the seafloor substrate (from sediment to hydrate and underlying liquid CO_2), and through the formation of density stratified CO_2 rich bottom waters (see for example the 200 m^2 hydrate zone at Yonaguni Knoll in the Okinawa Trough, where benthic fauna were rarely observed, Inagaki et al., 2006; Appendix 3.A).

Under other circumstances, the impact of leakage on the benthos may be considerably less. For example, low flow rates and/or multiple CO_2 flow paths through the overburden and sediment column may result in a patchy and temporally variable delivery of CO_2 to the seafloor, leading to CO_2 release as intermittent and itinerant droplet streams, and the potential formation of small and transient seafloor hydrate deposits (see Section 6.1). Under these conditions, the benthos would be exposed to fluctuating chemical conditions, and would likely exhibit a degree of tolerance.

Hashimoto et al. (1995) report CO_2 droplet streams emerging from dense mussel beds at Minami-Ensei Knoll in the Okinawa Trough (see Appendix 3.A). The presence of CO_2 venting within these live mussel beds suggests one or more of the following: (i) the mussels are tolerant of high CO_2/depressed pH; (ii) venting is itinerant – thus individual mussels are not exposed to perturbed chemical conditions for prolonged periods; (iii) venting in this specific area (i.e. within the mussel bed) was a recent phenomenon at the time of observation, such that the health of the mussel population had not yet been noticeably impacted; (iv) CO_2 is flowing along confined pathways (e.g. through hydrate lined pipes) – thus the mussels are protected from (extremely) high porewater CO_2. Similarly, Shitashima & Maeda (2005) observed live clam beds in close proximity to seafloor CO_2 hydrate outcrops, where Galatheid crabs were also seen on the clam bed and sediment surface close to the hydrate deposit (See Chapter 5, Figure 5.6). While the presence of mobile crabs near the hydrate is perhaps not particularly notable, again the occurrence of the clam beds suggests that these animals are either tolerant of high CO_2 conditions, and/or that the chemistry of bottom seawater and surface sediment porewaters are not significantly perturbed at a short distance from the hydrate deposit (some 10s of cm or less). The latter hypothesis may indeed be the correct interpretation, where in-situ pH measurements made above hydrate deposits and pools of liquid CO_2 on the seafloor during small scale release experiments typically do not register a decrease in pH until the sensor is almost brought into contact with the CO_2 surface, or held near the seafloor on the downstream side of the CO_2 deposit (personal observation). Given that the clams inhabit an area lying to one side of the hydrate outcrop (see Figure 5.6, Chapter 5), they may well be located on the upstream side of the deposit. A physical barrier (e.g. a rock) may also be separating the substrate in which the clams are located from the hydrate bearing sediments.

The dominant effect on the benthos at CO_2 vent sites appears to be the exclusion of less tolerant species, and the increase in abundance of opportunistic species with high tolerance (see Appendix 3.A). A number of studies report that the majority of sedimentary infauna and epifauna common to the general geographical area are excluded from the immediate location of CO_2 release, and that polychaetes and nematodes become abundant or dominant (see Appendix 3.A). At other sites, while dense populations of infauna and epifauna do occur in close proximity to locations of CO_2 release, diversity within the immediate vicinity of the vents remains reduced in comparison to the local ambient population (see Appendix 3.A). However, it is noted that these changes are likely related to factors such as elevated sedimentary temperatures, high particulate loadings/low light levels, and high concentrations of other toxic species (e.g. H_2S or As), either in addition to, or as opposed to, elevated CO_2 (see Appendix 3.A; compound effects may also be significant but generally have not been explored – for example the combined impact of high temperatures and elevated CO_2 (Portner et al., 2005)). Similarly, the increase in species abundance and diversity reported in the peripheral region of some vent fields is most likely related to factors other than elevated CO_2 (e.g. an elevated food source arising from chemosynthetic production at hydrothermal vents; see Appendix 3.A). Nevertheless, that significant alteration to the benthic community structure is normally constrained to the vent field and its immediate periphery, with a return to 'typical' community structure beyond this, strongly suggests that the impact of CO_2 leakage to the ocean at slow to moderate flow rates will be similarly restricted. The notable exception to this is when venting occurs within an area with restricted or semi-restricted circulation (see Section 6.2.2.3).

6.2.2.2 Alteration of Ecosystem Function

The impact that changes in community structure would exert on biological productivity and ecosystem services is unclear. However, some potential consequences can be highlighted through examination of an example bottom boundary level ecosystem model, as shown in Figure 6.12.

Figure 6.12: An example bottom boundary layer (BBL) ecosystem model based on carbon flux, and including both the sedimentary and water column pools. After the BBL carbon budget of Smith (1992) and the mesopelagic ecosystem model of Kita & Ohsumi (2005). This simple model does not include the photic zone. Purple arrows show feeding, blue arrows show egestion and/or mortality, green arrows denote the microbial loop. Respiration is not shown. For further discussion see text.

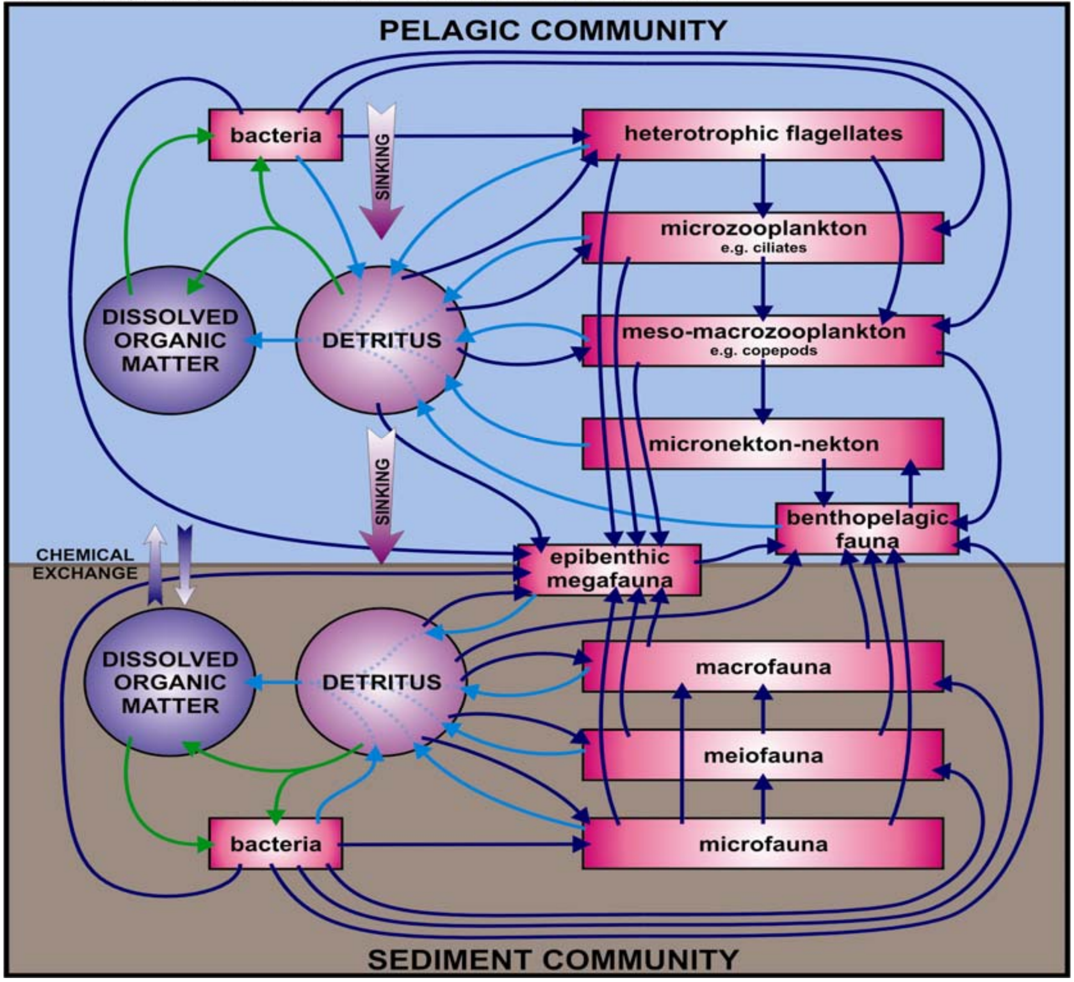

Benthic communities play a vital role in the processing of organic detritus, and thusare an important component in the recycling of carbon and nutrients (see Figure 6.12; Gage & Tyler, 1991; Smith 1992). Large changes to, or indeed the exclusion of, entire benthic groups such as the infauna or epifauna (as discussed above), in addition to the potential exclusion of benthopelagic scavengers (due to avoidance of elevated CO_2 levels), would exert a profound effect on the structure of the food web and the cycling of material within these ecosystems (e.g. Tamburri et al., 2000; Vetter & Smith, 2005). Indeed, some evaluations of ocean storage scenarios (e.g. CO_2 lakes) suggest that the widespread destruction of benthic environments could lead to a significant reduction in rates of nutrient cycling, and thus a decline in primary production and consequent overall decrease in the biomass of higher organisms (e.g. Shirayama, 1995). However, in the leakage case impacts seem likely to remain local in their influence, unless catastrophic leakage occurs at multiple storage sites.

In addition to effects on benthic fauna, elevated CO_2 levels due to leakage could also influence all other components of this ecosystem model. For example, Kita & Ohsumi (2004) emphasize the importance of the microbial loop in nutrient and carbon cycling (where dissolved inorganic matter is directly used as a carbon and energy source by heterotrophic prokaryotes, which are then grazed by flagellates, ciliates, copepods and filter feeders), and highlight the need for further studies investigating the impacts of elevated CO_2 on the performance of the microbial loop within these fundamentally important biogeochemical cycles (e.g. in response to changes in the speciation of nutrients and the carbonate system – see also the impact on nitrification – Section 6.2.1.4). Inagaki et al., (2006) recently reported the first investigation of the microbial communities inhabiting liquid CO_2 and hydrate bearing sediments, finding that this extreme environment was populated by a community of microorganisms assimilating CO_2 and CH_4. An important question remains as to how these communities and their functioning respond to changes in CO_2 concentration and in-situ pH (Inagaki et al., 2006). Elevated CO_2 can also impact the pelagic community. For example, in their study of the Loihi vent site, Vetter & Smith (2005) conclude that there is an enhanced fallout of dead or moribund pelagic animals that have become intoxicated by the CO_2 plumes. At Loihi, this elevated supply of organic detritus supports high numbers of scavengers (Vetter & Smith, 2005), although conceivably, such an impact could lead to the formation of a dead zone – as discussed in the following section.

6.2.2.3 Creation of a Mortality Sink or Dead Zone

One of the specific issues raised with respect to ocean storage of CO_2 was the possible creation of a mortality sink or 'dead zone' (e.g. Ohsumi, 1995; Tamburri et al., 2000).

This concern arises from a general acknowledgement that immobile or slow moving animals in the immediate area of a seafloor CO_2 deposit (e.g. a CO_2 lake), or within the footprint of a dense CO_2 rich seawater plume propagating along the seafloor, will be unable to escape and will be killed. As most deep-sea animals feed (at least partially) on carrion or detritus, mobile scavengers may then be attracted to the region of elevated CO_2 by the odour plumes released from the recently deceased animals (e.g. Tamburri & Barry, 1999). If these scavengers were then also overcome by high CO_2, their bodies would serve as bait to attract yet more scavengers, and so on. Consequently, while CO_2 release might initially affect only the immediate locale, it is feasible that the eventual disturbance would be considerably greater (Ohsumi, 1995; Tamburri et al., 2000).

For a dead zone to form, mobile animals must remain within an area of elevated CO_2 long enough to be rendered unconscious and eventually killed. Whether or not this occurs will be dependent on the following inter-related points (e.g. Tamburri et al., 2000; Vetter & Smith, 2005):

(i) an animals ability to sense and avoid a CO_2 rich plume
(ii) whether or not an animal can escape a CO_2 plume if entered
(iii) whether the animal remains within the CO_2 rich plume once unconscious
(iv) the ability of the animal to recover from exposure to elevated CO_2

These points are discussed below with reference to in-situ experiments, observations at natural vent sites, and the likely nature of CO_2 release in a leakage event.

In a small scale CO_2 release experiment, Tamburri & Brewer (2000) attracted Hagfish to a release location by pumping fish odour solution into seawater. Once the animals had reached the release point, pumping was switched to a CO_2 saturated fish odour solution (pH ~5.3). Following the switch, all individuals displayed an avoidance response and moved away from the immediate release location (Tamburri & Brewer, 2000). However, in a companion experiment several species of fish (including Hagfish, Sablefish and Dover Sole) and invertebrates (sea urchins and gastropods) did not avoid a release location when fish odour solution was pumped through porous CO_2 hydrate material (pH ~5.6; Tamburri et al., 2000). Indeed, one Hagfish entered the vessel containing the hydrate material, was rapidly rendered unconscious (within 5 seconds), fell to the seafloor, recovered, and repeated the experience twice more (Tamburri et al, 2000).

In a similar experimental approach Vetter & Smith (2005) used the naturally CO_2 rich vent plumes at Loihi seamount (up to 418 mmolCO_2/kg, Sedwick et al., 1992) to explore the effects of elevated CO_2 on the feeding behaviour of deep sea scavengers. Odour plumes were created by placing bait (dead fish) within the CO_2 rich vents (pH ~6) and at control locations removed from the venting fluids. At control sites the bait was consumed within 24 hours. Conversely, while bait placed within the CO_2 rich vents attracted the interest of pre-adapted vent shrimp, it appeared generally untouched after ~6-8 days, indicating avoidance[11] by other local scavengers (Vetter & Smith, 2005). Direct observations of avoidance[†] behaviour similar to that reported by Tamburri & Brewer (2000) were also made, where an eel approached a bait parcel, then at a distance of ~1m 'it abruptly reversed its sinusoidal swimming, shaking its head violently as it moved rapidly away from the bait and out of sight' (Vetter & Smith, 2005). In addition, amphipods trapped and held within the CO_2 rich vents exhibited an avoidance[†] response, swimming at increased speeds within 30 seconds of immersion (Vetter & Smith, 2005). Active swimming continued for a period of a few minutes, with the amphipods entering a state of torpor after 10-25 minutes of exposure, suggesting these animals could avoid/swim out of a CO_2 plume (Vetter & Smith, 2005).

The different responses observed in these experiments most likely relate to the strength of the dissolved CO_2 signal (Tamburri & Brewer, 2000; Vetter & Smith, 2005). In the release of a CO_2 saturated solution and at the Loihi vents, the CO_2 rich solutions were well mixed. However, in the hydrate experiment, while pH at the vessel opening was initially 5.6, the odour solution may not have been thoroughly mixed with the CO_2 rich seawater, or the hydrate may have stabilized over time (resulting in a slower dissolution of CO_2), thus pH in the odour plume may have approached near ambient values (Tamburri & Brewer, 2000).

These results suggest that when an animal enters a well mixed plume rich in CO_2 with a depressed pH it can (a) can detect the plume and (b) remain conscious for long enough to swim away from the plume. However, attracted by food odour may enter regions of high CO_2 and be quickly rendered unconscious.

The abruptness of an animal's transition from ambient seawater to the CO_2 plume on entry, and from the plume to seawater on exit, may be a critical factor in determining the physiological response (Kikkawa et al., 2006). The mortality of animals exposed to a gradient in CO_2 is likely to be significantly lower than that of animals exposed to an abrupt transition (either a sharp increase when entering high CO_2 conditions, or a sharp decrease on return to ambient conditions; see Kikkawa et al., 2006). Thus animals may be able to tolerate transit into or out of the plume along gradients downstream from the release point, but unable to tolerate the more abrupt changes in CO_2 that would be experienced upstream from the release point (see illustrative distributions of seawater pH in Figures 6.7 and 6.9).

---

[11] Although the avoidance cue at this site may have been other (non-CO_2 related) differences between the vent fluids and ambient seawater, given the generally low concentrations of other chemical stressors in the vent fluids and the moderately increased temperatures (0.3-3.0°C above ambient), it seems most likely to have been the elevated CO_2 (Vetter & Smith, 2005).

If rendered unconscious, an animal will eventually die if it remains within a high CO_2 plume. However, if it exits the plume it may recover (to either re-enter the plume or escape). For example, in the hydrate experiment when the Hagfish lost consciousness and sank to the seafloor it was fortuitously removed from the high pCO_2 seawater and recovered consciousness after ~20 seconds (Tamburri et al., 2000). Similarly, amphipods exposed to CO_2 rich vent fluids for 60 minutes recovered consciousness approximately 30 minutes after being removed from the vents (Vetter & Smith, 2005).

In the potential leakage case, the question of whether or not an animal that is overcome by high CO_2 remains within the CO_2 rich seawater plume when rendered unconscious will depend on both the rate of CO_2 release and the local hydrographic conditions.

In an open system, that is leakage in a location with unrestricted hydrodynamics, the rate of leakage must exceed a certain value (depending on local conditions) for a dense sinking plume of CO_2 rich seawater to form. Thus for slow to moderate leakage rates (which may continue unmitigated over some considerable length of time) and typical abyssal current speeds, dilution factors will tend to be large, and the area of seafloor over which a large decrease in ΔpH is experienced is likely to be fairly small (see for example Section 6.1.5 and Figure 6.9). Furthermore, the footprint of the CO_2 rich plume may not be fixed, but rotate about the release point due to tidally dominated currents (Chapter 3 Box 3.6; Barry et al., 2005). Under these conditions if an animal fails to detect and escape the plume and is instead rendered unconscious at the seafloor within the plume, within a period of 30 minutes to 1 hour it would lie outside of the plume. Targeted experiments indicate that at least one species of amphipod is capable of recovering from exposure to seawater with a ΔpH of ~1 for this duration (Vetter & Smith, 2005). Similarly, small scale release experiments with caged animals have demonstrated that Benthoctopus and eelpout can survive a month long exposure to tidally oscillating CO_2 plumes (Barry & Drazen, 2007). Although all Grenadier (rat-tails) died in this experiment, this may have been due to predation or stress from being caged, rather than CO_2 stress (Barry & Drazen, 2007). It therefore seems unlikely that a large mortality sink (defined here as an area where mortality rates are such that numerous nekton carcasses are found at the seafloor) will form in an open system. This conclusion is broadly supported by observations at natural vent sites with unrestricted hydrodynamics, where reported biological impacts tend to be restricted to the immediate vicinity of the vents and no direct evidence of enhanced carrion fall-out has been reported (see Appendix 3.A).

Nevertheless, there are some observational indications of an increased fall-out flux of organic detritus in the vicinity of CO_2 vent sites. For example, Vetter & Smith (2005) highlight the ‘extraordinarily high’ numbers of scavengers present at Loihi, noting that there must be a correspondingly high flux of food into this system to support such a large population. While this abundant food source could ultimately be supported by high rates of chemosynthetic production (as yet undiscovered), and/or be related to enhanced productivity over the seamount (yielding a high carrion flux that is independent of CO_2 venting), the authors conclude that the most likely source is the enhanced fallout of dead or moribund animals that have become intoxicated by the CO_2 vent plumes (Vetter & Smith, 2005). Thus while recognisable dead-zones may not form in open systems, alteration of ecosystem structure and function due to an enhanced delivery of organic detritus to the seafloor may still occur.

In a restricted system, that is leakage into a stagnant water column (no flow) or a confined volume of seawater, such as a topographic depression, the situation is somewhat different. Under these conditions, there is limited exchange of seawater and dilution factors are low, thus even a slow leak could result in a significant build up of dense CO_2 laden bottom waters. Furthermore, the CO_2 plume can be viewed as static, thus if an animal is rendered unconscious, it will remain within the plume at the seafloor and will die. A small number of natural CO_2 vent sites fall in the restricted or semi-restricted system category, the most notable of which are the Vailulu’u Seamount (Samoan hotspot) and the Kraternaya Bight (Yankich Island, Central Kurile Arc) vent sites respectively.

At Vailulu’u Seamount, a biological dead-zone has formed within the summit crater (Staudigel et al., 2006). At depths below 750 m in the crater bottom, confined waters form a moat that encircles Nafanua, a 300 m tall volcanic cone located on the crater floor (Staudigel et al., 2006).

Hydrothermal smoker vents located within the moat emit fluids with extremely low pH (2.7) in addition to the release of immiscible fluid droplets inferred to be liquid CO_2 (North Moat Hydrothermal Complex - Staudigel et al., 2006). As a result, the confined waters in the moat are highly acidic and turbid, where seawater sampled near the vents had a significantly depressed pH of 5.1 (Staudigel et al., 2006). This region was dubbed the 'Moat of Death' by the authors, where 'abundant carcasses of midwater fish, squid, and crustaceans littered the seafloor' and the only living animals observed were polychaetes (see description of Habitat Type III in Staudigel et al., 2006). At depths above 750 m, some seawater flushing occurs via breaches in the crater walls; creating locations alternately bathed by clean seawater and the toxic waters from the 'Moat of Death', where the authors hypothesize that these regions may play an important role in trapping life within the Vailulu'u crater (see description of Habitat Type IV in Staudigel et al., 2006). While the specific cause of death is at present unknown, the authors identify most probable cause as a combination of low pH and asphyxiation from the combined effect of reduced dissolved oxygen and Fe oxide particulates coating gills, citing similar cases reported for nekton mortality in submarine volcanic settings (Staudigel et al., 2006 and references therein).

At Kraternaya Bight the situation is somewhat different, where the impact of CO_2 rich gasohydrothermal venting at this site provides an interesting comparison to the deep water enclosed system of Vailulu'u. Firstly, Kraternaya Bight is a shallow system, thus saturation concentrations for CO_2 are lower than at high pressure, and exchange of CO_2 with the atmosphere (loss to the atmosphere) will occur. Secondly, at this semi-restricted site, limited exchange of seawater occurs through a narrow shallow strait that links the Bight to the open ocean. The exchange of water is tidal (irregular semi-diurnal tides), where on average ~700,000 m^3 of seawater (2.5 to 3.5°C) flows into the bight at high tide with the same volume flowing out at low tide (warmed to 9 to 12°C), in comparison to an estimated influx of hydrothermal fluids of ~20,000 m^3/day (Zhirmunsky & Tarasov, 1990). Here, although gasohydrothermal activity exerts a strong influence on the biological community, the system supports a diverse and rich macrofauna (Tarasov et al., 1990; Gamo and Glasby, 2003). In general, the macrofaunal community exhibits significant differences to that found outside the bight, where several common bight species have changed in morphology and adapted to the extreme conditions (Zhirmunsky & Tarasov, 1990; see Appendix 3.A for further details). Nevertheless, periodic high mortality events, apparently in response to increased hydrothermal activity, have been reported (e.g. Kamenev et al., 2004; see Appendix 3.A for further details). Thus it would appear that population health is strongly dependent on the balance between the input of toxic compounds and the flushing rate of system, where the 'normal' state is a healthy population (adapted to given conditions). Thus either increased hydrothermal activity at a constant flushing rate, or a decreased rate of flushing at constant hydrothermal input, leads to decreased health.

Although there are other factors that exert a profound influence on the local biota at the hydrothermal vents sites discussed above (e.g. temperature, H_2S concentrations, particle loadings), it seems reasonable to conclude that for a given rate of leakage (and assuming all other factors are equal), the impact of CO_2 leakage on local biota will depend on the dilution of the CO_2 signal, which is in turn dependent on local hydrodynamics, where impacts are likely to be greatest in topographically confined areas, and least in areas of unrestricted circulation.

It is noted that of the numerous CO_2 vent sites discussed in this report (see Chapter 3 and Appendix 3.A), dead-zone formation has only been reported at the Vailulu'u site. Furthermore, leakage to a seafloor depression could be considered unlikely, as subsurface flow tends to be directed over basement highs. Nevertheless, this possibility should be taken into consideration during site selection and formulation of monitoring programmes (see Section 6.3), where any potential leakage pathways that exit to the seafloor within topographically confined areas should be identified as high priority 'watch points'.

6.2.3 Placing the Biological Impacts of CO_2 Leakage in Context

As noted elsewhere in this report, it is important to consider the potential impacts of CO_2 leakage from subseafloor geological storage sites in context. That is, in comparison to what would happen to marine systems if any stored CO_2 had instead been released directly to the atmosphere (e.g. Shirayama & Thornton, 2005). However, comparison of the two cases (impacts on ocean biota from emissions to the atmosphere versus impacts on ocean biota from leakage) is difficult, given:

(i) comparing the two cases can be thought of as comparing apples and oranges, as opposed to apples and apples. Taking a simplistic viewpoint, atmospheric release will result in long term exposure of the surface ocean to moderately elevated CO_2 and depressed pH, while leakage would likely result in comparatively short term exposure of localized areas at a range of water depths (near surface to deep ocean) to higher levels of CO_2 and more severely depressed pH.

(ii) the current poor level of understanding regarding how marine ecosystems will be affected, including uncertainties regarding the relative sensitivities of surface ocean and deep water ecosystems to elevated CO_2.

(iii) uncertainties in the future uptake of sub-seafloor geological storage, and therefore in the CO_2 emissions abatement achieved and the overall probability (and locations) of leakage.

Nevertheless, if CO_2 is released to the atmosphere it will equilibrate with the surface ocean, while if CO_2 is stored in subseafloor geological reservoirs the likelihood is that the vast majority of that CO_2 will remain isolated from the ocean and atmosphere over at least 1000 years (given proper site selection and monitoring). While the current mass of CO_2 stored in subseafloor geological reservoirs is small in comparison to anthropogenic emissions, the potential storage capacity is large (see Chapter 1). Indeed, utilization of this capacity could make a significant contribution to the global emissions abatement effort over the course of the 21st Century (e.g. IPCC, 2005), thereby helping to minimize the increase in atmospheric and surface ocean CO_2 concentrations that is experienced. Furthermore, should leakage occur, the total area impacted will be comparatively small when considered on a global basis. For example, at CO_2 vent sites, the size of the vent field (which typically describes the area of seafloor influenced by the vents) ranges from a few 100s of m^2 to 10s of km^2 (see Appendix 3.A), where the lower end of this range could be considered analogous to leakage at a single location (e.g. a wellbore), while the upper end could be analogous to numerous leakage points distributed across the entire footprint of a storage reservoir. Even if we consider the upper end of this range, then simultaneous leakage occurring across the footprint of 1000 storage sites of reasonable size (~25 km^2 - 5 km x 5 km) would impact less than 0.01% of the total seafloor, whilst leakage at 1000 discrete sites, each influencing an area some 10,000 m^2 (100 m x 100 m) would impact a total area of 10 km^2, or around 30 billionths of the seafloor area. While it is noted that the fraction of total seafloor area exposed to elevated CO_2 conditions does not directly translate to the fraction of marine biota impacted, it nevertheless seems reasonable to suggest that although local impacts of leakage from subseafloor storage reservoirs to the ocean may be comparatively severe, the global impact is likely to be less severe than that of the alternative; that is simply releasing the CO_2 to the atmosphere and suffering the consequent changes to surface ocean chemistry.

6.3 Monitoring of Leakage

Monitoring of CO_2 in the context of direct ocean sequestration is discussed in Chapter 6 of the IPCC SRCCS (IPCC, 2005). The guidance given states that a monitoring programme should “attempt to quantify the mass and distribution of CO_2 from each point source, and could also record related biological and geochemical parameters” (IPCC, 2005). The report also notes that these same issues may relate to monitoring of potential leakages from sub-sea geologic storage, or for verification that such leakage does not occur (IPCC, 2005).

In the case of subseafloor storage of CO_2 there are multiple motivations for carrying out an effective monitoring programme. These include (adapted from Winthaegen et al., 2005):

- To increase understanding of the behaviour and fate of CO_2 injected into subseafloor geological reservoirs. For a specific project, direct observations of CO_2 behaviour allows model testing and refinement and thus increases confidence in the ability to predict the fate of CO_2 in the long term. Furthermore, all experience and knowledge makes an important contribution to development of general models that can be applied to new potential storage sites.
- To verify storage. This is a vital issue if sub-seafloor storage of CO_2 is to be accepted as a creditable carbon sink under the terms of international agreements (Kyoto Protocol and future agreements).
- To ensure early detection of any leakage. Early detection allows the possibility of remedial action.
- The development and testing of techniques & methodologies relevant to the monitoring of subseafloor storage of CO_2 and any seepage to the water column.
- To safeguard the environment.

These motivations then inform what an effective monitoring programme should deliver. If leakage were to occur, an effective monitoring programme should shed light on how and why leakage occurred, thus allowing existing storage sites to be assessed for the same weakness and informing the decision making process at new potential storage sites. In order to verify storage, monitoring should enable the detection of relatively small leaks, where timely detection of leakage would allow remedial action to be taken and thus limit both the total mass of leaked CO_2 and the severity of any biological impacts.

In general, the magnitude of the leakage 'signal', and therefore the number of techniques (e.g. discrete sampling, in-situ chemical sensors, acoustic detection, etc.) that could be employed to detect the leak, will increase with the size of the leak, while the required spatial resolution of the monitoring survey and cost of detection will decrease. Thus large leaks are more likely to be detected in a timely and cost effective fashion than small leaks.

It may be deemed desirable to define the required leak detection threshold for a given project as a percentage of the total amount of CO_2 to be stored, taking into account the number of potential leakage points (i.e. wellbores) within the footprint of the reservoir. Similarly, monitoring programmes should consider the timeframe within which it is desirable to detect leakage at a given rate, again allowing for the possibility of multiple leakage events over the lifetime of the storage reservoir.

To meet recommended performance criteria (a minimum of 99% of the total injected CO_2 is retained over a period of at least 1000 years), the maximum allowable (i.e. undetected) annual leakage rate would be 0.001% of the final volume to be stored. Given the possibility of multiple small leaks, the leak detection threshold should be set somewhat below the total 'allowable' leakage rate. For example, undetected leakage at 2 to 3 wellbores at a rate of around 200 tCO_2/yr would result in a 50 $MtCO_2$ storage reservoir failing to meet performance standards, suggesting a desirable detection threshold on the order of 100 tCO_2/yr.

To determine timeframes for detection, storage projects could consider a gold performance standard somewhat more stringent than minimum operating requirements, and apply a worst case leakage scenario. For example, a desirable threshold could be set of 99.9% of total injected CO_2 to be retained over a period of 10,000 years. Allowing for the possibility of ~100 leakage events[12] (1 event every 100 years over a 10,000 year period), then for a storage reservoir with a capacity of ~50 $MtCO_2$, leakage at rates on the order of 100s tCO_2/yr would need to be detected and mitigated on a timescale of ~10 years, while leakage at rates on the order of 1000s tCO_2/yr would need to be detected and mitigated on a timescale of ~1 year. The increasing severity of chronic biological impacts over time should also be considered when determining preferable timescales for detection and mitigation.

---

[12] This number is provided for illustrative purposes and is based on the probability of leakage via a wellbore, which is on the order of 0.1 events per item per 1000 years (see Chapter 4). If in a worst case scenario the probability is considered to be 10 times higher, then for a project with10 wellbores located within the footprint of the storage reservoir this would indicate the monitoring programme should allow for 100 leakage events. Detailed analysis would have to consider all potential leakage mechanisms and expected rates of leakage via each mechanism.

In the ocean storage case, the location and amount of CO_2 released (or rate of release) would be known. This would allow the design and implementation of a directed monitoring programme, incorporating placement of chemical and biological sensors along pipelines, at the release site and on moorings within the expected footprint of the CO_2 dissolution plume (IPCC, 2005). In addition, periodic surveys could be carried out to more accurately map the CO_2 plume, utilising autonomous underwater vehicles in the near field, towed (from a research ship) undulating pumping systems at distances of a few km, and discrete sampling approaches on hydrographic section cruises conducted every 2-5 years in the very far field (IPCC, 2005).

Applying a similar approach to the leakage case is somewhat problematic as these techniques typically require either the location of release to be known, or the quantity of added CO_2 to be large, in order to enable detection. Thus while the monitoring programme outlined by the IPCC (2005) is indeed relevant once a leakage point has been identified, the costs (time and money) of establishing and maintaining an array of sensors, or of conducting mapping surveys, at a resolution sufficient to ensure detection of a small leak located at an unknown point within the spatial footprint of the storage site would likely be prohibitive. For example, to detect a CO_2 droplet stream leaking at a rate of 200 tCO_2/yr using chemical techniques (e.g. pH probes, pCO_2 sensors, or discrete sampling and analysis for TCO_2) may require a sampling grid with a spatial resolution better than 100 m. For a storage reservoir with a footprint of 25 km^2 (e.g. 5 km x 5 km) this equates to a minimum of ~2600 sampling stations or sensor locations – were installation of an array of this size would itself have a significant environmental impact.

A more pragmatic approach to leakage detection is therefore necessary, using the identification of potential leakage points (e.g. wellbores, faults) to determine those sites where detailed baseline surveys and continuous monitoring should be carried out (following an approach similar to that described for injection sites in the IPCC report). Tracking the movement of CO_2 in the subsurface and performing mass balance checks (i.e. is the mass of CO_2 contained in the reservoir equal to that injected?) should also provide prior warning of penetration or bypassing of the cap-rock seal and may lead to the identification of unexpected CO_2 migration pathways and additional possible leakage points. Detailed monitoring of identified ‘watch points’ should be combined with periodic surveys across the entire footprint of the storage reservoir.

The principal techniques available to identify and track additional CO_2 in the ocean are chemical detection of the dissolved CO_2 load (e.g. measurements of TCO_2 (pCO_2) or pH), and acoustic detection of CO_2 droplets and bubbles. Of these options, acoustic monitoring may represent the most promising approach for leakage detection. Numerous shallow water gas vent sites have been located using this technique (see Appendix 3.A), and recent experiments have shown clear detection of a small cloud of CO_2 at a depth of 1000 m using shipboard sonar (Brewer et al., 2006). It would seem this method lends itself to long term monitoring of identified ‘watch points’. Furthermore, in regions with a high volume of shipping traffic, this technique could potentially make use of ships of opportunity in order to achieve a high spatial and temporal monitoring resolution across the footprint of the storage reservoir. While the use of narrow highly penetrating single beams would require a ship to pass within reasonably close proximity to a leakage site (for a cone angle of 8-12° and leakage at a depth of 1000 m, the ship would need to pass within 140-210 m of the leakage point), the use of multiple beams would greatly increase the covered area.

Mapping of pH and TCO_2 plumes has been carried out at vent sites that are naturally rich in CO_2, such as Hatoma Knoll (hydrothermal vents with associated liquid CO_2 venting, see Chapter 3, Box 305; Shitashima & Maeda, 2005) and Axial Volcano (hydrothermal vents rich in dissolved CO_2; IPCC, 2005). However, there are a number of limitations to the use of chemical mapping for detecting leakage. Firstly, given the natural background variability in ocean carbon concentrations, this technique would require a detailed (high resolution) survey of TCO_2 distribution over the footprint of the storage reservoir prior to any storage activities to determine the background CO_2 concentration & distribution. Secondly, variability in the upper ocean mixed layer would make it difficult to directly monitor small changes in CO_2 in waters shallower than the annual maximum mixed-layer depth, thus this technique would only be appropriate for monitoring potential leakage to relatively deep waters (seasonal mixing from the surface can extend as deep as 800 m in some places, but is less than 200 m in most regions of the ocean;

IPCC, 2005). Finally, the utility of these techniques is ultimately limited by the current analytical accuracy. For example, analytical techniques for measuring the TCO_2 of discrete samples are (at present) accurate to about ±0.05% (Johnson et al., 1998). For typical seawater TCO_2 (2.0 to 2.4 mmol/kg), this corresponds to 1-1.2 µmol/kg, indicating a detection limit for additional CO_2 of 3-3.6 µmol/kg, or ~130-160 tCO_2/km^3. Thus while discrete sampling could identify and locate a comparatively large leak, a 'small' leak is unlikely to be detected unless the hydrographic survey happens to pass in the immediate vicinity of the leakage site. For illustration, consider the detectable dissolved CO_2 signal from a rising droplet plume under the following assumptions and approximations (i) that (near) complete dissolution occurs over a vertical mixing height of ~150-200 m; (ii) a constant current velocity of ~5 cm/s; (iii) a lateral mixing rate one tenth of the along flow current speed (0.5 cm/s); (iv) that the total dissolved CO_2 load is constant per unit distance of along flow transport (i.e. the plume becomes increasingly dilute with distance from source) and is well mixed both vertically and laterally. Then leakage at a rate of ~200 tCO_2/yr would only be detectable at distances up to ~50-66 m from the source, while leakage at a rate of ~1000 tCO_2/yr would be detectable at distances up to 250-325 m. For detection at a distance of ~1 km from source would require a leakage rate on the order of 3000-4000 tCO_2/yr.

Since the potential impact of CO_2 leakage on ocean ecosystems is a significant concern, it seems reasonable to state that an effective monitoring programme must include biological monitoring in addition to the tracking of any leaked CO_2, rather than this being considered an optional extra. The role of habitat mapping in assessing potential site specific impacts of leakage, and in particular the need to identify any vulnerable/high value ecosystems located within the footprint of the storage reservoir, are discussed elsewhere in this report (see Chapters 3 and 7). A ground-state biological survey should be carried out at identified 'watch points' prior to any injection, with periodic repeat assessments to evaluate any ecosystem changes over time. Plans should also be formulated for a responsive higher intensity monitoring programme in the event of detected leakage. Since the use of acoustics for biological detection is well established, this tool may offer a unique way to detect both leakage of CO_2 and any water column biological responses to that leakage (Brewer et al., 2006).

As noted by Winthaegen et al. (2005), effective monitoring during both the injection and storage phase of a project is important for all of these reasons, and considerable amounts of time and money should be spent on monitoring the reservoir, the overburden, wells, injection facilities, the surface and the atmosphere, and in this case we can also add the water column. To achieve timely identification of leakage at relatively slow leakage rates will require significant investment to optimise existing detection techniques, develop new technologies, and design efficient monitoring methodologies. Field trials and the development and testing of new monitoring techniques and methods will lead to an increased ability to detect leaks in a timely and cost effective manner.

7: Vulnerable Objects & High Risk Scenarios

When discussing potential leakage or seepage, a distinction can be made between the susceptibility of a storage reservoir to leakage, the possibility of a leakage event occurring, and the risks associated with a potential leakage event. Within this context:

Susceptibility: is a function of the probability of potential leakage/seepage occurrence and leakage/seepage related factors. For example, a storage reservoir located in a tectonically active area where entrapment of CO_2 relied on a sealing fault, or a reservoir with numerous decommissioned wellbores could be classified as being highly susceptible to leakage.

Possibility: depends on the susceptibility and on impact factors (both natural and human) such as frequency of earthquakes, well site maintenance (quality of seals), or over-pressuring (among others).

Risk: depends on the possibility and on the presence or absence of vulnerable objects.

Thus the risks of leakage are high when a high possibility of leakage is combined with the presence of a vulnerable object in the leakage path.

Here we consider a leakage scenario where CO_2 migrates out of a storage reservoir via a mid to high permeability flow path, such as an unsealed fault. While this type of leakage could be relatively benign (if for example efficient secondary trapping mechanisms are operating in the sediment column), if a preferential pathway exists that links the leakage point to a vulnerable object, then it would represent a high risk event. A number of 'vulnerable objects' can be imagined. For example, a topographic depression protected from bottom currents, such that leakage of CO_2 would result in high levels of dissolved CO_2 building up in the water column (c.f. the 'moat of death' at Vailulu'u Seamount; Staudigel et al., 2006). However, as flow tends to be directed over basement highs, leakage to a seafloor depression could be considered unlikely. Two examples of high risk scenarios are considered here where the presence of a vulnerable object may in fact indicate the presence of a preferential flow path – these are deep water coral reefs and methane gas hydrate deposits.

7.1 Fragile Ecosystems – Coral Reefs

If leakage of CO_2 occurred in the vicinity of a coral reef, the inhibition of carbonate precipitation and/or dissolution of carbonate could have a devastating impact on the local ecosystem.

The global distribution of shallow water tropical and subtropical coral reefs is shown in Figure 7.1, while the currently known distribution of deepwater coral reefs is shown in Figure 7.2. Comparison of these Figures to those regions where sub-seafloor storage of CO_2 is occurring, or is expected to occur in the near future, shows that coral reefs occur in the vicinity of nearly all of these sites. For example, the extensive shallow water reefs of Indonesia and Australia, and the cold water reefs of the Northeast Atlantic.

Figure 7.1: Global distribution of tropical and subtropical coral reefs (data from www.reefbase.org)

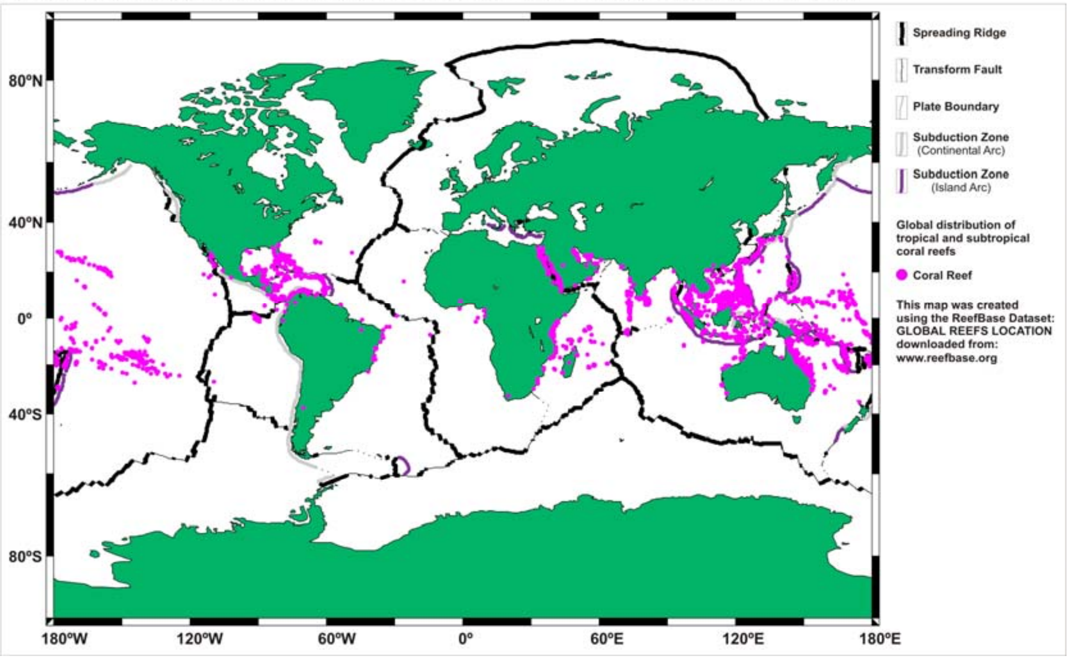

Figure 7.2: Global distribution of cold water coral reefs (after Freiwald et al., 2004)

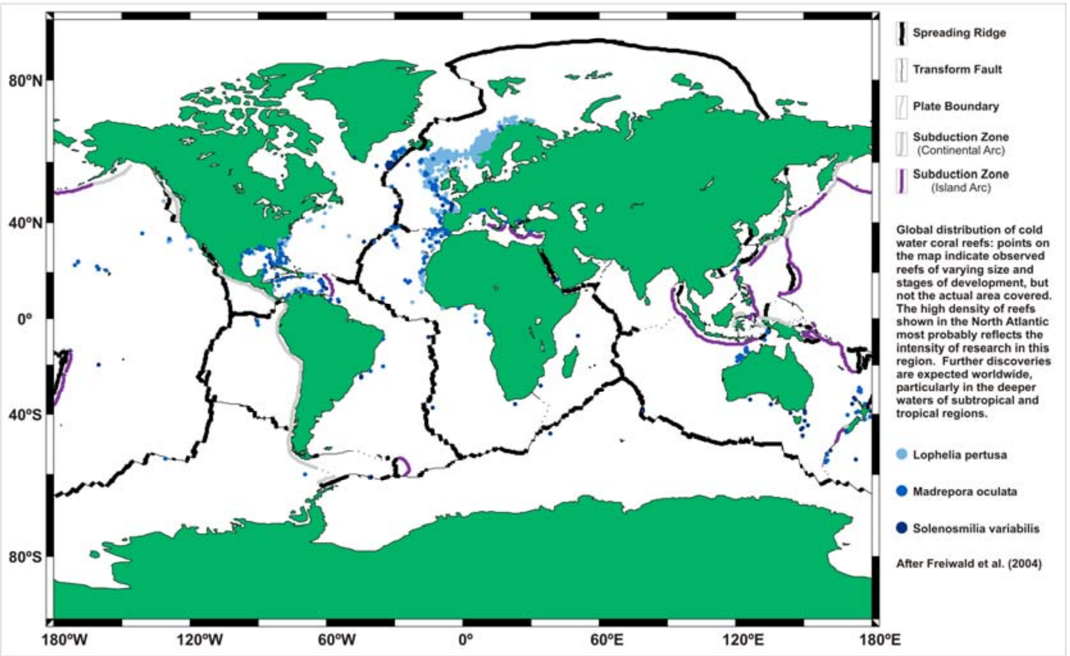

7.1.1 Acknowledging and Addressing Risks to Coral Reefs

This report is not suggesting that CO_2 storage should not be carried out in reservoirs underlying coral reefs. Rather, the potential for leakage into coral ecosystems should be carefully assessed and the risks duly recognised and addressed during site selection and the preparation of Environmental Impact Assessments (EIAs) and risk management strategies. It is noted that risks or damage to coral reefs may have a strong negative impact on public perceptions of (and therefore support for) geological sequestration of CO_2 under the seafloor. This report therefore recommends that all information pertaining to the assessment of risks to coral reefs should be made public and included in published EIAs, even when leakage is considered highly unlikely and risks to coral habitat very low. For example, in the Draft Environmental Impact Assessment for the Gorgon Project (ChevronTexaco Australia Pty Ltd., 2005), the Gorgon Joint Venturers (GJV) follow this model in their assessment of risks to the terrestrial environment, making the statement (Chapter 10: Terrestrial Environment - Risks & Management):

> *While atmospheric emissions and a major leak of CO_2 present low risks to flora and vegetation, these issues are discussed in the following sections in recognition of stakeholder interest.*

However, this approach is not followed in the assessment of risk to the marine environment, where the discussion of risks to coral reefs (Chapter 11: Marine Environment – Risks and Management) does not include any mention of CO_2 leaks, while in the assessment of possible leakage pathways (Chapter 13: Greenhouse Gas Emissions - Risks and Management, Table 13-18) leakage along offshore faults to the north and east of Barrow Island is classed as possible, with an associated risk statement '*Impacts on marine fauna are not anticipated as faults are only identified from seismic and do not extend to the surface*.'

A comparative assessment of the global risk to coral reefs from increasing atmospheric CO_2 concentrations versus the localised risk in the instance of a CO_2 leakage event might also prove interesting and useful. Coral reefs likely represent one of the most vulnerable ecosystems to the future high CO_2-low pH ocean, thus the mitigation of CO_2 emissions through CO_2 storage should confer considerable benefits to the health of coral reefs when compared to a 'no storage' future scenario. Potential impacts of elevated CO_2 levels on tropical coral reefs have been discussed widely in the literature with respect to increasing atmospheric CO_2 concentrations and the future high CO_2-low pH Ocean (e.g. Royal Society, 2005 and references therein). In the discussion below we focus on the deep water reefs common to the Northeast Atlantic Ocean.

7.1.2 Deep Water Coral Reefs – A Fragile Ecosystem

Recent deep-ocean exploration using advanced acoustics and submersibles has revealed unexpectedly widespread and diverse coral ecosystems in deep waters on continental shelves, slopes, seamounts, and ridge systems around the world.

Scleractinian (stony) deep water corals (also referred to as deep sea or cold water corals), have an aragonite skeleton, and may be either solitary or compound (reef forming). The distribution of three reef building cold water corals, *Lophelia pertusa, Madrepora oculata and Solenosmilia variabilis, are* shown in Figure 7.2 (after Freiwald et al., 2004).

To date, the majority of cold-water coral reefs have been found in the Northeast Atlantic Ocean, and are usually dominated by *Lophelia*. *Lophelia* is a primary framework-building coral, which produces large, highly branched bushy colonies with branches that join together where they touch. This structure is incredibly strong, producing a long-lasting reef framework. *Madrepora* is often found on *Lophelia* reefs in the Northeast Atlantic. This species produces a more delicate skeleton, with slender branches that form a secondary reef framework. *Solenosmilia* can also occur in the *Lophelia* reefs of the Northeast Atlantic contributing to the coral framework.

The occurrence of *Lophelia* in the Northeast Atlantic varies from scattered groups of colonies to vast reef complexes (Roberts et al., 2003). The Norwegian Shelf has the highest known density of *Lophelia* reefs in the world, with hundreds of large coral reefs located in water depths of 40 to 400m and an estimated spatial coverage on the order of 2,000 km^2. In UK and Irish waters *Lophelia* occurs along the continental shelf, and on offshore seamounts and banks, such as the Rockall Bank and the Porcupine Seabight. *Lophelia* has also been found growing on the legs of some North Sea Oil Rigs (e.g. Gass & Roberts, 2006).

Lophelia colonies grow at very slow rates of ~5-30 mm/yr, taking hundreds of years to form moderate sized colonies and thousands of years to build a large reef structure (see Gass & Roberts (2006) and references therein). For example, a large reef complex on the Sula Ridge off the Norwegian coast (14 km in length and up to 30m in height) is estimated to be ~9,000 years old (Hovland & Risk, 2003).

These reefs are of both ecological and economic importance. The coral habitat is known to support many associated species, with a high diversity of benthic species and megafauna (Fosså et al., 2002; Hovland & Risk, 2003; Roberts et al., 2003). The UK Biodiversity Group (2000) estimates that species diversity is about three times higher on *Lophelia* reefs compared to the surrounding soft-bottomed sediments. The reefs have traditionally been rich fishing grounds, with higher landing rates compared to surrounding waters (Fosså et al., 2002). They also act as a nursery area for many juvenile animals, including commercially valuable species such as redfish, and may play a key role as spreading centres for associated faunas, particularly those species which exhibit high reef abundance but are scare elsewhere (Fosså et al., 2002; Rogers, 2004). Degradation of a significant part of the *Lophelia* reefs may therefore dramatically change the distribution of species diversity along the whole shelf and slope (Fosså et al., 2002).

Existing threats to these ecosystems are considerable. In particular, intensive trawling has resulted in widespread damage to deep water reefs (Fosså et al., 2002; Rogers, 2004; Roberts et al., 2003, 2006). For example, it is estimated that between 30 and 50% of *Lophelia* reefs on the Norwegian continental shelf have been damaged or impacted by trawling (Fosså et al., 2002). Due to their depth habitat, they perhaps also represent the ecosystem that is most vulnerable to the effects of ocean acidification, where shoaling of the aragonite saturation horizon could not only prevent further precipitation of aragonite but also lead to extensive dissolution (Guinotte et al. 2006; Roberts et al., 2006; Turley et al., 2007).

The slow growth rate and long life of cold water corals makes them particularly vulnerable to damage, where it could take hundreds or thousands of years (if at all) for reefs to recover and for the restitution of ecological function (Fosså et al., 2002). The ecological importance of these reefs in combination with their fragility and the already extensive damage they have sustained has led to numerous calls and proposals for deep water coral reefs to be protected by law. Globally, a number of cold water reefs are now protected, either with full protection from all human activities as designated Marine Protected Areas or Habitat Conservation Areas, and/or closed to bottom contact fishing in order to protect coral habitat (e.g. WWF, 2004; Rogers, 2006). On the Norwegian Shelf, deliberate destruction of coral reefs is banned and a number of reefs have more rigorous protection. The Darwin Mounds in the Rockall Trough have been protected by an emergency measure under the European Habitats Directive and might be designated as a Special Area of Conservation (SAC), with several other sites in UK and Irish waters being candidate or draft SACs.

7.1.3 Deep Water Coral Reefs – Coupling to Preferential Flow Paths

It has been suggested that the occurrence of *Lophelia* reefs on the continental shelf of the North East Atlantic is correlated with sub-surface faults and other structures associated with low level hydrocarbon seepage, including gas hydrate fuelled methane seeps (Hovland & Thomsen, 1997; Hovland et al., 1998; Henriet et al., 1998; Hovland & Risk, 2003).

This theory was put forward based on the assumption that light hydrocarbon seeps (mainly methane) feed a chemosynthetic food chain which in turn supports cold-water corals and their associated fauna (Hovland and Thomsen, 1997; Hovland et al., 1998; Hovland & Risk, 2003). However, this hypothesis is somewhat controversial (Rogers, 1999), and there is no definitive proof that deep-water coral reefs are directly fuelled by seepage (Hovland & Risk, 2003). It may be that the formation of seafloor carbonate crusts and concretions as a by-product of microbial chemosynthesis (e.g. Roberts & Aharon, 1994) simply provides the hard substrata required for larval settlement (e.g. Freiwald, 2002).

Regardless of whether *Lophelia* reefs explicitly require hydrocarbon seepage, there are numerous indicators documented by German, British, and Norwegian researchers over the last 10-15 years that all suggest a close link between the location of Norwegian reef structures on the continental shelf and the seepage of fluids through the seabed (Hovland & Risk, 2003). These include (Hovland & Risk, 2003):

- seaward-dipping sedimentary permeable strata
- enhanced acoustic seismic reflectors
- adjacent pockmark craters
- locally elevated light hydrocarbon sediment content
- locally elevated seawater methane content

Although all the listed indicators do not necessarily occur at each of the respective reef locations simultaneously (Hovland & Risk, 2003), it seems clear that a large proportion of reefs are located in areas where seepage either has occurred, is occurring, or might occur. As such, *Lophelia* reefs are highly likely to be linked to preferential flow paths for CO_2 migration through the subsurface.

If leakage of CO_2 to a deep water reef should occur, the consequent decease in seawater pH could prevent calcification and even lead to dissolution of the reef structure. It is noted that the extent to which local pH is affected will be dependent on the scale of leakage. Nevertheless, the coupling of a preferential flow path with a fragile and valuable ecosystem, where the impact of leakage is potentially devastating, means that the possibility of leakage to sediments underlying a cold water reef should be classed as a High Risk scenario.

7.2 GeoHazards – Methane Gas Hydrates

The second example of a high risk scenario considered here is the possibility of CO_2 leakage into methane hydrate bearing sediments.

Gas hydrates are naturally occurring compounds found in permafrost and ocean margin regions. These materials form when water and small "guest" molecules, such as methane, react at low temperature, high pressure conditions. The water crystallizes into a network of hydrogen-bonded molecular cages that contain the guest molecules (Sloan, 1998a).

Large amounts of methane (CH_4) in the form of solid hydrates are stored on the continental shelves (see Figure 7.3), and are often associated with hydrocarbon vents, seeps, or mud volcanoes. The CH_4 may be of either biogenic or thermogenic origin, produced by the microbial degradation of organic matter at low temperatures, and/or the thermal cracking of kerogens at high temperatures and burial depths (e.g. Kvenvolden, 1995; Milkov, 2005). While some hydrate deposits form from biogenic gas produced in-situ (i.e. within the CH_4 hydrate stability zone), a significant proportion are formed by gases (either biogenic and/or thermogenic) sourced from depth, where the gases migrate long distances (i.e., hundreds to thousands of meters) into the stability zone along faults or through permeable sand/silt layers, gas chimneys, or mud volcanoes (Milkov, 2005 and references therein). The presence of a hydrate deposit thus indicates a high probability of preferential flow paths in the underlying sediment.

Figure 7.3: Global distribution of methane hydrate deposits on the continental shelf (known and inferred).

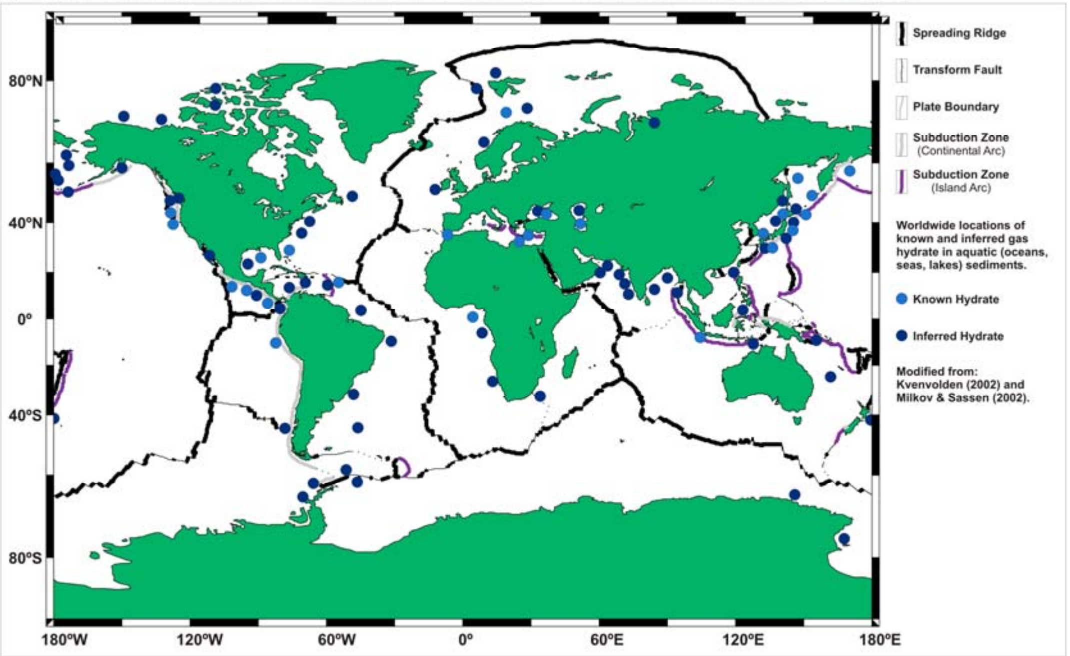

Hydrate deposits are of considerable interest for three reasons: (1) as a submarine geohazard (2) as a factor in global climate change, and (3) as a potential energy resource (Kvenvolden, 2000). All of these factors are of relevance here as CO_2 leakage into methane hydrate bearing sediments has the potential to (1) trigger a submarine landslide, possibly leading to tsunami generation (2) release large volumes of methane – a potent greenhouse gas - to the atmosphere, and (3) destroy potentially valuable hydrocarbon reserves.

7.2.1 Links between Gas Hydrates and Submarine Sediment Slides

A geohazard is shorthand for a geophysical or geological hazard, and is typically used to refer to rapid onset events. Methane gas hydrates are considered a geohazard due to the possible connection between hydrate dissociation and submarine sediment failures – or slides.

Risks associated with decomposition of methane gas hydrates have been widely addressed in the literature (for an excellent overview see Maslin, 2004) and a brief summary is given here.

There is strong circumstantial evidence that the dissociation of methane hydrates due to ongoing, natural geological processes may play a key role in promoting large-scale seafloor slumps along the continental margins. Regionally, there are many examples of this connection - surficial slides and slumps on the continental slope and rise of West Africa; slumps and collapse features on the U.S. Atlantic continental slope; large submarine slides on the Norwegian continental margin; sediment blocks on the sea floor in fjords of British Columbia; and massive bedding-plane slides and rotational slumps on the Alaskan Beaufort Sea continental margin (Kvenvolden, 1993, 1999, 2000).

7.2.1.1 Sediment Slide Triggering Mechanism

When hydrate forms in unconsolidated sediments it hinders the normal sediment compaction process. If exposed to lower pressure and/or increased temperature, the decomposition of the hydrate can disrupt the poorly compacted host sediment and trigger a slide.

Gases are highly concentrated in the solid hydrate phase, thus the decomposition of hydrates can release large volumes of gas. 1 m^3 of CH_4 hydrate can contain the equivalent of 164 m^3 of CH_4 at standard temperature and pressure (Sloan, 1998a). However, the immediate volume increase that occurs on hydrate decomposition is dependent on temperature and pressure conditions in the sediment column. The volume expansion factor increases as water depth (hydrostatic pressure) decreases. For example, at 1000m water depth (and typical seafloor temperatures), the volume of released CH_4 and water is little over twice the original gas hydrate volume, whereas at 500m water depth, the volume increases by a factor of 3.5, and in very shallow hydrate deposits (<300m water depth), expansion factors may exceed 6.0 (see Figure 7.4, Panel A). This volume expansion causes the pore fluids to become highly pressurised and essentially pushes the sediment apart, leading to a loss of sediment compactness, the formation of large pore spaces, and potentially triggering a sediment slide. As would be expected, the steeper the sediment slope, the more likely it is that a slide will occur, where slides are more likely to be promoted by gas hydrate breakdown on slopes of more than 4 degrees.

Figure 7.4: Volume increases (at T, P conditions in the sediment column) arising from decompositon of methane hydrate or an exchange reaction with carbon dioxide (assuming 100% replacement). Data only shown within the hydrate stability field.

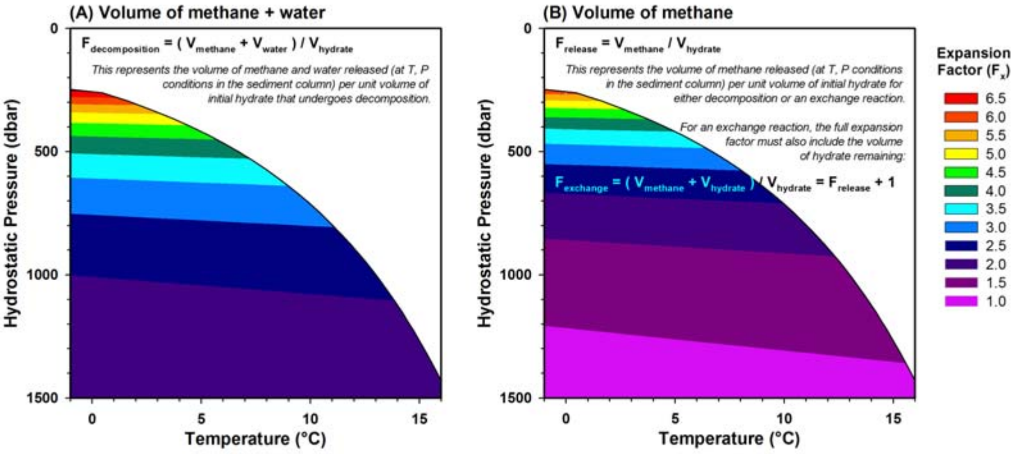

(A) Volume of methane + water

$F_{decomposition} = (V_{methane} + V_{water}) / V_{hydrate}$

This represents the volume of methane and water released (at T, P conditions in the sediment column) per unit volume of initial hydrate that undergoes decomposition.

(B) Volume of methane

$F_{release} = V_{methane} / V_{hydrate}$

This represents the volume of methane released (at T, P conditions in the sediment column) per unit volume of initial hydrate for either decomposition or an exchange reaction.

For an exchange reaction, the full expansion factor must also include the volume of hydrate remaining:

$F_{exchange} = (V_{methane} + V_{hydrate}) / V_{hydrate} = F_{release} + 1$

7.2.1.2 Impacts of Submarine Sediment Failures

Submarine sediment failures may have a direct impact on oil and gas industry engineering structures (e.g. sea bottom installations, pipelines, production facilities) and pose a serious risk to personnel (Kvenvolden, 2000).

Sediment slides also have the potential to generate tsunamis (Maslin, 2004 and references therein). Tsunamis are caused by the rapid perturbation of the seabed or of the water column above it, which either lift the sea surface up above its normal level or depress it. Submarine landslides involve the movement of sub-seafloor material from one place to another, generating a reverse flow of water (‘dipole mechanism’). In general, the size of the generated wave will increase with sediment slide volume and velocity. Sediment slide velocity depends on both the slope and the mechanism of movement. The greater the slope, the greater the component of gravitational force acting down it and so the greater the accelerating force. Coherent sliding blocks usually move more slowly than avalanche-like mass movements. However, in ancient submarine landslides, the very largest blocks, with dimensions of kilometres to tens of kilometres, moved as far (and, by inference, as fast) as the rest of the rock avalanches with which they are associated. Geological evidence indicates that this is because these blocks trap a layer of pressurised mud and debris beneath them upon which they effectively float by a "hovercraft" effect and so slide without basal friction.

One consequence of a large slope failure event may be the complete loss of methane-gas-hydrate and free gas to the oceans and eventually the atmosphere (see Figure 7.5). As methane is a potent greenhouse gas, hydrate formation and dissociation is thus thought to play an important role in past and future climate change (e.g. Sloan, 1998b; Henriet & Mienert, 1998; Kennett et al., 2003; Maslin et al., 2004).

Figure 7.5: Illustration of what happens when a sediment slope failure occurs above a gas hydrate layer and how large quantities of gas may be released (after Maslin, 2004; adapted from Kvenvolden, 1998).

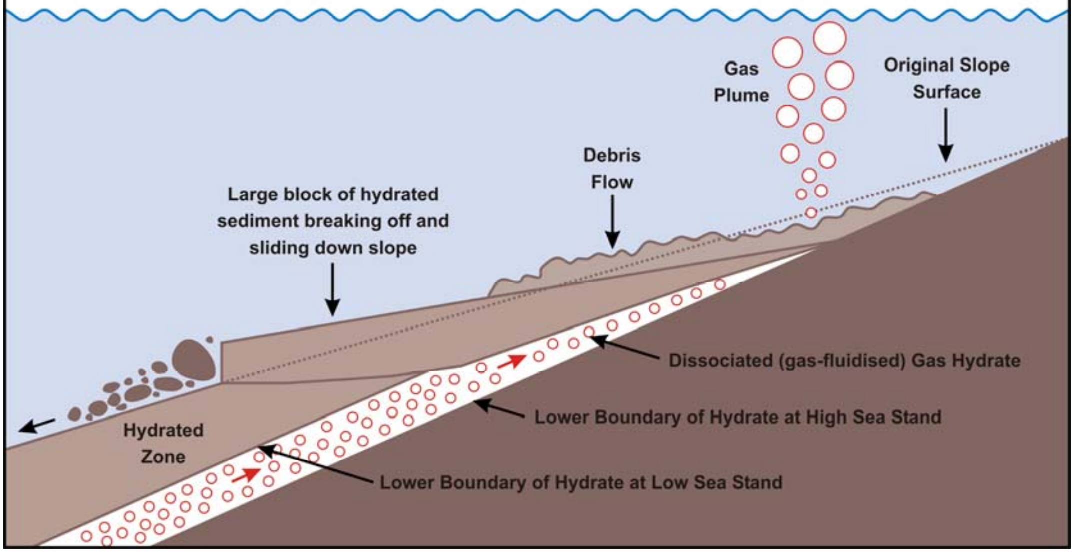

7.2.2. Exchange Reaction betwee CO_2 and CH_4 Hydrate

Thermodynamic arguments suggest that CO_2 will replace CH_4 in the hydrate structure, i.e. CO_2 hydrate is more stable than CH_4 hydrate. This raises the possibility that simply bathing a CH_4 hydrate mass in liquid or gaseous CO_2 could result in an exchange reaction, with conversion of CO_2 to the solid hydrate and concomitant release of CH_4 gas. Indeed, this reaction has recently gained much interest as it offers the potential double benefit of sequestering captured fossil fuel CO_2 with recovery of liberated CH_4 gas as an additional energy source. However, in the case of unintended leakage or seepage of CO_2 from a sub-seafloor storage reservoir into hydrate bearing sediments if an exchange reaction takes place it would result in the liberation of free methane gas without capture and recovery.

7.2.2.1 How Likely is it that an Exchange Reaction will Occur?

Several recent laboratory studies have explored the exchange reaction between CH_4 hydrate and CO_2. Komai et al. (2002) used Raman spectroscopy to observe the reaction between structure I (sI) CH_4 hydrate and gaseous CO_2 in a small pressure cell. They observed slow conversion rates (several hours), where CO_2 hydrate formed both at the surface and within the interior of the CH_4 hydrate, and water ice crystals were also produced. In a following study, Yoon et al. (2004) reported that surface shielding by CO_2 hydrate formed in the outer layers of the sample plays a key role in retarding the dissociation of CH_4 hydrate in the interior. Lee et al. (2003) carried out a similar reaction using finely ground sI CH_4 hydrates to increase the surface area available for reaction, and ^{13}C NMR to investigate details of cage occupancy. They observed that CO_2 replaces CH_4 in the large cages of the sI hydrate structure, where replacement was complete in less than 5 hours with recovery of ~64% of the CH_4 present in the initial hydrate. In an extension to this work, Park et al. (2006) reported an increased CH_4 yield of ~85% when a binary CO_2-N_2 gas mixture was used as the reactant, since N_2 could replace CH_4 present in the small cages of the sI hydrate structure.

Park et al. (2006) also presented results from the first experiment using a structure II (sII) CH_4 + C_2H_6 hydrate and CO_2 in both the gas (274.15K, 35 bar; 1°C, 350 dbar) and liquid (274.15 K, 42 bar; 1°C, 420 dbar) phases. They reported near identical results for the exchange reaction with CO_2 gas (recovery: 92% CH_4 & 99% C_2H_6) versus CO_2 liquid (recovery: 90% CH_4 & 97% C_2H_6). Interestingly, CO_2 was found to replace CH_4 in both the sII-large and sII-small cages where this replacement induced a continuous structural change to sI hydrate as the reaction proceeded and the critical guest composition limit for sII hydrate was exceeded.

In a novel study, Graue et al. (2006) provide the first example of liquid CO_2 displacement of CH_4 from sI hydrate resident within a porous sandstone (277.15K, 81.6 bar) using 3D MRI to monitor the exchange process over time. These authors report initially rapid CH_4 production rates that decrease with time, where CH_4 production continued over 4 days, and flushing of the hydrate/sandstone plug with additional liquid CO_2 resulted in further CH_4 liberation.

However, there are significant differences between laboratory studies, and natural hydrate deposits. In particular, in the natural environmental the hydrate composition and structure are defined by the deposit and the physical properties of the experiment cannot be controlled. While laboratory studies have focused on simple synthetic sI CH_4 hydrates or sII CH_4 + C_2H_6 hydrates, naturally occurring hydrates are more complex and may exhibit significant heterogeneity in terms of guest gas composition and hydrate structure. The P-T field is set by the external environment, and the hydrate surface area available for reaction is dependent on the naturally occurring hydrate fabric. Dunk et al. (2006) recently reported results from the first in-situ oceanic experiment on this reaction, carried out at the massive thermogenic hydrate mounds that outcrop from the seafloor at water depths of 850 m in Barkley Canyon, offshore Vancouver Island (48°18.642' N, 126°3.903' W). The experiment was performed as a feasibility test to determine if measurable exchange occurred between a macroscopic natural gas hydrate and liquid CO_2 under the P-T conditions at the sea-floor (Figure 7.6).

Figure 7.6: Investigating the exchange reaction between a complex natural gas hydrate and liquid CO_2 at the seafloor
(A) Collecting a core of hydrate (B) Adding CO_2 to the reaction chamber - note the sharply defined boundaries of the hydrate cores (C) Observed visual changes to the hydrate cores, with increased 'fluffiness' over time (after Dunk et al., 2006).

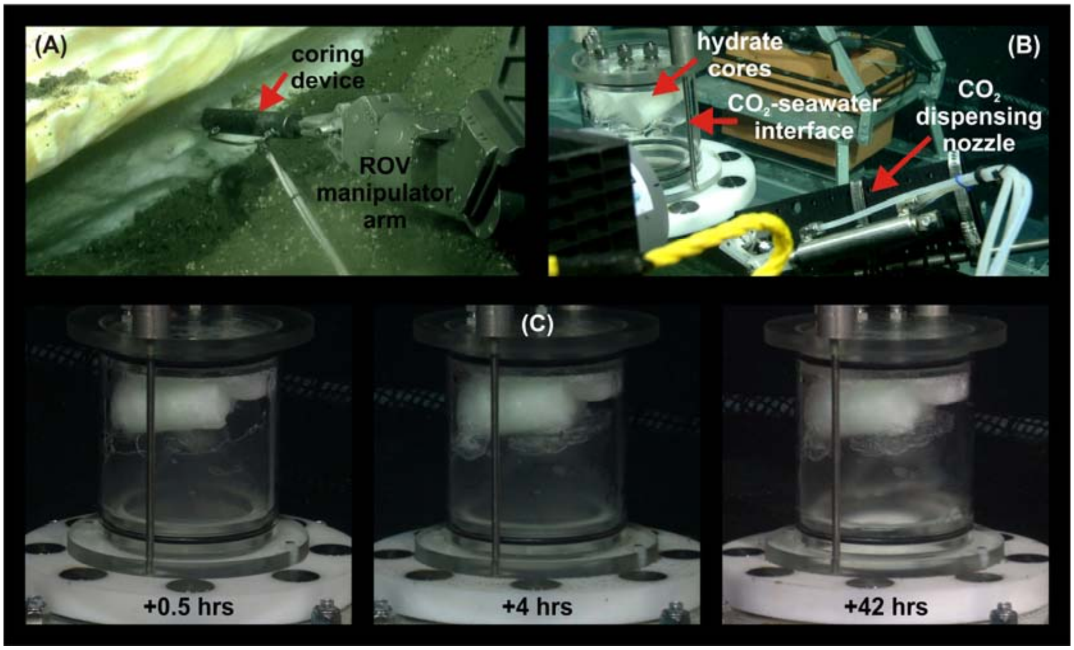

Two small cores (10 cm length, 4 cm diameter) of hydrate were collected from the exposed outcrops using an ROV operated tool. The release of some small gas bubbles was observed during coring. The cores were ejected into a glass walled, closed top, reaction chamber. Approximately 2L of liquid CO_2 were dispensed into the chamber. Under ambient conditions (T = 4.0 °C, P = 870 dbar, S = 34.2), the densities of the gas hydrate and liquid CO_2 were closely matched and less than that of seawater, where the hydrate cores floated at the top of the chamber fully immersed within the buoyant liquid CO_2. The chamber was then placed on a base plate to seal the system. Over the following ~48 hours, the system was periodically inspected with the ROV HDTV camera, and at the end of the experiment the sample was interrogated using in-situ Raman spectroscopy. Initially, the boundaries of the hydrate cores were sharply defined. 30 minutes following addition of liquid CO_2, the core boundaries had taken on a 'fluffy' appearance, where the extent of 'fluffiness' increased with time. This increase in 'fluffiness' appears to reflect an ongoing process occurring at the core boundary such as exchange leading to restructuring of the hydrate and/or dissolution of the hydrate with re-growth of a secondary hydrate. Raman interrogation after 48 hours reaction time identified gaseous CH_4 and CO_2 hydrate in addition to the initial CH_4 hydrate and CO_2 liquid.

These initial results suggest that an exchange reaction will occur under in-situ conditions, although the extent of exchange may be limited to external surfaces (c.f. Yoon et al., 2004). This suggests that more exchange may occur in hydrate deposits where the hydrate fabric is highly porous, or discrete nodules of hydrate are dispersed throughout the sediment column, with more limited reaction occurring at massive hydrate deposits.

7.2.2.2 Consequences of an Unintended Exchange Reaction

An unintended exchange reaction between CO_2 that has leaked from a storage reservoir into methane hydrate bearing sediments would result in the liberation of a free CH_4 gas phase. If complete exchange is assumed, the volume of CH_4 released under in-situ P-T conditions per unit volume of reacted hydrate is shown in Figure 7.4(B). As the initial hydrate still remains (but with CO_2 as the replacement guest molecule), the total volume increase is higher by 1 unit volume (although this does not account for the consumption of the CO_2). As with other mechanisms that result in hydrate dissociation (e.g. changes in P,T conditions), the resulting pressurisation of the pore fluids would destabilise the seafloor and could result in large scale sediment slides, leading to both widespread hydrate dissociation and the release of buoyant gas trapped beneath the hydrate capping layer (see Figure 7.5). Thus the overall release of methane could be significantly higher than that initially replaced by CO_2.

In addition to the direct impacts of sediment slides and possible tsunami generation, the impact of releasing methane to the ocean and eventually the atmosphere must also be considered. Given that the purpose of storing CO_2 is as a climate change mitigation strategy, for a leakage/seepage event to result in release of methane should be considered an extremely serious negative consequence.

Methane is a more potent greenhouse gas than CO_2. Global Warming Potentials (GWPs) are used to compare the abilities of different gases to trap heat in the atmosphere. The GWP is the radiative forcing that results from adding 1 kg of a gas to the atmosphere relative to the effect of 1 kg of CO_2, and is based on both the radiative efficiency (heat absorbing ability) and the decay rate of the gas (the amount removed from the atmosphere) over a given number of years. The GWP for methane is 62 over 20 years, 23 over 100 years, and 7 over 500 years. Noting that replacement in a hydrate structure does not occur on a weight for weight basis, and accounting for the molecular masses of CO_2 (44g/mole) and CH_4 (16g/mole), on a mole to mole basis, the increased atmospheric forcing factors become 22.5, 8.4 and 2.5. Thus, even in the absence of sediment slope failure, if methane gas is released to the atmosphere as a result of CO_2 leakage from a geological storage site it would negate the benefit of 22.5 times the amount of CO_2.

Finally, as some CH_4 hydrate deposits could be viewed as potentially mineable hydrocarbon reserves, the loss of the original deposit could also represent a significant economic loss.

7.3 Summary & Recommendations

The risks of leakage are high when a high possibility of leakage is combined with the presence of a vulnerable object in the leakage path. Two vulnerable objects are identified that may signal the presence of preferential flow paths in the underlying sediments; deep water coral reefs and natural gas hydrate deposits.

Deep water coral reefs are a fragile ecosystem of both ecological and economic value, sustaining high levels of biodiversity, and acting as a nursery ground for many species including commercially important fish stocks. The occurrences of deep water reefs on the continental shelf of the North East Atlantic are often associated with indictors of hydrocarbon seepage or possible fluid migration pathways. These pathways could act as preferential flow conduits for leaked CO_2, delivering CO_2 from the subsurface to the reef. Leakage of CO_2 to a deep water reef is potentially devastating, where the resultant decease in seawater pH could prevent calcification and even lead to dissolution of the reef structure. In turn, destruction of reef habitat could dramatically change the distribution and diversity of species along the entire shelf and slope. As the corals are very slow growing, it may take hundreds or thousands of years for reefs to recover from damage, or they may not recover at all.

The coupling of a preferential flow path with a fragile and valuable ecosystem means that the possibility of leakage to sediments underlying a cold water reef should be classed as a High Risk scenario.

Large amounts of methane (CH_4) in the form of solid hydrates are stored on the continental shelves. A significant proportion of natural gas hydrate deposits are formed by gases (either biogenic and/or thermogenic) sourced from depth, where the gases migrate long distances into the stability zone along faults or through permeable sand/silt layers, gas chimneys, or mud volcanoes. These gas migration pathways could act as conduits, delivering leaked CO_2 into CH_4 hydrate bearing sediments. As CO_2 hydrate is more stable than CH_4 hydrate, this could lead to an unintended exchange reaction, where CO_2 replaces CH_4 in the hydrate structure, releasing large volumes of CH_4 gas. The resultant pressurisation of the pore fluids could destabilise the seafloor and cause a sediment slide, leading to further hydrate dissociation and the release of buoyant gas trapped beneath the hydrate capping layer, and potentially triggering a tsunami.

The potential release of large volumes of methane, a potent greenhouse gas, combined with the risk of causing a submarine land slide, and possibly triggering a tsunami, means that the possibility of leakage to sediments underlying a natural gas hydrate deposit should be classed as a High Risk scenario.

APPENDIX 1A: Hendriks et al. (2004) Estimates of Reservoir Storage Capacity ($GtCO_2$).

Region	Depleted Oil Fields							Remaining Oil Fields							Total Oil Fields				ECBM		
	Onshore			Offshore				Onshore			Offshore				Onshore	Offshore		All		All	
	Low	Best	High	Low	Best	(%)	High	Low	Best	High	Low	Best	(%)	High	Best	Best	(%)	Best	Low	Best	High
Canada	0.7	1.1	1.5	0.0	0.0	(0)	0.0	0.0	0.4	3.1	0.0	0.3	(43)	3.2	1.5	0.3	(17)	1.8	0.0	8.5	51.0
U.S.A.	2.5	3.7	4.9	1.0	3.0	(45)	5.4	0.8	6.2	44.5	0.1	0.5	(7)	4.8	9.9	3.5	(26)	13.4	0.0	31.7	190.2
Central America	0.5	0.8	1.0	2.1	6.3	(89)	11.2	0.1	2.1	14.5	0.2	2.8	(57)	20.5	2.9	9.1	(76)	12.0	0.0	0.0	0.0
South America	2.3	3.4	4.5	2.1	6.3	(65)	11.2	0.7	8.3	53.8	0.3	5.8	(41)	52.4	11.7	12.1	(51)	23.8	0.0	2.0	11.7
Northern Africa	1.2	1.8	2.4	0.9	2.7	(60)	4.8	0.4	4.5	23.8	0.1	0.9	(17)	6.4	6.3	3.6	(36)	9.9	0.0	0.0	0.0
Western Africa	0.2	0.3	0.3	2.6	7.8	(96)	13.9	0.1	1.6	17.8	0.4	6.1	(79)	67.4	1.9	13.9	(88)	15.8	0.0	0.2	1.3
Eastern Africa	0.0	0.0	0.0	0.0	0.0	–	0.0	0.0	0.0	0.2	0.0	0.1	(100)	0.6	0.0	0.1	(100)	0.1	0.0	0.0	0.0
Southern Africa	0.0	0.0	0.0	0.2	0.5	(100)	1.0	0.0	0.1	0.6	0.0	1.0	(91)	10.6	0.1	1.5	(94)	1.6	0.0	7.4	44.6
Western Europe	0.1	0.2	0.2	3.4	10.3	(98)	18.2	0.0	0.1	1.1	0.3	4.0	(98)	39.9	0.3	14.3	(98)	14.6	0.0	1.0	5.7
Eastern Europe	0.3	0.4	0.6	0.0	0.0	(0)	0.0	0.1	0.9	5.1	0.0	0.0	(0)	0.0	1.3	0.0	(0)	1.3	0.0	0.7	4.2
Former S.U.	4.8	7.2	9.6	1.7	5.1	(41)	9.0	1.7	21.8	132.4	0.2	2.9	(12)	19.3	29.0	8.0	(22)	37.0	0.0	25.0	150.1
Middle East	7.9	11.8	15.7	3.4	10.3	(47)	18.4	5.1	62.0	405.8	0.8	9.3	(13)	61.1	73.8	19.6	(21)	93.4	0.0	0.0	0.0
Southern Asia	0.1	0.1	0.2	0.4	1.3	(93)	2.3	0.0	0.4	2.1	0.1	0.6	(60)	3.0	0.5	1.9	(79)	2.4	0.0	2.0	11.9
Eastern Asia	1.0	1.5	2.0	0.4	1.2	(44)	2.2	0.2	3.0	23.0	0.0	0.5	(14)	3.4	4.5	1.7	(27)	6.2	0.0	158.0	840.7
South East Asia	0.6	0.9	1.2	1.3	3.8	(81)	6.7	0.1	1.0	6.0	0.1	1.4	(58)	10.9	1.9	5.2	(73)	7.1	0.0	19.0	113.9
Oceania	0.0	0.0	0.0	0.5	1.5	(100)	2.6	0.0	0.0	0.2	0.0	0.5	(100)	5.0	0.0	2.0	(100)	2.0	0.0	11.3	54.1
Japan	0.0	0.0	0.0	0.0	0.0	–	0.0	0.0	0.0	0.0	0.0	0.0	–	0.0	0.0	0.0	–	0.0	0.0	0.1	0.5
Greenland	0.0	0.0	0.0	0.0	0.0	–	0.0	0.0	0.0	0.0	0.0	0.0	–	0.0	0.0	0.0	–	0.0	0.0	0.0	0.0
TOTAL	**22.2**	**33.2**	**44.1**	**20.0**	**60.1**	(64)	**106.9**	**9.3**	**112.4**	**734.0**	**2.6**	**36.7**	(25)	**308.5**	**145.6**	**96.8**	(40)	**242.4**	**0.0**	**266.9**	**1479.9**

Region	Depleted Gas Fields							Remaining Gas Fields							Total Gas Fields				Aquifers		
	Onshore			Offshore				Onshore			Offshore				Onshore	Offshore		All		All	
	Low	Best	High	Low	Best	(%)	High	Low	Best	High	Low	Best	(%)	High	Best	Best	(%)	Best	Low	Best	High
Canada	0.1	6.6	8.1	0.0	0.0	(0)	0.0	6.6	8.1	10.2	0.7	0.8	(9)	1.3	14.7	0.8	(5)	15.5	2.2	17.3	77.7
U.S.A.	1.8	6.0	7.7	1.2	1.3	(18)	1.9	6.0	7.7	15.3	0.7	0.8	(9)	1.4	13.7	2.1	(13)	15.8	2.2	17.3	77.6
Central America	0.2	0.8	1.2	1.3	0.8	(50)	1.8	0.8	1.2	4.4	5.6	9.4	(89)	26.7	2.0	10.2	(84)	12.2	0.9	7.3	32.7
South America	0.2	8.7	17.6	0.4	0.5	(5)	0.9	8.7	17.6	49.4	3.6	14.3	(45)	60.4	26.3	14.8	(36)	41.1	2.9	23.0	103.4
Northern Africa	0.1	13.8	19.4	0.1	0.1	(1)	0.2	13.8	19.4	42.6	1.5	3.1	(14)	9.8	33.2	3.2	(9)	36.4	1.7	13.4	60.5
Western Africa	0.1	1.1	2.7	0.4	0.5	(31)	0.9	1.1	2.7	6.7	4.7	11.7	(81)	28.5	3.8	12.2	(76)	16.0	1.9	15.1	68.0
Eastern Africa	0.0	0.1	0.4	0.0	0.0	(0)	0.0	0.1	0.4	1.3	0.2	1.2	(75)	4.0	0.5	1.2	(71)	1.7	0.7	5.5	24.6
Southern Africa	0.0	0.0	0.1	0.0	0.0	–	0.0	0.0	0.1	0.2	0.5	1.2	(92)	4.5	0.1	1.2	(92)	1.3	1.8	14.0	63.1
Western Europe	0.2	4.7	10.4	10.3	10.1	(68)	13.3	4.7	10.4	16.9	12.9	26.8	(72)	111.9	15.1	36.9	(71)	52.0	0.9	7.0	31.7
Eastern Europe	0.0	2.9	3.9	0.0	0.0	(0)	0.0	2.9	3.9	6.6	0.0	0.0	(0)	0.0	6.8	0.0	(0)	6.8	0.4	3.4	15.2
Former S.U.	0.3	71.0	126.3	2.1	2.2	(3)	5.3	71.0	126.3	331.5	24.0	71.3	(36)	287.3	197.3	73.5	(27)	270.8	4.1	33.0	148.5
Middle East	0.3	92.3	168.1	0.7	0.7	(1)	1.4	92.3	168.1	372.6	69.9	85.0	(34)	116.3	260.4	85.7	(25)	346.1	1.2	9.7	43.6
Southern Asia	0.2	3.9	9.5	0.6	0.6	(13)	1.2	3.9	9.5	24.0	1.3	4.6	(33)	12.9	13.4	5.2	(28)	18.6	2.7	21.2	95.5
Eastern Asia	0.1	3.9	7.8	0.1	0.1	(3)	0.1	3.9	7.8	23.5	0.2	0.3	(4)	1.0	11.7	0.4	(3)	12.1	1.7	13.4	60.3
South East Asia	0.1	2.8	7.0	2.6	3.0	(52)	4.4	2.8	7.0	17.9	16.5	31.9	(82)	61.3	9.8	34.9	(78)	44.7	0.8	6.4	28.8
Oceania	0.0	0.1	0.2	0.3	0.4	(80)	0.8	0.1	0.2	0.5	6.9	16.9	(99)	39.9	0.3	17.3	(98)	17.6	3.5	28.1	126.3
Japan	0.0	0.0	0.0	0.0	0.0	–	0.0	0.0	0.0	0.0	0.0	0.0	–	0.0	0.0	0.0	–	0.0	0.2	1.9	8.4
Greenland	0.1	0.0	0.3	0.0	0.0	–	0.0	0.0	0.3	1.5	0.0	1.9	(86)	10.4	0.3	1.9	(86)	2.2	0.4	3.3	15.0
TOTAL	**3.8**	**218.7**	**390.7**	**20.1**	**20.3**	(8)	**32.2**	**218.7**	**390.7**	**925.1**	**149.2**	**281.2**	(42)	**777.6**	**609.4**	**301.5**	(33)	**910.9**	**30.2**	**240.3**	**1080.9**

APPENDIX 1B: Hendriks et al. (2004) Calculations of Storage Capacity

Calculations of potential CO_2 storage capacity (in Gt CO_2) for Storage Reservoir Types (Hendriks et al., 2004).			**Values used for Estimates**		
			Low	**Best**	**High**
Depleted Oil Fields Assumes part of the volume that was occupied by oil will have been occupied by water and cannot be replaced by CO_2. $CO_2\ (Gt) = O_P \times V_{BO} \times S_O \times \rho_{CO2} \times 10^{-12}$					
O_P	(BO)	Total oil produced in the past in Barrels of Oil			
V_{BO}	(m^3/BO)	Volume of a Barrel of Oil	0.159	0.159	0.159
S_O		Fractional volume of the original space occupied by oil that can be replaced with CO_2	0.4	0.6	0.8
ρ_{CO2}	(kg/m^3)	Density of CO_2 at depth	750	750	750
Remaining Oil Fields Assumes all future oil is produced via EOR and relates extra oil production via EOR to CO_2 storage capacity. $CO_2\ (Gt) = EOR \times R_{CO2:EOR} \times 10^{-12}$ *where* $EOR = [O_R + O_U] / [(g_{API}+5)/100] \times F_{EOR} \times C$					
EOR	(BO)	Enhanced Oil Recovery due to CO_2 injection in Barrels of Oil			
$R_{CO2:EOR}$	(kg/BO)	Ratio of net CO_2 injection to EOR	150	450	800
O_R	(BO)	Total known remaining oil reserves in Barrels of Oil			
O_U	(BO)	Total undiscovered oil reserves in Barrels of Oil	F5[b]	F50[b]	F95[b]
g_{API}		API gravity of oil (specific values used represent the composition of the oil)	maximum	median	minimum
F_{EOR}		Fractional extra oil recovery due to CO_2 injection (dimensionless)	0.05	0.12	0.2
C		Contact Factor - fraction of oil amenable to miscible or immiscible flooding with CO_2	0.75	0.75	0.75
Depleted Gas Fields Conservatively assumes 75% of void space created can be occupied by CO_2. $CO_2\ (Gt) = G_P \times S_G \times R_{CO2:CH4} \times \rho_{CO2(STP)} \times 10^{-12}$ $R_{CO2:CH4} = 2\times10^{-7}d^2 - 0.0015d + 4.1707$					
G_P	(m^3)	Total volume of gas produced in the past			
S_G		Fractional volume of original space occupied by gas that can be replaced with CO_2	0.75	0.75	0.75
$R_{CO2:CH4}$		The molar ratio of CO_2 to CH_4 for a fixed volume at depth (ratio of volumes @ STP[a])			
d	(m)	Reservoir depth	maximum	median	minimum
$\rho_{CO2(STP)}$	(kg/m^3)	Density of CO_2 @ STP[a]	1.98	1.98	1.98
Remaining gas Fields Most likely this will not become available until reservoirs are depleted. $CO_2\ (Gt) = [G_R + G_U] \times S_G \times R_{CO2:CH4} \times \rho_{CO2(STP)} \times 10^{-12}$ *where*					
G_R	(m^3)	Total volume of known gas reserves @ STP[a]			
G_U	(m^3)	Total volume of undiscovered gas reserves @ STP[a]	F5[b]	F50[b]	F95[b]
All other variables as for Depleted Gas Fields					
Unmineable Coal Beds Excluded lignite. Main constraint on utilisation of ECMB considered to be the number of injection wells required. $CO_2\ (Gt) = ECMB \times E_{CO2:CH4} \times \rho_{CO2(STP)} \times 10^{-12}$ *where* $ECMB = A_C \times X_C \times T_C \times \rho_C \times G_C \times F_{ECMB}$					
ECMB	(m^3)	Producible gas from Enhanced Coal bed Methane Recovery (ECMB) @ STP[a]			
$E_{CO2:CH4}$		Exchange ratio - moles of CO_2 that replace 1 mole of CH_4	2	2.5	3
$\rho_{CO2(STP)}$	(kg/m^3)	Density of CO_2 @ STP[a]	1.98	1.98	1.98
A_C	(m^2)	Surface area of coal basins			
X_C		Fraction of A_C that could be utilised for ECMB	0.1	0.1	0.1
T_C	(m)	Cumulative thickness of coal (estimated for each region)	0	expected	2 × expected
ρ_C	(Mg/m^3)	Density of coal			
G_C	(m^3/Mg)	Gas content of coal @ STP[a]	4	8	20
F_{ECMB}		Fractional recovery factor - that part of the gas in place that can be recovered	0.4	0.4	0.4
Aquifers[c] Assumes only aquifers below 750m depth will be used. $CO_2\ (Gt) = A_A \times X_A \times T_A \times (\phi_A/100) \times S_A \times \rho_{CO2} \times 10^{-12}$ *where*					
A_A	(m^2)	Surface area of sedimentary basins			
X_A		Fraction of sedimentary basins that form aquifers that are part of a structural trap	0.01	0.01	0.01
T_A	(m)	Aquifer thickness m	50	100	300
ϕ_A		Aquifer porosity (%)	5	20	30
S_A		Fractional volume of aquifer trap that can be filled with CO_2	0.02	0.02	0.02
ρ_{CO2}	(kg/m^3)	Density of CO_2 at depth	750	750	750

[a] STP = standard temperature and pressure

[b] F5, F50 and F95 are the values of undiscovered resources with a *certainty* of 95%, 50% and 5% respectively that the amount of oil or gas is at least as high as the reported value.

[c] Note 2 typographic errors in this equation (not followed through to calculations) in the text of Hendriks et al. (2004): (1) ρ_{CO2} is quoted at STP, where it should be at depth (2) ρ_{CO2} is quoted in units of Mg/m^3, which means the exponential factor should be $\times10^{-9}$ not $\times10^{-12}$.

APPENDIX 1C: Dooley et al. (2005) Estimates of Reservoir Storage Capacity ($GtCO_2$).

Region	Coal Basins	Depleted Oil	Depleted Gas	Saline Aquifers		
				Onshore	Offshore (%)	All
USA	58.7	11.0	36.7	2731.7	909.3 (25)	3641.0
Canada	3.7	0.0	3.7	1001.0	249.3 (20)	1250.3
Western Europe	3.7	7.3	40.3	73.3	143.0 (66)	216.3
Japan	0.0	0.0	0.0	0.0	0.0 –	0.0
Australia and New Zealand	29.3	0.0	11.0	205.3	476.7 (70)	682.0
Former S.U.	18.3	22.0	256.7	370.3	1386.0 (79)	1756.3
China	14.7	3.7	7.3	330.0	33.0 (9)	363.0
Middle East	0.0	33.0	190.7	223.7	14.7 (6)	238.3
Africa	7.3	14.7	62.3	117.3	231.0 (66)	348.3
Latin America	3.7	14.7	47.7	187.0	55.0 (23)	242.0
Southeast Asia	25.7	3.7	29.3	121.0	179.7 (60)	300.7
Eastern Europe	3.7	0.0	7.3	106.3	11.0 (9)	117.3
Korea	0.0	0.0	0.0	0.0	0.0 –	0.0
India	7.3	0.0	7.3	187.0	187.0 (50)	374.0
TOTAL	**176.0**	**110.0**	**700.3**	**5654.0**	**3875.7 (41)**	**9529.7**

These estimates of regional capacity of potential geological CO_2-storage reservoirs were derived from the technical literature supplemented by the authors technical judgment. Details are given in: Dooley, J.J. and S.J. Friedman, (2004). *A Regionally Disaggregated Global Accounting of CO_2 Storage Capacity: Data and Assumptions*. Battelle, Pacific Northwest Division Technical Report Number PNWD-3431, 15p.

APPENDIX 3.A CO$_2$ Vent Sites – Summary of Current Knowledge.

This appendix provides a summary of current knowledge regarding known CO$_2$ vent sites. The extent of knowledge regarding these sites ranges from well investigated, to largely unknown (i.e. where gas venting has been observed but detailed biological or geochemical surveys have not yet been carried out and/or reported). CO$_2$ vent sites are now receiving a high degree of attention within the research community – with recognition that cross disciplinary investigations are needed to provide vital information regarding potential impacts of leakage from sub-seafloor CO$_2$ storage sites and/or oceanic CO$_2$ storage and/or the high CO$_2$/low pH ocean. As such, the number of expeditions to study these sites appears to be increasing and the quality and extent of information is improving all the time. This appendix briefly summarises currently available information, providing key references for each site and a basis upon which a future CO$_2$ vent site database can be established. The focus is on sites where venting of a separate CO$_2$ rich gas or liquid phase is known to occur, thus this appendix does not include descriptions of sites where hydrothermal aqueous fluids rich in CO$_2$ (e.g. Loihi seamount, Hawaii; Axial volcano, JdFR), or where venting of a gas/liquid phase inferred to be CO$_2$ (e.g. Vailulu'u Seamount, Samoan Hotspot) occurs.

List of Sites

Shallow Water & Mid Depth Sites

3.A.1 The Mediterranean Vent Systems
3.A.2 The Atlantic Ocean: Iceland and the Azores
3.A.3 The Caribbean Sea: Dominica, Lesser Antilles
3.A.4 The Eastern Pacific Margin: Baja California Peninsula & Mexico
3.A.5 The Western Pacific Margin I: Kurile Islands & Japan
3.A.6 The Western Pacific Margin II: Papua New Guinea & New Zealand

Deep Water Sites

3.A.7 The Okinawa Trough
3.A.8 The Champagne Vent Site, NW Eifuku, Mariana Arc

3.A.1 The Mediterranean Vent Systems

Type of Volcanic Activity:	**Subduction related**
Depth of Venting:	**Shallow water gasohydrothermal systems**
Type of CO_2 Venting:	**Gas phase, CO_2 dominant**

Hydrothermal activity in the Mediterranean Sea represents one of the most studied and better described gasohydrothermal systems. Reviewing the considerably body of literature available for the numerous Mediterranean vent sites is beyond the scope of this appendix and the reader is referred to the review by Dando et al. (1999) and references therein, and for the Aegean Sea in particular to Dando et al. (2000). A very brief synopsis of key findings (based largely on these reviews) is given below.

Hydrothermalism in this region results from the subduction of the oceanic part of the African plate below the European Plate, where the subduction zone is delineated by trenches ~3 km deep. High heat flows in the resulting volcanic arc and back-arc extensional areas have set up hydrothermal convection systems. Most of the known vent sites are in shallow coastal waters (<300m depth), where gasohydrothermal activity has been observed in the Tyrrhenian Sea, in the Northern Aegean, and in the Southern Aegean along the Hellenic Island Arc (see Table 3.1, Chapter 3).

Hydrothermal Fluids

Mediterranean hydrothermal fluids range from entirely marine to entirely meteoric (rain water) in origin, and exhibit varying salinities due to both the input of meteoric water and phase separation as a result of seawater boiling at low pressure (Dando et al., 1999 and references therein). The chemistry of the vent fluids reflects alteration of the source fluid due to interactions with sediments at elevated temperatures and the entrainment of sediment pore waters. Rising gas bubbles can initiate water circulation within the sediment so that the released water is recharged by overlying bottom water (O'Hara et al., 1995), where studies in the Aegean have reported a concentric inflow area between 2 and 2.5 m distant from the vent site (Robinson et al., 1997; Dando et al., 2000).

In the Tyrrhenian Sea vent fluids have been analysed from Vulcano and Panarea. With respect to ambient seawater, Vulcano fluids exhibited low pH (minimum = 5.2) and high TCO_2 (65 mmol), with sulphide concentrations of up to 0.27mM, and were enriched in phosphate (30-fold), Si (19-fold), Li (1.6-fold), Rb (3.7-fold), Fe (112-fold), Mn (16-fold) and NH_3 (17-fold) (Sedwick & Stuben, 1996). Similarly, Panarea fluids exhibited low pH (minimum = 4.26) and high TCO_2 (45-53 mmol), and were enriched in Li (1 to 5-fold), Ca (1 to 3.8-fold), K (1 to 2.4-fold), and depleted in Mg, Na, and sulphate (Italiano & Nuccio, 1991). In the Aegean Sea, water from a submarine brine pool at Palaeochori Bay, Milos, and pore waters from the area exhibited low pH (minimum = 5.24) and moderately elevated TCO_2 (2.6-11.8 mmol), and were enriched in phosphate (13-fold), Si (up to 2300-fold), Na (up to 2.6 fold), K (13-fold), Ca (5-fold), and depleted in Mg and sulphate (Fitzsimons et al., 1997). Sulphide concentrations of 1.8 mmol have been reported (Sedwick & Stuben, 1996). Dando et al. (2000) report that vents close to the shore showed up to 340-fold enrichments in Li, Rb, Sr, Ba and Si, while at deeper vents only 3-fold enrichments were found. In other areas where gas venting occurs (but gas compositional data are not available) there have been more detailed studies on fluid composition, including analysis of metal concentrations. For example, Santorini and Methana hydrothermal fluids are enriched in Fe, Mn, As, Cd, Cu and Zn (Varnavas & Cronan, 1988). Overall, the chemical characteristics of these vent fields are similar to others occurring along the Hellenic Volcanic Arc, including the Yali, Kos, and Milos hydrothermal systems (Smith & Cronan, 1983; Varnavas & Cronan, 1991; Cronan & Varnavas, 1993).

Gas Venting

CO_2 is the dominant gas at most of the Mediterranean vent sites, accounting for 75-100% by volume of the total gas released (Baubron et al., 1990; Italiano & Nuccio, 1991; Calanchi et al., 1995; Minissale, 1989; Dando et al., 1995a). The CO_2 is derived from both dissociation of marine carbonates and degassing of subducted slab and magma (Botz et al., 1996; Calanchi et al., 1995; Dando et al., 1995a; Fytikas et al., 1989; Minisale, 1989). Paradisos, off the Greek island of Xanthi, is the single reported exception, where H_2 comprises 96.6% of the total gas (Minissale, 1989).

In the CO_2 dominated systems, minor gas components include significant quantities of nitrogen (N_2), hydrogen sulphide (H_2S), methane (CH_4), and hydrogen (H_2). In particular, H_2S can reach concentrations up to 6.5% in the Calabrian Arc (Italiano & Nuccio, 1991) and 8.1% in the Hellenic Arc (Dando et al., 1995a). Dando et al., (1995a) suggest that the trace gas composition may reflect interaction with microbially active sediments, where the rising hydrothermal gases strip biogenic gases from the sediment column. In particular, the authors note that high CH_4 contents were consistently observed in gas samples collected from vents situated in a seagrass bed in Palaeochori Bay (Milos) where biogenic CH_4 is formed through the decomposition of leaf debris.

The total CO_2 flux (submarine & subaerial; gaseous & dissolved) from the Mediterranean volcanic systems is significant on a global basis, where Dando et al. (1999) estimate a flux on the order of 10^7-10^8 kgCO_2/day (3.65-36.5 MtCO_2/yr). The uncertainty on this estimate is large due to the general paucity of data from which to calculate robust flux estimates and the inherent variability of the system (Dando et al., 1999). In particular, episodic events such as earthquakes result in a large release of gas and the contribution made by such events cannot easily be determined (Hasiotis et al., 1996). For example, during the March 1992 earthquake south-east of Milos there were large releases of gas, where the numbers of submarine gas vents along a 1km transect increased by 65% within an hour of the earthquake (Delibasis & Drakopoluos, 1993; Dando et al., 1995b).

For the submarine hydrothermal systems, individual bubble stream and/or site estimates are available for Panarea (Tyrrhenian), Kos (Aegean) and Milos (Aegean). Of these, the estimates of total CO_2 released in the free gas phase appear to be best constrained for the extensive gasohydrothermal systems of Milos (Dando et al., 1995a, 2000).

The CO_2 flux from the Panarea hydrothermal field is estimated to be 1.8×10^4 kgCO_2/day (6.6 ktCO_2/yr; Italiano & Nuncio, 1991). For the Aegean systems at Kos and Milos, measurements of gas exhalation rates at individual bubble streams show considerable variation both within and between sites, and over time, ranging from weak or moderate to very rapid venting (Dando et al., 1995a, 2000). The most recent surveys reported ranges (corrected to STP) of 1.7 to 65.2 L/hr (average of 16.4 L/hr, sample number not stated) at Kos and 0.1 to 56.6 L/hr (average 8.1 L/hr, sample number not stated) at Milos (Dando et al., 2000). Note the slightly different flow rates for Milos in comparison to an earlier survey, which reported a range of 0.16 to 26.23 L/hr, and mean of 8.56 L/hr (38 seeps, 56 measurements; Dando et al., 1995a).

The total area around Milos over which gas venting occurs is around 34 km^2, including an extensive area to the south and east of Milos running from Zefiros Point in the south, around Paleochori Bay and Spathi Point to Boudia Bay in the North, with additional areas both at the opening to and within the Gulf of Milos (Dando et al., 1995a, 2000). The density of bubble streams within the vent fields varies widely, ranging from areas of no venting, to scattered individual bubble streams, to areas with multiple vents at a high density. Strongly degassing vents are scattered throughout the area and are likely concentrated in highly fractured regions (Dando et al., 2000). In the region of most vigorous venting at Paleohori Bay sediments appeared to be “boiling” over an area of ~30m^2 due to the intensity of the gas release, where flow rates at this site could not be measured (described as similar to a fluid reactor bed; Dando et al., 1995a). In an area of moderate venting in Paleohori Bay, SCUBA diver surveys indicated an approximate vent density of 6-7 outlets per m^2 (Dando et al., 1995a). Comparisons between the number of vents observed in SCUBA surveys to the number identified from echo-sounding transects suggest that echo-sounding underestimates the number of bubble streams by a factor of 7 to 10 (Dando et al., 1995a, 2000). Dando et al. (1995a) conclude it is reasonable to suppose that for every bubble stream identified using an echo-sounder there are in actuality 2 to 10 times more bubble streams present.

Dando et al. (1995a) estimated the total CO_2 gas flux from the Milos vent field by (i) conducting an echo-sounding survey of a significant area of the vent field (ii) determining the average number of bubbles streams per m^2 from the echo-sounding survey and correcting for the underestimation (i.e. multiplying by a factor of 2 to 10) (iii) extrapolating the number of bubble streams to the area of the entire site (streams per m^2 multiplied by total field area) (iv) multiplying the number of streams by the mean gas flux observed at an individual bubble stream (v) multiplying the total gas flux by the mean fractional CO_2 content. Estimates of the flux of free CO_2 gas determined in this manner give a range of 0.7-3.7 $MtCO_2$/yr (Dando et al., 1995a). Note Dando et al. (2000) report a slightly revised estimate of 0.9 to 3.5 $MtCO_2$/yr, which has presumably been calculated in a similar fashion.

Biota

An overview of the biota of Mediterranean gasohydrothermal vent sites is given in Dando et al., (1999). The brief notes provided below are from this article, and the reader is referred to this article (and references therein) for further information.

Dando et al. (1999) note that the Mediterranean vents represent sites at which the impact of pollution on marine ecosystems can be studied. However, the specific influence of elevated CO_2 is not directly discussed.

The Mediterranean vents support many prokaryotes (archea and bacteria) including sulphur and sulphate reducers, methanogens and iron oxidisers among others. A number of species are similar to those found at the Ocean Spreading Ridges (OSRs), while others are novel, including giant sulphur oxidisers and new groups of thermophiles and hyperthermophiles.

Vent obligate taxa are not found at the shallow water Mediterranean vent sites, and the direct effect of gasohydrothermal venting on the macrobiota is to exclude many of the less tolerant local species (Dando et al., 1995a; Fitzsimons et al., 1997). Although many species are unable to survive close to the most toxic of the vents others have adapted to these conditions (Dando et al., 1999).

In the neighbourhood of vent outlets, seagrasses are absent and algal distributions are changed. There is a reduced diversity of infauna within sediments at the vents, and many common infaunal species are absent, although opportunistic species of polychaetes and nematodes that exhibit a degree of sulphide and temperature tolerance colonise vent vicinities in large numbers, and nematodes tend to become dominant in the meiofauna (0.1-1mm size class). The only macrofaunal species to be found at the vent outlets and living on top of brine seeps (Milos) was a euryhaline and eurythermal (wide salinity and temperature tolerance) nassariid gastropod. In contrast, the epifauna near the vent sites is particularly diverse and the vent sites are areas of settlement for exotic thermophilic species. At the periphery of the vent fields, the fauna is characterised by filter feeders and surface deposit feeders (Gimenez & Marin, 1991).

Mediterranean References

Baubron, J.C., Allard, P., & Toutain, J.P., (1990). Diffuse volcanic emissions of carbon dioxide from Vulcano Island, Italy. *Nature*, **344**: 51-53.

Botz, R., Stüben, D., Winckler, G., Bayer, R., Schmitt, M., Faber, E., (1996). Hydrothermal gases offshore Milos Island, Greece. *Chemical Geology*, **130**: 161-173.

Calanchi, N., Capaccioni, B., Martini, M., Tassi, F., Valentini, L., (1995). Submarine gas-emission from Panarea Island (Aeolian Archipelago): distribution of inorganic and organic compounds and inference about source conditions. *Acta Vulcanologica*, **7**: 43-48

Cronan, D.S., Varnavas, S.P., (1993). Submarine fumarolic and hydrothermal activity off Milos, Hellenic Volcanic Arc. *Terra Abstracts*, **5**: 569.

Dando, P.R., Hughes, J.A., Leahy, Y., Niven, S.J., Taylor, L.J., & Smith, C. (1995a). Gas venting rates from submarine hydrothermal areas around the island of Milos, Hellenic Volcanic Arc. *Continental Shelf Research*, **15**: 913-929

Dando, P.R., Hughes, J.A., Leahy, Y., Taylor, L.J., Zivanovic, S., (1995b). Earthquakes increase hydrothermal venting and nutrient inputs into the Aegean. *Continental Shelf Research*, **15**: 655-662

Dando, P.R., Stüben, D., Varnavas, S.P., (1999). Hydrothermalism in the Mediterranean Sea. *Progress in Oceanography*, **44**: 333-367.

Dando, P.R., Aliani, S., Arab, H., Bianchi, C.N., Brehmer, M., Cocito, S., Fowler, S.W., Gundersen, J., Hooper, L.E., Kölbi, R., Kuever, J., Linke, P., Makropoulos, K.C., Meloni, R., Miquel, J.-C., Morri, C., Müller, S., Robinson, C., Schlesner, H., Sievert, S., Stöhr, E., Stüben, D., Thomm, M., Varnavas, S.P., Ziebis, W., (2000). Hydrothermal studies in the Aegean Sea. *Physics & Chemistry of the Earth* (B), **25**: 1-8.

Delibasis, N.D., Drakopoluos, J.C., (1993). The Milos island earthquake of March 20, 1992 and its tectonic significance. *Pageoph*, **141**: 131-153.

Fitzsimons, M.F., Dando, P.R., Hughes, J.A., Thiermann, F., Akoumianaki, I., Pratt, S.M., (1997). Submarine hydrothermal brine seeps off Milos, Greece: observations and geochemistry. *Marine Chemistry*, **57**: 325-340.

Fytikas, M., Kavouridis, T., Leonis, C., Marini, L., (1989). Geochemical exploration of the three most significant geothermal areas of Lesbos Island, Greece. *Geothermics*, **18**: 465-475.

Giaccone, G., (1969). Associazioni algali e fenomeni secondary di vulcanismo nelle acque marine di Vulcano (Mar Tirreno). *Giornale Botanico Italiano*, **68**: 353-366. In Italian (cited in Dando et al., 1999).

Gimenez, F., Marin, A., (1991). The polychaete annelids from a shallow-water gasohydrothermal vent of the Gulf of Naples. *Anales de Biologia, Madrid*, **17**: 143-151.

Gugliandolo, C., Maugeri, T.L., (1993). Chemolithotrophic, sulfur-oxidizing bacteria from a marine, shallow hydrothermal vent of Vulcano (Italy). *Geomicrobiology Journal*, **11**: 109-120.

Hasiotis, T., Papatheodorou, G., Kastanos, N.A., (1996). Pockmark field in the Patras Gulf (Greece) and its activation during the 14/7/93 seismic event. *Marine Geology*, **130**: 333-344.

Italiano, F., Nuccio, P.M., (1991). Geochemical investigations of submarine volcanic exhalations to the east of Panarea, Aeolian Islands, Italy. *Journal of Volcanology and Geothermal Research*, **46**: 125-141.

Mattison, R.G., Abbiati, M., Dando, P.R., Fitzsimons, M.F., Pratt, S.M., Southward, A.J., Southward, E.C., (1998). Chemoautotrophic microbial mats in submarine caves with hydrothermal sulphidic springs at Cape Palinuro, Italy. *Microbial Ecology*, **35**: 58-71.

Minissale, A. (1989). Geochemical characteristics of Greek thermal springs. *Journal of Volcanology and Geothermal Research*, **39**: 1-16.

O’Hara, S.C.M., Dando, P.R., Schuster, U., Bennis, A., Boyle, J.D., Chui, F.T.W., Hatherell, T.V.J., Niven, S.J., Taylor, L.J., (1995). Gas seep induced interstitial water circulation - observations and environmental implications. *Continental Shelf Research,* **15**: 931-948.

Robinson, C., Ziebis, W., Mu¨ller, S., Eichstadt, K., Dando, P., Linke, P., Varnavas, S., Megalovasilis, P., & Panagiotaras, D., (1997). In situ investigations of shallow water hydrothermal vent systems, Palaeochori Bay, Milos, Aegean Sea. In *Proceeding of the Fourth Underwater Science Symposium*, pp. 85–100.

Sedwick, P., Stuben, D., (1996). Chemistry of shallow submarine warm springs in an arc-volcanic setting: Vulcano Island, Aeolian Archipelago, Italy. *Marine Chemistry*, **53**: 147-161.

Smith, P.A., Cronan, D.S., (1983). The geochemistry of metalliferous sediments and waters associated with shallow submarine hydrothermal activity (Santorini, Aegean Sea). *Chemical Geology*, **39**: 241-262.

Varnavas, S. P., & Cronan, D. S. (1988). Arsenic, antimony and bismuth in sediments and waters from the Santorini hydrothermal field, Greece. *Chemical Geology*, **67:** 295-305.

Varnavas, S.P., Cronan, D.S., (1991). Hydrothermal metallogenic processes off the islands of Nisiros and Kos in the Hellenic Volcanic Arc. *Marine Geology*, 99: 109-133.

3.A.2 The Atlantic Ocean: Iceland and the Azores

Gasohydrothermal activity has been reported in two locations in the Atlantic Ocean, where the Mid Atlantic Ridge intersects Iceland, and in the Azores.

3.A.2.1 The Iceland Hotspot

Type of Volcanic Activity: **Hotspot influenced OSR**
Depth of Venting: **Shallow to Mid-Depth**
Type of CO_2 Venting: **Gas phase, low to intermediate CO_2**

In Iceland the Mid-Atlantic Ridge (MAR) is superimposed on the large Iceland hot spot. Phase separation (boiling of sea water) leading to the formation of free gas bubbles emerging from the sea floor has been reported at two hydrothermal fields in the Kolbeinsey Ridge area. Kolbeinsey Ridge, named after the Island of Kolbeinsey, is part of the MAR extending from the Tjörnes Fracture Zone at ~66ºN to the Jan Mayen Fracture Zone at ~71ºN. The southern part of the Ridge is volcanically active (Fricke et al., 1989) with the latest documented eruption in the year 1372.

Kolbeinsey Hydrothermal Field – Shallow water depth & low CO_2

The Kolbeinsey Hydrothermal Field (KHF) is located to the south of Kolbeinsey Island at ~67°05'N and 18°43W (Fricke et al., 1989; Botz et al., 1999). The vents are located at 104-113 m water depth, with maximum fluid exit temperatures of 100-130°C (Botz et al., 1999). This site was first described by Fricke et al. (1989), who observed gas bubbles venting from the seafloor. Although gas samples were not collected on this first visit, it had been suggested that these vents might be CO_2 rich based on the reported gas composition of an onshore geothermal system (Dando et al., 1995b). However, later sample collection and analysis demonstrated that these vents have a comparatively low CO_2 content of <2 mol% (Botz et al., 1999 – see notes below regarding reporting of gas contents).

Grimsey Hydrothermal Field – Mid water depth & low to intermediate CO_2

The Grimsey Hydrothermal Field (GHF) is located to the northeast of Grimsey Island at 66°36'N and 17°39W, about 30 km offshore from Iceland. Gas vents at a depth of ~400m have a reported CO_2 content of 1-41 mol% (Botz et al., 1999). The general characteristics of this site have been well described by Hannington et al. (2001), while Botz et al. (1999) and Riedel et al. (2001) explore the composition and source of the vent gas in more detail. The main findings from these papers are briefly summarised below.

General Site Description

The GHF was located by strong acoustic scattering in the water column caused by a large gas rich plume. Although bubbles were not observed at the sea surface, the plume was readily detected in 18 kHz echo-sounding profiles over the vent field. Subsequent observations with the submersible vehicle JAGO confirmed the presence of gas rich vents at the seafloor (Hannington et al., 2001).

The main vent field occurs at a depth of ~400m (395-407m) and covers an area of ~1km^2. It consists of about 20 large diameter (up to 10m) mounds and 1-3m chimneys and spires of anhydrite and talc. The north-south alignment of the mounds over a 1km strike length of the valley floor suggests that their distribution is controlled by a buried fault. Actively boiling hydrothermal vents occur on most of the mounds and extensive two phase venting indicates that the field is underlain by a large boiling zone (200x300m). Widespread shimmering water and extensive white patches of anhydrite in the sediment between the mounds indicates that the entire 1 km^2 area occupied by the vents is thermally active.

The site is characterised by low salinity, low sulphur, metal depleted fluids. Most of the high temperature fluid is discharged through narrow candlestick chimneys protruding from large anhydrite spires. Fluid exit temperatures ranged from ~200-250°C, with almost all toward the upper limit of this range and close to the boiling point of water at this depth. The absence of 'smoke' in the venting fluids indicates that the concentrations of metal and sulphur are low. High temperature vent fluids have pH 5.9-6.8 and high alkalinity (2.4-3.0 meq/L). Magnesium (Mg) and sulphate (SO_4^{2-}) concentrations are 37-44 and 20.6-25.7 mmol and most likely reflect mixing of hydrothermal fluids with seawater. End member chlorinity is 274 mmol, about half that of seawater, supporting the observation of phase separation in the vents.

Surface temperatures in the sediments on top of the mounds are between 50 and 80°C (Hannington et al., 2001). Higher shallow subsurface temperatures of 110-150°C have been reported at sediment depths of ~10cm, suggesting that the entire mound may be inflated with hydrothermal fluid. A number of 3-4m long sediment cores were collected across the field, and these sediments were probed for temperature measurements. Although not an accurate measure of in-situ temperature, this exercise demonstrated high heat flow across the site, with all but one reported core temperatures in the range 25-102°C, compared to ambient bottom water temperatures of 1.5°C. The highest temperature cores (65-102°C) map out an area of extremely high heat flow surrounding the main central hydrothermal mounds and are thought to delineate the extent of the sub-seafloor boiling zone (Hannington et al., 2001). Away from the subsurface boiling zone, temperatures remained significantly above ambient at ~20-50°C, with the exception of single measurement at near ambient (2°C) on the boundary of the gas plume.

Gas Venting

As noted above, the GHF was located by strong acoustic scattering in the water column caused by a large gas rich plume.

The plume is located above the centre of the hydrothermal field, covering an area of ~0.2 km^2, or around 1/5th the total extent of the GHF (from Figure 9 in Hannington et al., 2001). The acoustic profile shows most intense scattering near the seafloor, where the signal appears to disperse at depths of 150-50m (Hannington et al., 2001). This suggests complete dissolution of the gas bubbles in the water column on a length-scale of 250-350m. This inference is supported by the lack of breaking bubbles at the sea surface (Hannington et al., 2001).

At the seafloor, gas was observed streaming from small holes in the sediments surrounding the vents and in places large gas pockets were found trapped in the sediments (Hannington et al., 2001). The presence of bubble streams well away from the high temperature chimneys suggests that the gas may have originated at greater depth below the seafloor (Hannington et al., 2001).

Although the temperature of the gas vents was not reported, the location of the plume coincides with the sediment core temperature measurements noted above, indicating elevated subsurface temperatures of +25°C.

Gas bubble samples were collected using a water-filled (1.5 L, inverted) glass bottle positioned in the gas stream. The water in the bottles was partly replaced by gas which further expanded during uplift. When the submersible reached the surface a diver closed the sample bottle under water and then disconnected it from the submersible (Botz et al., 1999).

Appreciable amounts of both CO_2 and CH_4 were present in the gas bubbles, with reported CO_2 concentrations between 1.1 mol% and 41.2 mol%, and CH_4 concentrations between 7.2 and 24.3 mol% (Botz et al., 1999 – see notes below regarding reporting of gas concentrations). The CO_2 is most likely of magmatic origin which is slightly influenced by subsurface carbonate dissociation, while the CH_4 is derived mainly from thermal decomposition of sedimentary organic matter (Botz et al., 1999; Reidel et al., 2001).

Biota

A detailed biological survey of this site does not appear to have been carried out.

However, Hannington et al. (2001) report that no vent specific macrofauna were observed at the seafloor, and comment on a single scale worm recovered on an active chimney. For a mid-depth site the absence of vent specific fauna site is somewhat unusual, as some vent obligate taxa would be expected. They also note that biological activity was notably absent in all of the sediment cores collected from this site. This reflects the high temperatures in the cores due to the presence of a subsurface boiling zone and generally high heat flow in this area.

Notes

High subsurface temperatures and associated lack of sediment in-fauna indicate that this site is unsuitable as an analogue for investigating the impacts of CO_2 on local benthic biota. However, this site may yield further valuable information regarding the impact of gas venting on the water column.

As yet, no gas flux estimates have been reported, and insufficient information is available to calculate even a provisional estimate (e.g. number of gas streams and rate of gas venting). The influence of CO_2 on the water column has not been investigated, i.e. there is no site scale survey of water column pH, TCO_2 or alkalinity.

For the GHF, Riedel et al. (2001) make the statement that 'apart from boiling water most of the hydrothermal gas consists of CO_2 which dissolves on its way to the sea surface', referencing this statement to Botz et al. (1999) who report a maximum CO_2 content of 41%. In a personal communication Dr Botz noted that at the time this site was investigated, in-situ gas sampling devices (such as are used today) had not yet been developed, hence it is not possible to really quantify the total gas phase. Based on macroscopic observations the bubbles dissolved on their way to the sea surface due to cooling water steam probably accompanied by the dissolution of CO_2 (Botz, personal communication).

It seems plausible that the balance 'gas' in this case is water vapour (c.f. estimates of the gas:steam ratio for San Felipe, Gulf of California) – thus under the classification system used here this may actually be a CO_2 dominant site (concentrations on dry gas basis).

Iceland References

Botz, R., Winckler,G., Bayer, R., Schmitt,M., Schmidt, M., Garbe-Schönberg, D., Stoffers, P., Kristjansson, J.K., (1999). Origin of trace gases in submarine hydrothermal vents of the Kolbeinsey Ridge, north Iceland. *Earth and Planetary Science Letters* **171**: 83–93.

Fricke, H., Giere, O., Stetter, K., Alfredsson, G.A., Kristjansson, J.K., Stoffers, P., Svavarsson, J., (1989). Hydrothermal vent communities at the shallow subpolar Mid-Atlantic Ridge, *Marine Biology* **102**: 425-429.

Hannington, M., Herzig, P., Stoffers, P., Scholten, J., Botz, R., Garbe-Schonberg, D., Jonasson, I.R., Roset, W., and the Shipboard Scientific Party, (2001). First Observations of high-temperature submarine hydrothermal vents and massive anhydrite deposits off the north coast of Iceland. *Marine Geology* **177**: 199-220.

Riedel, C., Schmidt, M., Botz, R., Theilen, F., (2001). The Grimsey hydrothermal field offshore North Iceland: crustal structure, faulting and related gas venting. *Earth and Planetary Science Letters* **193:** 409-421.

3.A.2.2 D. Joao de Castro Seamount, Azores

Type of Volcanic Activity:	**OSR influenced Hotspot**
Depth of Venting:	**Shallow water gasohydrothermal system**
Type of CO_2 Venting:	**Gas phase venting, CO_2 dominant**

The D. João de Castro Seamount (also referred to as D. João de Castro Bank) is located in the Azores archipelago (38°13.3'N, 26°36.2'W) between the islands of Terceira and São Miguel, on the hyper slow spreading Terceira Rift. It is classified as a Natura 2000 site (protected area recognised as a 'site of Community importance' under the EC Habitats Directive). This site has been explored and surveyed by scuba divers and an autonomous underwater vehicle (AUV), and has been well described by Cardigos et al. (2005), with additional analysis of the seamount biota by Colaço et al. (2006) and Ávila et al. (2007).

General Site Description

The D. João de Castro Seamount has an elevation of 1000m, where the upper part of the seamount has its base at 50 m water depth and shoals to 13m below sea-level at the summit. The area of the seamount shallower than 50m is ~0.35 km^2. The summit is a volcanic caldera (300 x 600 m, 0.18 km^2), with a depth of 40 m inside the caldera.

Shallow gasohydrothermal activity occurs near the top of the seamount on the western caldera rim and wall at depths of 20-45 m. The area covered by hydrothermal activity extends to ~ 0.011 km^2 and both hydrothermal fluids and gases discharge from cracks and fissures in the rocky strata (Cardigos et al., 2005). Of 44 vents examined in detail, 4 discharged only fluids, and 40 discharged fluids and gas bubbles. Temperatures measured at discrete vents over a 3 year period were relatively constant.

Two distinct zones or types of hydrothermal venting were described (the white area and the yellow area), where these zones are separated by ~50 m and are characterized by different physical and chemical properties (Cardigos et al., 2005). The distinct characteristics of these fluids suggest that phase separation may have occurred in the subsurface, with the yellow and white systems being fed by different plumbing systems (Cardigos et al., 2005).

The white area is defined by vents surrounded by white bacterial mats *(Beggiatoa* sp., a filamentous proteobacteria). This area extends to ~ 9000 m^2 between 20 and 45 m depth. Fluid temperatures at the point of discharge are relatively low, ranging from 26.5-42.6°C with an average of 35.8°C. The fluids have low pH (4.32-5.62, mean 5.01) and are enriched in sulphide (12-242 μM, mean 82 μM), dissolved gases and Pb (Cardigos et al., 2005).

The yellow area is defined by vents with yellowish coloured openings. This area extends to ~2000 m^2 between 18 and 25m depth. Fluid temperatures at the point of discharge are moderately higher than those in the white area, ranging from 58.2-63.3°C, with an average of 61.2°C. The fluids have low pH (4.12-5.47, mean 5.09) and low sulphide (0.7-3 μM, mean 1 μM) and are enriched in Ba, Fe and Mn (Cardigos et al., 2005).

Gas Venting

The gas is released across a small area (100 x 50 m, 5000 m^2) in the western part of the caldera at water depths of 16–45 m. The gas bubbles discharge through fissures in the rock in combination with the discharge of low to mid temperature hydrothermal fluids.

Gas samples were collected by SCUBA divers using inverted funnels in a plastic bag or glass bottle. The gas is dominated by CO_2 (90%) with minor amounts of H_2S (9-36 ppm), H_2 (94-21749 ppm) and CH_4 (0-84.2 ppm), and is sourced from a magmatic chamber located between 1 and 5 km under the seafloor (Cardigos et al., 2005).

No gas flux estimates have been reported, and insufficient information is available to calculate a provisional estimate.

Water column profiles of CH_4 and H_2 together with echo-sounder survey indicate deeper vents located on the south east flanks of the seamount at depths ranging from 150m to more than 400m (Cardigos et al., 2005).

Biota

The biological information available for this site is extensive (Cardigos et al., 2005; Colaço et al., 2006; Ávila et al., 2007), and includes analysis of the effects of shallow water venting on marine biota (Colaço et al., 2006) and a comparison of the mollusk community structure between the seamount and typical inshore habitats (Ávila et al., 2007).

Overall, the macro species composition at the shallow vents of the D. Joao de Castro seamount is typical of that found in shallow water environments of the Azores region with no endemic vent species present (Cardigos et al., 2005; Colaço et al., 2006). In total 156 benthic species were identified on the seamount including 41 macro-algae (seaweeds), 10 Porifera (sponges), 9 Cnidaria (e.g. sea anemones, corals, jellyfish, sea pens, hydra), 5 Annelida (segmented worms), 20 Arthropoda (e.g. crabs, sea spiders, shrimps, mites) and 44 Mollusca (e.g. sea slugs, snails, bivalves, octopus) , 7 Echinodermata (e.g. starfish, brittle stars, sea urchins, sea cucumbers), 11 Pisces (fish) and 9 other species (bacteria, comb jellies, sea spiders, bryozoans, nematodes, salps, turtles, dolphins, marine birds) (Cardigos et al., 2005). In the immediate proximity of the vents, species diversity was significantly lower, where the species found closest to the vents were a temperature and/or sulphide tolerant subset of these local species (Cardigos et al., 2005). However, abundances of some species were higher, with for example, fish being generally more abundant in areas of venting (Cardigos et al. 2005). Protists and bacteria adapted to the metal rich waters of this ecosystem were present (Colaço et al., 2006).

The heterogeneity of the vent fluids in the two contrasted areas is reflected by the differences found in the organisms collected (Colaço et al., 2006). For example, at the white vents, the green alga *Codium elisabenthae* (endemic to Macronesian Islands) was found closest to the vents at distances from 0-140cm from vent outlets (Cardigos et al., 2005). At the yellow vents the closest species was *Sargassum* cf. *vulgare,* which occurred at distances of 0-70 cm from the vent outlets, where this species had a high density on the seamount compared to the rest of the Azores (Cardigos et al., 2005).

A more detailed analysis of the molluscs indicated a smaller number of molluscan taxa and a different community structure compared to shore environments on the Azores (Ávila et al., 2007). Average numbers and densities of species were lower at hydrothermal vents than at similar sites without hydrothermal activity (Ávila et al., 2007).

Notes

Vents appear to be located on the caldera rim, and the outer caldera wall. Strong currents in this area result in rapid dilution of the hydrothermal effluent. For example, Cardigos et al. (2005) note that sulphide concentrations at the white vents are sufficient to support a chemosynthetic dependent ecosystem, however strong currents cause rapid dilution of fluids and probably create an unstable system. This accounts for notable difference between this site and others regarding negative impacts on local biota.

For example if we take a very simplistic view of this site, there is a small area of hydrothermal venting, where CO_2 gas is also being released. In the immediate confines of this small area, species diversity is low and represents a subset of sulphide and temperature tolerant local species. However, due to strong currents/rapid dilution, the influence of the vents is confined to the immediate area, with no evident wider impact on the seamount biota.

This contrasts with observations at ‘restricted’ type sites - e.g. Vailulu’u (Samoan hotspot) or the Kraternaya Bight (Kuriles), where build up of both CO_2 and other toxic compounds (metals, H_2S) in the water column occurs, with marked impacts in local ecosystems.

Azores References

Cardigos, F., Colaço, A., Dando, P.R., Ávila, S.P., Sarradin, P.-M., Tempera, F., Conceicao, P., Pascoal, A., Serrao Santos, R., 2005. Shallow water hydrothermal vent field fluids and communities of the D. Joao de Castro Seamount (Azores). Chemical Geology ***224****: 153-168.*

Colaço, A., Raghukumar, C., Mohandass, C., Cardigos, F., Santos, R.S., (2006). Effect of shallow-water venting in Azores on a few marine biota. *Cahiers de Biologie Marine* **47**: 359-364.

Ávila, S.P., Cardigos, F., Santos, R.S., (2007). Comparison of the community structure of the marine molluscs of the "Banco D. Joao de Castro" seamount (Azores, Portugal) with that of typical inshore habitats on the Azores archipelago. *Helgoland Marine Research* **61**: 43-53.

3.A.3 The Caribbean Sea: Dominica, Lesser Antilles

Type of Volcanic Activity:	**Subduction related (Island Arc)**
Depth of Venting:	**Very shallow water - gasohydrothermal system**
Type of CO_2 Venting:	**Gas phase, CO_2 dominant**

Dominica is one of the islands of the Lesser Antilles archipelago, one of only two active island arc systems in the Atlantic Ocean. Champagne Hot Springs (CHS) is located on the southwest flank of the Morne Plat Pays volcanic complex, on the southern tip of Dominica, approximately 2km south of the coastal community of Pointe Michel and just offshore from Point Guignard (McCarthy et al., 2005). This site has been described by McCarthy et al. (2005). A summary is provided below (all information accredited to McCarthy et al., 2005).

General Site Description

Submarine hydrothermal venting occurs at the CHS in 1-5m water along the submerged flank of the Plat Pays volcanic complex. The vent field extends approximately 40m seaward and is 22m at its maximum width, covering a total area of $880m^2$, where venting occurs along two east-west trending fissures in the lava rock.

Two types of discharge are observed (i) Focused discharge of a clear fluid at discrete vent ‘ports’ 2-6 cm in diameter (ii) Diffuse discharge of vent fluid and streams of bubbles emerging directly through the fractured volcanic rocks and unconsolidated sediment.

Six discrete vent sites were identified. Fluid temperatures at the point of discharge ranged from 41-71.4°C, with an average of 56.6°C. The fluids have low pH (5.95 to 6.15, mean 6.04) and are enriched in Fe, Mn and As, Si and Li.

Sediments in this region are enriched in Na, Fe, As and Sb and depleted in Mn when compared to average Caribbean seafloor sediments. Hydrothermal hydrous iron oxide precipitates occur in the immediate vicinity of the discrete vent sites, forming layers up to 5cm thick close to the vent orifices and ranging in colour from dark brown to bright orange. At distances greater than ~2m, they are only present only as a thin orange coating on the volcanoclastic sediments.

Gas Venting

Diffuse venting and abundant gaseous discharge occurred throughout the area, with streams of bubbles emerged directly through the fractured volcanic rocks and unconsolidated sediment. Venting through the sediment was intermittent, with shifts in stream location of a few cm.

Gas samples were collected into Giggenbach sampling bottles. All gas samples have CO_2 as the major component, accounting for 74-93 mol% of the total analyzed gas. N_2 is the second most abundant gas, ranging from 4 to 21 mol%. H_2S levels are significant, comprising 1.6-3.9 mol%, while CH_4, HCl, O_2 and Ar are minor constituents. The elevated CO_2 concentrations, along with N_2/Ar and N_2/He ratios suggest both magmatic and meteoric gas contributions and are typical of arc type settings.

Minimum and maximum gas fluxes for individual bubble streams (as determined by fluid displacement by gas) were 0.1-0.4 L/min respectively.

Biota

No discussion of the biota in relation to vent distribution is available (to the best of the authors knowledge).

Notes

Although gas fluxes for individual bubbles streams are provided, an estimate of the density of bubble streams is not given.

The measured total gas release rate (of which 74-93% is CO_2) ranges from 6-24 L per hour per bubble stream under in-situ conditions.

In-situ conditions are not explicitly stated for those vents where the flux measurements were made. However, vents occur over a water depth range of 1-5m, approximately equal to 1.1-1.5 atm, and it is assumed that measurements are at (or near) the ambient seawater temperature of 29.2°C. Under these conditions, the reported flux is equivalent to 6.0 to 32.5 L/hr at STP, or 76-520 kgCO_2/yr. Noting the description of abundant venting throughout the area, it would seem that an average vent density of ~1 stream per m^2 across the entire vent field would provide a conservative estimate of 880 streams, suggesting a total CO_2 flux on the order of 67-458 tCO_2/yr.

Dominica References

McCarthy, K.T., Pichler, T., Price, R.E., (2005). Geochemistry of Champagne Hot Springs shallow hydrothermal vent field and associated sediments, Dominica, Lesser Antilles. *Chemical Geology* **224**: 55-68.

3.A.4 The Eastern Pacific Margin: Baja California Peninsula & Mexico

Coastal shallow water hydrothermal activity has been reported at a number of sites along the shores of the Baja California Peninsula and Mexico (e.g. Vidal et al., 1981; Barragán et al., 2001; Prol-Ledesma et al., 2002; Forrest et al., 2005). Of these sites, CO_2 is dominant at San Felipe (Barragán et al., 2001) and intermediate at Bahía Concepción (Forrest et al., 2005), both of which are located in the Gulf of California. At the other sites, N_2 and CH_4 are dominant, with minor amounts of CO_2 (2 mol% at Punta Banda on the Pacific Coast of Baja California, Vidal et al., 1981; 0.15 mol% at Punta Mita on the coast of Central Mexico, Prol-Ledesma et al., 2002).

3.A.4.1 San Felipe, Gulf of Mexico

Type of Volcanic Activity:	**EPR associated Fault Zone**
Depth of Venting:	**Very shallow water - gasohydrothermal system**
Type of CO_2 Venting:	**Gas phase, CO_2 dominant**

The description of this site formed part of a wider study of geothermal fluids in the Gulf of California and Mexico (Barragán et al., 2001) and available information is limited.

Barragán et al. (2001) report that the hot springs of this system boil at various places along the shoreline. These authors also provide further information from an unpublished report (Gastil and Bertine, 1982). According to Gastil & Bertine (1982) the springs are located on the south side of a ridge of oxide-bearing meta-carbonic rocks, where some of the springs are accessible only during low tide. In addition fishermen have reported the existence of submarine hot springs. Thus San Felipe is a shallow coastal system, with venting occurring in the inter-tidal (littoral) zone, and possibly extending into the sublittoral zone.

Barragán et al. (2001) report coastal spring fluid temperatures of 48°C and a pH of 5.8. They also present analysis of a gas sample from San Felipe, which consists of 99.2 mol% CO_2, with minor N_2 (0.65 mol%), CH_4 (993 ppmv), Ar (410 ppmv) and H_2S (38 ppmv). Details of sampling are not provided.

Notes

Barragán et al. (2001) also provide the dry gas to steam ratio from their gas analysis. This is the only paper I have seen where this is reported. Gas to steam ratio is quoted as 472,700 mg gas per kg steam.

3.A.4.2 Bahía Concepción, Gulf of Mexico

Type of Volcanic Activity: **EPR associated Fault Zone**
Depth of Venting: **Very shallow water - gasohydrothermal system**
Type of CO_2 Venting: **Gas phase, intermediate CO_2**

Prol-Ledesma et al. (2004) and Forrest et al (2005) report investigations of active hydrothermal venting associated with the El Requesón fault zone (ERFZ) along the western shore of the Bahía Concepción, in the Gulf of California.

General Site Description

Hydrothermal venting in this area occurs along an NW-SE trending onshore-offshore normal fault near Punta Santa Barbara. In this fault controlled system, hydrothermal fluids and gas are being released in the intertidal and shallow subtidal zones (to 15m depth) through rocks and sediment in a roughly linear trend extending over 750m of coastline (Prol-Ledesma et al., 2004; Forrest et al., 2005).

Both diffuse and focused venting of hydrothermal fluids and gas occurs, although water flow is mostly diffuse (Prol-Ledesma et al., 2004). Temperatures in the fluid discharge area vary from ~50°C at the sea bottom up to 87°C at a depth of 10 cm in the sediments (Prol-Ledesma et al., 2004). In the intertidal zone, fluid flow occurs through fractures, most of which are aligned with the onshore fault (Forrest et al., 2005). In the subtidal zone, fluid flow occurs through cracks in bedrock and boulders, pebble-cobble conglomerates and through sediments, where in some areas fluid flow is vigorous enough to create a shimmering effect in the water column (Forrest et al., 2005).

Prol-Ledesma et al. (2004) present analysis of hydrothermal fluids sampled from vents with vigorous flow at 5m water depth. The pH of the fluids ranged from 5.95-6.02, and the waters had elevated concentrations of Ca, As, Hg, Mn, Ba, HCO_3, Li, Sr, B, I, Cs, Fe and Si, and lower concentrations of Cl, Na, SO_4 and Br with respect to ambient seawater. The geochemistry of the vent fluids indicate that it is meteoric water mixed with seawater (Prol-Ledesma et al., 2004). The thermal fluids are formed by infiltration and subsequent heating of meteoric water, where vent fluid is generated by further mixing with seawater (Prol-Ledesma et al., 2004). The hydrothermal activity is altering the rocks, modifying sediments, and precipitating calcite, cinnabar, manganese, and opal-A (Canet et al., 2003).

A temperature logger deployed for a 48 hour period in the vicinity of a vent at 7m depth recorded significant fluctuations in temperature with tidal height (Forrest et al., 2005). The highest temperature (44.4°C) was recorded at the lowest water level (6.04m) and the lowest temperature (33.1°C) at the highest water level (7.21m). This reflects mixing between the vent fluids (exit temperature of 81.0°C) and ambient seawater (31.5°C), indicating that fluid fluxes are negatively correlated with tidal height, with the highest flow rates occurring at low tide (Forrest et al., 2005). This is likely due to variations in hydrostatic pressure related to tidal loading (Boles et al., 2001; Aliani et al., 2004).

Gas Venting

Gas discharge takes place within an area of more than 1 km^2. Prol-Ledesma et al. (2004) report that gas flow is intermittent and concentrates along small fractures covered by detrital sediments. However, Forrest et al. (2005) note that in some areas of the subtidal zone there are numerous persistent streams of gas bubbles emanating from the seafloor (see Figure 4 in Forrest et al., 2005).

Forrest et al. (2005) report analysis of the gas composition. Samples were collected at 7m water depth in the same area of vigorous venting where temperature logging was carried out. Gas was collected from several different sites within this area using plastic funnels placed over the gas vents to fill inverted glass vials.

The Bahía Concepción gas samples consisted primarily of N_2 (54.1-52.6 mol%) and CO_2 (42.9-44.1 mol%) with minor amounts of CH_4 (2.1-2.3 mol%), Ar (0.68-0.72%), O_2 (0.12-0.24 mol%), He (413-439 ppmv), H_2 (45-91 ppmv), C_2H_6 (177-179 ppmv), and C_3H_8 (20-22 ppmv) (Forrest et al., 2005).

The high concentration of N_2 may be partially derived from the thermal alteration of sedimentary organic matter (Jenden et al., 1988). Gases from other coastal hydrothermal systems in Mexico also show enrichment in N_2, with concentrations as high as 87.4 mol% at Punta Mita (Prol-Ledesma et al., 2002).

The isotopic composition of CH_4 ($\delta^{13}C$ = -34.3‰) and high CH_4/C_2H_6 ratio indicate that the gas is thermogenic in origin, consistent with derivation of CH_4 by thermal cracking of marine algal kerogens ($\delta^{13}C$ between -25‰ and -45‰) (Forrest et al., 2005).

Forrest et al. (2005) identify 4 potential sources of CO_2 in this system which could be consistent with the measured isotopic composition ($\delta^{13}C$ = -5.9‰):

(1) Geothermal fluids dissolving rhodolith calcium carbonates ($\delta^{13}C$ = -0.2‰ to -5.2‰).

(2) Decarboxylation of kerogens, which can be expected to be accompanied by corresponding shifts in the isotopic composition of the CO_2 released (Giggenbach, 1997), where at low maturity levels, the CO_2 generated is slightly depleted in the heavy isotope compared to the associated source kerogen (Andresen et al., 1994).

(3) CO_2 derived from an 80/20 mixture of seawater dissolved inorganic carbon (DIC $\delta^{13}C$ = 0‰) and DIC from buried organic matter that has been broken down by sulfate reduction ($\delta^{13}C$ = -25‰).

(4) Exsolution of mantle-derived volatiles from magma ($\delta^{13}C$ values between -4‰ and -7‰; Craig et al., 1981; Botz et al., 2002).

However, the $CO_2/^3He$ ratio ratio of the gases is 1.83x10^8, significantly lower than the typical $CO_2/^3He$ ratio of mantle gases, which does not depart significantly from ~2x10^9 at spreading zones (Marty and Jambon, 1987). Thus Forrest et al. (2005) conclude that a significant portion of the CO_2 is likely generated by thermal decomposition of organic and carbonate-rich sediments (e.g. Vaselli et al., 2002) or some combination of mantle and sedimentary processes.

Biota

The diversity and abundance of biota on rocky habitats adjacent to diffuse venting sites appears to be enhanced, particularly in fish and epifaunal filter-feeding invertebrate assemblages, while infaunal animals are significantly less diverse and abundant in areas of active venting through the soft sediment (Forrest and Melwani, 2003).

A rhodolith bed borders the vent area (Forrest et al., 2005). Rhodoliths are free-living non-geniculate coralline algae, and are the major carbonate producers throughout the Gulf of Mexico (Halfar et al., 2001).

Gulf of California & Mexico References

Barragán R.R.M., Birkle, P. Portugal M.E., Arellano G.V.M., Alvarez R.J., (2001). Geochemical survey of medium temperature geothermal resources from the Baja California Peninsula and Sonora, México. *Journal of Volcanology and Geothermal Research*, **110**: 101-119.

Canet, C., Prol-Ledesma, R.M., Rubio-Ramos, M.A., Forrest, M., Torres-Vera, M.A., 2003b. Mn–Ba–Hg mineralization related to the shallow hydrothermal vents in Bahı´a Concepcı´on, Baja California Sur, Mexico. GSA General Meeting Abstracts with Programs, Seattle, WA. Geological Society of America, p. 237-3. Cited in Forrest et al. (2005).

Forrest, M.J., Ledesma-Vzaquez, J., Ussler III, W., Kulongoski, J.T., Hilton, D.R., Greene, H.G., (2005). Gas geochemistry of a shallow hydrothermal vent associated with the El Requesón fault zone, Bahía Concepción, Baja California Sur, Mexico. Chemical Geology ***224**: 82-95.*

Forrest, M.J., Melwani, A., (2003). Ecological consequences of shallow water hydrothermal venting along the El Requesón fault zone, Bahía Concepción, B.C.S., Mexico. Geological Society of America Abstracts with Programs, Seattle, pp. 557-578. Cited in Forrest et al. (2005).

Gastil, R.G., Bertine, K., (1982) Estudio geoquímico termal de Baja California y sur de California. (Thermal geochemical study of Baja California and South California). University of San Diego, CA., unpublished report, pp 58-61. Cited in Barragán et al., (2001).

Prol-Ledesma, R.M., Canet, C., Melgarejo, J.C., Tolson, G., Rubio-Ramos, M.A., Cruz-Ocampo, J.C., Ortega-Osorio, A., Torres-Vera, M.A., Reyes, A., (2002). Cinnabar deposition in submarine coastal hydrothermal vents, Pacific Margin of central Mexico. *Economic Geology* **97**: 1331-1340.

Prol-Ledesma, R.M., Canet, C., Torres-Vera, M.A., Forrest, M.J., Armienta, M.A., (2004). Vent fluid chemistry in Bahía Concepción coastal submarine hydrothermal system, Baja California Sur, Mexico. *Journal of Volcanology and Geothermal Research* **137**: 311 – 328

Vidal V.M.V., Vidal, F.V., Isaacs, J.D., (1981). Coastal submarine hydrothermal activity off Northern Baja, California: 2. Evolutionary History and isotope geochemistry. *Journal of Geophysical Research* **86 (B10)**: 9451-9468.

Supporting References

Aliani, S., Meloni, R., Dando, P.R., (2004). Periodicities in sediment temperature time-series at a marine shallow water hydrothermal vent in Milos Island. *Journal of Marine Systems* **46**: 109–119.

Andresen, B., Thorondsen, T., Barth, T., Bolstad, J., (1994). Thermal generation of carbon dioxide and organic acids from different source rocks. *Organic Geochemistry* **21:** 1229– 1242.

Boles, J.R., Clark, J.F., Leifer, I., Washburn, L., (2001). Temporal variation in natural methane seep rate due to tides, Coal Oil Point area, California. *Journal of Geophysical Research* **106 (C11):** 27077-27086.

Botz, R., Wehner, H., Scmitt, M., Worthington, T.J., Schmidt, M., Stoffers, P., (2002). Thermogenic hydrocarbons from the offshore Calypso hydrothermal field, Bay of Plenty, New Zealand. *Chemical Geology* **186:** 235-248.

Craig, H., Welhan, J.A., Kim, K.R., Poreda, R., Lupton, J.E., 1981. Geochemical studies of the 218N EPR hydrothermal fluids. *Eos (Transactions - American Geophysical Union)* **61:** 992.

Giggenbach, W.F., (1997). Relative importance of thermodynamic and kinetic processes in governing the chemical and isotopic composition of carbon gases in high-heatflow sedimentary basins. *Geochimica et Cosmochimica Acta* **61:** 3763-3785.

Halfar, J., Godinez-Orta, L., Goodfriend, G.A., Mucciarone, D.A., Ingle Jr., J.C., Holden, P., (2001). Holocene-Late Pleistocene non-tropical carbonate sediments and tectonic history of the western rift margin basin of the southern Gulf of California. *Sedimentary Geology* **144:** 149-178.

Marty, B., Jambon, A., (1987). C/^{3}He in volatile fluxes from the solid Earth: implications for carbon geodynamics. *Earth and Planetary Science Letters* **83:** 16-26.

3.A.5 The Western Pacific Margin I: Kurile Islands & Japan

The Kurile Island Arc stretches for ~600 km from Kamchatka in the north to Hokkaido in the south. The arc is very seismically active, particularly in the south, and is characterized by extensive volcanism and hydrothermal activity (see review by Glasby et al., 2006). The proportion of subaerial and submarine volcanoes are approximately equal, with 105 subaerial volcanoes, 100 submarine volcanoes, and a further 5 submarine calderas (Glasby et al., 2006 and references therein).

Submarine gas venting has been reported at a number of locations along the Kurile Arc (Namsarev et al., 1989; Zhirmunsky & Tarasov, 1990; Zonenshayn et al., 1987). However, most gas vents in this hydrocarbon rich area are dominated by methane (e.g. Gaedicke et al., 1997; Sahling et al., 2003), and significant CO_2 gas contents have only been reported at a single site, Kraternaya Bight, Yankich Island (Namsarev et al., 1989; Zhirmunsky & Tarasov, 1990). Nevertheless, CO_2 dominated vents have been reported for on-land systems in the region, such as the Yuzhno-Sakhalinsky Mud Volcano on Sakhalin Island (lying along the boundary between the Sea of Japan and the Sea of Okhotsk) which vents gases with a CO_2 content of 73-86 mol% (Shakirov et al., 2007). Thus it seems likely that additional vents with significant CO_2 contents (if not CO_2 dominated) might well be discovered along the Kurile Arc and/or in the sea of Okhotsk.

3.A.5.1 Kraternaya Bight, Yankich Island, Ushishir volcano, Central Kurile Arc

Type of Volcanic Activity:	**Subduction Related – Island Arc**
Depth of Venting:	**Very shallow water - gasohydrothermal system**
Type of CO_2 Venting:	**Gas phase, intermediate CO_2**

Kraternaya Bight has been extensively studied (see for example Tarasov et al., 1990; Zhirmunsky & Tarasov, 1990; Kamenev et al., 2004 and references therein, and the site description given in Glasby et al., 2006) and a brief overview is given below.

General Site Description

Ushishir is a partially submerged volcano now in the stage of solfatar activity[13] (Gavrilenko et al., 1989). The subaerial parts of the volcano form a group of three islands, known as the Ushishir Islands. Yankich Island is the circular caldera rim (~1.5km in diameter) that almost completely encloses Kraternaya Bight, a submerged caldera with a diameter of ~1 km and maximum depth of 63 m that is connected to the open ocean through a narrow and shallow straight (depth of 0.2-0.4m at low tide). The Kraternaya Bight is characterized by gasohydrothermal activity associated with fault zones.

In the southeastern part of the bight, boiling springs (92-96°C) occur in the intertidal zone with warm (40-60°C) vents at depths of 0-23m (Kamenev et al., 2004; Glasby et al., 2006). These fluids are strongly acidic (pH of 2–3.5) and contain high concentrations of H_2S (up to 340 μM), other reduced sulphur compounds, ammonia, silica (up to 3mM), phosphorus, and 2-3 orders of magnitude higher concentrations of Mn, Fe, Zn, Cu, Cd, Ni, and Cr than seawater (Kamenev et al., 2004; Glasby et al., 2006). In the northern part of the bight, and in the strait, there are numerous relatively cold (5-15°C), gasohydrothermal vents at depths of 1-15m (Kamenev et al., 2004; Glasby et al., 2006). The lower temperature of these vents most likely result from mixing with seawater and ground water. These vent fluids are also less acidic (pH of 6-7) and do not contain H_2S (Kamenev et al., 2004; Glasby et al., 2006).

The restricted communication between waters held in the bight and the open ocean means that the gasohydrothermal activity exerts a strong influence on the characteristics of the water column, as well as on both planktonic and benthic communities of marine organisms (Tarasov et al., 1990; Gamo and Glasby, 2003). The effects of the hydrothermal fluid inflow are reflected as distinctive peaks of CO_2, pH, and H_2S in the water column (Tarasov et al., 1990; Zhirmunsky & Tarasov, 1990), and the anomalously high concentrations of heavy metals in both the water column and bottom sediments (Shulkin, 1989, 1991).

Gas Venting

The major component of the vented gas is CO_2 (54-66%), with secondary N_2 (27-42%). The rate of gas venting has been measured at three vents at 12-30 L/hr (Namsarev et al., 1989). Thus a single vent at this location expels CO_2 at a rate of 2500-7750 mol/yr or 110-340 kg/yr.

Biota

Volcanic activity in Kraternaya Bight exerts a significant impact on the structure and specific composition of the biotic community, where the influx of gasohydrothermal vents into shallow waters results in a mixture of photosynthetic and chemosynthetic primary production, leading to complex metabolic and energy cycles (see for example Tarasov et al. 1985, 1986, 1990; Tarasov and Zhirmunskaya, 1989; Zhirmunsky & Tarasov, 1990).

The planktonic community is characterized by high rates of production and destruction of organic matter in the upper surface waters (0-5m). 'Red tides' occur due to the daily vertical migration of the ciliate *Mesodinium rubrum* harbouring a symbiotic microalgae, *Chroomonas* (Tarasov et al., 1990; Zhirmunsky & Tarasov, 1990). Bacterial, algobacterial and diatom mats occur in areas where hydrothermal fluids are seeping though the sloping crater floor as well as near gasohydrothermal vents (Tarasov et al., 1990). These mats were thought to serve as biogeochemical filters which transform the hydrothermal trace elements and reduced compounds into sedimentary organic matter. In particular, the 5 mm thick algobacterial mats have a multi-layered structure which includes many microorganisms (different kinds of sulfur oxidizing bacteria and thermophylic archaebacteria) and are characterized by extremely high rates of CO_2 fixation and organic matter production (up to 33.4 $gC/m^2/d$, Starynin et al., 1989).

---

[13] A volcanic area that gives off sulphurous gases and steam

Kraternaya Bight supports a rich and diverse macroflora and macrofauna, with high population density and biomass (Zhirmunsky & Tarasov, 1990). Over 200 species have been identified, including macro-algae (seaweeds), Porifera (sponges), Cnidaria (corals), Annelida (segmented worms - polychaetes), Arthropoda (crustaceans, barnacles), Mollusca (snails, bivalves), and Echinodermata (starfish, sea urchins, sea cucumbers) (Zhirmunsky & Tarasov, 1990). Seaweed biomass was high, reaching up to 30 kg wet/m^2 in the northern part of the bight that is not influenced by fluids with high H_2S (Zhirmunsky & Tarasov, 1990). In general, the macrofaunal community exhibits significant differences to that found outside the bight, where several species which are common in the bight do not occur outside the island or on other Kurile Islands – they have changed in morphology and adapted to the extreme conditions (Zhirmunsky & Tarasov, 1990). The intertidal zone was dominated by barnacles and gastropods. At depths of 2-5m, sea urchins predominated, forming dense aggregations of up to 1500 indivudals/m^2. The sea urchins were found to be only ~1/3rd the size of those from outside of the bight and lay in several layers. Zhirmunsky & Tarasov (1990) hypothesised that this may indicate a short lifecycle, most likely due to exposure to extreme conditions. They also noted that the polychaetes were generally smaller inside the bight compared to outside. At greater water depths, holuthurians (sea cucumbers) dominated, and colonies of solitary corals predominated on muds at depths of 15 to 30m, with population densities reaching 540 individuals/m^2. Bottom sediments were also inhabited by several bivalve molluscs, nematodes and other invertebrates.

A specific study on two bivalve molluscs within Kraternaya Bight examined their distribution in relation to the intensity and type of gasohydrothermal activity (Kamenev et al., 2004). The bivalve molluscs *Macoma golikovi* and *Macoma calcarea* are the dominant macrobenthos species of Kraternaya Bight, and inhabit all the zones of underwater volcanic activity. The studies conducted between 1987 and 1997 on the quantitative distribution of these species in four areas of the bight, which had different intensity, temperature and chemical composition of gasohydrothermal vents and seep fluids, showed that both species were most abundant in areas not directly influenced by volcanic activity, and formed settlements with lower densities in the area of the gasohydrothermal vents containing H_2S. In 1993 and 1995, population mortality was observed in the areas of H_2S containing gasohydrothermal vents and fluid seeps. In other areas of the bight, abundances decreased sharply suggesting a relationship to the gasohydrothermal activity of the volcano in those years. That maximal concentrations of the metals Fe, Zn, Cd, and Mn were observed in the tissues of both species in 1993 provides circumstantial evidence to support this suggestion.

Notes

At first sight the high influx of toxic gases such as H_2S and heavy metals suggests that this site would not provide a good analogue for leakage of CO_2 from a subseafloor storage site. Nevertheless, while the effect of high CO_2 on the biological community has not been specifically addressed, apparent differences regarding the impacts on biota between the H_2S containing (south east vents) and H_2S free (northern vents) vents may provide some information to assist in separating the effects of CO_2 and H_2S on biota in the immediate vicinity of the vents (note researchers report lower population densities of both macroalgae and molluscs in regions of vents containing H_2S, but not those containing high CO_2 and low/no H_2S).

This shallow water semi enclosed system provides an interesting comparison to the deep water enclosed system of Vailulu'u – which exhibits high mortality in the region of CO_2 vents ('moat of death'). That this system supports a diverse and rich macrofauna is intriguing. In this system exchange of bight water is tidal (irregular semi-diurnal tides) – on average 700,000 m^3 of seawater (2.5 to 3.5°C) flows into the bight at high tide with the same volume flowing out at low tide (warmed to 9 to 12°C), and the influx of hydrothermal fluids has been estimated to be ~20,000 m^3/day (Zhirmunsky & Tarasov, 1990). It is a shallow system, therefore saturation concentrations for CO_2 are lower than at high pressure, and exchange with atmosphere (loss to atmosphere) will occur.

Note also the apparently periodic high mortality events in response to increased hydrothermal activity. i.e. population health is strongly dependent not only on the input of toxic compounds, but the balance between the input rate of toxic compounds versus the flushing rate of system.

In this system, the ‘normal’ state is a healthy population (adapted to given conditions), where increased hydrothermal activity at a constant flushing rate leads to decreased health.

Kurile Island References

Gaedicke, C., Baranov, B.V., Obzhirov, A.I., Lelikov, E.P., Belykh, I.N., Basov, E.I. (1997). Seismic stratigraphy, BSR distribution, and venting of methane-rich fluids west off Paramushir and Onekotan Islands, northern Kurils. *Marine Geology,* **136:** 259-276.

Gamo, T., Glasby, G.P., (2003). Submarine hydrothermal activity in coastal zones. In: Taneguchi, M.,Wang, K., Gamo, T. (Eds.), Land and Sea Hydrogeology. Elsevier, Amsterdam, pp. 151–163.

Gavrilenko, G.M., Bondarenko, V.I., Sazonov, A.P., 1989. Marine volcanological explorations at Kraternaya Bay. Mar. Biol. 3, 19–28 (In Russian). Cited in Glasby et al. (2006). Also cited as Marine volcanological research in Kraternaya Bight (Kurile Islands). Biologiya Morya 3: 19-28 in Zhirmunsky & Tarasov (1990)

Glasby G.P. Cherkashov G.A. Gavrilenko G.M. Rashidov V.A. Slovtsov I.B. (2006). Submarine hydrothermal activity and mineralization on the Kurile and western Aleutian island arcs, N.W. Pacific. *Marine Geology*, **231:** 163-180.

Kamenev G.M., Kavun, V.Y., Tarasov, V.G., Fadeev, V.I., (2004). Distribution of bivalve mollusks Macoma golikovi Scarlato and Kafanov, 1988 and Macoma calcarea (Gmelin, 1791) in the shallow-water hydrothermal ecosystem of Kraternaya Bight (Yankich Island, Kuril Islands): connection with feeding type and hydrothermal activity of Ushishir Volcano. *Continental Shelf Research*, **24:** 75–95.

Namsarev, B.B., Karnachuk, O.V., Borzenkov, I.A., Starynin, D.A. (1989). Microbiological processes in the bottom sediments of Kraternaya Bight. *Biologiya Morya*, **3:** 52-58 (in Russian). Cited in Zhirmunsky & Tarasov (1990).

Sahling, H., Galkin, S.V., Salyuk, A., Greinert, J., Foerstel, H., Piepenburg, D., Suess, E., (2003). Depth-related structure and ecological significance of cold-seep communities - a case study from the Sea of Okhotsk. *Deep-Sea Research,* 50: 1391-1409.

Shakirov, R., Obzhirov, A., Tsunogai, U., Biebow, N., (2007). Geological types of methane emission on the Sakhalin Island and Sea of Okhotsk. Proceedings of the International Symposium Asian Collaboration in IPY 2007-2008. 1st March 2007, Tokyo, Japan. Paper 54 (pages 155-158).

Shulkin, V.M., (1989). Geochemistry of metals in the Kraternaya Bight ecosystem. *Biologiya Morya*, **3:** 29-36 (in Russian). Cited in Kamenev et al. (2004).

Shulkin, V.M., (1991). Bio-geochemistry of metals in Kraternaya Bight. In: Zhirmunsky, A.V., Tarasov, V.G. (Eds.), Shallow-Water Hydrothermal Vents and the Ecosystem of Kraternaya Bight (Ushishir Volcano, Kurile Islands). Book I. Functional characteristics. Part I. Far East Branch USSR Academy of Sciences, Vladivostok, pp. 75–96 (in Russian). Cited in Kamenev et al. (2004).

Starynin D.A., Gorlenko V M Ivanov M V Karnachuk O V Namsarev B B (1989). Algobacterial mats of Kraternaya Bight. *Biologiya Morya,* **3:** 70-76. In Russian. Cited in Zhirmunsky & Tarasov (1990)

Tarasov, V.G., Propp, M.V., Propp, L.N., Kamenev, G.M., Blinov, S.V., 1985. Shallow-water hydrothermal vents and a unique ecosystem of Kraternaya Caldera (Kurile Islands). DVNC AN SSSR, Vladivostok, 29pp (in Russian).

Tarasov, V.G., Propp, M.V., Propp, L.N., Blinov, S.V., Kamenev, G.M., 1986. Shallow-water hydrothermal vents and a unique ecosystem of Kraternaya Caldera, Kurile Islands. Biologiya Morya (Marine Biology) 2, 72–74 (in Russian).

Tarasov, V.G., Propp, M.V., Propp, L.N., Zhirmunsky, A.V., Namsaraev, B.B., Gorlenko, V.M., Starynin, D.A., 1990. Shallow-water gasohydrothermal vents of Ushishir Volcano and the ecosystem of Kraternaya Bight (The Kurile Islands). Marine Ecology, 11, 1–23.

Zhirmunsky A V & Tarasov V G (1990). Unusual marine ecosystem in the flooded crater of Ushisher volcano. *Marine Ecology Progress Series*, 65: 95-102.

Zonenshayn, L.P., Murdmaa, I.O., Baranov, B.V., Kuznetsov, A.P., Kuzin, V.S., Kuz'min, M.I., Avdeyko, G.P., Stunzhas, P.A., Lukashin, V.N., Barash, M.S., Valyashko, G.M., Demina, L.L., (1987). An underwater gas source in the Sea of Okhotsk west of Paramushir island. *Oceanology*, **27:** 598–602.

3.A.5.2 Wakamiko Caldera, Kagoshima Bay, Kyushu, Japan

Type of Volcanic Activity:	**Subduction Related – Island Arc**
Depth of Venting:	**Shallow water - gasohydrothermal system**
Type of CO_2 Venting:	**Gas phase, CO_2 dominant**

Gasohydrothermal venting has been recorded in the shallow waters of Kagoshima Bay, located at the southern tip of Kyushu (Ossaka et al., 1992). Numerous studies of this site have been made (note some of the findings are published in Japanese), and a brief summary of available information is given below.

General Site Description

The submarine Wakamiko caldera is situated on the northeastern foot of the Sakurajima volcano, in northern Kagoshima Bay, Kyushu. Sakurajima is one of the most active volcanoes in Japan where the main magma chamber is located beneath the Wakamiko caldera (Takahashi, 1997; Yamanaka et al., 1999).

The flat caldera floor lies at approximately 200 m water depth and is covered by layers of recent sediments up to 80 m thick composed mainly of pyroclastics with a small amount of plant remains (Yamanaka et al., 1999, 2000). Hydrothermal petroleum generation resulting from pyrolysis of organic matter in caldera floor sediments has been reported (Yamanaka et al., 1999; Yamanaka et al., 2000).

Extensive fumarolic activity (gas venting) occurs both across the caldera floor (25 to >200°C) and at the summit of a shallow knoll like structure (25-30°C) that rises to a depth of ~80 m on the eastern edge of the caldera floor (Ossaka et al., 1992; Yamanaka et al., 2000; Yamanaka et al., 2001; Miura et al., 2002). Shimmering fluids have been observed around the vents on the caldera floor, where fluid chemistry suggests hydrothermal circulation is occurring in the subsurface (Yamanaka et al., 2001) and hydrothermal minerals such as gypsum, carbonate, native sulphur, barite, kaolinite, and sulphides rich in Fe, Hg, As and Sb are also present in the sediments and in veins near vent outlets (Nedachi et al., 1991; Sakamoto, 1985; Sakamoto et al., 1997). However, the chemistry of waters collected from the knoll site suggest hydrothermal fluid flow is not occurring at this location (Yamanaka et al., 2001).

Bottom water stratification develops within the caldera during the summer months due to restricted circulation and the pH and dissolved oxygen level of waters below 150 m decreases (pH=6.5, DO<0.5 ml/l) due to the input of acidic and anoxic gas and hydrothermal fluids (Kamata et al., 1978).

Gas Venting

Extensive gas venting occurs on the caldera floor, where vents appear to be concentrated in the north-western quadrant within an area some 2 km by 2km (see Figure 1 in Ossaka et al., 1992).

At the knoll site gas venting occurs to the south east of the knoll summit. Vigorous venting is restricted to an area some 50 m by 25 m which is characterised by coarse sandy bottom sediments and exposed rocks (see Figure 1 in Miura et al., 2002). Individual and groups of weaker vents also extend to the north and south east of this region covering a total field area of ~100m by 100m.

Volcanic gases were collected in 1977, 1978, 1990 and 1991 at the caldera floor and in 1977 and 1978 at the knoll (Ossaka et al., 1992). The reported composition of the gas is uniform between the sites and over time, and is thought to be sourced from the Sakurajima magma chamber (Ossaka et al., 1992). The gas is dominantly CO_2 (caldera floor = 77.2-92.6 mol%; knoll = 80.6-84.3 mol%), with minor CH_4 (caldera floor = 4.9-19.9 mol%; knoll = 12.5-15.3 mol%) and N_2 (caldera floor = 1.7-7.4 mol%; knoll = 2.6-4.0 mol%) and a small amount of H_2S (caldera floor = 0.15-1.37 mol%; knoll = 0.07-0.47 mol%) (Ossaka et al., 1992).

Gases were also sampled from both sites in the period 1995-1998, however to the authors knowledge only the sulphur isotopic values have been reported (Miura et al., 2002).

Biota

Due to the restricted circulation and depletion of oxygen in summer months there are no ‘remarkable’ megabenthos associated with the caldera floor vent sites (Miura et al., 2002).

In contrast the shallow knoll site supports a chemosynthetic community, including sulphate reducing bacteria, sulphur oxidizing bacteria, numerous clusters of tubeworms and other fauna such as a solemyid bivalve with a symbiotic polychaete (Hashimoto et al., 1993; Miura & Hashimoto, 1996; Miura et al., 1997; Miura et al., 2002).

The tubeworm clusters occur at depths of 80-110m in the region of weak venting to the north and south-east of the vigorous gas seep area, where most clusters contain a single or a few small gas seeps (Miura et al., 2002). Solitary worms were also observed within the region of vigorous venting (Miura et al., 2002). The absence of hydrothermal circulation and sulphur isotope analysis suggests that the tube-worms depend on biogenic sulphide derived from bacterial sulphate reduction, possibly using fumarolic methane as an electron donor, implying a life style comparable with that of communities at cold water methane seeps (Yamanaka et al., 2001; Miura et al., 2002).

Notes

The presence of a ‘seep’ type tube worm community in close proximity to CO_2 dominant gas vents is of significant interest. The CH_4 content of the vent gases is quite low – at 5-20 mol%. It is feasible that ‘leaked’ CO2 could have a CH4 content of this order under certain circumstances (potentially leakage from an EGR project) – suggesting the potential for leakage to result in the development of a chemosynthetic community.

Kagoshima Bay References

Hashimoto, J., Miura, T., Fujikura, K. & Osaka, J., (1993). Discovery of vestimentiferan tube-worms in euphotic zone. *Zoological Science,* **10:** 1063-1067.

Horibe, Y., Gamo, T., Baba, Y., (1980). Estimation of carbon dioxide flux from submarine volcano in Kagoshima Bay, Japan. In: Goldberg, E.D., Horibe, Y., Saruhashi, K. (eds.), Isotope Marine Chemistry. Uchida Rokaakuho Publishing Co. Ltd, Tokyo, pp. 327-337.

Kamata M., Yonehara N., Sakamoto H., Ohnishi T., (1978). Distribution of the trace elements and the circulation process of sea water in the inner bay sea water-an example at the Kagoshima Bay. In: Takahashi, A. (Ed.) Collected Reports of Special Project Research ``Preservation of Marine Environment", pp. 49-54 (in Japanese).

Miura, T. & Hashimoto, J., (1996). Nautiliniellid polychaetes living in the mantle cavity of bivalve mollusks from cold seeps and hydrothermal vents around Japan. *Publication of Seto Marine Biological Laboratory,* **37:** 257-274. Cited in Miura et al. (2002).

Miura, T., Nedachi, M., Hashimoto, J., (2002). Sulphur sources for chemoautotrophic nutrition of shallow water vestimentiferan tubeworms in Kagoshima Bay. *Journal of Marine Biological Association of the UK*, **82:** 537-540.

Nedachi, M., Ueno, H., Oki, K., Shiga, Y., Hayasaka, S., Ossaka, J., Nogami, K., Ito, N., Hashimoto, J., (1991). Sulfide veinlets and the surrounding marine sediments in the fumarole area in the Wakamiko Caldera, northern Kagoshima Bay. *JAMSTEC Journal of Deep Sea Research,* **7:** 235-243. (In Japanese with English Abstract.)

Ossaka, J., Hirabayashi, J., Ozawa, T., Onishi, T., Sakamoto, H., (1977). Study of the submarine volcanic activity, in the northern area of Sakurajima. Tokyo Institute of Technology, Tokyo (in Japanese).

Ossaka, J., Hirabayashi, J., Nogami, K., Kurosaki, M. & Hashimoto, J., (1992). Variation of chemical composition of volcanic gases from the northern part of Kagoshima Bay. *JAMSTEC Journal of Deep Sea Research,* **8:** 75-80. (In Japanese with English Abstract.)

Sakamoto, H., (1985). The distribution of mercury, arsenic, and antimony in sediments of Kagoshima Bay. *Bulletin of the Chemical Society of Japan,* **58:** 580-587.

Sakamoto, H., Tomiyasu, T., Yonehara, N., (1997). The contents and distributions of copper, zinc, cadmium and lead in sediments of Kagoshima Bay. Reports of the Faculty of Science, Kagoshima University, *Earth and Planetary Sciences,* **30:** 71-83.

Takahashi, M., (1997). The structure of high level crustal magmatic plumbing systems beneath the Quaternary arc volcanoes in Japanese Islands. *Kazan,* **42:** S175-S187, (in Japanese with English abstract).

Yamanaka, T., Mizota, C., Murae, T., Hashimoto, J., (1999). A currently forming petroleum associated with hydrothermal mineralization in a submarine caldera, Kagoshima Bay, Japan. *Geochemical Journal,* **33:** 355-367.

Yamanaka, T., Ishibashi, J., Hashimoto, J., (2000). Organic geochemistry of hydrothermal petroleum generated in the submarine Wakamiko caldera, southern Kyushu, Japan. *Organic Geochemistry,* **31**: 1117-1132.

Yamanaka, T., Ishibashi, J., Nakano, A., Ueki, Y., Hashimoto, J., (2001). Geochemical study of seafloor hydrothermal system and chemosynthetic animal community around a submarine caldera, southern part of Kagoshima Bay, southern Kyushu, Japan. *JAMSTEC Journal of Deep Sea Research,* **19:** 9-14.

3.A.6 The Western Pacific Margin II: Papua New Guinea & New Zealand

3.A.6.1 Luise Harbour, Lihir Island, Papua New Guinea

Type of Volcanic Activity:	**Subduction Related – Island Arc**
Depth of Venting:	**Very shallow water - gasohydrothermal system**
Type of CO_2 Venting:	**Gas phase, CO_2 dominant**

Gasohydrothermal venting in the shallow waters of Luise Harbour, Lihir Island, has been described by Pichler et al. (1999) and Pichler & Humphrey (2001), with a focus on mineral precipitation as a result of seawater-gas-sediment interaction. The principal characteristics of this site are described briefly below and unless otherwise stated, all information below is attributed to these papers.

General Site Description

Luise Harbour lies on the eastern shore of Lihir, one the islands in the Tabar-Feni island chain. Lihir itself comprises the remnants of 3 Pliocene to Holocene volcanoes, Kinami, Huniho and Luise (Wallace et al., 1983).

Several geothermal areas are located within the caldera of Luise volcano, including hot mud pools, chloride and acid sulphate water springs, and low temperature fumaroles with temperatures of 39-99C and pH of 1.6 to 2.8 (Wallace et al., 1983). Submarine gasohydrothermal vents are located in shallow water (3-10 m) approximately 100m offshore along the north side of Luise Harbour within an area of ~5,000 m^2, where venting occurs through fine to medium sized volcanoclastic sand. Venting is dominated by gas discharge.

Two types of venting have been observed: (1) six focused gas vents were found, with vigorous discharge of gas and possible associated minor discharge of clear fluid (inferred from shimmering observed above vent orifices) through vent ports 20-50cm in diameter, with temperatures at port outlets of 60-96°C. At these sites of focused gas exhalation the point of discharge was marked by small conical pockmarks in the sandy bottom and sediments were cemented due to hydrothermal precipitation; (2) dispersed discharge of gas bubbles emanating through the sandy bottom throughout the hydrothermal area with less vigorous flow rates and without the formation of a vent orifice (e.g. pockmarks were not present) or hydrothermal precipitation.

Hydrothermal fluid discharge (it is occurs) was too weak to sample. Dominant precipitates at the focused vent ports are Fe sulphides and dolomite, with smectites, chlorite and Ca-sulphate also present. Fe sulphides form 1-2 cm thick colloform bands (1-2 cm) and coat and or replace primary volcaniclastic sediment grains. Dolomite forms as cement in pore spaces and as massive veinlets that crosscut already cemented sediment. These minerals precipitate 10-20cm below the seafloor and form layers up to 10cm thick that extends around discharge sites for several m.

Two gas samples were collected from the submarine vents and were comprised dominantly of CO_2 (94.9-97.5 mol%), with minor H_2S (0.32-1.28 mol%), CH_4 (0.24-0.67 mol%), O_2 (0.34-0.59 mol%) and N_2 (1.57-2.41).

Notes

This site may represent a particularly good target for studies of the impact of CO_2 gas venting on local ecosystems. Note the absence of significant hydrothermal fluid flow, that precipitation of hydrothermal minerals is restricted to the shallow sub surface, and very high (~95-98%) CO_2 contents of the gas.

Pichler et al. (1999) note that O_2 and (part of) N_2 may be (i) inherent component of gas (ii) dissolved air stripped from seawater (iii) introduced during sampling.

References

Pichler, T., Humphrey, J.D., (2001). Formation of dolomite in recent island-arc sediments due to gas-seawater-sediment interaction. *Journal of Sedimentary Research*, 71: 394-399.

Pichler, T., Giggenbach, W.F., McInnes, B.I.A., Buhl, D., Duck, B., (1999). Fe sulfide formation due to seawater-gas-sediment interaction in a shallow-water hydrothermal systems at Lihir Island, Paua New Guinea. *Economic Geology*, 94: 281-288.

Supporting References

Wallace, D.A., Johnson, R.W., Chappell, B.W., Arculus, R.J., Perfit, M.R., Crick, I.H., (1983). Cainozoic volcanism of the Tabar, Lihir, Tanga, and Feni islands, Papua New Guinea: geology, whole-rock analyses, and rock-forming mineral compositions. *Sydney, Bureau of Mineral Resources Geology and Geophysics*. 62 p.

3.A.6.2 Tutum Bay, Ambitle Island, Papua New Guinea

Type of Volcanic Activity:	**Subduction Related – Island Arc**
Depth of Venting:	**Very shallow water - gasohydrothermal system**
Type of CO_2 Venting:	**Gas phase, CO_2 dominant**

Gasohydrothermal venting in the shallow waters of Tutum Bay (see notes), Ambitle Island, has been described by Pichler & Dix (1996) and Pichler et al., (1999), and unless otherwise stated, all information below is attributed to these papers. In addition, Pichler (2005) examines the source of the hydrothermal fluids in more detail, and Price & Pichler (2005) examine the biogeochemical cycling and bioavailability of vent sourced arsenic in Tutum Bay.

General Site Description

Tutum Bay lies on the south west margin of Ambitle Island, one of the Feni islands in the southernmost island group of the Tabar-Feni island chain. The island is part of a Quaternary stratovolcano with a central eroded caldera built on Oligocene marine limestone (Wallace et al., 1983).

Several geothermal areas are located along the western coast of Ambitle island, and gasohydrothermal venting also occurs in shallow waters (5-10 m) of the near shore region. The submarine vents lie on the inner shelf along a fault that intersects several of the on land geothermal areas within a patchy distribution of coral-algal reefs surrounded by medium to coarse grained mixed carbonate-volcanoclastic sand and gravel.

Two types of venting have been observed: (1) focused discharge of a clear two phase (boiling) fluid from discrete ports 1-15 cm in diameter, were phase separation occurs at the seafloor; (2) dispersed discharge of gas bubble streams that issue from the sandy to pebbly gravel sediments and through fractures in rocks.

Fluid venting at Tutum Bay is the result of subsurface heating of meteoric water (Pichler & Dix, 2006; Pichler et al., 1999; Pichler, 2005). Temperatures at vent outlets are 89-98°C, with estimated flow rates up to 300-400 L/min. The gas (steam) phase condenses within 2 to 3 m above the vent orifices, while shimmering extends for several metres from the seafloor. Four locations of focused venting were found. At three of the sites (2 single vents, and an assemblage of 3 vents within a small area) fluids exit at high flow rates through ports that are 10-15 cm in diameter. The fourth site is located to the north of the other vents and lies within an area of massive gas emanation. This site is characterised by a cluster of smaller vents within an area 1m by 3m that discharge fluids at lower flow rates through ports that are 1-5 cm in diameter.

Sampled vent fluids represent a mixture of hydrothermal fluid and seawater, where entrainment of seawater may happen in the shallow seafloor subsurface or during sampling. Vent waters are depleted in sulphate, Br, Cl, Na, K, Mg, Ca, Sr (slightly) and enriched in CO_2 (as bicarbonate - HCO_3^-), Si, Li, Rb, Cs, Fe, Mn, Sb, As and Tl with respect to ambient seawater.

Hydrothermal precipitates accumulate in areas surrounding the fluid vents and do not form chimney structures. The dominant precipitates are aragonite, and crusts of Fe-oxyhydroxides interlaminated with ferroan calcite ($(Ca,Fe)CO_3$), where isotope signatures suggest possible contribution of hydrothermal CO_2 to these cements.

Gas Venting

Gas venting in this area appears to be itinerant – with shifts in the location of gas stream outlets on the order of tens of cm, likely due to tortuous migration paths through surface sediments (Pichler et al., 1999).

Gas samples were collected into 600ml bottles via an inverted funnel placed over the vent outlets. The sampled gas was composed dominantly of CO_2 (92.6-97.9 mol%) with minor N_2 (2.2-4.7 mol%), O_2 (0.43-0.73 mol%), CH_4 (0.6-2 mol%) and He (~0.01-0.02 mol%). The gas has a magmatic/mantle origin with a minor contribution from subducted sediment (Pichler et al., 1999).

Pichler et al. (1999) also report an estimate of the total CO_2 gas flux from Tutum Bay of 100 L/s. Although raw data from which this estimate has been derived were not provided, it is stated that over 100 flux measurements were carried out by timing the replacement of a known volume of water from a graded cylinder – indicating that this is a comparatively robust estimate. As all measurements were normalised to 1 bar (Pichler et al., 1999), this flux is equivalent to ~200 gCO_2/s, ~17 tCO_2/day, or 6.2 $ktCO_2$/yr. Examination of Figure 2 in Pichler et al. (1999) shows gaseous discharge extending over an area some 50-75m by 100m, indicating an average flux of ~0.8-1.2 tCO_2/m^2/yr, although it is noted that the number of gas streams per unit area is not uniform within this field.

Biota

Pichler & Dix (1996) note that the Ambitle island gasohydrothermal vent site offers a natural laboratory to evaluate short and long term adaptation and/or mortality of biota in a tropical coral reef system due to changes in temperature, salinity or carbonate saturation state.

While dead coral colonies were observed in the immediate vicinity of the fluid vents, where hydrothermal precipitates accumulated on the dead corals, in general the diversity and health of the coral reef was found to be indiscernible from reefs that are not exposed to hydrothermal discharge (Pichler et al., 1999; Price & Pichler, 2005). The main focus of studies addressing input of toxic chemicals to this system has been an evaluation of the bioavailability of arsenic, where it was found that despite the amount of As released into the bay, corals, clams and fish do not show any direct response to the elevated values (Pichler et al., 1999; Price & Pichler, 2005). Indeed, fish were observed to hover over vent orifices, apparently bathing in the hydrothermal fluid (Price & Pichler, 2005).

Notes

Note Pichler & Dix (1996) refer to this site as Waramung Bay and location map shows slightly different position (to the south west) to that given in Pichler et al. (1999). However, both papers are discussing the same site.

Unlike restricted flow systems (e.g. Vailulu'u (Samoan hotspot); Kraternaya Bight (Kuriles); Matupi Harbour (New Britain Island)), this more open site exhibits little impact of gasohydrothermal venting on the local biota. See also D. Joao de Castro Seamount, (Azores).

References

Pichler, T., (2005). Stable and radiogenic isotopes as tracers for the origin, mixing and subsurface history of fluids in submarine shallow-water hydrothermal systems. *Journal of Volcanology and Geothermal Research*, 139: 211 – 226

Pichler, T., Dix, G.R., (1996). Hydrothermal venting within a coral reef ecosystem, Ambitle Island, Papua New Guinea. *Geology*, 24: 435-438.

Pichler, T., Pichler, T., Veizer, J., Hall, G.E.M., (1999). The chemical composition of shallow-water hydrothermal fluids in Tutum Bay, Ambitle Island, Papua New Guinea and their effect on ambient seawater. *Marine Chemistry*, 64: 229–252.

Price, R.E, Pichler, T., (2005). Distribution, speciation and bioavailability of arsenic in a shallow-water submarine hydrothermal system, Tutum Bay, Ambitle Island, PNG. *Chemical Geology*, 224: 122–135.

Supporting References

Wallace, D.A., Johnson, R.W., Chappell, B.W., Arculus, R.J., Perfit, M.R., Crick, I.H., (1983). Cainozoic volcanism of the Tabar, Lihir, Tanga, and Feni islands, Papua New Guinea: geology,

whole-rock analyses, and rock-forming mineral compositions. *Sydney, Bureau of Mineral Resources Geology and Geophysics*. 62 p.

3.A.6.3 Matupi Harbour, Rabaul Caldera, New Britain Island, Papua New Guinea

Type of Volcanic Activity:	**Subduction Related – Island Arc**
Depth of Venting:	**Very shallow water - gasohydrothermal system**
Type of CO_2 Venting:	**Gas phase, CO_2 dominant**

Gasohydrothermal venting in Matupi Harbour was first described by Obzhirov (1992), with further site details and an analysis of the effect of shallow water venting on the local biota presented by Tarasov et al., (1999). A brief summary is given below.

General Site Description

The Rabaul caldera is located on the northern most point of New Britain Island, where the island separates the Manus Basin in the North from the New Britain Trench in the south. The caldera forms Blanche Bay, a large elliptical, semi-isolated bay that opens in the south-east to the Bismark Sea. The bay is surrounded by subaerial volcanoes, including the recently active Rabalankaia, Tavurvur, and Vulcan volcanoes (see notes). Matupi Harbour lies in the north-eastern part of Blanche Bay and is a relatively sheltered basin of about 4 km^2 with a maximum depth of 65 m. The minimum depth in the southern part, where the harbour opens to the bay, is 24 m.

In 1990 an expedition mapped and sampled hydrothermal vent sites in Matupi Harbour (e.g. Tarasov et al., 1999). Gasohydrothermal fields were identified by visual observations of bubble release, and by temperature measurements of water and bottom sediments. At this time (see notes) intensive shallow-water (littoral and sublittoral zones) gasohydrothermal activity occurred within three distinct areas, two along the eastern shore of the harbour (Sites I and II, western slope of Tavurvur) and the third on the northern shore (Site III, southern slope of Rabalankaia) (Obzhirov, 1992; Tarasov et al., 1999).

Site I (Tavurvur) was characterised by seepage of hot volcanic fluids and the absence of gas venting at sublittoral depths (Tarasov et al., 1999). At Site II (Tavurvur) numerous gasohydrothermal vents and seeps with temperatures of 50-60°C were located on a steep slope in water depths of 1-10 m and covered an area of ~500 m^2. Venting occurs through the sandy gravely seafloor with intensive venting through lava blocks. Site III (Rabalankaia) was characterised by hotter vents with temperatures of 80-90°C that extended from the littoral zone to 27 m water depth and covered an area of ~1000 m^2. At 27 m depth hot fluids emanated from hard Fe-Mn conical structures up to 50cm high (chimneys) that were built on top of ring-like structures of loose yellow-green sediment some 1 m in diameter and 20-30 cm high. Sediment temperatures at all vent sites were 60-90°C.

Vent fluids had low pH (Tavurvur = 3.56; Rabalankaia = 6.1-7.25) and were enriched in dissolved gases and nutrients (CO_2, CH_4, H_2, H_2S, NH_4^+, SiO_3^{2-}) and metals with respect to ambient seawater, with metal enrichments of 2-5 fold for Fe and Mn, 2-10 fold for Cu, 5-20 fold for Pb and Cd, and 2-1000 fold for Zn (Tarasov et al., 1999). The highest concentrations of metals and sulphides were observed around Tavurvur volcano, with lower concentrations in the less acidic vent waters of Rabalankaia (Tarasov et al., 1999).

These emissions alter the chemical composition of the waters in Matupi Harbour, resulting in acidification and increased content of carbonic acid, silicate, ammonium and particulate matter, where the effect is most marked in near-bottom layers and in surface waters (0-3m; due to low density of warm fluids with respect to ambient seawater) in the vicinity of the gasohydrothermal vents (Tarasov et al., 1999).

Gas Venting

Gas samples in the sublittoral zone were collected (by SCUBA divers) into air-tight dark glass bottles using an inverted funnel placed over the vent outlet and analysed using gas chromatography (Obzhirov, 1992; Tarasov et al., 1999)).

At Site II (Tavurvur) samples were taken at depths of 2 to 9 m and consisted of CO_2 (62.3-88.4 mol%), with minor N_2 (9.5-28.8 mol%), O_2 (1.8-2.8 mol%), H_2S (0-7.0 mol%), H_2 (0.0006-0.0340 mol%) and CH_4 (0.007-0.010 mol%). At site III (Rabalankaia) samples were taken at depths of 7 and 27m, and consisted of CO_2 (82.7-86.5 mol%), N_2 (11.7-14.1 mol%), O_2 (1.5-2.9 mol%), H_2 (0.1430-0.1543 mol%) and CH_4 (0.040-0.045 mol%), with no H_2S present in these gases. The composition of vent gases at these sites reflected that of gases discharged at on-land fumaroles of the Tavurvur and Rabalankaia volcanoes, which are broadly similar, but with elevated CH_4 and decreased H_2S at Rabalankaia vents. High concentrations of CO_2 were also observed in near bottom waters, with an average CO_2 content in the range 0.16 to 0.36 ml/L, reaching up to 5.5 ml/L in the region of gas discharge.

Biota

Tarasov et al. (1999) provide a detailed analysis and discussion of the biota of Matupi Harbour. A brief summary of the main findings is given below and the reader is referred to this paper for further information.

Hydrothermal activity exerts a major effect on the composition of planktonic communities in Matupi Habour, which exhibit high numbers of cyanobacteria, sulphur bacteria and planktonic amoebas, particularly in the surface water layer over the gasohydrothermal fields.

Primary production in the centre of the Harbour was 1.63 $gC/m^2/d$, decreasing by over an order of magnitude in the vicinity of active venting to 0.03-0.13 $gC/m^2/d$. On the basis of chlorophyll a concentrations, the waters of Matupi Habour correspond to typical mesotrophic waters. The highest values of photosynthesis were an order of magnitude higher than that typically observed in the sublittoral zone around coral reef islands and were likely stimulated by high input of nutrients from the hydrothermal fluids. Chemosynthesis varied from 15 to 60% of primary production, with the highest values found in the surface and near-bottom layers. The highest values of bacterial production were recorded in the area of the Tavurvur gasohydrothermal vents: exceeding 216 $mgC/m^3/d$ (wet weight) at 14 m depth.

Despite the high values of primary production and a high ratio of conversion to biomass, the zooplankton community, dominated by cyclopoid copepods, was poor in species. The densest populations were found in the subsurface water layer in the vicinity of the vent fields.

Bacterial mats on the seafloor were observed only at the gasohydrothermal vent field of Tavurvur volcano (Site II). Here white bacterial mats were abundant in the littoral and sublittoral zones to water depths of 8-10 m. At depths of 0-1 m, the mats were ~0.5 cm thick, and were dominated by the filamentous colourless sulphur bacteria *Thiodendron* sp., with abundant *Thiovulum* sp. and *Beggiatoa* sp. At depths of 4-6 m, where volcanic gases and hydrothermal fluids were seeping intensively through the sediment, the mats were slightly thicker at 1-1.5 cm thick, and built mainly of *Thiodendron* sp, with common *Thiovulum* sp. and *Beggiatoa* sp., and numerous filamentous cyanobacteria present in the upper layers.

As at other shallow water hydrothermal vent sites, there was an absence of vent obligate fauna. Rather the principal effect of hydrothermalism was on species diversity, abundance, and distribution.

In general, vent sites had poor meiofauna and were almost devoid of macrofauna. However, the periphery of the vent fields were characterised by the richest (high density and diversity) benthic communities found in Matupi Harbour, where these communities were significantly different in composition to those in areas of Blanche Bay less exposed to volcanic fluids and gases.

In Blanche Bay outside Matupi Habour benthic communities had the usual structure for tropical inter-reef areas with loose substratum, sufficient light and tidal currents, and were dominated by solitary corals (e.g. *Fungia*, *Diaseris*, *Cycloseris* and other fungiids) with a low density of colonies growing on patches of hard substratum. In Matupi Harbour normal coral reefs were found only near the mouth of Blanche Bay.

High sediment temperature was a major factor limiting the distribution of benthic organisms within the vent fields. The usual infauna in Matupi Habour was dominated by nematodes, harpacticoid copepods and ostracods (80-90% of total). In contrast, zones of high sediment temperature in the hydrothermal vent fields were dominated by spinoid polychaetes (*Polydora* sp. - up to 2000 individuals/m^2 and 90% of total infauna at Site II) or a single oncholaimid nematode species (up to 131,000 indivudals/m^2 and 100% of total infauna at Site III), and epi-fauna were generally absent or low in abundance. Small mobile crabs were observed, forming small aggregations around the bacterial mats at Site II. Nassariid gastropods were also quite abundant at Site II (*Nassarius* sp.: 13 individuals/m^2)

The periphery of the vents were characterised by a rich fauna dominated by corals (52 species; 30 genera) and sponges, most of which were not found in the area outside Matupi Harbour. The large input of suspended particulate matter to the water column was one of the principal factors controlling the distribution of corals and other epifauna. Light penetration was also reduced by the hot and opaque hydrothermal fluid. As a result, coral species typically found at greater depth (lower light conditions) were present in shallow waters – for example the black coral *Antipathes* sp. was recorded at 3-5 m. At Site II, a scleractinian coral community was found at 3-10 m water depth where bubbling of gas through the coral structures was observed and coral growth was inhibited by ferrous silt covering the surface of the colonies. A diverse coral community was also found at water depths of 0.5-15 m on the steep slope in the eastern part of Site III. In regions were intensive venting occurred through the coral population the colonies were small and undeveloped with some parts dead. Bivalves, feather stars, sponges and anemones with symbiotic fish were also present. At depths of 15-20m corals were present, however the majority of the colonies had been killed by heavy sedimentation. The epifauna was most abundant in the Rabalankaia vent field at depths of 25-27 m, where the biomass of sponges and ascidians (sea squirts) on the ring structures reached 1 kg/m^2. It was hypothesised that the growth of the sponges (siliceous skeleton) may have been stimulated by volcanic solutions enriched in silicon

Notes

Tavurvur and Vulcan have erupted since the 1990 expedition. Both volcanoes erupted in 1994, with continued activity at Tavurvur (see eruption history at the Global Volcanism Program: http://www.volcano.si.edu/world/volcano.cfm?vnum=0502-14=&volpage=erupt).

Gas sampling and composition first reported by Obzhirov, A.L., (1992) and data given in Table 3.1, Chapter 3 is cited to this reference. However, note that a more detailed description of the vent sites including location, depth and temperature, are given in Tarasov et al. (1999).

References

Obzhirov, A.L., (1992). Chemistry of free and dissolved gases of Matupi Bay, Rabaul caldera, Papua New Guinea. *Geo-Marine Letters*, 12: 54-59.

Tarasov, V.G., Gebruk, A.V., Shulkin, V.M., Kamenev, G.M., Fadeev, V.I., Kosmynin, V.N., Malakhov, V.V., Starynin, D.A., Obzhirov, A.I., (1999). Effect of shallow-water hydrothermal venting on the biota of Matupi Harbour (Rabaul Caldera,New Britain Island, Papua New Guinea). *Continental Shelf Research*, 19: 79-116.

3.A.6.4 Bay of Plenty, North Island, New Zealand

Type of Volcanic Activity:	**Subduction Related**
Depth of Venting:	**Shallow water - gasohydrothermal system**
Type of CO_2 Venting:	**Gas phase, CO_2 dominant**

Extensive gas venting occurs in the Bay of Plenty within the offshore extension of the Taupo Volcanic Zone on the east coast of New Zealand's North Island. Bubble zones of shallow water gasohydrothermal vents extend for a distance of some 50 km along a line running through Whale Island, the submarine Calypso Mound, and White Island (e.g. Duncan & Pantin, 1969; Glasby, 1971; Sarano et al., 1989; Kamenev et al., 1993). Further geothermal activity also occurs at the Rurima Rocks, at a seamount to the west of White Island (Duncan & Pantin, 1969), and to the south-east of the Calypso Mound area (Glasby, 1971). A brief synopsis of gas venting in this area is provided below. For clarity a map is also included, showing the reported sites of gas venting in this region.

Sketch Map showing the distribution of gas venting in the vicinity of Whale and White Islands, Bay of Plenty, New Zealand. After Duncan & Pantin (1969; blue areas), with additional sites reported by Glasby (1971; purple stars) and Kamanev et al. (1993; pink stars). The majority of sites were identified by sonar. Observations of bubble bursting at the sea surface are indicated by a B. Note bubble bursting can only be observed in calm weather.

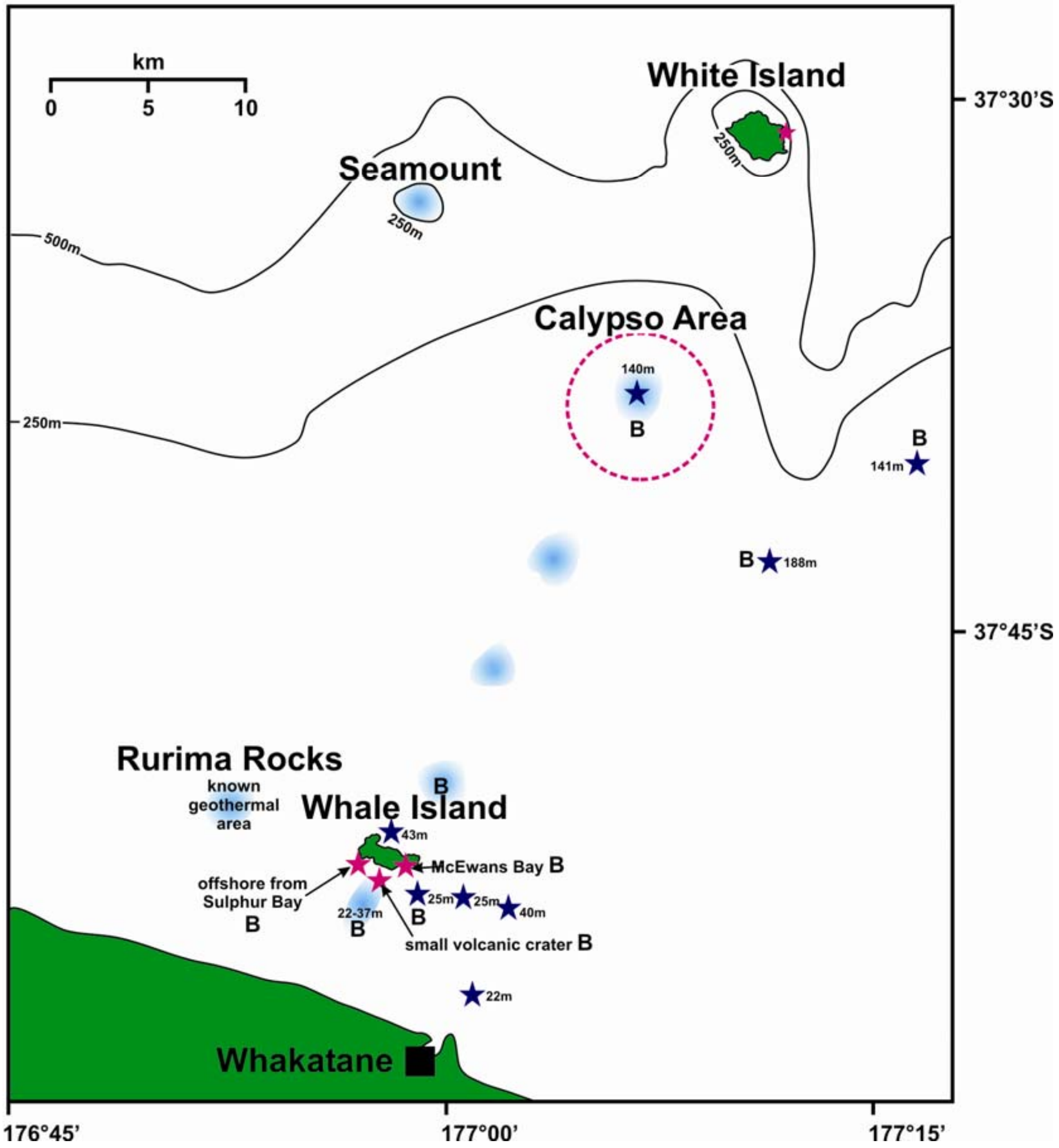

General Description & Distribution of Venting

Whale (Motuhora) Island forms the summit of a largely submerged Pleistocene complex volcano that lies offshore from Whakatane in the Bay of Plenty. Geothermal activity on the island includes acid hot springs, steaming ground, and fumaroles which occur primarily between the 354 m high central cone and the eastern tip of the island.

Extensive gasohydrothermal activity occurs in the shallow waters surrounding Whale Island (see map). Sites reported by Duncan & Pantin (1969) and Glasby (1971) were detected by sonar and/or bubble bursting at the sea surface. In 1990 an expedition explored 3 sites of venting, providing further descriptions of these areas with a focus on the biological communities (Kamenev et al., 1993). To the south-west, offshore from Sulphur Bay, venting occurred through the boulder covered seafloor at water depths of 12 m, where vents were spaced 1-2 m apart (Kamenev et al., 1993). To the south-east, at McEwans Bay, individual and multiple vents of volcanic gases and fluids were found on the silty sand seafloor at water depths of 5-12 m, with a vent density of 15-20 vents per m^2 (Kamenev et al., 1993). Bottom waters in this area were enriched in hydrocarbons (Propp et al., 1992). To the south of Whale Island, venting occurred at a small volcanic crater (150-200 m diameter, 25-45 m deep) located approximately 500 m offshore. At this site bubble bursting was observed at the sea-surface over the entire area of the crater (Kamenev et al., 1993). The bottom of the crater was covered by a homogeneous aleurite-pelite soft silt, dark-green in colour with a slight smell of H_2S, with bottom temperatures at the centre of the crater of 81°C, decreasing to 10-15°C at the periphery (Kamenev et al., 1993). Bottom waters in this area were enriched in oxygen, methane and ethane (Propp et al., 1992).

The crater site appears to correspond to the southern ‘bubble area’ described by Duncan & Pantin (1969) and revisited by Glasby (1971). It would appear that in the late 1960s this area was significantly larger, extending for 3 km in the NNE-SSW direction, with a width of 1.5 km, and centred 2 km offshore from the eastern end of Whale Island (Duncan & Pantin, 1969). Duncan & Pantin (1969) reported relatively vigorous bubble bursting activity which appeared patchy/periodic. They describe bubbles a few mm in diameter bursting at the surface in groups, with individual bubbles a few cm apart and the diameter of the group between 10 cm and 1 m, and one group appearing within an area of ~10 m^2 every 10 seconds to 2 minutes. Similarly, Glasby (1971) described bubbles ~10 mm in diameter, bursting at the surface at a rate of 5 bubbles per m^2 per second. This extended bubble zone appears to be associated with a fault zone lying off the eastern beach area of Whale Island (Glasby, 1971).

Duncan & Pantin (1969) also report a northern ‘bubble area’ centred 5 km NNE of the eastern end of Whale Island. This zone was ~1.5 km in diameter, with a bubble bursting rate around an order of magnitude lower than that observed at the southern bubble area (note whether this relates to an order of magnitude lower emission rate is dependent on the extent of bubble dissolution during ascent through the water column). In addition, Duncan & Pantin (1961) and Glasby (1971) report numerous other sites identified by strong columnar scattering (sonar) and/or visual observations of bubble bursting (see map). The deepest site where bubble bursting at the surface was reported was ~188 m water depth (Glasby, 1971).

Calypso Mound was discovered in February 1987 within one of these 'bubble zones' (Sarano et al., 1989; see map). The Calypso gasohydrothermal area is located at 160-180 m water depth, where the mound itself is a white gympsum ($CaSO_4$) and anhydrite ($CaSO_4.2H_2O$) cone some 10 m in diameter and 6-8 m high, formed at 167 m depth by discharge of thermal waters at the ocean floor (Sarano et al., 1989). In this area the near-bottom waters were saturated with ethane and methane, had slightly decreased salinity, and an increased amount of silicon (Propp et al. 1992). Bubble streams detected over Calypso Mound using an echogram originate at 167 m depth and terminate at 20 m depth, with no bubbles detected at the surface, indicating complete dissolution of the gas in seawater (W. Giggenbach and I. Menyailov, Bulletin of the Global Volcanism Network, 03/1990 Calypso Mound). Note however, Glasby (1971) reported visual observations of bubble bursting (from depths of ~140 m) in addition to discolouration of surface waters within the vicinity of the Calypso Mound area (see map).

White Island is the emergent summit of a 16 x 18 km submarine volcano, and is the most frequently active volcano in New Zealand. Kamenev et al. (1993) report a submarine gasohydrothermal vent site located of the eastern shore of White Island in water depths of 5-13 m. The seafloor in this location consists of a solid uneven lava flow with patches of dark coarse sand mixed with gravel. The lava flow had numerous cracks, with 2-3 m deep fissures, the bottom of which were covered with coarse sand and gravel. Individual gas vents were located on the lava flow and in sandy spots, with associated bottom temperatures of 30-40°C. Near-bottom waters in this region had elevated hydrogen and methane (Propp et al. 1992).

Vent Gas Composition

Gases collected from the seafloor near Whale Island at 34 m water depth are composed dominantly of CO_2 (68.0-73.4 mol%) with secondary CH_4 (12.0-19.3 mol%), N_2 (11.9-13.1 mol%), O_2 (0.7-1.4 mol%) and minor Ar (0.08-0.12 mol%) and H_2 (0.01-0.03 mol%) (Lyon et al., 1977). These samples may be air contaminated (W. Giggenbach and I. Menyailov, Bulletin of the Global Volcanism Network, 03/1990 Whale Island), where correction (based on the assumption that all O_2 derives from air contamination), gives a slightly increased CO_2 content of 70.5-78.7 mol%, and CH_4 content of 12.9-20.0 mol%. A similar composition of vent gases from this area was also reported by Giggenbach et al. (1993), with major CO_2 (88.0 mol%) and secondary CH_4 (9.5 mol%).

While vent gas compositions have not been reported (to the authors knowledge) for the majority of submarine vent sites in the Bay of Plenty, numerous analyses of the gases vented in on-land geothermal areas of both Whale and White Island have been made (e.g. W. Giggenbach and I. Menyailov, Bulletin of the Global Volcanism Network, 03/1990 Whale Island; Giggenbach & Matsuo, 1991; Giggenbach et al., 1993). In all cases, CO_2 is the dominant component, with varying amounts of secondary CH_4, N_2, H_2S and H. It therefore seems likely that the submarine vents within the Bay of Plenty are also CO_2 dominant.

Biota

The biota of hydrothermal vent sites in the Bay of Plenty has been described by Kamenev et al. (1993) for those sites marked by a pink star in the map provided. Unless otherwise stated, all information below is attributed to these authors.

In general, Kamenev et al. (1993) find that gasohydrothermal venting does not exert a negative effect on the local ecosystem. In this system, which has unrestricted hydrodynamic circulation, the macrobenthos is dominated by species that are common and widely distributed in New Zealand offshore waters. Areas of reduced species diversity and abundance are restricted to zones of high sediment temperature within the gasohydothermal vent fields, where the macrobenthos consists of motile animals, and animals adapted to the high temperature environment.

In the Sulphur Bay vent zone (Whale Island), large boulders at a depth of 6-9 m were colonised by macroalgae. The bivalve *Modiolus areolatus* was found among the macroalgae rhizoids (anchors) in high numbers, with population densities of ~70 individuals/m^2. A gastropod (*Cookia sulcata*) was also common in this area. Samples collected near the gas seepages contained one individual of the burrowing bivalve species *Tawera spissa*.

In the McEwans Bay gasohydrothermal zone (Whale Island), bacterial and algobacterial mats covering areas up to several m^2 were found. The mats were white to brown and 3-5 mm thick, consisting of thiobacilli and colourless filamentous sulphur oxidising bacteria *Thiodendron* sp. and *Thiothrix* sp. (Sorokin 1991). Algobacterial mats had formed around the margins of the bacterial mats, consisting of a mixture of colourless sulphur oxidising bacteria and benthic diatoms. Separate brown diatom mats were also observed, although these were considerably smaller (2-3 mm diameter) and less numerous.

Dense populations of the bivalve *T. spissa* occurred in this area, with an average density of 1581.0±134.5 individuals/m^2. Nearby was a gastropod (*Cominella adspersa*) community, with an average population density of 510.7±96.7 individuals/m^2. Other macrobenthos present in this area were individuals of a second gastropod species (*Penion dilatus*), star fish (*Astropecten polyacanthus*), polychaetes (Spionidae, Capitellidae, and Lumbrineridae families), isopods (*Exosphaeroma obtusum*), small soldier crabs, and young individual hexacorals. The meiobenthos was dominated by nematodes, with harpacticoid copepods, ostracods, amphipods, tanaids, and polychaetes also present. In general this community structure is very similar in composition to that found outside the zone of hydrothermal activity, but with a higher abundance and diversity of meiofauna within the hydrothermal areas.

In close proximity to the vent site at a depth of 6-7 m, were mussel beds of the commercially important species *Perna canaliculus*. The growth characteristics of these mussels were similar to those found for *P. canaliculus* from several areas in New Zealand, indicating no adverse health effects related to the hydrothermal activity.

At the small volcanic crater site (south of Whale Island), bottom temperature exerted a strong control on species diversity and distribution. At temperatures up to 30°C, the macrobenthos was dominated (~90% of macrofaunal biomass) by 3 species, the crab *Macropthalmus hirtipes,* the gastropod *Cominella maculosa,* and the amphipod *Proharpinia* sp. Individuals of a second gastropod species (*Pelicaria vermis*) and brittle stars (*Ophiuroidea*) were also present. Highest numbers of these animals were found at temperatures of 20°C or less. At higher temperatures sediment infauna disappeared. In silt above 50°C only the crab *M. hirtipes* was found , and at temperatures of 65°C a tube worm *Siboglinum* sp. was found. The meiobenthos in the crater consisted only of nematodes, where at temperatures of 81°C in the crater centre no meiofauna were observed.

Within the Calypso Mound area, samples from depths of 150-200 m showed a diverse benthic fauna typical for soft sediments that did not significantly differ from that observed beyond the vent zone. Polychaete, sipunculid, and echiurid worms, holothurians, starfishes, sea urchins, sea lilies, ophiurids (brittle stars), bivalves, scaphopods (tusk shells), and gastropods occurred in great numbers. Within the hydrothermal area tube worms of the genus Siboglinum were also present, and beyond this zone a priapulid worm was found.

In gasohydrothermal zones of White Island, bacterial mats with an area of 2-3 m^2 were found, where these mats were formed of giant cells (up to10 mm) of colourless sulphur-oxidising bacteria *Beggiatoa* sp. (Sorokin 1991). On the sandy bottom (temperatures of 30-40°C) both within and beyond the gasohydrothermal activity zone no macroinvertebrates were found, and the meiofauna consisted only of nematodes.

Bay of Plenty References

Duncan, A. R.; Pantin, H. M. 1969: Evidence for submarine geothermal activity in the Bay of Plenty. *New Zealand Journal of Marine and Freshwater Research*, 3: 602-606.

Giggenbach, W.F., Matsuo, S., (1991). Evaluation of results from second and third IAVCEI field workshop on volcanic gases, Mt. Usu, Japan and White Island, New Zealand. *Applied Geochemistry*, 6: 125-141.

Giggenbach, W.F., Sano, Y., Wakita, H., (1993). Isotopic composition of helium, and CO2 and CH4 contents in gases produced along the New Zealand part of a convergent plate boundary. *Geochimica et Cosmochimica Acta*, 57: 3427-3455.

Glasby, G.P., (1971). Direct observation of columnar scattering associated with geothermal gas bubbling in the Bay of Plenty, New Zealand. *New Zealand Journal of Marine and Freshwater Research*, 5: 483-496.

Kamenev, G.M., Fadeev, V.I., Selin, N.I., Tarasov. V.G., Malakhov, V.V., (1993). Composition and distribution of macro and meiobenthos around sublittoral hydrothermal vents in the Bay of Plenty, New Zealand. *New Zealand Journal of Marine and Freshwater Research*, 27: 407-418.

Lyon, G.L., Giggenbach, W.F., Singleton, R.J., and Glasby, G.P., (1977). Isotopic and Chemical composition of submarine geothermal gases from the Bay of Plenty, New Zealand. *New Zealand Department of Scientific and Industrial Research Bulletin*, 218: 65-67.

Propp, L.N., Obzhirov, A.I., Propp, M.V., (1992). The gas and hydrochemical anomalies in the bottom layer of water in an area of volcanic activity (Bay of Plenty, New Zealand). *Oceanology, 32:* 680-686 (in Russian, with summary in English).

Sarano, F., Murphy, R.C, Hougton, B.F., Hodenquist, J.W., (1989). Preliminary observation of submarine geothermal activity in the vicinity of White Island volcano, Taupo volcanic zone, New Zealand. *Journal of the Royal Society of New Zealand, 19:* 449-459.

Sorokin, D.Yu., (1991). Oxidation of reduced sulphur compounds in volcanic active regions in Bay of Plenty (New Zealand) and Matupy Harbor (New Britain, Papua-New Guinea). *Proceedings of the USSR Academy of Science. Series biological 3:* 376-387 (in Russian, with summary in English).

3.A.7 The Okinawa Trough

Type of Volcanic Activity:	**Subduction related (Back Arc)**
Depth of Venting:	**Deep water**
Type of CO_2 Release:	**Liquid and hydrate phases, CO_2 dominant**

Although the Okinawa Trough has been well studied, a large proportion of the results are published in Japanese (particularly within the JAMSTEC Journal of Deep-Sea Research). To aid accessibility of this material to the international community, Glasby & Notsu (2003) recently presented an excellent review of the Okinawa Trough, and the reader is referred to this article for a thorough overview of hydrothermalism in this region.

The Okinawa Trough is an intracontinental back arc basin in the early stages of rifting that formed as a result of the subduction of the oceanic Phillipine Sea Plate beneath the continental Eurasia Plate along the Ryukyu Trench (Glasby & Notsu, 2003 and references therein). The trough is a seafloor depression about 1200 km long, located to the southwest of Japan, behind the Ryukyu trench and Ryukyu Island Arc (see map below). In the north, the trough is ~230 km wide, with a maximum water depth of ~200m. In the south, the trough is ~60-100 km wide, with a maximum water depth of ~2300m. Arc volcanism is dominant in the northern Ryukyu Arc and back-arc volcanism is dominant in the middle and southern Okinawa Trough (Shinjo et al., 2000).

The Okinawa Trough is characterized by a thick sedimentary cover, up to 8 km thick in the north and about 2 km thick in the south (Sibuet et al., 1987). Sediments originate from five sources; (i) turbidity derived material from the East China Sea (ii) terrigenous material derived from the islands on the Ryukyu Arc (iii) volcanic fragments from submarine or neighbouring volcanoes (iv) hydrothermal precipitates (e.g. mounds, chimneys, plume particles) (v) fine grained pelagic sedimentation (Tsugara et al., 1991; Zhao et al., 1995).

Heat flow is high, with an estimated mean heat flow across the middle and southern Okinawa Trough of ~130 mW/m^2 (Yasui et al., 1970; Lu et al., 1981). The heat source is magmatic in origin, resulting from the subduction of the Philippine plate. Rifting-induced fracture systems facilitate hydrothermal circulation, where the advecting fluid is recycled seawater with a magmatic component (Ishibashi, 1991; Glasby & Notsu, 2003).

Four high temperature hydrothermal fields have been discovered in the middle Okinawa Trough; Minami-Ensei Knoll, the CLAM Site, Iheya North Knoll, and the JADE Site. More recently, hydrothermal venting has been discovered in the southern Okinawa Trough at Yonaguni Knoll and Hatoma Knoll. All of these sites exhibit vent fluids that are highly enriched in CO_2 in comparison to OSR vent sites. Furthermore, the venting of a separate CO_2 liquid phase, and/or the formation of CO_2 hydrate at the sediment-seawater interface, has been observed at five of these sites. Further details on these sites are provided below. Present studies in this region are directed towards the southern Okinawa Trough, and new sites may be discovered here in the future.

Bathymetric map of the Okinawa Trough showing locations of CO_2 vent sites (after Sibuet et al., 1987, Figure 1).

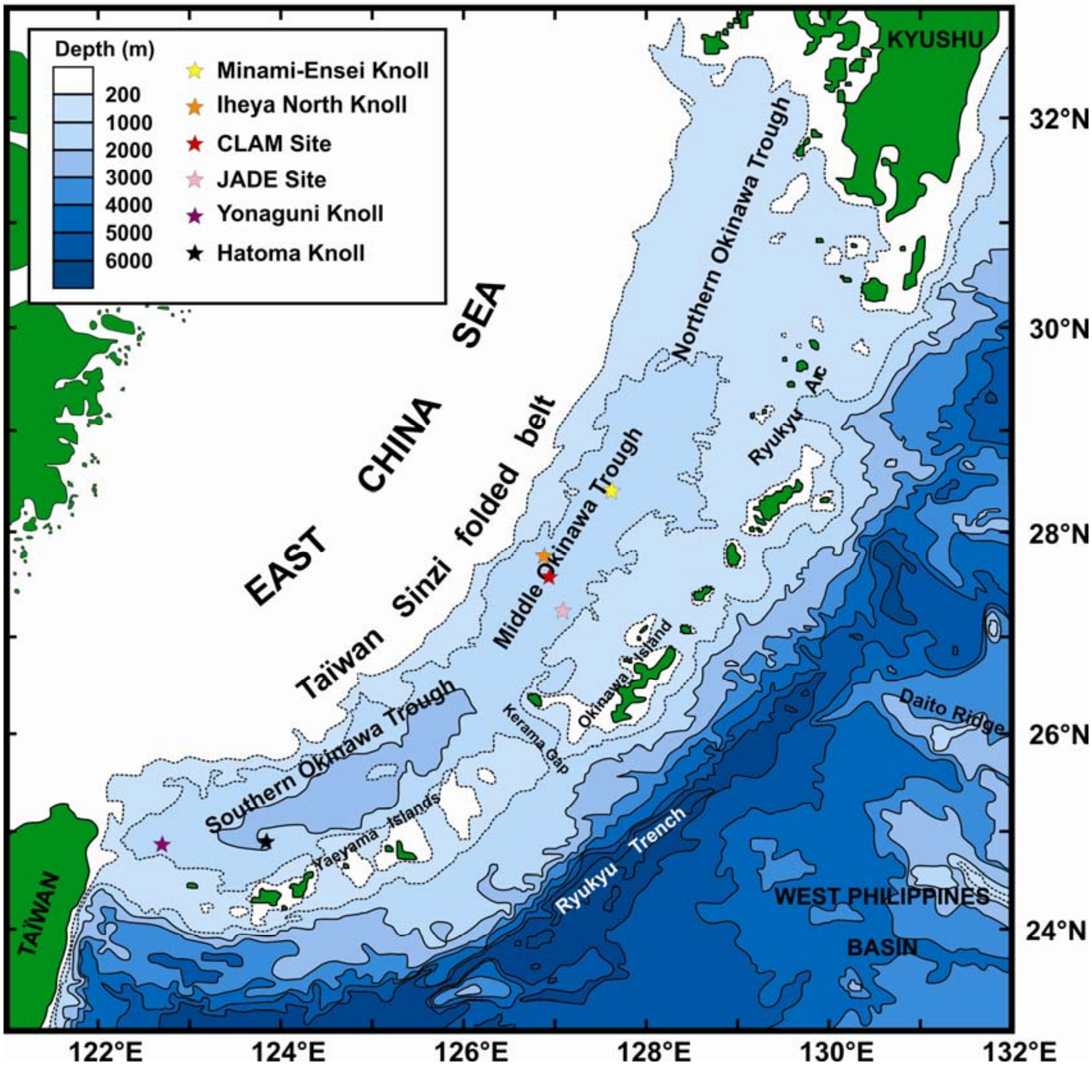

Site	Location	Latitude, Longitude
Minami-Ensei Knoll	Middle Okinawa Trough	28°23.7'N, 127°38.7'E
Iheya North Knoll	Middle Okinawa Trough	27°47.2'N, 126°53.9'E
CLAM Site	Middle Okinawa Trough	27°32.8'N, 126°57.9'E
JADE Site	Middle Okinawa Trough	27°15.0'N, 127°04.5'E
Yonaguni Knoll	Southern Okinawa Trough	24°50.9'N, 122°42.0'E
Hatoma Knoll	Southern Okinawa Trough	24°51.3'N, 123°50.5'E

3.A.7.1 Depression C, Minami-Ensei Knoll, Okinawa Trough

Type of Volcanic Activity:	**Subduction Related**
Depth of Venting:	**Deep water**
Type of CO_2 Release:	**Liquid and Hydrate phases, CO_2 dominant**

Buoyant liquid CO_2 droplets and a buoyant 'sherbert-like' hydrate material have been observed emerging from the seafloor at Minami-Ensei Knoll.

Minami-Ensei Knoll is located in the middle Okinawa Trough, approximately 140 km west of Amami-Ohshima Island (see map above). The knoll is elliptical in shape, reaching a water depth of 550m at its shallowest point (Hashimoto et al., 1995). Located on the western slope of the knoll are several small depressions which are thought to be calderas and range in size from ~100 to ~1000 m in diameter (Hashimoto et al., 1995). In 1991 intense hydrothermal activity and associated discharge of CO_2 was discovered in one of the larger depressions ('Depression C') during a dive of the Shinkai 2000 (Hashimoto et al., 1993).

Depression C is approximately 1000-1200 m in diameter with a maximum depth of ~720m, where the base of the depression is relatively flat and is encircled by a steep escarpment around 100 m high. A series of hydrothermal mounds ~5-6 m in height trend north-south across the centre of the depression floor. The mounds are topped by clusters of chimneys 0.2-2.5 m in height from which clear fluids with exit temperatures of 265-278°C emerge (Chiba et al., 1993; Chiba, 1997; Hashimoto et al., 1995). That the maximum exit temperature recorded is close to the boiling point of seawater at this depth suggests that hydrothermal activity at the knoll is violent with repeated explosions (Glasby & Notsu, 2003). The mounds comprise both sulphide (pyrite, sphalerite, galena and chalcopyrite) and nonsulphide (anhydrite, gypsum, calcite, dolomite and talc) minerals. The chimneys mainly consist of gypsum and anhydrite with minor sulphides, calcite, talc and amorphous silica. The mineral zoning in the chimneys resembles that of black smoker chimneys, with the inner walls comprising massive sulphides encased by the outer walls of anhydrite and gypsum. Detailed descriptions of the mineralogy and composition of these hydrothermal deposits have been presented by Nedachi et al. (1992) and Nakashima et al. (1993, 1995). Shimmering fluids and hot vents with associated rising streams of small buoyant 'bubbles' (droplets) were also observed emerging from the sandy bottom and fissures on outcrops elsewhere across the depression floor (Hashimoto et al., 1995).

The hydrothermal fluids have high CO_2 concentrations (64-96 mmol/kg) and low pH (4.9-5.1) (Gamo, 1995; Chiba et al., 1993). The concentration of CO_2 in the bottom water within the depression is ~38-39 mmol/kg (Hashimoto et al., 1995). The composition of the fluids, which appeared to be influenced by interaction with the sediment (high NH_4^+ and alkalinity), suggesting that Minami-Ensei Knoll is characterized by shallow circulation of hydrothermal fluids (Chiba et al., 1993).

CO_2 Discharge

Discharge of a distinct CO_2 rich phase has been reported at Minami-Ensei Knoll (Chiba et al., 1992; Hashimoto et al., 1995). Hashimoto et al. (1995) describe clear and cloudy 'gas bubbles' (droplets?) emerging from the sandy bottom of the depression and from the dense mussel beds among the crowded chimneys (Hashimoto et al., 1995). The 'bubbles' contained 87% CO_2, where the $\delta^{13}C$ value of the CO_2, the $^3He/^4He$ ratio, and the $\delta^{34}S$ of the H_2S, support a magmatic origin for these gases (Chiba et al., 1992). Hydrate formation at the seafloor has also been observed, where the hydrate texture is described as a 'sherbet-like' substance (Chiba et al., 1992; Hashimoto et al. 1995). The hydrate material emerged intermittently out of the seafloor to rise up through the water column, where this phenomenon decreased with increasing distance from the most active vent (Hashimoto et al. 1995). The positive buoyancy of the 'hydrate' phase indicates a composite hydrate-liquid particle (see Chapter 6 for discussion).

Biota

The biological community of Minami-Ensei Knoll has been described by Hashimoto et al. (1995). In brief, Depression C supports a mixed pelagic-hydrothermal community. There are vent organisms present, indicating the presence of H_2S, however, the trophic structure is complicated due to the presence of non-vent organisms (Hashimoto et al., 1993; Hashimoto et al., 1995). Hashimoto et al. (1995) remark on the similarities between the distribution of fauna at the Minami-Ensei vents and other Okinawa Trough vent sites, noting that there are differences between these sites and 'typical' OSR vent sites. Hashimoto et al. (1995) link these differences to the type of volcanism and thus indirectly to the CO_2 content of the vent fluids, where the Okinawa sites are characterized as 'arc-type' volcanism (as inferred from the high concentration of CO_2 in vent fluids). However, a specific discussion of the impact of high CO_2 concentrations on the biota, or an in depth exploration of the potential relationship between CO_2 venting and the biological community, is not presented.

Notes

There is no indication of a dead zone or mortality sink. The absence of a dead zone implies one (or both) of the following: (a) circulation is not restricted and the depression is well flushed (b) biota are either tolerant of high CO_2 levels or do not remain in areas with high CO_2 for long periods of time. With regards to these points:

Depression C is connected by a corridor ~670 m deep to a smaller depression to the NW, where Hashimoto et al. (1995) comment on ripple marks across the floor indicating a strong bottom current – thus this depression may be well flushed (although note reported CO_2 concentration in bottom waters approx 20 times that of seawater).

The presence of CO_2 venting within live mussel beds suggests one or more of the following (a) the mussels are tolerant of high CO_2 (b) venting is itinerant – thus individual mussels are not exposed to high CO_2 for prolonged periods (c) venting in this specific area (i.e. within the mussel bed) was a recent phenomenon (at the time of observation) such that the health of the mussel population was not yet noticeably impacted (d) CO_2 is flowing along confined pathways (e.g. through hydrate lined pipes) – thus the mussels are protected from (extremely) high porewater CO_2.

3.A.7.2 Iheya North Knoll, Okinawa Trough

Type of Volcanic Activity:	**Subduction Related**
Depth of Venting:	**Deep water**
Type of CO_2 Release:	**Hydrate phase**

Chiba et al. (1996) report the occurrence of CO_2 hydrates at the seafloor at Iheya North Knoll. However, no further information is currently available (in English to the authors knowledge) regarding the nature, fate and impact of CO_2 release at this site.

Iheya North Knoll is located approximately 25 km to the north of the CLAM site (Iheya Ridge). Hydrothermal activity was discovered at the foot of the Knoll in 1995, occurring at depths between ~970 and 1050 m within a restricted area about 250 m in diameter (Glasby & Notsu, 2003 and references therein). Many relict and active vent chimneys occur in this area. The relict sulphide chimneys contain abundant barite, sphalerite, common pyrite, marcasite, galena and chalcopyrite and rare wurtzite (Chiba et al., 1996). The active chimneys discharge clear fluids with exit temperatures of ~240-310°C and deposit mainly anhydrite (Chiba et al., 1996, 2000; Chiba, 1997; Kataoka et al., 2000, 2001). The hydrothermal fluids have Cl^- concentrations much lower than seawater, indicating phase separation of the fluid below the seafloor, where variations in fluid composition reflects the mixing of vapour and brine phases in different ratios (Chiba et al., 1996; Kataoka et al., 2000). In addition, the hydrothermal fluids have lower alkalinities and NH_4^+ concentrations than those from Minami-Ensei Knoll and the JADE site, indicating that the interaction of the hydrothermal fluids with sediment is less pronounced at this site (Chiba et al., 2000). This field also has a well-established hydrothermal vent community (Kim et al., 1989; Ohta, 1990; Momma et al., 1996; Tawara et al., 1997; Yamamoto et al., 1999).

3.A.7.3 CLAM Site, Iheya Ridge, Okinawa Trough

Type of Volcanic Activity:	**Subduction Related**
Depth of Venting:	**Deep water**
Type of CO_2 Release:	**Unknown**

The occurrence of a separate CO_2 phase (either droplets or hydrate) has not been reported for this site. However, the hydrothermal fluids from the CLAM Site exhibit high CO_2 concentrations, where Glasby & Notsu (2003) report a concentration of 74-86 mmol/kg, while Gamo (1995) extrapolates to an end-member concentration of 160-200 mmol/kg (based on an end member fluid with a Mg concentration of 20 mmol/kg).

3.A.7.4 The JADE hydrothermal Field, Izena Hole, Okinawa Trough

Type of Volcanic Activity:	**Subduction Related**
Depth of Venting:	**Deep water**
Type of CO_2 Release:	**Liquid and hydrate phases, CO_2 dominant**

Both venting of liquid CO_2 and CO_2 hydrate formation have been observed at the JADE site (Sakai et al., 1990).

The Izena Hole (also known as the Izena Cauldron) is a small rectangular graben (6 x 3 km with a maximum depth of 1665m) located in the middle Okinawa Trough (see map above; Kato et al., 1989; Halbach et al., 1993). In 1988 the JADE hydrothermal field was discovered on the steep rugged terrain of the northeastern slope of the Izena Hole, where the site occurs at water depths of 1300-1450 m and covers an area some 1.8 km long and 0.6 km wide (Halbach et al., 1989, 1993; Sakai et al., 1990).

The JADE field is one of the most active hydrothermal areas in the Okinawa Trough, and is characterized by extensive hydrothermal mineralization, with hundreds of active and inactive sulphide-sulphate mounds (up to 10s m in diameter and 15 m high) and chimneys (0.1 to 5 m high) irregularly distributed across the site (Halbach et al., 1989; Nakamura et al., 1989). Mounds and chimneys are composed of galena, sphalerite, tetrahedrite, native sulphur, barite and anhydrite (Kimura et al., 1990). A range of vent types have been reported, including a single 'black smoker' chimney with a vent fluid exit temperature of 320ºC (Nakamura et al., 1990), a number of chimneys and mounds emitting clear fluids with an exit temperature of ~220ºC (where sulphide minerals have precipitated prior to discharge; Sakai et al., 1990), and several large 'white smokers' discharging grey or white fluids at the lower temperature of ~130ºC (Kimura et al., 1989).

As with other sites in the Okinawa Trough, the hydrothermal fluids exhibit a very high CO_2 concentration (200 mmol/kg), significantly higher than that observed at OSR hydrothermal vents (Ishibashi et al., 1995). The concentration of CH_4 in bottom waters from the Izena Hole are also elevated (up to 0.7 mmol/kg) and vary across the site, suggesting a number of vents also emit CH_4 (Watanabe et al., 1995). The CO_2 and He in the hydrothermal fluids are magmatic in origin, while the CH_4 is thermogenic (Ishibashi, 1991; Ishibashi et al., 1995).

CO_2 Release

The JADE site was the first deep water site where venting of a discrete CO_2 dominated liquid phase and formation of hydrate were observed (Sakai et al., 1990). Two locations of CO_2 discharge were reported, the first approximately 100m to the N of the black smoker chimney, and the second approximately 500m to the SW (see Figure 1 in Sakai et al., 1990). At both sites, droplets emerged 'intermittently but freely' and when the sediment was disturbed during sampling (Sakai et al., 1990).

The buoyant liquid CO_2 droplets are expelled to the ocean through translucent hydrate 'horns' that grow out of the sediments, with the liquid CO_2 emerging from the top of the horns as hydrate coated buoyant CO_2 droplets (Sakai et al., 1990). The horns grew to lengths of ~10 cm, increasing in diameter from a narrow base to about 1 cm at the top, and periodically broke off and rose through the water column (Sakai et al., 1990). The droplets contained ~86% CO_2, 3% H_2S and 11% residual gas (CH_4 and H_2), where the chemical composition and isotopic ratios of the droplets indicated the same source as the dissolved gases in the black smoker vent fluids (Sakai et al., 1990; Ishibashi and Urabe, 1995).

Sakai et al. (1990) and Hou et al. (1999a,b) suggested that an impermeable CO_2 hydrate layer forms beneath the seafloor in the vicinity of these hydrate pipes, where this hydrate layer acts as a trap for buoyant liquid CO_2. However, Glasby & Notsu (2003) argued that temperatures in the sub-surface are likely to be too high for CO_2 hydrate to form as this site occurs in close proximity to a black smoker discharging hydrothermal fluids at a temperature of 320°C. Nevertheless, Sakai et al. (1990) report a temperature of 3.8°C at the sediment-seawater interface, with a temperature gradient of ~0.8°C/cm, indicating that hydrate formation would be possible in the upper 8cm of the sediments where temperatures are below 10°C. They suggest that leakage of droplets through the impeding hydrate layer occurs when the seal is ruptured, most likely due to shifts in hydrothermal fluid circulation patterns leading to elevation of the 10°C isotherm, where this hypothesis is consistent with the general observation that seepage of CO_2 is occurring in areas of high heat flow (Sakai et al., 1990).

Biota

Large colonies of vent fauna including Galtheidae (squat lobsters), crabs, shrimps and bivalves, polychaetes have been reported at the JADE site, where the stable isotope ratios of the animals reflect dependence on symbiotic chemoautotrophic bacteria which utilize H_2S in vent fluids and other reduced inorganic compounds (Kimura et al., 1989, 1990, 1991b; Kim et al., 1990; note all these publications are in Japanese with English abstract).

3.A.7.5 Yonaguni Knoll, Okinawa Trough

Type of Volcanic Activity:	**Subduction Related**
Depth of Venting:	**Deep water**
Type of CO_2 Release:	**Liquid phase, CO_2 dominant**

A seafloor lake of liquid CO_2, capped by a hydrate layer, has been reported at Yonaguni Knoll IV (Inagaki et al., 2006).

The Yonaguni Knoll IV hydrothermal field is located at ~1330-1410 m water depth in the southern Okinawa Trough (see map above, Inagaki et al., 2006).

The site is characterized by two active black smoker vents with vent exit temperatures of 323ºC, with other active and inactive chimneys throughout the site (Glasby & Notsu, 2001; Fujikura et al., 2001; Inagaki et al., 2006). The active chimneys consisted mainly of barite and anhydrite with minor amounts sulphides (J.-I. Ishibashi, personal communication, reported in Glasby & Notsu, 2001). Near the black smokers, vapour rich clear venting fluids and small liquid CO_2 droplets emerge from the seafloor (Inagaki et al., 2006).

Inagaki et al., (2006) report the discovery and exploration of a CO_2 zone – located some 50 m downslope to the south of one of the black smoker chimneys (Tiger chimney). The CO_2 zone comprises a liquid CO_2 pool covering an area greater than 200 m^2, capped by a thin layer (<10cm) of CO_2 hydrate, and covered by 20-40 cm layer of pavement sediments with abundant white patches (Inagaki et al., 2006). Small droplets of liquid CO_2 were emanating from cracks in the pavement structure, and after collection of a sediment core from one of the white patches, continuous emission of CO_2 was observed from the cored hole (Inagaki et al., 2006). The *in situ* temperature in this area increased from 3.9°C in the overlying bottom water to 9.9°C at 35 cm sediment depth (Inagaki et al., 2006), consisted with the formation of a thin near surface hydrate layer (see also JADE site; Sakai et al., 1990).

Seawater pH was depressed around the pavement (6.3) and in sediment porewaters (6.6) with respect to bottomwaters outside the hydrate zone (7.3), where in-situ pH at the liquid CO_2 interface were likely considerably more depressed, potentially with values as low as 4 (Inagaki et al., 2006).

The CO_2 concentration of vent fluids was highly elevated (300 mmol/kg). The CO_2 droplets (2 samples analysed) consisted mainly of CO_2 (85.10±2.12%), with small amounts of CH_4 (13.95±2.05%), and H_2 concentrations were below the detection limit (Inagaki et al., 2006). The stable carbon isotopic compositions of CO_2 (7.0‰) and CH_4 (26.4‰) in the droplets were similar to those from the nearby Tiger vent fluids (7.6‰ and 26.3‰ respectively), indicating the same origin for the gases (Inagaki et al., 2006).

Biota

While the active hydrothermal vents support an associated vent community (Fujikura et al., 2001), benthic fauna were rarely observed in the CO_2 hydrate zone (Inagaki et al., 2006). Inagaki et al. (2006) have presented a detailed analysis of the microbial community at this site. High abundances of microbial cells (>10^9 cells/cm^3) were found in the pavement samples above the CO_2 lake, decreasing significantly to ~10^7 cells/cm^3 at the liquid CO_2-CO_2 hydrate boundary. Inagaki et al. (2006) conclude that the presence of functional genes related to C1 assimilation, in addition to the presence of highly ^{13}C-depleted archael and bacterial lipid biomarkers, suggest that the microbial communities in the CO_2 liquid and CO_2-hydrate-bearing sediments are dominated by microorganisms assimilating CO_2 and CH_4.

3.A.7.6 Hatoma Knoll, Okinawa Trough

Type of Volcanic Activity:	**Subduction Related**
Depth of Venting:	**Deep water**
Type of CO_2 Release:	**CO_2 liquid and hydrate, CO_2 dominant**

Seafloor CO_2 hydrate outcrops and venting of buoyant liquid CO_2 droplets have been reported at Hatoma Knoll (Shitashima & Maeda, 2005).

The Hatoma Knoll in the Okinawa Trough is located approximately 50 km to the North of Iriomote Island. The Knoll has caldera shaped topography, and is ~400-600 m in diameter. The hydrothermal site covers an area of ~16,800 m^2, including two large (~10 m tall) active chimneys in the centre of the crater bottom at a water depth of ~1500 m, and many vents along the crater wall (Tsuchida et al., 2000; Nakano et al., 2001; Watanabe, 2001). The site comprises both active and inactive chimneys, where the chimneys consist principally of anhydrite and barite (Watanabe, 2001). Active chimneys emit clear fluids (maximum vent exit temperature of 301°C) characterized by high alkalinity and NH_4 compared to seawater (due to interaction of the fluids with sedimentary organic matter) and significantly lower Cl- than seawater (370-540 mmol/kg with respect to 550 mmol/kg), indicating subcritical phase separation of the hydrothermal fluids beneath the seafloor (Tsuchida et al., 2000; Nakano et al., 2001).

CO_2 Release

Shitashima & Maeda (2005) reported on CO_2 venting at this site, and also carried out a number of experiments to determine droplet dissolution and rise characteristics, following techniques developed by Brewer and coworkers (see also Chapters 3 and 6). CO_2 droplets were observed emerging from the base of the active chimneys in the centre of the crater (Shitashima & Maeda, 2005). The liquid droplets were dominated by CO_2 (95-98%), with minor H_2S (2-3%) and other trace gas species (Shitashima & Maeda, 2005). CO_2 hydrate was also observed at the seafloor (Shitashima & Maeda, 2005).

The CO_2 droplets ranged in size from ~4 to 10 mm in diameter, and were tracked during their ascent, with droplet behaviour observed using an HDTV camera mounted on an ROV. The initial rise rate ranged from 13 cm/s to 26 cm/s. Both droplet size and rise rate decreased during ascent as the droplets (a) gradually dissolved and (b) converted to CO_2 hydrate while rising. A detailed mapping survey of pH distribution in the CO_2 vent area, using grid navigation of the ROV (400m X 400m, 3 layers) which was fitted with a pH/pCO_2 sensor, showed only a localized pH depression at the CO_2 vent site (Shitashima & Maeda, 2005).

Biota

The active hydrothermal vents support numerous associated vent fauna. These communities have been described in JAMSTEC (In Japanese with English Abstract only). Shitashima & Maeda (2005) state ‘many organisms such as crab, shrimp, shellfish and fish have lived at the CO_2 emission area’. See also Figure 5.6 in Chapter 5, from presentation of Shitashima & Maeda (2005)).

All Okinawa Trough References

Chiba, H., (1997). Geochemistry of active hydrothermal systems in Okinawa Trough backarc basin. Deep Sea Research in Subduction Zones, Spreading Centers and Backarc Basins. JAMSTEC Deep-Sea Res., Spec. Vol., pp. 63– 68.

Chiba, H., Sakai, H., Gamo, T., Ishibashi, J.-I., Nakashima, K., Minami, H., Dobashi, F., (1992). Chemistry and isotopic composition of bubbles emerging from the seafloor at the Minami-Ensei Knoll, Okinawa Trough. Proceedings of the JAMSTEC Symposium Deep-Sea Research, 8: 81-87 (in Japanese with English Abstract).

Chiba, H., Nakashima, K., Gamo, T., Ishibashi, J.-I., Tsunogai, U., Sakai, H., (1993). Hydrothermal activity at the Minami-Ensei Knoll, Okinawa Trough: chemical characteristics of hydrothermal solutions. Proceedings of the JAMSTEC Symposium Deep-Sea Research, 9: 271-282 (in Japanese with English Abstract).

Chiba, H., Ishibashi, J.-I., Ueno, H., Oomori, T., Uchiyama, N., Takeda, T., Takemine, C., Ri, J., Itomitsu, A., (1996). Seafloor hydrothermal systems at North Knoll, Iheya Ridge, Okinawa Trough. JAMSTEC Journal Deep-Sea Research, 12: 211-219 (in Japanese with English Abstract).

Chiba, H., Kataoka, S., Ishibashi, J., Yamananka, T., (2000). Distribution of hydrothermal vents, fluid chemistry, and phase separation at the Iheya North seafloor hydrothermal system, Mid-Okinawa Trough. EOS Transactions of the American Geophysical Union, 81 (22), Abstract WP86.

Fujikura, K., Fujiwara, Y., Ishibashi, J.-I., Katayama, S., Komatsu, T., Maezawa, Y., Maki, Y., Miyazaki, J.-I., Miyake, H., Okamoto, K., Okoshi, K., Toth, L.G., Tsuchida, S., Yamaguchi, T., Yamanaka, T., Watabe, H., Zielinski, S., Kato, K., (2001). Report on investigation of hydrothermal vent ecosystems by the crewed submersible ‘Shinkai 2000’ on Dai-Yon (No. 4) Yanaguni Knoll and the Hatoma Knoll, the Okinawa Trough. JAMSTEC Journal of Deep-Sea Research, 19: 141–154 (in Japanese with English Abstract).

Gamo, T., (1995). Wide variation of chemical characteristics of submarine hydrothermal fluids due to secondary modification processes after high temperature water– rock interaction: a review. In: Sakai, H., Nozaki, Y. (Eds.), Biogeochemical Processes and Ocean Flux in the Western Pacific. Terra Scientific Publ., Tokyo, pp. 425–451.

Glasby, G.P., Notsu, K., (2003). Submarine hydrothermal mineralization in the Okinawa Trough, SW of Japan: an overview. Ore Geology Reviews, 23: 299-339.

Halbach, P., Nakamura, K.-I., Wahsner, M., Lange, J., Sakai, H., Käselitz, L., Hannsen, R.-D., Yamano, M., Post, J., Prause, B., Seiffert, R., Michaelis, W., Teichmann, F., Kinoshita, M., Ma¨rten, A., Ishibashi, J., Czerwinski, S., Blum, N., (1989). Probable modern analogue of Kuroko-type massive sulphide deposits in the Okinawa Trough back-arc basin. Nature, 338: 496-499.

Halbach, P., Pracejus, B., Märten, A., (1993). Geology and mineralogy of massive sulfide ores from the central Okinawa trough, Japan. Economic Geology, 88: 2210-2225.

Hashimoto, J., Fujikura, K., Ohta, S., Miura, T., (1993). Observation of hydrothermal vent communities at the Minami-Ensei Knoll-II. Proc. JAMSTEC Symposium of Deep-Sea Research, 9: 327–336 (in Japanese with English Abstract).

Hashimoto, J., Ohta, S., Fujikura, K., Miura, T., (1995). Microdistribution pattern of the hydrothermal vent communities of the Minami-Ensei Knoll in the Mid-Okinawa Trough, Western Pacific. Deep-Sea Research, Part 1, 42: 577-599.

Hou, Z., Ai, Y., Qu, X., Zhang, Q., Tang, S., (1999a). Possible contribution of magmatic fluids to seafloor ore-forming hydrothermal systems in the Okinawa Trough. Acta Geologica Sinica, 73: 57-65 (in Chinese with English Abstract).

Hou, Z., Zhang, Q., Qu, X., (1999b). Hydrothermal fluid evolution and ore-forming processes of submarine hydrothermal systems in the Okinawa Trough. Exploration and Mining Geology, 8: 257-272.

Inagaki, F., Kuypers, M.M.M., Tsunogai, U., Ishibashi, J., Nakamura, K., Treude, T., Ohkubo, S., Nakaseama, M., Gena, K., Chiba, H., Hirayama, H., Nunoura, T., Takai, K., Jørgensen, B.B., Horikoshi, K., Boetius, A., (2006) Microbial community in a sediment-hosted CO_2 lake of the southern Okinawa Trough hydrothermal system. Proceedings of the National Academy of Sciences, 103: 14164-14169.

Ishibashi, J.-I., (1991). Geochemical studies of hydrothermal fluids in the middle Okinawa Trough Back Arc Basin. Unpublished DSc thesis. University of Tokyo. 131 pp.

Ishibashi, J.-I., (1995). Geochemistry of phase-separated hydrothermal fluids of the North Fiji Basin, southwest Pacific. In: Sakai, H., Nozaki, Y. (Eds.), Biogeochemical Processes and Ocean Flux in the Western Pacific. Terra Scientific Publ., Tokyo, pp. 453-467.

Ishibashi, J.-I., Urabe, T., (1995). Hydrothermal activity related to arc-back arc magmatism in the western Pacific. In: Taylor, B. (Ed.), Backarc Basins Tectonics and Magmatism. Plenum, New York, pp. 451-495.

Kataoka, S., Ishibashi, J.-I., Yamanaka, T., Chiba, H., (2000). Topography and fluid geochemistry of the Iheya North Knoll seafloor hydrothermal system in the Okinawa Trough. JAMSTEC Journal of Deep-Sea Research, 16: 1-7 (in Japanese with English Abstract).

Kataoka, S., Ishibashi, J.-I., Chiba, H., (2001). Time series study of chemical composition of hydrothermal fluids from the North Knoll at the Iheya Ridge in the Okinawa Trough. JAMSTEC Journal of Deep-Sea Research, 19: 123-129 (in Japanese with English Abstract).

Kato, Y., Nakamura, K.-I., Iwabuchi, Y., Hashimoto, J., Kaneko, Y., (1989). Geology and topography in the Izena Hole of the middle Okinawa Trough—results of diving surveys in 1987 and 1988. JAMSTECTR Deep-Sea Research, 5: 163-182 (in Japanese with English Abstract).

Kim, E.S., Sakai, H., Hashimoto, J., Yanagisawa, F., Ohta, S., (1989). Sulfur isotopic ratios of hydrothermal vent animals at Ogasawara Arc and Mid-Okinawa Trough—evidence for microbial origin of hydrogen sulfide at low-temperature hydrothermal areas. Geochemistry Journal, 23: 195-208.

Kimura, M., Tanaka, T., Kyo, M., Ando, M., Oomori, T., Izawa, E., Yoshikawa, I., (1989). Study of topography, hydrothermal deposits and animal communities in the middle Okinawa Trough hydrothermal areas using the submersible ‘‘SHINKAI 2000’’ system. JAMSTECTR Deep-Sea Research, 5: 223-244 (in Japanese with English Abstract).

Lu, R.S., Pan, J.J., Lee, T.C., (1981). Heat flow in the southern Okinawa Trough. Earth and Planetary Science Letters, 55: 299-310.

Momma, H., Iwase, R., Mitsuzawa, K., Kaiko, Y., Fujiwara, Y., Amitani, Y., Aoki, M., (1996). Deep tow survey in Nanseisyoto region (K95-07-NSS). JAMSTEC Journal of Deep-Sea Research, 12: 195-210 (in Japanese with English Abstract).

Nakamura, K.-I., Kato, Y., Kimura, M., Ando, M., Kyo, M., (1989). Occurrence and distribution of the hydrothermal ore deposits at the Izena Hole in the Okinawa Trough—summary of knowledge in 1988. JAMSTECTR Deep-Sea Research, 5: 183-189 (in Japanese with English Abstract).

Nakamura, K.-I., Marumo, K., Aoki, M., (1990). Discovery of a black smoker vent and a pockmark emitting CO_2-rich fluid on the seafloor hydrothermel mineralization field at the Izena Cauldron in the Okinawa Trough. JAMSTECTR Deep-Sea Research, 6: 33-50 (in Japanese with English Abstract).

Nakano, A., Matsumura, M., Ishibashi, J.-I., (2001). Geochemistry of hydrothermal fluids from the Hatoma Knoll in the South Okinawa Trough. JAMSTEC Journal of Deep-Sea Research, 18: 139-144 (in Japanese with English Abstract).

Nakashima, K., Sakai, H., Yoshida, H., Chiba, H., Tanaka, Y., Gamo, T., Ishibashi, J.-I., Tsunogai, U., (1993). Mineralogical and fluid inclusion studies on some hydrothermal deposits at the Iheya Ridge and Minami-Ensei Knoll, Okinawa Trough: report of Research Dive 621 and hydrothermal precipitates collected by Dives 487 and 622 of ‘‘Shinkai 2000’’. Proceedings of the JAMSTEC Symposium Deep-Sea Research, 9: 253-269 (in Japanese with English Abstract).

Nakashima, K., Sakai, H., Yoshida, H., Chiba, H., Tanaka, Y., Gamo, T., Ishibashi, J.-I., Tsunogai, U., (1995). Hydrothermal mineralization at the Okinawa Trough. In: Sakai, H., Nozaki, Y. (Eds.), Biogeochemical Processes and Ocean Flux in the Western Pacific. Terra Scientific Publ., Tokyo, pp. 487–508.

Nedachi, M., Ueno, H., Ossaka, J., Nogami, K., Hashimoto, J., Fujikura, K., Miura, T., (1992). Hydrothermal ore deposits on the Minami-Ensei Knoll of Okinawa Trough–Mineral assemblages. Proceedings of the JAMSTEC Symposium of Deep-Sea Research, 8: 95-106 (in Japanese with English Abstract).

Ohta, S., (1990). Deep-sea submersible survey of the hydrothermal vent community on the northeastern slope of the Iheya Ridge, Okinawa Trough. JAMSTECTR Deep-Sea Research, 6: 145-156 (in Japanese with English Abstract).

Sakai, H., Gamo, T., Kim, E.-S., Tsutsumi, M., Tanaka, T., Ishibashi, J.-I., Wakita, H., Yamano, M., Oomori, T., (1990). Venting of carbon dioxide-rich fluid and hydrate formation in mid-Okinawa Trough backarc basin. Science, 248: 1093-1096.

Shinjo, R., Woodhead, J.D., Hergt, J.M., (2000). Geochemical variation within the northern Ryukyu Arc: magma source compositions and geodynamic implications. Contributions to Mineralogy and Petrology, 140: 263-282.

Shitashima, K., Maeda, Y., (2005). Fate of liquid CO_2 discharged from the hydrothermal area in the Okinawa Trough. EOS Transactions, American Geophysical Union 86(52), Fall Meeting Supplement, Abstract B33A-1018.

Sibuet, J.-C., Letouzey, J., Barbier, F., Chavret, J., Foucher, J.-P., Hilde, T.W.C., Kimura, M., Chiao, L.-Y., Marsset, B., Muller, C., Ste´phan, J.-F., (1987). Back arc extension in the Okinawa Trough. Journal of Geophysical Research, 92: 14041-14063.

Tawara, K., Yamamura, T., Tazaki, K., Chiba, H., Ishibashi, J.-I., (1997). Microorganisms of hydrothermal vents at Iheya Ridge. Journal of the Mineralogical Society of Japan, 26: 81–85 (in Japanese with English Abstract).

Tsuchida, S., Watanabe, K., Ishibashi, J.-I., Miyake, H., Watabe, H., Yamaguchi, T., Katajima, T., Nakano, A., Matsumura, M., Watanabe, H., (2000). Preliminary report on a biological, geological, and geochemical survey on hydrothermalism at the Hatoma and Minna Knolls. JAMSTEC Journal of Deep-Sea Reseach, 17: 35-42 (in Japanese with English Abstract).

Tsugaru, R., Tamaki, Y., Sako, M., Kimura, M., Shimamura, K., (1991). Report on DELP 1988 cruises in the Okinawa Trough: Part 4. Preliminary report on the sediment samples. Bulletin of the Earthquake Research Institute, 66: 71-89.

Watanabe, K., (2001). Mapping of hydrothermal activity area on the Hatoma Knoll in the southern Okinawa Trough. JAMSTEC Journal of Deep-Sea Research, 19: 87–94 (in Japanese with English Abstract).

Watanabe, S., Tsurushima, N., Kusakabe, M., Tsunogai, S., (1995). Methane in Izena Cauldron, Okinawa Trough. Journal of Oceanography, 51: 239–255.

Yamamoto, T., Kobyashi, T., Nakasone, K., Nakao, S., (1999). Chemosynthetic community at North Knoll, Iheya Ridge, Okinawa Trough. JAMSTEC Journal of Deep-Sea Research, 15: 19-24 (in Japanese with English Abstract).

Yasui, M., Epp, D., Nagasaka, K., Kishii, T., (1970). Terrestrial heat flow in the seas around the Nansei Shoto (Ryukyu Islands). Tectonophysics, 10 : 225-234.

Zhao, Y.-Y., Yan, M.-C., Jiang, R.-H., (1995). Abundance of chemical elements in continental shelf sediment of China. Geo-Marine Letters, 15: 71-76.

3.A.8 Champagne Vent Site, NW Eifuku, The Mariana Arc

Type of Volcanic Activity:	**Subduction related – Island Arc**
Depth of Venting:	**Deep water**
Type of CO_2 Release:	**Liquid phase, CO_2 dominant**

Liquid CO_2 venting has been reported at the Champagne Vent Site, NW Eifuku, on the Mariana Arc (Lupton et al., 2006).

NW Eifuku is a small volcanic cone located at 21.49°N, 144.04°E on the Mariana Arc. It is the smallest and deepest in a cluster of 3 volcanoes (neighbouring Daikoku and Eifuku), rising to a water depth of ~1535m at its shallowest point (Lupton et al., 2006).

Hydrothermal activity on NW Eifuku was inferred from identification of water column anomalies in the area, where excess H_2, CO_2, CH_4, Fe and Mn and depressed pH and light backscattering, were observed within the depth range 1490-1620m (Lupton et al., 2003; Resing et al., 2003). Later exploration located several sites of hydrothermal discharge on NW Eifuku, where the Champagne Vent Site (CVS), located ~80 m WNW of the volcano summit at a water depth of 1604 m, is the most intense of these sites (Lupton et al., 2006).

The CVS is characterised by a number of small white chimneys that discharge a buoyant milky fluid (Lupton et al., 2006). The most vigorous vents emit fluids with exit temperatures of ~103-108ºC, while several other vents discharge at lower temperatures of 11-68ºC (Lupton et al., 2006). Vent fluids exhibited depressed pH (3.4 to 4.8) and very high CO_2 concentrations (up to ~2700 mmol/kg – approximately an order of magnitude greater than the highest concentrations reported at the Okinawa Trough), where the very high CO_2 contents are most likely due to entrainment of the liquid CO_2 phase (Lupton et al., 2006)

CO_2 Release

In addition to hydrothermal vent fluids, liquid CO_2 droplets coated with a milky hydrate skin were also observed rising slowly from the seafloor around the chimneys, percolating from crevices in the seafloor (Lupton et al., 2006). The droplets were approximately 1.5 cm in diameter and were coated with a milky skin assumed to be CO_2 hydrate, and were sticky, adhering to each other and the ROV like 'clumps of grapes' (Lupton et al., 2006). The area of seafloor where active venting of CO_2 occurred was characterized by pumice and whitish/yellow sulphur-rich material (Lupton et al., 2006). The flux of CO_2 droplets increased dramatically whenever the seafloor was disturbed, consistent with the presence of a layer of liquid CO_2 beneath the surface capped by an impeding layer of hydrate, where any penetration of the hydrate cap released the buoyant liquid CO_2 beneath (Lupton et al., 2006).
Careful probing of the seafloor where the liquid droplets were forming found temperatures less than 4°C, consistent with the presence of CO_2 hydrate (c.f. Okinawa Trough sites - Yonaguni Knoll (Inagaki et al., 2006) and JADE hydrothermal field (Sakai et al., 1990)).

The droplets consisted mainly of CO_2 (98.6-99.6%), with secondary H_2S (0.5-0.8%) and other trace gases (CH_4 and H_2 <0.01%, He ~6 ppm) (Lupton et al., 2006). The $\delta^{13}C$ and $CO_2/^3He$ ratios are within the range typical for volcanic arc settings, and indicate that the carbon is derived from ~90% marine carbonates, with small contributions from mantle carbon and organic matter (Lupton et al., 2006). Lupton et al. (2006) also note that the fact that the radiocarbon is "dead" (age ≥ 50,000 years) suggests that the source is subducted carbonates incorporated into the melt at depth in the subduction zone and not local carbonates on the volcano edifice.

Biota

Lupton et al., (2006) report few vent animals right at Champagne vent site, although an extensive biological community was found within the surrounding few hundred m, including mussels, shrimps, crabs, and limpits.

References

Lupton, J. E., Baker, E.T., Embley, R.W., Resing, J.A., Massoth, G.J., Nakamura, K., Greene, R., Walker, S., Lebon, G., (2003). Hydrothermal helium plumes over submarine volcanoes of the Mariana Arc, Eos Trans. AGU, 84(46), Abstract T32A-0916.

Lupton, J., Butterfield, D., Lilley, M., Evans, L., Nakamura, K.I., Chadwick, W., Resing, J., Embley, R., Olson, E., Proskurowski, G., Baker, E., de Ronde, C., Roe, K., Greene, R., Lebon, G., Young, C., (2006). Submarine venting of liquid carbon dioxide on a Mariana Arc volcano. Geochemistry Geophysics Geosystems, 7: Art. No. Q08007.

Resing, J. A., Lebon, G., Baker, E., Lupton, J., Nakamura, K., Massoth, G., Embley, R., (2003), Geochemical characterization of hydrothermal plumes above hydrothermally active volcanoes on the Mariana Arc, Eos Trans. AGU, 84(46), Abstract T32A-0915.

B1: The Physical and Chemical Behaviour of CO_2 in the Ocean

The physical and chemical properties of CO_2 in seawater affect its fate upon release to the deep-sea environment. In this section a brief review is given of CO_2 phase transitions, buoyancy, hydrate formation, dissolution rates, chemistry of CO_2 in seawater, and the kinetics of CO_2 hydration and hydroxylation.

B1.1 CO_2 Phase Transitions

The phase transitions of CO_2 in the ocean are shown in Figure 1 as a function of temperature and hydrostatic pressure. Also shown for comparison are typical water column temperature-pressure profiles for the major ocean basins (from WOCE profiles).

Pure CO_2 exists as a gas in shallow surface waters, where the gas to liquid transition occurs at approximately 400-500m, depending on location and thus the water column temperature profile (see Table 1 & Figure 1 below). In the cold North and Barents Seas, off the coast of Norway, this transition occurs at slightly shallower depths of ~350-380m. (North Sea Hydrographic profiles from Norway Institute of Marine Research, via BODC database).

TABLE 1: Depth Of Gas To Liquid Transition In Worlds Oceans

Region	Pressure (dbar)	Depth (m)	Temperature (°C)
North/Barents Sea (64.7°N, 0.07°E)	345	341	0.7
North/Barents Sea (64.4°N, 0.7°E)	360	356	2.3
North/Barents Sea (62.7°N, 3.9°E)	381	377	4.5
North Pacific Ocean (E)	402	399	6.5
Indian Ocean 436	433	9.6	
North Atlantic Ocean (E)	461	457	11.8
North Pacific Ocean (W)	464	460	12.1
North Atlantic Ocean (W)	530	510	17.5

FIGURE 1: CO_2 Phase Diagram

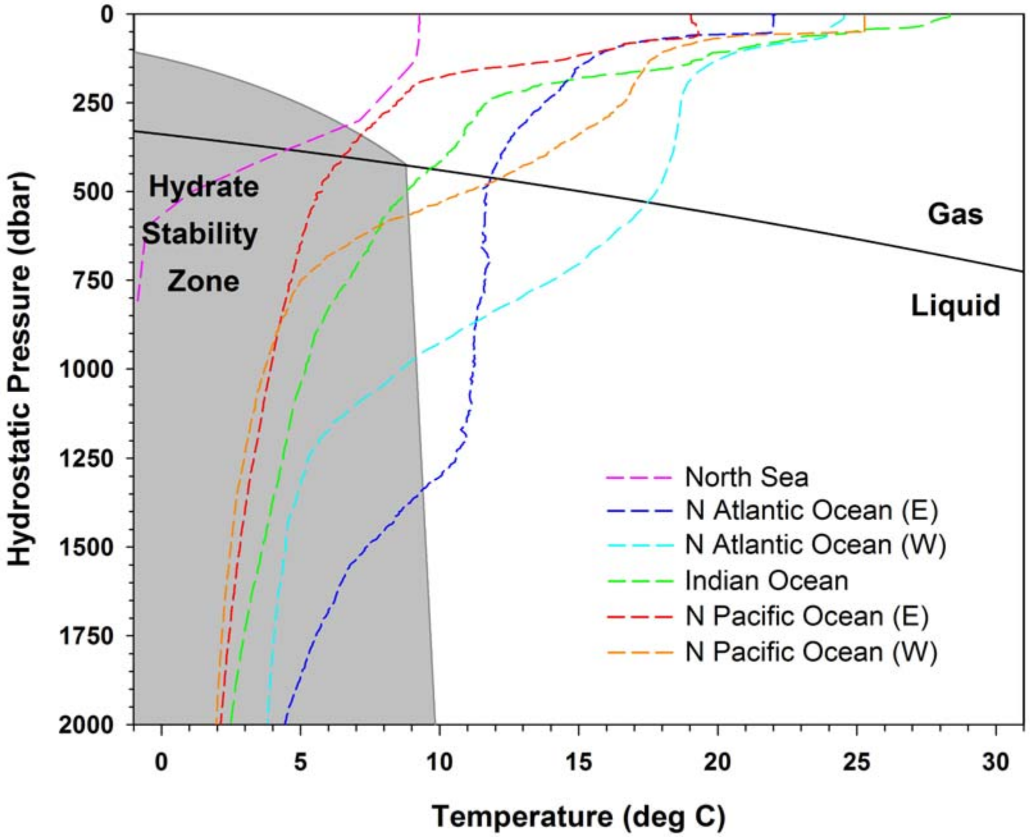

B1.2 CO_2 Density

CO_2 is a highly compressible fluid.

The density of CO_2 can be calculated from the equation of state (Span & Wagner, 1996). A software package, CO2Tab, based on this equation of state is commercially available. Under this approach, the properties of CO_2 are determined from fundamental equations, with no interpolation or curve fits to raw data. When densities calculated using CO2Tab are compared to CO_2 compressibility data available for the P-T conditions of interest here (Perry, 1950), a minor offset is observed (Figure 2a), where the application of a simple correction factor results in excellent agreement between the calculated and experimental values (Figure 2b; E. Peltzer pers. comm.). Within this report, all calculated CO_2 densities are the theoretical value determined from CO2Tab divided by the correction factor of 0.9956.

FIGURE 2: Comparison of the Theoretical and Observed Density of Liquid CO_2

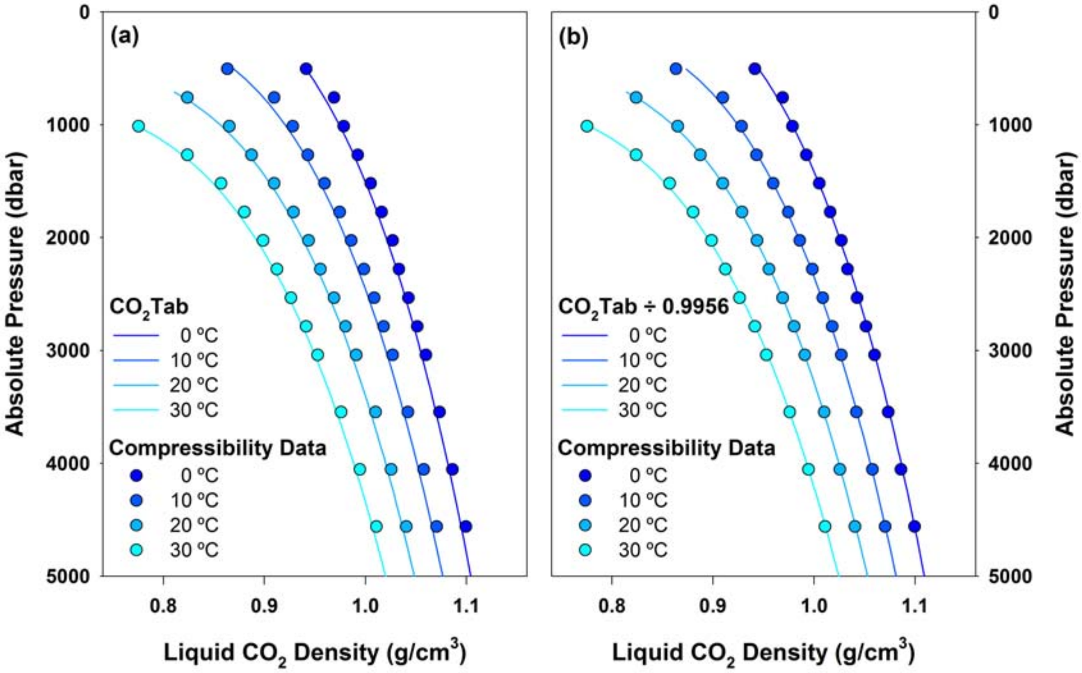

The increase in density of liquid CO_2 (ρ_{CO2}) with increasing hydrostatic pressure (depth) is shown in Figure 3 in comparison to the density of seawater (ρ_{SW}). The point of neutral buoyancy ($\rho_{CO2} = \rho_{SW}$) occurs at ~2600 dbar (see Table 2 and Figure 3). Thus at depths below this point CO_2 is more dense than seawater and will form a sinking plume, and at depths above this point CO_2 is less dense the seawater and will form a rising plume.

TABLE 2: Depth at which CO_2 is Neutrally Buoyant in the Worlds Oceans

Region	Pressure (dbar)	Depth (m)
North/Barents Sea	2277	2243
North Pacific Ocean (W)	2561	2528
North Pacific Ocean (E)	2576	2543
Indian Ocean 2584	2554	
North Atlantic Ocean (E)	2725	2688
North Atlantic Ocean (W)	2765	2727

FIGURE 3: COMPARISON OF SEAWATER & CO_2 DENSITIES

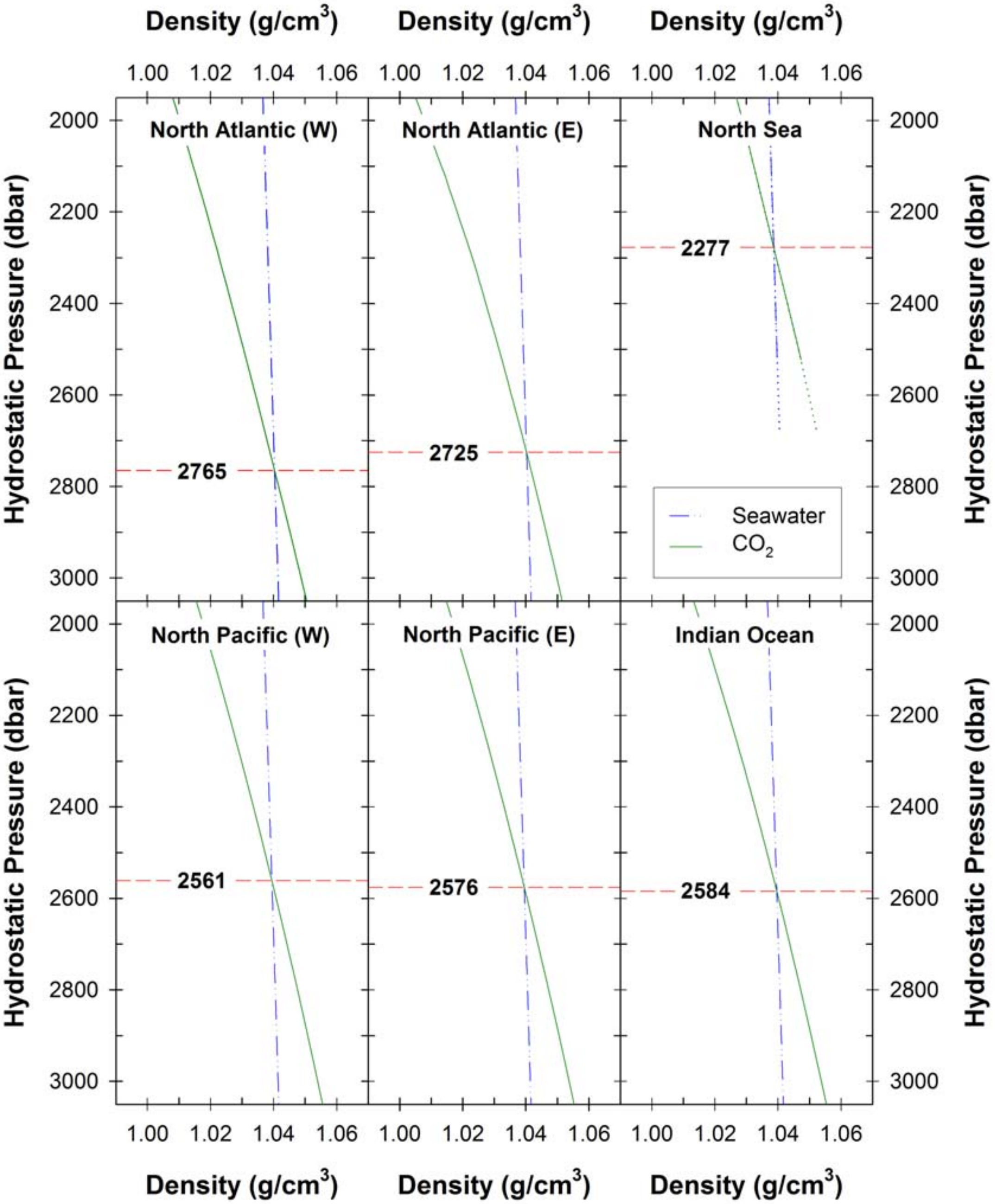

B1.3 CO_2 Hydrate

CO_2 readily forms a gas hydrate (or clathrate), where the phase boundary is well known, and in the Pacific Ocean typically occurs at ~325m depth (see Figure 1). Hydrates are a solid ice-like phase formed at low temperature and high pressure between a mixture of water and low molecular weight gases, where the 'host' water forms a molecular cage that traps the 'guest' gas. The water molecules that form the lattice are strongly hydrogen bonded with each other, and the gas molecules interact with the water molecules through Van der Waals forces. CO_2 forms a structure 1 hydrate (see Figure 4), which consists of 2 small water cages (5 pentagons, 5^{12}) and 6 large cages (5 pentagons & 6 hexagons, $5^{12}6^2$).

The reaction for CO_2 hydrate formation is:

CO_2 (g or l) + nH_2O (l) → $CO_2 \cdot nH_2O$ (s)

Where n is the hydration number (average moles of water required to cage one mole of CO_2). For the ideal hydrate, n has a value of 5.75, however the actual value of n for CO_2 hydrate typically varies from 6.07 to 7.8 (Yamamuro and Suga, 1989; Sloan 1991). In a review of the physical properties of CO_2 hydrate, Uchida et al. (1995) report a mean hydration number of 7.30±0.13.

A fully formed crystalline CO_2 hydrate (i.e. no void space/gas pockets) has a density of 1.112 g/cm^3 (recommended value of Chen (1972) and Bozzo et al. (1975); range in reported values is 1.054 to 1.134 g/cm^3 (Uchida et al., 1995 and references therein; Aya et al., 1997)). CO_2 hydrate is thus denser than seawater at all depths. Hydrate formation within the sediment column or at the sediment-seawater interface at a CO_2 vent site may therefore form a barrier to the rise of buoyant liquid or gaseous CO_2 (e.g. Lupton et al., submitted; Inagaki et al., submitted). Figure 5 shows a mass of CO_2 hydrate formed at the seafloor at a depth of ~3600m.

FIGURE 4: Structure 1 Hydrate consists of 2 small cages and 6 large cages. (a) Cages are formed by hydrogen bonding between water molecules shown in red (O) and white (H). The guest gas molecule is shown in green (CO_2). (b) Small cage geometry (5^{12}) (c) Large cage geometry ($5^{12}6^2$).

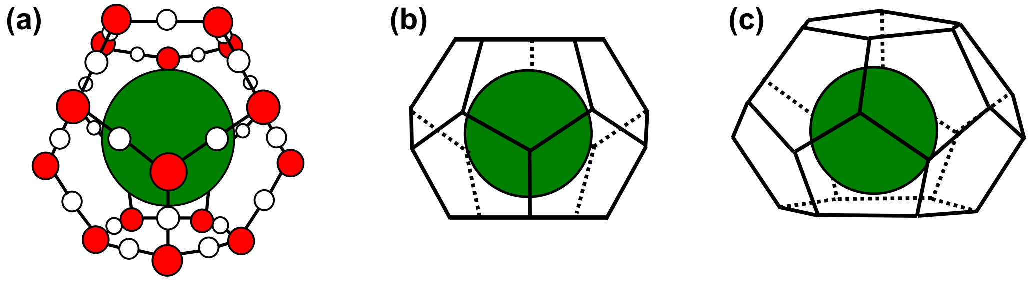

FIGURE 5: CO_2 Hydrate at the Seafloor (3600m water depth). (a) A pool of liquid CO_2 dispensed at the seafloor and contained within a white plastic corral. Note the presence of a thin hydrate film at the CO_2-seawater interface (b) The same corral 24 hours later showing formation of solid CO_2 hydrate. Note the 'frost-heave' appearance with sediments covering the surface of the CO_2 hydrate. This suggests that the dense liquid CO_2 penetrated into the sediment pore-space, leading to super-saturation of the pore-fluids, and enabling the rapid formation of a massive hydrate to erupt from the sediment column (Dunk et al., 2002).

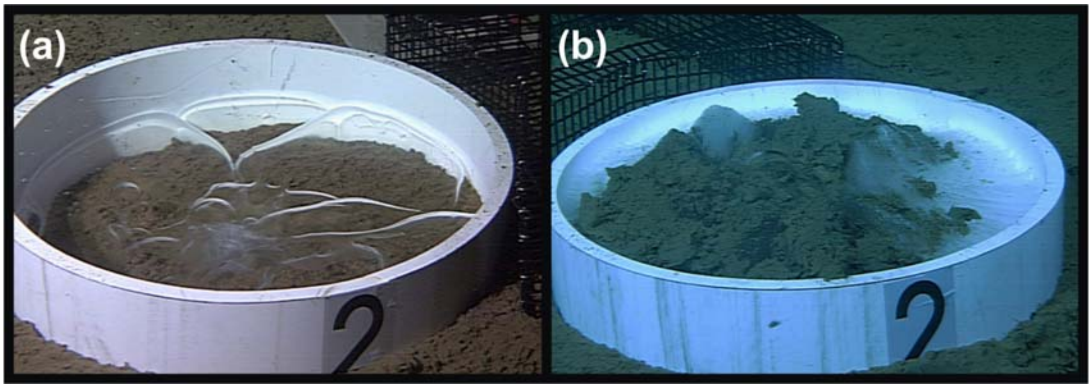

B1.4 Dissolution rate of CO_2 in the ocean

Exposed to an excess of seawater, CO_2 will eventually dissolve forming an aqueous phase with density higher than the surrounding seawater. The dissolution rate of liquid CO_2 can vary greatly with the vigor of mixing, which changes the surface area exposed, the thickness of the diffusive boundary layer, and potentially the thickness of the hydrate membrane formed. Measurements of the dissolution rate of liquid CO_2 and CO_2 hydrate have been made under varying conditions both in the laboratory and in-situ (see Table 3 for summary).

In a pressure vessel experiment, Aya et al (1997) measured the dissolution rate of a liquid CO_2 droplet at 30 MPa (absolute pressure, approximately equivalent to ~3000 m water depth) and 4.5 °C in the presence and absence of a hydrate membrane, determining rates of 1.7 and 2.8 $\mu mol/cm^2s$ respectively. Under comparable conditions in an in-situ experiment (3600m water depth, 1.6°C), Dunk et al. (2002) determined the dissolution rate of liquid CO_2 through a hydrate membrane under static conditions (i.e. shielded from seafloor currents) from pH perturbations, giving a dissolution rate of 1.7 $\mu mol/cm^2s$, in excellent agreement with the pressure vessel data.

In a dynamic water column experiment, Brewer et al. (2002) tracked buoyant CO_2 droplets (sheathed with a hydrate membrane) released at a depth of 800m and temperature of 4.4°C. The initial rise rate for 0.9 cm diameter droplets was 10 cm/s at 800m, and the dissolution rate (calculated from droplet shrinkage rates) was 3.0 $\mu mol/cm^2s$, where 90% of the mass loss occurred within 30 minutes over a 200m ascent from the release point. This moderately faster dissolution rate most likely reflects the dynamic conditions surrounding the plume droplets (i.e. thin boundary layer, under-saturation of seawater with respect to CO_2).

In contrast, Dunk et al. (2005) reported a slower dissolution rate of ~0.5 $\mu mol/cm^2s$ for liquid CO_2 through a hydrate membrane at 500m water depth and a temperature of 6°C. Although this experiment was conducted in-situ, the dissolution rate was determined in a closed vessel experiment, where the CO_2 was in contact with seawater that became progressively enriched in CO_2, and slow mixing rates were intermittently applied. Furthermore, visual observations indicated the formation of a comparatively thick hydrate membrane at the CO_2-seawater interface. Indeed, this dissolution rate is more comparable to that determined for solid CO_2 hydrate by Rehder et al. (2004). These authors transported cylindrical specimens of pure polycrystalline CO_2 hydrate ($CO_2{\cdot}5.75H_2O$) to the seafloor (1028m, 3.5°C) and measured the hydrate shrinkage rate under natural boundary conditions (variable flow field and undersaturation of seawater with respect to CO_2 hydrate), determining a dissolution rate of 0.4 μmol/cm^{2}s (Rehder et al., 2004).

TABLE 3: Dissolution rate of CO_2 in Seawater

Location	CO_2 Phase (L=liquid, H=hydrate)	Conditions	Dissolution Rate (μmol/cm^{2}s)
Pressure Vessel	L + H membrane	30MPa, 4.5°C1.7	
	L	30MPa, 4.5°C2.8	
Monterey Bay			
Seafloor	L + H membrane	3600m, 1.6°C, static	1.7
Water Column	L + H membrane	800m, 4.4°C, dynamic	3.0
Closed Vessel	L + H membrane	500m, 6.0°C, variable	0.5
Seafloor	H (n=5.75)	1000m, 3.5°C, dynamic	0.4

B1.5 Ocean Chemistry of CO_2

- **CO_2 Thermodynamics**

Following addition of CO_2 (gaseous, liquid or hydrate) to under-saturated seawater, the CO_2 will dissolve to form the aqueous phase:

CO_2 (g, l, h) → CO_2 (aq) **[1]**

Aqueous CO_2 then reacts with water to form carbonic acid (H_2CO_3):

CO_2 (aq) + H_2O $\Re$ H_2CO_3 **[2]**

Carbonic acid dissociates rapidly to form the bicarbonate ion (HCO_3^-) and a hydrogen ion (H^+, N.B. will actually be present as hydronium ions H_3O^+):

H_2CO_3 $\Re$ HCO_3^- + H^+ **[3]**

It should be noted that H_2CO_3 as a distinct chemical species has not been spectroscopically detected, and that the majority of dissolved CO_2 is present in the aqueous form (~99.7%, Langmuir, 1997). The direct reaction pathway from aqueous CO_2 to bicarbonate may also be significant:

CO_2 (aq) + H_2O $\Re$ HCO_3^- + H^+ **[4]**

As the two species CO_2 (aq) and H_2CO_3 cannot be distinguished from each other, for the purposes of equilibrium calculations these terms are combined as total dissolved CO_2 (referred to in the literature as both CO_2* and H_2CO_3*):

CO_2^* = CO_2 (aq) + H_2CO_3 **[5]**

Where the solubility of CO_2 is dependent on the fugacity of CO_2 (*f* = partial pressure of CO_2 corrected for non-ideal behavior. The fugacity is about 0.3% to 0.4% lower than the partial pressure over the conditions of interest) and K_0 (the solubility coefficient of CO_2 in seawater):

$$K_0 = \frac{[CO_2^*]}{f(CO_2)} \qquad [6]$$

And reactions [3] and [4] are approximated to an overall reaction with equilibrium constant K_1 (first dissociation constant of carbonic acid):

$CO_2^* \rightleftharpoons HCO_3^- + H^+$ **[7]**

$$K_1 = \frac{[HCO_3^-][H^+]}{[CO_2^*]} \qquad [8]$$

The bicarbonate ion can undergo a further dissociation to form carbonate and a second hydrogen ion, with equilibrium constant K_2 (second dissociation constant of carbonic acid):

HCO_3^- $\Re$ CO_3^{2-} + H^+ **[9]**

$$K_2 = \frac{[CO_3^{2-}][H^+]}{[HCO_3^-]} \qquad [10]$$

K_1 and K_2 have been determined for various temperatures and salinities by several different investigators. The data presented by Merbach et al. (1973) are based on experiments conducted using real seawater, and the values of K_1 and K_2 preferred here are the recent refits of this data presented by Lueker et al. (2000). The preferred value of K_0 is from Weiss (1974).

The total dissolved inorganic carbon in seawater (referred to within the literature variably as DIC, TCO_2, TC, or ΣCO_2) is the sum of carbon contained within this system:

$$TCO_2 = CO_2^* + HCO_3^- + CO_3^{2-} \quad \textbf{[11]}$$

- **Buffering & Alkalinity**

The oceans have a large chemical capacity to take up CO_2 due to the extensive buffering capacity of the seawater carbonate system.

The oceans are described as a highly buffered system since relatively large quantities of acid or base can be added to seawater without causing a large change in pH, i.e. the concentration of chemical species whose equilibria controls pH ($\log_{10}\{H^+\}$) is significantly higher than the concentrations of either H^+ or OH^-.

The alkalinity of seawater is its capacity to act as a base by reacting with protons (hydrogen ions). In this respect, alkalinity can be considered as the ability of seawater to neutralize added acids, and is sometimes referred to as the acid neutralisation capacity (ANC). Several anions in seawater can act as buffers, where total alkalinity (TAlk) is measured in milli-equivalents per litre (meq/L). Various definitions of alkalinity (differing in the seawater ions included) have been given in the literature. The definition presented here is that given by Dickson (1981):

$$\begin{aligned} TAlk = {} & [HCO_3^-] + 2[CO_3^{2-}] + [B(OH)_4^-] + [OH^-] + [HPO_4^{2-}] + 2[PO_4^{3-}] + \\ & [SiO(OH)_3^-] + [HS] + 2[S] + [NH_3] - [H^+] - [HSO_4^-] - [HF] - [H_3PO_4] \quad \textbf{[12]} \end{aligned}$$

At circumneutral pH, the pKas of boric, phosphoric, silicic, and sulfuric acids are such that these acids make a small contribution to TAlk (i.e. these acids are dominantly present in the protonated forms), and the concentration of the hydrogen and hydroxide ions are near negligible. The Carbonate Alkalinity (CAlk) can therefore be used to approximate seawater alkalinity. As the concentration of carbonate is also significantly lower than that of bicarbonate, unless there are significant amounts of organic acids present, seawater alkalinity is largely dependent on the concentration of the bicarbonate ion.

$$CAlk = [HCO_3^-] + 2[CO_3^{2-}] \approx [HCO_3^-] \quad \textbf{[13]}$$

- **Effect of adding CO_2 to Seawater**

Adding CO_2 increases TCO_2 without changing TAlk (no change in total charge).

The principal effect of adding CO_2 to seawater is to consume the carbonate ion and to form the bicarbonate ion:

$$CO_2 + H_2O + CO_3^{2-} \rightarrow 2HCO_3^- \quad \textbf{[14]}$$

In addition, some CO_2 undergoes simple reaction with water

$$CO_2 + H_2O \rightarrow H^+ + HCO_3^- \quad \textbf{[15]}$$

In either case, TAlk does not change. The combined reactions produce bicarbonate, and lower both ocean pH (increase acidity) and carbonate ion concentration (see Figure 7 below).

The speciation of the TCO_2 system in seawater as a function of pH is shown in Figure 6. Although it may appear that pH controls the relative proportions of the CO_2 system species, this is somewhat misleading. Rather it is the TCO_2 that controls the speciation of the CO_2 system and thus the pH of seawater. This is illustrated in Figure 7, which shows the pH, CO_2^*, HCO_3^- and CO_3^{2-} concentrations for a parcel of seawater that is progressively enriched in TCO_2.

FIGURE 6: Speciation of the CO_2 System in Seawater as a function of pH.

Pacific Ocean water (WOCE Line P17N, Station 10) at P = 458.1 dbar , S = 34.1, T = 6.0°C, TCO_2 = 2886.9 mmol/kg, TAlk = 2306.4 meq/kg, pH = 7.614 (total scale).

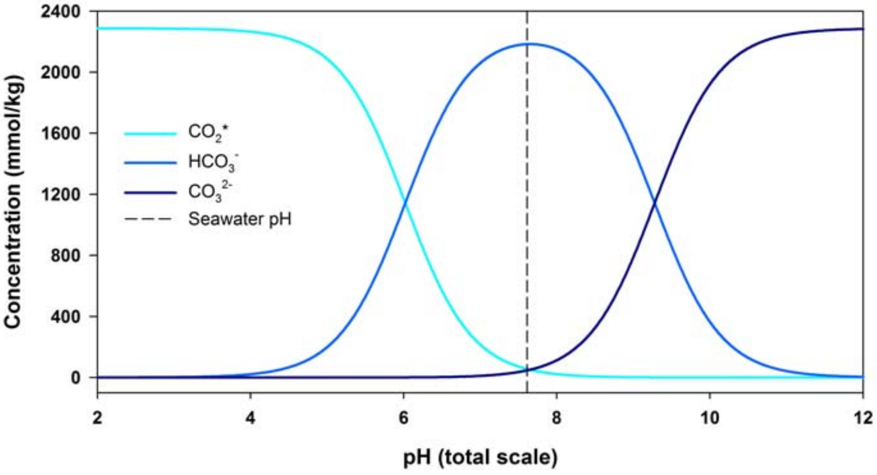

FIGURE 7: Change in CO_2 system speciation and seawater pH on enrichment of seawater TCO_2 (i.e. addition of CO_2 up to 5 times seawater concentration).

Pacific Ocean water (WOCE Line P17N, Station 10) at P = 458.1 dbar , S = 34.1, T = 6.0°C, TCO_2 = 2886.9 mmol/kg, TAlk = 2306.4 meq/kg, pH = 7.614 (total scale).

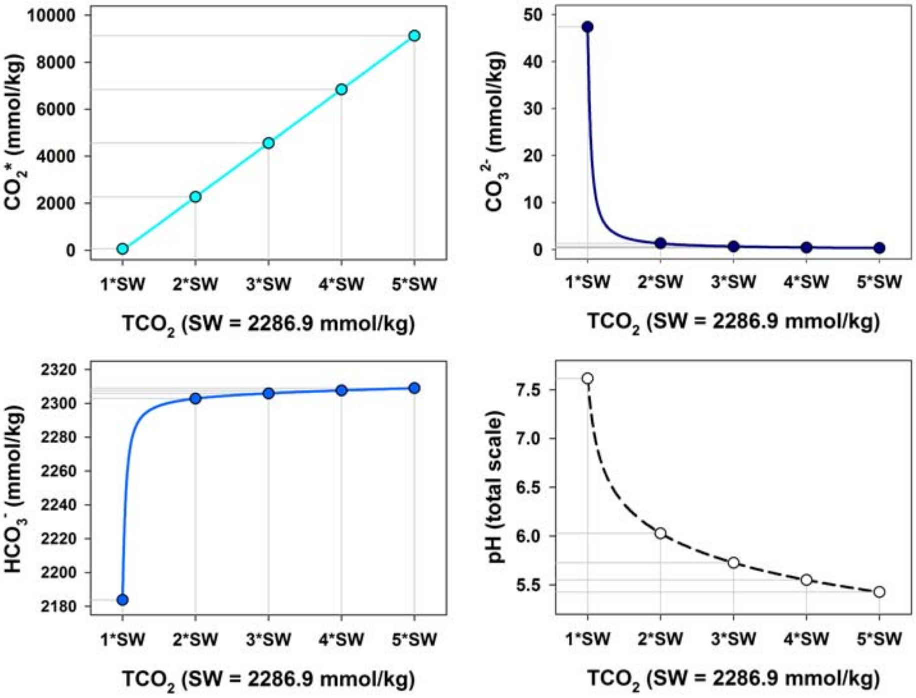

- **Dissolution of Calcium Carbonate**

The solubility product, K_{SP}, defines the solubility of a mineral. K_{SP} is the product of the concentration of the constituent ions of the mineral in solution when at equilibrium with the solid phase, and will vary with T and P. For calcium carbonate ($CaCO_3$):

$$K_{SP} = [Ca^{2+}][CO_3^{2-}] \qquad \textbf{[16]}$$

There are two polymorphs of calcium carbonate, calcite and aragonite. Aragonite is more soluble than calcite, thus K_{SP}(aragonite) > K_{SP}(calcite).

The saturation state of seawater with respect to calcium carbonate is described by the solubility ratio, Ω:

$$\Omega = [Ca^{2+}][CO_3^{2-}]/K_{SP} \qquad \textbf{[17]}$$

Where values of Ω <1 represent undersaturation ($CaCO_3$ will dissolve) and values of Ω >1 represent supersaturation ($CaCO_3$ will precipitate).

The consumption of CO_3^{2-} following the addition of CO_2 to seawater (see equation 14 above) will decrease Ω. Depending of the initial value of Ω, this will either make it more difficult to precipitate $CaCO_3$, or lead to dissolution of $CaCO_3$.

Dissolving $CaCO_3$ produces CO_3^{2-}, thus adding 2 mole equivalents of TAlk and one mole of TCO_2 to seawater through the reaction:

$$CaCO_3\,(s) \;\Re\; Ca^{2+} + CO_3^{2-} \qquad \textbf{[18]}$$

The carbonate ion will then react with CO_2 to form bicarbonate:

$$CO_2 + CO_3^{2-} + H_2O \;\Re\; 2HCO_3^{-} \qquad \textbf{[19]}$$

Thus increasing TAlk more than TCO_2 leads to a decrease in the partial pressure of CO_2, and the overall effect of dissolving $CaCO_3$ is:

$$CaCO_3\,(s) + CO_2 + H_2O \;\Re\; Ca^{2+} + 2HCO_3^{-} \qquad \textbf{[20]}$$

B1.6 Measurement of the CO_2 System in Seawater

- **Analysis of the CO_2 system at ambient concentrations**

At ambient seawater concentrations ($TCO_2 \approx 2$ mmol/kg), it is not currently possible to measure the individual concentrations of CO_2*, HCO_3^- and CO_3^{2-} in seawater, and the CO_2 system is characterized by four measurable parameters:

(1) Total Alkalinity, TAlk (equation 12 above)
(2) Total Inorganic CO_2, TCO_2 (equation 11 above)
(3) $pH = -\log_{10}\{H^+\}$
(4) the fugacity of CO_2 in air that is in equilibrium with the sample, $f(CO_2)$

The knowledge of any two of these parameters, along with temperature, pressure, abundances of other constituents of seawater (principally the concentrations of Si and PO_4^{3-}), and the relevant equilibrium constants, allows determination of the other two parameters, and the CO_2 system speciation. In practice, a third parameter is usually measured to check the internal consistency of any measurements and calculations.

NOTE: an excellent software package, CO2SYS, which calculates the CO_2 system speciation under user-defined conditions is available for download free of charge (Lewis & Wallace, 1998).

- **Analysis of the CO_2 system at elevated concentrations**

Although there are as yet no techniques available for the direct determination of the CO_2 system speciation at ambient concentrations ($TCO_2 \approx 2.0$-2.5 mmol/kg), new techniques are being developed for in-situ analysis at higher concentrations. In particular, Raman spectroscopy offers the unique promise of separate detection of the CO_2 system species, since each has a characteristic spectroscopic signal (Nakamoto, 1997; Davis & Oliver, 1972, Figure 8).

The rapid development of laser Raman spectrometers (LRS) for deep-sea science (Brewer et al., 2004a; Pasteris et al., 2004) provides new opportunities for advanced detection of the oceanic CO_2 system. In a recent deployment of a deep-sea LRS, Dunk et al. (2005) reported an in-situ detection limit for CO_2* of ~10 mmol/kg (at 500 m depth), improving considerably on the previously reported detection limits for the aqueous CO_2 system. Although direct comparisons between detection of CO_2*, HCO_3^-, and CO_3^{2-} should not be made due to different Raman scattering efficiencies of these species, laboratory analysis has demonstrated that the current DORISS system allows direct detection of 15mM HCO_3^-, where the use of a new generation of advanced high volume collection optics (product currently under development from Kaiser Optical Systems, Inc.) enables direct detection of 7mM HCO_3^- (Brewer et al., 2004b).

In summary, Raman detection of the oceanic CO_2 system ($TCO_2 = CO_2^* + HCO_3^- + CO_3^{2-}$) is capable of providing direct quantitative assessment of carbonate system speciation at elevated levels (ca. 5-10 times ambient seawater concentrations). The application of the Raman technique is therefore suitable for examination of natural deep-ocean volcanic CO_2 sources, and other sites where elevated CO_2 concentrations are expected (e.g. monitoring of oceanic CO_2 disposal sites or the seepage or leakage of CO_2 from sub-seafloor geologic sequestration sites). Furthermore, although the natural levels of CO_2 in the ocean are typically too low to detect with current instrument sensitivity, there are significant opportunities for signal enhancement (3,4). These techniques are currently under development for application in the ocean, and in-situ detection limits can be expected to improve substantially over the next 5-10 years.

FIGURE 8: Raman Spectra of CO_2*, HCO_3^- and CO_3^{2-}

The spectrum for CO_2* (136 mmol/kgwas acquired in-situ). The spectra for HCO_3^- and CO_3^{2-} were acquired in the laboratory from aqueous solutions of $NaHCO_3$-Na_2SO_4 (487 mmol/kg:31 mmol/kg) and Na_2CO_3-Na_2SO_4 (124 mmol/kg:31 mmol/kg), where the concentration of SO_4^{2-} is approximately equal to that of seawater. The peak at 1332 Δcm^{-1} is from a diamond wafer placed in the optical path of the instrument.

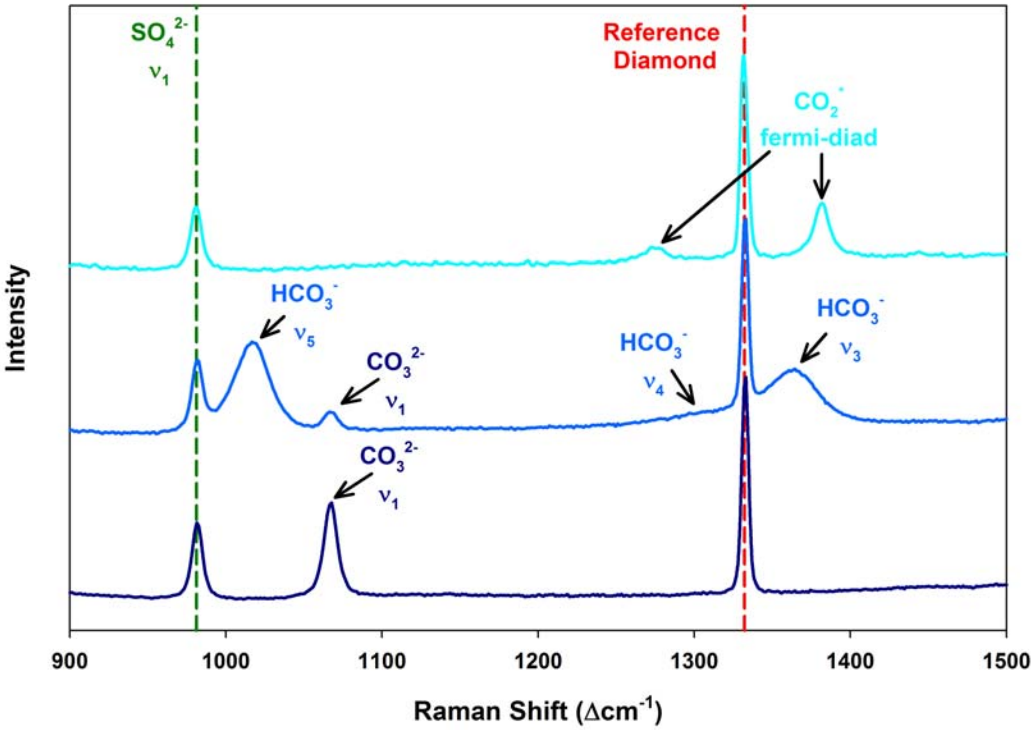

B1.7 CO_2 Rich Plumes, Perturbation of Seawater pH & the Kinetics of CO_2 Hydration and Hydroxylation.

The slow hydration and hydroxylation kinetics of carbon dioxide at ambient temperatures and pressures are well known to ocean chemists. This has serious implications both for the sensing of CO_2 rich plumes and the accurate estimation of the TCO_2 burden in the water column surrounding a CO_2 release site.

In investigations of CO_2 dissolution in seawater as part of an ocean CO_2 sequestration scenario, Brewer et al. (2005) artificially created a CO_2 rich plume of seawater by generating flow over a contained reservoir of liquid CO_2 placed on the seafloor. CTD & pH sensors were placed at various distances downstream from this “benthic flume”. When currents were favorable, the plume of CO_2 enriched seawater passed the sensors, and negative pH spikes were recorded. Although a decrease in pH is expected from the addition of CO_2 (see Figure 7 above), the low pH excursions were frequently accompanied by negative spikes in conductivity. Normally, one would expect that if sufficient CO_2 had dissolved to depress the pH, a proportional increase in the conductivity would occur due to the presence of additional H^+ and HCO_3^- ions. Brewer et al. (2005) attributed the negative spikes in conductivity to disequilibrium in the CO_2 system, where varying quantities of excess dissolved CO_2 were "diluting" the seawater salinity, and hence decreasing the conductivity.

The presence of unreacted CO_2 was confirmed by drawing a sample (~500 ml) of the CO_2 enriched seawater from the plume into a reaction vessel fitted with pH probe. The reaction vessel was then closed, and the trapped solution pumped around a small recirculation loop (to ensure thorough mixing) until the system had reached equilibrium (see Figure 9). While the initial pH of the plume water at the time it was drawn into the reaction cell was ~0.22-0.25 units below ambient, at equilibrium the ΔpH was much larger at 1.06-1.11 units (Figure 9). For this example, using the pH measured in the plume would suggest a TCO_2 enrichment of ~70-80 μmol/kg, underestimating the true TCO_2 enrichment by a factor of 6-7.

In summary, the slow hydration of CO_2 is such that at a CO_2 release site, local advection may remove the reactants far from the observing site before equilibrium is reached. A pH electrode senses only hydrogen ions, and thus will not detect the dissolved CO_2 signal until after the hydration step, and subsequent rapid de-protonation steps, are complete. This can result in significant underestimation of the true dissolved CO_2 burden. Corrections to this can be made by either (i) observing the reduction in conductivity caused by the large quantity of non-ionic CO_2 flowing by the sensor or (ii) trapping a sample of the CO_2 enriched water and allowing it to reach equilibrium.

FIGURE 9: Example of CO_2 System Disequilibrium

The pH record from a closed loop flow experiment carried out on water samples drawn from a CO_2 rich plume. Ambient seawater pH of 7.88 is measured above the plume (A). The intake tube is lowered into the plume, and a decreased varying pH of ~7.6 is observed (B). On closing the circulation cell, the pH signal quickly drops to a stable pH of ~6.77 (C). The sequence is repeated by opening the cell, recording once again higher, and rapidly varying, pH signals in the CO_2 rich plume (D). Upon closing the cell the pH again drops (E). On opening the cell and raising the intake tube into background seawater normal and stable ocean values are recorded (F).

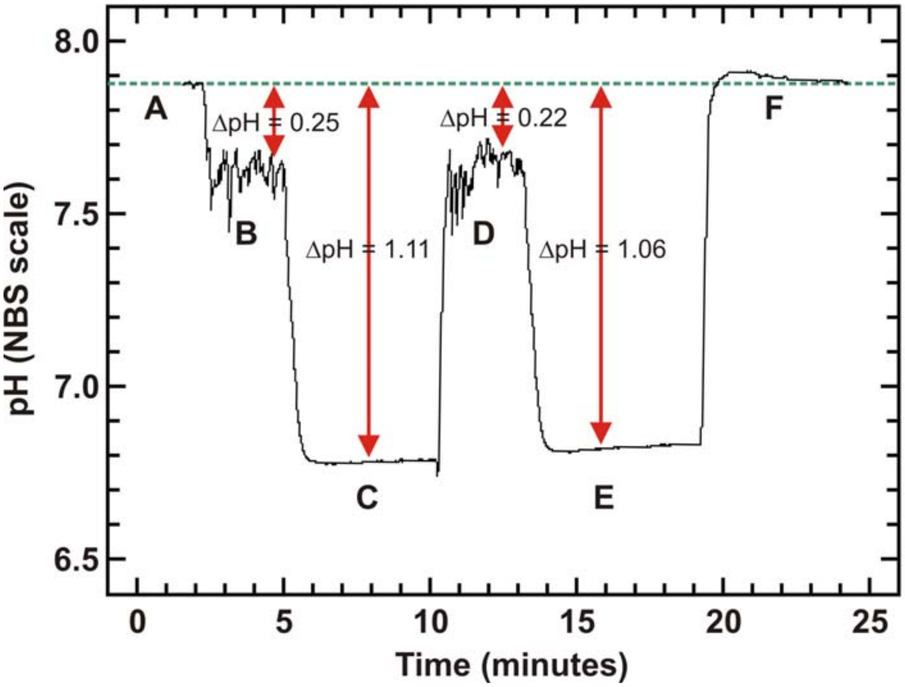

Johnson (1982) reported the rate constants for the hydration and hydroxylation of CO_2 in seawater as a function of temperature. Zeebe and Wolf-Gladrow (2001), have compiled an elegant and comprehensive kinetic model of CO_2 hydration and hydroxylation, which illustrates the strong impact of pH on the rate of reaction. In recent work the Zeebe and Wolf-Gladrow model has been compared to observed in-situ reaction rates measured at depths from 5 to 1000m in the Pacific Ocean (Peltzer et al., 2005; Dunk et al., in prep). Based upon these comparisons, it is clear that experimental measurements made in-situ are in very good agreement with the model of Zeebe and Wolf-Gladrow (2001). Likewise, for future measurements in dynamic environments, this model should be an excellent predictor of the time necessary to achieve equilibrium and thus provide an advance indication of the spatial and time frames for analyses. A MATLAB script file for performing these calculations is available (Dunk et al., in prep).

NOTES ON PRESSURE

Absolute Pressure = Hydrostatic Pressure + Pressure at sea-level (1 atm)

Hydrostatic pressure (dbar) is approximately equivalent to depth (m), where the absolute relationship between these parameters is dependent on latitude (Unesco, 1983).

References

Aya, I., Yamane, K., Narai, H., 1997. Solubility of CO_2 and density of CO_2 hydrate at 30 MPa. Energy 22, 263-271.

Bozzo, A.T., Chen, H-S., Kass, J.R., Barduhn, A.J., 1975. Dealination, 16 (303).

Brewer, P.G., Peltzer, E.T., Friedrich, G., Rehder, G., 2002. Experimental determination of the fate of rising CO_2 droplets in the water column. Environmental Science and Technology 36, 5441-5446.

Brewer, P.G.; Malby, G.; Pasteris, J.D.; White, S.N.; Peltzer, E.T.; Wopenka, B.; Freeman, J.; Brown, M.O. Development of a laser Raman spectrometer for deep-ocean science. Deep-Sea Res. I, 2004a, 51, 739-753.

Brewer, P.G.; Dunk, R.M.; White, S.N.; Peltzer, E.T.; Bowie, B.; Walz, P.M. First attempts at direct Raman detection of the oceanic carbonate system. Eos. Trans. AGU. 2004b, Fall Meet. Suppl., Abstract OS43B-0557.

Chen, H-S., Res. Develop. Prog. Report No. 830, Office of Saline Water, U.S. Dept. of Interior, Washington, D.C., 1 (1972).

Davis, A.R.; Oliver, B.G. A vibrational-spectroscopic study of the species present in the CO_2-H_2O system. J. Sol. Chem. 1972, 1, 329-339.

Dickson, A.G., 1981. An exact definition of total alkalinity and a procedure for the estimation of alkalinity and total inorganic carbon from titration data. Deep-Sea Res. 28A, 609–623.

Dunk, R. M., Peltzer, E. T., Rehder, G., Brewer, P. G., 2002. Dissolution rate of liquid CO_2 at 3600m depth as determined by pH measurements. EOS, Trans. AGU, Ocean Sciences Meeting Suppl., Abstr. OS51F-06.

Dunk, R. M., Peltzer, E. T., Walz, P.M., Brewer, P. G. 2005. Seeing a deep ocean CO_2 enrichment experiment in a new light: Laser Raman detection of dissolved CO_2 in seawater. Environmental Science and Technology 39,9630-9636.

Dunk, R.M., Peltzer, E.T., Walz, P.M., Brewer, P.G., in prep. The hydration rate of CO_2 in the ocean: effects of pH, temperature, and pressure. To be submitted to Marine Chemistry.

Gabitto, J., Tsouris, C., 2004. Dissolution mechanisms of CO_2 hydrate droplets in deep seawaters. Energy Conservation and Management.

Johnson, K. S. 1982. Carbon dioxide hydration and dehydration kinetics in sea water. Limnol. Oceanogr., 27, 849–855.

Langmuir, D., 1997. Aqueous Environmental Geochemistry: Prentice Hall, New Jersey, 600 p.

Lewis, E., Wallace, D., 1998. Program developed for CO_2 system calculations. Program developed for CO2 system calculations. Rep. 105, 33 pp., Oak Ridge Natl. Lab., U.S. Dep. of Energy, Oak Ridge, Tenn. (Available at http://cdiac.esd.ornl.gov/oceans/co2rprt.html)

Lueker, T.J., Dickson, A.G., Keeling, C.D., 2000. Ocean pCO2 calculated from dissolved inorganic carbon, alkalinity, and equations for K1 and K2: validation based on laboratory measurements of CO_2 in gas and seawater at equilibrium. Marine Chemistry 70, 105-119.

Merbach, C., Culberson, C.H., Hawley, J.E., Pytkowitcz, R.M., 1973. Measurement of the apparent dissociation constants of carbonic acid in seawater at atmospheric pressure. Limnol. Oceanogr. 18, 897-907.

Nakamoto, K. Infrared and Raman Spectra of Inorganic and Coordination Compounds, Part A.: Theory and Applications in Inorganic Chemistry. 1997, Wiley.

Peltzer, E.T., Brewer, P.G., Dunk, R.M., Fuchs, M.P., Walz, P.M., 2006. Deep Ocean CO_2 Hydration Kinetics. AGU Ocean Sciences Meeting, Abstract OS45B-20.

Pasteris, J.D.; Wopenka, B.; Freeman, J.J.; Brewer, P.G.; White, S.N.; Peltzer, E.T.; Malby, G. Raman spectroscopy in the deep ocean: successes and challenges. Appl. Spectrosc. 2004, 58, 195A – 208A.

Perry, J.H., 1950. Chemical Engineers Handbook. McGraw-Hill Book Company, Inc. New York, Toronto, and London. Table 155, Compressibility Factors of Carbon Dioxide, pg 206.

Rehder, G., Kirby, S.H., Durham, W.B., Stern, L.A., Peltzer, E.T., Pinkston, J., Brewer, P.G., 2004. Dissolution rates of pure methane hydrate and carbon-dioxide hydrate in undersaturated seawater at 1000-m depth. Geochimica et Cosmochimica Acta 68, 285-292.

Sloan Jr., E.D., 1991. Clathrate Hydrates of Natural Gases, Marcel Dekker, New York.

Span, R., Wagner, W., A New Equation of State for Carbon Dioxide Covering the Fluid Region from the Triple Point Temperature to 1100 K at Pressures up to 800 Mpa. J. Phys. Chem. Ref. Data, Vol. 25, No. 6, 1996.

Uchida, T., Hondoh, T., Mae, S., Kawabata, J., 1995. Physical data of CO_2 Hydrate. In: Handa, N., and Ohsumi, T., (Eds.), Direct Ocean Disposal of Carbon Dioxide. Terra Scientific Publishing Company, Tokyo. pp.45-61.

Unesco, 1983. Algorithms for computation of fundamental properties ofseawater, 1983. _Unesco Tech. Pap. in Mar. Sci, No. 44, 53 pp. Eqn 25, p26.

Weiss, R.F., 1974. Carbon dioxide in water and seawater, the solubility of a non-ideal gas. Marine Chemistry 2, 203-215.

Yamamuro, O., Suga, H., 1989. Thermal Analysis 35, 2025.

Zeebe, R., Wolf-Gladrow, D., (2001). CO2 in seawater: Equilibrium, Kinetics, Isotopes. Elsevier. Amsterdam. 346pp.

References

Chapter 1

Akimoto K., Kotsubo H., Asami T., Li X., Uno M., Tomoda T., Oshumi T., (2004). Evaluation of Carbon Sequestration in Japan with a Mathematical Model. Energy, 29: 1537-1549.

Bachu, S., (2003). Screening and ranking of sedimentary basins for sequestration of CO_2 in geological media. Environmental Geology, 44: 277-289.

Bachu, S., (2005). Module 13 - Current potential for CO_2 capture and geological storage in the APEC region. In: Harwood, J., (Ed.), Building capacity for CO_2 capture and storage project in the APEC region: A training manual for policy makers and Practitioners. The Delphi Group, APEC Reference #205-RE-01.3

Bøe, R., Magnus, C., Osmundsen, P.T., Rindstad, B.I., (2002). CO_2 point sources and subsurface storage capacities for CO2 in aquifers in Norway. Norsk Geologische Undersogelske, Trondheim, Norway, NGU Report 2002.010.

Bradshaw, J., Dance, T., (2005). Mapping geological storage prospectivity of CO_2 for the world's sedimentary basins and regional source to sink matching. In: Rubin, E.S., Keith, D.W., Gilboy, C.F., Wilson, M., Morris, T., Gale J., Thambimuthu K., (Eds.), Greenhouse Gas Control Technologies 7 (Proceedings of the 7th International Conference on Greenhouse Gas Control Technologies (GHGT-7), 5-9 September 2004, Vancouver, Canada), v1: p. 583-592, Elsevier.

Bradshaw, J., Rigg, A.J., (2001). The GEODISC Program: Research into geological sequestration of CO_2 in Australia. Environmental Geosciences, 8: 166-176.

Bradshaw, J. B., Bradshaw, E., Allinson, G., Rigg, A.J., Nguyen, V., Spencer, A., (2002). The potential for geological sequestration of CO_2 in Australia: preliminary findings and implications to new gas field development. Australian Petroleum Production and Exploration Association Journal, 42: 24-46.

Bradshaw, J., Allinson, G., Bradshaw, B.E., Nguyen, V., Rigg, A.J., Spencer, L., Wilson, P., (2004). Australia's CO_2 geological storage potential and matching of emissions sources to potential sinks. Energy, 29: 1623-1631.

Chargin, A., Socolow, R., (1997). Fuels decarbonisation and carbon sequestration: report of a workshop. Rep. PU/CEES 302, Princeton Univ. Cent. Energy Environ. Stud., Princeton, NJ

ChevronTexaco Australia Pty Ltd., (2005). Draft Environmental Impact Statement/Environmental Review and Management Programme for the Proposed Gorgon Development: Main Report. ChevronTexaco Australia Pty Ltd.

Curtin University of Technology (2004). A Technical Appraisal of the feasibility for the Sequestration of Gorgon Gas Field Carbon Dioxide at Barrow Island (Phase 2). Curtin University of Technology, Perth.

Dooley, J.J., Friedman, S.J., (2004). A regionally disaggregated global accounting of CO_2 storage capacity: Data and assumptions. Battelle, Pacific Northwest Division Technical Report Number PNWD-3431.

Dooley, J.J., Kim, S.H., Edmonds, J.A., Friedman, S.J., Wise, M.A., (2005). A first-order global geologic co_2 storage potential supply curve and its application in a global integrated assessment model. In: Rubin, E.S., Keith, D.W., Gilboy, C.F., Wilson, M., Morris, T., Gale J., Thambimuthu K., (Eds.), Greenhouse Gas Control Technologies 7 (Proceedings of the 7th International Conference on Greenhouse Gas Control Technologies (GHGT-7), 5-9 September 2004, Vancouver, Canada), v1: p. 573-581, Elsevier.

Hanisch, C., (1998). The pros and cons of carbon dioxide dumping. Environmental Science and Technology, 32: 20A-24A

Hendriks, C., Graus, W., van Bergen, F., (2004). Global carbon dioxide storage potential and costs. Report by Ecofys in cooperation with TNO. EEP-02001 by order of the: Rijksinstituut voor Volksgezondheid en Milieu (Dutch National Institute for Public Health and the Environment).

Herzog, H., Drake, E., Adams, E., (1997). CO_2 capture, reuse, and storage technologies for mitigating global climate change. White Paper Final Report, Energy Laboratory, Massachusetts Institute of Technology, US Department of Energy Order No: DE-AF22-96PC01257.

Holloway, S. (Ed.), (1996): The underground disposal of carbon dioxide. Final report of Joule 2 Project No. CT92-0031. British Geological Survey, Keyworth, Nottingham, UK.

Holloway, S., (2005). Underground sequestration of carbon dioxide—a viable greenhouse gas mitigation option. Energy, 30: 2318–2333.

IEA-GHG (2002). Building the cost curves for CO_2 storage, Part 1: sources of CO_2, Greenhouse Gas R&D Programme Report No. PH4/9.

IEA-GHG (2004). A review of global capacity estimates for the geological storage of carbon dioxide. IEA Greenhouse Gas R&D Programme Technical Review (TR4).

Imbus, S.W., Katz, B.J., Urwongse, T., (1998). Predicting CO_2 occurrence on a regional scale: Southeast Asia example. Organic Geochemistry, 29: 325-345.

IPCC, (2005). IPCC Special Report on Carbon Dioxide Capture and Storage. Prepared by Working Group III of the Intergovernmental Panel on Climate Change. Metz, B., Davidson, O., de Coninck, H.C., Loos, M., Meyer, L.A., (Eds.), Cambridge University Press, Cambridge, United Kingdom and New York, NY, USA, 442 pp.

IPCC, (2007). Climate Change 2007: Mitigation. Contribution of Working Group III to the Fourth Assessment Report of the Intergovernmental Panel on Climate Change. Metz, B., Davidson, O.R., Bosch, P.R., Dave, R., Meyer, L.A., (Eds.), Cambridge University Press, Cambridge, United Kingdom and New York, NY, USA., 851 pp.

JAPEX (Japan Petroleum Exploration Co., Ltd) website: http://www.japex.co.jp/english/technology/gtl.html (accessed October 2007).

Kaya, Y., Koide, H., Nakaya, T., Ohsumi, T., Takita, K., Yoshimura, S., (2001). Underground sequestration of carbon dioxide in tectonically active area. In: Durie, R.A., Williams, D.J., Smith, A.V., McMullan, P.,

Li, X., Ohsumi, T., Koide, H., Akimoto, K., Kotsubo, H., (2005). Near-future perspective of CO_2 aquifer storage in Japan: Site selection and capacity. Energy, 30: 2360-2369.

Matter, J.M., Assayag, N., Goldberg, D., (2006). Basaltic rocks and their potential to permanently sequester industrial carbon dioxide emissions. Proceedings of the 8th International Conference on Greenhouse Gas Control Technologies (GHGT-8), 19-22 June 2006, Trondheim, Norway. Paper 02_01_04.

Manancourt, A., Gale, J., (2005). A review of capacity estimates for the geological storage of CO_2. In: Rubin, E.S., Keith, D.W., Gilboy, C.F., Wilson, M., Morris, T., Gale J., Thambimuthu K., (Eds.), Greenhouse Gas Control Technologies 7 (Proceedings of the 7th International Conference on Greenhouse Gas Control Technologies (GHGT-7), 5-9 September 2004, Vancouver, Canada), v2: p. 2051-2054. Elsevier.

Mignot, V., Le Gallo, Y., Lecomte, J-C., Euzen, T., Vallaure, T., Mallo, J., (2006). Casablanca Field, a depleted karstic oil reservoir for geological storage of CO2. Proceedings of the 8th International Conference on Greenhouse Gas Control Technologies (GHGT-8), 19-22 June 2006, Trondheim, Norway. Paper 02_04_11.

Oen, P.M., (2003): The development of the Greater Gorgon Gas Fields. APPEA Journal, 43: 167-177.

Paulson, C.A.J., (Eds.), Greenhouse Gas Control Technologies (Proceedings of the 5th International Conference on Greenhouse Gas Control Technologies (GHGT-5), 13-16 August 2000, Cairns, Australia). CSIRO Publishing, p. 296-8.

RCEP (2000). Energy: The Changing Climate. The 22nd Report Issued By The Royal Commission On Environmental Pollution. HMSO.

Tanaka, S., Koide, H., Sasagawa, A., (1995). Possibility of underground CO_2 sequestration in Japan, Energy Conversion and Management, 36: 527-530.

Thrasher, J., Fleet, A.J. (1995). Predicting the risk of carbon dioxide 'pollution' in petroleum reservoirs. In: Grimalt, J.O., Dorronsoro, C., (Eds.), Organic Geochemistry: Developments and Applications to Energy, Climate, Environment and Human History - Selected papers from the 17th International Meeting on Organic Geochemistry, San Sebastian, AIGOA, pp. 1086-1088.

USGS (1996). 1995 National Assessment of United States Oil and Gas Resources. United States Geological Survey Digital Data Series 30 (http://pubs.usgs.gov/dds/dds-030/)

USGS (2000). US Geological Survey World Petroleum Assessment, Description and Results, United States Geological Survey Digital Data Series 60 (http://pubs.usgs.gov/dds/dds-060/)

van Bergen, F., Gale, J., Damen, K.J., Wildenborg, A.F.B., (2004). Worldwide selection of early opportunities for CO_2-enhanced oil recovery and CO_2-enhanced coal bed methane production. Energy, 29: 1611-1621.

van der Meer, L.G.H., Hartman, J., Geel, C., Kreft, E., (2005). Re-injecting CO_2 into an offshore gas reservoir at a depth of nearly 4000 metres sub-sea. In: Rubin, E.S., Keith, D.W., Gilboy, C.F., Wilson, M., Morris, T., Gale J., Thambimuthu K., (Eds.), Greenhouse Gas Control Technologies 7 (Proceedings of the 7th International Conference on Greenhouse Gas Control Technologies (GHGT-7), 5-9 September 2004, Vancouver, Canada), v1: p. 521-530. Elsevier.

van der Meer, L.G.H., Kreft, E., Gell, C., Hartman, J., (2005). K12-B a test site for CO_2 storage and enhanced gas recovery. SPE Europe/EAGE Annual Conference, 13-16 June 2005, Madrid, Paper SPE94128.

van der Meer, L.G.H., Kreft, E., Gell, C.R., Hoore, D.D., Hartman, J., (2006). Enhanced gas recovery testing in the K12-B reservoir by CO2 injection, a reservoir engineering study. Proceedings of the 8th International Conference on Greenhouse Gas Control Technologies (GHGT-8), 19-22 June 2006, Trondheim, Norway. Paper 02_04_05.

Wildenborg, T., Gale, J., Hendriks, C., Holloway, S., Brandsma, R., Kreft, E., Lokhorst, A., (2005). Cost curves for CO_2 storage: European sector. In: Rubin, E.S., Keith, D.W., Gilboy, C.F., Wilson, M., Morris, T., Gale J., Thambimuthu K., (Eds.), Greenhouse Gas Control Technologies 7 (Proceedings of the 7th International Conference on Greenhouse Gas Control Technologies (GHGT-7), 5-9 September 2004, Vancouver, Canada), v1: p. 603-610. Elsevier,

Yamazaki, T., Aso, K., Chinju, J., (2006). Japanese potential of CO_2 sequestration in coal seams. Applied Energy, 83: 911-920.

References Chapter 2

Anderson, D.L., (1998). A model to explain the various paradoxes associated with mantle noble gas geochemistry. Proceedings of the National Academy of Sciences of the USA, 95: 9087-9092.

Anderson, D.L., Schramm, K.A., (2005), Global hotspot maps. In: Foulger, G.R., Natland, J.H., Presnall, D.C., Anderson, D.L., (Eds.), Plates, plumes, and paradigms: Geological Society of America Special Paper 388, p. 19-29.

Aubaud, C., Pineau, F., Hékinian, R., Javoy, M., (2005). Degassing of CO_2 and H_2O in submarine lavas from the Society hotspot. Earth and Planetary Science Letters, 235: 511- 527.

Baker, E.T., German, C.R., (2004). On the global distribution of hydrothermal vent fields. In: C.R. German, C.R., Lin, J., Parsons, L.M., (Eds.), Mid-Ocean Ridges: Hydrothermal Interactions Between the Lithosphere and Oceans. Geophysical Monograph Series 148, 245-266. American Geophysical Union.

Bargar, K.E., Jackson, E.D., (1974). Calculated volumes of individual shield volcanoes along the Hawaiian-Emperor Chain. Journal of Research of the U.S. Geological Survey, 2: 545-550.

Batiza, R., (1982). Abundances, distribution and sizes of volcanoes in the Pacific Ocean and implications for the origin of non-hot spot volcanoes. Earth and Planetary Science Letters, 60: 195-206.

Bird, P., (2003). An updated digital model of plate boundaries. Geochemistry Geophysics Geosystems, 4: 1027. (doi:10.1029/ 2001GC000252)

Bjarnason, I.T., Menke, W., Flovenz, O.G., Caress, D., (1993). Tomographic image of the Mid-Atlantic plate boundary boundary in southwestern Iceland. Journal of Geophysical Research, 98: 6607-6622.

Caress, D.W., McNutt, M.K., Detrick, R.S., Mutter, J.C., (1995). Seismic imaging of hotspot-related crustal underplating beneath the Marquesas Islands. Nature, 373: 600-603.

Carracedo, J.C., Day, S.J., Gravestock, P., Guillou, H., (1999). Later stages of volcanic evolution of La Palma, Canary Islands: Rift evolution, giant landslides, and the genesis of the Caldera de Taburiente. Geological Society of America Bulletin, 111: 755-768.

Chevallier, L., (1987). Tectonic and structural evolution of Gough Volcano: A volcanological model. Journal of Volcanology and Geothermal Research, 33: 325-336.

Clarke, W.B., Beg M.A., Craig,H., (1969). Excess ^{3}He in the sea: evidence for terrestrial primordial helium. Earth and Planetary Science Letters, 6: 213-220.

Clift, P., Vannucchi, P., (2004). Controls on tectonic accretion versus erosion in subduction zones: Implications for the origin and recycling of the continental crust. Review of Geophysics, 42: RG2001. (doi: 2003RG000127)

Clor, L.E., Fischer, T.P., Hilton, D.R., Sharp, Z.D., Hartono, U., (2005). Volatile and N isotope chemistry of the Molucca Sea collision zone: Tracing source components along the Sangihe Arc, Indonesia. Geochemistry Geophysics Geosystems, 6: Q03J14 (doi:10.1029/2004GC000825)

Craig, H., Lupton, J.E., (1976). Primordial neon, helium and hydrogen in oceanic basalts. Earth and Planetary Science Letters, 31: 369-85.

Craig, H., Clarke, W.B., Beg, M.A., (1975). Excess ^{3}He in deep water on the East Pacific Rise. Earth and Planetary Science Letters, 26: 125-132.

Crisp, J.A., (1984). Rates of magma emplacement and volcanic output. Journal of Volcanology and Geothermal Research, 20: 177-211.

Dando, P.R., Stuben, D., Varnavas, S.P., (1999). Hydrothermalism in the Mediterranean Sea. Progress in Oceanography, 44: 333-367.

Darbyshire, F.A., Bjarnason, I.T., White, R.S., Flovenz, O.G., (1998). Crustal structure above the Iceland mantle plume imaged by the ICEMELT refraction profile. Geophysical Journal International, 135: 1131-1149.

Denman, K.L., Brasseur, G., Chidthaisong, A., Ciais, P., Cox, P.M., Dickinson, R.E., Hauglustaine, D., Heinze, C., Holland, E., Jacob, D., Lohmann, U., Ramachandran, S., da Silva Dias, P.L., Wofsy, S.C., Zhang, X., (2007). Couplings between changes in the climate system and biogeochemistry. In: Solomon, S., Qin, D., Manning, M., Chen, Z., Marquis, M., Averyt, K.B., Tignor, M., Miller, H.L., (Eds.), Climate Change 2007: The Physical Science Basis. Contribution of Working Group I to the Fourth Assessment Report of the Intergovernmental Panel on Climate Change Cambridge University Press, Cambridge, United Kingdom and New York, NY, USA.

De Ronde, C.E.J., Massoth, G.J., Baker, E.T., Lupton, J.E., (2003). Submarine hydrothermal venting related to volcanic arcs, Giggenbach Memorial Volume, In: Simmons, S.F., Graham, I.J., (Eds.), Volcanic, geothermal and ore-forming fluids: Rulers and witnesses of processes within the Earth. Society of Economic Geologists Special Publication 10: 91-110.

Des Marais, D.J., Moore, J.G., (1984). Carbon and its isotopes in mid-oceanic basaltic glasses. Earth and Planetary Science Letters, 69: 43-57.

Dick, H.J.B., Lin, J., Schouten, H., (2003). An ultraslow-spreading class of ocean ridge. Nature, 426: 405-412.

Dimalanta, C.B., Taira, A., Yumul, G.P., Tokuyama, H., (2000). Seismic and gravity constraints on the crustal structure and thicknesses of some island arcs in the Western Pacific region. Western Pacific Geophysic Meeting, 27-30 June 2000, Tokyo, Japan. Abstract S52G-12.

Dvorak, J. J., Dzurisin, D., (1993). Variations in magma supply rate at Kilauea Volcano, Hawaii. Journal of Geophysical Research, 98: 22,255-22,268.

Elderfield, H., Greaves, M.J., Rudnicki, M.D., Hydes, D.J., (1993). Aluminium reactivity in hydrothermal plumes at the Mid Atlantic Ridge. Journal of Geophysical Research, 98: 9667-9670.

Elderfield, H., Schultz, A., (1996). Mid-Ocean Ridge hydrothermal fluxes and the chemical composition of the ocean. Annual Reviews of Earth and Planetary Science, 24:191-224.

Farley, K.A., Maier-Reimer, E., Schlosser, P., Broecker, W.S., (1995). Constraints on mantle ^{3}He fluxes and deep-sea circulation from an oceanic general circulation model. Journal of Geophysical Research, 100: 3829-3839.

Freundt, A. H., Schmincke, H.-U., (1995). Eruption and emplacement of a basaltic welded ignimbrite during caldera formation on Gran Canaria. Bulletin of Volcanology, 56: 640-659.

Gerlach, D.C., (1990). Eruption rates and isotopic systematics of ocean islands: Further evidence for small-scale heterogeneity in the upper mantle. Tectonophysics, 172: 273-289.

Gerlach, T.M., (1989). Degassing of carbon dioxide from basaltic magma at spreading centers: II, Mid-oceanic ridge basalts. Journal of Volcanology and Geothermal Research, 39: 221-232.

Gerlach, T.M., (1991). Present-day CO_2 emission from volcanoes. EOS, Transactions, American Geophysical Union, 72: 249-251.

Glasby, G.P., Notsu, K., (2003). Submarine hydrothermal mineralization in the Okinawa Trough, SW of Japan: an overview. Ore Geology Reviews, 23: 299-339.

Glasby, G.P., Cherkashov, G.A., Gavrilenko, G.M., Rashidov, V.A., Slovtsov, I.B., (2006). Submarine hydrothermal activity and mineralization on the Kurile and western Aleutian island arcs, N.W. Pacific. Marine Geology, 231: 163-180.

Graham, D., Sarda, P., (1991). Reply to comment by T.M. Gerlach on “Mid-coean Ridge popping rocks: implications for degassing at ridge crests”. Earth and Planetary Science Letters, 105: 568-573.

Guillou, H., Carracedo, J.C., Day, S.J., (1998). Dating of the Upper Pleistocene-Holocene volcanic activity of La Palma using the unspiked K-Ar technique. Journal of Volcanology and Geothermal Research, 86: 137–149.

Hagstrum, J.T. (2005). Antipodal hotspots and bipolar catastrophes: Were oceanic large-body impacts the cause? Earth and Planetary Science Letters, 236: 13-27.

Hoernle, K., Schmincke, H.-U., (1993). The role of partial melting in the 15 Ma geochemical evolution of Gran Canaria: A blob model for the Canary Hotspot. Journal of Petrology, 34: 599-626.

Jakobsson, S.P., (1972). Chemistry and distribution pattern of recent basaltic rocks in Iceland. Lithos, 5: 365-386.

Jamous, D., Memery, L., Andrie, C., Jeanbaptiste, P., Merlivat, L., (1992). The distribution of He-3 in the deep Western and Southern Indian-Ocean. Journal Of Geophysical Research, 97: 2243-2250.

Javoy, M., Pineau, F., Allégre, C.J., (1982). The carbon geodynamic cycle. Nature, 300: 171-173.

Jenkins, W.J., Beg, M.A., Clarke, W.B., Wangersky, P.J., Craig, H., (1972). Excess ^{3}He in the Atlantic Ocean. Earth and Planetary Science Letters, 16: 122-126.

Jicha, B.R., Scholl, D.W., Singer, B.S., Yogodzinski, G.M., Kay, S.M., (2006). Revised age of Aleutian Island Arc formation implies high rate of magma production. Geology, 34: 661-664.

Jokat, W., Ritzmann, O., Schmidt-Aursch, M.C., Drachev, S., Gauger, S., Snow, J., (2003). Geophysical evidence for reduced melt production on the Arctic ultraslow Gakkel mid-ocean ridge. Nature, 423: 962-965.

Kingsley, R.H., Schilling, J-G., (1995). Carbon in mid-Atlantic ridge basalt glasses from 28°N to 63°N: evidence for a carbon enriched Azores mantle plume. Earth and Planetary Science Letters, 129: 31-53.

Klein, F.W., (1982). Patterns of historical eruptions at Hawaiian volcanoes. Journal of Volcanology and Geothermal Research, 12: 1-35.

Kurz, M.D., Jenkins, W.J., (1981). The distribution of helium in oceanic basalt glasses. Earth and Planetary Science Letters, 53: 41-54.

Lilley, M.D., Butterfield, D.A., Lupton, J.E., Olson, E.J., (2003). Magmatic events can produce rapid changes in hydrothermal vent chemistry. Nature, 422: 878-881.

Lipman, P.W., (1995). Declining growth of Mauna Loa during the last 100,000 years: Rates of lava accumulation vs. gravitational subsidence. In: Rhodes, J.M., Lockwood, J.P., (Eds.), Mauna Loa Revealed: Structure, Composition, History, and Hazards. Geophysical Monograph Series 92, 45-80. American Geophysical Union.

Lister, C.R.B., (1972). On the thermal balance of a mid-ocean ridge. Geophysical Journal of the Royal Astronomical Society, 26: 515-535.

Lupton, J.E., (1983). Terrestrial Inert Gases: Isotope tracer studies and clues to primordial components in the mantle. Annual Review of Earth and Planetary Sciences, 11: 371-414.

Lupton, J.E., (1998). Hydrothermal helium plumes in the Pacific Ocean. Journal of Geophysical Research, 103: 15,853-15,868.

Lupton, J., Butterfield, D., Lilley, M., Evans, L., Nakamura, K.I., Chadwick, W., Resing, J., Embley, R., Olson, E., Proskurowski, G., Baker, E., de Ronde, C., Roe, K., Greene, R., Lebon, G., Young, C., (2006). Submarine venting of liquid carbon dioxide on a Mariana Arc volcano. Geochemistry Geophysics Geosystems, 7: Art. No. Q08007.

Marty, B., Jambon, A., (1987). C/^{3}He in volatile fluxes from the solid Earth: Implication for carbon geodynamics. Earth and Planetary Science Letters, 83: 16-26.

Marty, B., Tolstikhin, I.N., (1998). CO_2 Fluxes from mid-ocean ridges, arcs, and plumes. Chemical Geology, 145: 233-248.

Marty, B., Zimmerman, L., (1999). Volatiles (He, C, N, Ar) in mid-ocean ridge basalts: assessment of shallow-level fractionation and characterisation of source composition. Geochimica Cosmochimica Acta, 63: 3619-3633.

Marty, B., Sano, Y., France-Lanord, C., (2001). Water-saturated oceanic lavas from the Manus Basin: volatile behaviour during assimilation-fractional crystallisation-degassing (AFCD). Journal of Volcanology and Geothermal Research, 108: 1-10.

Maund, J.G., Rex, D.C., Leroex, A.P., Reid, D.L., (1988). Volcanism on Gough Island: A revised stratigraphy. Geological Magazine, 125: 175-181.

Menard, H.W., (1964). Marine geology of the Pacific. McGraw-Hill, New York, N.Y., 271 pp.

Menke, W., West, M., Brandsdottir, B., Sparks, D., (1998). Compressional and shear velocity structure of the lithosphere in northern Iceland. Bulletin of the Seismological Society of America, 88: 1561-1571.

Muller, M.R., Minshull, T.A., White, R.S., (1999). Segmentation and melt supply at the Southwest Indian Ridge. Geology, 27: 867-870.

Nicolaysen, K., Frey, F.A., Hodges, K.V., Weis, D., Giret, A., (2000). 40Ar/39Ar geochronology of flood basalts from the Kerguelen Archipelago, southern Indian Ocean: Implications for Cenozoic eruption rates of the Kerguelen plume. Earth and Planetary Science Letters, 174: 313-328.

Nielson, D.L., Sibbett, B.S., (1996). Geology of Ascension Island, South Atlantic Ocean. Geothermics, 25: 427-448.

Nishio, Y., Sasaki, S., Gamo, T., Hiyagon, H., Sano, Y., (1998). Carbon and helium isotope systematics of North Fiji Basin basalt glasses: carbon geochemical cycle in the subduction zone. Earth and Planetary Science Letters, 154: 127-138.

Östlund, H.G., Craig, H., Broecker, W.S., Spencer, D., (Eds.) (1987). GEOSECS Atlantic, Pacific and Indian Ocean Expeditions; Shorebased data and Graphics, v7, 230 p., National Science Foundation, Washington, D.C.

Pairault, A.A., Hall, R., Elders, C.F., (2003). Structural styles and tectonic evolution of the Seram trough, Indonesia. Marine and Petroleum Geology, 20: 1141-1160.

Paris, R., Guillou, H., Carracedo, J.C., Perez-Torrado, F.J., (2005). Volcanic and morphological evolution of La Gomera (Canary Islands), based on new K-Ar ages and magnetic stratigraphy: Implications for ocean island evolution. Journal of the Geological Society, London, 162: 501-512.

Plank, T., Langmuir, C.H., (1993): Tracing trace elements from sediment input to volcanic output at subduction zones. Nature, 362: 739-743.

Plesner, S., Holm, P.M., Wilson, J.R., (2002). 40Ar-39Ar geochronology of Santo Antao, Cape Verde Islands. Journal of Volcanology and Geothermal Research, 120: 103-121.

Quane, S. L., Garcia, M.O., Guillou, H., Hulsebosch, T.P., (2000). Magmatic history of the East Rift Zone of Kilauea Volcano, Hawaii based on drill core from SOH1. Journal of Volcanology and Geothermal Research, 102: 319-338.

Raven, J., Caldeira, K., Elderfield, H., Hoegh-Guldberg, O., Liss, P., Riebesell, U., Shepherd, J., Turley, C., Watson, A., (2005). Ocean acidification due to increasing atmospheric carbon dioxide. The Royal Society, Policy Document 12/05.

Resing, J.A., Lupton, J.E., Feely, R.A., Lilley, M.D., (2004). CO_2 and ^{3}He in hydrothermal plumes: implications for mid-ocean ridge CO_2 flux. Earth and Planetary Science Letters, 226: 449-464.

Reymer, A., Schubert, G., (1984). Phanerozoic addition rates to the continental crust and crustal growth. Tectonics, 3:63-77.

Rüth, C., Well, R., Roether, W., (2000). Primordial ^{3}He in South Atlantic deep waters from sources on the Mid-Atlantic Ridge. Deep-Sea Research, Part 1, 47: 1059-1075.

Sabine, C.L., Feely, R.A., Gruber, N., Key, R.M., Lee, K., Bullister, J.L., Wanninkhof, R., Wong, C.S., Wallace, D.W.R., Tilbrook, B., Millero, F.J., Peng, T.H., Kozyr, A., Ono, T., Rios, A.F., (2004). The oceanic sink for anthropogenic CO_2. Science, 305: 367-371.

Sakai, H., Gamo, T., Kim, E-S., Tsutsumi, M., Tanaka, T., Ishibashi, J., Wakita, H., Yamano, M., Oomori, T., (1990a). Venting of carbon dioxide-rich fluid and hydrate formation in Mid-Okinawa Trough Backarc Basin. Science, 248: 1093-1096.

Sakai, H., Gamo, T., Kim, E-S., Shitashima, K., Yanagisawa, F., Tsutsumi, M., (1990b). Unique chemistry of the hydrothermal solution in the Mid-Okinawa Trough backarc basin. Geophysical Research Letters, 17: 2133-2136.

Sano, Y., Marty, B., (1995). Origin of carbon in fumarolic gas from island arc. Chemical Geology, 119: 265-274.

Sano, Y., Williams, S.N., (1996). Fluxes of mantle and subducted carbon along convergent plate boundaries. Geophysical Research Letters, 23: 2749–2752.

Sano, Y., Nishio, Y., Gamo, T., Jambon, A., Marty, B., (1998). Noble gas and carbon isotopes in Mariana Trough basalt glasses. Applied Geochemistry, 13: 441-449.

Sapper, K., (1927). Vulkankunde. J. Engelhorns Nachf., Stuttgart, 424 pp. Cited in Crisp (1984).

Sarda, P., Graham, D., (1990). Mid-ocean ridge popping rocks: implications for degassing at ridge crests. Earth and Planetary Science Letters, 97: 268-289.

Schilling, J.-G., Unni, C.K., Bender, M.L., (1978). Origin of chlorine and bromine in the oceans. Nature, 273: 631-636.

Shaw, A.M., Hilton, D.R., Fischer, T.P., Walker, J.A., Alvarado, G.E., (2003). Contrasting He-C relationships in Nicaragua and Costa Rica: insights into C cycling through subduction zones. Earth and Planetary Science Letters, 214: 499-513.

Shaw, A.M., Hilton, D.R., Macpherson, C.G., Sinton, J.M., (2004). The CO_2-He-Ar-H_2O systematics of the Manus back-arc basin: Resolving source composition from degassing and contamination effects. Geochimica et Cosmochimica Acta, 68: 1837-1856.

Snyder, G., Poreda, R., Hunt, A., Fehn, U., (2001). Regional variations in volatile composition: Isotopic evidence for carbonate recycling in the Central American volcanic arc. Geochemistry Geophysics Geosystems, 2: Paper 2001GC000163.

Staudigel, H., Hart, S.R., Pile, A., Bailey, B.E., Baker, E.T., Brooke, S., Connelly, D.P., Haucke, L., German, C.R., Hudson, I., Jones, D., Koppers, A.P., Konter, J., Lee, R., Pietsch, T.W., Tebo, B.M., Templeton, A.S., Zierenberg, R., Young, C.M., (2006). Vailulu'u Seamount, Samoa: Life and death on an active submarine volcano. Proceedings of the National Academy of Sciences of the USA, 103: 6448-6453.

Stern, R., (2006). Perspectives on the Andean Arc from the Izu-Bonin-Mariana Arc System in the Western Pacific. Backbone of the Americas – Patagonia to Alaska, 3-7 April 2006, Geological Society of America Abstracts with Programs, Speciality Meeting No. 2, Paper 16-2., p. 115.

Taira, A., Saito, S., Aoike, K., Morita, S., Tokuyama, H., Suyehiro, K., Takahashi, N., Shinohara, M., Kiyokawa, S., Naka, J., Klaus, A., (1998). Nature and growth rate of the Northern Izu-Bonin (Ogasawara) arc crust and their implications for continental crust formation. The Island Arc, 7: 395-407.

Torgersen, T., (1989). Terrestrial helium degassing fluxes and the atmospheric helium budget: Implications with respect to the degassing processes of the continental crust. Chemical Geology, 79: 1-14.

Trull, T., Nadeau, S., Pineau, F., Polve, M., Javoy, M., (1993). C-He systematics in hotspot xenoliths: implications for mantle carbon contents and carbon recycling. Earth and Planetary Science Letters, 118: 43-64.

Van Soest, M.C., Hilton, D.R., Kreulen, R., (1998). Tracing crustal and slab contributions to arc magmatism in the Lesser Antilles island arc using helium and carbon relationships in geothermal fluids. Geochimica et Cosmochimica Acta, 62: 3323-3335.

Varekamp, J.C., Kreulen, R., Poorter, R.P.E., Van Bergen, M.J., (1992) Carbon sources in arc volcanism, with implications for the carbon cycle. Terra Nova, 4: 363-373.

Vidal, V., Bonneville, A., (2004). Variations of the Hawaiian hot spot activity revealed by variations in the magma production rate. Journal of Geophysical Research, 109: B03104 (doi:10.1029/2003JB002559).

Well, R., Lupton, J., Roether, W., (2001). Crustal helium in deep Pacific waters. Journal of Geophysical Research, 106: 14165-14177.

White, R.S., McKenzie, D., O'Nions, R.K., (1992). Oceanic crustal thickness from seismic measurements and rare earth element inversions. Journal of Geophysical Research, 97: 19,683-19,715.

White, R.S., Minshull, T.A., Bickle, M.J., Robinson, C.J., (2001). Melt generation at very slow-spreading oceanic ridges: Constraints from geochemical and geophysical data. Journal of Petrology, 42: 1171-1196, 2001.

White, S.M., Crisp, J.A., Spera, F.J., (2006). Long-term volumetric eruption rates and magma budgets. Geochemistry Geophysics Geosystems, 7: Q03010. (doi:10.1029/2005GC001002).

Chapter 3 References

Alendal, G., Drange, H., (2001). Two-phase, near-field modelling of purposefully released CO_2 in the ocean. Journal of Geophysical Research, 106: 1085–1096.

Anitescu, G., Tavlarides, L.L., (2006). Supercritical extraction of contaminants from soils and sediments. Journal of Supercritical Fluids, 38: 167-180.

Babel, S., del Mundo Dacera, D., (2006). Heavy metal removal from contaminated sludge for land application: A review. Waste Management, 26: 988-1004.

Baker E. T., German, C. R., Elderfield, H., 1995. Hydrothermal plumes over spreading-center axes: global distributions and geological inferences. In: Humphris, S. E., Zierenberg, A., Mullineaux, L. S., Thomson, R. E. (Eds.), Seafloor hydrothermal systems. Geophysical Monograph Series 91, pp. 47-71. American Geophysical Union.

Barragan, R.R.M., Birkle, P., Portugal, M.E., Arellano, G.V.M., Alvarez, R.J., (2001). Geochemical survey of medium temperature geothermal resources from the Baja California Peninsula and Sonora, México. Journal of Volcanology and Geothermal Research, 110: 101-119.

Barry, J.P., Drazen, J.C., (2007). Response of deep-sea scavengers to ocean acidification and the odor from a dead grenadier. Marine Ecology Progress Series, 350: 193-207.

Barry, J.P., Seibel, B.A., Lovera, C., (2001). Deep-Sea field studies of the biological consequences of direct ocean CO_2 sequestration. EOS Transactions, American Geophysical Union 82(47), Fall Meeting Supplement, Abstract U32B-09.

Barry, J.P., Buck, K.R., Lovera, C.F., Kuhnz, L., Whaling, P.J., Peltzer, E.T., Walz, P., Brewer, P.G., (2004). Effects of direct ocean CO_2 injection on deep-sea meiofauna. Journal of Oceanography, 60: 759-766.

Barry, J.P., Buck, K.R., Lovera, C., Kuhnz, L., Whaling, P.J., (2005). Utility of deep sea CO_2 release experiments in understanding the biology of a high-CO_2 ocean: Effects of hypercapnia on deep sea meiofauna. Journal of Geophysical Research - Oceans, 110: C09S12.

Baubron, J.C., Allard, P., & Toutain, J.P., (1990). Diffuse volcanic emissions of carbon dioxide from Vulcano Island, Italy. Nature, 344: 51-53.

Botz, R., Winckler, G., Bayer, R., Schmitt, M., Schmidt, M., Garbe-Schönberg, D., Stoffers, P., Kristjansson, J.K., (1999). Origin of trace gases in submarine hydrothermal vents of the Kolbeinsey Ridge, north Iceland. Earth and Planetary Science Letters, 171: 83-93.

Bradshaw, J., Dance, T., (2005). Mapping geological storage prospectivity of CO_2 for the world's sedimentary basins and regional source to sink matching. In: Rubin, E.S., Keith, D.W., Gilboy, C.F., Wilson, M., Morris, T., Gale J., Thambimuthu K., (Eds.), Greenhouse Gas Control Technologies 7 (Proceedings of the 7th International Conference on Greenhouse Gas Control Technologies (GHGT-7), 5-9 September 2004, Vancouver, Canada), v1: p. 583-592. Elsevier.

Brewer, P.G., Peltzer, E.T., Friederich, G., Aya, I., Yamane, K., (2000). Experiments on the ocean sequestration of fossil fuel CO_2: pH measurements and hydrate formation. Marine Chemistry, 72: 83-93.

Brewer, P.G., Peltzer, E.T., Friederich, G., Rehder, G., (2002). Experimental determination of the fate of rising CO_2 droplets in sea water. Environmental Science & Technology, 36: 5441-5446.

Brewer, P.G., Malby, G., Pasteris, J.D., White, S.N., Peltzer, E.T., Wopenka, B., Freeman, J., Brown, M.O., (2004a). Development of a laser Raman spectrometer for deep-ocean science. Deep-Sea Research Part 1 – Oceanographic Research Papers, 51: 739-753.

Brewer, P.G., Dunk, R.M., White, S.N., Peltzer, E.T., Bowie, B., Walz P.M., (2004b). First attempts at direct Raman detection of the oceanic carbonate system. EOS Transactions, American Geophysical Union, 85(47), Fall Meeting Supplement, Abstract OS43B-0557.

Brewer, P.G., Peltzer, E.T., Walz, P., Aya, I., Yamane, K., Kojima, R., Nakajima, Y., Nakayama, N., Haugan, P., Johannessen, T., (2005a). Deep ocean experiments with fossil fuel carbon dioxide: Creation and sensing of a controlled plume at 4 km depth. Journal of Marine Research, 63: 9-33.

Brewer, P.G., Kirkwood, W., Barry, J., Dunk, R.M., (2005b). Enabling the assessment of a high CO_2-low pH ocean: Is a Free Ocean CO_2 Enrichment (FOCE) experiment possible? . EOS Transactions, American Geophysical Union, 86(18), Joint Assembly Supplement, Abstract U23B-02.

Brewer, P.G., Chen, B.X., Warzinki, R., Baggeroer, A., Peltzer, E.T., Dunk, R.M., Walz, P., (2006). Three-dimensional acoustic monitoring and modeling of a deep-sea CO_2 droplet cloud. Geophysical Research Letters, 33: L23607.

Butterfield, D.A., Massoth, G.J., McDuff, R.E., Lipton, J.E., Lilley, M.D., (1990). Geochemistry of hydrothermal fluids from ASHES vent field, axial seamount, Juan de Fuca ridge: Subseafloor boiling and subsequent fluid-rock interaction. Journal of Geophysical Research, 95: 12,895-12,921.

Calanchi, N., Capaccioni, B., Martini, M., Tassi, F., Valentini, L., (1995). Submarine gas-emmision from Panarea Island (Aeolian Archipelago): distribution of inorganic and organic compounds and inference about source conditions. Acta Vulcanologica, 7: 43-48.

Cardigos, F., Colaço, A., Dando, P.R., Ávila, S.P., Sarradin, P.-M., Tempera, F., Conceição, P., Pascoal, A., Serrão Santos, R., (2005). Shallow water hydrothermal vent field fluids and communities of the D. João de Castro Seamount (Azores). Chemical Geology, 224: 153-168.

Carman, K.R., Thistle, D., Fleeger, J.W., Barry, J.P., (2004). Influence of introduced CO_2 on deep-sea metazoan meiofauna. Journal of Oceanography, 60: 767-772.

Chadwick, A., Noy, D., Lindeberg, E., Arts, R., Eiken, O., Williams, G., (2006). Calibrating reservoir performance with time-lapse seismic monitoring and flow simulations of the Sleipner CO_2 plume. . Proceedings of the 8th International Conference on Greenhouse Gas Control Technologies (GHGT-8), 19-22 June 2006, Trondheim, Norway. Paper 02_07_03.

Chen, B., Song, Y., Nishio, M., Akai, M., (2003). Large-eddy simulation of double cloud formation induced by CO_2 dissolution in the ocean. Tellus Series B, 55: 723– 730.

Chen, C.T.A., Zeng, Z., Kuo, F.W., Yang, T.F., Wang, B.J., Tu, Y.Y., (2005). Tide-influenced acidic hydrothermal system offshore NE Taiwan. Chemical Geology, 224: 69-81.

Chiba, H., Sakai, H., Gamo, T., Ishibashi, J-I., Nakashima, K., Minami, H., Dobahi, F., (1992). Chemistry and isotopic composition of bubbles emerging from the seafloor at the Minami-Ensei Knoll, Okinawa Trough. Proceedings of JAMSTEC, Symposium of Deep-Sea Research, 8: 81-87.

Chiba, H., Ishibashi, J.-I., Ueno, H., Oomori, T., Uchiyama, N., Takeda, T., Takemine, C., Ri, J., Itomitsu, A., (1996). Seafloor hydrothermal systems at North Knoll, Iheya Ridge, Okinawa Trough. JAMSTEC Journal of Deep-Sea Research, 12: 211- 219 (in Japanese with English Abstract).

Cooper, M.J., Elderfield, H., Schultz, A., (2000). Diffuse hydrothermal fluids from Lucky Strike hydrothermal vent field: Evidence for a shallow conductively heated system. Journal of Geophysical Research, 105: 19369-19375.

Dando, P.R., Hughes, J.A., Thiermann, F., (1995a). Preliminary observations on biological communities at shallow hydrothermal vents in the Aegean Sea. In: Parson, L.M., Walker, C.L., Dixon, D., (Eds.), Hydrothermal Vents and Processes, Geological Society, London, Special Publication, 87, pp. 303-317.

Dando, P.R., Hughes, J.A., Leahy, Y., Niven, S.J., Taylor, L.J., & Smith, C. (1995b). Gas venting rates from submarine hydrothermal areas around the island of Milos, Hellenic Volcanic Arc. Continental shelf Research, 15: 913-929.

Dando, P.R., Hughes, J.A., Leahy, Y., Taylor, L.J., Zivanovic, S., (1995c). Earthquakes increase hydrothermal venting and nutrient inputs into the Aegean. Continental Shelf Research, 15: 655-662.

Dunk, R.M., Peltzer, E.T., Rehder, G., Brewer, P.G., (2002). Dissolution rate of liquid CO_2 at 3600m depth as determined by pH measurements. EOS Transactions, American Geophysical Union, 83(4) Ocean Sciences Meeting Supplement, Abstract OS51F-06.

Dunk R.M., Peltzer, E.T., Walz, P.M., Brewer, P.G., (2005). Seeing a deep ocean CO_2 enrichment experiment in a new light: Laser Raman detection of dissolved CO_2 in seawater. Environmental Science & Technology, 39: 9630-9636.

Dunk R.M., Peltzer, E.T., Walz, P.M., Brewer, P.G., (in prep). The fate of mixed methane-hydrogen sulphide gas bubbles in the water column. To be submitted to Limnology and Oceanography.

Edmond, J.M., Campbell, A.C., Palmer, M.R., Klinkhammer, G.P., German, C.R., Edmonds, H.N., Elderfield, H., Thompson, G., Rona, P., (1995). Time series studies of vent fluids from the TAG and MARK sites (1986, 1990) Mid-Atlantic Ridge: a new solution chemistry model and mechanism for Cu/Zn zonation in massive sulphide ore bodies. In: Parson, L.M., Walker, C.L., Dixon, D., (Eds.), Hydrothermal Vents and Processes, Geological Society, London, Special Publication, 87, pp. 77-86.

Edmond, J.M., Measures, C.I., McDuff, R.E., Chan, L.H., Collier, R., Grant, B., Gordon, L.I., Corliss J.B., (1979). Ridge crest hydrothermal activity and the balance of the major and minor elements in the ocean; the Galapagos data. Earth and Planetary Science Letters, 46: 1-18.

Elderfield, H., Schultz, A., (1996). Mid-ocean ridge hydrothermal fluxes and the chemical composition of the ocean. Annual Reviews of Earth and Planetary Science, 24: 191-224.

Embley, R.W., and the shipboard scientific party (2006). Submarine Ring of Fire 2006 – Mariana Arc Submarine Volcanoes. R/V Melville, Cruise MGLN02MV.

Erkey, C., (2000). Supercritical carbon dioxide extraction of metals from aqueous solutions: A review. Journal of Supercritical Fluids, 17: 259-287.

Feely, R.A., Lewison, M., Massoth, G.J., Robert-Baldo, G., Lavelle, J.W., Byrne, R.N., Von Damm, K.L., Curl, H.C., (1987). Composition and dissolution of black smoker particles from active vents on the Juan de Fuca Ridge. Journal of Geophysical Research, 92: 11347-11363.

Feely, R.A., Massoth, G.J., Trefry, J.H., Baker, E.T., Paulson, A.J., Lebon, G.T., (1994). Composition and sedimentation of hydrothermal plume particles from North Cleft Segment, Juan de Fuca Ridge. Journal of Geophysical Research, 99: 4985-5006.

de Figueiredo, M.A., Reiner, D.M., Herzog, H.J., (2003). Ocean carbon sequestration: A case study in public and institutional perceptions. In: Gale, J., Kaya, Y., (Eds.), Greenhouse Gas Control Technologies (Proceedings of the 6th International Conference on Greenhouse Gas Control Technologies (GHGT-6), 1-4 October 2002, Kyoto, Japan). Permagon, p. 799–804.

Fisher, C.R., Childress, J.J., Arp, A.J., Brooks, J.M., Distel, D., Favuzzi, J.A., Felbeck, H., Fritz, L.W., Hessler, R., Johnson, K.S., Kennicutt, M.C., Lutz, R.A., Macko, S.A., Newton, A., Powell, M.A., Somero, G.N., Soto, T., (1988). Variation in the hydrothermal vent clam, Calyptogena magnifica, at Rose Garden vent on the Galapagos rift. Deep-Sea Research, 35: 1811-1832.

Fleeger, J.W., Carman, K.R., Welsenhorn, P.B., Sofranko, H., Marshall, T., Thistle, D., Barry, J.P., (2006). Simulated sequestration of anthropogenic carbon dioxide at a deep-sea site: Effects on nematode abundance and biovolume. Deep-Sea Research Part I - Oceanographic Research Papers, 53: 1135-1147.

Forrest, M.J., Ledesma-Vázquez, J., Ussler III, W., Kulongoski, J.T., Hilton, D.R., Greene, H.G., (2005). Gas geochemistry of a shallow hydrothermal vent associated with the El Requesón fault zone, Bahía Concepción, Baja California Sur, México. Chemical Geology, 224: 82-95.

Fujikura, K., Fujiwara, Y., Ishibashi, J.-I., Katayama, S., Komatsu, T., Maezawa, Y., Maki, Y., Miyazaki, J.-I., Miyake, H., Okamoto, K., Okoshi, K., Toth, L.G., Tsuchida, S., Yamaguchi, T., Yamanaka, T., Watabe, H., Zielinski, S., Kato, K., (2001). Report on investigation of hydrothermal vent ecosystems by the crewed submersible ‘Shinkai 2000’ on Dai-Yon (No. 4) Yanaguni Knoll and the Hatoma Knoll, the Okinawa Trough, JAMSTEC Journal of Deep-Sea Research, 19: 141-154 (in Japanese with English Abstract).

Gangstø, R., Haugan, P.M., Alendal, G., (2005). Parameterization of drag and dissolution of rising CO_2 drops in seawater. Geophysical Research Letters, 32: L10612, doi:10.1029/2005GL022637.

Gastil, R.G., Bertine, K., (1982). Estudio geoquímico termal de Baja California y sur de California. University of San Diego, CA., unpublished report, pp. 58-61.

German, C.R., Campbell, A.C., Edmond, J.M., (1991). Hydrothermal scavenging at the Mid-Atlantic Ridge: Modification of trace element dissolved fluxes. Earth and Planetary Science Letters, 107: 101-114.

Giggenbach, W.F., Matsuo, S., (1991). Evaluation of results from second and third IAVCEI field workshop on volcanic gases, Mt. Usu, Japan and White Island, New Zealand. Applied Geochemistry, 6: 125-141.

Giggenbach, W.F., Sano, Y., Wakita, H., (1993). Isotopic composition of helium, and CO_2 and CH_4 contents in gases produced along the New Zealand part of a convergent plate boundary. Geochimica et Cosmochimica Acta, 57: 3427-3455.

Glasby, G.P., Notsu, K., (2003). Submarine hydrothermal mineralization in the Okinawa Trough, SW of Japan: an overview. Ore Geology Reviews, 23: 299-339.

Heikoop, J.M., Tsujita, C.J., Risk, M.J., Tomascik, T., Mah, A.J., (1996). Modern iron ooids from a shallow-marine volcanic setting; Mahengetang, Indonesia. Geology, 24: 759-762.

Hessler, R.R., Smithey, W.M., Keller, C.H., (1985). Spatial and temporal variation of giant clams, tubeworms and mussels at deep-sea hydrothermal vents. Bulletin of the Biological Society of Washington, 6:465-474.

Hester, K.C., White, S.N., Peltzer, E.T., Brewer, P.G., Sloan, E.D., (2006). Raman spectroscopic measurements of synthetic gas hydrates in the ocean. Marine Chemistry, 98: 304-314.

Hester, K.C., Dunk, R.M., Walz, P.M., Peltzer, E.T., Sloan, E.D., Brewer, P.G., (2007a). Direct measurements of multi-component hydrates on the sealoor: Pathways to growth. Fluid Phase Equilibria, 261: 396-406 Sp. Iss. SI.

Hester, K.C., Dunk, R.M., White, S.N., Brewer, P.G., Peltzer, E.T., Sloan, E.D., (2007b). Gas hydrate measurements at Hydrate Ridge using Raman spectroscopy. Geochimica et Cosmochimica Acta, 71: 2947-2959.

Holland, P., (1997). Offshore blowouts - Causes and controls. Gulf Publishing Company, 1997.

Hughey, C.A., Rodgers, R.P., Marshall, A.G., Walters, C.C., Qian, K., Mankiewicz, P., (2004). Acidic and neutral polar NSO compounds in Smackover oils of different thermal maturity revealed by electrospray high field Fourier transform ion cyclotron resonance mass spectrometry. Organic Geochemistry, 35: 863-880.

Hughey, C.A., Rodgers, R.P., Marshall, A.G., Qian, K., Robbins, W.K., (2003). Identification of acidic NSO compounds in crude oils of different geochemical origins by negative ion electrospray Fourier transform ion cyclotron resonance mass spectrometry. Organic Geochemistry, 33: 743-759.

Inagaki, F., Kuypers, M.M.M., Tsunogai, U., Ishibashi, J., Nakamura, K., Treude, T., Ohkubo, S., Nakaseama, M., Gena, K., Chiba, H., Hirayama, H., Nunoura, T., Takai, K., Jorgensen, B.B., Horikoshi, K., Boetius, A., (2006). Microbial community in a sediment-hosted CO_2 lake of the southern Okinawa Trough hydrothermal system. Proceedings of the National Academy of Sciences of the USA, 103: 14164-14169.

Italiano, F., & Nuccio, P.M., (1991). Geochemical investigations of submarine volcanic exhalations to the east of Panarea, Aeolian Islands, Italy. Journal of Volcanology and Geothermal Research, 46: 125-141.

Kadko, D., (1993). An assessment of the effect of chemical scavenging within submarine hydrothermal plumes upon ocean geochemistry. Earth and Planetary Science Letters, 120: 361-374.

Kirkwood, W., Graves, D., Conway, M., Pargett, D., Scholfield, J., Walz, P., Dunk, R., Peltzer, E., Barry, J., Brewer, P., (2005). Engineering development of the Free Ocean CO_2 Enrichment (FOCE) experiment. MTS/IEEE Oceans 2005 (September 18-23). Technical Paper 050304-93.

Kirkwood, W.J., Peltzer, E.T., Brewer, P.G., (2007). In situ ocean acidification environmental observations: MBARI’s cabled observatory technology for controlled studies of changing ocean pH. Symposium on Underwater Technology and Workshop on Scientific Use of Submarine Cables and Related Technologies, 17-20 April 2007, Tokyo, Japan: Abstract TP1.5, p. 627-633.

Langdon, C., Broecker, W.S., Hammond, D.E., Glenn, E., Fitzsimmons, K., Nelson, S.G., Peng, T.H., Hajdas, I., Bonani, G., (2003). Effect of elevated CO_2 on the community metabolism of an experimental coral reef. Global Biogeochemical Cycles, 17: 1011.

Librando, V., Hutzinger, O., Tringali, G., Aresta, M., (2004). Supercritical fluid extraction of polycyclic aromatic hydrocarbons from marine sediments and soil samples. Chemosphere, 54: 1189-1197.

Lilley, M.D., Feely, R.A., Trefry, J.H., (1995). Chemical and biochemical transformations in hydrothermal plumes. In: Humphris, S.E., Zierenberg, A., Mullineaus, L.S., Thomson, R.E., (Eds.) Seafloor Hydrothermal Systems: Physical, Chemical, Biological and Geological Interactions. Geophysical Monograph Series 91, pp. 369-391. American Geophysical Union.

Lister, C.R.B., (1972). On the thermal balance of a mid-ocean ridge. Geophysical Journal of the Royal Astronomical Society, 26: 515-535.

Lupton, J. E., 1995. Hydrothermal plumes: Near and far field. Special publication- seafloor hydrothermal systems: physical, chemical, biological and geological interactions. Geophysical Monograph Series 91, pp. 317-343. American Geophysical Union.

Lupton, J., Butterfield, D., Lilley, M., Evans, L., Greene, R., Resing, J., Embley, R., Massoth, G., Christenson, B., de Ronde, C., Olson, E., Proskurowski, G., Nakamura, K., Schmidt, M., Stoffers, P., Worthington, T., Hannington, M., (2005). Carbon Fluxes from Submarine Arc Volcanoes - examples from the Mariana and Kermadec Arcs. EOS Transactions, American Geophysical Union 86(52), Fall Meeting Supplement, Abstract V51C-1498.

Lupton, J., Butterfield, D., Lilley, M., Evans, L., Nakamura, K.I., Chadwick, W., Resing, J., Embley, R., Olson, E., Proskurowski, G., Baker, E., de Ronde, C., Roe, K., Greene, R., Lebon, G., Young, C., (2006). Submarine venting of liquid carbon dioxide on a Mariana Arc volcano. Geochemistry Geophysics Geosystems, 7: Art. No. Q08007.

Lyon, G.L., Giggenbach, W.F., Singleton, R.J., and Glasby, G.P., (1977). Isotopic and Chemical composition of submarine geothermal gases from the Bay of Plenty, New Zealand. New Zealand Department of Scientific and Industrial Research Bulletin, 218: 65-67.

MacDonald, K.C., Becker, K., Spiess, F.N., Ballard, R.D., (1980). Hydrothermal heat flux of the “black smoker” vents on the East Pacific Rise. Earth and Planetary Science Letters, 48: 1-7.

McCarthy, K.T., Pichler, T., Price, R.E., (2005). Geochemistry of Champagne Hot Springs shallow hydrothermal vent field and associated sediments, Dominica, Lesser Antilles. Chemical Geology, 224: 55-68

McLeod, A.R., Long, S.P., (1999). Free-Air Carbon Dioxide Enrichment (FACE) in global change research: A review. Advances in Ecological Research, 28: 1-26.

Mills, R.A., Elderfield, H., (1995). Hydrothermal activity and the geochemistry of metalliferous sediment. In: Humphris, S.E., Zierenberg, A., Mullineaus, L.S., Thomson, R.E., (Eds.) Seafloor Hydrothermal Systems: Physical, Chemical, Biological and Geological Interactions. Geophysical Monograph Series 91, pp. 392-405. American Geophysical Union.

Minissale, A. (1989). Geochemical characteristics of Greek thermal springs. Journal of Volcanology and Geothermal Research, 39: 1-16.

Minissale, A., Duchi, V., Kolios, N., Nocenti, M., Verrucchi, C., (1997). Chemical patterns of thermal aquifers in the volcanic islands of the Aegean Arc, Greece. Geothermics, 26: 501-518.

Murton, B.J., Van Dover, C., Southward, E., (1995). The geological setting and ecology of the Broken Spur Hydrothermal Vent Field: 29º10’N on the Mid Atlantic Ridge, In: Parson, L.M., Walker, C.L., Dixon, D., (Eds.), Hydrothermal Vents and Processes, Geological Society, London, Special Publication, 87, pp. 33-43.

Murton, B.J., Redbourn, L.J., German, C.R., Baker, E.T., (1999). Sources and fluxes of hydrothermal heat, chemicals and biology within a segment of the Mid-Atlantic Ridge. Earth and Planetary Science Letters, 171: 301-317.

Obzhirov, A.L., (1992a). Chemistry of free and dissolved gases of Matupi Bay, Rabaul caldera, Papua New Guinea. Geo-Marine Letters, 12: 54-59.

Obzhirov (1992b). Dissolved gases of the near-bottom water layer in the area of Epi Island, Vanuatu. Geo-Marine Letters, 12: 232-235.

Ossaka. J., Hirabayashi, J., Nogami, K., Kurosaki, M., Hashimoto, J., (1992). Variation of chemical composition of volcanic gases from the northern part of Kagoshima bay. Proceedings of JAMSTEC, Symposium of Deep-Sea Research, 8: 75-80.

Peltzer, E.T., Brewer, P.G., Dunk, R.M., Erickson, J., Rehder, G., Walz, P., (2002). Recent advances in deep-sea CO_2 sequestration experiments. ACS Fuel Chemistry Division Preprints, 47: 23-24.

Pichler, T., Dix, G.R., (1996). Hydrothermal venting within a coral reef excosystem, Ambitle Island, Papua New Guinea. Geology, 24: 435-438.

Pichler, T., Giggenbach, W.F., McInnes, B.I.A., Buhl, D., Duck, B., (1999). Fe sulfide formation due to seawater-gas-sediment interaction in a shallow-water hydrothermal systems at Lihir Island, Paua New Guinea. Economic Geology, 94: 281-288.

Pichler, T., Pichler, T., Veizer, J., Hall, G.E.M., (1999b). The chemical composition of shallow-water hydrothermal fluids in Tutum Bay, Ambitle Island, Papua New Guinea and their effect on ambient seawater. Marine Chemistry, 64: 229–252.

Prol-Ledesma, R.M., Canet, C., Melgarejo, J.C., Tolson, G., Rubio-Ramos, M.A., Cruz-Ocampo, J.C., Ortego-Osorio, A., Torres-Vera, M.A., Reyes, A., (2002). Cinnabar deposition in submarine coastal hydrothermal vents, Pacific Margin of central Mexico. Economic Geology, 97: 1331-1340.

Rehder, G., Kirby, S.H., Durham, W.B., Stern, L.A., Peltzer, E.T., Pinkston, J., Brewer, P.G., (2004). Dissolution rates of pure methane hydrate and carbon-dioxide hydrate in undersaturated seawater at 1000-m depth. Geochimica et Cosmochimica Acta, 68: 285-292.

Riebesell, U., (2004). Effects of CO_2 enrichment on marine phytoplankton. Journal of Oceanography, 60: 719-729.

Sakai, H., Gamo, T., Kim, E-S., Tsutsumi, M., Tanaka, T., Ishibashi, J., Wakita, H., Yamano, M., and Oomori, T., (1990). Venting of carbon dioxide-rich fluid and hydrate formation in Mid-Okinawa Trough Backarc Basin. Science, 248: 1093-1096.

Saldana, M.D.A., Nagpal, V., Guigard, S.E., (2005). Remediation of contaminated soils using supercritical fluid extraction: A review (1994-2004). Environmental Technology, 26: 1013-1032.

Sato, T. (2004), Numerical simulation of biological impact caused by direct injection of carbon dioxide in the ocean, Journal of Oceanography, 60: 807– 816.

Sedwick, P. N., G. M. McMurtry, and J. D. MacDougall (1992). Chemistry of hydrothermal solutions from Pele's Vents, Loihi Seamount, Hawaii. Geochimica et Cosmochimica Acta, 56: 3643–3667

Schultz, A., Delaney, J.R., McDuff, R.E., (1992). On the partitioning of heat flux between diffuse and point source seafloor venting. Journal of Geophysical Research, 97: 12299-12314.

Shitashima, K., Maeda, Y., (2005). Fate of liquid CO_2 discharged from the hydrothermal area in the Okinawa Trough. EOS Transactions, American Geophysical Union 86(52), Fall Meeting Supplement, Abstract B33A-1018.

Shitashima, K., Koike, Y., Kyo, M., Henmi, H., (2005). Development electrochemical in-situ pH-pCO_2-ORP sensor. EOS Transactions, American Geophysical Union 86(52), Fall Meeting Supplement, Abstract B41B-0201.

Someya, S., Bando, S., Song, Y.C., Chen, B.X., Nishio, M., (2004). Laser-dye imaging of the pH field in a laboratory experiment. Journal of Oceanography, 60: 789-795.

Staudigel, H., Hart, S.R., Pile, A., Bailey, B.E., Baker, E.T., Brooke, S., Connelly, D.P., Haucke, L., German, C.R., Hudson, I., Jones, D., Koppers, A.P., Konter, J., Lee, R., Pietsch, T.W., Tebo, B.M., Templeton, A.S., Zierenberg, R., Young, C.M., (2006). Vailulu'u Seamount, Samoa: Life and death on an active submarine volcano. Proceedings of the National Academy of Sciences of the USA, 103: 6448-6453.

Stuben, D., Bloomer, S.H., Taibi, N.E., Neumann, T. Bendel, V., Puschel, U., Barone, A., Lange, A. Shiying, W., Cuizhong, L., Deyu, Z., (1992). First results of study of sulphur-rich hydrothermal activity from an island-arc environment: Esmeralda Bank in the Mariana Arc. Marine Geology, 103: 521-528.

Tamburri, M.N., Peltzer, E.T., Friederich, G.E., Aya, I., Yamane, K., Brewer, P.G., (2000). A field study of the effects of CO_2 ocean disposal on mobile deep-sea animals. Marine Chemistry, 72: 95-101.

Tarasov, V.G., Gebruk, A.V., Mironov, A.N., Moskalev, L.I., (2005). Deep-sea and shallow-water hydrothermal vent communities: Two different phenomena? Chemical Geology, 224: 5-39.

Thistle, D., Carman, K.R., Sedlacek, L., Brewer, P.G., Fleeger, J.W., Barry, J.P., (2005). Deep-ocean, sediment-dwelling animals are sensitive to sequestered carbon dioxide. Marine Ecology Progress Series, 289: 1-4.

Thistle, D., Sedlacek, L., Carman, K.R., Fleeger, J.W., Brewer, P.G., Barry, J.P., (2006). Simulated sequestration of industrial carbon dioxide at a deep-sea site: Effects on species of harpacticoid copepods. Journal of Experimental Marine Biology and Ecology, 330: 151-158.

Thistle, D., Sedlacek, L., Carman, K.R., Fleeger, J.W., Brewer, P.G., Barry, J.P., (2007). Exposure to carbon dioxide-rich seawater is stressful for some deep-sea species: an in situ, behavioral study. Marine Ecology-Progress Series, 340: 9-16.

Thompson, G., Humphies, S.E., Schroeder, B., Sulanowska, M., Rona, P., (1988). Active vents and massive sulfides at 26º N (TAG) and 23º N (Snakepit) on the Mid- Atlantic Ridge. Canadian Mineralogist, 26: 697-711.

Tivey, M.K., Humphris, S.E., Thompson, G., Hannington, M.D. , Rona, P.A., (1995). Deducing patterns of fluid flow and mixing within the TAG active hydrothermal mound using mineralogical and geochemical data. Journal of Geophysical Research, 100: 12527-12555.

Tyler, P.A., (2002). Deep-sea eukaryote ecology of the semi-isolated basins off Japan. Journal of Oceanography, 58: 333-341.

Tyler, P.A., (2003). Disposal in the deep sea: analogue of nature or faux ami? Environmental Conservation, 30: 26-39.

Vetter, E.W., Smith, C.R., (2005). Insights into the ecological effects of deep ocean CO_2 enrichment: The impacts of natural CO_2 venting at Loihi seamount on deep sea scavengers. Journal of Geophysical Research, 110: C09S13, doi: 10.1029/2004JC002617.

Vidal, V.M.V., Vidal, F.V., Isaacs, J.D., (1981). Coastal submarine hydrothermal activity off Northern Baja California 2. Evolutionary history and isotope geochemistry. Journal of Geophysical Research, 86: 9451-9468.

Von Damm, K.L., (1990). Seafloor hydrothermal activity; black smoker chemistry and chimneys. Annual Reviews of Earth and Planetary Science, 18: 173-205.

White, S.N., Kirkwood, W., Sherman, A., Brown, M., Henthorn, R., Salamy, K., Walz, P., Peltzer, E.T., Brewer, P.G., (2005). Development and deployment of a precision underwater positioning system for in situ laser Raman spectroscopy in the deep ocean. Deep-Sea Research Part I-Oceanographic Research Papers, 52:: 2376-2389.

White, S.N., Brewer, P.G., Peltzer, E.T., (2006a). Determination of gas bubble fractionation rates in the deep ocean by laser Raman spectroscopy. Marine Chemistry, 99: 12-23.

White, S.N., Dunk, R.M., Peltzer, E.T., Freeman, J.J., Brewer, P.G., (2006b). In situ Raman analyses of deep-sea hydrothermal and cold seep systems (Gorda Ridge and Hydrate Ridge). Geochemistry Geophysics Geosystems, 7: Q05023.

Zeebe, R. E., Wolf-Gladrow, D.A., (2001). CO_2 in Seawater: Equilibrium, Kinetics, Isotopes, 345 pp., Elsevier, New York

Zhirmunsky, A.V., Tarasov, V.G., (1990). Unusual marine ecosystem in the flooded caldera of Ushishir Volcano. Marine Ecology Progress Series, 65: 95-102.

Chapter 4 References

Araktingi, R.E., Benefield, M.E., Bessenyei, Z., Coats, K.H., Tek, M.R., (1984). Leroy storage facility, Uinta County, Wyoming—a case history of attempted gas migration control. Journal of Petroleum Technology, 36: 132-140.

Bachu, S., (2005). Module 6 - Screening of sites for CO_2 storage in geological media. In: Harwood, J., (Ed.), Building capacity for CO_2 capture and storage project in the APEC region: A training manual for policy makers and Practitioners. The Delphi Group, APEC Reference #205-RE-01.3

Bachu, S., Watson, T., (2006). Possible indicators for CO_2 leakage along wells. Proceedings of the 8th International Conference on Greenhouse Gas Control Technologies (GHGT-8), 19-22 June 2006, Trondheim, Norway. Paper 02_09_04.

Barlet-Gouédard, V., Rimmelé, G., Goffé, B., (2006). Well technologies for CO_2 geological storage: Construction, repair, plugging material and procedures for long term integrity. Proceedings of the 8th International Conference on Greenhouse Gas Control Technologies (GHGT-8), 19-22 June 2006, Trondheim, Norway. Paper 02_09_03.

Beauheim, R.L., Roberts, R.M., (2002). Hydrology and hydraulic properties of a bedded evaporite formation. Journal of Hydrology, 259: 66-88.

Bentham, M., Kirby, G., (2005). CO_2 Storage in saline aquifers. Oil & Gas Science and Technology – Revue de l'IFP, 60: 559-567

Busch, A., Alles, S., Krooss, B.M., Dewhurst, D., (2007). Potential of caprocks as CO_2 storage reservoirs. Geophysical Research Abstracts, 9 (Proceedings of the 4th European Geosciences Union General Assembly, 15-20 April, 2007, Vienna, Austria): 06734.

Carey, J.W., Wigand, M., Chipera, S., WoldeGabriel, G., Pawar, R., Lichtner, P., Wehner, S., Raines, M., Guthrie, G., (2006). Analysis and performance of oil well cement with 30 years of CO_2 exposure from the SACROC Unit, West Texas, USA. Proceedings of the 8th International Conference on Greenhouse Gas Control Technologies (GHGT-8), 19-22 June 2006, Trondheim, Norway. Paper 02_09_05.

Celia, M.A., Bachu, S., Nordbotten, J.M., Gasda, S.E., Dahle, H.K., (2004). Quantitative estimation of CO_2 leakage from geological storage—analytical models numerical models, and data needs. In: Rubin, E.S., Keith, D.W., Gilboy, C.F., Wilson, M., Morris, T., Gale J., Thambimuthu K., (Eds.), Greenhouse Gas Control Technologies 7 (Proceedings of the 7th International Conference on Greenhouse Gas Control Technologies (GHGT-7), 5-9 September 2004, Vancouver, Canada). Elsevier, v1: p. 663-671.

Celia, M.A., Bachu, S., Nordbotten, J.M., Kavetski, D., Gasda, S., (2006). A risk assessment tool to quantify CO_2 leakage potential through wells in mature sedimentary basins. Proceedings of the 8th International Conference on Greenhouse Gas Control Technologies (GHGT-8), 19-22 June 2006, Trondheim, Norway. Paper 02_09_01.

ChevronTexaco Australia Pty Ltd., (2005). Draft Environmental Impact Statement/Environmental Review and Management Programme for the Proposed Gorgon Development: Main Report. ChevronTexaco Australia Pty Ltd.

Circone, S., Stern, L.A., Kirby, S.H., Durham, W.B., Chakoumakos, B.C., Rawn, C.J., Rondinone, A.J., (2003). CO_2 hydrate: Synthesis, composition, dissociation behavior, and a comparison to structure I CH_4 hydrate. Journal of Physical Chemistry B, 107: 5529-5539.

Clarke, R.H., Cleverly, R.W., (1991). Petroleum seepage and post-accumulation migration. In: England, W.A., Fleet, A.J., (Eds.), Petroleum Migration, Geological Society, London, Special Publication, 59, pp. 265-271.

Czernichowski-Lauriol, I., Sanjuan, B., Rochelle, C., Bateman, K., Pearce, J., Blackwell, P., (1996). Inorganic geochemistry. *In*: Holloway, S. (Ed.) *The Underground Disposal of Carbon Dioxide,* Final Report of Joule II Project Number CT92-0031. British Geological Survey, Keyworth, Nottingham, UK.

Davis, K.E., McDonald, L.K., (2005). Potential corrosion and microbiological mechanisms and detection techniques in solution mining and hydrocarbon storage wells. In: Tsang, C-F., Apps, J.A., (Eds.), Underground injection science and technology. Elsevier, p. 177-192.

Deffeyes, K.S, (2005). Beyond Oil: The View from Hubbert's Peak. Hill and Wang. pp. 224.

Downey, M.W., (1984). Evaluating seals for hydrocarbon accumulations. American Association of Petroleum Geologists Bulletin, 68: 1752-1763.

Dusseault, M.B., Rothenburg, L., Bachu, S., Rothenburg, L.,. (2002). Sequestration of CO_2 in salt caverns. Petroleum Society's Canadian International Petroleum Conference, June 11-13 2002, Calgary, Canada, Paper 2002-237.

Ehgartner, B., Tidwell, V., (2000). Multiphase flow and cavern abandonment in salt. Sandia National Laboratories, Albuquerque, NM, September 2000. Report SAND2000-1495C.

Fisher Q.J., Knipe R.J., (2001). The permeability of faults within siliciclastic petroleum reservoirs of the North Sea and Norwegian Continental Shelf. Marine and Petroleum Geology, 18: 1063-1081.

FutureGen, (2007). Final Risk Assessment Report for the FutureGen Project Environmental Impact Statement. Contract No. DE-AT26-06NT42921.

Grunau, H.R., (1987). A worldwide look at the cap-rock problem. Journal of Petroleum Geology, 103: 245-266.

Haszeldine, R.S., Quinn, O., England, G., Wilkinson, M., Graham, C.M., Shipton, Z.K., Ballentine, C.J., Crossey, L., Evans, J.-P., Heath, J., (2005). Natural geochemical analogues for carbon dioxide storage and sequestration in deep geological porous reservoirs. Oil & Gas Science and Technology - Revue de l'IFP, 60: 33-49.

Haszeldine, S., Lu, J., Wilkinson, M., Macleod, G., (2006). Long-timescale interaction of CO_2 storage with reservoir and seal: Miller and Brae natural analogue fields North Sea. Proceedings of the 8th International Conference on Greenhouse Gas Control Technologies (GHGT-8), 19-22 June 2006, Trondheim, Norway. Paper 02_01_05.

Hildenbrand, A., Kroos, B.M., (2003). CO_2 migration processes in argillaceous rocks: pressure-driven volume flow and diffusion. Journal of Geochemical Exploration, 78-79:169-172.

Holland, P., (1997). Offshore blowouts – Causes and controls. Gulf Publishing Company.

Hooper, B., Muray, L., Gibson-Poole, C., (2005). Latrobe Valley CO_2 Storage Assessment, Final Report. CO2CRC Report No RPT05-0108.

IPCC, (2005). The IPCC Special Report on Carbon Dioxide Capture and Storage. Metz, B., Davidson, O., de Coninck, H., Loos, M., Meyer, L., (Eds.). Cambridge University Press.

Katz, D.L., Tek, M.R., (1981). Overview on underground storage of natural gas: Journal of Petroleum Technology, June 1981, 943-951.

Kharaka, Y.K., Cole, D.R., Hovorka, S.D., Gunter, W.D., Knauss, K.G., Freifeld, B.M., (2006). Gas-water-rock interactions in Frio Formation following CO_2 injection: Implications for the storage of greenhouse gases in sedimentary basins. Geology, 34: 577-580.

Liteanu, E., Spiers, C., Peach, C., (2007). Effect of CO_2 injection on compaction of carbonate rocks. Geophysical Research Abstracts, 9 (Proceedings of the 4th European Geosciences Union General Assembly, 15-20 April, 2007, Vienna, Austria): 06824.

Macgregor, D.S., (1996). Factors controlling the destruction or preservation of giant light oil fields. Petroleum Geoscience, 2: 197-217.

Maldal, T., Tappel, I.M., (2004). CO_2 underground storage for Snøhvit gas field development. Energy, 29: 1403-1411.

Pawar, R., Carey, J., Chipera, S., Fessenden, J., Kaszuba, J., Keating, G., Lichtner, P., Olsen, S., Stauffer, P., Viswanathan, H., Ziock, H., Guthrie, G., (2006). Development of a framework for long-term performance assessment of geologic CO2 sequestration sites. Proceedings of the 8th International Conference on Greenhouse Gas Control Technologies (GHGT-8), 19-22 June 2006, Trondheim, Norway. Paper 02_08_02.

Scherer, G.W., Celia, M.A., Prévost, J-H., Bachu, S., Bruant, R., Duguid, A., Fuller, R., Gasda, S. E., Radonjic, M., Vichit-Vadakan, W., (2005). Leakage of CO_2 through abandoned wells: role of corrosion of cement. In: Thomas, D.C., Benson, S.M., (Eds.), Carbon dioxide capture for storage in deep geologic formations – results from the CO_2 capture project. Elsevier, v2: p. 827-848.

Shi, J.Q., Durucan, S., (2005). CO_2 storage in caverns and mines. Oil & Gas Science and Technology **-** Revue de l'IFP, 60: 569-571.

Shipton, Z.K., Evans, J.P., Dockrill, B., Heath, J., Williams, A., Kirchner, D., Kolesar, P.T., (2005). Natural leaking CO_2-charged systems as analogs for failed storage reservoirs. In: Thomas, D.C., Benson, S.M., (Eds.), Carbon Dioxide Capture for Storage in Deep Geologic Formations, v2: pp. 699-712. Elsevier.

Stewart, S.A., (2007). Salt tectonics in the North Sea Basin: a structural style template for seismic interpreters. Geological Society, London, Special Publications, 272: 361-396.

van der Meer, B., (2005). Carbon dioxide storage in natural gas reservoirs. Oil & Gas Science and Technology - Revue de l'IFP, 60: 527-536.

Vu-Hoang, D., Vrignaud, Y., Jammes, L., Van Kuijk, R., Froelich, B., Schilling, K., Hori, H., Pistre, V., (2006). Assessing the integrity of downhole CO_2 storage using in-situ sonic, advanced ultrasonic, and electromagnetic measurements. Proceedings of the 8th International Conference on Greenhouse Gas Control Technologies (GHGT-8), 19-22 June 2006, Trondheim, Norway. Paper 02_09_02

Warren, J.K., (2007). Evaporites: Sediments, Resources and Hydrocarbons. Springer. 1035 pp.

Watson, T.L., Getzlaf, D., Griffith, J.E., (2002). Specialized cement design and placement procedures prove successful for mitigating casing vent flows – case histories. Gas Technology Symposium, 30 April - 2 May 2002, Calgary, Canada. Paper SPE 76333.

Watson, M.N., Daniel, R.F., Tingate, P.R., Gibson-Poole, C.M., (2004). CO_2 related seal capacity enhancement in mudstones: Evidence from the Pine Lodge natural CO_2 accumulation, Otway Basin, Australia. In: Rubin, E.S., Keith, D.W., Gilboy, C.F., Wilson, M., Morris, T., Gale J., Thambimuthu K., (Eds.), Greenhouse Gas Control Technologies 7 (Proceedings of the 7th International Conference on Greenhouse Gas Control Technologies (GHGT-7), 5-9 September 2004, Vancouver, Canada), v2: p. 2313-2316. Elsevier.

Chapter 5 References

Archer, D.E., (1996). An atlas of the distribution of calcium carbonate in sediments of the deep sea. Global Biogeochemical Cycles, 10: 159-174.

Archer, D., Kheshgi, H., Maier-Reimer, E., (1998). Dynamics of fossil fuel CO_2 neutralization by marine $CaCO_3$. Global Biogeochemical Cycles, 12: 259-276.

Ardvison, R.S., Ertan, I.E., Amonette, J.E., Luttge, A., (2003). Variation in calcite dissolution rates: a fundamental problem? Geochimica et Cosmochimica Acta, 67: 1623-1634.

Avraam, D.G., Payatakes, A.C., (1995). Flow regimes and relative permeabilities during steady-state 2-phase flow in porous-media. Journal of Fluid Mechanics, 293: 207-236.

Ballard, A.L., Sloan, E.D., (2004). The next generation of hydrate prediction. Part III. Gibbs energy minimization formalism. Fluid Phase Equilibria, 218: 15-31.

Bateman, K., Turner, G., Pearce, J.M., Noy, D.J., Birchall, D., Rochelle, C.A., (2005). Large-scale column experiment: Study of CO_2, porewater, rock reactions and model test case. Oil & Gas Science and Technology – Revue de l'IFP, 60: 161-175.

Bradshaw, A., (1973). The effect of carbon dioxide on the specific volume of seawater. Limnology and Oceanography, 18: 95-105.

Brunauer, S., Emmett, P.H., Teller, E., (1938). Absorption of gases and multimolecular layers. Journal of the American Chemical Society, 60: 309-319.

Bryant, W.R., Rack, F.R., (1990). Consolidation characteristics of Weddell Sea sediments. In: Barker, P.F., Kennet, J.P., (Eds.), Proceedings of the Ocean Drilling Program, Scientific Results, Vol. 113, College Station, TX: Ocean Drilling Program, pp. 211–223.

Camps, A., Rochelle, C., Milodowski, T., Long, D., Lovell, M., Bateman, K., Gunn, D., Jackson, P., Rees, J., 2006. The underground storage of CO_2 at low temperatures and its trapping in solid phases. Proceedings of the 8th International Conference on Greenhouse Gas Control Technologies (GHGT-8), 19-22 June 2006, Trondheim, Norway. Paper 02_01_10.

ChevronTexaco Australia, (2003). *Gorgon Development Summary Metocean Data Book.* ChevronTexaco Australia, Perth, WA.

Chiba, H., Sakai, H., Gamo, T., Ishibashi, J-I., Nakashima, K., Minami, H., Dobahi, F., (1992). Chemistry and isotopic composition of bubbles emerging from the seafloor at the Minami-Ensei Knoll, Okinawa Trough. Proceedings of JAMSTEC, Symposium of Deep-Sea Research, 8: 81-87.

Chiba, H., Ishibashi, J.-I., Ueno, H., Oomori, T., Uchiyama, N., Takeda, T., Takemine, C., Ri, J., Itomitsu, A., (1996). Seafloor hydrothermal systems at North Knoll, Iheya Ridge, Okinawa Trough. JAMSTEC Journal of Deep-Sea Research, 12: 211- 219 (in Japanese with English Abstract).

Dickens, G.R., Quinby-Hunt, M.S., (1997). Methane hydrate stability in pore water: A simple theoretical approach for geophysical applications. Journal of Geophysical Research, 102: 773-783.

Doughty, C., (2007). Modeling geologic storage of carbon dioxide: Comparison of non-hysteretic and hysteretic characteristic curves. Energy Conversion and Management, 48: 1768–1781.

Enos, P., Sawatsky, L.H., (1981). Pore networks in Holocene carbonate sediments. Journal of Sedimentary Petrology, 51: 961-985.

Fujikura, K., Fujiwara, Y., Ishibashi, J.-I., Katayama, S., Komatsu, T., Maezawa, Y., Maki, Y., Miyazaki, J.-I., Miyake, H., Okamoto, K., Okoshi, K., Toth, L.G., Tsuchida, S., Yamaguchi, T., Yamanaka, T., Watabe, H., Zielinski, S., Kato, K., (2001). Report on investigation of hydrothermal vent ecosystems by the crewed submersible 'Shinkai 2000' on Dai-Yon (No. 4) Yanaguni Knoll and the Hatoma Knoll, the Okinawa Trough, JAMSTEC Journal of Deep-Sea Research, 19: 141-154 (in Japanese with English Abstract).

Gehlen, M., Bassinot, F.C., Chou, L., McCorkle, D., (2005). Reassessing the dissolution of marine carbonates: II. Reaction kinetics. Deep-Sea Research I, 52: 1461-1476.

Glasby, G.P., Notsu, K., (2003). Submarine hydrothermal mineralization in the Okinawa Trough, SW of Japan: an overview. Ore Geology Reviews, 23: 299-339.

Hashimoto, J., Ohta, S., Fujikura, K., Miura, T., (1995). Microdistribution pattern and biogeography of the hydrothermal vent communities of the Minami-Ensei Knoll in the Mid-Okinawa Trough, Western Pacific. Deep-Sea Research I, 42: 577-598.

Haszeldine, R.S., Quinn, O., England, G., Wilkinson, M., Graham, C.M., Shipton, Z.K., Ballentine, C.J., Crossey, L., Evans, J.-P., Heath, J., (2005). Natural geochemical analogues for carbon dioxide storage and sequestration in deep geological porous reservoirs. Oil & Gas Science and Technology - Revue de l'IFP, 60: 33-49.

Haugan, P.M., Drange, H., (1992). Sequestration of CO_2 in the deep ocean by shallow injection. Nature, 357: 318-320.

Hou, Z., Ai, Y., Qu, X., Zhang, Q., Tang, S., (1999a). Possible contribution of magmatic fluids to seafloor ore-forming hydrothermal systems in the Okinawa Trough. Acta Geologica Sinica, 73: 57- 65 (in Chinese with English Abstract).

Hou, Z., Zhang, Q., Qu, X., (1999b). Hydrothermal fluid evolution and ore-forming processes of submarine hydrothermal systems in the Okinawa Trough. Exploration and Mining Geology, 8: 257-272.

House, K.Z., Schrag, D.P., Harvey, C.F., Lackner, K.S., (2006). Permanent carbon dioxide storage in deep-sea sediments. Proceedings of the National Academy of Sciences of the USA, 103: 12291-12295.

Hovland, M., Risk, M., (2003). Do Norwegian deep-water coral reefs rely on seeping fluids? Marine Geology, 198: 83-96.

Inagaki, F., Kuypers, M.M.M., Tsunogai, U., Ishibashi, J., Nakamura, K., Treude, T., Ohkubo, S., Nakaseama, M., Gena, K., Chiba, H., Hirayama, H., Nunoura, T., Takai, K., Jorgensen, B.B., Horikoshi, K., Boetius, A., (2006). Microbial community in a sediment-hosted CO_2 lake of the southern Okinawa Trough hydrothermal system. Proceedings of the National Academy of Sciences of the USA, 103: 14164-14169.

Koide, H., Takahashi, M., Tsukamoto, H., Shindo, Y., (1995). Self-trapping mechanisms of carbon dioxide in the aquifer disposal. Energy Conversion and Management, 36: 505-508.

Koide, H., Shindo, Y., Tazaki, Y., Iijima, M., Ito, K., Kimura, N., Omata, K., (1997a). Deep sub-seabed disposal of CO_2 - The most protective storage. Energy Conversion and Management, 38: S253-S258.

Koide, H., Takahashi, M., Shindo, Y., Tazaki, Y., Iijima, M., Ito, K., Kimura, N., Omata, K., (1997b). Hydrate formation in sediments in the sub-seabed disposal of CO_2. Energy, 22: 279-283.

Ligtenberg, H., Connolly, D., (2003). Chimney detection and interpretation, revealing sealing quality of faults, geohazards, charge of and leakage from reservoirs. Journal of Geochemical Exploration, 78-9: 385-387.

Liu, X., Flemings, P.B., (2007). Dynamic multiphase flow model of hydrate formation in marine sediments. Journal of Geophysical Research, 112: B03101.

Llamedo, M., Anderson, R., Tohidi, B., (2004). Thermodynamic prediction of clathrate hydrate dissociation conditions in mesoporous media. American Mineralogist, 89: 1264-1270.

Lupton, J., Butterfield, D., Lilley, M., Evans, L., Nakamura, K.I., Chadwick, W., Resing, J., Embley, R., Olson, E., Proskurowski, G., Baker, E., de Ronde, C., Roe, K., Greene, R., Lebon, G., Young, C., (2006). Submarine venting of liquid carbon dioxide on a Mariana Arc volcano. Geochemistry Geophysics Geosystems, 7: Art. No. Q08007.

Naeth, J., di Primio, R., Horsfield, B., Schaefer, R.G., Shannon, P.M., Bailey, W.R., Henriet, J.P., (2005). Hydrocarbon seepage and carbonate mound formation: A basin modelling study from the porcupine basin (offshore Ireland). Journal of Petroleum Geology, 28: 147-165.

Millero, F.J. (1995). The thermodynamics of the carbonate system in seawater. Geochimica et Cosmochimica Acta, 43: 1651-1661.

Morse, J.W., Berner, R.A., (1972). Dissolution kinetics of calcium carbonate in seawater: II. A kinetic origin for lysocline. American Journal of Science, 272: 840-851.

Morse, J.W., Arvidson, R.S., (2002). The dissolution kinetics of major sedimentary carbonate minerals. Earth-Science Reviews, 58: 51–84.

Mucci, A., (1983). The solubility of calcite and aragonite in seawater at various salinities, temperatures, and one atmosphere total pressure. American Journal of Science, 283: 780-799.

Sakai, H., Gamo, T., Kim, E-S., Tsutsumi, M., Tanaka, T., Ishibashi, J., Wakita, H., Yamano, M., and Oomori, T., (1990). Venting of carbon dioxide-rich fluid and hydrate formation in Mid-Okinawa Trough Backarc Basin. Science, 248: 1093-1096.

Schroot, B.M., Klaver, G.T., Schuttenhelm, R.T.E., (2005). Surface and subsurface expressions of gas seepage to the seabed - examples from the Southern North Sea. Marine and Petroleum Geology, 22: 499-515.

Shitashima, K., Maeda, Y., (2005). Fate of liquid CO_2 discharged from the hydrothermal area in the Okinawa Trough. EOS Transactions, American Geophysical Union 86(52), Fall Meeting Supplement, Abstract B33A-1018.

Sjöberg, E.L., Rickard, D.T., (1985). The effect of added dissolved calcium on calcite dissolution kinetics in aqueous solutions at 25°C. Chemical Geology, 49: 405-413.

Sloan., E.D., (1991). Clathrate Hydrates of Natural Gases, Marcel Dekker, New York.

Someya, S., Saito, K., Chen, B., Nishio, M., Song, Y., Tsutsui, K., (2006). CO_2 sequestration under an artificial impermeable layer with clathrate hydrate in sediments. Proceedings of the 8th International Conference on Greenhouse Gas Control Technologies (GHGT-8), 19-22 June 2006, Trondheim, Norway. Paper 02_05_01.

Song, Y., Nishio, M., Chen, B., Someya, S., Uchida, T., Akai, M., (2002). Measurement of the density of CO_2 solution by Mach-Zehnder Interferometry. Annals of the New York Academy of Sciences, 972: 206-212.

Uchida, T., Hondoh, T., Mae, S. Kawabata, J., (1995). Physical Data of CO_2 Hydrate. In: Handa, N., Ohsumi, T., (Eds.), Direct Ocean Disposal of Carbon Dioxide, Proceedings of ICO-2 – The Second International Symposium on Interaction between CO_2 and Ocean, 1-2 June 1993, Tsukuba, Japan, Terrapub, Tokyo, pp.45-61.

Walter, L.M., Morse, J.W., (1984). Reactive surface area of skeletal carbonates during dissolution: effect of grain size. Journal of Sedimentary Petrology, 54: 1081-1090.

Yamamuro, O., Suga, H., (1989). Thermodynamic Studies of Clathrate Hydrates, Journal of Thermal Analysis, 35: 2025-2064.

Chapter 6 References

Abe, Y., Abe, Y., Aya, I., Yamane, K., (2007). The optical measurement of CO_2 clathrate hydrate membrane thickness. Journal of Thermal Science and Technology, 2: 13-18 .

Alendal, G., Drange, H., (2001). Two-phase, near-field modeling of purposefully released CO_2 in the ocean. Journal of Geophysical Research, 106: 1085-1096.

Auerbach, D.I., Caulfield, J.A., Adams, E., Herzog, H.J., (1997). Impacts of ocean CO_2 disposal on marine life: A toxicological assessment integrating constant-concentration laboratory data with variable-concentration field exposure. Environmental Modeling & Assessment, 2: 333-343.

Aya, I., Yamane, K., Yamada, N., (1992). Stability of clathrate-hydrate of carbon dioxide in highly pressured water. In: Kroeger, P.G., Bayazitoglu, Y., (Eds.), Fundamentals of Phase Change: Freezing, Melting and Sublimation, ASME-HTD v215: p17–22.

Aya, I., Yamane, K., Nariai, H., (1997). Solubility of CO_2 and density of CO_2 hydrate at 30 MPa. Energy, 22: 263-271.

Barry, J.P., Drazen, J.C., (2007). Response of deep-sea scavengers to ocean acidification and the odor from a dead grenadier. Marine Ecology Progress Series, 350: 193-207.

Barry, J.P., Buck, K.R., Lovera, C., Kuhnz, L., Whaling, P.J., Peltzer, E.T., Walz, P., Brewer, P.G., (2004). Effects of direct ocean CO_2 injection on deep-sea meiofauna. Journal of Oceanography, 60: 759-766.

Barry, J.P., Buck, K.R., Lovera, C., Kuhnz, L., Whaling, P.J., (2005). Utility of deep sea CO_2 release experiments in understanding the biology of a high-CO_2 ocean: Effects of hypercapnia on deep sea meiofauna. Journal of Geophysical Research - Oceans, 110: C09S12.

Bigalke, N.K., Rehder, G., Gust, G., (2008). Experimental investigation of the rising behavior of CO_2 droplets in seawater under hydrate-forming conditions. Environmental Science and Technology, 42: 5241-5246.

Borowitzka, M.A., (1981). Photosynthesis and calcification in the articulated coralline red algae *Amphiroa anceps* and *A. foliacea.* Marine Biology, 62: 17-23.

Botz, R., Winckler,G., Bayer, R., Schmitt,M., Schmidt, M., Garbe-Schönberg, D., Stoffers, P., Kristjansson, J.K., (1999). Origin of trace gases in submarine hydrothermal vents of the Kolbeinsey Ridge, north Iceland. Earth and Planetary Science Letters, 171: 83–93.

Bozzano & Dente (2001) in Gangsto

Bradshaw, A., (1973). The effect of carbon dioxide on the specific volume of seawater. Limnology and Oceanography, 18: 95-105.

Brewer, P.G., Orr, Jr., F.M., Friederich, G., Kvenvolden, K.A., Orange, D.L., McFarlane, J., Kirkwood, W., (1998). Gas hydrate formation in the deep sea: In situ experiments with controlled release of methane, natural gas and carbon dioxide. Energy and Fuels, 12: 183-188.

Brewer, P.G., Friederich, G., Peltzer, E.T., Orr Jr., F.M., (1999). Direct experiment on the ocean disposal of fossil fuel CO_2. Science, 284: 943-945.

Brewer, P.G., Peltzer, E.T., Friedrich, G., Rehder, G., (2002). Experimental determination of the fate of rising CO_2 droplets in seawater. Environmental Science and Technology, 36: 5441-5446.

Brewer, P.G., Peltzer, E.T., Walz, P., Aya, I., Yamane, K., Kojima, R., Nakajima, Y., Nakayama, N., Haugan, P., Johannessen, T., (2005). Deep ocean experiments with fossil fuel carbon dioxide: Creation and sensing of a controlled plume at 4 km depth. Journal of Marine Research, 63: 9-33.

Brewer, P.G., Chen, B.X., Warzinki, R., Baggeroer, A., Peltzer, E.T., Dunk, R.M., Walz, P., (2006). Three-dimensional acoustic monitoring and modelling of a deep-sea CO_2 droplet cloud. Geophysical Research Letters, 33: L23607.

Bruland, K.W., Lohan, M.C., (2004). Controls on trace metals in seawater. In: Elderfield, H., (Ed.), Treatise on Geochemistry vol. 6, The Oceans and Marine Geochemistry. Elsevier, London. pp. 23-49.

Burleson, M.L., Smatresk, N.J., (2000). Branchial chemoreceptors mediate ventilatory response to hypercapnic acidosis in channel catfish. Comparative Biochemistry & Physiology, A: 125: 403-414.

Byrne, R.H., (2002). Inorganic speciation of dissolved elements in seawater: the influence of pH on concentration ratios. Geochemical Transactions, 3: 11-16.

Caulfield, J.A., Adams, E.E., Auerbach, D.I., Herzog, H.J., (1997). Impacts of ocean CO_2 disposal on marine life: II. Probabilistic plume exposure model used with a time-varying dose-response analysis. Environmental Modeling and Assessment, 2: 345-353.

Carman, K.R., Thistle, D., Fleeger, J.W., Barry, J.P., (2004). Influence of introduced CO_2 on deep-sea metazoan meiofauna. Journal of Oceanography, 60: 767-772.

Caulfield, J.A., Auerbach, D.I., Adams, E.E., Herzog. H.J., (1997). Near field impacts of reduced pH from ocean CO_2 disposal. Energy Conversion and Management, 38: S343-S348.

Chen, B., Akai, M., (2004). Modelling dispersion from direct injection of carbon dioxide in the water column. Presented at 'The Ocean in a High CO_2 World', An International Science Symposium, 10-12 May 2004, UNESCO, Paris, France.

Chen, B., Song, Y., Nishio, M., Akai, M., (2003). Large-eddy simulation of double cloud formation induced by CO_2 dissolution in the ocean. Tellus (B), 55: 723– 730.

Chen, B., Song, Y., Nishio, M., Akai, M., (2004). A Eulerian-Eulerian physical-biological impacts model of zooplankton injuring due to CO_2 ocean sequestration. Journal of Oceanography, 60: 797-805.

Chen, B., Song, Y., Nishio, M., Akai, M., (2005). Modelling of CO_2 dispersion from direct Injection of CO_2 in the Water Column, Journal of Geophysical Research, 11: doi 1029/2004JC002567.

Childress, J.J., (1995). Are there physiological and biochemical adaptations of metabolism in deep-sea animals?, Trends in Ecology & Evolution, 10: 30-36.

Clift, R., Grace, J.R., Weber, M.E., (1978). Bubbles, Drops and Particles. Academic Press, New York.

Crocker, C.E., Cech Jr., J.J., (1996). The effects of hypercapnia on the growth of juvenile white sturgeon, Acipenser transmontanus. Aquaculture, 147: 293-299.

Dunk, R.M., Brewer, P.G., Peltzer, E.T., Walz, P.M. (in preparation). The hydration rate of CO_2 in the ocean: effects of pH, temperature, and pressure.

Egorov, A.V., Crane, K., Vogt, P.R., Rozhkov, A.N., (1999). Gas hydrates that outcrop the sea floor: Stability models. Geo-Marine Letters, 19: 68-75.

Enstad, L.I., Alendal, G., Haugan, P.M., (2006). Dissolution of CO_2 from the sea-floor to oceanic waters. Proceedings of the 8th International Conference on Greenhouse Gas Control Technologies (GHGT-8), 19-22 June 2006, Trondheim, Norway. Paper 02_06_01

Evans, D.H., (1984). The roles of gill permeability and transport mechanisms in euryhalinity. In: Haar, W.S., Randall, D.J., (Eds.), Fish Physiology, Vol. XA, Academic Press, New York. pp. 239-283.

Feely, R.A., Sabine, C.L., Lee, K., Berelson, W., Kleypas, J., Fabry, V.J., Millero, F.J., (2004). Impact of Anthropogenic CO_2 on the $CaCO_3$ System in the Oceans. Science, 305: 362-366

Fer, I., Haugan, P.M., (2003). Dissolution from a liquid CO_2 lake disposed in the deep ocean. Limnology and Oceanography, 48: 872-883.

Gage, J.D., Tyler, P.A., (1991). Deep-sea biology: a natural history of organisms at the deep-sea floor. Cambridge University Press, Cambridge, UK. p. 504.

Gamo, T., Glasby, G.P., (2003). Submarine hydrothermal activity in coastal zones. In: Taneguchi, M., Wang, K., Gamo, T., (Eds.), Land and Sea Hydrogeology. Elsevier, Amsterdam, pp. 151-163.

Gangstø, R., (2004). Single CO_2 drops in seawater. Cand. Scient. Thesis in Physical Oceanography. University of Bergen.

Gangstø, R., Haugan, P.M., Alendal, G., (2005). Parameterization of drag and dissolution of rising CO_2 drops in seawater. Geophysical Research Letters, 32: L10612, doi:10.1029/2005GL022637.

Gao, K., Aruga, Y., Asada, K., Ishihara, T., Akano, T., Kiyohara, M., (1993). Calcification in the articulated coralline alga *Corallina pilulifera*, with special reference to the effect of elevated CO_2 concentration. Marine Biology, 117: 129-132.

Gattuso, J.-P., Frankignoulle, M., Bourge, I., Romaine, S., Buddemeier, R. W., (1998). Effect of calcium carbonate saturation of seawater on coral calcification. Global and Planetary Change, 18: 37-46.

Gilmour, K.M., (2001). The CO_2/pH ventilatory drive in fish. Comparative Biochemistry & Physiology A, 130: 219-240.

Glasby, G.P., (1971). Direct observation of columnar scattering associated with geothermal gas bubbling in the Bay of Plenty, New Zealand. New Zealand Journal of Marine and Freshwater Research, 5: 483-496.

Haedrich, R.L., (1997). Distribution and population ecology. In: Randall, D.J., Farrell, A.P., (Eds.), Fish Physiology, vol. 16, Deep-Sea Fishes. Elsevier, New York, pp. 79-114,

Haljasmaa, I.V., Vipperman, J.S., Lynn, R.J., Warzinski, R.P., (2005). Control of a fluid particle under simulated deep-ocean conditions in a high-pressure water tunnel. Review of Scientific Instruments, 76: 1-11.

Hannington, M., Herzig, P., Stoffers, P., Scholten, J., Botz, R., Garbe-Schonberg, D., Jonasson, I.R., Roset, W., and the Shipboard Scientific Party, (2001). First Observations of high-temperature submarine hydrothermal vents and massive anhydrite deposits off the north coast of Iceland. Marine Geology, 177: 199-220.

Hashimoto, J., Ohta, S., Fujikura, K., Miura, T., (1995). Microdistribution pattern of the hydrothermal vent communities of the Minami-Ensei Knoll in the Mid-Okinawa Trough, Western Pacific. Deep-Sea Research, Part 1, 42: 577-599.

Haugan, P.M., Alendal, G., (2005). Turbulent diffusion and transport from a CO_2 lake in the deep ocean. Journal of Geophysical Research, 110: C09S14.

Haugan, P.M., Drange, H., (1992). Sequestration of CO_2 in the deep ocean by shallow injection. Nature, 357: 318-320.

Heisler, N., (1986). Acid-base regulation in fishes. In: Heisler, N., (Ed.), Acid-Base Regulation in Animals, Elsevier, New York. pp. 309-356.

Herzog, H., Golomb, D., Zemba, S., (1991). Feasibility, modelling and economics of sequestratering power plant CO_2 emissions in the deep ocean. Environmental Progress, 10: 64-74.

Hirai, S., Okazaki, K., Tabe, Y., Hijikata, K., Mori, Y., (1997). Dissolution rate of liquid CO_2 in pressurized water flows and the effect of clathrate films. Energy, 22: 285-293.

Holder, G.D., Cugini, A.V., Warzinski, R.P., (1995). Modeling clathrate hydrate formation during carbon dioxide injection into the ocean. Environmental Science and Technology, 29: 276-278.

Holder, G. D. & Warzinski, R. P. (1996). Formation and growth of CO2 clathrate hydrate shells around gas bubbles or liquid drops. ACS Fuel Chemistry Division Preprints, 41: 1452.

Hooper, B., Muray, L., Gibson-Poole, C., (2005). Latrobe Valley CO_2 Storage Assessment, Final Report. CO2CRC Report No RPT05-0108.

Huesemann, M.H., Skillman, A.D., Crecelius, E.A., (2002). The inhibition of marine nitrification by ocean disposal of carbon dioxide. Marine Pollution Bulletin, 44: 142-148.

IEA Greenhouse Gas Research & Development Programme (2004). Gas Hydrates for Deep Ocean Storage of CO_2. Report Number PH4/26.

Inagaki, F., Kuypers, M.M.M., Tsunogai, U., Ishibashi, J., Nakamura, K., Treude, T., Ohkubo, S., Nakaseama, M., Gena, K., Chiba, H., Hirayama, H., Nunoura, T., Takai, K., Jørgensen, B.B., Horikoshi, K., Boetius, A., (2006). Microbial community in a sediment-hosted CO_2 lake of the southern Okinawa Trough hydrothermal system. Proceedings of the National Academy of Sciences, 103: 14164-14169.

IPCC, (2005). The IPCC Special Report on Carbon Dioxide Capture and Storage. Metz, B., Davidson, O., de Coninck, H., Loos, M., Meyer, L., (Eds.). Cambridge University Press.

Ishimatsu, A., Kikkawa, T., Hayashi, M., Lee, K.-S., Kita, J., (2004). Effects of CO_2 on marine fish: larvae and adults. Journal of Oceanography, 60: 731-742.

Ishimatsu, A., Hayashi, M., Lee, K.-S., Kikkawa, T., Kita, J., (2005). Physiological effects on fishes in a high-CO_2 world. Journal of Geophysical Research, 110: C09S09.

Jähne, B., Henz, G., Dietrich, W., (1987). Measurement of the diffusion coefficients of sparingly soluble gases in water. Journal of Geophysical Research, 92: 10767-10776.

Johnson, K.M., Dickson, A.G., Eischeid, G., Goyet, C., Guenther, P., Millero, F.J., Purkerson, D., Sabine, C.L., Schottle, R.G., Wallace, D.W.R., Wilke, R.J., Winn, C.D., (1998). Coulometric total carbon dioxide analysis for marine studies: Assessment of the quality of total inorganic carbon measurements made during the US Indian Ocean CO_2 Survey 1994-1996. Marine Chemistry, 63: 21-37.

Kamenev G.M., Kavun, V.Y., Tarasov, V.G., Fadeev, V.I., (2004). Distribution of bivalve mollusks Macoma golikovi (Scarlato and Kafanov, 1988) and Macoma calcarea (Gmelin, 1791) in the shallow-water hydrothermal ecosystem of Kraternaya Bight (Yankich Island, Kuril Islands): connection with feeding type and hydrothermal activity of Ushishir Volcano. Continental Shelf Research, 24: 75-95.

Kikkawa, T., Kita, J., Ishimatsu, A., (2004). Comparison of the lethal effect of CO2 and acidification on red sea bream (Pagrus major) during the early developmental stages. Marine Pollution Bulletin, 48: 108-110.

Kikkawa, T., Sato, T., Kita, J., Ishimatsu, A., (2006). Acute toxicity of temporally varying seawater CO2 conditions on juveniles of Japanese sillago (Sillago japonica). Marine Pollution Bulletin, 52: 621-625.

Kita, J., Ohsumi, T., (2004). Perspectives on biological research for CO_2 ocean sequestration. Journal of Oceanography, 60: 695-703.

Kurihara, H., Shimode, S., Shirayama, Y., (2004). Sub-lethal effects of elevated concentration of CO_2 on planktonic copepods and sea urchins. Journal of Oceanography, 60: 743-750.

Kvamme, B., (2000). Phase transitions and stabilities in seawater containing carbon dioxide. In Recent Advances in Marine Science and Technology, pp. 279–289. Honolulu, Hawaii USA, monograph.

Kvamme, B., Tanaka, H., (1995). Thermodynamic stability of hydrates for ethane, ethylene, and carbon dioxide. Journal of Physical Chemistry, 99: 7114-7119.

Kvamme, B., Svandal, A., Buanes, T., Kuznetsova, T., Gránásy, L., (2005). Phase field approaches to the kinetic modeling of hydrate phase transitions Invited and reviewed chapter in a book related to AAPG. Hedberg Research Conference Natural Gas Hydrates: Energy Resource Potential and Associated Geologic Hazards, September 12-16, 2004, Vancouver, BC, Canada, submitted October 2005. (downloaded from http://hdl.handle.net/1956/1118).

Langdon, C., Atkinson, M.J., (2005). Effect of elevated pCO_2 on photosynthesis and calcification of corals and interactions with seasonal change in temperature/irradiance and nutrient enrichment. Journal of Geophysical Research, 110: C09S07.

Langdon, C., Takahashi, T., McConnaughey, T., Anderson, H., West, H., (1998). Effect of calcium carbonate saturation state on the rate of calcification of an experimental coral reef. American Zoologist, 37: abstract #254.

Langdon, C., Takahashi, T., Sweeney, C., Chipman, D., Goddard, J., Marubini, F., Aceves, H., Barnett, H., Atkinson, M. J., (2000). Effect of calcium carbonate saturation state on the calcification rate of an experimental coral reef. Global Biogeochemical Cycles, 14: 639-654.

Langenbuch, M., Pörtner, H.O., (2002). Changes in metabolic rate and N-excretion in the marine invertebrate *Sipunculus nudus* under conditions of environmental hypercapnia: identifying effective acid-base parameters. The Journal of Experimental Biology, 205: 1153-1160.

Langenbuch, M., Pörtner, H.O., (2003). Energy budget of hepatocytes from Antarctic fish (Pachycara brachycephalum and Lepidonotothen kempi) as a function of ambient CO_2: pH-dependent limitations of cellular protein synthesis?. The Journal of Experimental Biology, 206: 3895-3903.

Leclercq, N., Gattuso, J.-P., and Jaubert, J., (2000). CO_2 partial pressure controls the calcification rate of a coral community. Global Change Biology, 6: 329-334.

Liu, X., Flemings, P.B., (2007). Dynamic multiphase flow model of hydrate formation in marine sediments. Journal of Geophysical Research, 112: B03101.

Lupton, J., Butterfield, D., Lilley, M., Evans, L., Nakamura, K.I., Chadwick, W., Resing, J., Embley, R., Olson, E., Proskurowski, G., Baker, E., de Ronde, C., Roe, K., Greene, R., Lebon, G., Young, C., (2006). Submarine venting of liquid carbon dioxide on a Mariana Arc volcano. Geochemistry Geophysics Geosystems, 7: Art. No. Q08007.

Marubini, F., Atkinson, M., Effect of lowered pH and elevated nitrate on coral Calcification. Marine Ecology Progress Series, 188: 117-121.

Marubini, F., Thake, B., (1999). Bicarbonate addition promotes coral growth. Limnology & Oceanography, 44: 716-720.

Marubini, F., Ferrier-Pages, C., Cuif, J. P., (2003). Suppression of skeletal growth in scleractinian corals by decreasing ambient carbonate-ion concentration: a cross-family comparison. Proceedings of the Royal Society of London, Series B, 270: 179-184.

McCarthy, K.T., Pichler, T., Price, R.E., (2005). Geochemistry of Champagne Hot Springs shallow hydrothermal vent field and associated sediments, Dominica, Lesser Antilles. Chemical Geology 224: 55-68.

McKendry, J.E., Milsom, W.K., Perry, S.F., (2001): Branchial CO_2 receptors and cardiorespiratory adjustments during hypercarbia in Pacific spiny dogfish (Squalus acanthias). The Journal of Experimental Biology, 204: 1519-1527.

McKenzie, D.J., Taylor, E.W., Dalla Valle, A.Z., Steffensen, J.F., (2002). Tolerance of acute hypercapnic acidosis by the European eel (Anguilla anguilla). Journal of Comparative Physiology, 172B: 339-346.

Michaelidis, B., Ouzounis, C., Paleras, A., Pörtner, H.O., (2005): Effects of long-term moderate hypercapnia on acid-base balance and growth rate in marine mussels (Mytilus galloprovincialis). Marine Ecology Progress Series, 293: 109-118.

Miles, H., Widdicombe, S., Spicer, J.I., Hall-Spencer, J., (2007). Effects of anthropogenic seawater acidification on acid-base balance in the sea urchin Psammechinus miliaris. Marine Pollution Bulletin, 54: 89-96.

Milsom, W. K., (2002). Phylogeny of CO_2/H^+ chemoreception in vertebrates. Respiratory Physiology & Neurobiology, 131: 29–41.

Mori, Y.H., (1998). Clathrate hydrate formation at the interface between liquid CO_2 and water phases - A review of rival models characterizing ‘‘hydrate films’’. Energy Conversion & Management, 39: 1537-1557.

Morris, R., Taylor, E.W., Brown, D.J.A., Brown, J.A., (1989). Acid Toxicity and Aquatic Animals. Society for Experimental Biology Seminar Series, vol. 34. Cambridge Univ. Press, New York. 282 pp.

Nishikawa, N., Ishibashi, M., Ohta, H., Akutsu, N., Tajika, M., Sugitani, T., Hiraoka, R., Kimuro, H., Shiota, T., (1995). Stability of liquid CO_2 spheres covered with clathrate film when exposed to environment simulating the deep sea. Energy Conversion & Management, 36: 489-492.

Nishio, M., Masutani, S.M., Minamiura, J., Ozaki, M., (2005). Study of liquid CO_2 droplet formation under simulated mid-depth ocean conditions. Energy, 30: 2284-2297.

Ohsumi, T., (1995). CO_2 disposal options in the deep sea. Marine Technology Society Journal, 29: 58-66.

Opdyke, B.N., Gust, G., Ledwell, J.R., (1987). Mass transfer from smooth alabaster surfaces in turbulent flows. Geophysical Research Letters, 14: 1131-1134.

Oyama, C., Abe, Y., Nariai, H., Yamane, K., Kojima, R., Aya, I., (2004). Estimation of CO_2 hydrate membrane thickness. Proceedings of Thermal Engineering Conference, 177-178 (in Japanese with English abstract).

Ozaki, M. (1999). Annual Report of RITE 1999, 286–307 (in Japanese).

Ozaki, M., Ohsumi, T., Masuda, S., (1999). Dilution of released CO_2 in mid ocean depth by moving ship. In: Eliasson, B., Riemer, P.W.F., Wokaum, A., (Eds.),Greenhouse Gas Control Technologies. Elsevier, New York. p.275-280.

Pane, E.F., Barry J.P. (2007). Extracellular acid-base regulation during short-tem hypercapnia is effective in a shallow-water crab, but ineffective in a deep-sea crab. Marine Ecology Progress Series, 334: 1-9.

Peltzer, E.T., Brewer, P.G., Dunk, R.M., Fuchs, M.P., Walz, P.M., 2006. Deep Ocean CO_2 Hydration Kinetics. AGU Ocean Sciences Meeting, Abstract OS45B-20.

Pichler, T., Dix, G.R., (1996). Hydrothermal venting within a coral reef ecosystem, Ambitle Island, Papua New Guinea. Geology, 24: 435-438.

Pörtner, H.O., (1990): An analysis of the effects of pH on oxygen binding by squid (Illex illecebrosus, Loligo pealei) haemocyanin. The Journal of Experimental Biology., 150: 407–424.

Pörtner, H.O., (2002). Climate variations and the physiological basis of temperature dependent biogeography: systemic to molecular hierarchy of thermal tolerance in animals. Comparative Biochemistry and Physiology Part A, 132: 739-761.

Pörtner, H.O., Reipschläger, A., (1996): Ocean disposal of anthropogenic CO_2: physiological effects on tolerant and intolerant animals. In: Ormerod, B., Angel, M., (Eds.), Ocean Storage of CO_2. Environmental Impact. Massachusetts Institute of Technology and International Energy Agency, Greenhouse Gas R&D Programme. Boston/Cheltenham, UK., pp. 57-81.

Pörtner, H.O., Reipschläger, A., Heisler, N., (1998). Metabolism and acid-base regulation in Sipunculus nudus as a function of ambient carbon dioxide. Journal of Experimental Biology, 201: 43-55.

Pörtner, H.O., Langenbuch, M., Reipschläger, A., (2004). Biological Impact of Elevated Ocean CO_2 Concentrations: Lessons from Animal Physiology and Earth History. Journal of Oceanography, 60: 705-718.

Pörtner, H.O., Langenbuch, M., Michaelidis, B., (2005): Synergistic effects of temperature extremes, hypoxia and increases in CO_2 on marine animals: from earth history to global change. Journal of Geophysical research – Oceans, 110: C09S10.

Redfield, A.C., Goodkind, R., (1929). The significance of the Bohr effect on the respiration and asphyxiation of the squid, Loligo pealei. The Journal of Experimental Biology., 6: 340-349.

Rehder, G., Kirby, S.H., Durham, W.B., Stern, L.A., Peltzer, E.T., Pinkston, J., Brewer, P.G., (2004). Dissolution rates of pure methane hydrate and carbon-dioixde hydrate in understaturated seawater at 1000-m depth. Geochimica et Cosmochimica Acta, 68: 285-292.

Remmers, J. E., Torgerson, C., Harris, M., Perry, S.F., Vasilakos, K., Wilson, R.J.A., (2001). Evolution of central respiratory chemoreception: A new twist on an old story. Respiratory Physiology, 129: 211-217.

Riestenberg, D.E., Tsouris, C., Brewer, P.G., Peltzer, E.T., Walz, P., Chow, A.C., Adams, E.E., (2005). Field studies on the formation of sinking CO_2 particles for ocean carbon sequestration: effects of injector geometry on particle density and dissolution rate and model simulation of plume behavior. Environmental Science and Technology, 39: 7287-7293

Sadiq, M., 1992: Toxic Metal Chemistry in Marine Environments. Marcel Dekker, New York. 390 pp.

Sakai, H., Gamo, T., Kim, E.-S., Tsutsumi, M., Tanaka, T., Ishibashi, J.-I., Wakita, H., Yamano, M., Oomori, T., (1990). Venting of carbon dioxide-rich fluid and hydrate formation in mid-Okinawa Trough backarc basin. Science, 248: 1093-1096.

Salomons, W., Forstner, U., (1984): Metals in the Hydrocycle. Springer-Verlag, Heidelberg. 349 pp.

Santschi, P.H., Anderson, R.F., Fleisher, M.Q., Bowler, W., (1991). Measurements of diffusive sublayer thicknesses in the ocean by alabaster dissolution, and their implications for the measurements of benthic fluxes. Journal of Geophysical Research, 96: 10641-10657.

Sato, T., (2004). Numerical simulation of biological impact caused by direct injection of carbon dioxide in the ocean. Journal of Oceanography, 60: 807-816.

Scheid, P., Shams, H., Piper, J., (1989). Gas exchange in vertebrates. Verh. Dtsch. Zool. Ges., 82: 57-68.

Sedwick, P.N., McMurtry, G.M., MacDougall, J.D., (1992). Chemistry of hydrothermal solutions from Pele's Vents, Loihi Seamount, Hawaii. Geochimica et Cosmochimica Acta, 56: 3643-3667.

Seibel, B.A., Walsh, P.J., (2003). Biological impacts of deep-sea carbon dioxide injection inferred from indices of physiological performance. The Journal of Experimental Biology, 206: 641-650.

Shirayama, Y., (1995): Current status of deep-sea biology in relation to the CO_2 disposal. In: Handa, N., Ohsumi, T., (Eds.), Direct Ocean Disposal of Carbon Dioxide. Terra Scientific Publishing Company. Tokyo, Japan. pp. 253-264.

Shirayama, Y., (1998). Biodiversity and biological impacts of ocean disposal of carbon dioxide. Waste Management, 17: 381-384.

Shirayama, Y., Thornton, H., (2005). Effect of increased atmospheric CO_2 on shallow water marine benthos. Journal of Geophysical Research – Oceans, 110: C09S08.

Shitashima, K., Maeda, Y., (2005). Fate of liquid CO_2 discharged from the hydrothermal area in the Okinawa Trough. EOS Transactions, American Geophysical Union 86(52), Fall Meeting Supplement, Abstract B33A-1018.

Smith, K.L., (1992). Benthic boundary layer communities and carbon cycling at abyssal depths in the central North Pacific. Limnology and Oceanography, 37: 1034-1056.

Snelgrove, P.V.R., Smith, C.R., (2002). A riot of species in an environmental calm: The paradox of the species-rich deep-sea floor. Oceanography and Marine Biology, 40: 311-342.

Song, Y., Nishio, M., Chen, B., Someya, S., Uchida, T., Akai, M., (2002). Measurement of the density of CO_2 solution by Mach-Zehnder Interferometry. Annals of the New York Academy of Sciences, 972: 206-212.

Spicer, J.I., Raffo, A., Widdcombe, S., (2007). Influence of CO_2 related seawater acidification on extracellular acid-base balance in the velvet swimming crab Necora puber. Marine Biology, 151: 1117-1125.

Staudigel, H., Hart, S.R., Pile, A., Bailey, B.E., Baker, E.T., Brooke, S., Connelly, D.P., Haucke, L., German, C.R., Hudson, I., Jones, D., Koppers, A.P., Konter, J., Lee, R., Pietsch, T.W., Tebo, B.M., Templeton, A.S., Zierenberg, R., Young, C.M., (2006). Vailulu'u Seamount, Samoa: Life and death on an active submarine volcano. Proceedings of the National Academy of Sciences of the USA, 103: 6448-6453.

Tamburri, M.N., Barry, J.P., (1999). Adaptations for scavenging by three diverse bathyal species, Eptatretus stouti, Neptunea amianta and Orchomene obtusus. Deep-Sea Research, 46: 2079-2093.

Tamburri, M.N., Brewer, P.G., (2000). Determining the effects of CO_2 ocean disposal on deep-sea organisms. Proceedings of the International Symposium on Deep Sea Sequestration of CO_2 (Deep Sea & CO_2 2000). 1-2 February 2000, Tokyo, Japan. Conference Paper 3-5.

Tamburri, M.N., Peltzer, E.T., Friederich, G.E., Aya, I., Yamane, K., Brewer, P.G., (2000). A field study of the effects of CO_2 ocean disposal on mobile deep-sea animals. Marine Chemistry, 72: 95-101.

Tarasov, V.G., Propp, M.V., Propp, L.N., Zhirmunsky, A.V., Namsaraev, B.B., Gorlenko, V.M., Starynin, D.A., (1990). Shallow-water gasohydrothermal vents of Ushishir Volcano and the ecosystem of Kraternaya Bight (The Kurile Islands). Marine Ecology, 11: 1-23.

Teng, H., Yamasaki, A., Shindo, Y., (1996). The fate of liquid CO_2 disposed of in the ocean. International Energy, 21: 765-774.

Teng, H., Yamasaki, A., Shindo, Y., (1999): The fate of CO_2 hydrate released in the ocean. International Journal of Energy Research, 23: 295-302.

The Royal Society (2005). Ocean acidification due to increasing atmospheric carbon dioxide. Policy document 12/05.

Thistle, D., Sedlacek, L., Carman, K.R., Fleeger, J.W., Brewer, P.G., Barry, J.P., (2007). Exposure to carbon dioxide-rich seawater is stressful for some deep-sea species: an in situ, behavioral study. Marine Ecology-Progress Series, 340: 9-16.

Tsouris, C., Brewer, P., Peltzer, E., Walz, P., Riestenberg, D., Liang, L., West, O.R., (2004). Hydrate composite particles for ocean carbon sequestration: field verification. Environmental Science and Technology, 38: 2470-2475.

Vetter, E.W., Smith, C.R., (2005). Insights into the ecological effects of deep ocean CO_2 enrichment: The impacts of natural CO_2 venting at Loihi seamount on deep sea scavengers. Journal of Geophysical Research, 110: C09S13.

Walsh, P.J., Milligan, C.L., 2989. Coordination of metabolism and intracellular acid-base status: ionic regulation and metabolic consequences. Can J Zoo. 67: 2994-3004.

Wheatly, M.G., Henry, R.P., (1992). Extracellular and intracellular acid–base regulation in crustaceans. Journal of Experimental Zoology, 263: 127-142.

Wickins, J.F., (1984). The effect of hypercapnic sea water on growth and mineralization in penaeid prawns. Aquaculture, 41: 37-48.

Winthaegen, P., Arts, R., Schroot, B., (2005). Monitoring subsurface CO_2 storage. Oil & Gas Science and Technology – Revue de l'IFP, 60: 573-582.

Yoshii, K., Yotsui, C., (1997), NH_3- and CO_2-induced suppression of taste nerve responses in clawed toads and eels. Brain Research, 757: 202-208.

Zeebe, R., Wolf-Gladrow, D., (2001). CO2 in seawater: Equilibrium, Kinetics, Isotopes. Elsevier. Amsterdam. 346pp.

Zhang, Y., (2005). Fate of rising CO_2 droplets in seawater. Environmental Science and Technology, 39: 7719-7724.

Zhirmunsky, A.V., Tarasov, V.G., (1990). Unusual marine ecosystem in the flooded crater of Ushisher volcano. Marine Ecology Progress Series, 65: 95-102.

Chapter 7 References

Dunk. R.M., Peltzer, E.T., Walz, P.M., Brewer, P.G., (2005). Seeing a deep ocean CO_2 enrichment experiment in a new light. Environmental Science & Technology, 39: 9630-9636.

Dunk, R.M., Brewer, P.G., Peltzer, E.T., Walz, P.M., Hester, K.C., Sloan, E.D., (2006). The exchange reaction between methane hydrate and carbon dioxide: An oceanic feasibility test. . EOS Transactions, American Geophysical Union 87(52), Fall Meeting Supplement, Abstract MR43A1070

Fosså, J.H., Mortensen, P.B., Furevik, D.M., (2002). The deep-water coral Lophelia pertusa in Norwegian waters : distribution and fishery impacts. Hydrobiologia, 471: 1-12.

Freiwald, A., (2002). Reef-forming cold-water corals. In: Wefer, G., Billett, D., Hebbeln, D., Jorgensen, B.B., Schluter, M., Van Weering, T. (Eds.), Series Ocean Margin Systems. Springer-Verlag, Berlin, pp. 365-385.

Freiwald, A., Fosså, J.H., Grehan, A., Koslow, T., Roberts, J.M., (2004). Cold-water Coral Reefs. UNEP-WCMC, Cambridge, UK.

Gass, S.E., Roberts, J.M., (2006). The occurrence of the cold-water coral *Lophelia pertusa* (Scleractinia) on oil and gas platforms in the North Sea: Colony growth, recruitment and environmental controls on distribution. Marine Pollution Bulletin, 52: 549–559.

Graue, A., Kvamme, B., Baldwin, B.A., Stevens, J., Howard, J., Ersland, G., Husebø, J., Zornes, D.R., (2006). Magnetic Resonance Imaging of methane - carbon dioxide hydrate reactions in sandstone Pores. SPE Annual Technical Conference, 24–27 September 2006, San Antonio, Texas, USA., Paper SPE 102915.

Guinotte, J.M., Orr, J., Cairns, S., Freiwald, A., Morgan, L., George, R., (2006). Will human induced changes in seawater chemistry alter the distribution of deep-sea scleractinian corals? Frontiers in Ecology and the Environment, 4:141-146.

Henriet, J-P., Mienert, J., (1998). Gas Hydrates: Relevance to world margin stability and climate change. Geological Society Special Publication No. 137, pp338, London.

Henriet, J., De Mol, B., Pillen, S., Vanneste, M., Van Rooiji, D., Versteeg, W., Croker, P.F., Shannon, P.M., Unnithan, V., Bouriak, S., Chachkine, P., (1998). Gas hydrate crystals may help build reefs. Nature 391, 648–649.

Hovland, M., Thomsen, E., (1997). Cold-water corals—are they hydrocarbon seep related? Marine Geology, 137: 159-164.

Hovland M, Risk, M., (2003). Do Norwegian deep-water coral reefs rely on seeping fluids? Marine Geology, 198: 83-96.

Hovland, M., Mortensen, P., Brattegard, T., Strass, P., Kokeongen, K., (1998). Ahermatypic coral banks off Mid-Norway: evidence for a link with seepage of light hydrocarbons. Palaios, 13: 189-200.

IPCC Third Assessment Report (Climate Change 2001: The Scientific Basis) (Cambridge UK: Cambridge University Press, 2001)

Kennett, J., Cannariato, K.G., Hendy, I.L., Behl, R.J., (2003), Methane Hydrates in Quaternary Climate Change: the clathrate gun hypothesis. American Geophysical Union (Washington, DC, USA), 216 pp.

Kvenvolden, K.A., (1993). Gas hydrates—geological perspective and global change. Reviews of Geophysics, 31: 173-187.

Kvenvolden, K.A., (1999). Potential effects of gas hydrate on human welfare: Proceedings of the National Academy of Sciences of the USA, 96: 3420-3426.

Kvenvolden, K.A., (2000). Gas Hydrate and Humans. In Gas Hydrates: Challenges for the Future. Annals of the New York Academy of Sciences, 912:17-22.

Komai, T., Kawamura, T., Kang, S., Nagashima, K., Yamamoto, Y., (2002). In situ observation of gas hydrate behaviour under high pressure by Raman Spectroscopy. Journal of Physics: Condensed Matter, 14: 11395-11400.

Lee, H., Seo, Y., Seo, Y.-T., Moudrakovski, I.L., Ripmeester, J.A., (2003). Recovering methane from solid methane hydrate with carbon dioxide. Angewandte Chemie International Edition, 42: 5048-5051.

Maslin, M.A., (2004). Gas Hydrates: A Hazard for the 21st Century. Issues in Risk Science 03, Benfield Hazard Research Centre

Maslin, M.A., Owen, M., . Day, S,, Long, D., (2004). Linking continental slope failure to climate change: Testing the Clathrate Gun Hypothesis. Geology, 32: 53-56.

MASSON, D.G., HARBITZ, C.B., WYNN, R.B., PEDERSEN, G., LØVHOLT, F., (2006). Submarine landslides: processes, triggers and hazard prediction. Philosophical Transactions of the Royal Society of London Series A, 364: 2009-2039.

Mortensen, P.B., Rapp, H.T., (1998). Oxygen- and carbon isotope ratios related to growth line patterns in skeletons of *Lophelia pertusa* (L) (Anthozoa: Scleractinia): Implications for determination of linear extension rates. Sarsia, 83: 433–446.

Park, Y., Kim, D.-Y., Lee, J.-W., Huh, D.-G., Park, K.-P., Lee, J., Lee, H., (2006). Sequestering carbon dioxide into complex structures of naturally occurring gas hydrates. Proceedings of the National Academy of Sciences of the USA, 103: 12690-12694.

Roberts, H.H., & Aharon, P., (1994). Hydrocarbon-derived carbonate buildups of the northern Gulf of Mexico continental slope; a review of submersible investigations. In: Aharon, P. (Ed), Hydrocarbon seeps and vents. Geo-Marine Letters, 14: 135-148.

Roberts, J.M., Long, D., Wilson, J.B., Mortensen, P.B., Gage J.D., (2003). The cold-water coral Lophelia pertusa (Scleractinia) and enigmatic seabed mounds along the north-east Atlantic margin: are they related? Marine Pollution Bulletin, 46: 7–20

Roberts, J.M., Wheeler, A.J., Freiwald A (2006). Reefs of the deep: The biology and geology of cold-water coral ecosystems. Science, 312: 543-547.

Rogers, A.D., (1999). The biology of Lophelia pertusa (Linnaeus 1758) and other deep-water reef-forming corals and impacts from human activities. International Review of Hydrobiology, 84, 315-406.

Rogers, A., (2006). The biology, ecology and vulnerability of deep-water coral reefs. International Union for Conservation of Nature & Natural Resources.

Sloan, E.D., (1998a). Clathrate Hydrates of Natural Gases, second edition. Marcel Dekker.

Sloan, E.D., (1998b). Physical/chemical properties of gas hydrates and application to world margin stability and climate change. Geological Society of London Special Publication, 137: 31-50.

Turley, C.M., Roberts, J.M., Guinotte, J.M., (2007). Corals in deep-water: will the unseen hand of ocean acidification destroy cold-water ecosystems? Coral Reefs, 26: 445-448.

UK Biodiversity Group, (2000). Tranche 2 Action Plans. Volume V – Maritime Species and Habitats. Peterborough, English Nature.

WWF, (2004). Cold water corals: Fragile havens in the deep. WWF-World Wide Fund For Nature.

Yoon, J.H., Kawamura, T., Yamamoto, Y., Komai, T., (2004). Transformation of methane hydrate to carbon dioxide hydrate: In situ Raman spectroscopic observations. Journal of Physical Chemistry A, 108: 5057-5059.